CLIMATE AND CARBON-CYCLING IN THE EARLY CRETACEOUS

KATE LITTLER

DEPARTMENT OF EARTH SCIENCES, UCL

THESIS SUBMITTED FOR THE AWARD OF DOCTOR OF PHILOSOPHY

MAY 2011

DECLARATION

I, Kate Littler confirm that the work presented in this thesis is my own. Where information has been derived from other sources, I confirm that this has been indicated in the thesis.

ABSTRACT

The Cretaceous (~145–65 Ma) is widely regarded as a greenhouse period with warm, equable climates and elevated atmospheric CO_2 relative to the modern. However, the earliest Cretaceous (Berriasian–Barremian; 145–125 Ma) is commonly characterised as a relatively colder "coolhouse" interval, typified by lower global temperatures than the mid-Cretaceous. Unfortunately, the lack of absolute sea surface temperature (SST) estimates prior to the Barremian has hampered efforts to definitively reconstruct Early Cretaceous climate. Here, the TEX_{86} palaeotemperature proxy, for which a detailed review is provided, has been used to generate a 13 myr record of SST estimates for the Early Cretaceous, based on sediments from assorted deep-sea drilling sites. A consistent offset in the TEX_{86} ratio between transported mudstones and pelagic carbonates in the low-latitude marine sediments (DSDP Sites 603 and 534) has been identified, which may be linked to post-burial diagenesis or a difference in organic matter type between lithologies. Mindful of these apparent lithological effects on TEX_{86}, only the pelagic sediments were used to subsequently reconstruct Early Cretaceous SSTs. These TEX_{86} records demonstrate both elevated SSTs (>27 ºC) at low and mid-latitudes relative to the modern, and the apparent stability of these high temperatures over long timescales. This lack of SST variation in the low-latitudes during the Valanginian positive carbon-isotope event (CIE; ~135–138 Ma), casts doubt on the warming-weathering feedback model put forward to explain this major perturbation. Additionally, new paired bulk organic ($\delta^{13}C_{org}$) and bulk carbonate ($\delta^{13}C_{carb}$) carbon-isotope records from North Atlantic DSDP sites, have been used to reconstruct relative changes in pCO_2 across the CIE. These observed fluctuations in $\Delta^{13}C$ imply changes in carbon-cycling and a possible drawdown in CO_2, due to excess organic matter burial associated with the CIE.

ACKNOWLEDGEMENTS

I'd like to wholeheartedly thank my supervisors Stuart Robinson and Paul Bown for three years of excellent guidance and support. For always having their doors open, and their red pens poised to correct my numerous mistakes with endless patience.

Three and half years of financial support for this project from NERC, is gratefully acknowledged, as is support from the UCL Grad School and UKIODP which enabled me to attend international conferences.

I'm indebted to Sandra Nederbragt for taking the time to train me in the TEX_{86} technique, and for introducing me to the world of organic geochemistry. I'd also like to thank Richard Pancost, for the many helpful discussions about various aspects of organic geochemistry, and for the tireless editing of the many versions of our paper.

Thanks to John Hill for helping me keep the temperamental HPLC-MS happily generating data over the last three years. Thanks to Rindy Ostermann for assistance in generating carbon-isotope data, and to Tony Osborn and Jim Davy for additional lab support.

I'm grateful to Kyle Taylor at Bristol for kindly producing additional GCMS data, and to Luke Handley and Ian Harrison at Newcastle for help with producing pyrolysis data.

My friends from UCL, London and beyond certainly deserve a mention, for coping with the endless stream of complaining about the horrors of writing-up, and for coaxing me out of the lab from time to time for some fresh air and a pint. Thanks to Raki and Tash in particular for the lunchtime gossip sessions and words of encouragement. Good luck with finishing your own PhDs girls. You can do it!

Thanks to Sam for being an absolute rock. For providing numerous cups of tea and pep-talks, and for not saying a word when I'm home two hours later than I said I would be. One day soon you'll know what all the fuss was about.

Mum, you've been an inspiration for submitting your PhD (just) before me. Dad you've been a soldier for putting up with both of our PhD-related whinging over the years. Christine, thanks for always reminding me that there is life beyond academia in the real world.

"If we knew what we were doing, it wouldn't be called research"
-Albert Einstein

CONTENTS

FIGURES

CHAPTER 1: INTRODUCTION

CHAPTER 3: A LITHOLOGY EFFECT ON THE TEX_{86} PROXY?

TABLES

CHAPTER 1. INTRODUCTION

1. 1. AIMS

The overarching aim of this thesis is to investigate climate and carbon-cycling in the earliest Cretaceous (Berriasian to Barremian; ~145 – 125 Ma), with particular reference to the enigmatic Valanginian carbon-isotope excursion. This will be achieved by producing new palaeotemperature and carbon-isotope records from globally distributed deep-sea marine sediments, to generate sea-surface temperature and pCO_2 estimates.

1. 2. SCIENTIFIC RATIONALE

The Cretaceous (~145 – 65 Ma) is widely thought to have been a "greenhouse" interval, typified by both high atmospheric CO_2 levels and warm average global temperatures relative to the modern (e.g. Herman & Spicer, 1996; Skelton *et al*., 2003; Hay, 2008; Jenkyns, 2010). Understanding the climate dynamics of past greenhouse worlds is of great importance, considering the large projected increase in atmospheric CO_2 due to anthropogenic activities, and the likely subsequent increase in global temperatures (IPCC, 2007). It may be that the Cretaceous–Early Cenozoic interval is the closest analogy to the warm, potentially ice-free world we are creating for our near future, and therefore warrants detailed investigation.

While the Cretaceous Period as a whole is universally accepted to have been characterised by elevated temperatures and low meridional temperature gradients, the Late Jurassic – earliest Cretaceous interval has often been portrayed as a relatively cooler interval, characterised by intermittent cold snaps and even transient glaciations (e.g. Price, 1999). Evidence to support this theory has come in the form of sedimentological observations, geochemical studies based on biogenic carbonate, and changes in palaeontological trends (e.g. Frakes & Francis, 1988; Kessels *et al*., 2006; McArthur *et al*., 2007a; Price & Nunn, 2010). All of these threads of evidence have been used to suggest that the Late Jurassic – Early Cretaceous was a "coolhouse" interval prior to the onset of true "hothouse" conditions in the mid

Cretaceous (e.g. Price, 1999). However, this theory stands at odds with the reconstructed high pCO_2 estimates for this interval, and challenges our understanding of the role of CO_2 in forcing the climate system (e.g. Tajika *et al*., 1999; Veizer *et al*., 2000; Robinson *et al*., 2002; Royer *et al*., 2004, 2007). Deconvolving this issue is complicated by both widely differing estimates of Early Cretaceous pCO_2 and a lack of quantitative SST estimates prior to the Early Barremian (Mutterlose *et al*., 2010; Jenkyns *et al*., 2011).

The earliest Cretaceous is notable for the large perturbation to the carbon-cycle that occurred during the Valanginian–Hauterivian period, known as the "Valanginian positive carbon-isotope event" (CIE; ~135–138 Ma) (e.g. Lini *et al*., 1992; Weissert *et al*., 1989; 1998; Erba *et al*., 2004). This prominent excursion, of ~+1.5‰ in carbonate ($\delta^{13}C_{carb}$) and ~+4‰ in organic-matter ($\delta^{13}C_{org}$) records, has been documented from many sections around the World, including Tethyan, North Atlantic and Central Pacific regions (e.g. Weissert *et al*., 1998; Erba *et al*., 2004). While the CIE itself is well-documented, there is a lack of evidence for organic-rich marine sediments ("black shales") in the Valanginian, which are commonly accompany large positive excursions in the Mesozoic carbon-isotope record (e.g. Weissert *et al*., 1998; Erba *et al*., 2004; Jenkyns, 2010). Therefore the mechanisms put forward to explain the Valanginian CIE remain controversial (e.g. Weissert *et al*., 1998; Erba *et al*., 2004; Westermann *et al*., 2010). The influx of volcanic pCO_2 from activity in the Paraná-Etendeka Large Igneous Province has been identified as the possible trigger mechanism, but little evidence has been put forward to support the hypothesised large changes in temperature or atmospheric pCO_2 at this time (e.g. Erba *et al*., 2004; McArthur *et al.,* 2007a; and references therein).

There is, therefore, a need for both new pCO_2 and SST records from the Berriasian–Barremian to aid in the interpretation of the Valanginian CIE and to constrain climate more closely during the earliest Cretaceous. It is possible to produce pCO_2 estimates using paired bulk carbonate ($\delta^{13}C_{carb}$) and bulk organic-matter ($\delta^{13}C_{org}$) records from the same samples, but there is currently a dearth of such records in the earliest Cretaceous. Many high-resolution $\delta^{13}C_{carb}$ records have been generated but there are comparatively fewer $\delta^{13}C_{org}$ records, very few of which are based on the same samples as are used in the bulk-carbonate records. Ergo, there is a

need for more high-resolution paired $\delta^{13}C_{carb}$ and $\delta^{13}C_{org}$ records from the earliest Cretaceous.

The TEX_{86} palaeotemperature proxy can be applied to marine sediments in order to generate SST estimates for the earliest Cretaceous. The TEX_{86} proxy makes use of the relationship between the ratio of different GDGT (glycerol dialkyl glycerol tetraether) lipids in non-thermophilic crenarchaeotal membranes, and the temperature of the seawater in which the organisms lived (e.g. Schouten *et al*., 2002). The proxy is based on the distribution of GDGT molecules preserved in marine sediments, and is thought to best correlate with the mean annual SST of the overlying water column at the time of deposition (e.g. Schouten *et al*., 2002; Kim *et al*., 2008; 2010). TEX_{86}–derived SST estimates already exist for the Barremian and have been shown to be applicable as far back as the Late Jurassic (Mutterlose *et al*., 2010; Jenkyns *et al*., 2011). This technique therefore offers the opportunity to reconstruct SSTs in the Berriasian–Barremian, as it can be used in a variety of marine settings, is independent of initial seawater chemistry and can be calibrated to absolute temperatures (e.g. Schouten *et al*., 2002; Kim *et al*., 2008; Kim *et al*., 2010).

However, before the TEX_{86} proxy can be used to reconstruct palaeotemperatures in the earliest Cretaceous, it is necessary to ascertain its suitability for generating SST estimates in Berriasian–Barremian marine cores. TEX_{86} is considered to be a SST proxy, however there are many assumptions inherent in this supposition and other factors such as lateral transport of GDGTs and possible post-depositional modulation of the TEX_{86} ratio must be considered before robust SST estimates can be made.

1. 3. THESIS STRUCTURE

Chapter 1: *Introduction.* This chapter outlines the background to Late Jurassic–Early Cretaceous palaeogeography and climate, provides a brief overview of the carbon-cycle and carbon-isotopes and gives a detailed explanation of the TEX_{86} proxy. The proxy and modelling evidence for climate in the Early Cretaceous will be explored in greater detail in Chapter 4. Similarly, a more in-depth discussion of earliest Cretaceous carbon-cycle perturbations and carbon-isotope interpretation will be given in Chapter 5. Chapter 1 includes an extended section on the TEX_{86} proxy, as

this is a recently developed technique, which requires greater explanation and justification than other more established proxies.

Chapter 2: *Materials and Methods*. This chapter outlines the location and lithostratigraphy of the deep-sea marine sediments studied in this thesis, and the biostratigraphy and magnetostratigraphy used to constrain the age-models for these cores. The geochemical and palaeontological techniques used throughout this thesis are outlined in detail in this chapter, and will not be repeated in subsequent chapters.

Chapter 3: *A lithological effect on the TEX_{86} proxy?* This chapter probes the use of the TEX_{86} palaeotemperature proxy in low-latitude, proto-North Atlantic cores of earliest Cretaceous age. In an effort to understand the effects of transportation on TEX_{86} in the earliest Cretaceous, co-occurring pelagic and transported turbiditic sediments from Deep Sea Drilling Program (DSDP) Sites 603 and 534 in the palaeo-North Atlantic are investigated. Any differences between the two lithologies in terms of their TEX_{86} ratios can be interpreted in a number of ways: 1) primary SST variations between the two sediment source areas; 2) different populations of marine Crenarchaeota in the shelf and deep-sea environments; 3) secondary diagenesis of the GDGT molecules by oxic degradation during transport or deposition. Analysis of geochemical and calcareous nannofossil assemblage data is used to narrow down the origin of the offset in TEX_{86}.

Chapter 4: *Sea-surface temperatures in the Early Cretaceous.* In Chapter 4, the first absolute SST estimates for the earliest Cretaceous, from multiple DSDP and ODP sites, are presented. The SST data produced using this technique are used to comment on both the absolute temperature and likely meridional temperature gradients during this period, as well as the relative stability of the climate over a >10 Myr timescale.

Chapter 5: *Organic carbon-isotope records from the western proto-North Atlantic: $\delta^{13}C$ excursions and pCO_2 estimates.* In this chapter the carbon-cycle of the Berriasian – Barremian is investigated, by generating bulk-organic carbon-isotope records for the western proto-North Atlantic, and comparing these values to existing bulk-carbonate data. This provides information on pCO_2 fluctuations in the earliest

Cretaceous. The trends in calcareous nannofossil assemblages from Chapter 3 and the SST records from Chapter 4 are combined with the new pCO_2 record from this chapter, to allow potential mechanisms for the Valanginian positive carbon-isotope excursion to be explored.

Chapter 6: *Conclusions and further work.* This chapter will provide a synthesis of the results presented in Chapters 3 to 5, and a summary of the overall conclusions of this thesis. Suggestions for future work will be outlined in brief.

1. 4. PALAEOGEOGRAPHIC AND CLIMATIC SETTING OF THE EARLY CRETACEOUS

1. 4. 1. INTRODUCTION

The Mesozoic Era incorporates the Triassic to Cretaceous Periods, ~245 – 65 Ma, and is considered to have been a time of elevated temperatures, equable climates and weakly developed climatic zones (e.g. Frakes, 1979; Hallam, 1985; Skelton *et al*., 2003). The Cretaceous in particular is often regarded as the warmest Period of the Mesozoic, characterised by long-term global warmth, shallow meridional temperature gradients, and a paucity of high-latitude ice (e.g. Herman & Spicer, 1996; Skelton *et al*., 2003). Atmospheric pCO_2 levels during the Cretaceous are thought to have been greatly elevated with respect to the modern, although placing constraints on absolute values remains difficult, and periods of lower pCO_2 have been proposed (e.g. Berner, 1994; Tajika *et al*., 1999; Wallmann *et al*., 2001; Berner & Kothavala, 2001; Haworth *et al*., 2005; Royer *et al*., 2007). However, despite the consensus for a largely warm and equable Mesozoic, it has been suggested that several intervals were characterised by cooler climates and steeper meridional temperature gradients (e.g. Frakes *et al*., 1992). The Late Jurassic – Early Cretaceous is one such interval, and is often regarded as a time of relatively cool conditions within the Mesozoic, prior to the onset of true Cretaceous "greenhouse" conditions in the mid-Cretaceous (e.g. Hallam, 1985; Price, 1999). There is also evidence to suggest that the relatively dry climate of the Late Jurassic, characterised by widespread evaporitic deposits and presumed aridity, was replaced by progressively more humid conditions in Eurasia and North America during the earliest Cretaceous,

which triggered the deposition of large-scale coal deposits in these regions (Hallam, 1984; Hallam, 1987; Westermann *et al*., 2010; Figure 1).

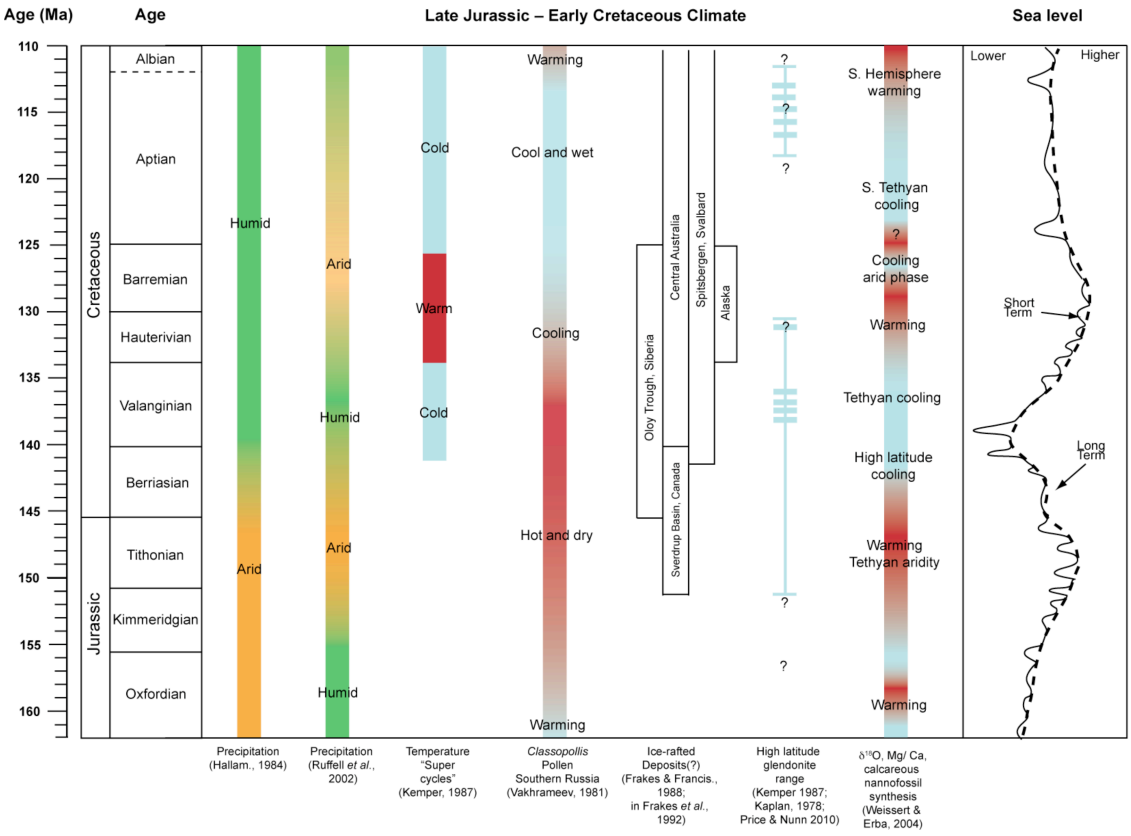

Figure 1. *Overview of broad trends in Late Jurassic to Early Cretaceous sea-level (Haq et al., 1987; Hardenbol et al., 1998) and climate, in terms of both temperature and precipitation (bars 1 – 6). Blue and red colours indicate relatively cooler periods and warmer temperatures respectively. Timescale after Gradstein et al. (2004) and McArthur et al. (2007a). Correlation between studies is complicated by the differing age models which the various studies are tied to.*

Importantly in terms of climate and ocean circulation, the Late Jurassic – Early Cretaceous witnessed the prelude to the final break-up of the Late Palaeozoic supercontinent, Pangaea. The increased volcanism and ocean spreading rates associated with the demise of Pangaea, coupled with the well-documented changes in sea level and the reorganisation of ocean gateways, would have had a profound influence on global climate and ocean circulation at this time (e.g. Parrish, 1993). The palaeogeography of the Early Cretaceous was dominated by the fragmenting supercontinent, with the northern Eurasian landmasses grouped together in the subsidiary supercontinent of Laurasia and the southern landmasses of South

America, Africa, Antarctica, India and Australia, which formed the core of the Gondwanan landmass (Figure 2). More than half the globe was occupied by the Panthalassic Ocean, with the large Tethyan Ocean incising into Pangaea from the east. The proto-North Atlantic, which had begun to rift apart in the Jurassic, was, by the earliest Cretaceous, a fully marine and unrestricted environment, which continued to open and widen throughout the mid-Cretaceous, while the South Atlantic was yet to form between Africa and South America.

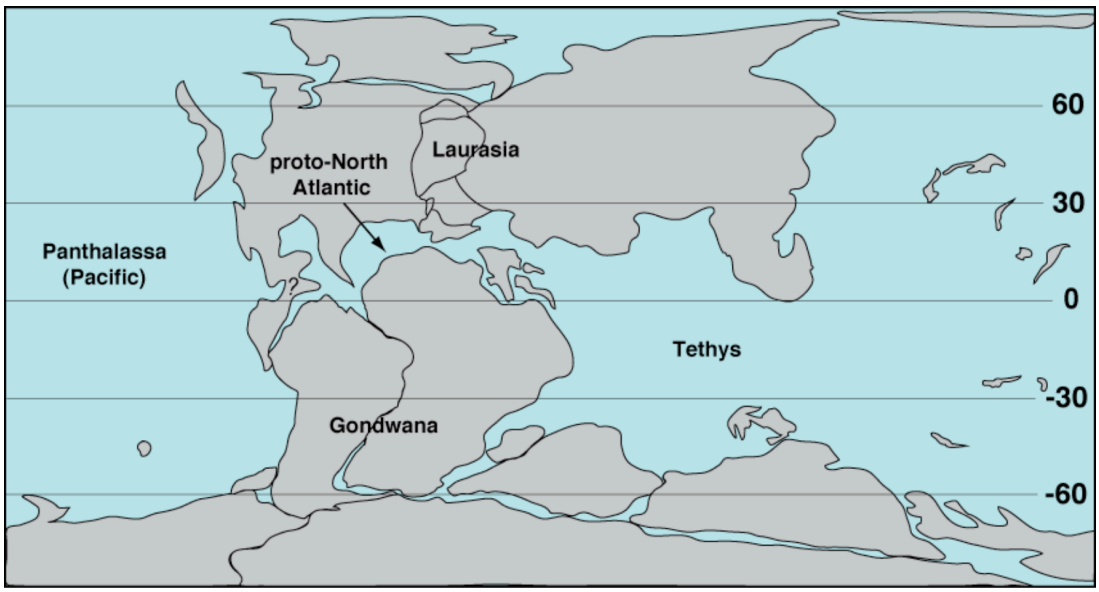

Figure 2. *Reconstructed continental arrangement at ~133 Ma (Early Hauterivian) based on the Ocean Drilling Stratigraphic Network plate tectonic reconstruction service (http://www.odsn.de/odsn/services/paleomap/paleomap.html).*

The Early Cretaceous is thought to have been punctuated by large fluctuations in sea-level (of up to 90 m), with several minor transgressive and regressive phases set against a background of generally rising sea levels between the Berriasian and the Early Valanginian (Haq *et al.,* 1987; Hardenbol *et al*., 1998; Figure 1). Some authors have suggested that these rapid sea-level variations could be the result of fluctuating global climate, and in particular changes in continental ice volume, superimposed on the long-term rise due to evolving ocean-spreading rates (e.g. McArthur *et al*., 2007a; Price, 1999; Stoll & Schrag, 1996). Some of the Valanginian and Hauterivian sea-level fluctuations have also previously been related

to platform drowning events in the Tethys and changes in provincialism of fauna between the Tethyan and Boreal realms (Weissert *et al*., 1998; Melinte & Mutterlose, 2001).

1. 4. 2. SEDIMENTOLOGICAL AND PALAEONTOLOGICAL EVIDENCE FOR CLIMATE CHANGE

The evidence for important climatic variations during the Berriasian–Barremian comes from a variety of sedimentological, palaeontological and geochemical evidence (e.g. Frakes & Francis, 1988; Kemper, 1989; Follmi *et al*., 1994; Price, 1999; Price *et al*., 2000; Mutterlose & Kessels, 2000; Pucéat *et al*., 2003; Price & Mutterlose 2004; Kessels *et al*., 2006; McArthur *et al*., 2007a; Price & Nunn, 2010; Duchamp-Alphonse), and is discussed in detail in Chapter 3, so only a brief summary will be presented here.

Sedimentological evidence was the first to be put forward in support of a "coolhouse" earliest Cretaceous (e.g. Price, 1999). Physical indicators of land-based ice such as tills and glacial striations are rare, but more indirect indicators such as purported dropstones are much more common (e.g. Frakes & Francis, 1988). Dropstones are outsized clasts within finer-grained sediment, which are often interpreted as being transported to the site of deposition by rafted continental ice, although other non-glacial explanations are also possible (e.g. Price, 1999). Some angular conglomeratic or brecciated deposits of Mesozoic age are interpreted as tills and diamictites, and are assumed to have a meltwater outflow or other glacial origin, but could also be the result of non-glacial debris flows (e.g. Alley & Frakes, 2003).

Other sedimentological evidence includes the presence of glendonites, thought to be indicative of cool bottom waters, in high-latitude locations such as Svalbard and Arctic Canada (e.g. Kemper *et al*., 1987; Price & Nunn, 2010). Glendonites are stellate calcite psuedomorphs of the low-temperature mineral ikaite ($CaCO_3 \cdot 6H_2O$), which, by analogy to modern ikaite deposits in the high Arctic, are thought to crystallize at cold bottom-water temperatures between −1.9 to 7°C, in high alkalinity and phosphate-rich environments (e.g. De Lurio & Frakes, 1999; Selleck *et al*., 2007; Price & Nunn, 2010). Clay mineral data from the Northern Hemisphere, shows changes in the ratio of kaolinite (warm and humid formation) to smectite (cool and arid formation), which seems to suggest both warming and cooling intervals

within the earliest Cretaceous (Price *et al*., 2000; Ruffell *et al*., 2002; Mutterlose *et al*., 2003; Duchamp-Alphonse *et al*., 2011).

In addition to the sedimentological evidence for cool earliest Cretaceous conditions, occasional low-latitude occurrences of biota, such as calcareous nannofossils and ammonites, normally associated with cool higher-latitude zones, have been put forward as palaeontological evidence for climatic variation (e.g. Mutterlose & Kessels, 2000; Erba *et al*., 2004; Kessels *et al*., 2006). General discussions of faunal endemism, or lack thereof, of various genera has also been proposed in support of the theory for the establishment of latitudinal climatic zones in the earliest Cretaceous, controlled by changes in temperature, but the effect of sea-level change must also be taken into account in these interpretations (e.g. Melinte & Mutterlose, 2001).

1. 4. 3. GEOCHEMICAL PALAEOTEMPERATURE PROXIES APPLIED TO THE EARLY CRETACEOUS

Geochemical evidence for climate change in the earliest Cretaceous also exists, and is regarded by some palaeoclimatologists as the most compelling evidence for climatic variation during this interval. One of the key pieces of evidence in the argument for cool and variable temperatures in the earliest Cretaceous, has been the application of oxygen-isotopes and Mg/Ca ratios to fossil carbonate materials such as belemnites to obtain absolute and relative temperature estimates (e.g. Ditchfield, 1997; Podlaha *et al*., 1998; Price *et al*., 2000; 2011; van de Schootbrugge *et al*., 2000; Puceat *et al*., 2003; Price & Mutterlose, 2004; McArthur *et al*., 2007a). Details of individual studies are given in Chapter 3, but a discussion of the theory and implications of the proxies is outlined here.

Oxygen isotopes

There are three stable isotopes of oxygen, ^{16}O, ^{17}O and ^{18}O, with natural abundances of 99.759 %, 0.0374 % and 0.2039 % respectively (Nier, 1950). The oxygen-isotope ratio is most often displayed in permil (‰) units relative to a standard (usually Vienna Standard Mean Ocean Water (VSMOW) for aqueous

samples or Vienna PeeDee Belemnite (VPDB) for solid samples), in the delta notation:

Eq. 1.
$$\delta^{18}O = \left(\frac{\delta^{18}O_{sample} - \delta^{18}O_{std}}{\delta^{18}O_{std}} \right) * 1000$$

The varying atomic weights of these isotopes when bound up in water molecules, leads to differential fractionation by evaporation-precipitation processes related to large-scale changes in climate, such as continental ice build–up. This "Rayleigh fractionation" process leads to differing values of the oxygen-isotope ratio in residual seawater ($\delta^{18}O_{sw}$), when different volumes of continental ice are present on the land, as high-latitude ice will be preferentially enriched in the lighter ^{16}O isotope, leaving the residual seawater with a heavier signal (Craig & Gordon, 1965; Shackleton, 1967). This seawater oxygen-isotope value ($\delta^{18}O_{sw}$) is incorporated into the carbonate skeletons of calcareous organisms such as belemnites and calcareous nannofossils, which can then be preserved in sediment archives. However the $\delta^{18}O$ value of carbonates also incorporates a temperature-controlled kinetic fractionation, where the isotopic composition is shifted towards more negative ("lighter") values in warmer temperatures, such that an increase of 4 ºC in temperature will be reflected in a ~1 ‰ decrease in $\delta^{18}O$ (e.g. Marshall, 1992). Thus it is necessary to deconvolve the physical equilibrium (Rayleigh) fractionation effects from the temperature (kinetic) effects in any one $\delta^{18}O$ ratio measurement, which is no trivial matter (e.g. Price *et al*., 2000).

Some authors have attempted to reconstruct absolute temperatures from biogenic calcite using modified modern calibrations, but there are several complicating factors in the construction of palaeotemperature records using this technique. In the modern ocean the $\delta^{18}O$ of seawater ($\delta^{18}O_{sw}$) varies with latitude due to global precipitation patterns, which are difficult to reconstruct in the deep past (e.g. Broecker, 1989; Zachos *et al*., 1994; LeGrande & Schmidt, 2006). Additionally, the biological fractionation imposed by the organism itself when precipitating calcite from seawater, known as the species-specific "vital effect", is also unknown for extinct taxa. This can be corrected for in extant species, but is impossible to determine in extinct clades such as belemnites (e.g. McArthur *et al*., 2007b). The

depth habit of nektonic belemnites is also not well constrained, unlike brachiopods or bivalves that are known to be epifaunal, which may influence the $\delta^{18}O$ value and therefore the temperature estimates from these fossils (e.g. Mutterlose *et al*., 2010). Belemnites are thought to have predominantly inhabited thermocline depths, where the temperature of the water is substantially less than that of surface waters, therefore $\delta^{18}O$ estimates from belemnites are best regarded as minimum estimates of SSTs (van de Schootburgge *et al*., 2000; Price *et al*., 2000; McArthur *et al*., 2007a; Mutterlose *et al*., 2010). However, some evidence suggests that at least some species of belemnites may have had nekto-benthonic life-habits, further complicating their use as recorders of upper-ocean temperatures (Anderson *et al*., 1994; Dutton *et al*., 2007; Price *et al*., 2009). Additionally, belemnites, like all carbonate sedimentary materials, are subject to diagenetic overprinting of their oxygen-isotopic ratios in the sedimentary pile, which must be assessed by visual or geochemical techniques, (e.g. Weissert *et al*., 1989; Marshall, 1992; McArthur *et al*., 2007a). Visual screening techniques include examining thin sections under cathodoluminescence, which make use of the fact that diagenetic calcite enriched in Mn will fluoresce under luminescence light (providing the sample is not also too rich in Fe), and so areas of alteration will become obvious and can be avoided (e.g. Marshall, 1992; Price & Sellwood, 1997). Similarly, determining the concentration of Fe and Mn in calcite using ICP-MS (Inductively Coupled Plasma-Mass Spectrometry) techniques can also be used to identify and remove diagenetic calcite, as both these elements are more enriched in more altered samples (Price & Sellwood, 1997).

Despite these many complications, attempts have been made to reconstruct estimates of absolute temperatures from $\delta^{18}O_{belemnite}$ data, with equations such as Eq. 1 (e.g. Anderson & Arthur, 1983).

Eq. 2. $$T^{o}C = 16.0 - 4.14(\delta^{18}O_{carb} - \delta^{18}O_{sw}) + 0.13(\delta^{18}O_{carb} - \delta^{18}O_{sw})^2$$

Where $\delta^{18}O_{carb}$ is the oxygen-isotope ratio in the sample (VPDB) and $\delta^{18}O_{sw}$ is the oxygen-isotope ratio of the sea-water (VSMOW) at the time of deposition. However, as this equation has three variables and two unknowns, temperature and $\delta^{18}O_{sw}$, the value for $\delta^{18}O_{sw}$ must be independently estimated. In the Mesozoic the value of -1‰ for $\delta^{18}O_{sw}$ based on the assumption of an "ice-free world" is often used after

Shackleton & Kennet 1975), however when excursions to heavy values of $\delta^{18}O$ are used to argue in favour of large continental ice build-up, the reasoning can become rather circular. Other studies have used different values for $\delta^{18}O_{sw}$, to account for effects such as high-latitude precipitation, but again this approach requires many assumptions about ancient hydrology that cannot be independently constrained (Price & Mutterlose, 2004). The paired $\delta^{18}O$ values of glendonites and belemnites have also been used to determine palaeotemperatures in the Early Cretaceous, but again, these estimates are complicated by unknown $\delta^{18}O_{sw}$ values and the uncertain transformation temperature of ikaiite to calcite (Price & Nunn, 2010).

Mg/Ca ratios

Another method of reconstructing seawater temperatures is to use the Mg/Ca ratio of biogenic calcites (e.g. Nürnberg *et al*., 1996; Elderfield & Ganssen, 2000; Lear *et al*., 2002; Lea, 2003). The substitution of calcium by magnesium in calcite tests and shells is governed by a combination of the inorganic distribution coefficient, as well as the physiological processes that affect the uptake of Mg, and as these are kinetic processes, will operate with more efficiency at higher temperatures (Lear *et al*., 2002; Lea, 2003). This technique was originally developed in Cenozoic foraminifera and has subsequently been used successfully in many palaeotemperature studies based on these organisms, from the Holocene to the mid-Cretaceous (e.g. Nürnberg & Müller, 2000; Lear *et al*., 2002; Erbacher *et al*., 2011). Absolute temperatures from other biogenic carbonate materials, such as belemnites, can be constructed using this approach, if modified equations are applied to the Mg/Ca ratio (e.g. McArthur *et al*., 2007a). There are however also many uncertainties associated with this process, such as the taxon-specific vital effect, which cannot be corrected for in extinct genera, and the assumption that the Mg/Ca ratio of the oceans has not changed with time or been unduly affected by salinity effects (McArthur *et al*., 2007a; b; Lea, 2003). In some studies, a combination of $\delta^{18}O$ and Mg/Ca data has been used to constrain $\delta^{18}O_{sw}$, with the Mg/Ca being used to account for the kinetic temperature effect and the remainder of the change in $\delta^{18}O$ being attributed to secular changes in $\delta^{18}O_{sw}$ due to changes in continental ice

volume (e.g. Hays & Grossman, 1991; Elderfield & Ganssen, 2000; McArthur *et al*., 2007a).

1. 5. THE CARBON-CYCLE AND CARBON-ISOTOPE EXCURSIONS

1. 5. 1. THE CARBON-CYCLE

The carbon-cycle consists of a number of large reservoirs of carbon, linked together by a series of geochemical or biogeochemical fluxes from one reservoir to another. These reservoirs include the hydrosphere, atmosphere, biosphere and geosphere, which can all act as either sources or sinks of carbon, acting on a variety of timescales (Figure 3. e.g. Weissert *et al*., 1989; Berner *et al*., 2003). The long-term, or endogenic, carbon-cycle is controlled by processes such as volcanic, metamorphic, erosional and depositional fluxes and operates on the timescales of tens of thousands to millions of years. In this geochemical cycle, volcanism and metamorphism act to increase the concentration of CO_2 in the atmosphere and surface oceans, while negative feedbacks such as silicate weathering and burial of organic matter in the sedimentary environment acts as a sink for CO_2. These long-term processes can be summarised in the following equations, as described by Berner *et al*., 2003:

Eq. 3. $$CO_2 + CaSiO_3 \leftrightarrow CaCO_3 + SiO_2$$

From left to right, this equation represents the drawdown of CO_2 by the weathering of silicate rocks, the transport of the products to the ocean, and their subsequent deposition as carbonate rocks. Going in the reverse direction the equation represents the release of CO_2 from the burial and thermal decomposition of these carbonates.

The long-term biotic carbon cycle can be represented by the equation:

Eq. 4. $$CO_2 + H_2O \leftrightarrow CH_2O + O_2$$

In the forward direction this represents fixation of carbon by photosynthesis, which is eventually stored as organic carbon in the deep sedimentary reservoirs, and may eventually become fossil fuels. The reverse equation represents the oxidative

weathering of organic-matter on the continents, or the burning of fossil fuels by humans, with the release of the CO_2 back into the atmosphere.

The surficial, exogenic or short-term carbon-cycle encompasses oceans, atmosphere, biosphere and soils, i.e. the most responsive sources and sinks of carbon, and includes reservoirs such as permafrost, methane hydrates and wetlands. The fluxes in and out of these reservoirs operate on much shorter timescales of hours to thousands of years, and therefore are more sensitive to perturbation than the long-term carbon-cycle feedback processes such as weathering (Berner *et al*., 2003). These long and short-term carbon cycles are linked through the small fluxes of carbon transferred from the exogenic cycle to the long-term rock record though sedimentation, and the small quantities of carbon released to the short-term reservoirs through volcanic degassing and metamorphism (Berner *et al*., 2003).

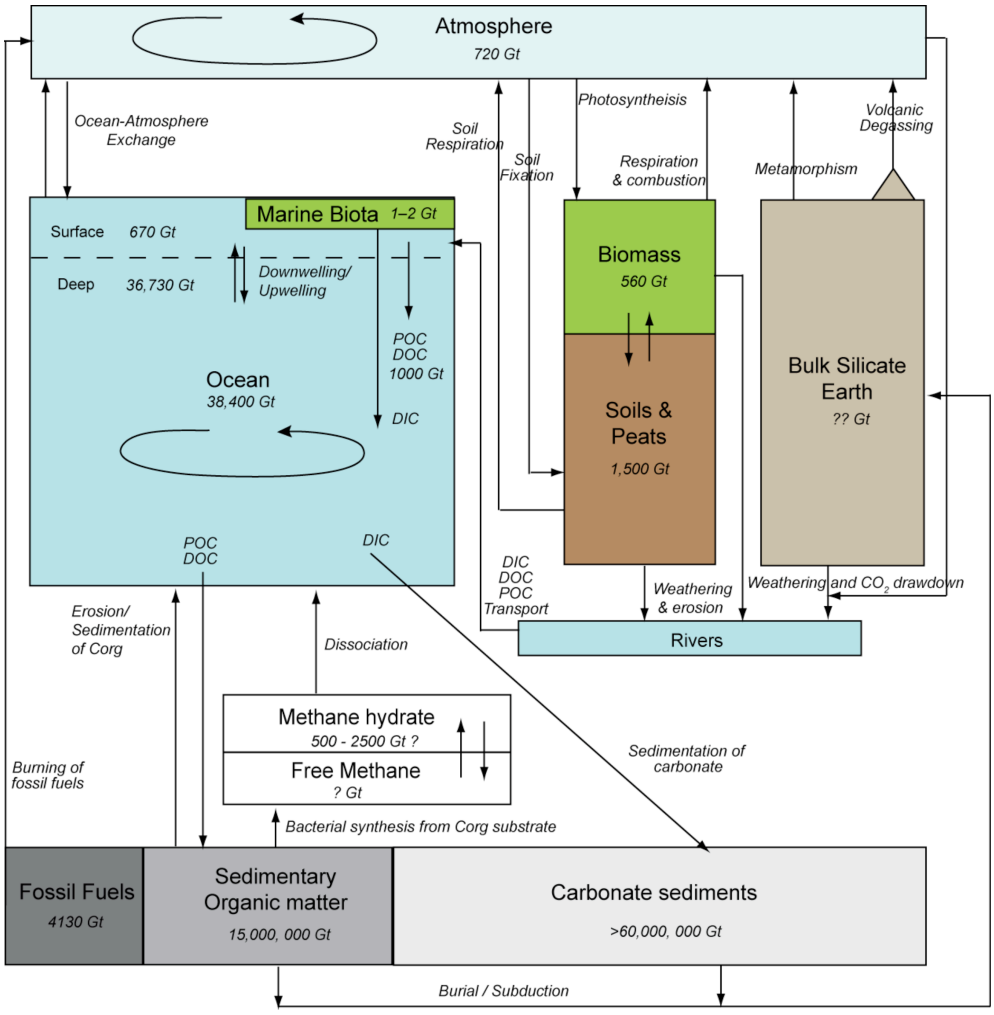

***Figure 3 (overleaf)**. A simplified diagram to show the long-term and exogenic carbon cycles. Modified after Weissert et al. (1989) with revisions after Dickens et al. (2001), Milkov (2004) and Berner (1999); (2003). DOC = Dissolved Organic Carbon, DIC = Dissolved Inorganic Carbon, POC = Particulate Organic Carbon. Mass of carbon in the bulk silicate Earth is very poorly constrained (hence is represented by "??"), with the estimates for carbon concentrations in the mantle anywhere between 1 ppm and 10,000 ppm (Deines, 2002).*

1. 5. 2. CARBON-ISOTOPE RECORDS AND EXCURSIONS

The carbon-cycle can be perturbed by natural or anthropogenic processes, by changing either the fluxes into or out of the system, or by creating or destroying carbon sinks. Natural perturbations have occurred countless times in Earth history, with major consequences for global climate and biota, and can be seen in the geological record in the form of changes in the carbon-isotope ratio with time. Carbon-isotope records, as recorded in biogenic carbonate or organic-matter, can reflect large-scale changes in the carbon-cycle at the time of deposition, and can be used to elucidate shifts in fluxes such as rates of carbonate production or organic-matter burial in the oceans (e.g. Scholle & Arthur, 1980; Weissert *et al*., 1989). There are two stable isotopes of carbon, ^{12}C and ^{13}C, which exist with natural abundances of 98.9 % and 1.1 % respectively (e.g. Nier, 1950; Farquhar *et al*., 1989). The ratio of these two different isotopes in a sample is usually expressed in the same manner as oxygen-isotopes, in permil relative to a standard (Vienna PeeDee Belemnite VPDB) in the delta notation.

Eq. 5.
$$\delta^{13}C = \left(\frac{\delta^{13}C_{sample} - \delta^{13}C_{std}}{\delta^{13}C_{std}} \right) * 1000$$

There are several kinetic and thermodynamic processes that lead to the fractionation of this natural carbon-isotopic abundance, in various natural materials. Chief amongst these is the light-isotope (^{12}C) preference that photosynthesizing organisms impose on the ambient carbon-isotopic composition of atmospheric CO_2. This leads to primary producers in both the terrestrial and marine realm having

relatively light $\delta^{13}C$ values, often within the range of ~-8 to ~-35 ‰ (e.g. O'Leary, 1988; Figure 4). In the oceans, these photosynthesizing organisms are then in-turn ingested by creatures higher up the trophic ladder, which transmits the light $\delta^{13}C$ signal to all parts of the organic food web. This leads to bulk organic-matter having more negative $\delta^{13}C$ values than contemporaneous marine carbonate, which usually has a $\delta^{13}C$ value of ~+1 to +2 ‰ in the modern oceans (Figure 4). Additionally, different plants types use different metabolic cycles to fix carbon from the atmosphere (e.g. C4 verses C3 plants), which leads to varying levels of fractionation of the ambient carbon-isotope ratio and therefore differing $\delta^{13}C$ ratios (e.g. O'Leary, 1988; Farquhar *et al*., 1989; Figure 4). There is also a broad difference in the $\delta^{13}C$ values of terrestrial higher plants and marine algae, due to physiological factors related to CO_2 diffusion in water (Farquhar *et al*., 1989).

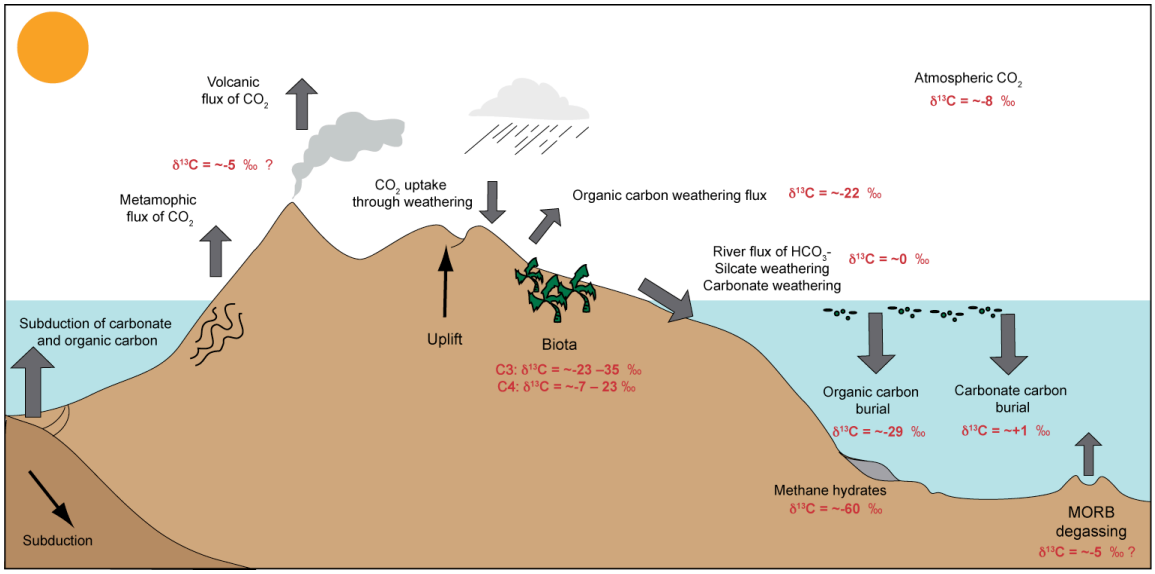

Figure 4. *A simplified diagram to show the carbon-isotopic composition (‰, VPDB) of important carbon reservoirs in the long-term, and elements of the exogenic carbon-cycle. Adapted from Kump & Arthur (1999).*

Other globally important processes, such as the production of biogenic methane (CH_4) from organic matter in anaeorobic environments, are also known to impose a strong light-isotope bias on the ambient carbon-isotope ratio, leading to very light $\delta^{13}C$ values of ~-60 ‰ in sedimentary methane clathrate deposits (Kvenvolden *et al*., 1995). Such well-constrained photosynthetic and methanogenic

fractionations, mean that changes in past carbon-cycling can be reconstructed when the $\delta^{13}C$ of the seawater or atmosphere is recorded by incorporation into carbonate or organic materials. Such materials may include fossil wood, bulk-organic matter, carbonate micro- and macro-fossils, and bulk carbonate. However, it is important to note that diagenesis of both organic matter and carbonates can lead to a skewing of the original $\delta^{13}C$ value (in a similar manner to the way the initial $\delta^{18}O$ value can be altered), which must be considered before inferences of large-scale changes in the carbon-cycle are made (e.g. Frank *et al*., 1999; Lehmann *et al*., 2002). However, as diagenetic environments have a much lower carbon content relative to oxygen, the carbon-isotope value is less prone to alteration than the oxygen-isotope value under such conditions.

1. 5. 3. CARBON-ISOTOPE EXCURSIONS AND OCEANIC ANOXIC EVENTS

During the Mesozoic, large perturbations to the carbon-cycle can be observed in the carbon-isotope record of both marine and terrestrial environments. These perturbations are referred to as "carbon-isotope excursions" (CIEs), and reflect large-scale reorganizations in the partitioning of carbon between organic and inorganic reservoirs (Scholle & Arthur, 1980; Weissert *et al*., 1989). Fluctuating global burial rates of isotopically light organic-matter (the "biological pump"), verses deposition of isotopically heavier carbonate in the sedimentary environment (the "carbonate pump"), are thought to lead to imbalances in the overall carbon-cycle which are expressed in the geological record as CIEs. These CIEs can be either positive or negative in nature, reflecting the different mechanisms involved, and can represent either long-term processes leading to broad excursions, or more short-term processes which can result in sudden, sharp excursions in the $\delta^{13}C$ record (Figure 5; e.g. Weissert *et al*., 1989).

In addition to the perturbations to the carbon-cycle seen in the $\delta^{13}C$ record, there are several periods during the Mesozoic which have been identified as so-called "Oceanic Anoxic Events" (OAEs), based on the widespread occurrence of marine sediments with elevated organic-matter contents, so-called "black shales" (e.g. Schlanger & Jenkyns, 1976; Jenkyns, 1980, 2010; Arthur *et al*., 1980). While these

black shale horizons were known from outcrop sections in the Tethyan region for decades, and had been associated with periods of regional anoxia, it was not until the discovery of contemporaneous black shales in the Central and North Pacific by the Deep Sea Drilling Project (DSDP), that the truly global distribution of these anoxic events became clear (Schlanger & Jenkyns, 1976). The discovery of organic-rich shales in mid-ocean settings such as the Central Pacific, also demonstrated that these anoxic periods were also not simply the result of deposition in locally restricted basins. OAEs are nearly always accompanied by positive CIEs, which can help to define these events chemostratigraphically, and which reflect the burial of organic carbon in black shales.

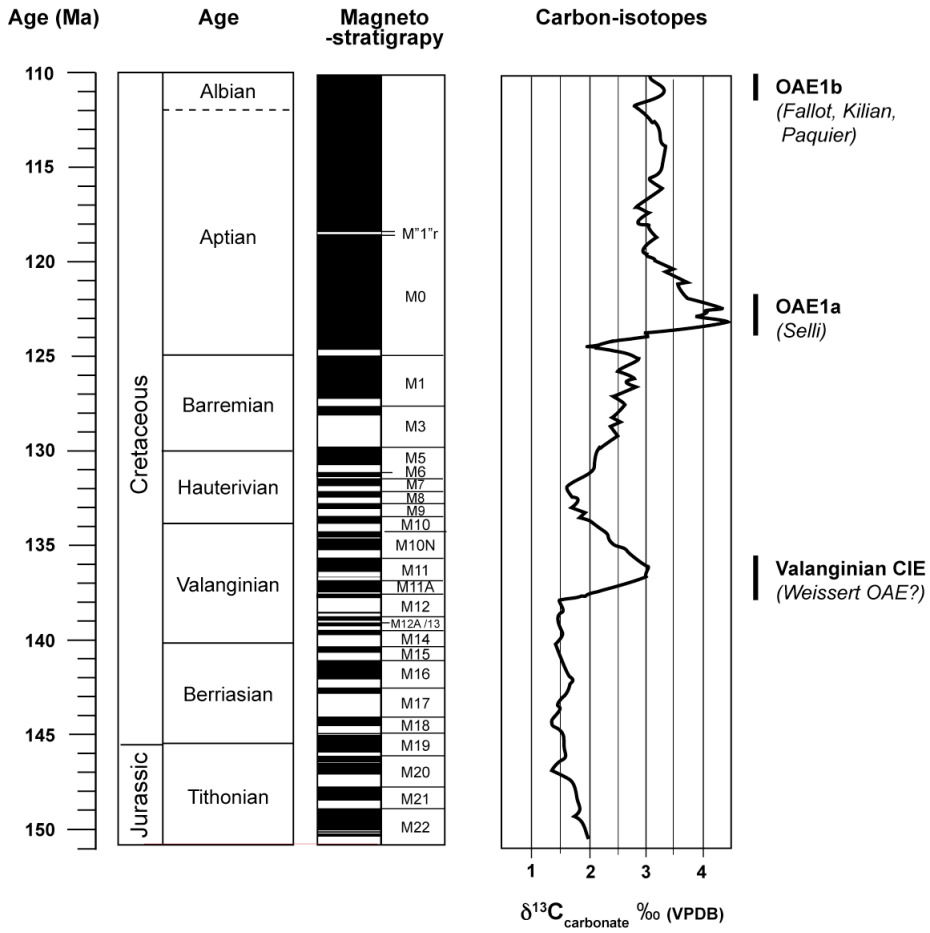

Figure 5*. An overview of the Late Jurassic–Early Cretaceous carbon-isotope record showing several perturbations (CIEs) and associated OAEs. Timescale (magnetostratigraphy and stage boundaries) is after Gradstein et al., (2004), with modifications after McArthur et al., (2007a) Carbon isotope curve is the generalized carbonate curve adapted from Weissert et al., (1998) and Leckie et al., (2002), with modifications to the Aptian-Albian curve after Herrle et al. (2010).*

Some OAEs are known to have disturbed the entire global atmospheric and oceanic carbon reservoirs, such as the Early Aptian, Selli Event (OAE 1a; ~120 Ma). This event is expressed as a globally widespread interval of black shale deposition in the Tethyan, Pacific and Atlantic Oceans, with a well-defined positive CIE recognizable in different geological materials from many sections around the world (e.g. Bralower *et al*., 1994; Menegatti *et al*., 1998; Grocke *et al*., 1999; Leckie *et al*., 2002; Méhay *et al*., 2009; Jenkyns, 2010; Figure 5). The Bonarelli Event at the Cenomanian-Turonian boundary (OAE2; ~93 Ma) is also an event of global significance, being characterized by a prominent positive CIE of ~2 ‰ in carbonates and by widespread global deposition of black shales (e.g. Sinninghe Damsté *et al*., 2010; Jenkyns, 2010; Leckie *et al*., 2002).

There are some periods of black shale deposition, however, that are not found globally, being more restricted to marginal or restricted basin settings, such as OAE1c and d (the Tollebuc and Breistroffer events respectively; Leckie *et al*., 2002) in the Late Albian; although the latter may have a limited record in the Pacific basin (Robinson *et al*., 2008). These events are more likely to be the result of regional processes, such as local basinal restriction and density stratification, related to local ocean circulation rather than worldwide productivity/preservation events, and therefore may not, in the strictest sense, represent OAEs (Jenkyns *et al*., 2010). However, even if the black shale deposition was not globally widespread, the amount of isotopically light organic-matter sequestered may still have been sufficient to cause globally-recognisable perturbations to the carbon-cycle and subsequent CIEs. In contrast some carbon-isotope events, such as the Valanginian positive CIE, are apparently not characterized by widespread black shale deposition, but have been ascribed OAE status on the basis of widely-recognised positive carbon-isotope excursions (e.g. Erba *et al*., 2004; Figure 5). The general absence of contemporaneous black shales in these chemostratigraphically-defined OAEs makes their classification, extent, and the mechanisms to explain their existence, somewhat controversial.

The mechanisms put forward to explain positive CIEs, and the associated OAEs, usually invoke increased burial rates of excess organic-matter in either the marine or terrestrial realms. This increased storage of isotopically depleted organic-matter in the marine environment can manifest itself as black shale deposits (e.g. Schlanger & Jenkyns, 1976; Jenkyns, 2010). In earlier studies it was proposed that

there were two end-member scenarios which could explain why global organic-matter burial in the oceans should have dramatically increased at certain times in the Mesozoic; increased productivity or increased preservation (e.g. Jenkyns, 1988). In the productivity model, an accelerated hydrological cycle leads to increased runoff of nutrients, which stimulates increased primary productivity and subsequently leads to a larger flux of organic matter to the sediments (e.g. Weissert *et al*., 1989). More recently, increased supply of biolimiting nutrients from active submarine volcanic centres have also been invoked as a cause of increased productivity in the Early Cretaceous, which would help to explain how mid-ocean settings far from coastal margins could also be affected by increased nutrification (e.g. Larson & Erba, 1999; Leckie *et al*., 2002; Weissert & Erba, 2004).

In the preservation model, the amount of primary productivity need not increase, but the amount of sinking organic matter which is oxidised and returned to the ocean is reduced due to the development of extended oxygen-minimum zones, thereby enhancing organic-matter preservation in the sediments (e.g. Jenkyns, 1988). The role of high sea level and the prevalence of shallow epicontinental seas in the Mesozoic, is thought to be particularly important with regards to the spread of oxygen-minimum zones in marginal basins in the preservation model. While the productivity model (invoking the "biological pump") is now thought to be the dominant mechanism for the initiation of OAE conditions, some combination of these two end-member models is also possible, and is perhaps more likely than either mechanism in isolation (Jenkyns, 2010).

Other explanations for positive CIEs that do not appear to have widespread black shales associated with them (such as the Valanginian CIE), include the increased storage of organic matter in the terrestrial environment in the form of peats and coal swamps, or in marginal marine basins, and/or decreased storage of ^{13}C in carbonates due to platform drowning events (e.g. Westermann *et al*., 2010). A combination of volume changes in these reservoirs would be expected to trigger a positive CIE, but would not require the presence of large-scale black shale deposits in the open ocean.

What all these mechanisms have in common is the need for a "trigger" for increased productivity (in the sea or on land) or marine anoxia, which is usually suggested to be a transient increase in global temperatures and the onset of "greenhouse conditions". While the independent evidence for these purported

temperature increases is not always unequivocal (e.g. Jenkyns, 2003), it remains the basis for many of the explanatory models put forward to explain positive CIEs and OAEs (e.g. Jenkyns, 2010; Mehay *et al*., 2009; Erba *et al*., 2004; Weissert *et al*., 1989). It becomes important, therefore, to constrain the temperature changes associated with OAEs and CIEs more closely, in order to determine the likely triggering mechanisms behind the perturbations.

Prominent negative CIEs are also known from the Mesozoic, which must represent an increased supply of ^{12}C to the ocean-atmosphere system from one or more of the reservoirs of isotopically light carbon. Such events in the Mesozoic include the negative isotopic excursion within the Toarcian OAE in the Early Jurassic (e.g. Jenkyns & Clayton 1997; Hesselbo *et al*., 2007; Jenkyns, 2003), and the sharp negative excursion that precedes OAE 1a in the earliest Aptian (Figure 4; e.g. Leckie *et al*., 2002; Keller *et al*., 2011). Indeed, both the Toarcian OAE and OAE 1a, are preceded by negative CIEs, which has led to speculation that the trigger mechanisms for some OAEs may be related to release of carbon from isotopically-light reservoirs (e.g. Jahren & Arens, 1998; Hesselbo *et al*., 2000; Mehay *et al*., 2009; Kuhnt *et al*., 2011). Negative CIEs are often attributed to large-scale releases of isotopically-depleted biogenic methane (e.g. Dickens *et al*., 1995; Hesselbo *et al*., 2000), which would rapidly decrease the $\delta^{13}C$ ratio of both the oceans and the atmosphere. The exact quantity of methane hydrate (clathrate) deposits which exist in the deep ocean is not known, but estimates place the figure between 500 and 2500 gigatons (Gt) of carbon, which is certainly enough to cause large changes to both the carbon-isotopic record and global climate if released suddenly (Milkov, 2004). Other proposed mechanisms to explain negative CIEs involve destruction of terrestrial carbon sinks such as peatlands (e.g. Zachos *et al*., 2010), generation of thermogenic methane from the intrusion of magmatic bodies into organic-rich sediments, associated with Large Igneous Province activity (e.g. Svensen *et al*., 2007), or isolation and desiccation of epicontinental seaways leading to respiration of the organic-matter within the sediments (Higgins & Schrag, 2006).

1. 6. THE TEX_{86} PALAEOTEMPERATURE PROXY

The difficulties with interpretation of oxygen-isotope and Mg/Ca records in the Early Cretaceous, outlined in Section 1. 3., emphasise the need for an SST proxy that is independent of the unknown initial seawater geochemistry. The U^{K}_{37} organic palaeothermometer, based on the distribution of alkenones produced by haptophyte algae, in part satisfies this need in the Cenozoic (Brassell *et al*., 1986; Conte *et al*., 2006). However, this proxy can probably only be used with confidence as far back as the Eocene (e.g. Liu *et al*., 2009; Bijl *et al*., 2009) even though rare alkenones are found in Cretaceous sediments (e.g. Farrimond *et al*., 1986; Brassell *et al*., 2004), and thus other techniques are needed to derive SST estimates for the Mesozoic. The TEX_{86} technique (TetraEther indeX of tetraethers consisting of 86 carbon atoms) is an alternative organic palaeotemperature proxy, which can be applied to sediments as old as Late Jurassic and thus provides an opportunity to reconstruct SSTs in the Early Cretaceous (Schouten *et al*., 2002; Mutterlose *et al*., 2010; Littler *et al*. 2011; Jenkyns *et al.*, 2011). This technique, first proposed nearly a decade ago, makes use of the relationship between the ratio of different GDGT (glycerol dialkyl glycerol tetraether) lipids in temperate crenarchaeotal membranes, and the temperature of the seawater in which the organisms lived. GDGTs are preserved in marine sediments, and can be analysed, quantified, and calibrated to reconstruct the temperature of the seawater at the time of deposition. Thus the TEX_{86} proxy has the potential to be a very powerful tool in the reconstruction of past climates, especially where traditional palaeotemperature proxies cannot be applied with confidence.

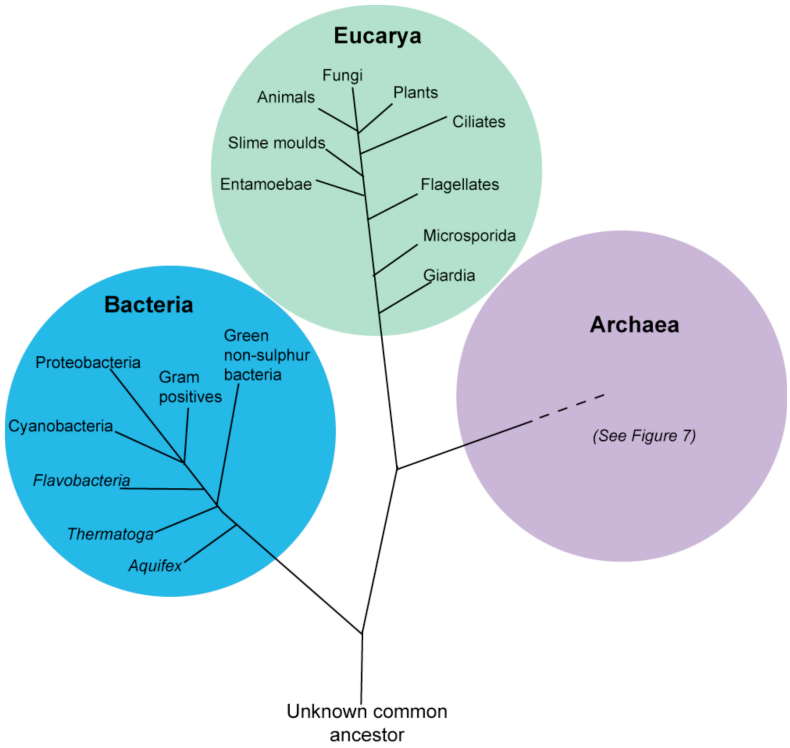

***Figure 6**. Simplified tree of life, showing the three Domains; Bacteria, Eucarya and Archaea. Adapted from Howland (2000). The details of Archaeal taxonomy, which are updated frequently as new information becomes available, are outlined in Figure 7 below.*

1. 6. 1. THE DISTRIBUTION AND ECOLOGY OF MARINE CRENARCHAEOTA

Non-thermophilic Crenarchaeota

Before using an organic proxy it is necessary to attempt to understand the organism(s) upon which the proxy is based, and specifically in the case of the TEX_{86} proxy, to provide evidence for GDGT production by temperate Crenarchaeota and to understand the relationship between these molecules and seawater temperature. The *Archaea* are microscopic, single-celled organisms which constitute the third domain of life, alongside the better-known domains of *Bacteria* and *Eucarya.* (Figure 6); (e.g. Woese *et al*., 1987; Schleper *et al*., 2005). Archaea have very simple morphologies, composed of a cell wall, cell membrane, simple organelles and a loop of DNA that contains all of their genetic information, and therefore appear superficially very similar to Bacteria even though they are genetically very distinct

forms of life (e.g. Howland, 2000). Archaea are thought to be part of a very ancient lineage, perhaps descended from the very earliest life on Earth, but until recently were thought to only survive in certain extreme environments in the modern World (e.g. Schleper *et al*., 2010). These so called "extremophiles" are able to exist and thrive in environmental conditions that would be impossible for other life forms to tolerate, such as hot geothermal springs, deep-sea hydrothermal vents and hypersaline environments (e.g. Grant *et al*., 1998; Pitcher *et al*., 2009; Zeng *et al*., 2009). As a result, the Crenarchaeota, which are one of the three recognised Kingdoms within the Archaea (Figure 7), were until recently thought to contain only thermophilic members (e.g. DeLong, 1998b).

Genetic surveys using new 16S ribosomal (rRNA) gene sequencing techniques (e.g. Fox *et al*., 1977; Fuhrman *et al*., 1992) revealed that archaea were not exclusively extremophiles, and marine representatives were present in both the open ocean and ocean margins (Fuhrman *et al*., 1992; DeLong, 1992; Fuhrman *et al*., 1993). Evidence for the presence of non-extremophile archaea in the marine environment, has also come from biomarkers. Temperate archaea synthesise specific cyclized lipids, glycerol dialkyl glycerol tetraethers (GDGTs), as part of their cell membrane structures (see Section 1-6-2). The majority of these cyclized GDGTs are not thought to be widely synthesised by other organisms, which suggests they can be regarded as biomarkers for the Crenarchaeota (e.g. Sinninghe Damsté *et al*., 2000; see Section 1-6-2). Therefore the presence and concentration of these GDGTs in modern seawater and sediments can be used to infer the relative importance and depth habitat of marine Crenarchaeota at that particular location. A combination of genetic and biomarker studies have revealed that Crenarchaeota are a ubiquitous and important part of many diverse modern marine environments, including the Arabian Sea (Sinninghe Damste *et al*., 2002b), Black Sea (Hoefs *et al*., 1997; Wakeham *et al*., 2003), Mediterranean Sea (Ouverney & Fuhrman, 2000), North Sea (Wutcher *et al*., 2004), the waters off Antarctica (DeLong *et al*., 1994; Murray *et al*., 1998; Church *et al*., 2003), the Cariaco Trench (Hoefs *et al*., 1997; DeLong *et al*., 1998a), and the North Atlantic and Pacific Oceans (Wutcher *et al*., 2005). The presence of Crenarchaeota in such a diversity of geographical locations and habitats suggests that planktonic temperate archaea are capable of thriving in a variety of marine ecological niches.

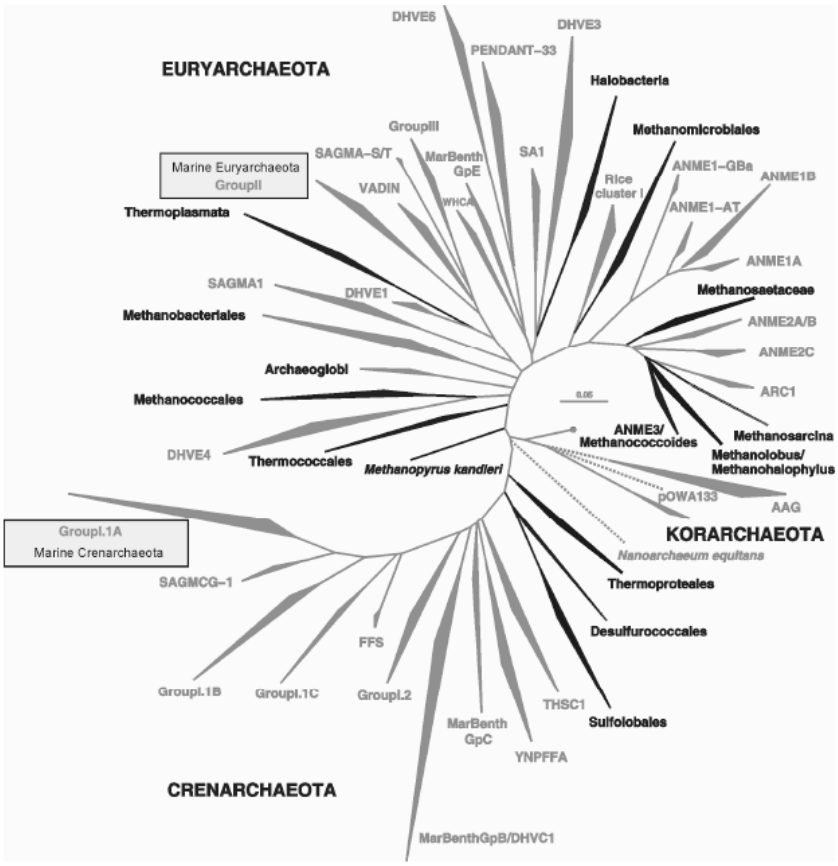

Figure 7*. Phylogenetic tree based on the 16S rRNA gene, to show the three Kingdoms of the Archaea (Crenarchaeota, Euryarchaeota and Korarchaeota) and their genetic relationships to one another, based on genetic surveys of ocean-dwelling populations of marine microbiota and culture studies. Taken from C. Wuchter (2006) PhD dissertation, University of Utrecht, (available online at http://igitur-archive.library.uu.nl/dissertations/2006-0412-200011/index.htm); originally adapted from Schleper et al., (2005).*

It has subsequently been estimated that temperate Crenarchaeota are actually one of the dominant prokaryotes in the deep Atlantic Ocean (Herndl *et al*. 2005). Some have gone so far as to suggest that marine Crenarchaeota make up ~20% of the entire picoplankton in the Pacific Ocean and that, by extrapolation, World oceans may contain as many as 1.3 x 10^{28} crenarchaeotal cells (Karner *et al*., 2001).

The marine Crenarchaeota are now thought to be predominantly planktonic chemoautotrophs, specifically chemolithoautotrophs (e.g. Schleper & Nicols, 2010; Martens-Habbena *et al*. 2009; Wuchter *et al*. 2006; Könneke *et al*. 2005; Francis *et al*. 2005), although some studies have suggested that some Crenarchaeota may be heterotrophs, on the basis of radiocarbon studies (Pearson *et al*., 2001; Shah *et al*., 2008; Ingalls *et al*., 2006), amino-acid tracer data (Ouverney & Fuhrman, 2000) and

genetic studies (Schouten *et al*., 2006). Field and laboratory work is still ongoing, but many of the described marine Crenarchaeota are now known to be important nitrifiers, converting ammonia into nitrite, which is then utilised by other organisms as a nutrient source (Hoefs *et al*., 1997; Pearson *et al*., 2001; Sinninghe Damste *et al.,* 2002b; Wutcher *et al*., 2003; 2006; Venter *et al*., 2004; Francis *et al*., 2005; Könneke *et al*., 2005; Mincer *et al*., 2007; Shah *et al*., 2008; Martens-Habbena *et al*., 2009). The carbon substrate needed for ammonia oxidation by the Crenarchaetoa is thought to be bicarbonate, on the basis of the carbon-isotopic composition of the Crenarchaeotal cell membranes (Sinninghe Damste *et al.,* 2002b; Wuchter *et al*., 2003). The one cultured member of the marine Crenarchaeota to date, "'*Candidatus* Nitrosopumilus maritimus', has been shown to be an effective nitrifier under conditions of extreme nutrient limitation, and as such can be regarded as an open-ocean oligotrophic specialist (Martens-Habbena *et al*., 2009). It is, however, unknown whether this species is representative of mesophilic marine Crenarchaeota in general.

Regardless, the widespread and ubiquitous nature of the Crenarchaeota, combined with the known ability of some members as nitrifiers, suggests the marine archaea have a previously unrecognised but possibly pivotal role in the marine nitrogen cycle (Könneke *et al*. 2005; Martens-Habbena *et al*., 2009). Recent evidence suggests Archaea could also be important nitrifiers in hot groundwater systems (e.g. De la Torre *et al*., 2008; Hatzenpichler *et al*., 2008; Zhang *et al*., 2008; Pitcher *et al*., 2009) and in the terrestrial soil environment (e.g. Treusch *et al*., 2005), making it likely the Archaea have a significant role in the global nitrogen cycle. Importantly in terms of the TEX_{86} proxy, if most marine Crenarchaeota can be regarded as having a chemoautotrophic habit, this denotes an ability to make their own food in the absence of light meaning they would not be restricted to the shallow photic zone of the oceans.

Where in the water column are marine Crenarchaeota living?

It is important to constrain the depth habit of marine Crenarchaeota, as the TEX_{86} proxy based on these organisms is proposed as a sea-surface temperature proxy, and therefore the Crenarchaeota might be expected to predominantly live at

shallow depths in the oceans (e.g. Schouten *et al*., 2002). The depth habit of the marine Crenarchaeota can be deduced from genetic surveys or from sampling the concentration of GDGTs at various depths. From the genetic surveys (Figure 8) it can be seen, barring some seasonal complications in the higher latitudes, that although temperate Crenarchaeota are found throughout the water column, they occur in highest abundances in relatively shallow ocean depths between 0 and 500 m, often peaking at ~150 m, at the base of the photic zone (e.g. Fuhrman *et al*., 1992; DeLong 1992; Massana *et al*., 2000; Karner *et al*., 2001; Sinnginghe Damste *et al*., 2002b; Herndl *et al*., 2005, Wuchter *et al*., 2006; Mincer *et al*., 2007). However, the Crenarchaeota show a strong subsurface preference, often becoming a *proportionately* more important part of the picoplankton with increasing depth (e.g. Herndl *et al*., 2005; Murray *et al*., 1999; Mincer *et al*., 2007; Figure 8).

In the Antarctic, the trend of depth habit is complicated by a strong seasonality (see below), but the basic trend of increasing crenarchaeotal productivity with depth holds true, at least during the summer months (Massana *et al*., 1998; Murray *et al*., 1998; Church *et al*., 2003; Figure 8). The trend for subsurface dominance of Crenarchaeota can also be seen in the GDGT biomarker depth transects, which mirrors the pattern seen in the genetic surveys (Figure 9). Sinninghe Damste *et al*. (2002b) examined the flux of GDGTs in the water column in the Arabian Sea and found the highest concentrations at depths between 0 and 500 m, generally peaking at 500 m depth near the top of the strong regional oxygen-minimum zone (OMZ). Similarly several depth habitat studies in the Santa Monica Basin, Equatorial Pacific Ocean and northeastern Pacific Ocean, demonstrated similar patterns of subsurface GDGT distribution, with low surface-water concentrations which increased markedly at depths > 100 m (Wuchter *et al*., 2005).

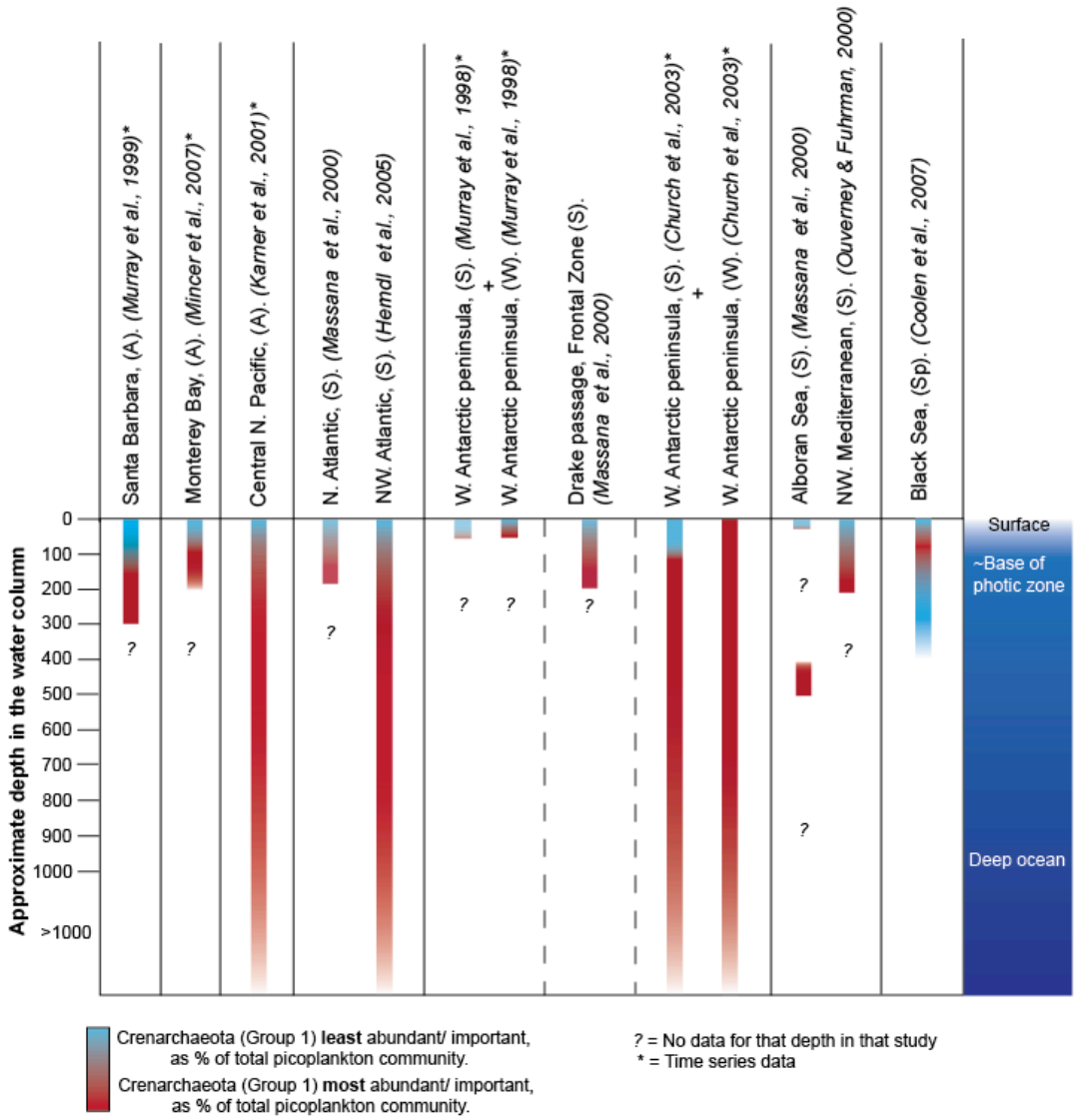

Figure 8. *Synthesis figure to summarise the depth habits of marine Crenarchaeota from selected genetic studies. Some of these studies were conducted over several months or even years (* symbol). Where there is a lack of seasonality an averaged trend is shown, "A", whereas in the seasonal high-latitudes," S" = summer collection and "W" = winter collection.*

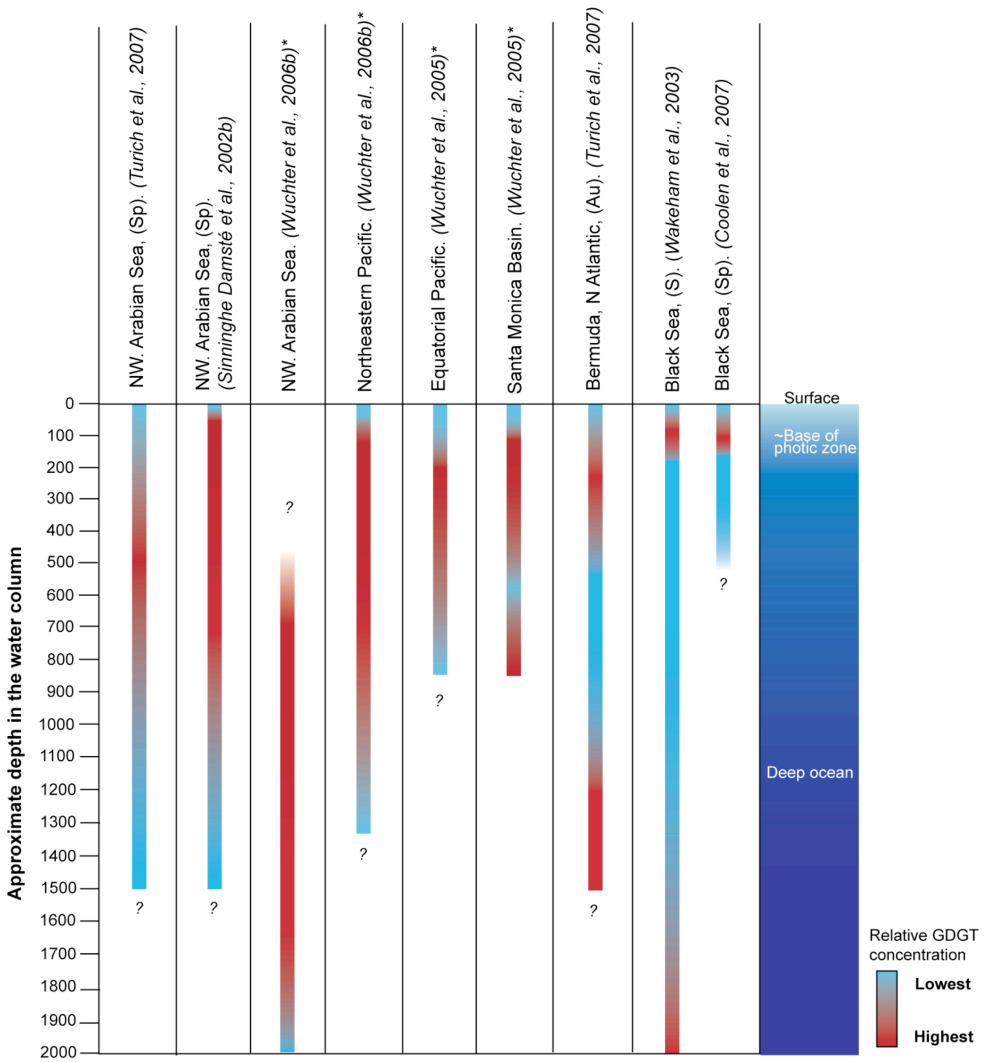

Figure 9. *Synthesis figure showing the results of relative GDGT concentration vs. depth studies in the northwestern Arabian Sea, the Black Sea, the North Atlantic, the Santa Monica Basin, Equatorial Pacific and northeastern Pacific. Some of these studies were conducted over several months or years as indicated by asterix (*) symbol. S = collected in summer months, Au = collected in autumn months, Sp = collected in spring months.*

Some exceptions do exist however, which suggest that there may also be a deep-water source of GDGTs in some basins, such as in the largely anoxic waters of the Black Sea. Here, the concentration of GDGTs at various depths in the water column was examined by Wakeham *et al*. (2003) and, in broad agreement with genetic study by Cohen *et al*. (2007), was found to be highest between 100 and 130 m water depth, in the transition zone between the oxic and suboxic zones (Figures 8, 9). However, significant GDGT production was also found to be occurring

throughout the water column, particularly at depths greater than 1500 m, where the relative proportion of GDGTs as a percentage of the organic carbon increased substantially. Turich *et al*. (2007) have also reported a similar trend in the North Atlantic waters off Bermuda.

In summary, both genetic and GDGT surveys in modern World Oceans suggests Crenarchaeota are living at a range of depths in the water column, but are present in only very low abundances in the surface ocean, often with maximum concentrations at the base of the photic zone, and variable concentrations in the deeper ocean.

Seasonality in marine Crenarchaeota populations

Potential seasonality in the abundance of microbial populations is an important issue when developing an organism-based palaeotemperature proxy that is supposed to represent mean annual average SSTs (e.g. Schouten *et al*., 2002). It appears that in regions where there are relatively low seasonal variations in environmental parameters, like temperature and nutrient abundance, such as the oligotrophic North Pacific subtropical gyre, the relative abundances of Crenarchaeota in the water column appears to lack a clear seasonal signal (Karner *et al*., 2001). However, this lack of coherent seasonality is also evident from a ~3 year study in the nearby Santa Barbara Basin, which does experience contrasting seasonal conditions and periods of increased upwelling and productivity (Murray *et al*., 1999; Figure 10).

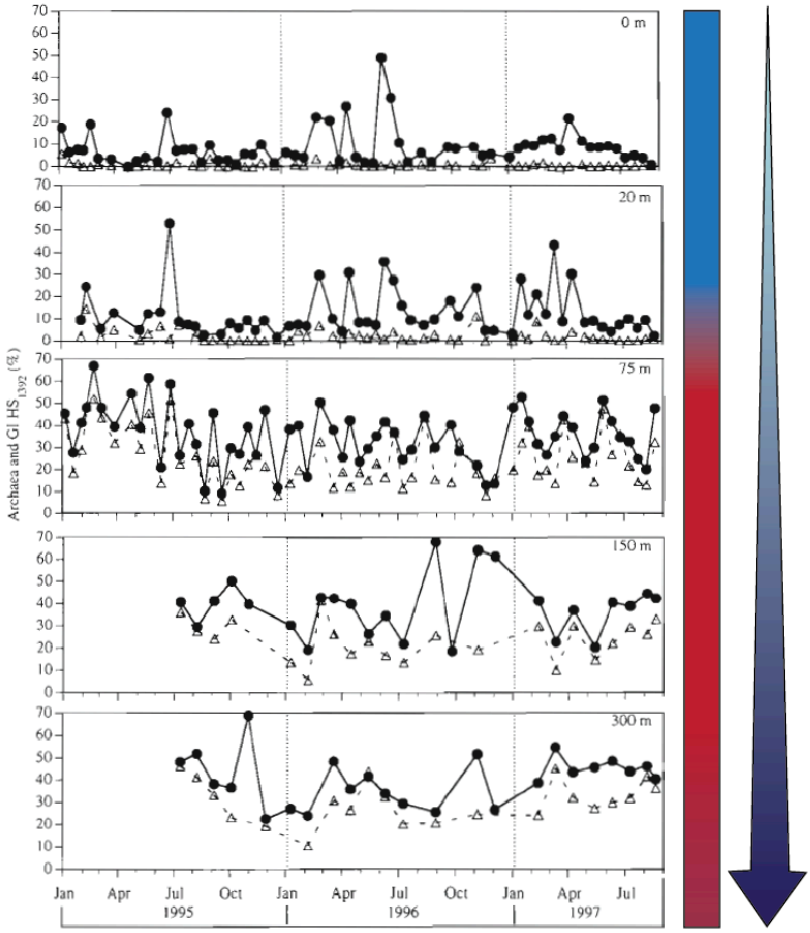

Figure 10. *Adapted from Murray et al., (1999). A three year time-series showing the relative abundance of the Group I Crenarchaeota (open triangles) in the Santa Barbara Basin, and how this varies with depth. Arrow denotes increasing depth, coloured bar denotes greatest relative abundance of the Group1 crenarchaeota at that depth (red = more abundant).*

Seasonality in the concentration and distribution of Crenarchaeota in seawater has been seen in some time-series field studies, usually where there are large seasonal contrasts in temperature and nutrient supply (e.g. Church *et al*., 2003; Wuchter *et al*., 2005; Mincer *et al*., 2007). In the North Sea, which is a highly seasonal environment, a distinct peak in shallow water (~1 m depth) GDGT production in the shallow coastal waters was observed during the winter and spring months (November – April), further supported by genetic evidence for a winter bias in crenarchaeotal abundance (Figure 11; Wuchter *et al*., 2005; 2006; Herfort *et al*., 2006). This winter-spring bias is not restricted to the North Sea, and can also be seen in a four-year time-series study in North Atlantic waters near Bermuda (Wuchter *et al*., 2005) and in the Monterey Bay time-series, where greater absolute cell counts of

Group I archaea are observed during the winter months (Mincer *et al*., 2007). In the Antarctic region several studies (e.g. Murray *et al*., 1998; Church *et al*., 2003) have shown that the pattern of crenarchaeotal production is strongly seasonal, which is perhaps not unexpected in a region where for several months of the year the surface of the ocean is covered by sea ice, and light and temperature levels vary considerably. For example, it has been estimated that Archaeal rRNA constituted only ~1% of total microbial rRNA in the surface waters around the Antarctic Peninsula during the summer, but this proportion rose to 14 -29% during the winter season (Murray *et al*., 1998; Figure 12).

The peak in crenarchaeotal abundance in the winter-spring months seen in some mid- and high-latitude studies, is thought to be related to both the increased abundance of ammonium (a crenarchaeotal food source) in the water during the winter, and perhaps the reduced competition from organisms such as cyanobacteria, which are not well-adapted to growing in cool, low-light conditions of the winter (e.g. Wuchter *et al*., 2006). Strong mixing of surface waters during the winter at these latitudes may also have an effect on the microbial concentration, by stirring up both nutrients and the organisms themselves from their usual depths in the water column.

In summary, the issue of seasonality in marine crenarchaeotal abundance is clearly complex, with different trends reported from different ocean basins and environmental settings. Seasonality appears to be minor in open-ocean oligotrophic settings (e.g. Karner *et al*., 2001), while more marginal basins such as Monterey Bay (Mincer *et al*., 2007) may experience some winter biasing in GDGT production. Perhaps not unexpectedly, higher latitude regions that experience large seasonal changes in environmental conditions, such as the North Sea and the Antarctic, are affected more strongly by winter-spring biasing in crenarchaeotal abundances (e.g. Murray *et al*., 1998). This finding suggests that care should be taken in the interpretation of crenarchaeotal-based temperature records (TEX_{86}), in the high latitudes and areas thought to be affected by large seasonal contrasts.

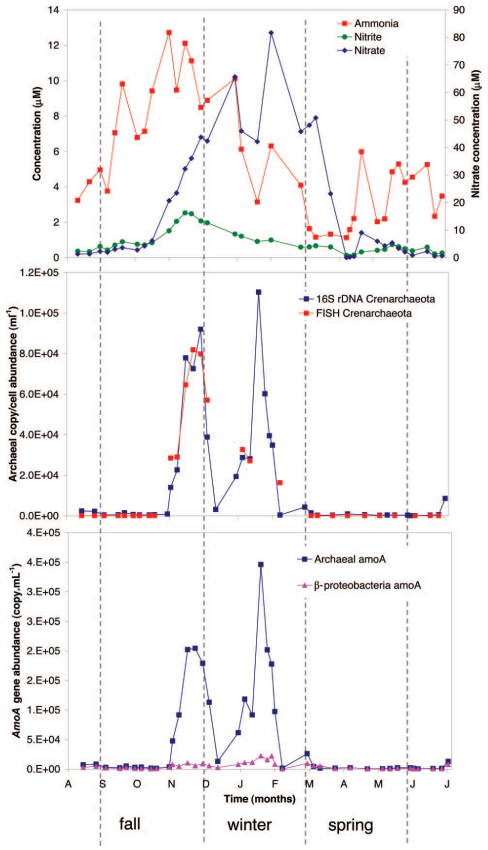

Figure 11. *Time series data from surface waters of the coastal North Sea (near Texel Island, Netherlands), showing the concentration of Crenarchaeota and nutrients throughout the year (Wuchter et al., 2006).*

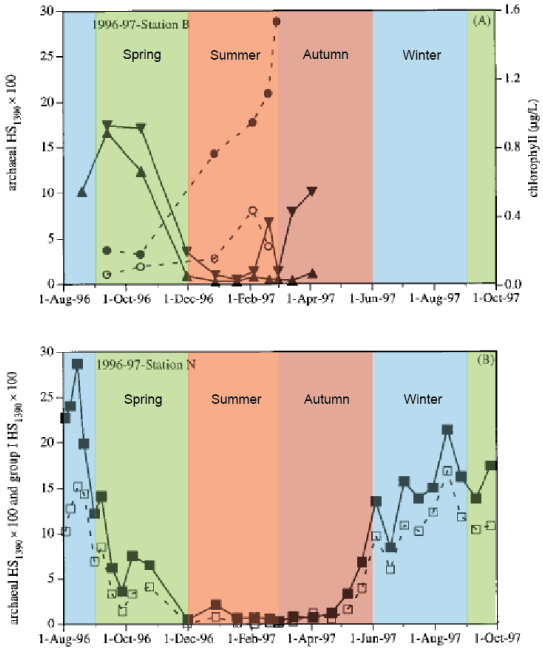

Figure 12. *Archaeal concentrations around the Antarctic Peninsula, adapted from Murray et al. (1998). Top panel: Black circles = chlorophyll levels at the surface; open circles = chlorophyll levels at 50 m depth; upright triangles = Archaea concentration at the surface; upsidedown triangles = Archaea concentration at 50 m. Bottom panel: Black squares = Archaeal concentrations, open squares = Group I Crenarchaeota concentrations.*

1. 6. 2. CRENARCHAEOTAL GDGTS AND TEMPERATURE

Unlike eukaryote or bacterial membranes, which are predominantly composed of diacyl membrane lipids, archaeal membranes are composed of either dialkyl glycerol diethers (DGD) or glycerol dialkyl glycerol tetraethers (GDGT) lipids (Figures 13, 14; Schouten *et al*., 2000; Sinninghe Damste *et al*., 2002). While all Archaea have this basic GDGT or DGD configuration, it is predominently non-thermophilic Crenarchaeota, in both the marine and terrestrial realms, along with some soil-dwelling bacteria and marine euryarchaeota which synthesis the four specific GDGTs which are made use of in the TEX_{86} proxy (e.g. Schouten *et al*., 2007; 2008).

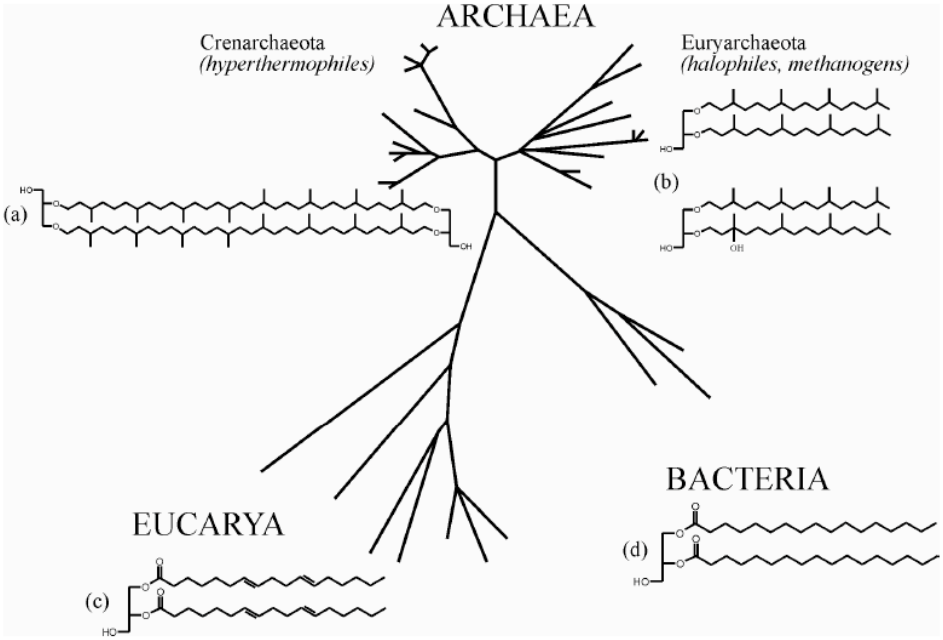

Figure 13. *The structure of the different lipid types used in the cell membranes of various organisms, divided on the basis of Domain and Kingdom. (a) glycerol dibiphytanyl (dialkyl) glycerol tetraethers (GDGTs), (b) diphytanyl glycerol diethers (DGDs), (c) and (d) fatty acids glycerol diesters. Taken from C. Wuchter (2006) PhD dissertation, University of Utrecht, (available online at http://igitur-archive.library.uu.nl/dissertations/2006-0412-200011/index.htm); originally adapted from Schleper et al. (2005).*

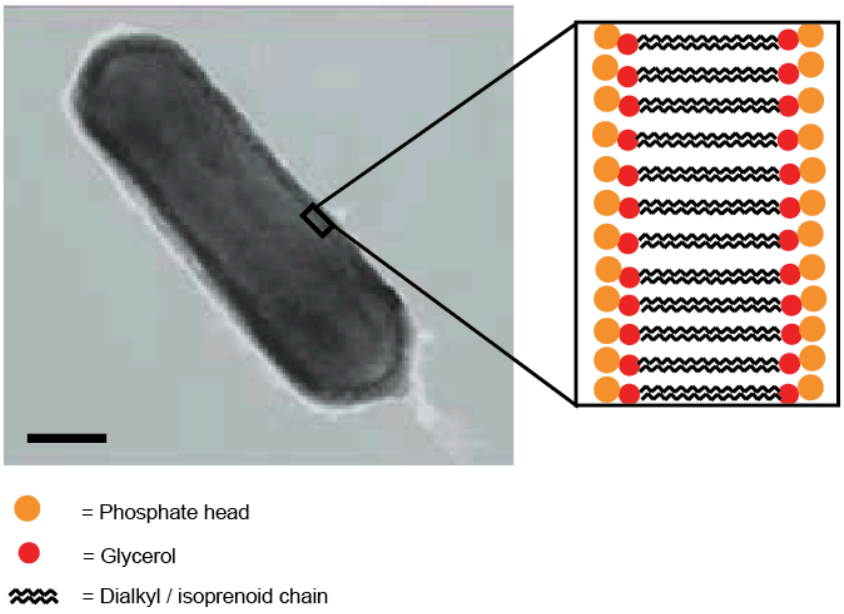

Figure 14. *Simplified structure of the cell membrane of a typical Archaea (right), showing the core GDGT structures with the polar phosphate head groups still attached (Intact Polar Lipid; IPL). Archaea pictured (left) is the cultured marine nitrifier, candidatus Nitrosopumilus maritimus, taken from Könneke et al. (2005). Scale bar represents 0.1 μm.*

With regard to the TEX_{86} proxy, marine Crenarchaeota synthesise five key isoprenoid GDGTs (GDGT 0 to 4) and one regioisomer (GDGT 4'), where the number refers to the number of cyclopentane moieties in each dialkyl chain (see Figure 15). Within these dialkyl chains there may be up to four cyclopentane moieties, or in the case of "crenarchaeol" (GDGT 4), four cyclopentane moieties and a cyclohexane moiety. Crenarchaeol, with its extra cyclohexane moiety, has been thought of as a retrospective adaptation to temperate conditions, where the more open structure it affords allows the cell membrane to retain its fluidity in the cooler waters of the marine or lacustrine environment (Sinnginghe Damste *et al*., 2002).

Early culture experiments showed that the distribution and abundance of different ether lipids within the cell membranes of thermophilic Crenarchaeota and euryarchaeota, is temperature dependant (e.g. Gliozzi *et al*., 1983; Uda *et al*., 2001). For example, when the thermophilic euryarchaeota *Thermoplasma acidophilum* was subjected to different growth temperatures between 40ºC and 60ºC, the degree of cyclization of the membrane lipids was seen to be affected, with more cyclized

(cyclopentane moieties) being added to the lipid structures with increased temperature (Uda *et al*., 2001). This addition of cyclopentane rings with temperature is thought to be an adaptation by the organisms as they adjust the structure of their membranes to retain optimum fluidity in the environmental conditions in which they finds themselves (e.g. Pitcher *et al*., 2009).

It has subsequently been shown that temperate Crenarchaeota also adapt the composition of their membranes in response to the temperature of the water in which they are grown (Sinninghe Damste *et al*., 2002; Schouten *et al*., 2002), a fact which has been exploited in the development of the TEX_{86} proxy. In general, as the temperature of the water is increased, the ratio of GDGTs containing more cyclopentane moieties within their dialkyl chains also increase, i.e. there is an increase in the relative abundance of GDGTs 4', 3, and 2, relative to GDGT 1 (Figure 15). Additionally, the composition of membrane GDGTs in temperate Crenarchaeota has been demonstrated in mesocosm studies to be largely independent of external factors such as nutrient flux or salinity (e.g. Wutcher *et al*., 2004). This, if true, is extremely important, as these external geochemical parameters are difficult to constrain in past oceans. This apparent independence from initial conditions, coupled with the apparently remarkably durable nature of fossil GDGTS in the sedimentary record, makes the analysis of GDGT ratios a robust basis for a palaeotemperature proxy.

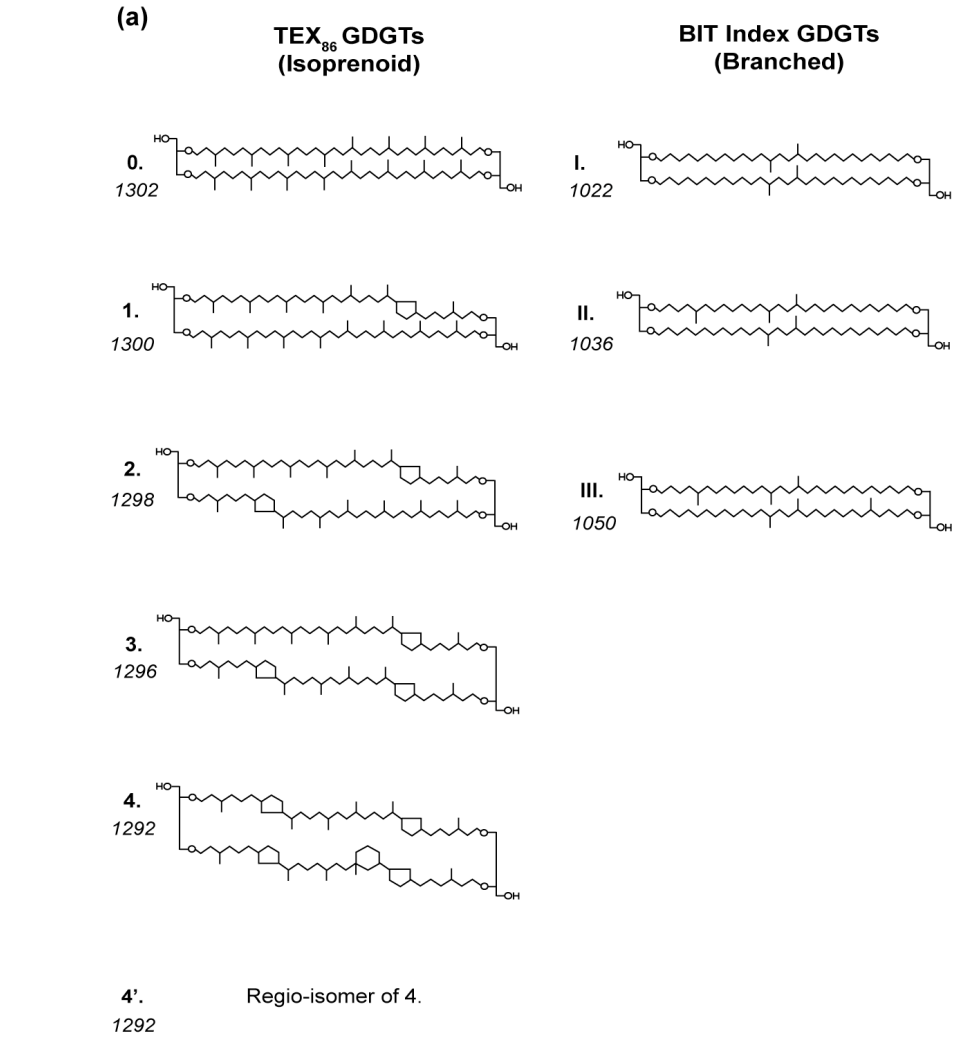

Figure 15. ***(a)*** *The structure of GDGT (glycerol dialkyl glycerol tetraether) molecules used to construct both the TEX_{86} ratio (the isoprenoid GDGTs) and the BIT Index (the branched GDGTs). Molecules are shown here with their $[M+H^+]^+$ values (e.g. 1292).* ***(b)*** *Idealised chromatogram for a marine sediment sample. Numbered peaks correspond to the lipid structures shown above.*

1. 6. 3. DEVELOPMENT OF THE TEX_{86} PROXY

The development of the TEX_{86} palaeotemperature proxy has largely been conducted in an empirical "trial and error" fashion, built upon the basic observation that the composition of GDGTs in Archaeal membranes appears to be influenced by increasing temperature (see above). These GDGTs had already been shown to be resistant to degradation in sediments on geological timescales (Chappe *et al*., 1982; Hoefs *et al*. 1997) and were therefore excellent candidates for the development of a palaeotemperature proxy. Although the effect of temperature on GDGTs in marine Crenarchaeota was first explored in Sinninghe Damste *et al*. (2002), the potential for a palaeo-SST proxy was first documented in Schouten *et al*. (2002). This study examined 44 core-top sediment samples from 15 different marine locations, including samples from the Atlantic and Pacific Oceans, and the Arabian, North, Aegean and Black Seas. The distribution of GDGTs 0 – 4' in each core-top sample was analysed and this data was compared to World Ocean Database (1998) measurements of temperature at various depths in the water column, for the same location the sediment cores were taken from (Schouten *et al*., 2002).

When the number of weighted average cyclopentane rings in each sediment sample (encompassing all isoprenoid GDGTs 0 to 4'), was plotted against the documented annual average SST, a general positive trend was observed with a relatively high r^2 value of 0.63 (Figure 16). This suggested that the trend seen in thermophilic Archaea of a positive relationship between number of cyclopentane moieties and growth temperature was also generally applicable to the temperate marine Crenarchaeota.

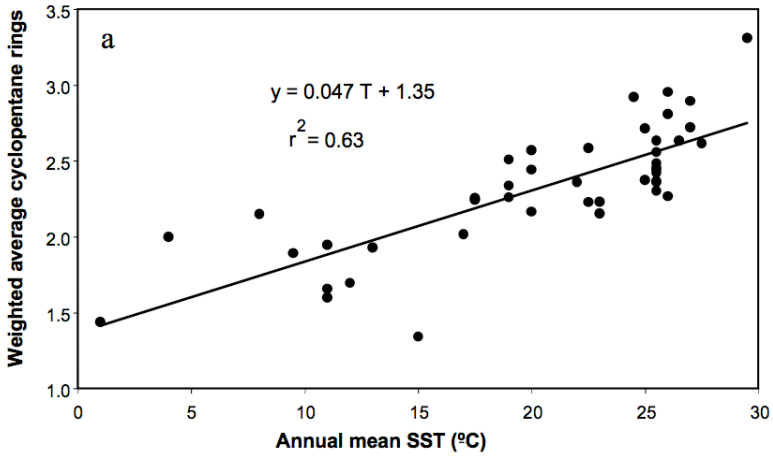

Figure 16. *The core-top calibration set (n = 44) of Schouten et al., (2002). Black circles = weighted average number of cyclopentane moieties found in GDGT molecules in each sediment sample, plotted against the annual average SST (ºC) for that location.*

However, when GDGTs 4 ("crenarchaeol") and GDGT 0 ("calderarchaeol") were excluded from consideration, the correlation between GDGT distribution and seawater temperature increased considerably (see below). The so-called "TEX_{86} ratio" was therefore defined as:

Eq. 6. $$TEX_{86} = \frac{[GDGT\ 2] + [GDGT\ 3] + [GDGT\ 4']}{[GDGT\ 1] + [GDGT\ 2] + [GDGT\ 3] + [GDGT\ 4']}$$

with the exclusion of both GDGTs 0 and 4. It can be seen that the TEX_{86} ratio is most sensitive to the proportion of GDGT 1 as this is the only molecule present in the denominator but not the numerator of the equation.

When the TEX_{86} ratios of the 44 core-top samples studied by Schouten *et al*. were plotted against the SST or temperature at 100 m depth for that location, a strong positive correlation was observed (Figure 17). On the basis of this limited global dataset, the r^2 values of the SST and deeper water calibrations are very similar (0.92 and 0.86 respectively), with a slightly better fit observed between TEX_{86} and annual average SST. This then suggested that the TEX_{86} proxy is best suited to estimating surface water temperatures, when averaged out over the whole year, despite the known subsurface depth preference and issues with seasonality (see below).

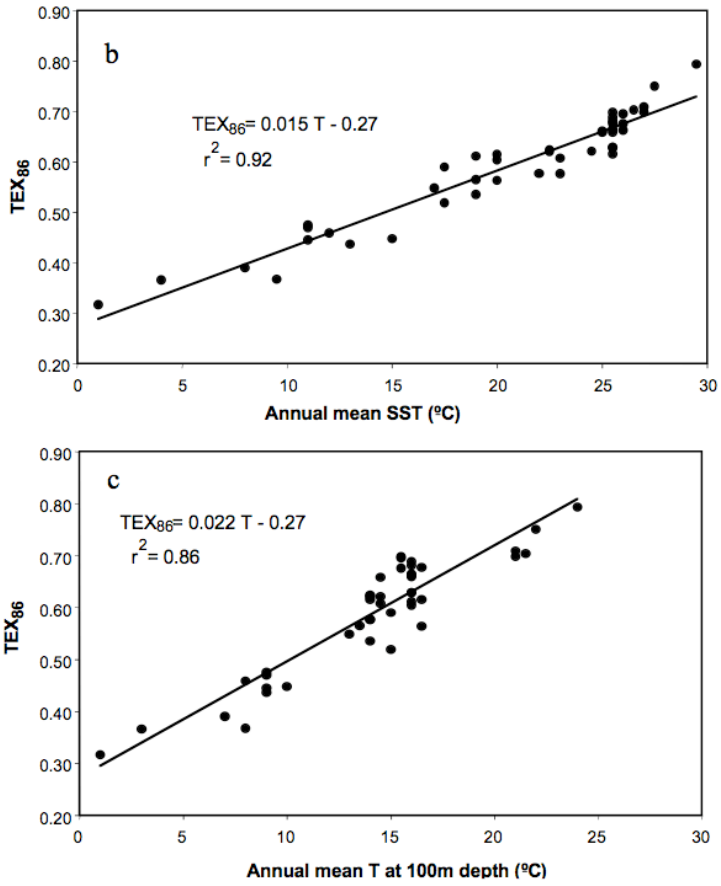

Figure 17*. The modern core-top calibration set (n = 44)of Schouten et al., (2002), and the linear regressions as calculated in that paper. Panel b is plotted against average annual SST and panel c is plotted against annual mean T at 100 m depth in the water column.*

On the basis of this initial study and the linear regression through the dataset, the relationship between TEX_{86} and SST was defined as:

Eq. 7. $$T = \frac{(TEX_{86} - 0.28)}{0.015}$$

The analytical error, using the methodology outlined in Schouten *et al*., (2002), was estimated to be ±0.022 (~±1.5 ºC), while the additional standard error of the calibration is on the order of ±2ºC. This calibration would be expected to give SST estimates that were within "reasonable" boundaries (~0–30 ºC) of expected SSTs for *recent* ocean samples, as the TEX_{86} ratio would always be likely to fall within the

modern core-top calibration range. However, when the calibration was applied to TEX_{86} ratios from low-latitude ancient greenhouse Worlds (e.g. the Cretaceous), the reconstructed temperatures were found to often exceed 40 ºC, far above the SST estimates suggested by other SST proxies or model outputs (Schouten *et al*., 2003). This highlighted the problem with using the simplistic linear regression as an extrapolation of Eq.7 when the TEX_{86} ratio was considerably above the range seen in the modern ocean (> ~0.750).

Although the presence of GDGTs in organic-rich Cretaceous rocks was first documented by Kuypers *et al*. (2001), the first study to use the new TEX_{86} proxy to reconstruct palaeotemperatures for ancient greenhouse oceans was Schouten *et al*. (2003), who applied the proxy to mid-Cretaceous black-shale core samples from various Deep Sea Drilling Program (DSDP) sites. The GDGT spectra from the low-palaeolatitude sites was strikingly different to most modern samples, particularly in that the relative proportions of GDGTs 0 and I relative to GDGT 2, 3, 4 and 4' were generally much lower than those observed in the global calibration set (Schouten *et al*., 2002). This translated to TEX_{86} ratios that were ~0.690 – 0.960 for Aptian to Cenomanian-Turonian samples, meaning that they were, on the whole, beyond the range of the modern core-top calibration set. This presented a dilemma; if the original regression (Eq. 7) was used to calculate SST from these highest TEX_{86} values, then the estimated temperatures were in the range of 40 – 45ºC. These were much warmer than SSTs suggested by other proxies such as oxygen-isotopes and were considered unrealistic estimates even in the low-latitudes of the Cretaceous world. The compromise solution in Schouten *et al*., (2003) was to construct a so-called "high temperature calibration", which only used data points with values >20ºC from that existing modern core-top calibration set to create a new linear regression (Figure 18), which has a much steeper gradient and therefore yielded significantly lower SST estimates than the original calibration (Eq. 8).

Eq. 8

$$T = \frac{(TEX_{86} + 0.016)}{0.027}$$

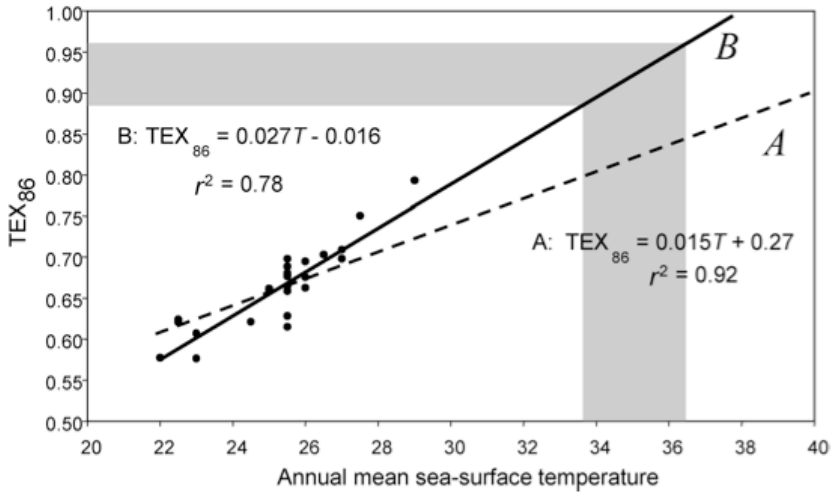

Figure 18. *The high temperature calibration of Schouten et al. (2003). Line A is the Schouten et al., (2002) linear calibration based on the entire dataset (n= 44). Line B is the adapted high temperature calibration based on 22 of the warmest of these datapoints. Grey band represents the range of Cretaceous low-latitude TEX_{86} values seen in the Schouten et al., (2003) study.*

Although, or arguably because, the Schouten *et al*. (2003) high temperature calibration was only based on 22 points, it has a relatively high correlation coefficient ($r^2 = 0.78$). Importantly, use of this calibration for the mid-Cretaceous TEX_{86} samples in Schouten *et al*. (2003) yields SST estimates of 27º to 36ºC which, while still very warm for annual average values, are less unreasonable than the >45ºC temperatures suggested by the original calibration.

While the initial Schouten *et al*. (2002) calibration dataset, and subsequent modifications in Schouten *et al*. (2003), illustrated the potential for the TEX_{86} proxy to be used as a palaeothermometer, the core-top dataset was too small and too restricted geographically to be truly globally comprehensive, nevertheless, several subsequent TEX_{86} studies used the high temperature calibration as the basis of their palaeotemperature reconstructions (e.g. Jenkyns *et al*., 2004; Forster *et al*., 2006; Pearson *et al*., 2007). However, for the TEX_{86} calibration to be as broadly applicable as possible to various marine settings, it was necessary to increase the size of the calibration dataset. Kim *et al*. (2008) produced a much more comprehensive and globally representative core-top study, which had a total of 287 data points from all the major oceans (Figure 19). However, the final calibration was generated based on

a smaller subset of the total data (n = 223), where all the data from the polar oceans (Arctic and Southern Oceans) and the Red Sea was excluded, as well as any data that fell outside of 2 times the standard deviation of the linear regressions (cross symbols in Figure 22). The TEX_{86} data were compared with temperature data from several different depths (0–4000 m range), and varying seasonal temperature ranges in the surface waters; however, the best correlation was still found to be with mean annual SST (Figure 20). When a linear regression was fitted to this data (TEX_{86} *vs*. SST) the resulting equation was:

Eq. 9 $$T = -10.78 + (56.2 * TEX_{86})$$

which has a very high correlation coefficient of 0.935, and an estimated standard calibration error of ±1.7ºC, in addition to the smaller analytical error due to improved techniques of ±0.3ºC.

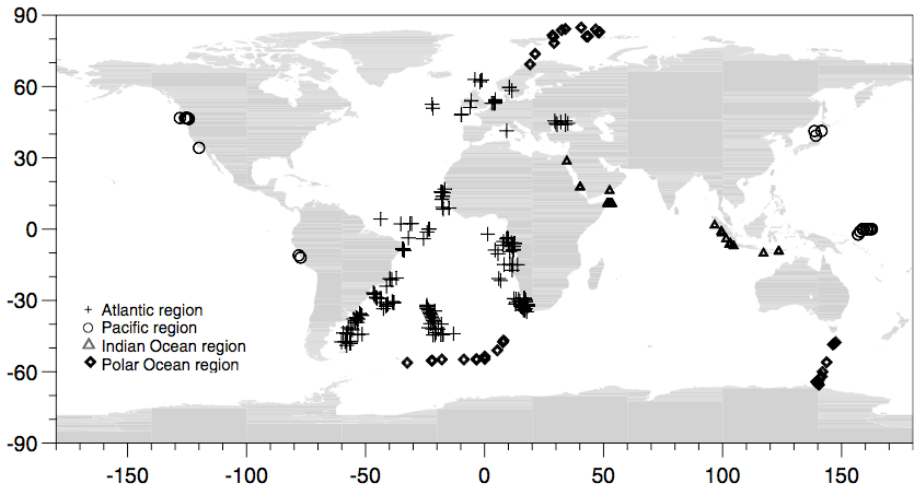

Figure 19. *Location of core-top calibration samples used in that study, grouped by geographic location in the modern oceans (n =287), taken from Kim et al., (2008). X axis is degrees longitude, y axis is degrees latitude.*

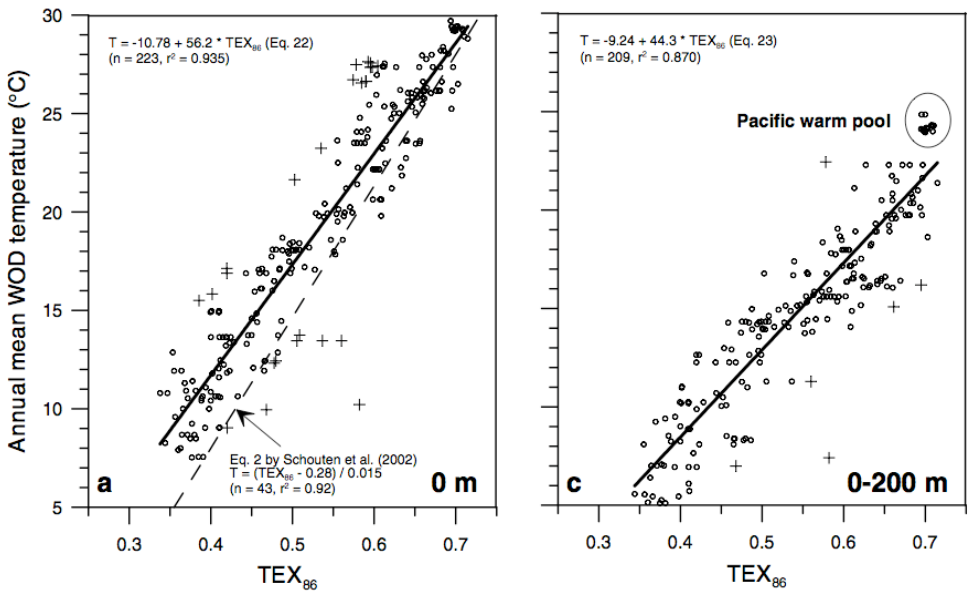

Figure 20. *(a) Annual mean temperature at 0 m water depth (SST) against TEX_{86} values, (c) cross plot of depth-averaged annual mean temperature above 200 m against TEX_{86} values, taken from Kim et al. (2008). The data from the Polar Oceans and the Red Sea were excluded. Cross symbols indicate excluded data points which deviated more than 2 times from the standard deviation of the linear regression models. The stippled line in (a) indicates the calibration line by Schouten et al. (2002). Note SST is now on the y-axis and TEX_{86} is on the x-axis.*

This new linear calibration was thought to be applicable to both modern and ancient sediments for the reconstruction of annual average SSTs, in the same manner as the original Schouten *et al*. (2002) equation. Although it should be noted the new study also highlighted the relatively good correlation ($r^2 = 0.670$) between TEX_{86} and the integrated temperature signal across the whole 0–200 m shallow ocean depth range (Figure 20). The proxy was not recommended for use below 5 ºC, as the data appeared to become non-linear with temperature below this point, hence the decision to exclude the polar ocean data from the calibration set. The Red Sea data consistently plotted away from the main ocean calibration set, and was excluded on the basis that the unique chemistry and physical oceanography of the Red Sea probably leads to the Crenarchaeota there having a specialized or non-linear response to temperature (Kim *et al*., 2008). It was also suggested that the archaeal population living in the Red Sea may be thriving during the summer months (as opposed to the winter-spring months elsewhere), therefore skewing the sedimentary GDGT-derived temperatures in that region towards warmer temperatures than the true annual

average mean SST (Kim *et al*., 2008).

The major issue with the Kim *et al*., (2008) calibration, as with the Schouten *et a*l., (2002) linear calibration, is in the estimation of SST when the calibration is extrapolated beyond the range of the modern core top data set (~>0.70). At such high TEX_{86} values the estimates for mean annual SST become very warm indeed (>40ºC), which many palaeoclimatologists regard as unrealistic, even during periods of greenhouse warmth. Not satisfied with the exclusion of so much of the global calibration set (22% of the total) and with the statistical treatment of the data in Kim *et al*. (2008), Liu *et al*. (2009) suggested an alternative calibration:

Eq. 10 $$T = 50.475 - (16.332 * (1/TEX_{86}))$$

This calibration includes all of the 287 data points in the Kim *et al*. (2008) core-top calibration set, but assumes a non-linear, reciprocal relationship between TEX_{86} and SST. The root mean square calibration error of ±3.7 ºC is therefore much higher than the error associated with the linear Kim *et al*. (2008) calibration, mostly due to the inclusion of the highly scattered cool (sub)polar data. The main differences between the reciprocal calibration and the linear assumption are in the high (>25 ºC) and low (<15 ºC) temperature ranges, while in the central regions of the calibration (TEX_{86} of 0.45–0.70) the two calibrations produce very similar temperature estimates. Below the TEX_{86} value of 0.45 the curve is considerably steeper, leading to SST estimates that are up to 7.5 ºC degrees cooler than the linear equation predicts (Figure 21). Below 0.3 the curve is nearly vertical, reflecting the large scatter in the calibration data in the polar-regions, meaning the proxy cannot be used. In the >0.70 TEX_{86} range, the reciprocal calibration has the effect of substantially flattening the curve, thus reducing the sensitivity to temperature changes as well as the absolute SST values predicted by the proxy, which now cannot theoretically exceed 34.1 ºC. Liu *et al*. (2009) argued that these changes to the high TEX_{86} portion of the calibration brought the TEX_{86} SST estimates more in-line with other SST proxies, such as oxygen-isotopes and Mg/Ca ratios, in greenhouse World palaeoclimate reconstructions. These proxies do not support the >40 ºC estimates suggested by the linear calibration, and therefore cooler temperature estimates from the TEX_{86} proxy are generally more parsimonious with the existing data. These two calibrations, one

linear and suggesting very high temperatures in the >0.75 range and the other suggesting very low sensitivity and cooler temperatures in the same range, can be regarded as upper and lower limits on the range of plausible temperatures respectively.

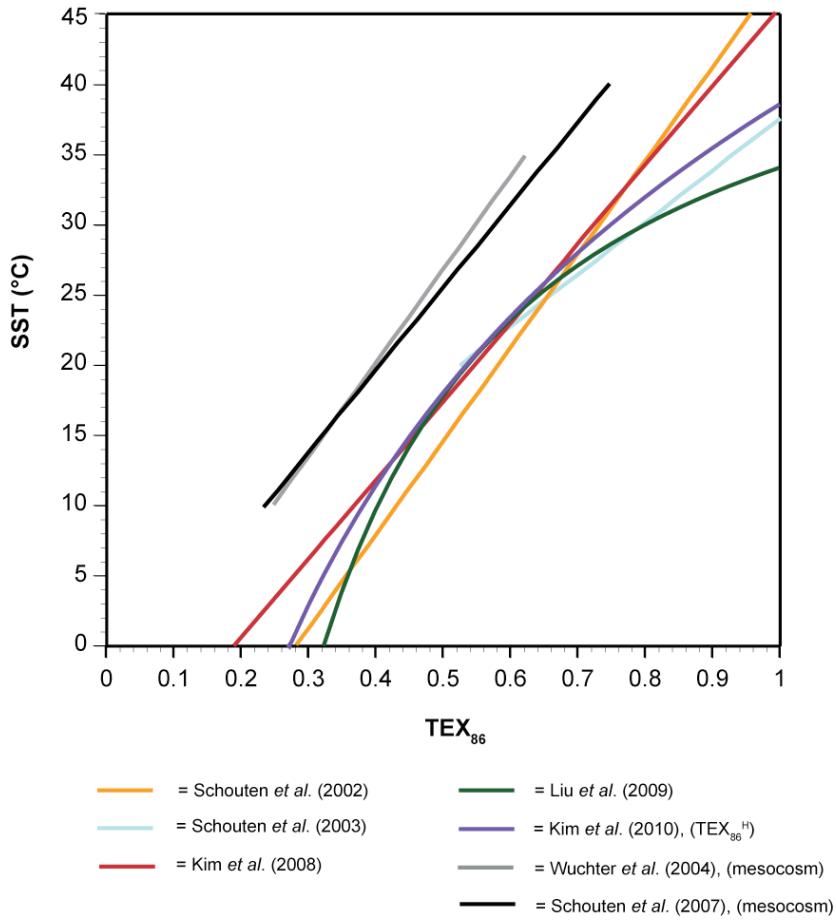

Figure 21. *Graph to show five different TEX_{86} calibrations and their relative effects on SST estimates. The comparison between the mesocosm experiments with the core-top calibrations shows they have a very similar gradient but different y-intercepts.*

The obvious next step was to improve the core-top calibration by incubating Crenarchaeota at various elevated temperatures in mesocosm experiments. However, this was complicated by the apparent difficulty that cultured Crenarchaeota had in synthesizing the crenarchaeol regioisimer, GDGT 4' (Wuchter *et al*., 2004). While the TEX_{86} values from incubated North Sea samples generally followed a linear positive trend, and the gradient was the same as the Schouten *et al*. (2002) equation (0.015), the y-intercept was substantially lower in the mesocosm calibration equation

(see Figure 21). As the abundance of the GDGT 4' molecule is part of the definition of the TEX_{86} proxy, this meant the mesocosm calibration could not be used directly to supplement the original TEX_{86} core-top dataset. Similar trends were found when equatorial Indian Ocean water samples were incubated in 2 ºC temperature steps between 30ºC and 40ºC for 134 days (Schouten *et al*., 2007; Figure 22). When these newer data was combined with the existing data from Wuchter *et al*. (2004) and the combined regression calibration was calculated, the resulting equation was found to have a very similar gradient to the original Schouten *et al*. (2002) equation of 0.017, but a different y-intercept of +0.064. This again was due to the low levels of GDGT 4' which the incubated Crenarchaeota synthesized relative to the core-top populations.

Interestingly, DNA analysis of the incubation studies taken after 101 days, suggested that even though all the samples fell into the Group 1.1A Marine Crenarchaeota subgroup, there were at least three different sub-populations of crenarchaeota within the original Indian Ocean seawater, which appeared to have three different optimum growth temperatures at 25ºC, 34 – 36ºC and 40ºC (Schouten *et al*., 2007). This finding has implications for the use of the TEX_{86} proxy, which is based on an integrated sediment GDGT signal, as the response of each crenarchaotal population in the water column to SST may not be the same in each geographic location, and with changing long-term temperature.

Interestingly, a moderately thermophilic ammonia-oxidising crenarchaeote (*Candidatus. N. gargensis*), isolated from a geothermal hot spring, was found to contain all the GDGTs used in the original TEX_{86} proxy, including the crenarchaeol regioisomer (GDGT 4') (Pitcher *et al*., 2010). Cultures of this organism were grown in mesocosms at temperatures of 42 – 50ºC, and the subsequent TEX_{86} values at these temperatures were all found to be >0.985, in good agreement with the higher temperature linear calibrations such as Eq. 9 (Kim *et al*., 2008).

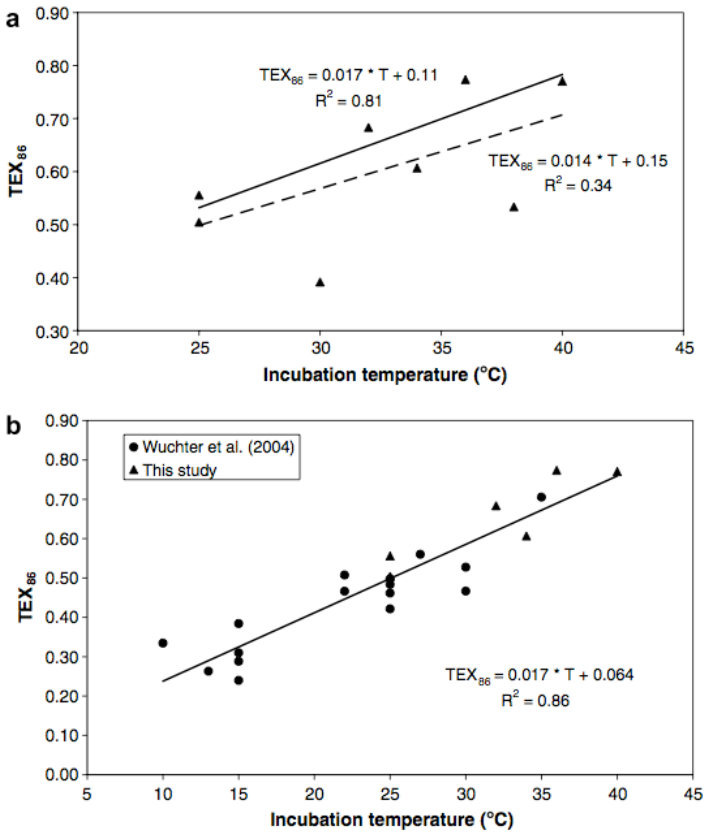

Figure 22. *(a) TEX_{86} against incubation temperature for all the T steps used in the Schouten et al. (2007) study. Dotted line = correlation line for all incubation experiments, solid line = the correlation for incubation experiments excluding those at 30° and 38°C. (b) TEX_{86} against incubation temperature of data from Schouten et al. (2007) (black triangles) and from Wuchter et al. (2004) (black circles).*

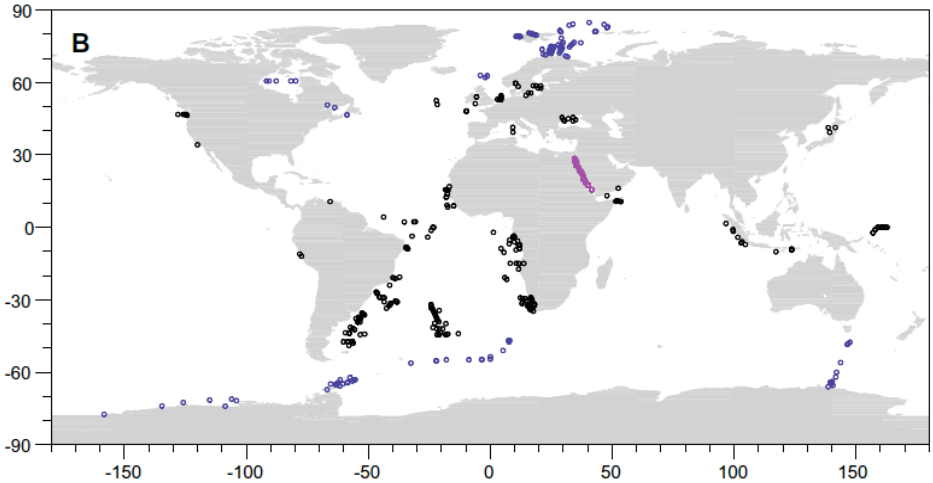

Figure 23. *The latest global core-top calibration set from Kim et al. (2010). Black symbols = data used in the TEX_{86}^{H} calibration and the blue and purple symbols represent (sub)polar and Red Sea data respectively which was excluded from consideration in the TEX_{86}^{H} calibration (see below).*

The global core-top calibration was recently updated with the publication of Kim *et al*. (2010), which expanded the modern core-top dataset to 426 samples from around the World (Figure 23). There were particular improvements in the spatial coverage of the polar and subpolar oceans, which were only poorly represented in the earlier core-top surveys. In contrast to the earlier studies, Kim *et al*. (2010) compared the calculated TEX_{86} ratios with SSTs estimated from satellite data, as opposed to *in situ* measurements from the World Ocean Database (WOD). The authors ultimately proposed two new calibrations based on this improved dataset, to try and reconcile the problems associated with high temperature estimates in the >0.7 TEX_{86} range. Two different variations of the TEX_{86} ratio, utilizing different GDGT combinations were proposed: TEX_{86}^{L} and TEX_{86}^{H}.

It was suggested that the TEX_{86}^{L} arrangement, defined below and based on the whole core-top dataset minus the Red Sea data, was likely to give the most accurate results when the palaeo-temperatures are thought to be below 15℃.

Eq. 11 $$TEX_{86}^{L} = \log\left(\frac{[GDGT-2]}{[GDGT-1]+[GDGT-2]+[GDGT-3]}\right)$$

The equation to convert TEX_{86}^{L} to SST is given as:

Eq. 12. $$T = (67.5 * TEX_{86}^{L}) + 46.9$$

which has a relatively high standard residual calibration error of ±4ºC.

The second GDGT calibration, TEX_{86}^{H}, is based on a more filtered dataset with the omission of all polar and subpolar, as well as all Red Sea, data points. It shows the best fit with the SST data above 15ºC, and is recommended as the preferred calibration for ancient greenhouse World palaeoclimate reconstruction. It is defined as:

Eq. 13. $$TEX_{86}^{H} = \log\left(\frac{[GDGT\ 2]+[GDGT\ 3]+[GDGT\ V']}{[GDGT\ 1]+[GDGT\ 2]+[GDGT\ 3]+[GDGT\ V']}\right)$$

which is, in fact, identical to the original TEX_{86} equation, except for the addition of a logarithmic term, e.g. $TEX_{86}^{H} = \log TEX_{86}$. The equation to convert TEX_{86}^{H} to SST is given as:

Eq. 14. $$T = (68.4 * TEX_{86}^{H}) + 38.6$$

which has a relatively lower standard residual calibration error of ±2.5℃.

The Kim *et al*. (2010) study also calculated what the resulting equation would be, if the reciprocal approach after Liu *et al*. (2009) was applied to this new dataset (minus the Red Sea data):

Eq. 15. $$T = (-19.1 * (1/TEX_{86})) + 54.5$$

Perhaps unsurprisingly, this new reciprocal calibration produced very similar results to the older equation (Eq. 10), with slightly warmer temperature estimates in the upper values of the TEX_{86} range, and a high standard residual error of ±5.4 ºC. The range of all the proposed calibrations from Kim *et al*. (2010), and other selected calibrations for comparison, are shown for information in Figure 24.

For completeness, it should be mentioned that additional calibrations based on regional calibrations or rearrangements of the original GDGT ratios used in the TEX_{86} ratio, have also been proposed in some studies. In order to address the issues with poor calibration potential in the high-latitudes, Shevenell *et al*. (2011) added seven new TEX_{86} data points from western Antarctic sediments to the existing global calibration set. The resultant linear equation (Eq. 16) was used to reconstruct temperature in the Holocene.

Eq. 16. $$T = \frac{(TEX_{86} - 0.3038)}{0.0125}$$

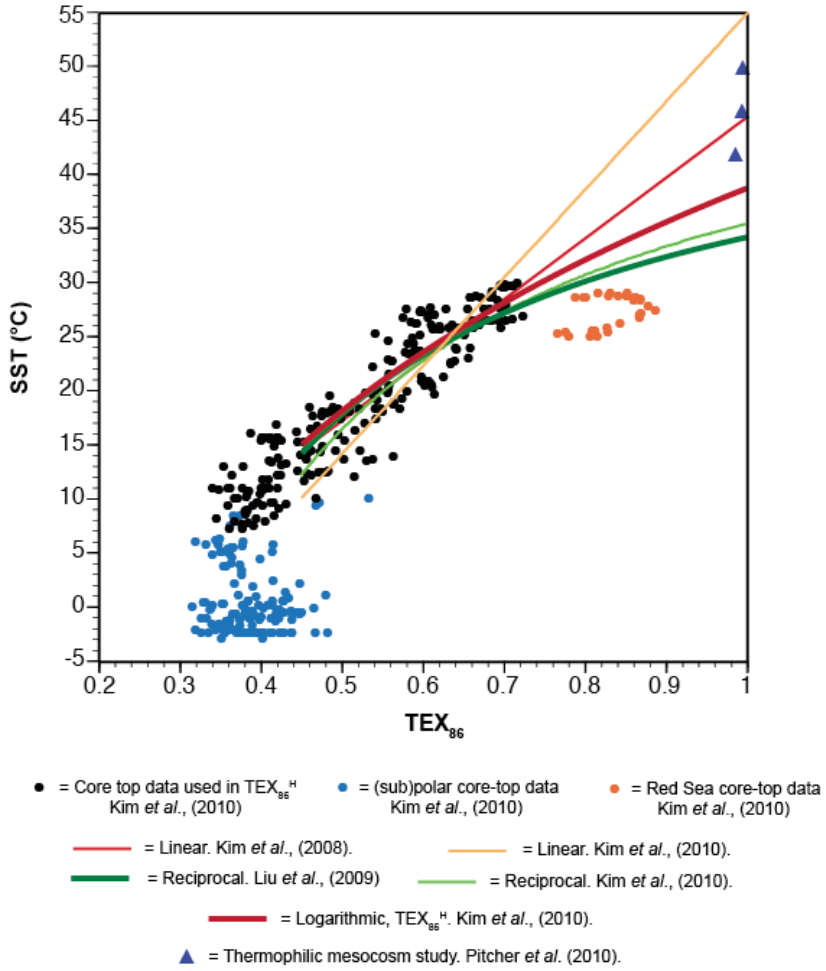

Figure 24. *Core-top data from Kim et al. (2010) and all the relevant calibrations applied to Early Cretaceous TEX_{86} values in this thesis: linear; logarithmic; and reciprocal. (Sub)polar and Red Sea data, highlighted in blue and orange respectively, are excluded from the Kim et al. (2010) logarithmic calculations (TEX_{86}^{H}), while the Red Sea data is excluded from the "Reciprocal. Kim et al. (2010)" equation, but not the original "Reciprocal, Liu et al. (2009)" calibration.*

Sluijs *et al*. (2006) analysed GDGT distributions in Eocene sediments from the Arctic, and hypothesised that an anomalously high abundance of GDGT-3 in the sediments was indicative of terrestrial contamination, and therefore devised as alternative calibration, "TEX_{86}' " which was defined as:

Eq. 17.
$$TEX'_{86} = \frac{[GDGT\ 2] + [GDGT\ 3] + [GDGT\ 4']}{[GDGT\ 1] + [GDGT\ 2] + [GDGT\ 4']}$$

This arrangement, which was converted to SST using the equation:

Eq. 18.

$$T = \frac{(TEX'_{86} - 0.2)}{0.016}$$

had a high correlation coefficient ($r^2 = 0.93$) when it was applied to 104 marine core-top sediment samples, which included data from Schouten *et al*. (2002). It appeared to predict "reasonable" SSTs for the Eocene sediments, and may have removed the effects of terrestrial contamination at this location.

In a later study based on recent sediments from the Santa Monica Basin, Shah *et al*. (2008) proposed that GDGT 4' (the crenarchaeol regioisomer) had a different biological origin, possibly deeper in the water column, than the other GDGTs, and therefore should be excluded from the SST proxy (see Section 1-4-5). This supposition was at least partly supported by Wuchter *et al*. (2004) and Schouten *et al*. (2007) who found that cultured Crenarchaeota have apparent difficulty in synthesising GDGT 4'. In Shah *et al*. (2008), the "TEX_{86}*" ratio was defined as:

Eq. 19.

$$TEX^{*}_{86} = \frac{[GDGT\ 2] + [GDGT\ 3]}{[GDGT\ 1] + [GDGT\ 2] + [GDGT\ 3]}$$

This arrangement, for which no SST conversion equation was given, is seen to reduce the gradient of the slope of the regression line when compared to the TEX_{86} equation for the same set of sedimentary samples, and is thought to be responsible for much of the sensitivity to temperature of the original TEX_{86} arrangement Shah *et al*. (2008).

These alternative calibrations may be applicable in certain regional studies, but are not regularly applied to palaeo-climate reconstructions, and are therefore not discussed further in the context of the Early Cretaceous study.

1. 6. 4. THE EFFECTS OF DEEP-WATER PRODUCTION, SEDIMENTARY PRODUCTION AND SEASONALITY ON TEX_{86}

As discussed above, the association of TEX_{86} with SST is based on empirical evidence, suggesting that the global core-top calibration dataset TEX_{86} values best correlate with mean annual SST, and not mean annual thermocline temperatures (e.g. Schouten *et al*., 2002; Kim *et al*., 2008). This has two main implications:

1) That the Crenarchaeota producing the GDGTs, are mostly concentrated in the surface waters (and therefore are influenced most strongly by SSTs), and/or the export of GDGTs from the surface waters to the sediment is more efficient than the export of GDGTs from deeper waters.

2) That the TEX_{86} ratio of the sediment represents an averaged yearly temperature signal, apparently unaffected by seasonal changes in either temperature or GDGT production.

Sea-surface or thermocline temperatures?

As already discussed above, numerous lines of evidence suggest that the majority of GDGT production by Crenarchaeota is concentrated in subsurface depths, and often becomes particularly pronounced around thermocline depths of 100 – 200 m. In which case the surface water temperature signal often associated with TEX_{86} is puzzling. Given that sedimentary TEX_{86} does seem to best correlate with SST and not thermocline temperatures (e.g. Schouten *et al*., 2002; Kim *et al*., 2008; Kim *et al*., 2010; Wuchter *et al*., 2005; 2006b), is it then possible then that the export of surface water GDGTs is somehow more efficient than export from the deeper waters? It would seem that the simple answer is yes (e.g. Sinnginghe Damste, *et al*., 2002; Wakeham *et al*., 2003; Wuchter *et al*., 2005).

It would be expected that scavenging of Crenarchaeota and other picoplankton through heterotrophic activity would be most intense in the shallow photic zone, where most marine productivity is concentrated. This scavenging would lead to organic material such as GDGTs, being biopackaging in the form of faecal pellets, thus facilitating their transport to the sediments (e.g. Schouten *et al*., 2002). One could certainly imagine a scenario where GDGT molecules produced in the deeper parts of the ocean are not as effectively scavenged and biopackaged, and

therefore have less chance of sinking to the seafloor before being remineralised (e.g. Wakeham *et al*., 2003). Indeed a study by Huguet *et al*. (2006) examined the gut contents of both pelagic and benthic marine decapod crustaceans in the Atlantic and Mediterranean and found GDGTs in nearly all specimens, suggesting these molecules are biopackaged by scavenging in both the photic and benthic environments.

This phenomenon of efficient surface-water transport is seen in the dysoxic waters of the Black Sea, where despite GDGT production throughout the water column, the sedimentary TEX_{86} values (~0.44) are very similar to the values seen in the upper 400 m of the water column (0.44 ± 0.05) (Wakeham *et al*., 2003; Schouten *et al*., 2002). This has also been observed in the oxic waters of the Arabian Sea, where sedimentary TEX_{86} (~0.71) values are identical to those seen near the sea surface (0.72 ± 0.06) (Sinnginghe Damste, *et al*., 2002; Schouten *et al*., 2002), thus suggesting the surface flux of GDGTs was the predominant source of GDGTs reaching the underlying sediment.

A further study based on data from several ocean basins, also observed that although the production of GDGTs occurs throughout the water column, (Figure 9), the TEX_{86} values from water samples >100 m did not match with *in situ* temperature, but rather with SST (Wuchter *et al*., 2005; Wuchter *et al*., 2006b; Figure 25). This was also true of TEX_{86} signal preserved in the underlying sediments (Wuchter *et al*., 2005). In sediment traps in the Arabian Sea, TEX_{86} values from 500 m depth followed the seasonal pattern of SST from the overlying waters, but with a 1 to 3 week time delay, which is attributed to the time taken for the particles to settle through the water column (Wuchter *et al*., 2006b). In deeper water traps at 1500 m and 3000 m, the seasonality signal was lost and the TEX_{86} values best reflected mean annual average SST, thus suggesting deeper waters (and by extrapolation, the sediments beneath) represent a homogenized, time averaged TEX_{86} signal.

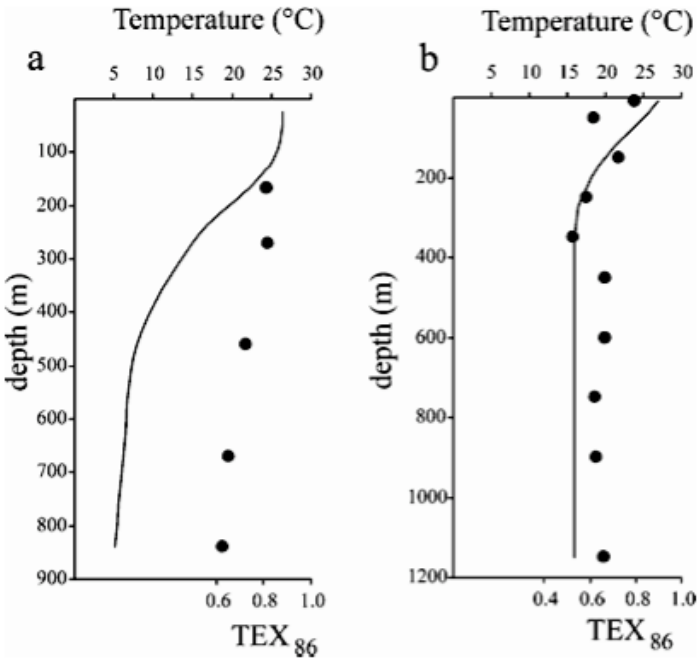

Figure 25. *TEX_{86} data from (a) The equatorial Pacific, and (b) the Cariaco Basin, taken from Wutcher et al. (2005). The TEX_{86} –derived temperatures (black circles) are relatively invariant in the water column at both sites, and seems to best correspond to SST, rather than in situ temperature at that depth (solid line).*

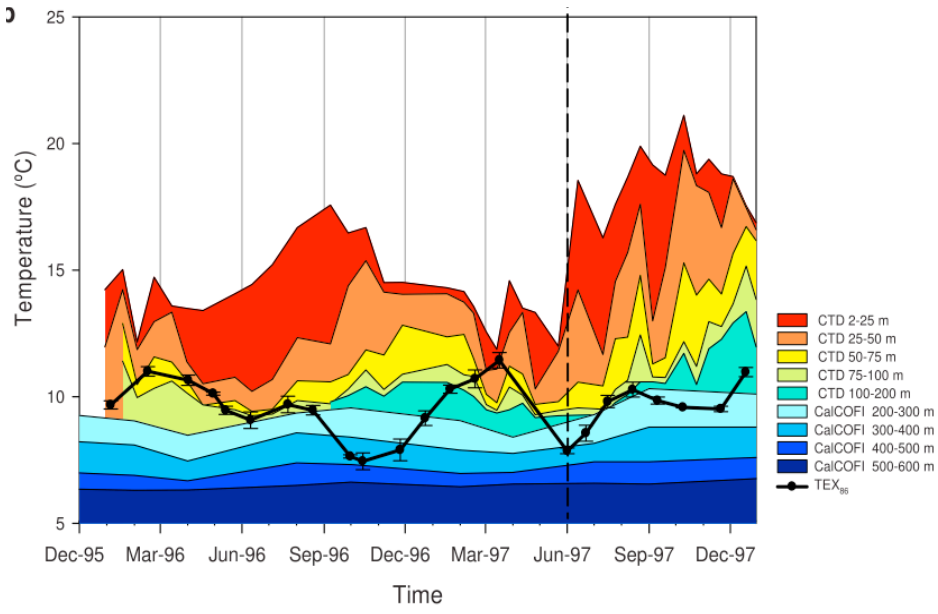

Figure 26. *Taken from Huguet et al. (2007). Time-series study over two years (1995 to 1997) in the Santa Barbara Basin, showing measured TEX_{86} ratios from a sediment trap at 490m water depth (50 m from the bottom) in black, compared to measured in situ temperatures from CTD casts (coloured sections). The lack of coherence between TEX_{86} temperatures and measured temperatures, at any depth, is clear.*

However, as alluded to above, core-top calibration studies by both Schouten *et al*. (2002) and later work by Kim *et al*. (2008) showed that correlation of TEX_{86} with an integrated 0 – 200 m water depth temperature signal, was almost as good as the correlation with SST (r^2 of 0.870 vs. 0.935 respectively, in Kim *et al*. (2008); (Figure 20). Therefore it may be that sedimentary TEX_{86} does indeed best reflect an integrated upper water signal, rather than strictly SSTs. In support of this theory, a time-series study by Huguet *et al*. (2007) in the Santa Barbara basin demonstrated a rather complex relationship between TEX_{86} and temperature, which suggests that sedimentary TEX_{86} actually best reflects subsurface (100 – 150 m) rather than SSTs in that basin (Figure 26). It may be that this reflects local oceanographic conditions or biota indigenous to the specific Santa Barbara Basin study area, which is heavily influenced by seasonal upwelling.

An additional complication was highlighted by Menzel *et al*. (2006), who upon examination of Mediterranean Sea sediments of Pliocene age, concluded that organic-rich sapropels with relatively cool TEX_{86} SST estimates of 15–17ºC, reflected GDGTs from a deeper part of the water column relative to the "normal" marine sedimentation which had warmer TEX_{86} SST estimates of 26–29ºC. Menzel *et al*. (2006) hypothesised, based on comparison with complementary U^k_{37} evidence, that the apparent change in SST during sapropel deposition was not real, and instead reflects either a change in depth habit of the crenarcheota due to the onset of anoxic and euxinic conditions, or a change in the season of dominant GDGT production.

So it would appear that, on balance, the TEX_{86} ratio does reflect an upper ocean (0–200 m) and perhaps a surface water temperature signal in most oligotrophic settings, and some seasonal settings (e.g. the Arabian Sea, Wuchter *et al*., 2006b), despite the preferred subsurface depth habitat of the source organisms. This is likely to be due to increased scavenging and formation of faecal pellets in the upper ocean, which aid the transport of GDGTs to the sediments. It appears that although subsurface, and indeed very deep, *in situ* production of GDGTs does occur in some ocean basins, it is the surface-water signal that is eventually incorporated into the sedimentary record. There are however some exceptions, particularly within modern partially-restricted organic-matter rich basins or during times of enhanced organic matter deposition, where the subsurface GDGT signal may predominate in the sediments (Menzel *et al*., 2006; Huguet *et al*., 2007).

Can sedimentary or deep water production of GDGTs affect the TEX_{86} ratio?

It is clear from many studies that archaea of both the Euryarchaeota and Crenarchaeota Kingdoms, as well as many bacteria, can live and thrive in the subsurface sedimentary environment, which is a very large but poorly understood ecosystem (Vetriani *et al*., 1998; Inagaki *et al*., 2003; Sorensen & Teske, 2006; Shah *et al*., 2008 and references within). As many of the archaeal groups are known to synthesise GDGTs, including GDGTs 0 – 4 used in the TEX_{86} proxy (e.g. Pancost *et al*., 2001; Biddle *et al*., 2006; Schouten *et al*., 2007), the potential for sedimentary GDGT biasing of the pelagic TEX_{86} record is an issue which must be considered. The good correlation between core-top TEX_{86} and upper water column temperatures in many oceanographic settings (e.g. Schouten *et al*., 2002; Wuchter *et al*., 2006; Kim *et al*., 2008), would suggest that contribution of deep-water or sedimentary GDGTs is minimal, however several studies have examined the issue of *in situ* GDGT production and have come to the conclusion that it may be a major issue in some high-productivity marine settings (e.g. Shah *et al*., 2008).

It appears that on the basis of both genetic and biomarker information, that the deep sedimentary biosphere under highly-productive upwelling regions such as offshore Peru, is dominated by chemoautotrophic archaea (Biddle *et al*., 2006). These organisms, and others living in marine sediments elsewhere, were found to be capable of synthesising the cyclized GDGTs (1-4') used in the TEX_{86} proxy (Pancost *et al*., 2001; Biddle *et al*., 2006). Marked differences between the archaeal populations in organic-rich and organic poor marine sediments in the western Pacific have also been reported (Inagaki *et al*., 2003). Furthermore, a study examining the $\Delta^{14}C$ values of concomitant planktonic foraminifera, alkenones and GDGTs samples from the Bermuda Rise (oligotrophic) and Santa Monica Basin (mesotrophic), concluded that some *in situ* production of GDGTs within the sediment could be occurring in the Santa Monica Basin, leading to overestimation of SST from TEX_{86} (Shah *et al*., 2008). This mismatch in the Santa Monica basin was attributed to possible lateral advection of GDGTs, or deep-water/ sediment production of GDGTs. These studies perhaps suggests that the potential contamination from sedimentary or deep water GDGTs is greater in high productivity, organic-rich settings than in oligotrophic settings, and may help to explain poor TEX_{86} performance in such settings (e.g. Huguet *et al*., 2007).

In conclusion, despite the very good empirical agreement between SSTs and sedimentary TEX_{86} values in many studies (e.g. Schouten *et al*., 2002; Kim *et al*., 2008), there appear to be some complications in certain restricted, dysoxic or marginal basins, possibly stemming from deep-water or sedimentary GDGT production in these organic- matter enriched settings (e.g Huguet et al., 2007; Menzel *et al*., 2006; Biddle *et al*., 2006; Shah *et al*., 2008). Therefore organic-matter rich settings, such as restricted basins, should perhaps be approached with a degree of care with regards to using the TEX_{86} proxy to reconstruct SSTs.

Seasonality effect on TEX_{86}

Core-top samples certainly represent a time-integrated signal, and in that sense one might expect the sedimentary TEX_{86} ratio to have a better fit with an average temperature rather than a seasonal one. A sedimentary sample would certainly be expected to give a more time-averaged representation of the water column GDGTs throughout the years(s) rather than the "snapshot" one might observe from water column filtrates (e.g. Schouten *et al*., 2002). However, several case studies have demonstrated a consistent seasonal bias or a poor correlation between TEX_{86} and SSTs in some strongly seasonal marine settings, e.g. the Angolan Basin (Schouten *et al*., 2002), the southern Atlantic (M. Clarkson. *UCL, unpublished MSc Dissertation, 2010*), the shallow North Sea (Herfort *et al*., 2006) and the Santa Barbara Basin (Huguet *et al*., 2007). Additionally, although not demonstrated specifically in terms of TEX_{86}, it is clear that winter-spring maximums in GDGT production occur in high-latitude settings, while scavenging is concentrated in the summer months, which may bias the SST reconstruction in such settings (Murray *et al*., 1998: Church *et al*., 2003). It is likely that seasonality effects on the TEX_{86} record are a potential issue in some marine settings, probably depending on factors such as light availability, warmth and the influence of upwelling and other seasonal oceanographic conditions. This clearly presents problems when considering deep time SST reconstructions using TEX_{86}, (such as the Cretaceous) where it is impossible to conduct modern calibration studies which are unique to that particular ancient basin.

However, no seasonality bias has been identified in open-ocean, low-latitude regions in GDGT production (e.g. Karner *et al*., 2001), suggesting that seasonality

effects may be a high-latitude, or marginal basin, issue with TEX_{86}. Furthermore, Kim *et al*. (2008) investigated the possible seasonality bias in detail by comparing the global TEX_{86} core-top ratios with winter, spring, summer and autumn mean temperature averages in surface waters. They found that although there was good correlation between TEX_{86} and SST at all times of the year (r^2 range of 0.813 to 0.872, with the highest values for the autumn), the best correlation was still with mean annual average SST overall. It was concluded that while seasonality (and depth habit) may have some influence on the scatter seen in the TEX_{86} calibration set, the overall trend suggests seasonality is a only a minor component. The combination of homogenization of the sinking GDGTs over the year, plus the possibility of lateral transfer of GDGTs from elsewhere in the region, appears to result in a sedimentary signal that best correlates with an annual average, despite peak surface water GDGT production during the southwestern monsoon (June – September); (Kim *et al*., 2008; Wuchter *et al*., 2006b).

1. 6. 5. TERRESTRIAL GDGTS AND THE BIT INDEX

An added complication to the use of the TEX_{86} proxy in marine environments is the fact that organisms that live in soils or peat bogs, such as bacteria and methanogenic archaea, also synthesize GDGTs (Pancost *et al*., 2000; Hopmans *et al*., 2004; Weijers *et al*., 2006a). These terrestrial GDGTs can potentially bias the palaeotemperature reconstruction if the terrestrial GDGTs are introduced into the marine realm through fluvial or aeolian transport (e.g. Hopmans *et al*., 2004; Weijers *et al*., 2006b; 2010). GDGT 0 ("caldarchaeol") is a ubiquitous component of both archaeal (thermophilic, halophilic, methanogenic and marine) and some bacterial (predominantly methanogenic) cell membranes, and is therefore not diagnostic of Group 1 Crenarchaeota in particular (e.g. Pancost *et al*., 2001), which was the main reason this molecule was omitted from the original TEX_{86} equation (Schouten *et al*., 2002). The problem is that the cyclized isoprenoid tetraethers (GDGTs 1 – 3) used in the TEX_{86} equations (see Figure 15) can also have various origins, both marine and terrestrial, and the relationship between GDGT cyclization and temperature is unlikely to be the same for these different organisms living in different habitats. The branched, uncyclized tetraethers on the other hand, are regarded as having a

predominantly terrestrial origin (Schouten *et al*., 2000; Hopmans *et al*., 2004; Figure 15). This conclusion of differing origins for branched and isoprenoid GDGTs, was supported by Pancost *et al*. (2000), who showed that acyclic and cyclic GDGTs from various peat bogs had different $\delta^{13}C$ compositions, and were therefore likely to be synthesized by different source organisms utilizing different metabolic pathways.

Crenarchaeol (GDGT 4), was regarded as a marker for the non-thermophilic marine Crenarchaeota, although it has now also been found to be synthesised by other archaea (e.g. Pearson, *et al*., 2004; De la Torre *et al*., 2008; Pitcher *et al*., 2009). It was therefore hypothesised that determining the ratio of crenarchaeol to branched GDGTs (I, II and III) would provide a measure of the terrestrial component in a sediment sample. The BIT (Branched and Isoprenoid Tetraether) Index was developed as a way of constraining this terrestrial GDGT flux into the marine realm by Hopmans *et al*. (2004), and is defined as:

Eq. 20
$$BIT\ Index = \frac{[GDGT\ I] + [GDGT\ II] + [GDGT\ III]}{[GDGT\ I] + [GDGT\ II] + [GDGT\ III] + [GDGT\ V]}$$

where a ratio of 0 would indicate no branched GDGTs (very low terrestrial input) and a ratio of 1 would indicate no crenarchaeol (very high terrestrial component). The BIT Index was tested in the Angola Basin, where it was found to track the outflow of the Congo River, and in the North Sea where the influence of large European rivers such as the Thames and the Humber was clearly seen in the elevated BIT Index values there (Hopmans *et al*., 2004).

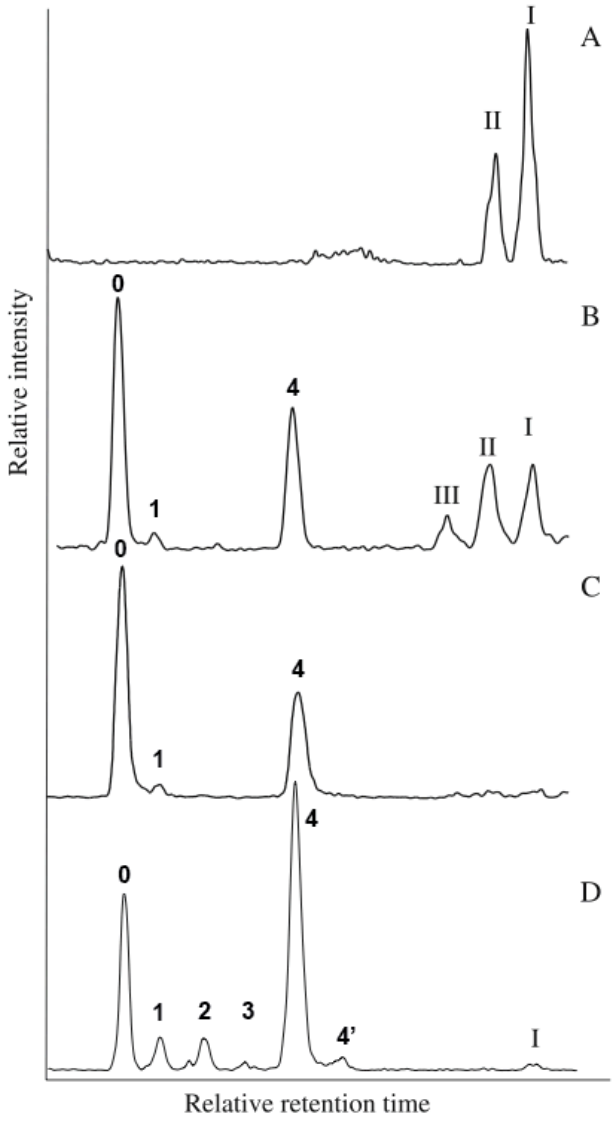

Figure 27*. Comparison of GDGT spectra from different modern environments, taken from Hopmans et al. (2004). (A) Soil from a deciduous tree forest, Texel, the Nederlands, (B) surface sediment from the Mok Bay, Texel, (C) water column sample of the Wadden Sea and (D) core top sample from the Congo River basin.*

Importantly, based on hypothetical mixing-models of terrestrial and marine GDGTs, it was suggested in (Weijers *et al*., 2006b) that an upper limit in the BIT Index of 0.4, and preferably 0.3, would be sufficient to assume that the TEX_{86} ratio had not been unduly influenced by terrestrial GDGT contamination (Figure 28). For example, in their model Weijers *et al*. (2006b) used a marine end member with a "TEX_{86} temperature" of 22.3ºC and a BIT index of 0.03, and a terrestrial end member with a "TEX_{86} temperature" of 32.2ºC and a BIT index of 0.92, and showed that the effect of increasing influence of the terrestrial contamination on the marine

TEX_{86} value was clear. In the model, a BIT Index of 0.4 would indicate that >30% of the GDGTs in the sample were derived from soils, leading to a temperature deviation of >2ºC. As this is a considerable potential temperature effect, it is clear that it is important to constrain the BIT Index in a marine sediment sample, by analyzing the branched GDGT abundances at the same time as determining the TEX_{86} ratio using the isoprenoid GDGTs.

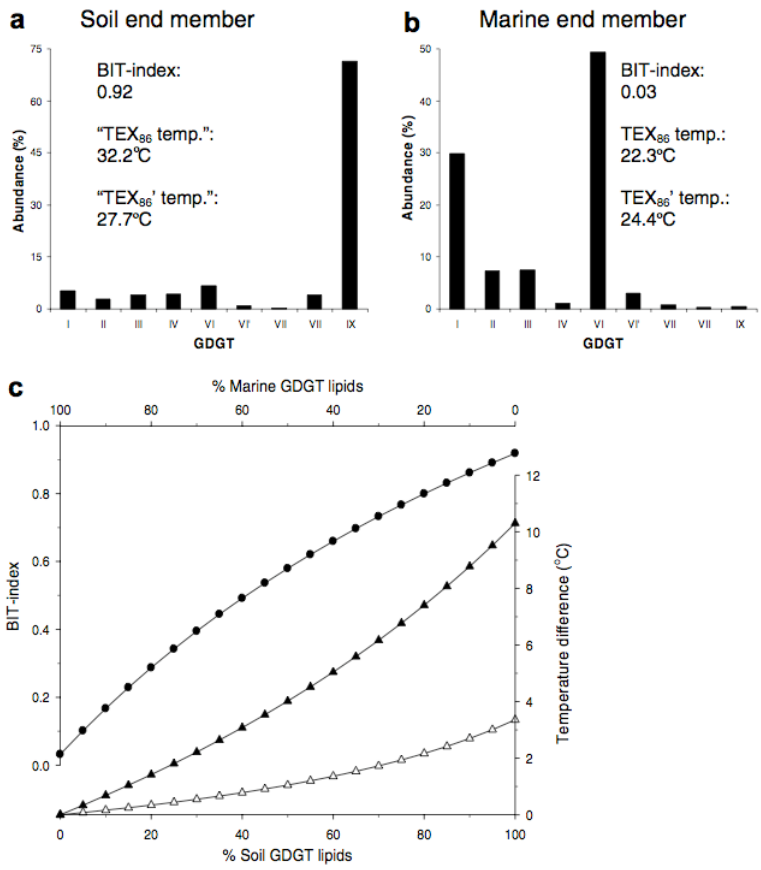

Figure 28. *(a) =Specific GDGT abundance in the soil end member; (b) =Specific GDGT abundance in the marine sediment end member; (c) hypothetical mixing model to show the effect of terrestrial GDGT contamination on the TEX_{86} temperature reconstruction; all taken from Weijers et al. (2006b).*

1. 6. 6. HOW DOES OXIC DEGRADATION AND THERMAL MATURATION AFFECT THE TEX_{86} PROXY?

If the TEX_{86} proxy is to be used to construct palaeotemperature records from sedimentary records, it is necessary to constrain the effect that both oxic degradation

and thermal maturation could have on the ratio, and therefore the reconstructed SST estimates. GDGTs are organic compounds synthesized predominantly in the water column, but they are broken down by degradation processes both within the water column prior to deposition, and in the sediments themselves (e.g. Huguet *et al*., 2009; Schouten *et al*. 2004). Additionally deep burial in the sedimentary pile would expose the sediments, and the GDGTs within, to elevated temperature regimes, which may cause the molecules to degrade.

Some studies have concluded, that while there is generally a significant reduction in the overall abundance of GDGTs in sediments that have been exposed to oxic degradation, there is no effect on the TEX_{86} ratio itself (Schouten *et al.* 2004; Kim *et al*., 2009). This has been demonstrated in one comparative field study of *in situ* recent marine sediments from the northern Indian Ocean, (Schouten *et al.* 2004) and in one study that examined recent marine sediments set out on moorings in various oxic and anoxic settings (Kim *et al*., 2009). Neither of these studies saw a significant difference in TEX_{86} despite the widely differing oxygen levels between samples.

One study examining Neogene turbidites, however, did observe changes in the TEX_{86} ratio, thought to be related to the effects of preferential oxic degradation on the GDGT molecules (Huguet *et al*., 2009). Contrary to the results from Schouten *et al*., (2004) or (Kim *et al*., 2009), this study showed that the oxidized parts of the turbidites often had substantially different TEX_{86} ratios (and greatly reduced GDGT concentrations) relative to the unoxidized portions of the turbidites. However neither the direction of the trend nor the magnitude of the change in absolute TEX_{86} value was consistent between the different turbidites studied (Figures 29). In a high-resolution study on a Pleistocene turbidite, the TEX_{86} value was shown to become unstable and generally increase slightly from 0.54 ± 0.003 in the unoxidized part to 0.57 ± 0.02 in the oxidized portion, which would correspond to a temperature change of ~1 – 2 ºC (depending on SST calibration) (Figure 29a). Interestingly, when other older turbidites are examined (Figure 29b), the trend is often reversed with a shift to lower TEX_{86} values in the oxidized part of the sediments, and the magnitude of the difference in the ratio can be as large as 0.06 (~3–4 ºC temperature difference). This scenario would lead to a "cold bias" in the TEX_{86} SST reconstruction (Huguet *et al*., 2009). The BIT index in all cases increases substantially in the oxidized part of the turbidites relative to the unoxidized parts (Figure 29), which suggests that the

branched GDGTs are more stable during oxic degradation than the isoprenoid GDGTs. In all turbidites analysed by Huguet *et al*., (2009), the amount of GDGTs in the sediment decreased radically from the unoxidized part of the turbidite to the oxidized portion, in agreement with the findings of Schouten *et al*., (2004).

The disparity between the findings of Kim *et al*., (2009) and Huguet *et al*., (2009) could be attributed to the short length of time (~1 year) which the GDGTs were subjected to oxic degradation in during the former study, relative to the presumed much longer term exposure of the turbiditic sediments to oxic conditions in the latter study. It may be that GDGTs are stable on the timescales of months to years, but begin to preferentially degrade on longer decadal timescales (Kim *et al*., 2009). Another factor to consider may be the effect of weathering and sub-aerial exposure on GDGT ratios in outcrop sections, which has not yet been investigated in detail (T. Herbert, *pers comm. 2010*). However, this scenario is not relevant within the context of the marine sediments examined in this thesis. Regardelss, clearly more work is needed to constrain the effects of oxic degradation on both modern and ancient sediments.

While the effects of oxic degradation on TEX_{86} are somewhat controversial, the effects of over-maturation appear to be well constrained. Experimental hydrous pyrolysis experiments at temperatures between 160ºC and 330ºC, which aimed to simulate the elevated conditions of deep burial and thermal maturation, showed an effect on the TEX_{86} ratio with increased temperature (Figure 30; Schouten *et al.,* 2004). It appears that GDGT 0 (caldarchaeol), and to a lesser extent GDGT 1, are more thermally stable than the other, more cyclized, GDGTs, as they were still present in detectable quantities at 280ºC, while the other GDGTs are below detection levels at this temperature. The effect of increasing burial temperature on the TEX_{86} ratio was minimal up to temperatures < 240ºC, with a fairly invariant TEX_{86} ratio of 0.60 ±0.01, however above this temperature a substantial shift was observed with values of 0.45 recorded at 260ºC. These results suggest that the TEX_{86} ratio is stable up to temperatures of ~240ºC but will be biased towards much cooler temperatures above this temperature due to thermal maturation of the GDGT molecules.

a)

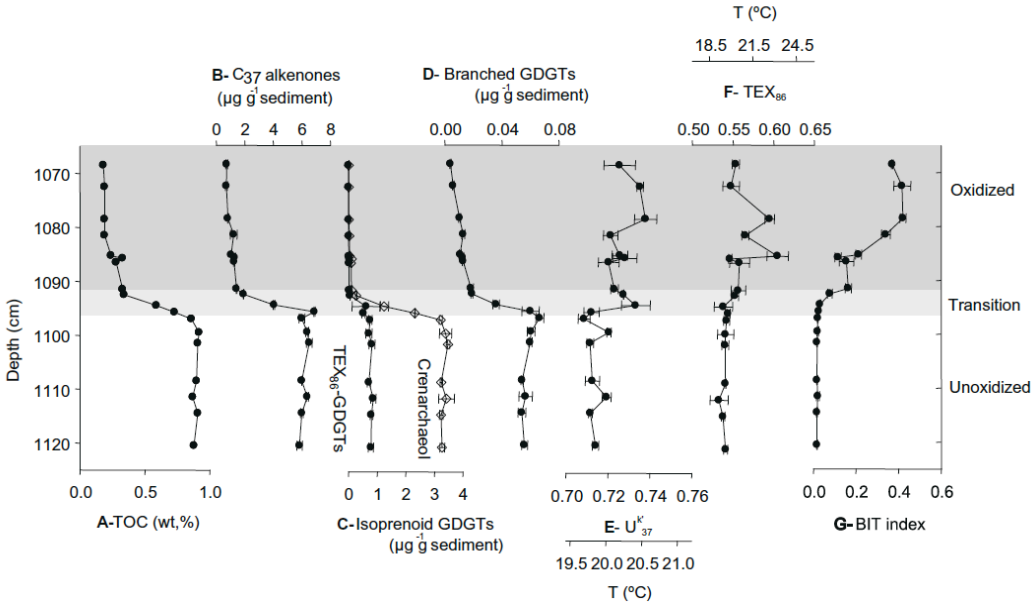

b)

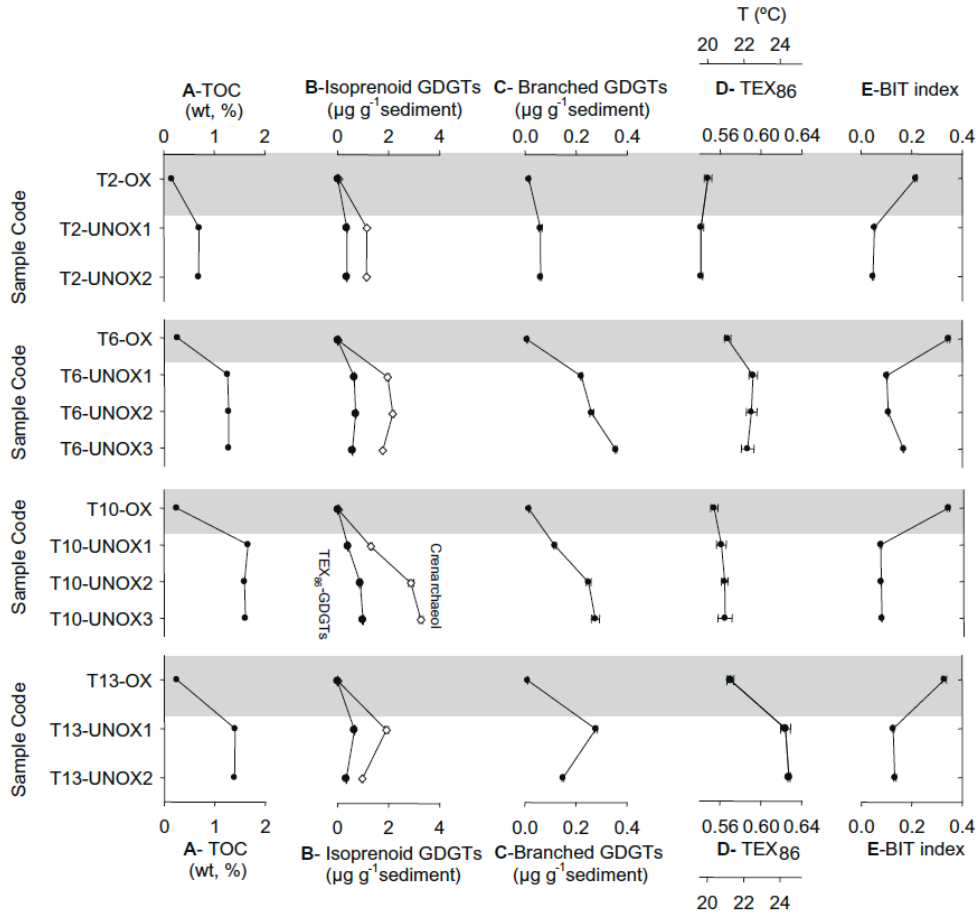

***Figure 29**. **(a)** Biomarker data from a Pleistocene turbidite in the Madeira Abyssal Plain (MAP) region, taken from Huguet et al. (2009). **(b)** Data from other Pliocene/Miocene turbidites in the MAP region. Grey bars denote oxidized parts of the turbidites.*

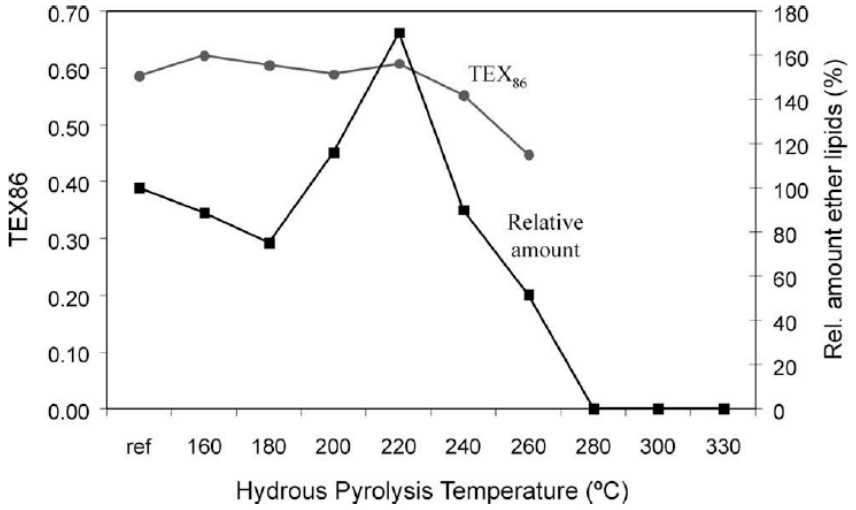

***Figure 30**. Artificial maturation data from Schouten et al., (2004), showing the effect on both GDGT concentration (black squares) and the TEX_{86} ratio (black circles) with increasing hydrous pyrolysis temperature.*

Clearly, the temperatures which ancient sediments have been exposed to will not always be known, so the use of a well-known biomarker indicator based on the relationship between thermal maturity and hopane composition was proposed in Schouten *et al*. (2004). When the ratio of hopanes bearing the biological 17β,21β(H) stereochemical configuration is low relative to the more thermally stable 17α,21β(H) and 17β,21α(H) isomers, the sediment is probably immature enough to not be unduly affected by thermal maturation. This is quantified by ensuring the ββ/(ββ + αβ + βα) ratio is <0.5, indicating the rocks are suitably immature (Schouten *et al*., 2004)

1. 6. 7. TEX_{86} SUMMARY

- Marine Crenarchaeota are abundant and ubiquitous throughout the modern World oceans.
- Most marine Crenarchaeota are probably chemoautotrophs, of which a sizable proportion may be ammonia-oxidizers. Some crenarchaeota may be heterotrophic.

- Marine Crenarchaeota, and GDGTs synthesised by Crenarchaeota, are generally of low abundance in surface waters (<100 m depth) and are most abundant between 100 and 500 m water depth. Although deep-water populations and production have been documented. TEX_{86} ratios in sediments probably represent SSTs because of preferential biopackaging in the photic zone.
- In oligotrophic settings no strong seasonal bias has been observed in crenarchaeotal or GDGT abundance. In more seasonal marine settings (high latitude, upwelling regions, etc) a winter-spring seasonal bias is often seen in productivity. This suggests that high latitude regions or areas affected by sustained upwelling should be treated with caution when applying the TEX_{86} proxy.
- *In situ* sedimentary production may occur in some settings, potentially biasing palaeo-SST reconstruction. This is most likely to happen in organic-rich marine settings in high productivity regions where sedimentary biosphere activity is highest.
- Only marine Crenarchaeota synthesise all of the (GDGTs) used in the TEX_{86} proxy, but many of the individual GDGTs can also be synthesised by certain bacteria and Crenarchaeota in the oceans and soils, and possibly by some marine euryarchaeaota. Therefore, sites near cold seeps where methanogenic bacteria may live, or contaminated by soil must be avoided. The BIT Index can be used to ascertain the degree of terrestrial contamination.
- Thermal maturation can influence the TEX_{86} proxy by skewing the SSTs to cooler values, but the effects of oxic degradation are more controversial. GDGTs are probably stable on timescales of ~years, but may become unstable on longer timescales under oxic conditions.

CHAPTER 2. METHODS AND MATERIALS

2. 1. SAMPLES

2. 1. 1. SITE LOCATION AND SAMPLING

Marine sediments of Berriasian–Barremian age (~142 to ~ 128 Ma) were sampled from cores recovered from various drilling sites in the World oceans, and were subsequently analysed using various geochemical and palaeontological techniques. These sediments were cored during six separate drilling expeditions by the Ocean Drilling Program (ODP) and its predecessor, the Deep Sea Drilling Program (DSDP), and one coring expedition by the British Geological Survey (BGS), between 1974 and 1990 (Table 1). Three of the sites are located in the North Atlantic, four sites in the Indian Ocean, one site in the Weddell Sea region of the Southern Ocean, and one in the North Sea (Figure 31). Eight sites in total were sampled as part of this project (DSDP 249, 534 and 603, ODP 763, 765, 766 and 692, and BGS 81/43). The palaeolatitude of these sites during the earliest Cretaceous was determined by reference to the Plate Tectonic Reconstruction Service (ODSN) Paleomap project. A summary of the palaeogeographic reconstruction and the location of the sampled sites during the Hauterivian is shown in Figure 32.

Initially, a small number of samples at a low resolution (~ one sample every 9 m) were taken from each site, as part of a TEX_{86} pilot study. A variety of different lithologies were sampled from Site 534 and 603 during the pilot-study stage, concentrating on mid-grey laminated marls (pelagic origin) and dark-grey mudstones (presumed turbiditic origin), throughout the cores. At all other sites lithological separation was not possible and sample selection was based predominantly on depth only. After the pilot study phase, sites that showed promising results (e.g. Sites 534 and 603) were subsequently sampled at a higher resolution, to increase the density of data across key intervals such as the Late Valanginian and Early Hauterivian.

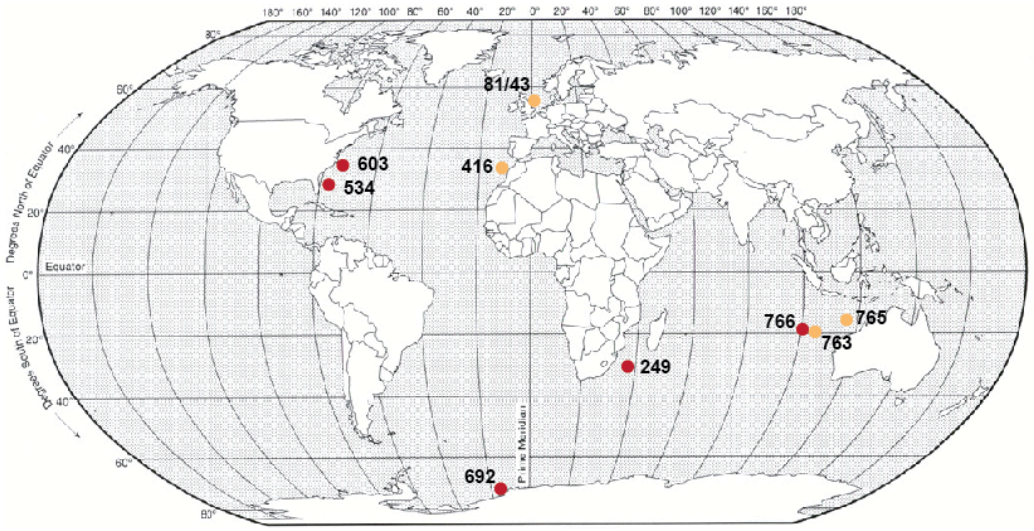

***Figure 31**: Map (Robert Projection) showing modern geographical location of the DSDP, ODP and BGS Sites sampled during this project. Red circles are sites where TEX_{86} and carbon-isotope data was successfully generated; yellow circles are sites which were also sampled, but which failed to yield promising TEX_{86} data and/or carbon-isotope data in the pilot study. The sampled sites cover a range of palaeolatitudes in the modern World, especially in the Southern Hemisphere.*

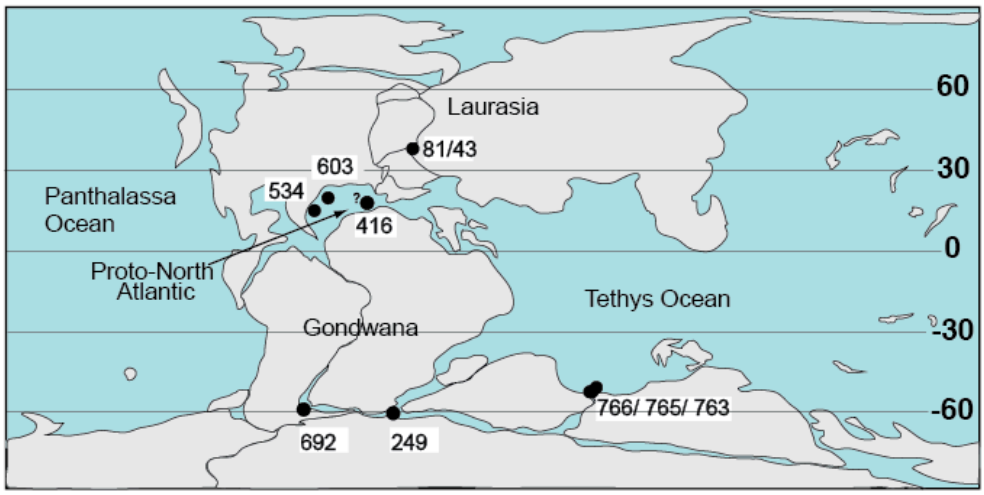

***Figure 32**: Simplified palaeogeographic reconstruction of the Early Hauterivian (~133 Ma), showing location of sampled core sites (black circles).*

HOLE*	MODERN GEOGRAPHICAL LOCATION (LATITUDE)	EXP YEAR	PRESENT WATER DEPTH	PALAEOGEOGRAPHIC LOCATION IN EARLY CRETACEOUS (~133 MA)	MODERN SETTING
25-249	**South-western Indian Ocean (30°S)**	**1974**	**2088 m**	**Southern Tethys Ocean ~61°S**	**Mozambique Ridge summit**
50-416-A	Eastern North Atlantic Ocean (33°N)	1976	4191 m	Proto-North Atlantic ~20 °N?	Deep Moroccan Basin
76-534-A	**Western North Atlantic Ocean (28°N)**	**1980**	**4971 m**	**Proto-North Atlantic ~15°N**	**Central Blake-Bahama Basin**
93-603-B	**Western North Atlantic Ocean (35°N)**	**1983**	**4633 m**	**Proto-North Atlantic ~20°N**	**Foot of lower continental rise terrace, Jersey margin**
113-692-B	**Weddell Sea, Southern Ocean (70°S)**	**1988**	**2875 m**	**Southern Tethys Ocean ~59°S**	**Mid slope bench, Weddell Sea margin**
122-763-B	South-eastern Indian Ocean (20°S)	1990	1367 m	Southeastern Tethys Ocean ~53°S	Central Exmouth Plateau
123-765-C	South-eastern Indian Ocean (16°S)	1990	5717 m	Southeastern Tethys Ocean ~50°S	Argo Abyssal Plain
123-766-A	**South-eastern Indian Ocean (20°S)**	**1990**	**3998 m**	**Southeastern Tethys Ocean ~53°S**	**Exmouth Plateau flank**
BGS 81/43	Southern North Sea (55 °N)	1981	66 m	Northwestern Tethys/ Boreal seaway ~ 40 °N	Continental shelf

Table 1: *Location and oceanographic setting of sampled sites. All location and water depth data taken from the respective DSDP/ODP Initial Reports or BGS Site Reports (see below). Exp year = Expedition year. *Core nomenclature: e.g. 93-603-B, refers to Leg 93, Site 603 and (where applicable) Hole B. Most important sites in the context of this thesis are highlighted in bold.*

In the North Atlantic, DSDP Hole 76-534A and DSDP Hole 93-603B were sampled from 960 to 1250 mbsf (meters below sea floor) and 1320 to 1570 mbsf respectively. In the Indian Ocean, ODP Hole 123-766-A was sampled between 260 to 450 mbsf. The resolution of sampling in these major sites was generally on the order of 2 to 3 samples per core section (~every 50 cm), although note that the resolution of the resulting successful TEX_{86} data is much lower on the order of 1 data point per 1.5 m Core). Hole 692B only contains five cores (53 to 98 mbsf) of earliest

Cretaceous age, so up to 3 samples per core section (every 50 cm) were taken for detailed analysis at this site. Site 249, 763 and 765 were sampled with a much lower resolution on the order of one sample per two core sections (every ~18 m), as these were not re-sampled after the original pilot study. The western Atlantic samples (Sites 534, 603 and 416) used in this study were collected in person from the Bremen Core Repository (BRC) in Germany by either Dr Stuart Robinson or myself. Core BGS 81/43 was sampled personally at the BGS Core Store at Gilmerton, Scotland. Cores taken from the Indian and Southern Oceans (Sites 249, 692, 763, 765 and 766) are held at the Kochi Core Repository (KCR) in Japan, and were sampled by curatorial staff at this institute and shipped to UCL upon request. Due to the age and depth of burial that the sediments have been subjected to, the material is usually well-lithified, and sampling of 15–20 cm^3 sized pieces is generally achieved using a hammer and chisel, or in the case of the Indian Ocean samples, a rock saw. The handling of the sediments is kept to a minimum and they are placed directly into labelled plastic samples bags once removed from the core, and stored in boxes at room temperature.

2. 1. 2. LITHOSTRATIGRAPHY

Sites 534 and 603

The sediments of Early Cretaceous age from the western North Atlantic Sites (603 and 534) represent part of the Berriasian–Barremian, regional Blake-Bahama Formation, which is designated as "Unit V" at both sites. These sites are dominated by radiolarian-bearing, carbonate sediments, which alternate between bioturbated limestones and laminated marls. Both sites also contain redeposited siliciclastic sediments (claystone, silt and sandstone), which are concentrated in the upper and middle sections of the Unit at each site (see Figures 33a and b); (Sheridan *et al.,* 1983; van Hinte *et al.,* 1987).

Site 534

Site 534 is located in the Blake-Bahama Basin, 870 km NE of the Bahamas (Sheridan *et al.,* 1983; Appendix Figure 1). The Lower Cretaceous sediments at Site

534 are divided into 4 lithological subunits. Unit V represents the regional Blake-Bahama Formation of earliest Cretaceous age, and is broken into 4 Subunits, a–d (Figure 33a; Sheridan *et al*., 1983). Unit V is dominated by calcareous sediments and contains a mixture of laminated marls, bioturbated chalks, carbonaceous claystones and some coarse terrigenous siliciclastics. The dominantly calcareous lithology throughout suggests deposition occurred above the CCD at all times, probably at palaeo-water depths of ~3500 m (Robertson & Bliefnick, 1983; Robertson, 1984).

The lower part of the section, Subunit Vc (Core ~81–76), is dominated by alternating bioturbated and laminated chalks and marls. There is an increasing amount of dark-coloured calcareous claystones and black shales up-section through Subunit Vb, peaking in Cores 61–62, (base of Subunit Va). There is a corresponding increase in the proportion of coarse siliciclastics from Core 65 upwards, which peaks in Core 59 (mid Subunit Va). Radiolarians are quite common throughout the section, especially in Subunits Vd and Vb (Robertson & Bliefnick, 1983).

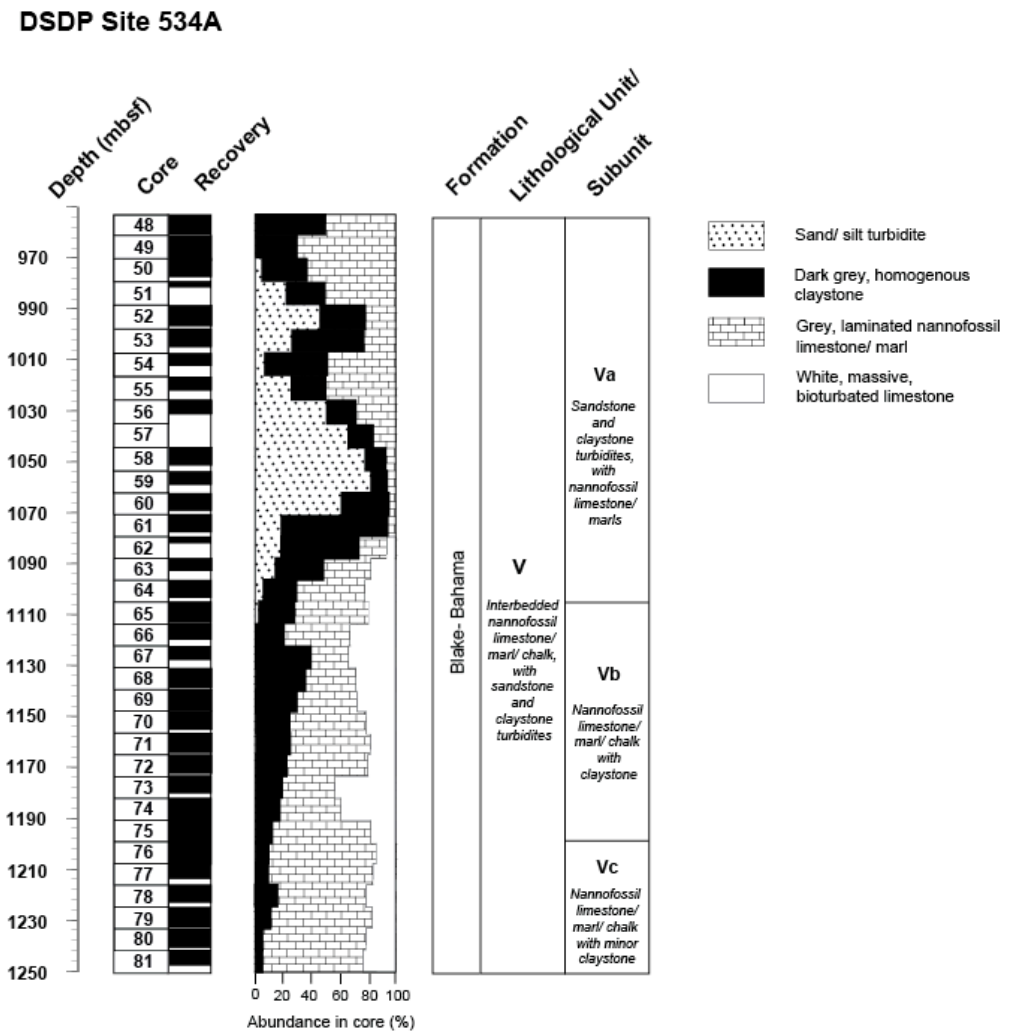

***Figure 33a**: Lithostratigraphy of the sampled section (Unit V) of Site 534A showing Berriasian to Barremian sediments, adapted from* Sheridan *et al.* (1983). *White areas in the recovery column indicate no recovery of sediments within that 9m interval. Sandy intervals show particularly poor recovery.*

Site 603

Site 603 is today located 435 km from the coast of eastern North America, and lies at the foot of the lower continental rise terrace (Appendix Figure 2), while in the Early Cretaceous the site was located ~320 km seaward of the shelf break (van Hinte *et al.,* 1987). The Berriasian–Barremian sediments at Site 603 are dominated by carbonate-rich pelagic marls and chalks, with subordinate claystones and sandstones of transported origin (Figure 33b). Cores 76 to 82 constitute Subunit Vb, which is exclusively formed of pelagic carbonates, while overlying Subunit Va contains transported sediments such as claystones and sandstones. Site 603 appears to have been at the edge of a large deep-sea fan complex during the Valanginian–Barremian

period, which periodically brought terrestrially-derived, coarse siliciclastic material down from the shelf into the newly opening proto-North Atlantic Ocean (van Hinte *et al.,* 1987). These transported deposits are not found below Core 75 (1510 mbsf), and the coarser sandstone influx does not occur below Core 71 (1480 mbsf) (Figure 33b). Within the Unit, the proportion of siliciclastics increases up-section, peaking in Cores 45-48, and within the sampled section peaking in Cores 55–56 (~1330 mbsf). Fine homogeneous claystones are the dominant transported sediments in Cores 75–68, whereafter the coarser sandstones increase in relative importance. Radiolarians are relatively abundant in the carbonates throughout the unit, particularly in the lower part of Unit V, but are frequently replaced by either calcite or pyrite (van Hinte *et al.,* 1987).

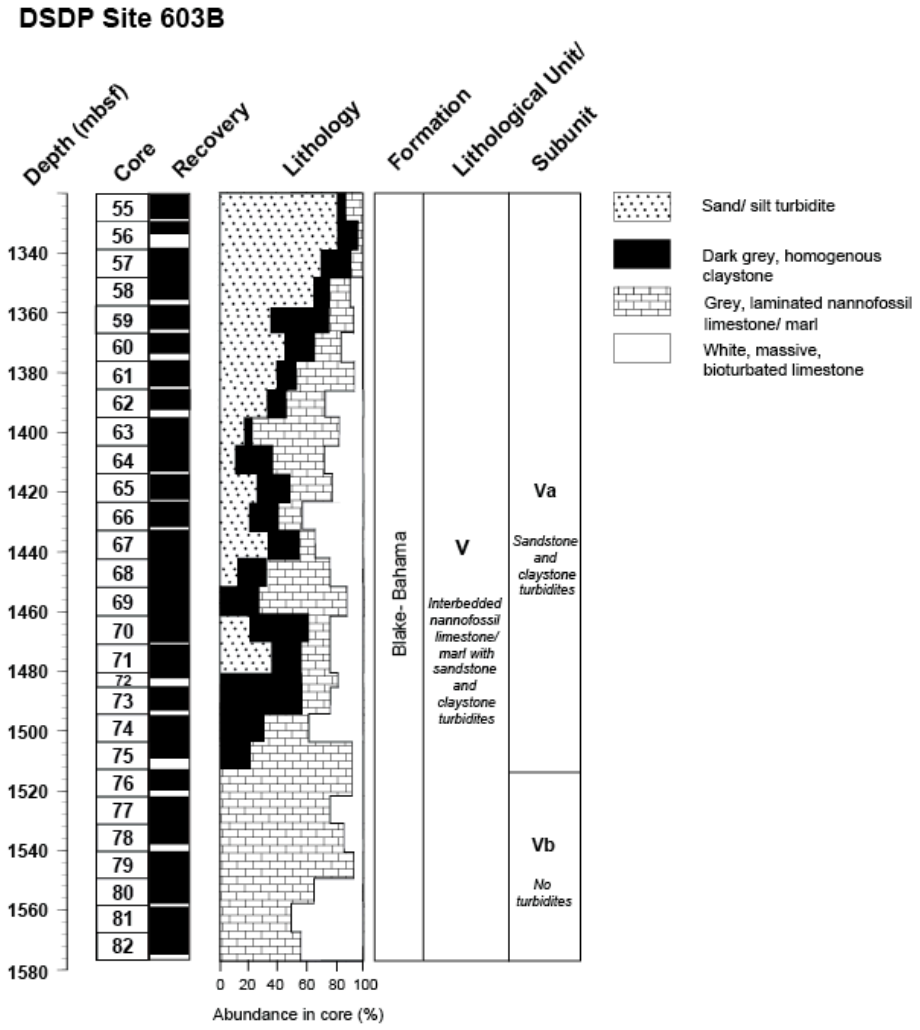

Figure 33b*: Lithostratigraphy of the sampled section (Unit V) of Site 603B showing Berriasian to Hauterivian sediments, adapted from* van Hinte *et al.* (1987)*. White areas in the recovery column indicate no recovery of sediments within that 9m interval.*

Site 766

Site 766 is today located ~350 km off the NW coast of Australia, on the flank of the Exmouth plateau, between the Gascoyne and Cuvier abyssal plains (Ludden *et al*., 1990b; Appendix Figure 3). This site occupied a more hemipelagic setting than the North Atlantic sites during the Early Cretaceous, and was clearly in close proximity to a terrestrial sediment source supplying sand and clay-sized material to the basin, as demonstrated by the dominance of siliciclastics throughout, and in places, neritic bioclastics (Ludden *et al*., 1990b). The lithostratigraphy at this site is divided into several Units, of which Unit III represents the Early Cretaceous regional "Barrow Group". Unit III is characterized by radiolarian-rich claystones, sandy siltstones and silty sandstones, and coarser polymictic sandstones, and is devoid of the nannofossil oozes or chalks which characterize the overlying Unit II (Figure 33c). This late Valanginian – Barremian siliciclastic sequence has been interpreted as a distal part of a submarine fan, which is thought to thicken toward the continental margin (Ludden *et al*., 1990b). Unit V is further divided into a lower Subunit, (IIIB, Cores 48–44), which is dominated by dark, occasionally graded, greenish grey sandstones and siltstones of Late Valanginian to Hauterivian age, and an upper Subunit, (IIIA, Cores 44 to 27), which predominantly consists of dark greenish grey claystones of Upper Hauterivian to Early Barremian age (Ludden et al., 1990b). The contact with basaltic (tholeiitic) basement is encountered in Cores 49 and 48 in the form of dolerite sills of various thickness at the base of Subunit IIIB. Radiolarians are present throughout the section, usually as glauconite-replaced moulds, and are particularly common in the claystones in Subunit IIIa. The sediments are far less carbonate-rich than at Sites 603 or 534, and the preservation and range of nannofossils for age constraint is much more limited. Both the available microfossil assemblages and dominant lithologies are suggestive of a relatively shallow site, deposited on basement at an original water depth of ~800m, before rapidly subsiding to greater depths of ~2000m by the Late Hauterivian (Ludden *et al*., 1990b; Mutterlose, 1992).

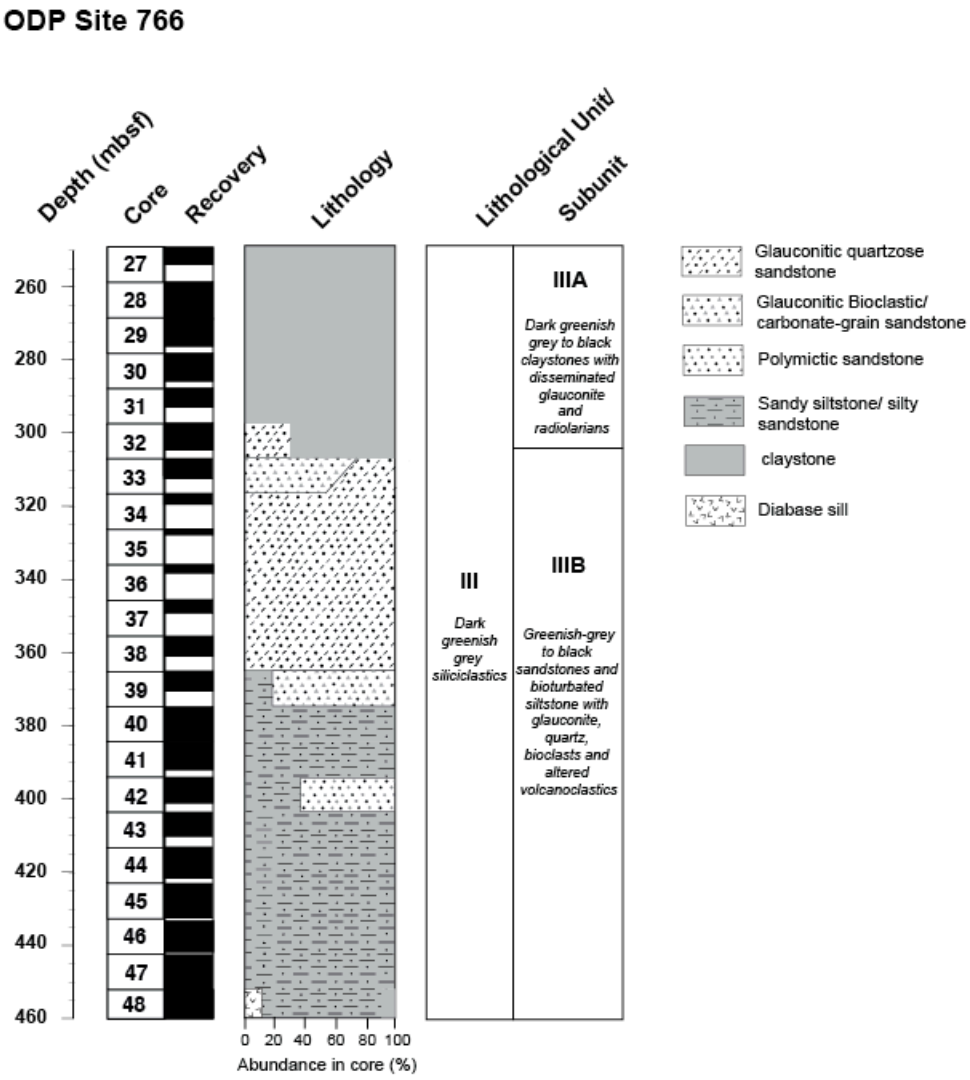

***Figure 33c**: Lithostratigraphy of the sampled section (Unit III) of Site 766, showing Upper Valanginian to Lower Barremian sediments, adapted from (Ludden et al., 1990b). White areas in the recovery column indicate no recovery of sediments within that 9m interval. Sandier intervals show particularly poor recovery.*

Site 692

Site 692 is today located in the Weddell Sea, on the continental slope of the Dronning Maud Land margin, East Antarctica (Barker *et al*., 1988). The lithology in Unit III (Valanginian – Hauterivian?) is dominated by nannofossil-bearing claystone and mudstone, with varying percentages of clay, mud, nannofossils, and organic

matter, with occasional calcareous nannofossils and radiolarians (See Figure 33d; Barker *et al*., 1988; O'Connell, 1990). The dominant clay type is smectite throughout and there is a small but persistent volcanic component in the form of ash lamellae and lenses in Cores 7–9. The clays often have exceptionally high organic-matter content with an average of ~8% and maximum values of up to 18%, which, together with the minimal evidence for bioturbation suggests deposition in a restricted, dysoxic to periodically anoxic environment. Benthic foraminiferal assemblages suggest deposition of these claystones and mudstones in water depths of ~500 m (Mutterlose & Wise, 1990).

Site 249

Site 249 is today located in the south-western Indian Ocean, on the summit of the Mozambique Ridge at a water depth of ~2100 m (Simpson *et al.,* 1974). The Early Cretaceous ("Neocomian") sediments recovered from this site (Cores 23 – 32; Unit III) are largely composed of dark grey claystones and siltstones, occasionally cemented with carbonate, with varying contributions from volcanic components (altered glass shards, ash bands etc), which generally increase up-section (See Figure 33e); (Simpson *et al.,* 1974). These sediments have a mixed terrigenous and volcanic origin and are interpreted as having been deposited in a partially restricted, but fully marine, environment, probably in part by the action of turbidites. The depositional area has been suggested to be a small rift or pull-apart basin (O'Connell, 1990). Basaltic basement was reached at the base of the Unit in Core 32.

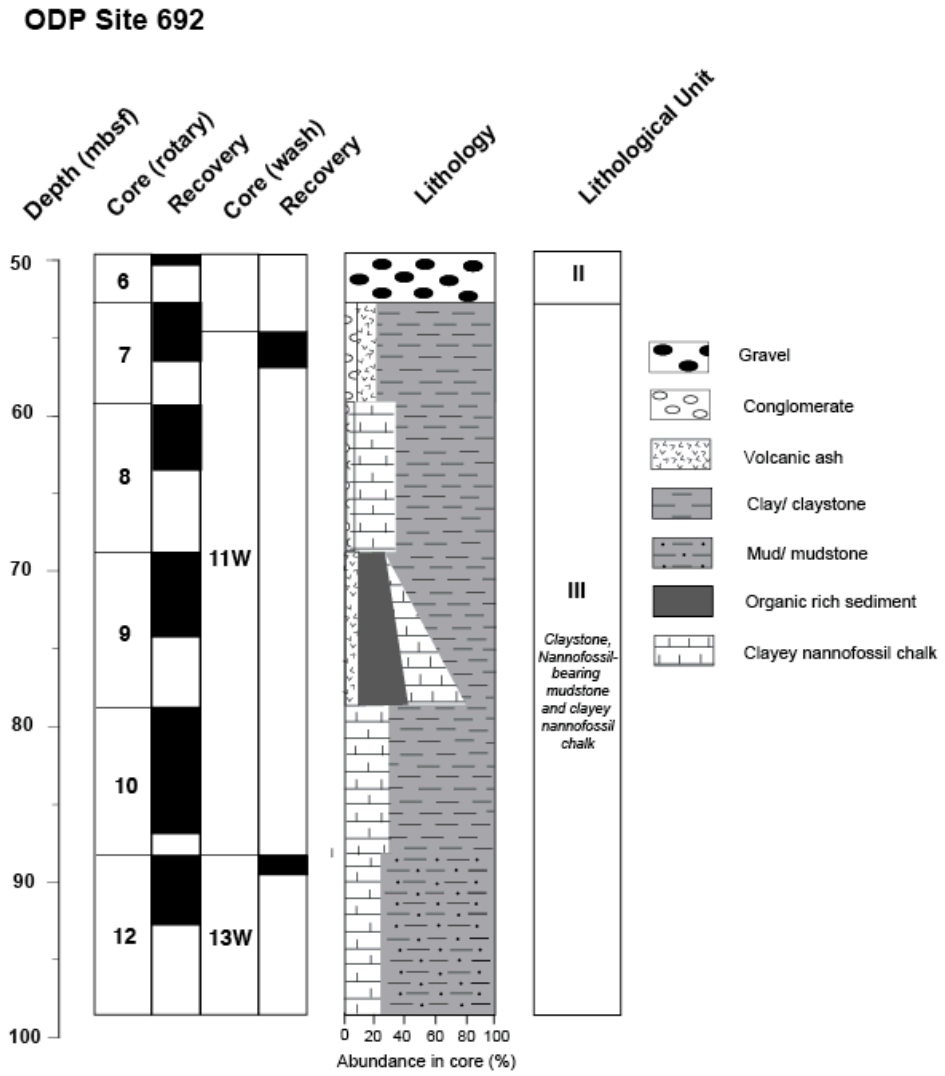

***Figure 33d**: Lithostratigraphy of the sampled section (Unit III) of Site 692, showing Neocomian (probable Valanginian to Hauterivian) sediments, adapted from Barker, Kennett et al. (1988).*

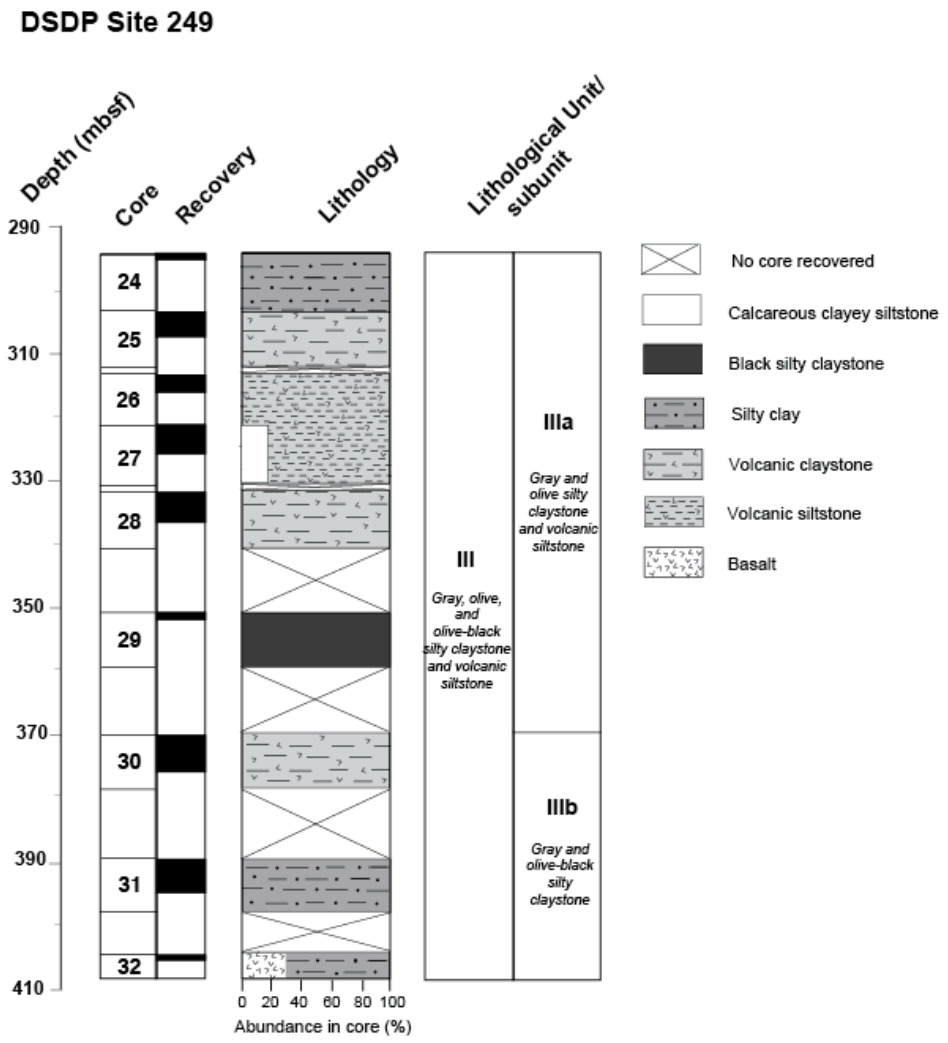

***Figure 33e**: Lithostratigraphy of the sampled section (Unit III) of Site 249, showing Neocomian sediments, adapted from Simpson et al. (1974).*

Sites 763, 765 and 416

Site 765, 763 and 416 are not described in detail (nor do they have figures outlining their lithology), as these sites were not investigated further beyond the initial, largely unsuccessful, TEX_{86} pilot study stage.

Sites 763 and 765

Sites 765 and 763 were drilled to the East of Site 766 off the NW margin of Australia, during Legs 123 and 122. Site 765 is a very deep site and is located in the modern day Argo Abyssal Plain at ~5700m water depth. Berriasian to Hauterivian sediments at this site are dominated by fine-grained siliciclastics, in particular varicoloured claystones in Unit VI and VII with some reddish brown, calcareous claystones and radiolarites in Unit VI (Ludden *et al.,* 1990a; Mutterlose, 1992). Deposition in the Early Cretaceous probably occurred in a deep pelagic to hemipelagic setting, on the basis of the reddish and greenish-tinged mudstones that dominate the lithological succession and the low organic-matter and carbonate content throughout. It is thought that this site was likely to have been below the CCD for much, if not all, of its depositional history (Ludden *et al.,* 1990b).

Site 763 is located on the western part of the central Exmouth Plateau, at the much shallower depth of ~1370 m. The Upper Berriasian – Hauterivian sediments (Units V to VI), which were recovered at this site, are predominantly composed of dark grey siliciclastics, including silty, glauconitic claystones and sandstones (Haq *et al*., 1990). The underlying Berriasian sediments (Unit VII) are interpreted as rapidly deposited prodelta deposits, on the basis of the high sedimentation rates in this unit and analysis of the terrigenous sediment within it, and corresponds to the regional "Barrow Group". The Upper Berriasian – Hauterivian sediments in Unit VI are composed of silty claystones with lesser siltstone, sandstones, and minor carbonates. The top of this unit is marked with a major unconformity of ~8 Myr, which is capped by the initiation of more silty claystone deposition in Unit V (Haq *et al*., 1990).

Site 416

Site 416 is located in the eastern North Atlantic, in the Moroccan Basin, at a modern water depth of ~4200m (Lancelot *et al*., 1980). Sediments of Berriasian – Hauterivian age (Units V and VI) are dominated by varying proportions of grayish/reddish/greenish siltstone, mudstone, sandstone and calcarenite turbidites (Lancelot *et al*., 1980; Wortmann & Weissert *et al*., 2000). These deposits are generally terrigenous in origin with a small proportion of redeposited calcareous claystones, and all have a distal turbiditic origin. Grading, rip-up structures and

laminations associated with various parts of the classic Bouma sequence are common throughout Units VI and VII.

2. 1. 3. CALCAREOUS NANNOFOSSIL BIOSTRATIGRAPHY

The identification of nannofossil species for biostratigraphic age control is achieved by observation of smear slides using high-powered light microscopes. Smear slides are prepared by scraping a small amount of sediment powder from a fresh, broken surface of the sample onto a glass slide. A few drops of distilled water are then carefully added and the resultant wet sediment mixture is smeared and scraped with a wooden toothpick, leaving only a thin residue of material on the slide. A small amount of optically invisible Norland glue is used to attach a clover slip to the glass, which is left to cure under ultraviolet light. The slide is examined under cross-polarised light at x1000 magnification. Identification of nannofossil taxa is made by reference to Bown (1998).

In addition, identification is confirmed by analysis of selected samples using a Jeol JSM-6480LV high-performance, Variable Pressure Analytical Scanning Electron Microscope (SEM), which also allows the degree of preservation of the coccoliths to be determined. For SEM analysis, sub-samples of <0.5 cm^3 are selected for examination, ensuring that a fresh, broken surface is exposed on each sample. These sub-samples are glued to stubs with silver glue, left to dry and then placed into a gold-coating vacuum device to sputter-coat the samples with a very thin layer of gold. The stubs are then placed into the SEM and examined at a variety of magnifications.

2. 1. 4. AGE MODELS

Ages were assigned to the samples using a combination of magneto- and biostratigraphy. Much of this work has already previously been done both by initial onboard stratigraphic analysis (which is documented in the DSDP/ODP Initial Reports), and in subsequent academic papers. The primary biostratigraphic control in Early Cretaceous core material is usually based on calcareous nannofossil assemblages, as these are often abundant and allow correlation between distant sites. Nannofossil zonation allows time to be subdivided into zones and finer resolution

subzones (Figure 34). In general, the original age assignments were found to be in agreement with the additional biostratigraphic assessments carried out in this study, with occasional modifications and additions, especially in the older sites where the numerical age of the zones may have changed since the Initial Reports were generated. In the case of Sites 603 and 534, particular attention was paid to the age models generated by Bornemann *et al.* (2008), which were based on calcareous nannofossil zonations.

In the Early Cretaceous (Berriasian – Barremian), magnetostratigraphy can also be used to constrain relative and absolute ages. The age-models for the most comprehensively studied sites 534, 603 and 766 were constructed by linear interpolation between magnetostratigraphic tie-points, and tied to an absolute timescale (Gradstein *et al*., 2004) with modifications to the placement of Valanginian–Hauterivian boundary after McArthur *et al*. (2007a).

Sites 534 and 603

The age control for Sites 534 and 603 is well constrained and based on magnetostratigraphic data integrated with calcareous nannofossil and other biostratigraphic data (Figure 35a, b). The magnetostratigraphic control is generally very good at both Sites 603 and 534, where Chrons M15, M10N – M5 (and at Site 534, Chron M3r) can be identified within the cores (Appendix Table 1; Ogg, 1987). Unfortunately, the Valanginian M11 – M14 Chrons cannot be identified at either site, which leaves a ~4.7 Myr gap in magnetostratigraphic control. However, there is some biostratigraphic control during this interval at both sites, which broadly support a linear interpolation between the bracketing magnetostratigraphic tie-points at these depths. Key calcareous nannofossil marker species such as *C. oblongata, C. cuvillieri, S. colligata* and, at Site 534, *L. bollii*, allow the assignment of nannozones NK2 to NC5 at both sites (Appendix Table 2; Bergen, 1994; Covington & Wise, 1987; Bornemann *et al*., 2008). While the defining of the NK2 Zone within each site is relatively straightforward, the placing of some boundaries (e.g. NK4 Zone) is more complicated, due to uncertainties in the last occurrence of marker species such as *T. veranae.*

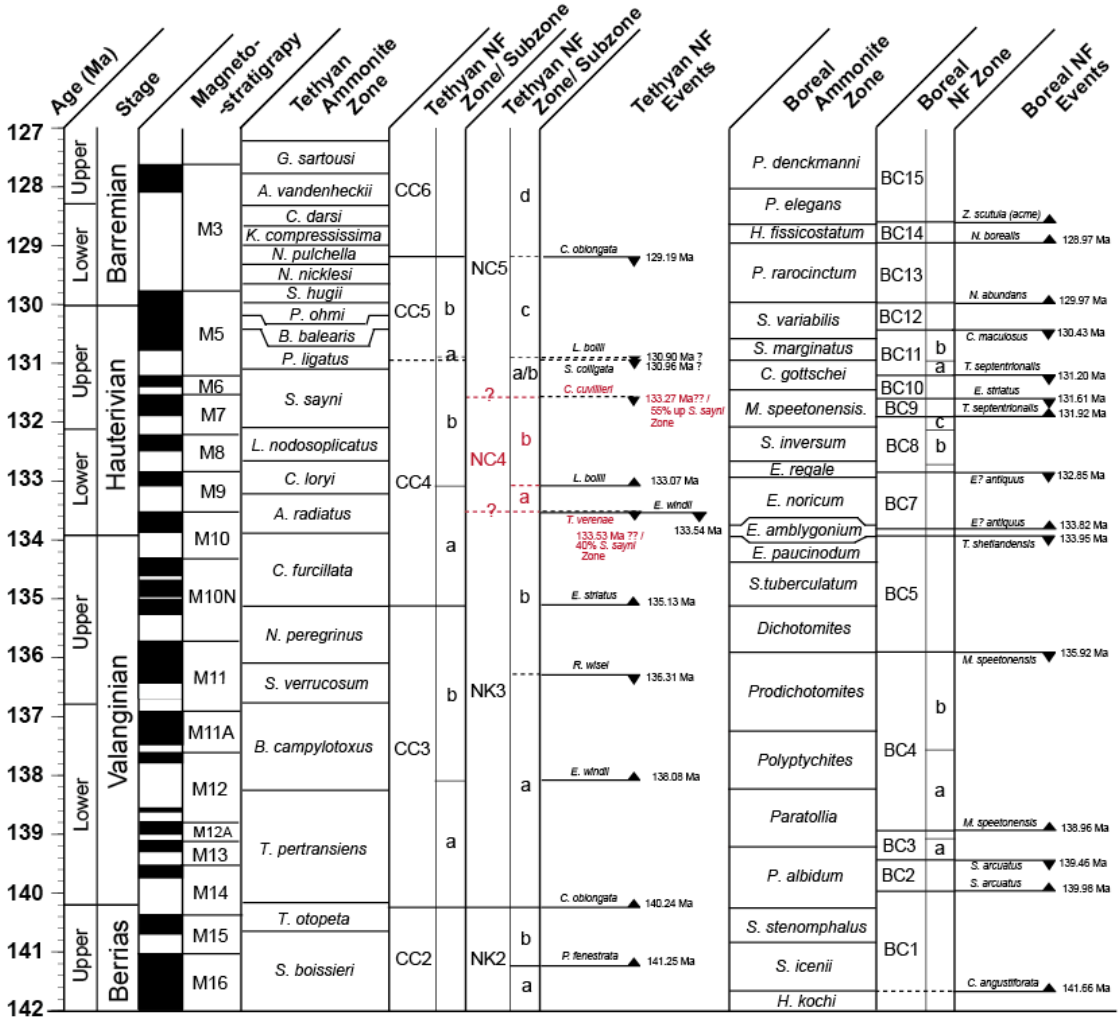

***Figure 34**: Early Cretaceous biostratigraphy and magnetostratigraphy for the Tethyan and Boreal realms, with absolute age information from Timescale Creator, v. 1.2. Berrias = Berriasian. NF = nannofossil. Arrows pointing up represent first occurrences, while arrows pointing down represent last occurrences. The Tethyan NC4 is difficult to tie to absolute and relative time, as its base is defined by the last occurrence (LO) of Tubodiscus venerae, which seems to vary depending on location, and its top (base of NC5) is defined by the LO of Crucielipsis cuvillieri, which despite certainly being Hauterivian in age, has variable absolute age estimates. These difficult regions of the age model are highlighted in red on the figure.*

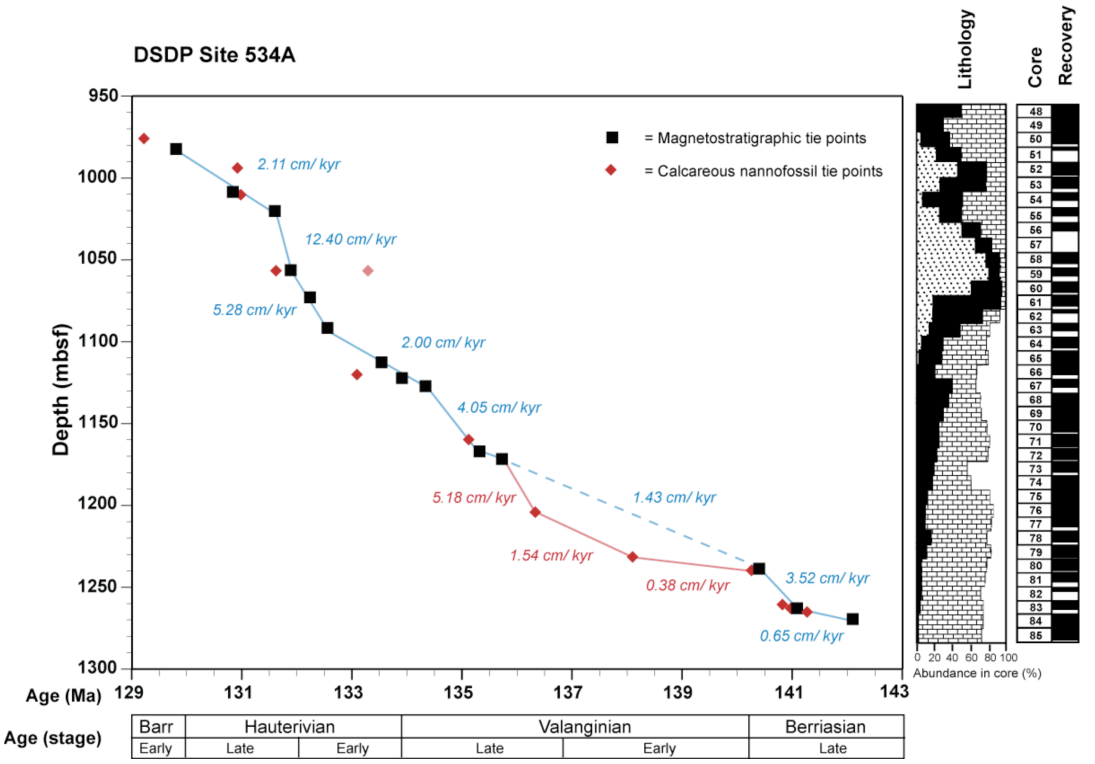

Fig 35a. *Age vs. depth plot for Site 534. Magnetostratigraphy is after* Ogg (1987), *biostratigraphy is after Bergen, (1994). Average sedimentation rate estimates are shown in blue (magnetostratigraphy) or red (biostratigraphy). Lithology as in Figure 33a.*

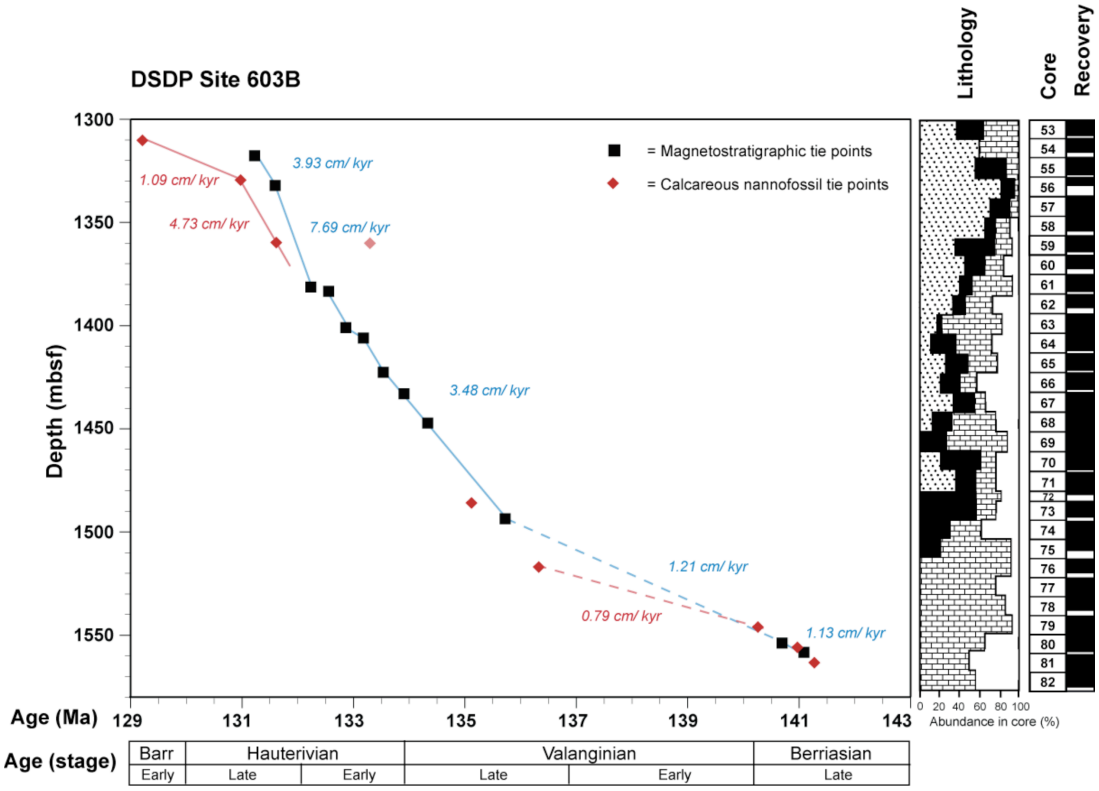

Figure 35b. *Age vs depth plot for Site 603. Magnetostratigraphy is after* Ogg (1987*; biostratigraphy is after Covington & Wise (1987). Lithology as in Figure 33b.*

Site 766

The age model for Site 766 in the Indian Ocean is predominantly based on magnetostratigraphic tie points with supporting biostratigraphic information (Appendix Table 1 & 2; Baumgartner *et al*., 1992; Kaminski *et al*., 1992). Magnetochrons M10N – M7 and M3 have been identified at this site, and provide good Late Valanginian–Early Barremian age control (Kaminski *et al*., 1992). Although the biostratigraphic age control is not as tightly constrained as for the North Atlantic sites, the age control at this location is deemed to be sufficiently robust to allow comparison with other sites (Figure 35c). Certain key species were present at Site 766, most importantly *C. cuvillieri*, which is an excellent marker for the Berriasian–Upper Hauterivian (Mutterlose *et al*., 1992). Its last occurrence (LO) in Core 31 at this site is a robust indicator of the base of the NC5 Zone at this level. The absence of *R. wisei*, while not as diagnostic, is suggestive of a Late Valanginian age for the lowermost part of the record (Cores 48 to 44), which is in agreement with the estimates of age provided by the magnetostratigraphy.

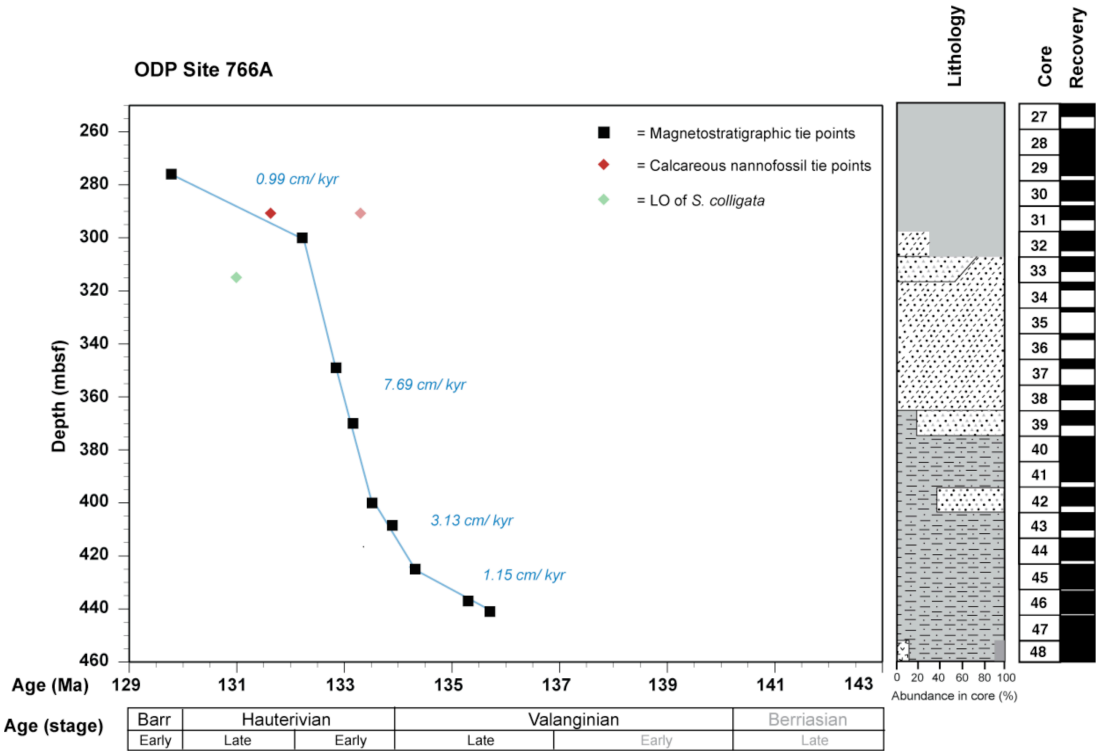

Figure 35c*. Age vs depth plot for Site 766. Magnetostratigraphy after Kaminski et al., (1992); biostratigraphy after Mutterlose, (1992). LO of S. colligata is not regarded as a reliable stratigraphic marker here and is not used in the age scheme.*

Site 692

The age of Site 692, which is located in modern day Weddell Sea, can only be constrained to Valanginian–Hauterivian on the basis of limited calcareous nannofossil and palynological evidence (Appendix Table 2) (Mutterlose & Wise, 1990). This is based on the occurrence of *C. cuvillieri* (limiting the section to Berriasian to Hauterivian in age) and the presence of *C. deflandrei* and *D. rectus,* which are identified as tentative indicators of a Valanginian age for Cores 7 to 12. There is no magnetostratigraphic age control.

Site 249

Site 249, in the modern day southwest Indian Ocean, has even poorer age control than at Site 692. The age constraints that do exist are based on limited calcareous nannofossil and foraminiferal biostratigraphy, and suggest a Neocomian, probably Berriasian–Hauterivian, age (Figure 5b); (Bukry, 1974; Simpson *et al*., 1974). A Cretaceous age is suggested by the dominance of *W. barnesae,* and the common occurrence of *Micanthrolithus sp.* suggests a pre-Aptian age. The absence of diagnostic Late Cretaceous genera such as *Cribrosphaera, Micula,* and *Prediscosphaera* suggest pre-Albian deposition, and the absence of *C. cuvillieri*, which can often be found in other Neocomian Indian Ocean sections such as Site 766 and 692, suggests Late Hauterivian or later deposition. However, it should be noted that the absence of species is not generally a reliable indicator of age, as other environmental factors could also exclude certain taxa from a depositional area.

SITES 765, 763 AND 416

Detailed age models were not constructed for Sites 765, 763 and 416, beyond the work already documented in the Initial Reports and subsequent literature. All the samples taken were from cores assigned a Berriasian–Hauterivian age on the basis of integrated biostratigraphy. All ages quoted when discussing these sites are taken from the literature without further modification, specifically, Site 765: Ludden *et al*. (1990a); Bown (1992); Site 763: Haq *et al.,* (1990); Bralower & Siesser (1992); (Brenner, 1992); Site 416: Lancelot *et al*. (1980); Cepek (1980).

2. 2. GEOCHEMICAL TECHNIQUES

2. 2. 1. TEX_{86} AND BIT INDEX

The entire process, from raw core sample, through chemical processing and mass spectrometery analysis, to end TEX_{86} value, takes 4–5 days. It is possible to generate up to twelve TEX_{86} values in a week by processing samples simultaneously.

2. 2. 1. 1. SAMPLE PREPARATION

Prior to analysis, the surface of the selected sediment sub-sample was scraped clean using a scalpel, to remove any loose rock debris, drilling-mud or large salt crystals. The sub-samples were then placed in clean glass beakers in a warm oven at 50°C overnight, to ensure there was no residual water remaining, as this can have a negative impact on lipid extraction. Lithified sediment samples were then powdered to a fine flour texture by hand, using an agate pestle and mortar.

2. 2. 1. 2. GDGT EXTRACTION

Work was carried out at the Biogeochemical Research Laboratory at UCL. Powdered samples were solvent extracted following the methods of Schouten *et al*. (2002), and the revised methodology of Schouten *et al*. (2007). In brief: between 6–8 g of powdered sediment was placed in each glass test-tube, to which ~5 ml of methanol was added using glass pipettes. The samples were then ultrasonically extracted using a sonic water bath and a centrifuge, using one times methanol, three times dichloromethane (DCM)/methanol (1:1, v/v), and three times DCM. The supernatants were evaporated to dryness under a continuous pure N_2 flow on a hotplate maintained at 40 ºC. Any water remaining in the total extract was removed by passing the extracts (dissolved in DCM/methanol (3:1, v/v)) over a column containing anhydrous Na_2SO_4. The total extract was then split into polar and apolar fractions by column chromatography, using hexane/DCM (9:1, v/v) and DCM/methanol (1:1, v/v) sequentially as the eluents and Al_2O_3 as the stationary phase. The apolar fraction can be washed off the Al_2O_3 column with three columns-full (3 ml) of the weaker hexane/DCM (9:1, v/v), and is collected at the base of the

column in vial "c". This fraction is not needed for TEX_{86}/ BIT index analysis but can be used to investigate other organic geochemical trends (see Section 2-2-1-6). The polar extract was then redissolved in hexane/propanol (99:1, v/v), before being filtered through a PTFE 0.45 μm filter attached to a gas syringe.

2. 2. 1. 3. GDGT QUANTIFICATION

Samples were analysed using an Agilent 1200 series High Performance Liquid Chromatography (HPLC), attached to a G6130A single quadrupole mass spectrometer (MS). An APCI-MS technique is used to achieve detection of the positive GDGT ions. The analytical protocol is as described in Schouten *et al*. (2007). Figure 36 illustrates and describes the HPLC/ APCI-MS protocol. The GDGTs are eluted isocratically using 99% hexane and 1% propanol for 5 minutes. The ratio is then increased over 45 minutes to 98.2% hexane: 1.8% propanol with a linear gradient. The abundance of both isoprenoid and branched GDGTs (Figure 15) is measured in selective ion monitoring (SIM) mode, which is more sensitive and gives better reproducibility than using full scan mode (Schouten *et al*., 2007). The nebuliser in the APCI chamber is maintained at a pressure of 60 psi, the vaporiser is maintained at 400°C, the drying gas (N_2) is maintained at 200°C at a flow rate of 6 L/min. The corona needle is maintained at 5 μA (-3.2 kV), the MS capillary is maintained at a voltage of -3 kV, the quadrupoles are maintained at 100°C, and there is a dwell time of 234 ms in SIM mode. Ion peaks of the respective GDGTs are integrated to determine the relative abundance of each molecule in the sample (Figure 15) and subsequently to determine the TEX_{86} index for that sample. It should be noted that a recent inter-laboratory study involving 15 separate laboratories, has shown that although there are reproducibility issues between the labs, the choice of mass spectrometer (Quad SIM, Ion trap or Time Of Flight) makes no systematic difference to the TEX_{86} or BIT Index values (Schouten *et al*., 2009).

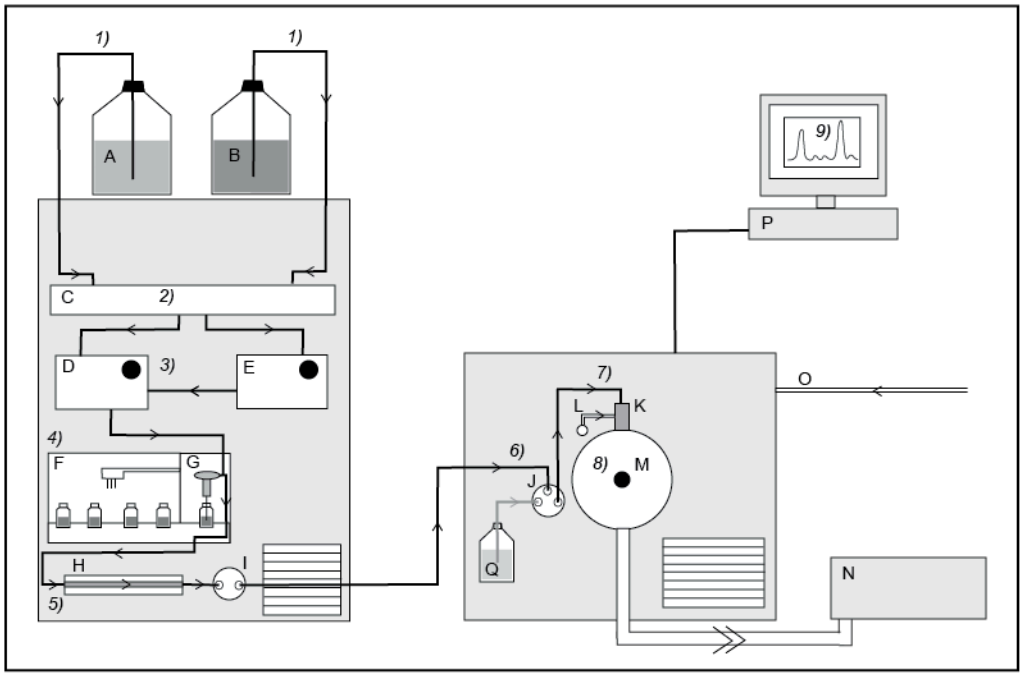

Figure 36a. *Schematic diagram of Agilent 1200, HPLC-MS showing key components and solvent flow. A = Solvent "A" bottle (hexane), B = Solvent "B" bottle (propan-2-ol), C = Degasser, D = hexane pump (primary), E = Propanol pump (secondary), F = autosampler, G = needle injection system, H = Prevail cyano column, (2.1 × 150 mm, 3 µm; Alltech, Deerfield, IL), I = LC Rheodyne valve, J = MS Rhyodyne valve, K = Nebuliser, L = N_2 input to nebuliser, M = APCI chamber, N = Rough pump (main vacuum generator, O = N_2 input from generator, P = computer connected to the HPLC-MS array with Chemstation ™ software, Q = MS tuning solution.*

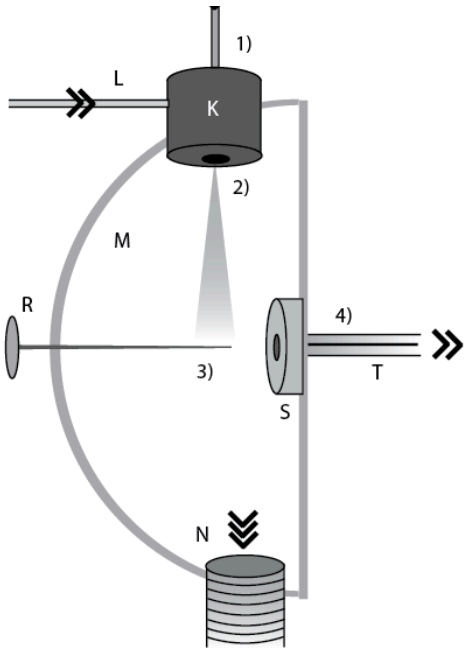

Figure 36b: *APCI (Atmospheric Pressure Chemical Ionisation) system detailed schematic. As for Figure 7a above; K = Nebuliser, L = N_2 input to nebuliser, M = APCI chamber, N = pipe leading to rough pump (vacuum generator). Additionally; R = corona needle, S = capillary shield, T = MS capillary.*

2. 2. 1. 4. TEX_{86} CALIBRATION

Once the relative abundance of each isoprenoid GDGT has been determined, the values can be used to reconstruct the SST by application of a calibration, as discussed in Section 1-6-3. Kim *et al*. (2010), using the most comprehensive modern core-top dataset available and statistical analysis of the GDGT distributions, have proposed two alternative indexes: TEX_{86}^{H} and TEX_{86}^{L}, which are thought to be most applicable to warmer and cooler temperature ranges respectively. For the Early Cretaceous the TEX_{86}^{H} proxy is the most suitable equation to use in this instance.

Eq. 13 $$TEX_{86}^{H} = \log\left(\frac{[GDGT\ 2] + [GDGT\ 3] + [GDGT\ 4']}{[GDGT\ 1] + [GDGT\ 2] + [GDGT\ 3] + [GDGT\ 4']}\right)$$

Which is converted to SST using the equation:

Eq.14 $$SST = 68.4(TEX_{86}^{H}) + 38.6$$

All measured GDGT ratios are converted to SST (°C) using this calibration throughout this thesis, but for comparison an alternative calibration which yields much cooler SST estimates (after Liu *et al*., 2009; using the core-top data from Kim *et al*., 2010) is discussed alongside the TEX_{86}^{H} estimates. This calibration is based on the original TEX_{86} ratio,

Eq.6 $$TEX_{86} = \frac{[GDGT\ 2] + [GDGT\ 3] + [GDGT\ 4']}{[GDGT\ 1] + [GDGT\ 2] + [GDGT\ 3] + [GDGT\ 4']}$$

which is converted to SST using the equation:

Eq.15 $$SST = (-19.1 * (1/TEX_{86}) + 54.5)$$

Due to unavoidable uncertainty in calibration to SST, the raw TEX_{86} data are presented along with both logarithmic and reciprocal temperature calibrations (Eq.

14 and 15), throughout Chapter 3. Taking into account trends in the latest calibration dataset and other high-temperature mesocosm evidence (e.g. Kim *et al*., 2010; Pitcher *et al*., 2010), the SST estimates generated by the reciprocal equation are regarded as minimum temperature estimates for the Early Cretaceous data.

2. 2. 1. 5. ERRORS IN TEX_{86} AND SST

Repeat analysis of an in-house standard and previous work (Schouten *et al*., 2007) suggest the analytical error associated with the TEX_{86} technique using SIM HPLC-MS techniques is on the order of ±0.01. This small analytical error equates to an error in SST of only ±0.6° to 0.9°C (TEX_{86}^{H}) or ±0.4° to 1°C ($1/TEX_{86}$) for the range of TEX_{86} values in this study. The greatest source of error in SST estimates undoubtedly comes from the calibrations themselves. The logarithmic equation of Kim *et al*. (2010), (TEX_{86}^{H}), (n = 255) has a relatively small standard error of ±2.5°C, but it should be noted that this is largely due to the exclusion of all data from the (sub)polar regions, where SST does not seem to be the dominant control on the TEX_{86} ratio. The standard error associated with the reciprocal calibration ($1/TEX_{86}$) is much larger (~ ± 5.4°C), which is partly attributable to the inclusion of the highly scattered (sub)polar data (n = 396) which has been excluded from the logarithmic equation.

2. 2. 1. 6. BIT INDEX

The BIT index (see Introduction Section 1-6-5) is determined at the same time as the TEX_{86} ratio for each sample, using the same analytical techniques described above. The abundance of branched GDGT molecules with an *m/z* ratio of 1050, 1036 and 1022, in addition to the isoprenoid GDGTs used in the TEX_{86} ratio, was quantified in order to construct the BIT Index ratio. In some cases (especially at Site 603) the abundance of the unbranched GDGTs was so low, that it was not possible to integrate the peaks and so the BIT index could not be determined.

2. 2. 2. TOC AND $CaCO_3$ % ANALYSIS

Samples are first cleaned and crushed to a fine powder in an agate pestle and mortar. For each sample, two sub-samples are selected and individually analysed for their carbon content. One sub-sample, of between 40 and 70 mg, is decarbonated by dropwise addition of 10% HCl directly onto the powder in silver analysis capsules, which are left at least overnight on a hot plate at 40 ºC until completely dry. The other half of the sample is left unprocessed and is analysed in tin capsules. Both silver and tin capsules are rolled to enclose the sediment within. The percentage total organic carbon (TOC) and carbonate ($CaCO_3$) in a sample, is determined by combustion of the sample in a Thermo Electron, 1112 series Flash EA. Samples are placed into the carousel, which drops them one at a time into a furnace maintained at 950 ºC.

The gases produced by the total combustion are then passed through a quartz column containing copper oxide, which oxidises the gases. A second column contains reduced Cu, reduces species NO to N_2. The gases then pass through a water trap containing magnesium perchlorate, which removes any residual water from the sample gas, which then passes through a GC column, separating out CO_2 from N_2. Determinations of %C (and %N, which is often below analytical resolution in Early Cretaceous carbonates), are made by reference to an internal UCL standard. Comparison of the carbon content of the raw and decarbonated sub-samples allows the amount of $CaCO_3$ and TOC to be determined. The raw sediment sample gives a measure of Total Carbon % while the decarbonated sample yields a value for TOC %. The equation:

Eq. 21. $$CaCO_3 = (Total\ Carbon - Total\ Organic\ Carbon) * 8.333$$

is used to calculate $CaCO_3$ % from Total Carbon% and TOC %.

2. 2. 3. CARBON-ISOTOPE ANALYSIS

2. 2. 3. 1. BULK-CARBONATE CARBON ISOTOPES

Isotope analyses were carried out at the Bloomsbury Environmental Isotope Facility (BEIF) at UCL. Samples were cleaned and dried and powdered using a fine drill. Powdered samples of ~300–500 μg were placed into borosilicate glass reaction test-tubes, and treated with enough peroxide to oxidize the organic matter. Acetone or methanol was then added to aid drying of the samples and they were left overnight to dry completely in a warm oven at 50ºC. Test-tubes were first flushed with He to remove any residual air, after which drops of purified phosphoric acid were dropped onto the carbonate samples and CO_2 gas was liberated. Samples were analysed on a GasBench connected to a ThermoFinnegan Delta V continuous flow IRMS. Reproducibility of internal and external standards suggest reproducibility is better than 0.1‰ for both for both $\delta^{13}C$ and $\delta^{18}O$. All stable-isotope data are reported in ‰ deviation from Vienna Peedee belemnite (VPDB).

2. 2. 3. 2. BULK-ORGANIC CARBON ISOTOPES

In order to remove any carbonate material from the sediment before analysis, the powdered samples must first be decarbonated. A thorough decarbonation regime is especially important in the Early Cretaceous samples used in this study, as many were limestones or marls with a $CaCO_3$ of >50%. Approximately 10 ml of 10% HCl is added to the samples in a dropwise fashion. These test-tubes are then placed in a water bath which is heated to ~60°C and left for 2 hours at a time to aid the reaction and to remove any dolomite. The sample is then placed into a centrifuge and spun at ~1200 rpm for 15 minutes to separate the sediment from the acid. This is repeated three times, using fresh acid each time, to ensure all the carbonate has been removed. Samples are then washed with distilled water until neutrality is reached (5 – 7 washes). The test-tubes are then placed into a warm oven at 50°C and left to dry overnight. Samples are then re-ground in the pestle and mortar back into a fine powder.

The decarbonated samples are analysed using a Flash EA connected to a ThermoFinnegan Delta V continuous-flow IRMS. Samples are weighed out according to their TOC%, such that there is approximately 70 μg of carbon (which should all be of organic origin) in each sample, in order to ensure that the resultant peak will be within the range of the calibration standards. The samples are placed into tin capsules (as used for TOC analysis), which are then rolled and placed into the carousel. These are then dropped into the furnace one by one and combusted. The gases pass a pure He stream into a reactor tube filled with a mixture of chromium oxide and cobaltic oxide, and then through a copper reducing column and a magnesium perchlorate water trap. The sample gas then passes into the IRMS to be analysed. The repeatability of internal standards is better than 0.1‰; however the repeatability of Early Cretaceous samples was often ~0.3‰, with occasionally very poor reproducibility of >1‰. All stable-isotope data are reported in ‰ deviation from Vienna Peedee belemnite (VPDB).

2. 2. 4. THERMAL MATURITY

To exclude thermal biasing of the records, a subset of samples (6 from 534A, 8 from 603B, 3 from 766A) were analysed to determine the proportion of hopanes bearing the biological 17β,21β(H) stereochemical configuration relative to the more thermally stable 17α,21β(H) and 17β,21α(H) isomers. Apolar fractions (generated as described above) were analysed using gas chromatography (GC) and GC-mass spectrometry, with hopane distributions determined using *m/z* 191 mass chromatograms generated during GC-MS. GC analysis was performed on a CarloErba Gas Chromatograph equipped with a flame ionisation detector (FID) and fitted with a Chrompack fused silica capillary column (50 m x 0.32 mm i.d.) coated with a CP Sil-5CB stationary phase (dimethylpolysiloxane equivalent, 0.12 μm film thickness). GC-MS analysis was performed on a Thermoquest Finnigan Trace GC (same column as used for GC) interfaced with a Thermoquest Finnigan Trace MS operating with an electron ionisation source at 70 eV and scanning over *m/z* ranges of 50 to 850 Daltons. For both GC and GC-MS, the temperature program was as follows: the oven temperature was increased to 130°C with an initial ramp of 20°C/min, then to 300°C at 4°C/min, followed by an isothermal hold for 20 min.

This analysis was carried out by Kyle Taylor, under the supervision of Professor Richard Pancost at the Organic Geochemistry Unit, Chemistry Department at Bristol University.

2. 2. 5. ROCK EVAL PYROLYSIS

Standard pyrolysis techniques and a Delsi Oilshow Analyser were used to ascertain the organic-matter type within a subset of Site 534 sediments (J. Harrison, *pers comm., 2011*). Powdered samples were placed into an air-tight pyrolysis chamber, which was then filled with He, and initially heated to 300 °C. This drives off any free hydrocarbons in the sample. The temperature is then increased to a maximum of 550 °C in order to thermally decompose the kerogen and release the hydrocarbons (HCs). Analysis of these hydrocarbons allowed both the T_{max} (temperature at which the most hydrocarbons were released from the kerogen) and Hydrogen Index (HI) to be determined. The HI is defined as:

Eq. 22 $$HI = (S2 * 100)/TOC$$

where S2 is the amount of hydrocarbons (mg HC/g dry rock) generated through thermal cracking of the kerogen during heating, and TOC is the total organic-carbon content (%). This analysis was carried out by Jim Harrison at the Civil Engineering and Geosciences Department, University of Newcastle.

CHAPTER 3. A LITHOLOGICAL EFFECT ON THE TEX_{86} PROXY?

3. 1. AIMS

The TEX_{86} proxy has been shown to be a robust SST proxy through modern calibration experiments and subsequent multiproxy palaeoclimate studies, however the effects of variables other than temperature on the TEX_{86} proxy must also be constrained where possible, to give confidence in the SST reconstructions. The aim of this chapter is to investigate an apparent effect on the TEX_{86} ratio related to lithology observed at proto-North Atlantic DSDP Sites 534 and 603, between alternating pelagic laminated marls and transported homogeneous claystones within the same core. Such an effect could be attributable to several causes, including primary oceanographic or climatic variability, a difference in crenarchaeotal population structure in the shelf or the deep-sea, or a secondary diagenetic effect related to oxic degradation of the GDGTs. The results of this study will determine whether these cores are suitable for subsequent palaeoclimate reconstruction using the TEX_{86} proxy.

3. 2. INTRODUCTION

3. 2. 1. THE TEX_{86} PROXY AND THE NORTH ATLANTIC STUDY SITES

As discussed in Chapter 1, in the last decade much has been discovered about the dynamics of the TEX_{86} proxy, and the ecology of the Archaea upon which it is based. TEX_{86} ratios in modern core-top sediments have been shown empirically to best correlate with annual average sea-surface temperature (SST) at the site of deposition (e.g. Schouten *et al*., 2002; Kim *et al.*, 2008; 2010; Wuchter *et al*., 2005). This is despite complications regarding both the depth habit and seasonality of the source organisms (e.g. Murray *et al*., 1998; Church *et al*., 2003; Wuchter *et al*., 2005; 2006b; Huguet *et al*., 2007; Herfort *et al*., 2006), and possible contributions from deep water or sedimentary production of GDGTs (e.g. Shah *et al*., 2008; Turich *et al*., 2007; 2008; Schouten *et al*., 2008). The long-term stability of GDGTs has been demonstrated by a record stretching back to at least the Late Jurassic (e.g. Jenkyns *et*

al., 2011), although some studies have suggested that processes such as oxic degradation or thermal maturation of the GDGTs are capable of altering the relative distribution of GDGTS over time (e.g. Schouten *et al*., 2004; Kim *et al*., 2009; Huguet *et al*., 2009). However, to-date there has been no systematic investigation of the effects that deposition of GDGTs in different lithologies within the marine environment may have on the TEX_{86} ratio. For example, there are no calibration studies in recent sediments examining the differences in TEX_{86} between pelagic and transported sediments in the same region, let alone any similar studies in ancient sediments. Such calibration studies are important, as deep-sea marine sediments, particularly the Early Cretaceous sediments studied in this thesis, frequently contain a mixture of authochthonous pelagic deposits and allochthonous sediments transported from the shelf by turbidites (e.g. Robertson & Bliefnick, 1983; Summerhayes, 1987). If there was found to be a "lithology effect" on the TEX_{86} ratio in such sediments, sampling and analysis of these various lithologies may lead to erroneous interpretations of fluctuating SSTs in palaeoclimate reconstructions.

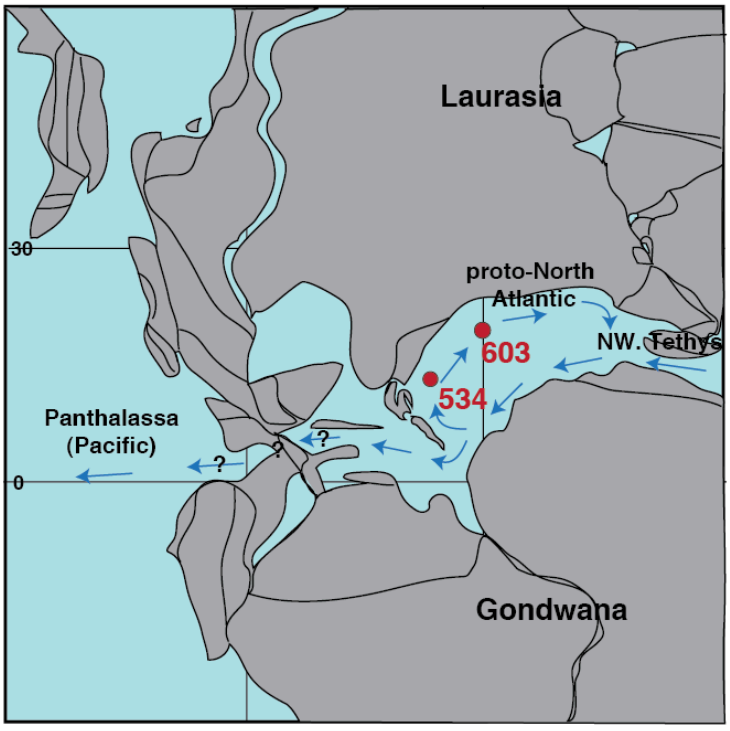

Figure 37*. Reconstructed palaeogeography of the proto-North Atlantic region in the Early Hauterivian (~133 Ma). Sites 534 and 603 shown in red; likely location and direction of surface currents shown in blue. Adapted from Puceat et al., 2005 and the Ocean Drilling Stratigraphic Network plate tectonic reconstruction service(http://www.odsn.de/odsn/ services/paleomap/paleomap.html).*

Sediments belonging to the regional Blake Bahama Formation were deposited in the western proto-North Atlantic in the earliest Cretaceous, at both DSDP Sites 534 and 603 (Figure 37; Sheridan *et al.,* 1983; van Hinte *et al.,* 1987). As outlined in Chapter 2, the Berriasian–Barremian sediments at Sites 534 and 603 are characterised by alternating pelagic bioturbated chalks and laminated marls, punctuated by homogeneous mudstones and graded sandstones, which are likely to have had a transported origin (Figures 38, 39; Section 2-1-2; Sheridan *et al.,* 1983; van Hinte *et al.,* 1987). The most common lithological type throughout the Neocomian at both Sites 534 and 603 is laminated, coccolith-rich, mid-grey marl, which is thought to have been deposited by pelagic sedimentation above the CCD in a largely dysoxic environment (Figure 38; Sheridan *et al.,* 1983; Robertson & Bliefnick, 1983; van Hinte *et al.,* 1987). These laminated marls often grade into bioturbated chalks, indicating fluctuating concentrations of oxygen at the water-sediment interface and perhaps changes in palaeoproductivity with time (Sheridan *et al.,* 1983; Robertson & Bliefnick, 1983; van Hinte *et al.,* 1987; Figure 38).

Sediments presumed to have an allochthonous transported origin include coarse sandstones, which peak in the Hauterivian at both sites, and finer homogeneous claystones, which increase in importance from the Late Valanginian onwards (Figure 38). The sharp contacts between the mudstones and the underlying laminated marls are suggestive of energetic lateral emplacement of the former, while the general lack of laminations in the mudstones suggests either intense bioturbation or turbulent mixing during emplacement (Figure 39; Sheridan *et al.,* 1983; Robertson & Bliefnick, 1983; Robertson, 1984; van Hinte *et al.,* 1987).

In addition to these sedimentological observations, the type of organic-matter has also been shown to be different between the laminated marls and the homogeneous mudstones at Site 603, with the latter being preferentially enriched in terrestrially-sourced organic-matter (Dean & Arthur, 1987). The composition of calcareous nannofossil assemblages between the marl and mudstones at Site 603 also suggest a different depositional origin for the laminated marls (pelagic) and the homogeneous mudstones (transported) (Covington & Wise 1987; Applegate *et al*., 1989; Bornemann *et al*., 2008), but no such observations have yet been made at Site 534. For these reasons, these two lithologies, the laminated marls and the presumed transported mudstones, will be the focus of the TEX_{86} calibration study at both Sites 534 and 603.

The first part of the study will examine calcareous nannofossil assemblage data from co-occurring laminated marls and homogeneous mudstones at Site 534, to establish whether the same trends as have previously been documented at Site 603, are also applicable at this site. Geochemical data, including carbonate and organic-matter content and type, will also be generated at Site 534 to establish if a different depositional origin for the marls and the mudstones can be confirmed at that site. The second part of the study will determine the TEX_{86} ratios and GDGT abundances in depth-paired samples at Site 534, to determine if there is any offset between the two lithologies in these values. Supporting calcareous nannofossil data, and geochemical data from Site 603 will also be generated, although the samples from this site are not depth-paired in terms of the alternating lithology.

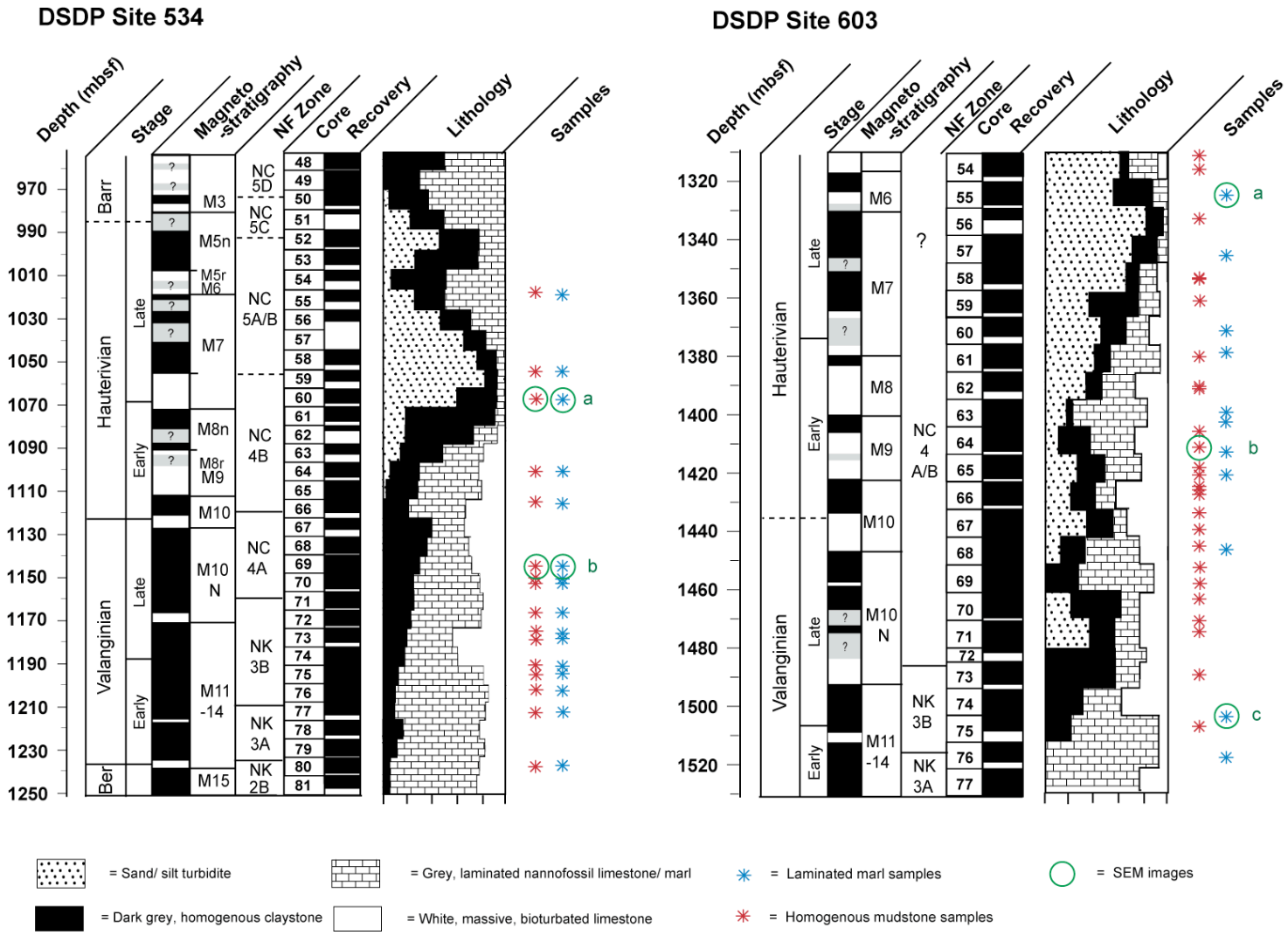

Figure 38. *Lithostratigraphy and age models at Sites 534 and 603. The location of samples with successful TEX_{86} data, presented below, is shown as stared symbols (see Section 3-4). Letters and circles represent samples with SEM images.*

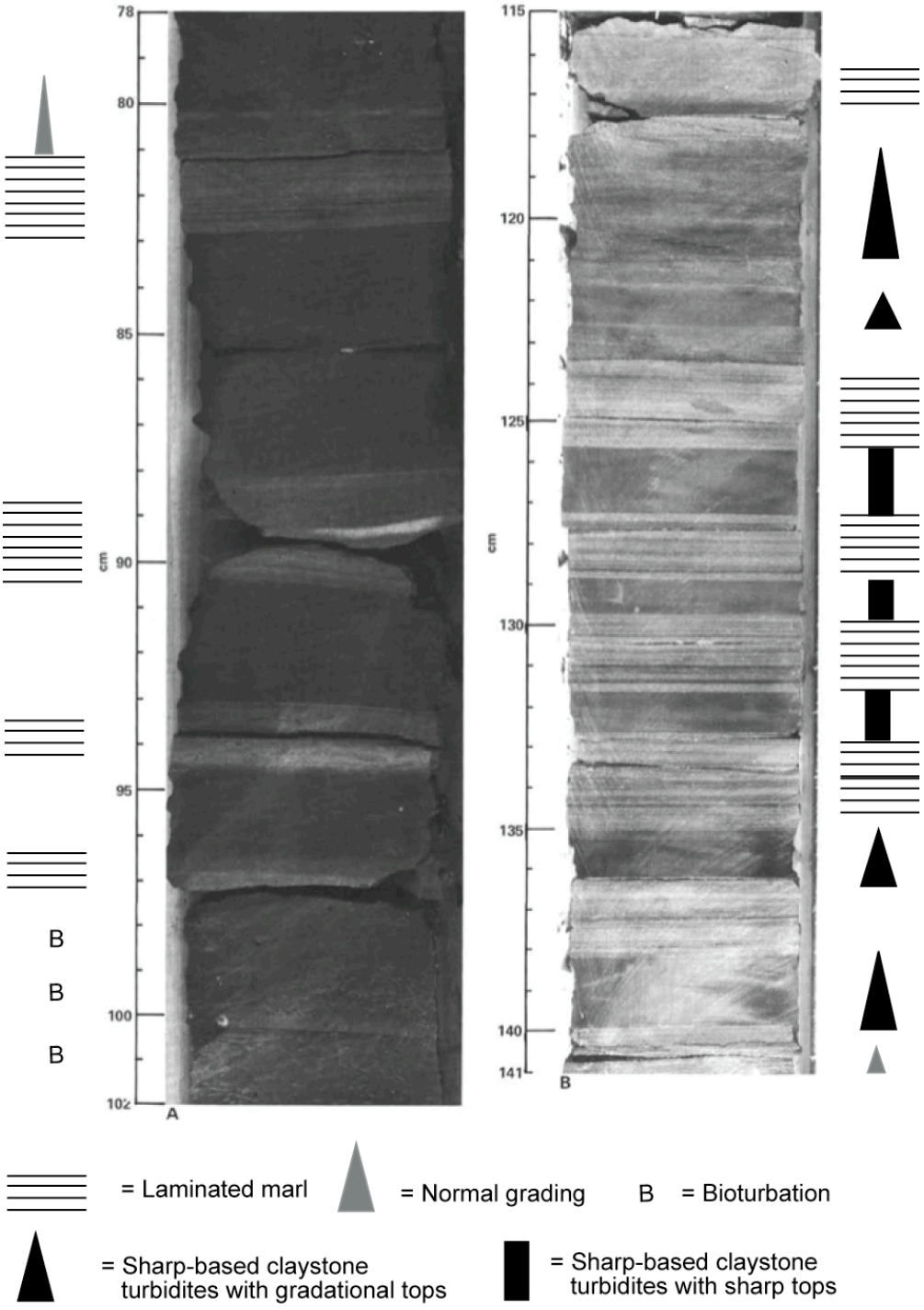

Figure 39. (a) *Lithological variations at Site 534 taken from Robertson & Bliefnick (1983). A = Thick turbiditic mudstone bed (Sample 534A-60-01, 78-102 cm; mid Hauterivian). Most of the claystones are massive and unburrowed. Some small-scale normal grading (~1 cm) can be seen (e.g., 80–81 cm) and some minor ripples. B = Thinly-bedded, turbiditic claystones intercalated with finely laminated nannofossil marl (Sample 534A-58-01, 115-141 cm; Late Hauterivian). Note the sharp bases to the claystone turbidites, but either the sharp or the gradational tops of the claystone turbidites.*

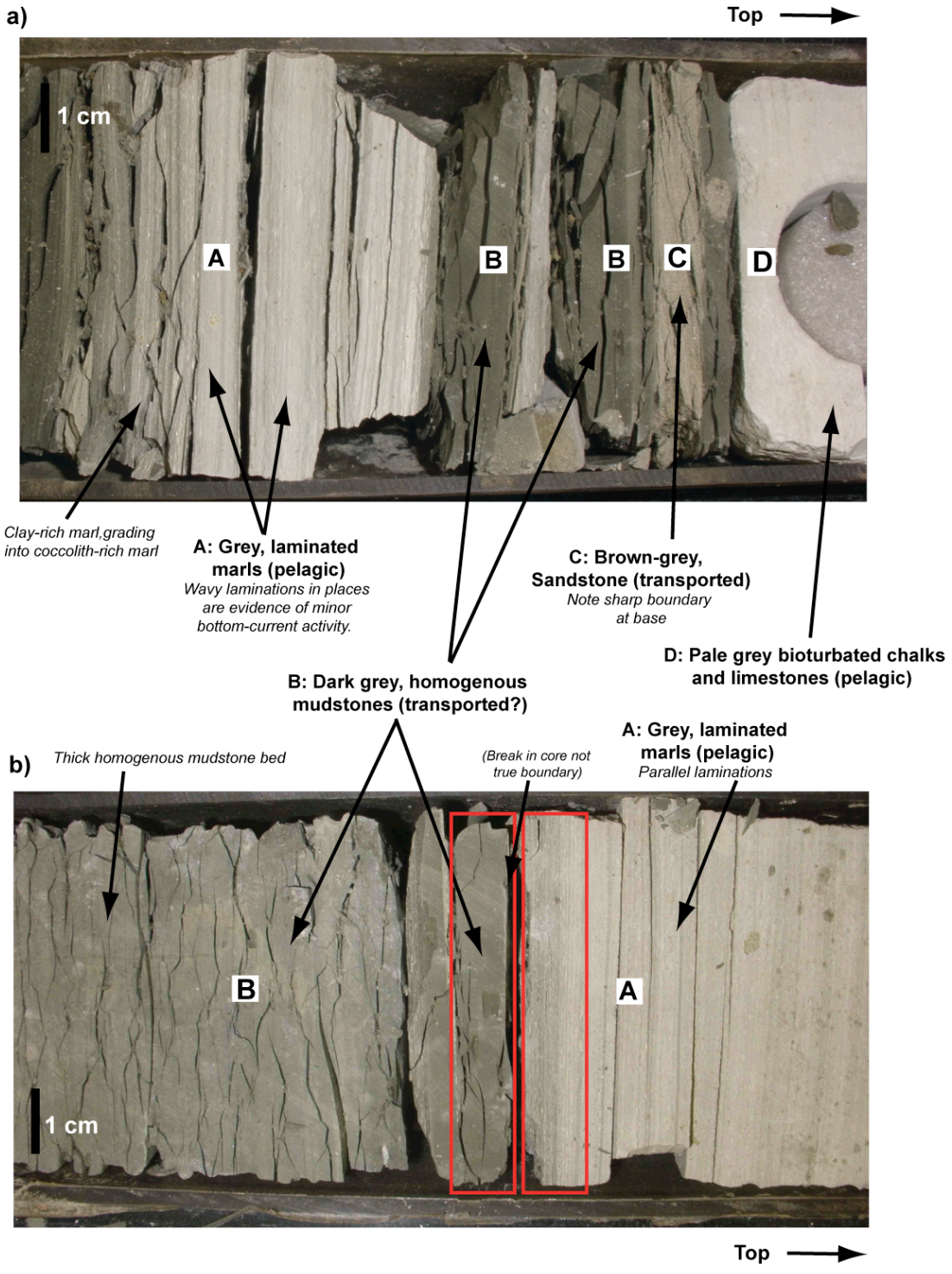

Figure 39b. *Lithological variations at Site 534. Image 1 = DSDP76-534A-64-02, 110–122 cm; image 2 = DSDP76-534A-72-01, 88–101 cm. Although obscured by fragmentation of the cores, sharp boundaries between the base of the homogeneous mudstones and the top of the laminated marls can be seen, with a more gradational boundary between the top of the mudstones and the base of the marls. Image 1 shows the pelagic sedimentation being interrupted by several small mudstone and sandstone turbidites, while in image 2 the mudstone bed is much thicker and represents a much more substantial turbiditic event. Red boxes in Image 2 indicate the location of a* TEX_{86} *lithology pair (see below).*

3. 3. METHODS AND MATERIALS

The main investigation was focused on depth-paired Site 534 sediments, with supporting evidence from analysis of Site 603 samples. Geochemical (TOC %, $CaCO_3$ %, $\delta^{13}C_{org}$) and palaeontological (calcareous nannofossil preservation and assemblage) data have been generated for some of the laminated marl and homogeneous mudstone samples, in addition to the TEX_{86} data. Geochemical and sample cleaning methods, as well as the age models for each site are outlined in detail in Chapter 2. Palaeontological and sampling methods specific to this study are outlined below.

At Site 534, 22 paired samples, each consisting of a mid-grey laminated marl and a stratigraphically adjacent dark-grey homogeneous mudstone sample, were successfully analysed at a resolution of approximately one pair per core, from Section 534A-55-01 to 534A-80-04, (1018 – 1238 mbsf; Late Berriasian – Early Barremian), (Figure 38). Samples were selected to be as close as possible to one another (preferably within 5 cm). At Site 603, the pairing is less precise because samples were not selected specifically to be adjacent to one another during sampling (Figure 38); 16 laminated marl samples and 39 homogeneous claystone samples were successfully analysed from Cores 603B-52–01 to 603B-82-04, (1311 – 1572 mbsf). At both sites, samples were selected on the basis of their visual appearance at the time of sampling to determine the lithology.

To examine variations in calcareous nannofossil preservation and assemblages at Sites 534 and 603, simple smear slides were prepared and examined for every sample (Section 2-1-3). At Site 534, SEM images were also taken from 4 samples (2 pairs) from the Late Valanginian and mid-Hauterivian respectively, while at Site 603, 2 laminated marls samples and 1 homogeneous marl sample were examined under the SEM (Figure 38; Section 2-1-3). In the smear slide observations, 150 fields of view (FOV) were examined for each sample, and the abundance of certain key species was determined: Abundant (“A”; >100 individuals per slide), Common (“C”; 30 – 99 individuals per slide), Few (“F”; 9 – 29 individuals per slide), Occasional (“O”; 3 – 8 individuals per slide) or Rare (“R”; 1 – 2 individuals per slide).

Preservation of the calcareous nannofossils was designated as, Poor, Poor–Moderate, Moderate, Moderate–Good, or Good, and was determined qualitatively by the degree of etching (dissolution) and the amount of secondary overgrowth (precipitation of secondary calcite) observed on the coccoliths. Diversity is the measure of the total number of species seen in the samples under the light microscope, within the 35 species that were included in the count. Very small species such as *Rotelapillus laffittei* and *Stradnerlithus geometricus,* and low birefringence taxa such as *Biscutum* spp. and *Axopodorhabdus* spp. have been omitted from the diversity count in all samples. Additionally, although several species were commonly observed in each genera, *Watznaueria* spp*., Assipetra* spp*., Nannoconus* spp. and *Micrantholithus* spp. are each counted as a single "species" in the diversity count.

3. 4. RESULTS

3. 4. 1. SITE 534

3. 4. 1. 1. CALCAREOUS NANNOFOSSIL ASSEMBLAGES AND PRESERVATION AT SITE 534

The composition and preservation of the calcareous nannofossil assemblages was examined in each of the samples analysed for TEX_{86} (see below), to investigate the difference in sediment provenance between the marls and the mudstones suggested by previous work at Site 603 (Figures 40–45; Covington & Wise 1987; Applegate *et al*., 1989; Bornemann *et al*., 2008). The average nannofossil composition of each lithology (Figure 40) is complicated by a considerable temporal variation in the distribution of taxa throughout the Early Cretaceous (Figure 43).

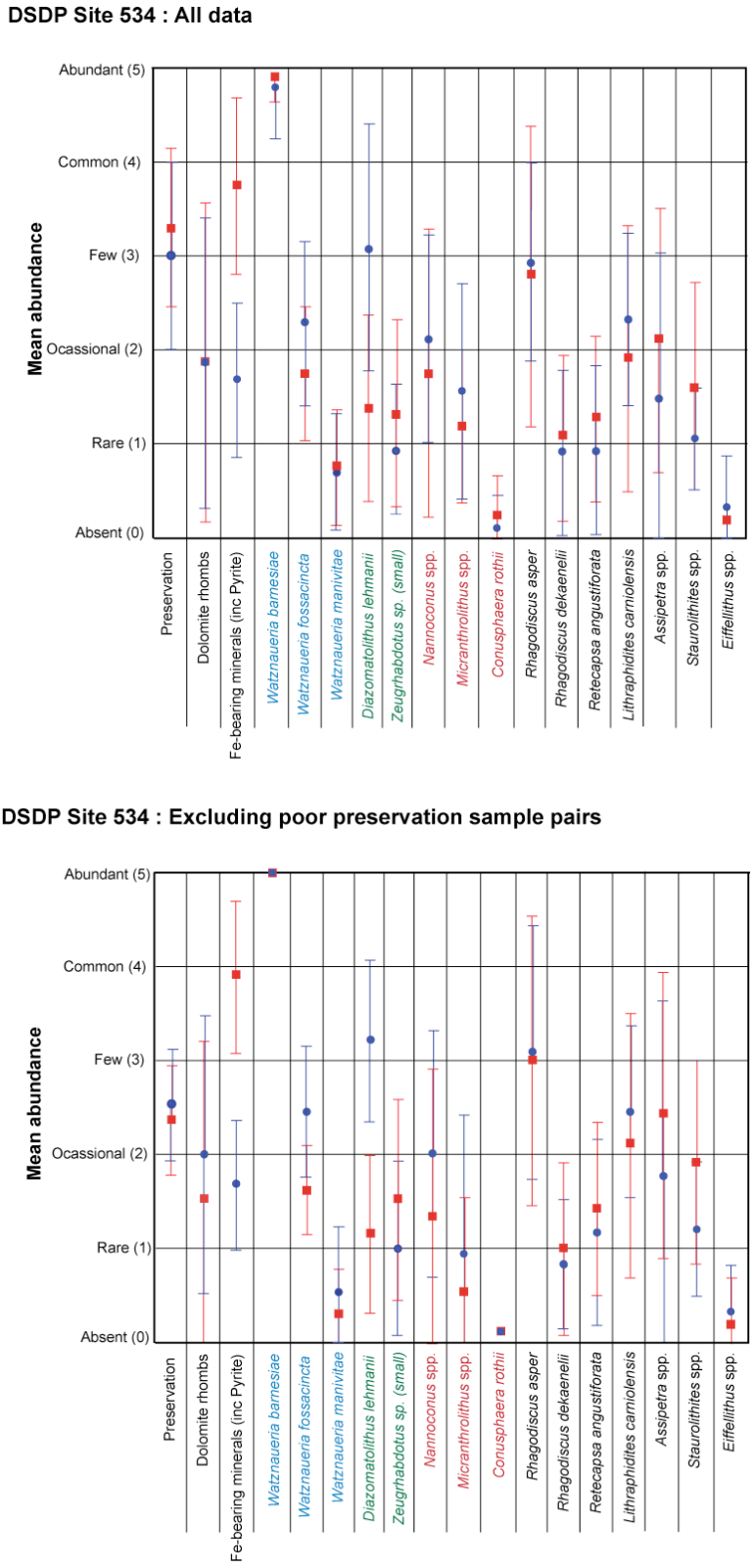

Figure 40. *Major palaeontological differences between the two lithologies at Site 534. Red squares = homogeneous mudstones, blue circles = laminated marls. Top chart represents mean values of all samples (16 pairs) across the Late Berriasian–Late Hauterivian, whereas bottom chart shows only those samples where both halves of the pair had at least "moderate" preservation (9 pairs in total). Colours of species' names indicated which group they belong to, e.g. pale blue are Watznaueria spp; red are nannoliths, etc. Error bars represent one standard deviation.*

534: 60-04-63
Pair "a"
Mid Hauterivian.
Dark grey, homogenous mudstone

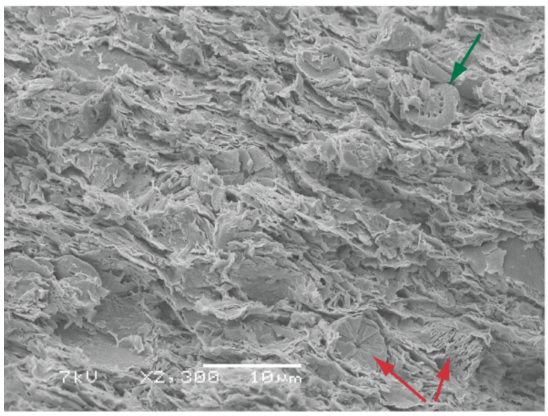

X 2300. Predominantly clay with coccoliths. Specimens of *Nannoconus* spp. indicated by red arrows. A *Retecapsa* sp. is indicated by the green arrow.

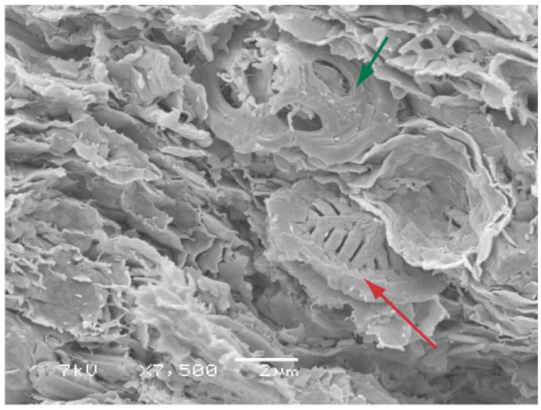

X 7500. Clay containing well-preserved coccoliths. A *Cretarhabdus striatus* is indicated by a red arrow, showing fine central structures, and a somewhat etched *Axopodorhabdus dietzmanii* is indicated by green arrow.

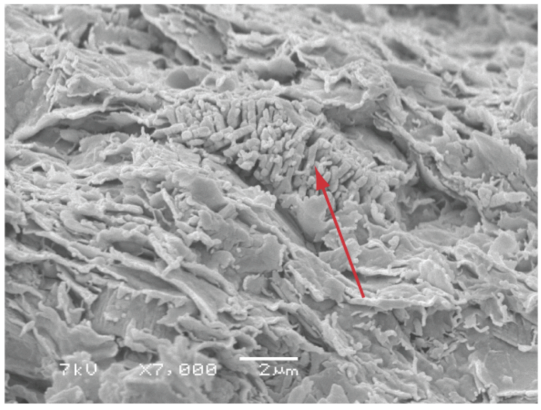

X 7000. A disintegrating *Nannoconus* spp. amongst the clay indicated by red arrow.

534: 60-04-66
Pair "a"
Mid Hauterivian.
Mid-grey, laminated marl

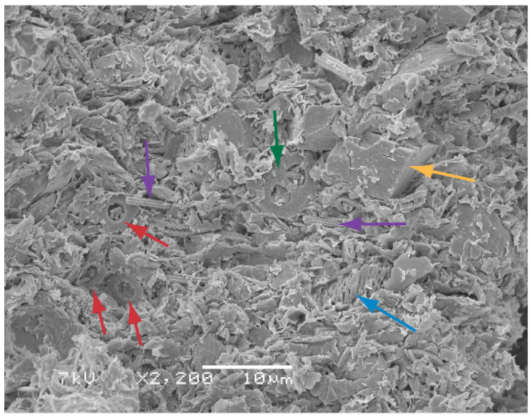

X 2200. Well-preserved coccoliths. Red arrows show *D. lehmanii*, purple arrows indicate *L. carniolensis*, green arrow indicates *S. colligata*, blue arrow indicates *Nannoconus* spp. and yellow arrow indicates dolomite rhomb.

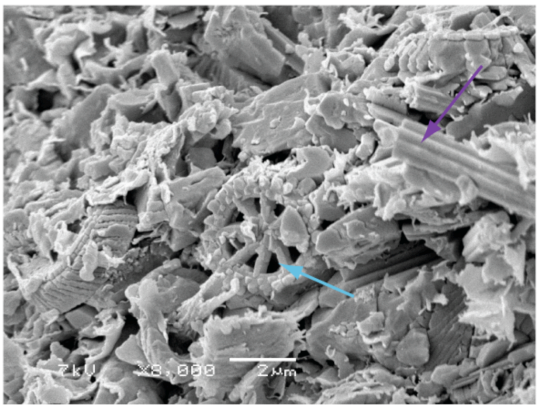

X 8000. Well preserved coccoliths and clay flakes. *L. carniolensis* is common throughout (purple arrow) and *R. laffittei* (pale blue arrow) is quite common and shows good preservation of the delicate central bars.

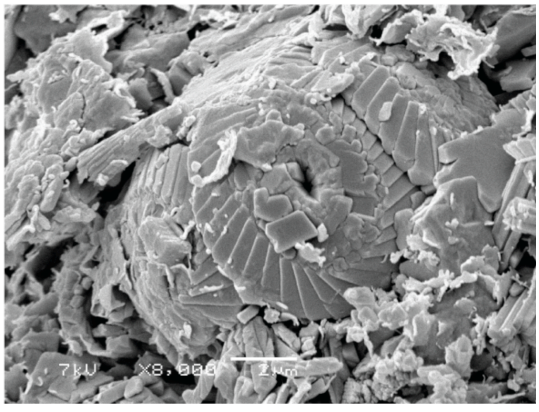

X 8000. *W. barnesiae* coccosphere. Some secondary calcite is visible, but coccoliths are generally well preserved.

***Figure 41**. SEM images of pair 'a' from core 534A-60-04, showing the texture, preservation and coccolith assemblages present in each lithology.*

534: 69-05, 35 cm
Pair "b"
Late Valanginian
Dk grey, Homogenous mudstone

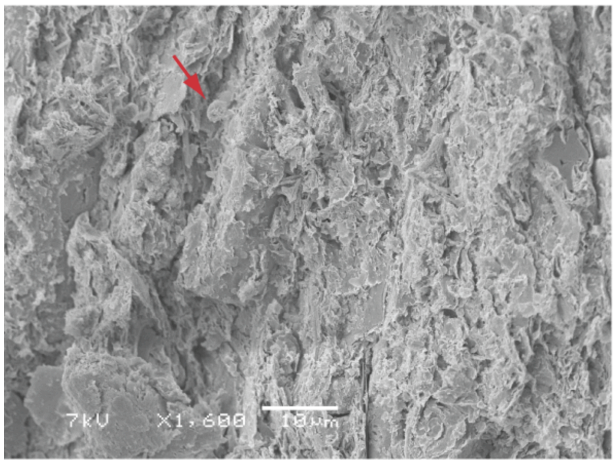

X 1600. Dominantly clay with opaque minerals and rare coccoliths (red arrow). Assemblage is sparse, but still quite diverse under the light microscope.

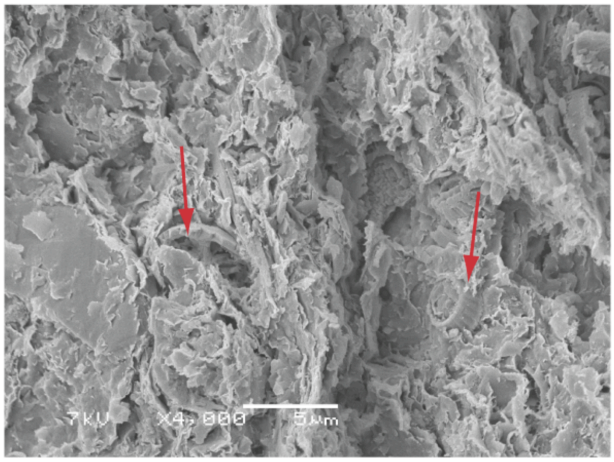

X 4000. Clay with poorly exposed and moderately preserved coccoliths. Some etching evident on the few coccoliths which are visible.

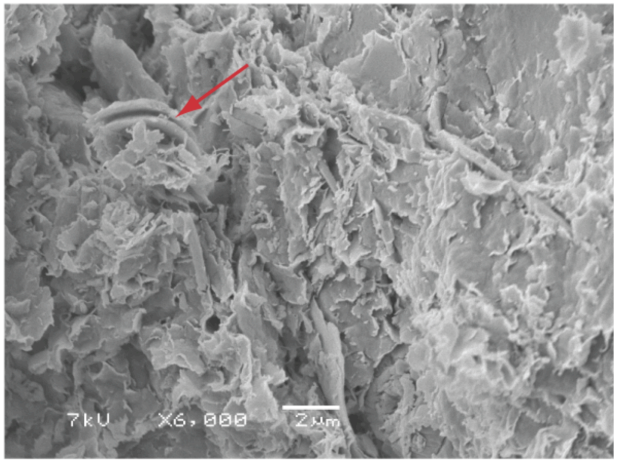

X 6000. Clay with poorly exposed coccolith (red arrow) of *W. barnesiae*? Preservation appears poor.

Figure 42a. *SEM images of the homogeneous mudstone half of pair 'b' from core 534A-69-05, showing the texture and preservation of the calcareous nannofossil assemblage. Preservation is moderate.*

534: 69-05, 34 cm
Pair "b"
Late Valanginian
Dark grey, laminated marl

Nannofossil-rich lamination:

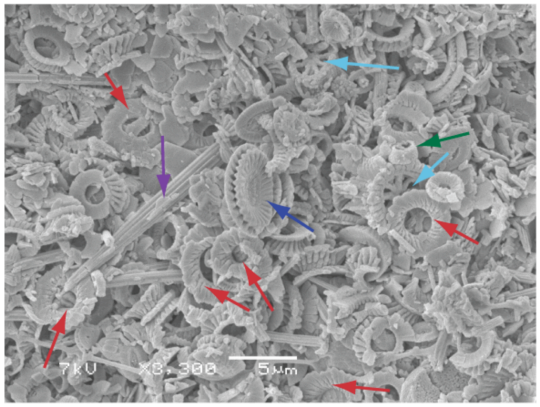

X 3300. Dominated by well-preserved and divserse coccoliths, predominantly of *D. lehmanii*, (red arrows), with *W. barnesiae* (blue arrow), *L. carniolensis* (purple arrows), *R. laffittei* (pale blue arrow), and rare small *Zeugrhabdotus* spp. (green arrow) and *T. jurapelagicus* (yellow arrow).

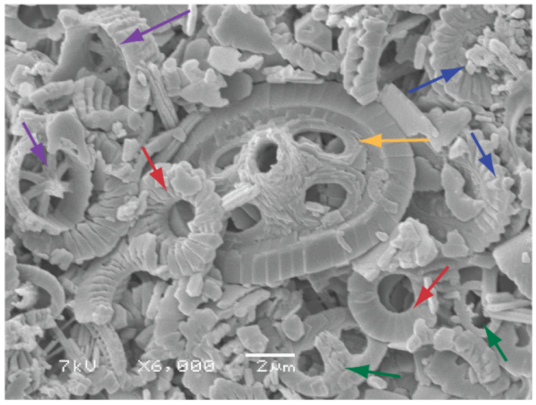

X 6000. Well-preserved coccoliths including *Axopodorhabdus dietzmanii* (yellow arrow), with *D. lehmanii*, (red arrows), with *W. barnesiae* (blue arrows), *Stradnerlithus geometricus* (purple arrows) and two different *Zeugrhabdotus* spp. (green arrows)

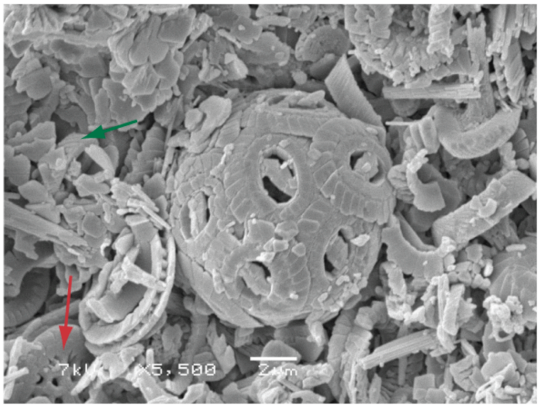

X 5500. Well preserved *Watznaueria* (new, unnamed species) coccosphere, surrounded by *W. barnesiae* and *D. lehmanii* fragments. *C. conicus*? visible in bottom left (red arrow), and small *Zeugrhabdotus* spp. (green arrow) to the left.

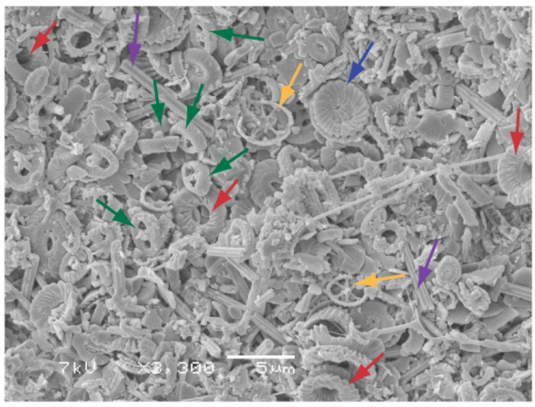

X 6000. Well-preserved coccoliths including *D. lehmanii* (red arrows), *W. barnesiae* (blue arrows), *Stradnerlithus geometricus* (yellow arrows) *L. carniolensis* (purple arrows) and several *Zeugrhabdotus* spp. (green arrows).

Clay-rich lamination:

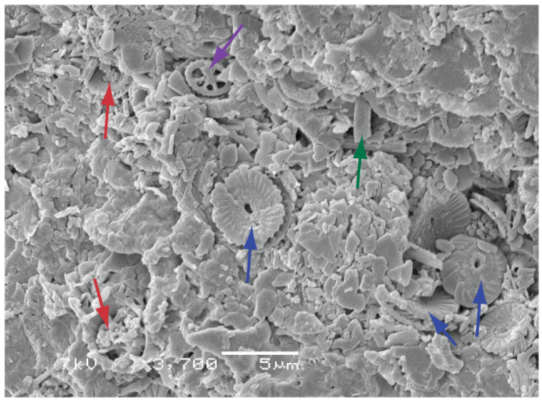

X 3700. Clay dominated. Etched *D. lehmanii* (red arrow) and *W. barnesiae* from a collapsed coccosphere (blue arrows), with occassional *Stradnerlithus geometricus* (purple arrow) and *Zeugrhabdotus* spp. (green arrow).

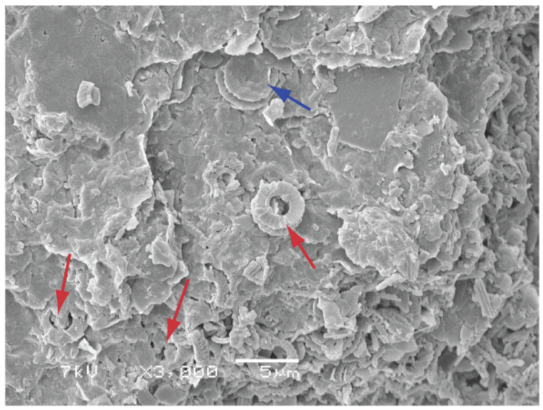

X 3000. Poorly preserved and much less abundant coccoliths. *D. lehmanii* (red arrows) and etched *W. barnesiae* (blue arrows) are visible.

***Figure 42b**. SEM images of the laminated marl half of pair 'b' from core 534A-69-05, showing the excellent preservation of the calcareous nannofossil assemblage. Top 4 panels are from a nannofossil-rich layer, whereas the bottom two panels are from clay-rich layers.*

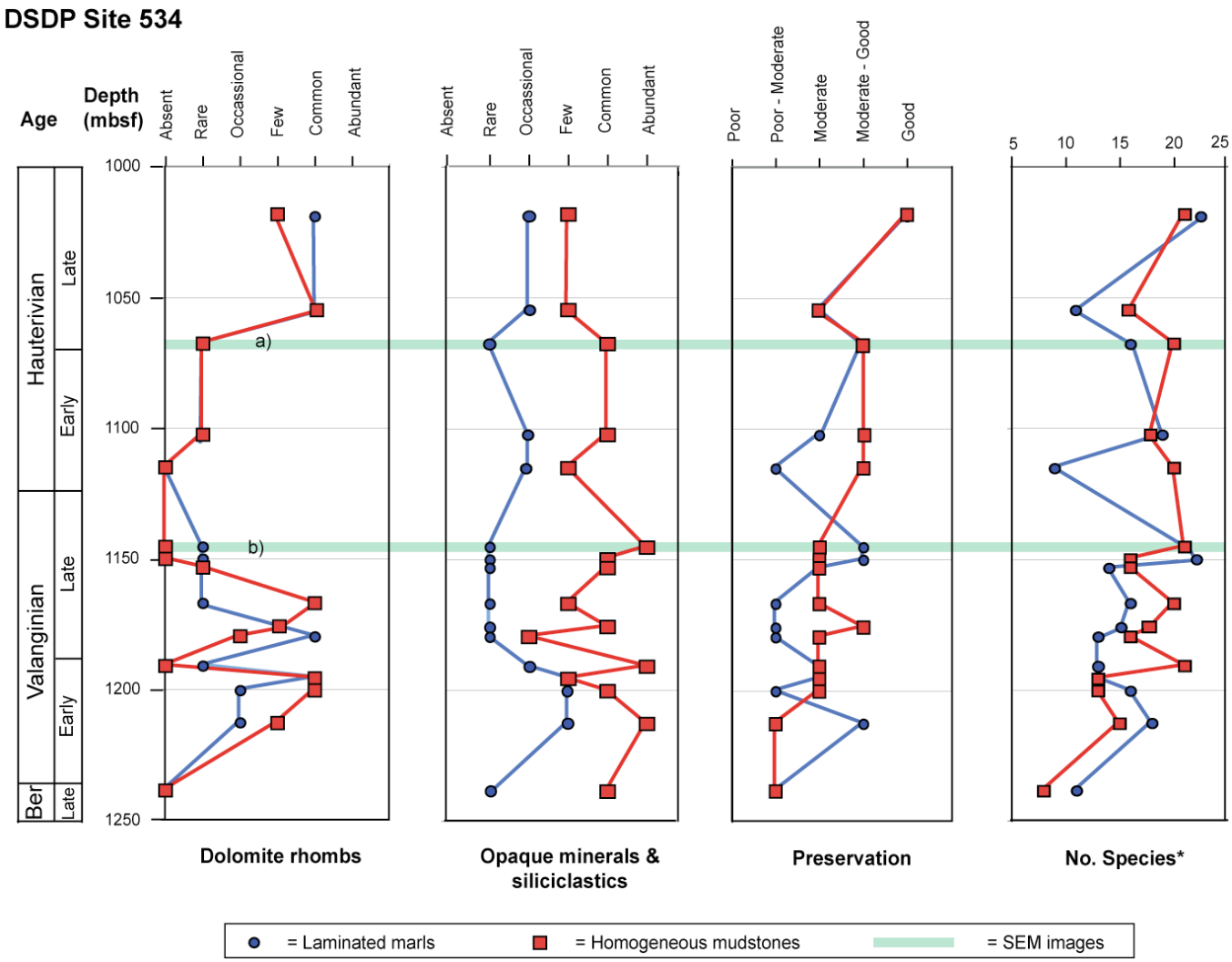

***Figure 43a**. Light microscope observations from all paired laminated marl and homogeneous mudstone samples at Site 534.*

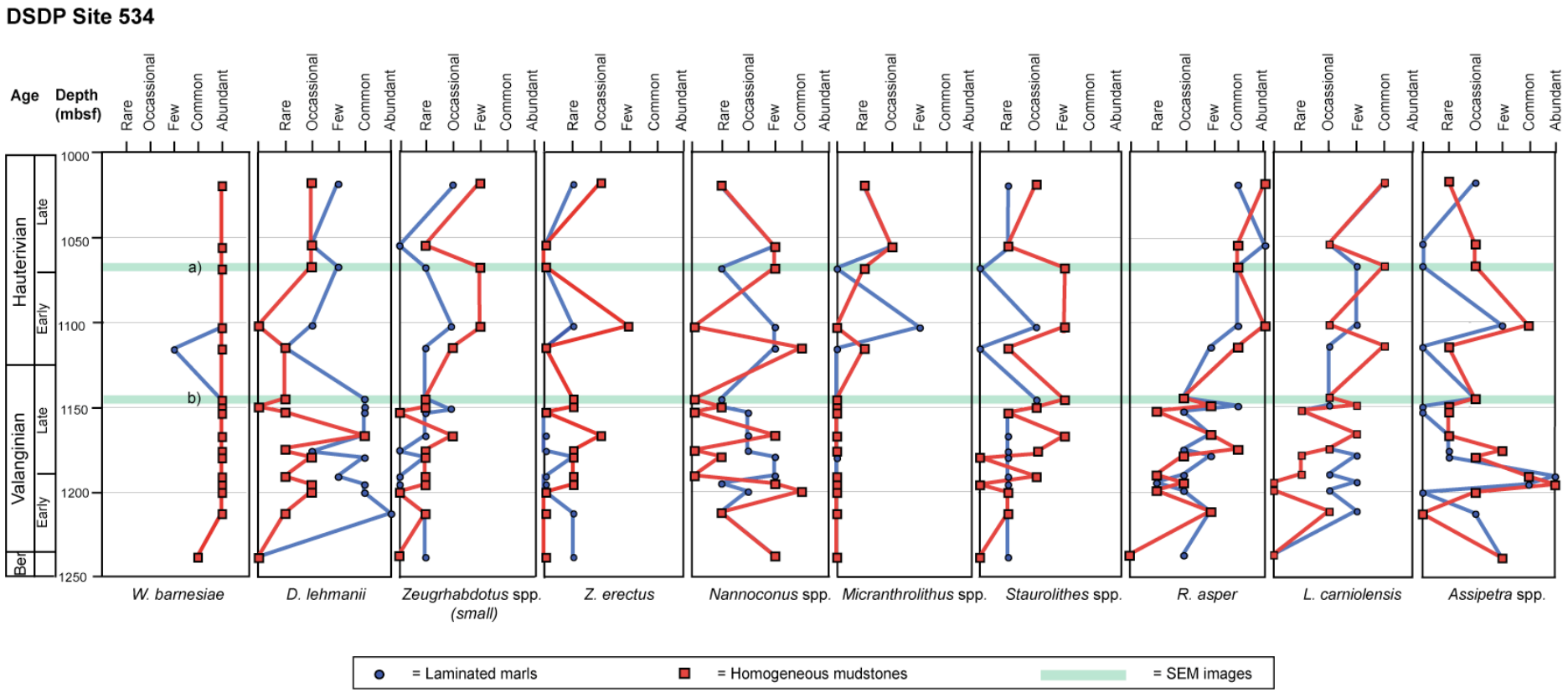

Figure 43b. *Light microscope observations from all paired laminated marls and homogeneous mudstones at Site 534.*

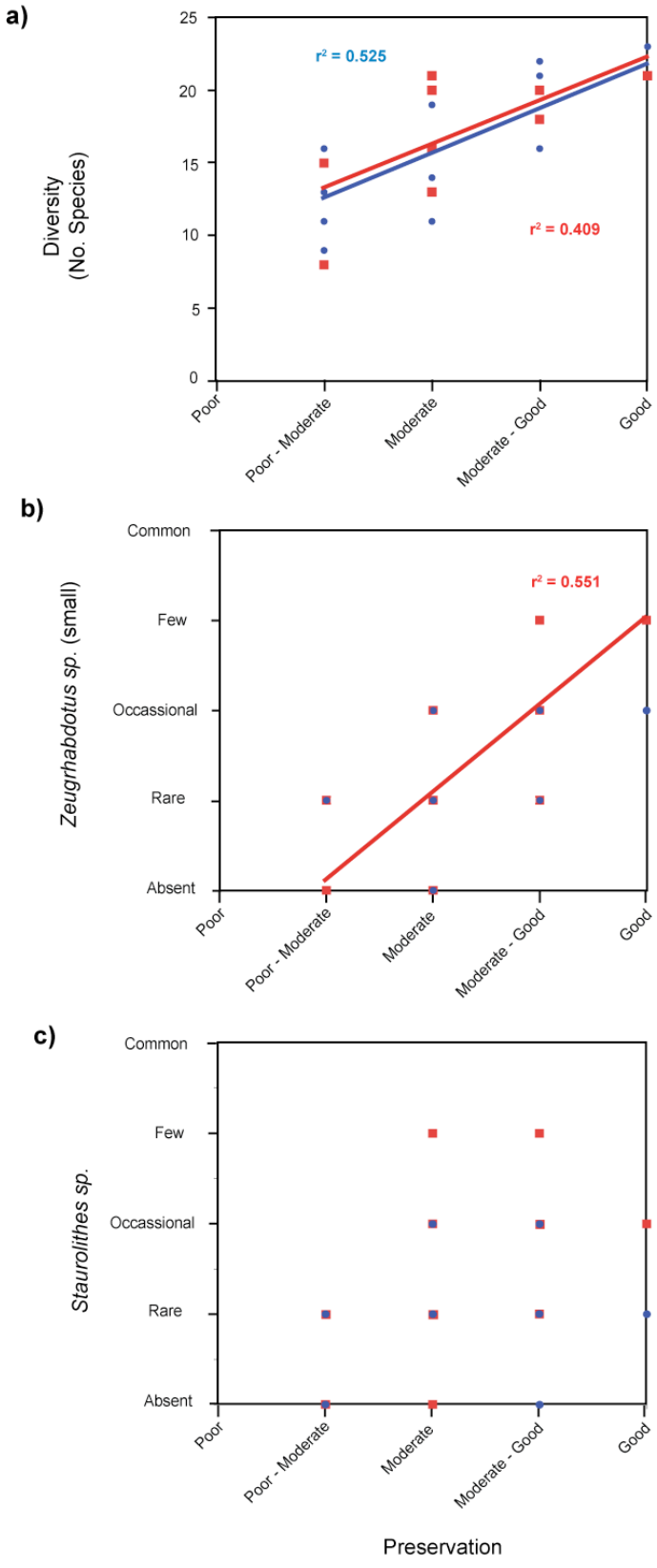

Figure 44. *Cross-plots of Site 534 data. (a) calcareous nannofossil preservation vs. diversity of assemblage; (b) abundance of small* Zeugrhabdotus spp. *vs. preservation;(c) abundance of* Staurolithites spp. *vs. preservation. Where* R^2 *values (numbers on plots) are <0.3, no linear regressions are shown.*

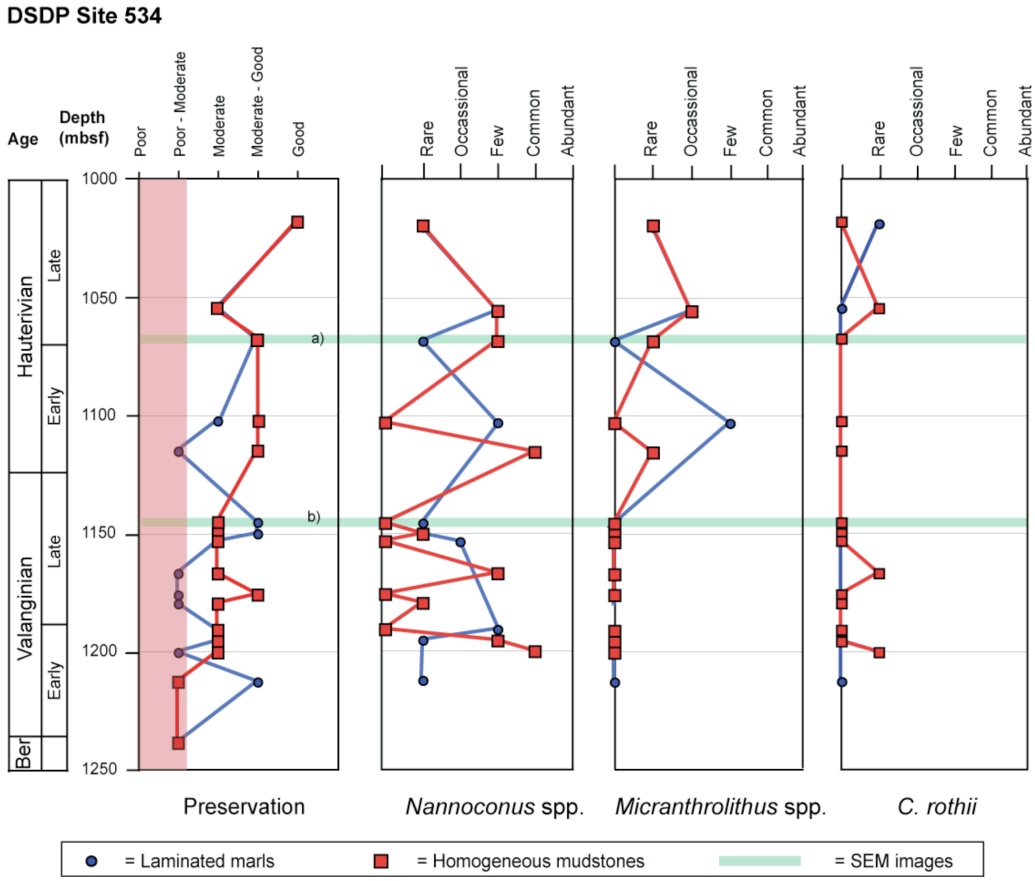

Figure 45. *Abundance of nannoliths in the Early Cretaceous sediments at Site 534, with 7 of the most poorly preserved samples removed (shaded in red on "preservation" plot).*

Similarities between the two lithologies

On the basis of calcareous nannofossil assemblages and preservation alone, it would be challenging to separate the homogenous mudstones from the laminated marls. The calcareous nannofossil preservation overall at Site 534 is moderate, with some samples displaying very good preservation characterised by the presence of fragile, dissolution-susceptible taxa and whole coccospheres, while other samples show a higher degree of etching and selective dissolution (Figure 40, 41, 42). Only minor differences were noted between the two lithologies in terms of nannofossil preservation, and the average values are within error of one another (Figure 40), however, there are considerable temporal variations in both lithologies throughout the record (Figures 43a).

The dominant calcareous nannofossil genus throughout all the earliest Cretaceous sediments at Site 534 is *Watznaueria* and in particular *Watznaueria barnesiae*, which often constitutes >50 % of the assemblage, particularly in some of the more poorly preserved samples (Figures 40, 43b). *Watznaueria barnesiae* is abundant in all samples relative to other species, and there is no discernable difference between the different lithologies (Figures 40, 43b). *Rhagodiscus asper* is a common component of many of the assemblages, and when the effects of dissolution are removed, is seen to be equally abundant in the marls and the mudstones (Figures 40, 43b).

Differences between the two lithologies

One of the few ways in which the two lithologies differ significantly is in the abundance of opaque minerals and siliciclastic fragments, which is consistently higher in the homogeneous mudstones than in the laminated marls (Figures 40, 43a). The homogeneous mudstones also have a slightly higher diversity overall (totally number of species in each slide) than the laminated marls (Figure 43a), however the average difference between the two lithologies in terms of this perameter is not statistically significant (>1 standard deviation apart). Moreover, the clear covariance between preservation and diversity in both lithologies, where better preservation leads to higher diversity, suggests the diversity trends should be regarded with some caution in terms of palaeoenvironmental interpretation (Figure 44).

Some minor differences in calcareous nannofossil assemblage between the marls and the mudstones are observed throughout the record (Figure 43b), but the average values for each species in each lithology are usually statistically indistinguishable from one another (Figure 40). This may be due in part to the large temporal variability in the abundances of these species from the Late Berriasian to the Late Hauterivian at Site 534. In fact, the only species which shows a significant average difference is the abundance of *Diazomatolithus lehmanii,* which is relatively common in the marls, but only rarely found in the mudstones (Figure 40, 43b). The abundance of *D. lehmanii* in the laminated marls also varies temporally, being much more common in the Valanginian than the Hauterivian (Figure 43b).

In contrast to the published trends from Site 603 (Applegate *et al*., 1989), the relative abundance of nannoliths in the two lithologies at Site 534 does not show a

particularly coherent pattern across the entire Berriasian–Hauterivian (Figures 43b, 45), and the mean abundances of *Nannoconus* spp. in each lithology are within error of one another (Figure 40). However, within the core there is considerable temporal variability in abundances between the pairs, with a general decline of nannoconids in the mid–Late Valanginian in the homogeneous mudstones (Figures 43b, 45). Such a decline is not obvious in the laminated marls, even when poor preservation is taken into account (Figures 40, 43b, 45). There is no statistically significant difference in average *Micrantholithus* spp., abundance between the marls and mudstones regardless of preservation (Figures 40, 43b, 45).

3. 4. 1. 2. GEOCHEMICAL VARIABLES AT SITE 534

At DSDP Site 534, the TOC and $CaCO_3$ contents, the bulk-organic carbon-isotope composition ($\delta^{13}C_{org}$), the organic-matter type (pyrolysis data), the TEX_{86} ratio, the BIT Index and the GDGT abundance in each sample was determined, the results of which are summarised in Table 2.

Lithology	**$CaCO_3$ %**	**TOC %**	**$\delta^{13}C_{org}$ (‰)**	**S2 (mg HC/ g)**	**HI (mg HC/ mg C_{org})**	**T_{max} °C**	**TEX_{86}**	**[GDGT] g^{-1}**	**BIT Index**
Laminated marl (n = 16)	73.03 [14.18]	0.75 [0.42]	-26.99 [0.89]	0.74 (n = 6) [0.71]	70 (n = 6) [47]	430 (n = 6) [2]	0.920 [0.01]	211,000 [178,000]	0.094 (n = 1)
Homogeneous mudstone (n = 16)	24.81 [11.94]	1.02 [0.54]	-25.45 [1.54]	0.48 (n = 5) [0.43]	44 (n = 5) [34]	477 (n = 5) [74]	0.896 [0.01]	44,700 [48,000]	0.015 (n= 3) [0.00]
T-test value	10.4 (2.75)	1.56 (2.75)	3.46 (2.75)	0.690 (3.25)	1.01 (3.25)	1.58 (3.25)	5.45 (2.75)	3.71 (2.75)	n/a
P value	<0.0001	0.1292	0.0016	0.5070	0.3389	0.1486	<0.0001	0.0011	n/a

***Table 2**. Summary of geochemical results from DSDP Site 534. n equals the number of analyses in each category, as not all samples yielded data for each geochemical parameter. S2 = mg of hydrocarbons released per gram of sediment during pyrolysis; HI = Hydrogen Index. Square brackets indicate standard deviations. GDGT values are shown to 3 significant figures. Round brackets indicate the unpaired, two-tailed T-test threshold at the P value = 0.01 level, for the relevant degrees of freedom.*

TOC % and $CaCO_3$ %

At DSDP Site 534, a clear difference is seen between the $CaCO_3$ content in the laminated marls compared to the homogeneous mudstones, with the laminated marls having on average three times as much carbonate as the mudstones (Table 2, Figure 46a). The significance of this difference is confirmed with a P value of <0.0001. There is also generally a strong covariance between the $CaCO_3$ content in each pair throughout the section, where a lower $\%CaCO_3$ in one lithology is mirrored by lower $\%CaCO_3$ in the other lithology of the pair (e.g. Figure 46a; 1018 – 1150 mbsf). There is a general trend for the homogeneous mudstones to have slightly higher TOC values than the laminated marls, which is demonstrated by the difference in average values (1.02% and 0.75% respectively), even though this difference is not statistically significant (P value of 0.13; Table 2). However, within each lithological pair there is a trend for higher TOC% in the mudstones (~0.6% average difference), with 11 out of the 16 pairs showing this trend. This trend is reversed in the two samples from the late Early Valanginian (1190 – 1195 mbsf), where the laminated marls are seen to have unusually high TOC contents of ~1.6 % (Figure 46a).

$\delta^{13}C_{org}$ data

The bulk organic carbon-isotope record ($\delta^{13}C_{org}$) shows a consistent offset between the two lithologies, with the homogeneous mudstones consistently having higher (more positive) values than the laminated marls (Figure 46a). This is reflected in the 2.54 ‰ difference in the average values between the two lithologies, which is far above the reproducibility of the standards of ±0.1 ‰, and in the low P value of 0.0016 (Table 2). There is a general covariance between the different lithologies in each pair throughout the section, where relatively more positive $\delta^{13}C_{org}$ values in one lithology are often mirrored by more positive values in the other half of the pair (Figure 46a).

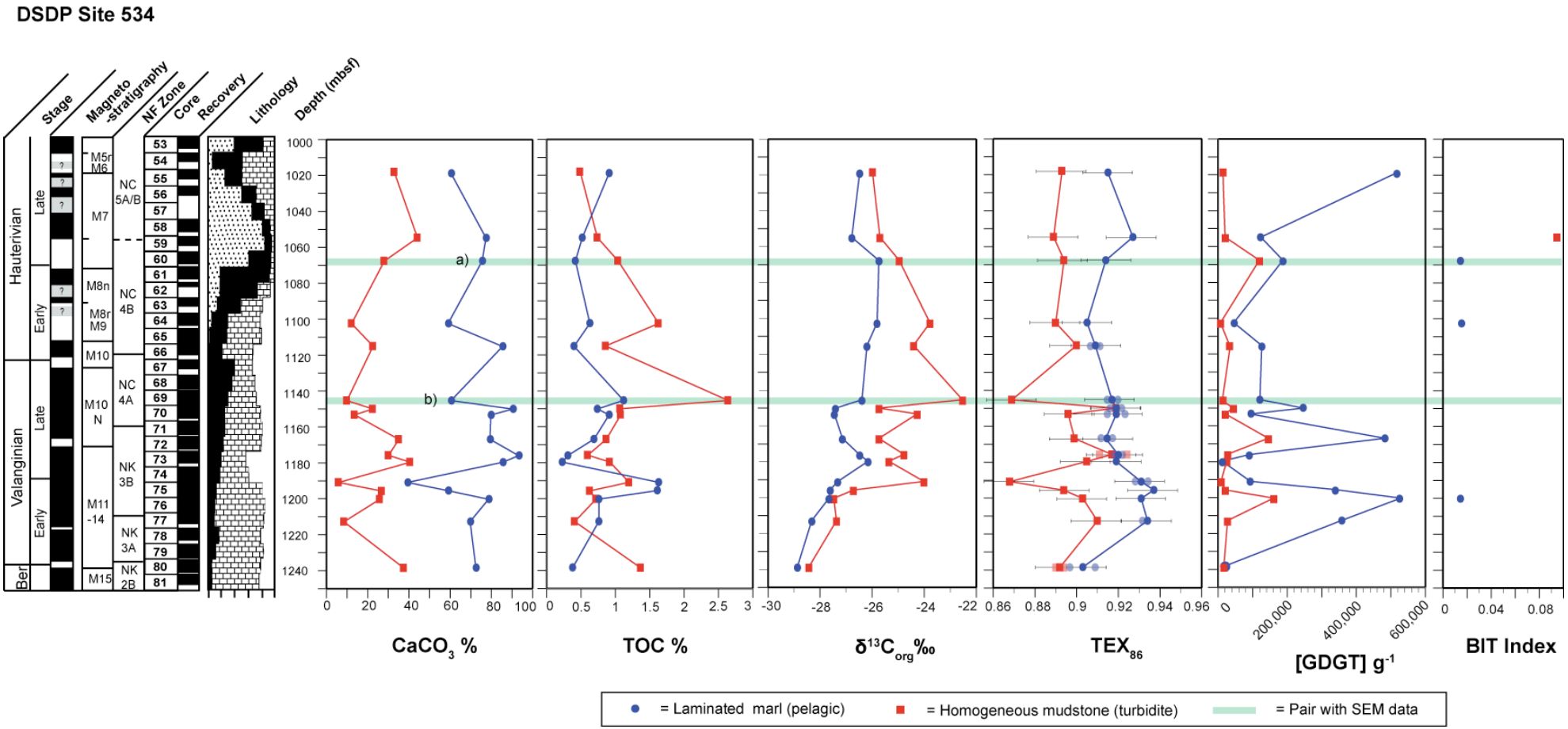

Figure 46a. *Geochemical results from the earliest Cretaceous of DSDP Site 534, showing $CaCO_3$ and TOC contents, $\delta^{13}C_{org}$ trends, TEX_{86} values, GDGT abundances and BIT Index values in each lithologically paired sample. In the TEX_{86} plot, the error bars denote the ±0.012 error seen in the long-term internal standard. The pale symbols represent the values determined in each reanalysis of the sample, with the solid symbols representing the average of the two analyses.*

Rock Eval pyrolysis data

The limited Rock Eval pyrolysis data from Site 534 shows some minor differences between the two lithologies, but it is difficult to ascribe general trends as only 11 samples (5 homogeneous marls and 6 laminated marls) were analysed, and none of the differences between the lithologies are statistically significant overall (Table 2). The majority of the samples are from the Valanginian (n = 9), with one laminated marl sample from the Upper Hauterivian and one homogeneous mudstone sample from the Upper Berriasian (Figure 46b). Overall the homogeneous mudstones have higher T_{max} values of 477 ºC, verses the laminated marl average of 430 ºC, but it should be noted that these higher mudstone values are skewed considerably by two very high Upper Valanginian points (Table 2, Figure 46b). The two paired Upper Valanginian samples at ~1153 mbsf and ~1176 mbsf both show a large offset between the ~430 ºC marl value and the 503–595 ºC mudstone values (Figure 46b). The sample with the highest TOC, 1190 mbsf (highlighted pink) has the highest amount of free hydrocarbons (S1 value), but the values are low for all samples overall (Figure 46b). The hydrogen indexes (HI) are low overall (<150) and do not reveal a coherent pattern of lithological offset, with the pair at 1153 mbsf showing higher HI values in the mudstone, but the marl and mudstone in the 1176 mbsf pair having very similar HI values to one another (Figure 46b).

Maturation

Four laminated marl samples from Site 534 (~1060 – 1240 mbsf) were analysed for their hopane index, to ascertain the degree of thermal maturation at Site 534 (Section 2-2-4). All were found to be below the critical 0.5 value, above which the TEX_{86} ratio can become distorted (Littler *et al*., 2011).

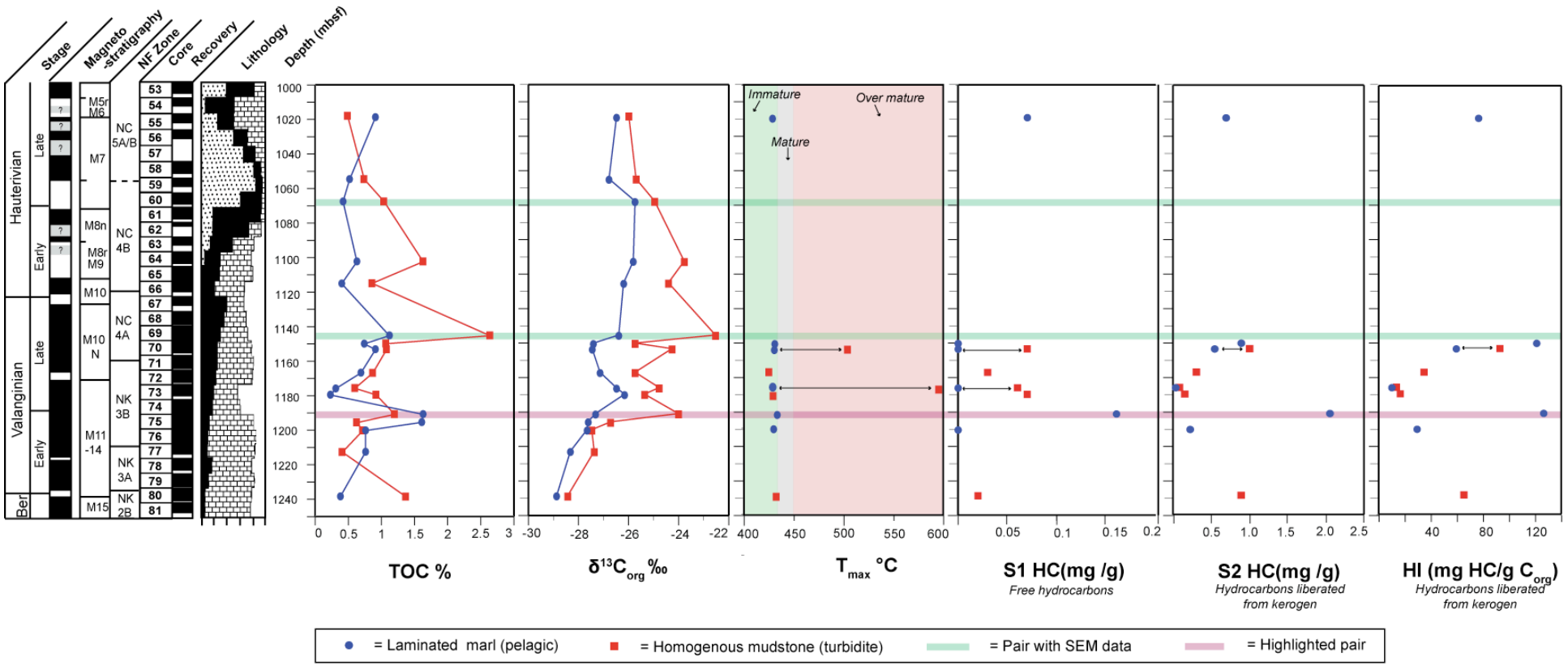

Figure 46b. *Rock Eval pyrolysis data for 11 of the Site 534 samples. Symbols as for Figure 46a.*

GDGT abundances, TEX_{86} ratios

At Site 534 TEX_{86} values in the laminated marls have an average value of 0.920, whereas the homogeneous mudstones have an average value of 0.896, leading to a small, but significant, average difference of 0.024. This is double the analytical error of 0.012 based on repeated analysis of an internal standard and corresponds to a temperature difference of ~0.8 ºC using the TEX_{86}^{H} calibration (Kim *et al*., 2010), and ~0.6 ºC using the less sensitive reciprocal calibration (Kim *et al*., 2010; after Liu *et al*., 2009). Importantly, the average difference between the two lithologies in terms of TEX_{86} is very statistically significant, with a P value of <0.0001.

Although the analytical error calculated using the long-term standard is relatively high, reflected in the large error bars in Figure 46a, reruns of the Site 534 samples, where reanalysis was possible, suggest that the reproducibility in these samples is actually much better. Average reproducibility of ±0.008 in the homogeneous marls (n = 2, where n equals the number of pairs where duplicate analyses were possible), and ±0.006 in the laminated marls (n = 5), suggests that although only 7 out of the 16 pairs had difference in TEX_{86} that were beyond the analytical error of ±0.12, it is likely that at least another three of the samples actually also have significant difference in TEX_{86} values within the pair (Figure 46a). Duplicate analysis was attempted for all samples, but the very low GDGT abundances in these earliest Cretaceous sediments made this impossible in most instances.

A difference in GDGT abundance was also observed between the two lithologies, with the laminated marls having higher abundances of GDGTs per gram of sediment extracted, normalised to a 100µl dilution ([GDGT g^{-1}]), than the corresponding homogeneous claystones in all but two of the pairs (Figure 46a). This is reflected in the difference in average GDGT abundance between the two lithologies, with the laminated marls having nearly 5x the abundances seen in the transported sediments (Table 2). This difference is statistically significant at the >99% probability level, with a P value of 0.0011 (Table 2). In contrast to the TEX_{86} values themselves, there is a covariance between the GDGT abundances between the lithologies in each pair, where a relatively higher GDGT abundance in one lithology is often matched by a correspondingly higher GDGT abundance in the other half of the pair (Figure 46a).

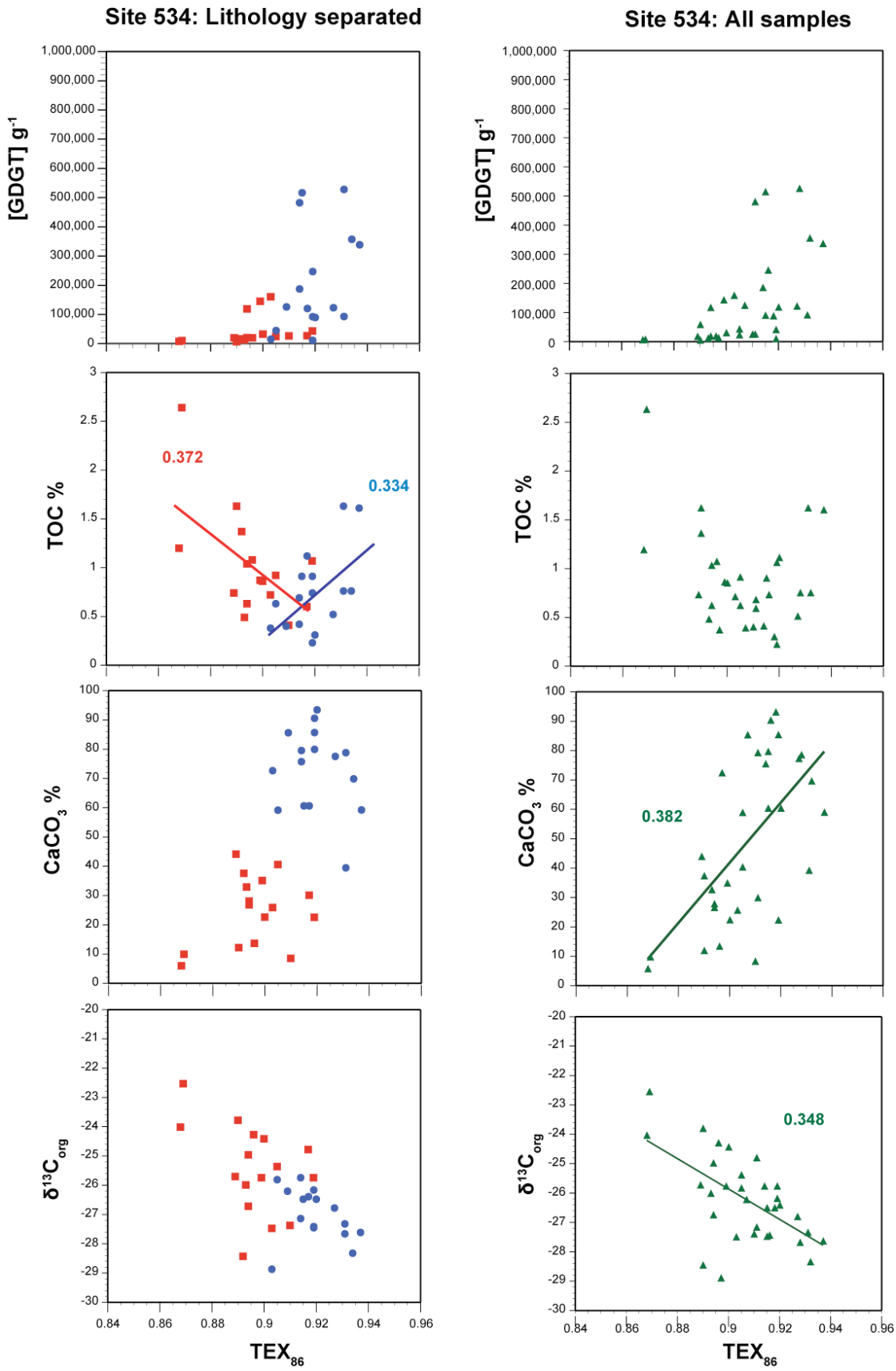

Figure 47a. *Cross-plots to show the relationships between TEX_{86}, and other geochemical variables such as GDGT concentrations, TOC%, $CaCO_3$% and $\delta^{13}C_{org}$. Where R^2 values (numbers on plots) are <0.3, no linear regressions are shown.*

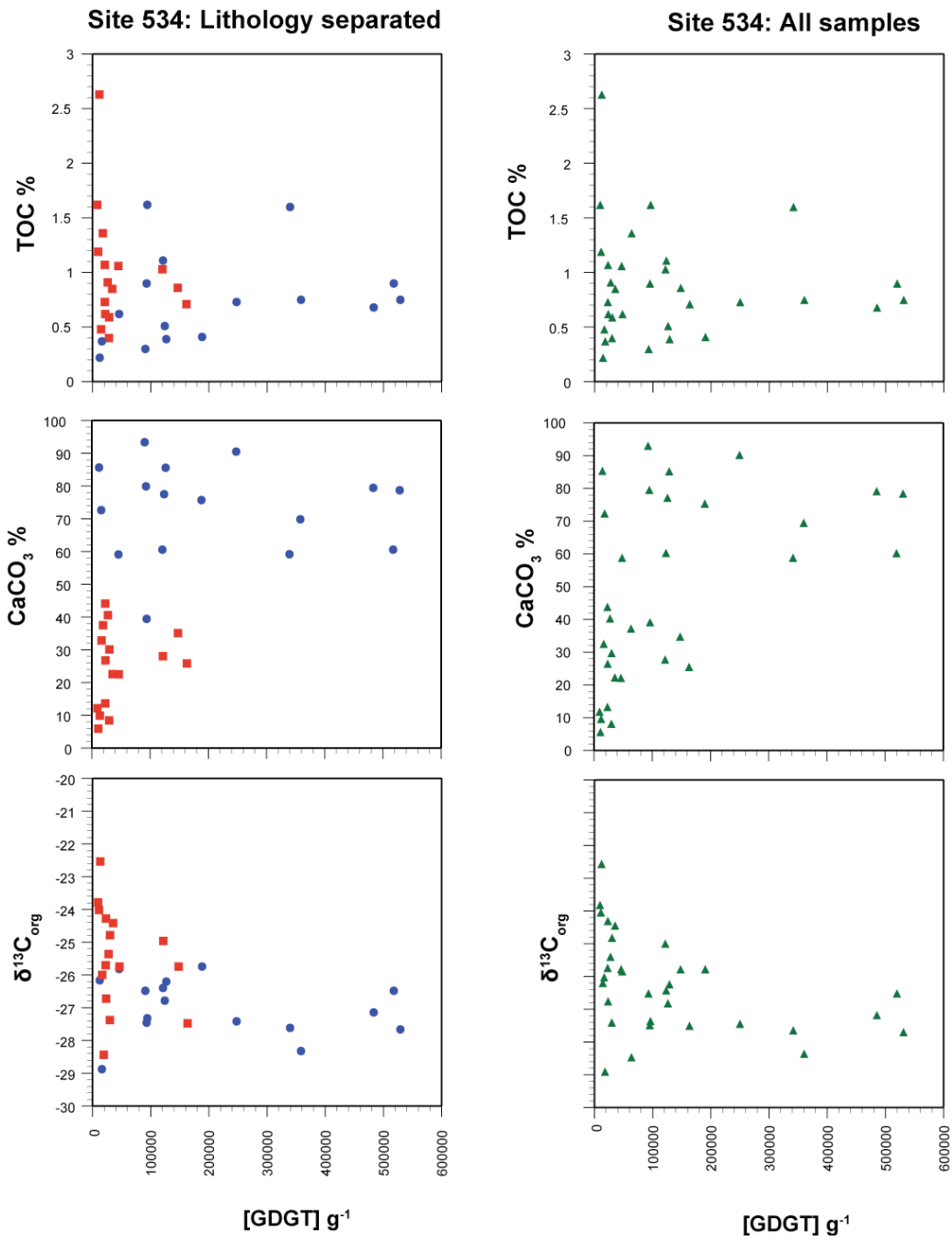

Figure 47b. *Cross-plots to show the relationships between GDGT concentrations and variables such as TOC%, CaCO3% and $\delta^{13}C_{org}$. Where R^2 values are <0.3 no linear regressions are shown.*

BIT Indices

Due to the very low concentrations of Branched GDGTs in all of the earliest Cretaceous sediments at Site 534, it was only possible to determine the BIT Index in three laminated marl samples, and one homogeneous mudstone sample (Table 2). The BIT Index in all other samples was therefore effectively 0. All samples had low BIT Indices suggesting a low input of terrestrial GDGTs at Site 534 overall, but average values of 0.015 in the laminated marl samples, contrasted with a somewhat higher value of 0.094 in the one homogeneous sample that yielded a value (Table 2, Figure 46a). There is no lithologically paired BIT Index data and none of the points were concentrated enough to be run in duplicate.

Geochemical cross-plots

Very little relationship is noted between TEX_{86} and any of the geochemical parameters at Site 534 (Figure 47). The strongest relationship is between TOC and TEX_{86}, which shows a weak negative correlation in the mudstones ($r^2 = 0.372$) and a weak positive correlation between TEX_{86} and TOC % in the laminated marls ($r^2 = 0.334$), (Figure 47a). There is no relationship between GDGT abundance and any of the geochemical variables, suggesting the strength of the signal in each sample is not responsible for the offset in the TEX_{86} ratios (Figure 47b).

3. 4. 2. DSDP SITE 603

3. 4. 2. 1. CALCAREOUS NANNOFOSSIL ASSEMBLAGES AND PRESERVATION AT SITE 603

In contrast to some of the findings at Site 534, there is a somewhat clearer distinction between the calcareous nannofossil assemblages in the homogeneous mudstones and the laminated marls at Site 603, (Figure 48). However, many of the mean abundances of the species are still statistically indistinguishable between the two lithologies, which is probably attributable to the complicated temporal patterns observed in the data (Figures 48, 52b).

Similarities between the two lithologies

The preservation of calcareous nannofossils in earliest Cretaceous sediments at Site 603 is moderate–good overall, and unlike the situation at Site 534, no samples display preservation worse than "moderate" (Figures 48–51). Some samples, particularly in the latest Valanginian and Hauterivian have excellent preservation, allowing the preservation of delicate taxa (Figure 49). The mean preservation between the two lithologies is exactly the same (Figures 48, 52a).

As at Site 534, the dominant species is the abundant *Watznaueria barnesiae*, and there is very little difference between the two lithologies in terms of its abundance (Figure 48, 52b). The distribution of other species between the two lithologies is somewhat different than at Site 534, but again, the majority of the species have mean abundances which are statistically indistinguishable from one another (Figure 48).

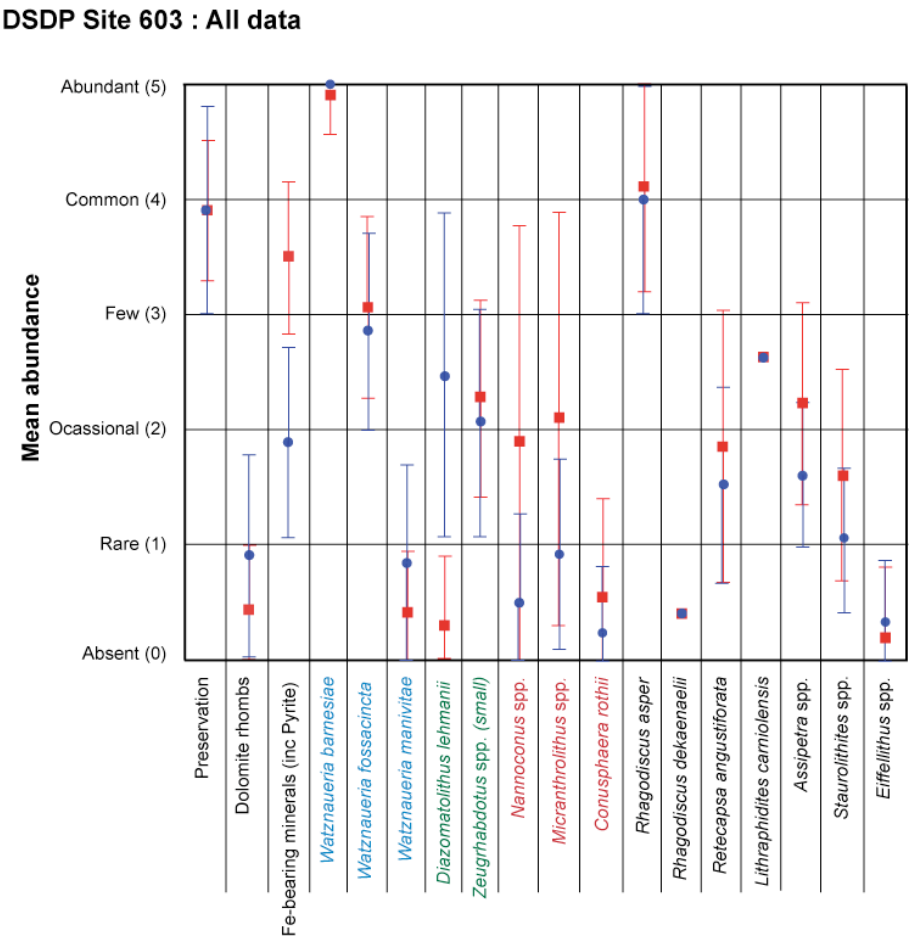

***Figure 48**. Major palaeontological differences between the two lithologies at Site 603. Mean values of all samples of Early Valanginian–Late Hauterivian age. Colours of species' names indicated which group they belong to, e.g. pale blue are Watznaueria spp; red are nannoliths, etc. Error bars represent one standard deviation.*

Differences between the two lithologies

As at Site 534, the abundance of opaque minerals and siliciclastic fragments is consistently higher in the homogeneous mudstones than in the laminated marls at Site 603 (Figure 48, 52a). The diversity of the nannofossil assemblage are similar in both lithologies, but marginally higher in the mudstones overall, mostly due to the higher diversity seen in this lithology in the Hauterivian samples (Figures 48, 52a). There is no covariance between preservation and diversity in either lithology, suggesting preservation is not a controlling factor on diversity at Site 603 (Figure 53).

As at Site 534, the only taxa which shows a statistically significant difference between the two lithologies is *D. lehmanii*, which is much more common in the

marls than the mudstones at Site 603 (Figure 48, 52b). The abundance of *D. lehmanii* in the marls also varies temporally, being much more common in the Late Valanginian than the Hauterivian, which again agrees with the peak in abundance seen at Site 534 at this time (Figures 43b, 52b).

The differences between the marls and mudstones in the relative average abundance of nannoliths, are somewhat greater than those observed at Site 534, but these differences are still not statistically significant (Figure 48). However, the general trends at Site 603 suggest that *Nannoconus* spp., *Micrantholithus* spp. and *C. rothii* are all marginally more common in the mudstones than the marls, and that the lack of significance in the average data is due to temporal variation during the Valanginian–Hauterivian (Figures 48, 52b, 54). The abundance of *Nannoconus* spp. and *Micrantholithus* spp. are fairly invariant with time in the laminated marls, constituting only a rare–occasional part of the assemblage, but there is considerable temporal variability in the homogeneous mudstones, with an increase in the abundance of both *Nannoconus* spp. and *Micrantholithus* spp. in the Hauterivian (Figures 48, 52b, 54). *Micrantholithus* spp. are present in the assemblage from the Late Valanginian onwards (Figures 48, 52b, 54). *C. rothii* is rare–occasional in abundance at Site 603, and is not seen until the Early Hauterivian (Figures 48, 52b, 54).

603B-57-05, 49 cm
Laminated marl
Late Hauterivian

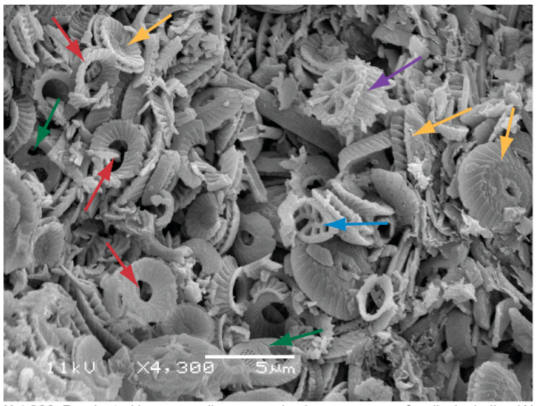

X 4,300. Dominated by very well-preserved calcareous nannofossils, including *W. barnesiae* (yellow arrows), *D. lehmanii* (red arrows), *Zeugrhabdotus* spp. (green arrow), *R. laffittei* (purple arrow), *Stradnerlithus asymmetricus* (blue arrow).

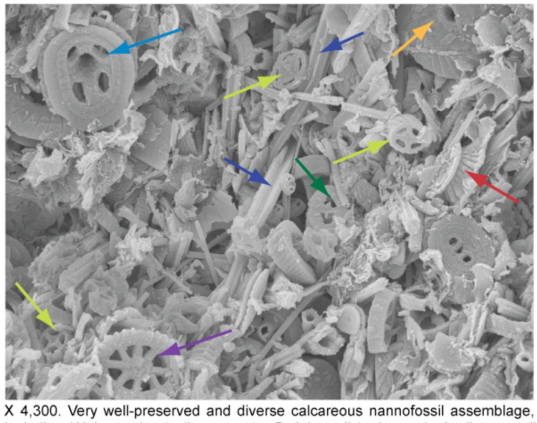

X 4,300. Very well-preserved and diverse calcareous nannofossil assemblage, including *W. barnesiae* (yellow arrow), *D. lehmanii* (red arrow), *A. dietzmannii (blue arrrow)*, *L. carniolensis* (dark blue arrow), *Zeugrhabdotus* spp. (green arrow), *R. laffittei* (purple arrow), *Staurolithites* spp. (lime green arrow).

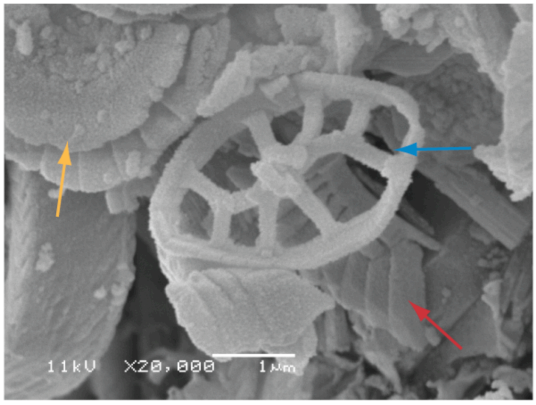

X 4,300. Well-preserved *Stradnerlithus asymmetricus* (blue arrow) surrounded by *W. barnesiae* (yellow arrow) and *D. lehmanii* (red arrow).

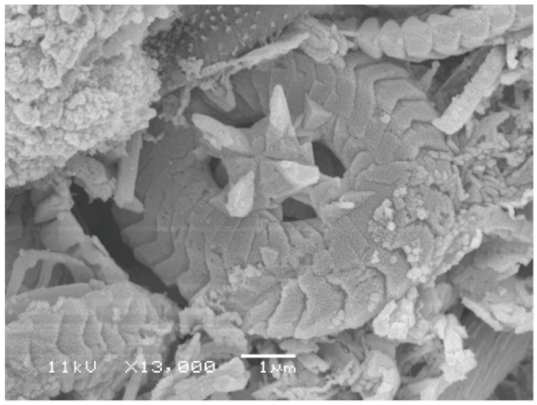

X 13,000. Well-preserved *H. chiastia*

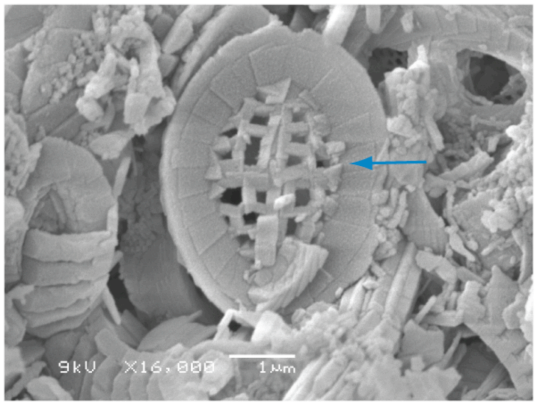

X 16,000. *Cretarhabdus inaequalis* showing well-preserved central grill structure.

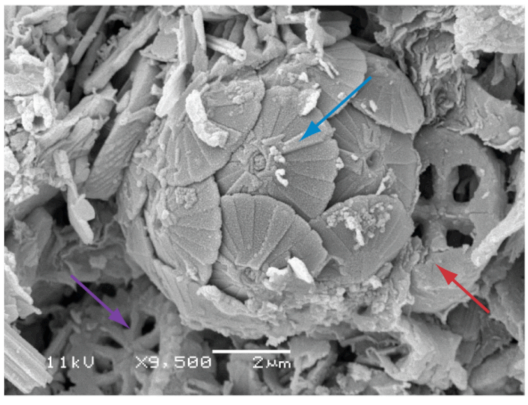

X 9,500. Well-preserved *Discorhabdus ignotus* coccosphere (blue arrow) with *R. laffittei* (purple arrow), *Staurolithites sp.* (red arrow).

Figure 49. *SEM images of a laminated marl sample ('a') from Core 603B-57-05, showing the excellent preservation and diversity of the calcareous nannofossil assemblage. [Images 2–6 were taken by P. Bown].*

603B-64-03, 105 cm
Homogenous mudstone
Early Hauterivian

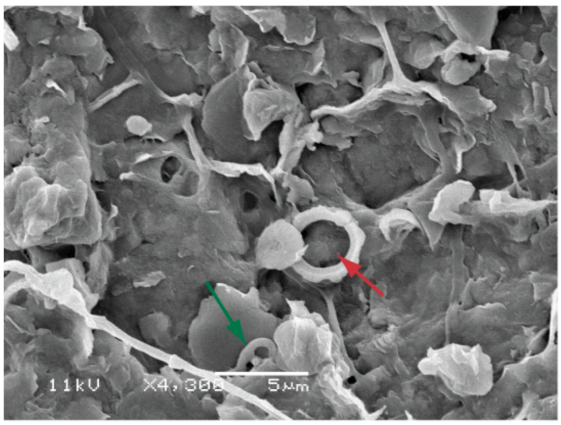

X 4300. Dominated by clay with occassional, coccoliths. *D. lehmanii* (red arrow), and a small *Zeugrhabdotus* spp. (green arrow) are visible. Preservation overall (from smear slide) is moderate–good with minor etching.

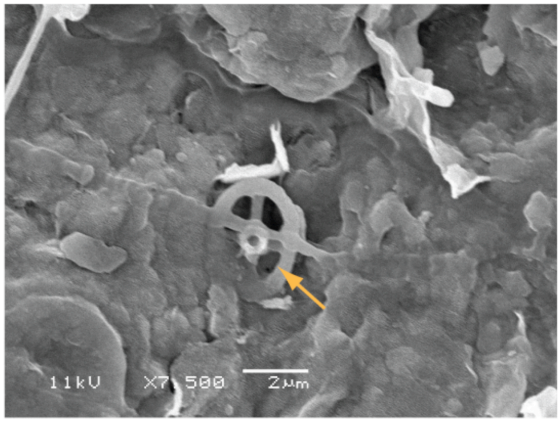

X 7500. An etched *Staurolithites* sp. (yellow arrow) surrounded by clay.

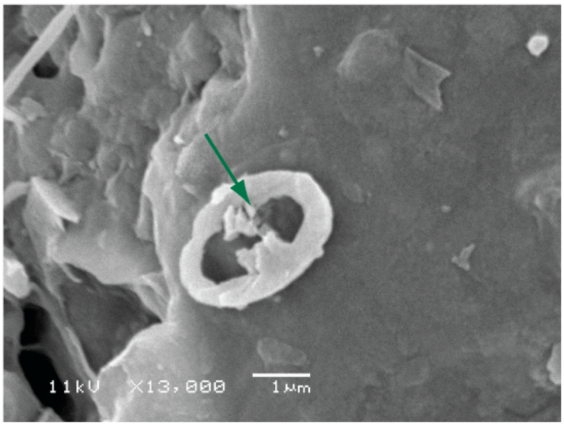

X 13,000. A very small *Zeugrhabdotus* sp. (green arrow) surrounded by clay.

Figure 50. *SEM images from a homogeneous mudstone sample from Core 603B-64-03. Although preservation may appear poor in these images, the overall preservation from light microscope observations is Moderate– Good, with only mild etching evident, as evidenced by the preservation of small taxa such as the Zeugrhabdotus* sp. *in the bottom panel. The disparity between these SEM and light microscope observations can be attributed to the difficulty in imaging relatively rare calcareous nannofossils within the clay matrix in the SEM, which can be compensated for using the smear-slide technique in the light microscope.*

603B-75-03, 85 cm
Homogenous mudstone
Mid Valanginian
[no geochemical data available]

603B-75-03, 109 cm
Laminated marl
Mid Valanginian

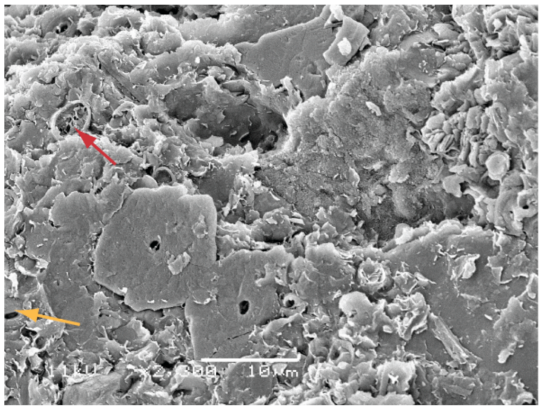

X 2300. Predominantly large clay flakes with occassional, poorly preserved coccoliths. Very etched unidentified coccolith (red arrow), and a moderately well preserved *W. fossacincta* (?) (yellow arrow) are visible.

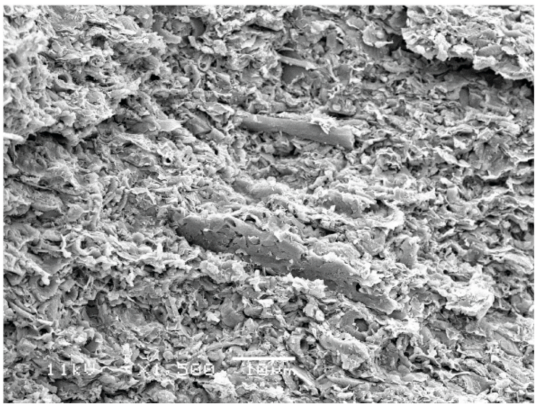

X 1500 Sample is dominated by coccoliths with minor clay. Dominant species include *D. lehmanii*, *W. barnesiae* and *W. fossacincta*. Preservation is moderate to good with some minor etching.

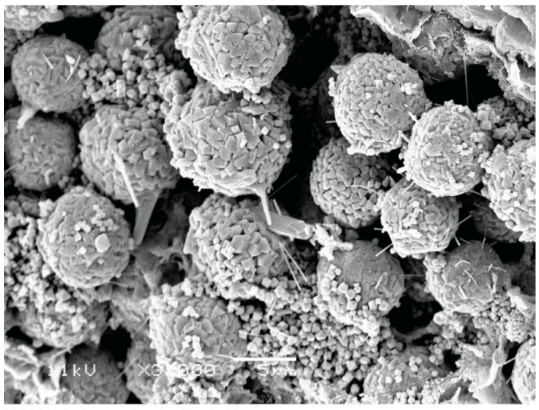

X 3000 A cluster of pyrite framboids.

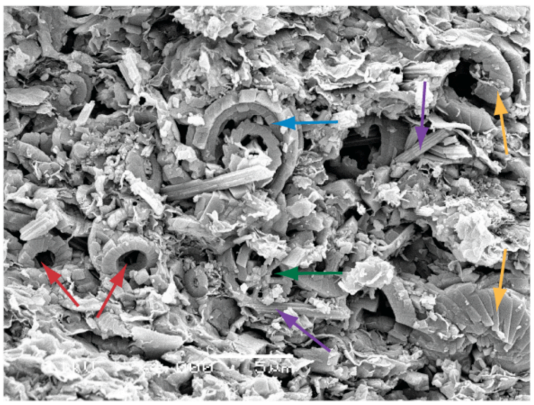

X 4000 Typical coccolith assemblage with examples of *D. lehmanii* (red arrows), *L. carniolensis* (purple arrows), *W. barnesiae* (yellow arrows), *R. laffittei (?)* (green arrow), and *Axopodorhabdus* sp. (?) (blue arrow).

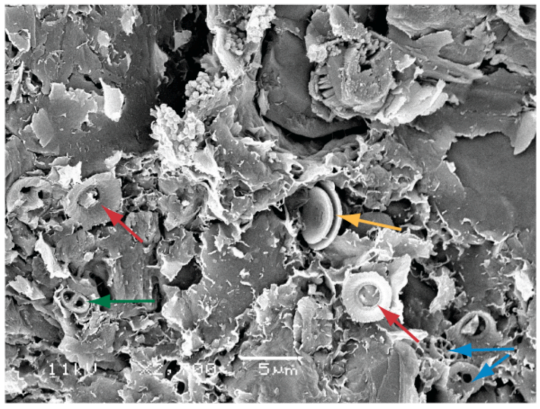

X 2700 A sparse and etched assemblage of coccoliths surrounded by clay. *D. lehmanii* (red arrows), *W. barnesiae* (yellow arrow), a small *Zeugrhabdotus* sp. (green arrow) and two unidentifiable coccoliths (blue arrows) are visible.

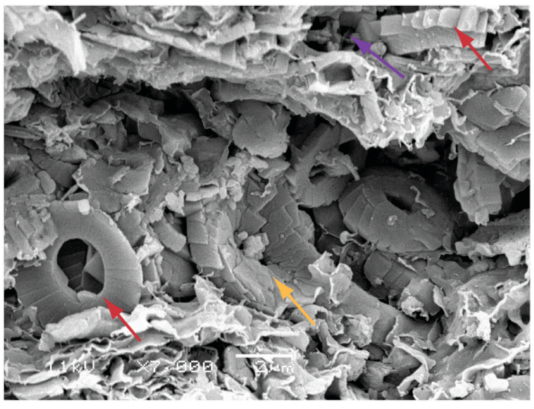

X 7000 Coccolith assemblage showing *D. lehmanii* (red arrows), *W. barnesiae* (yellow arrow), and an etched *Staurolithites* sp. (purple arrow). Secondary calcite and clay is also visible.

Figure 51*. SEM images of a laminated marl sample ('c') and a nearby homogeneous mudstone from Core 603B-75-03 (right). The marl shows moderate preservation overall, with well-preserved W. barnesiae coccoliths, but some etching and poor-preservation evident on the smaller and more fragile taxa. The mudstone (for which there are no geochemical data), has poor-moderate preservation, with etching and dissolution common.*

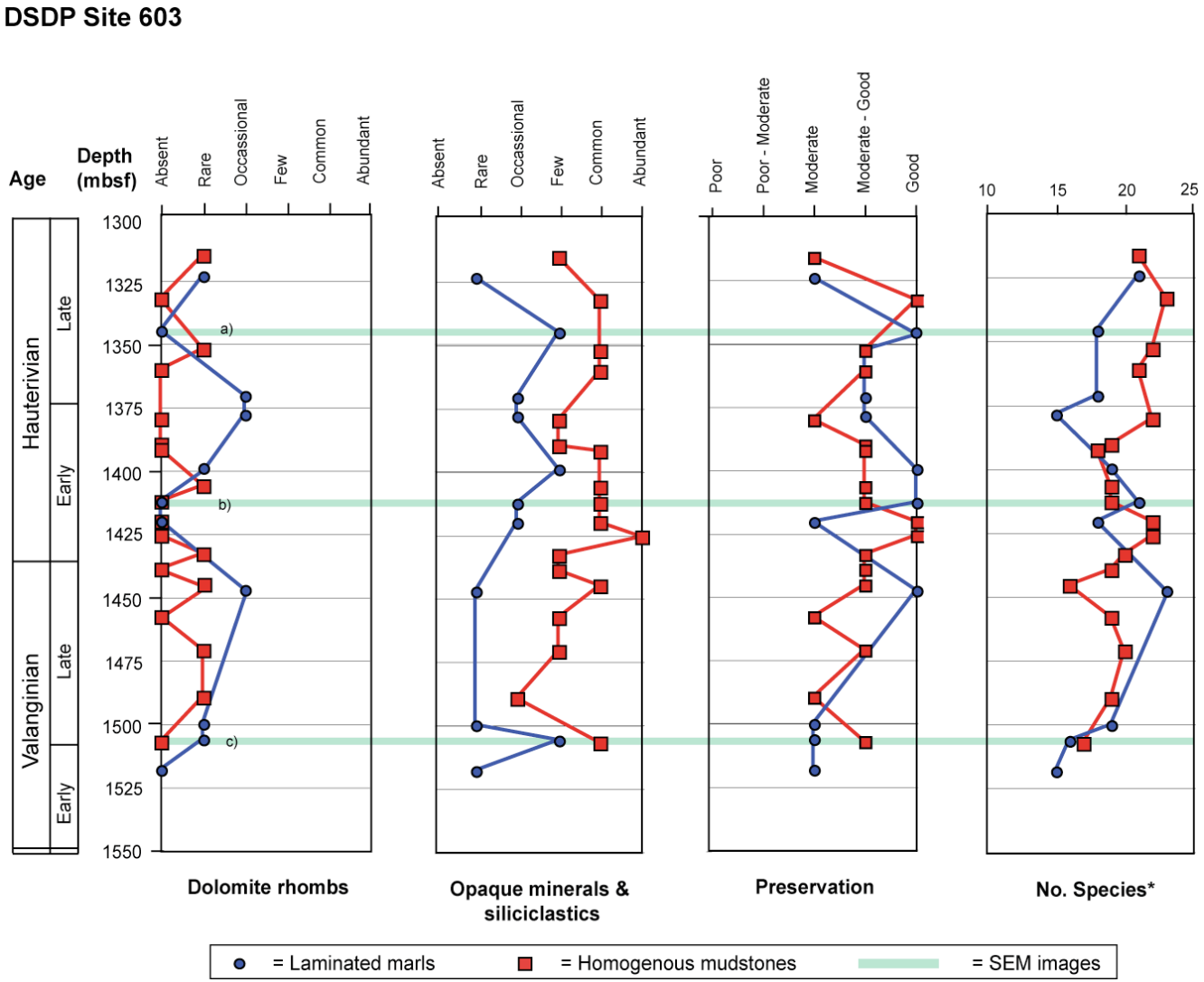

Figure 52a. *Light microscope observations from all paired laminated marl and homogeneous mudstone samples at Site 603.*

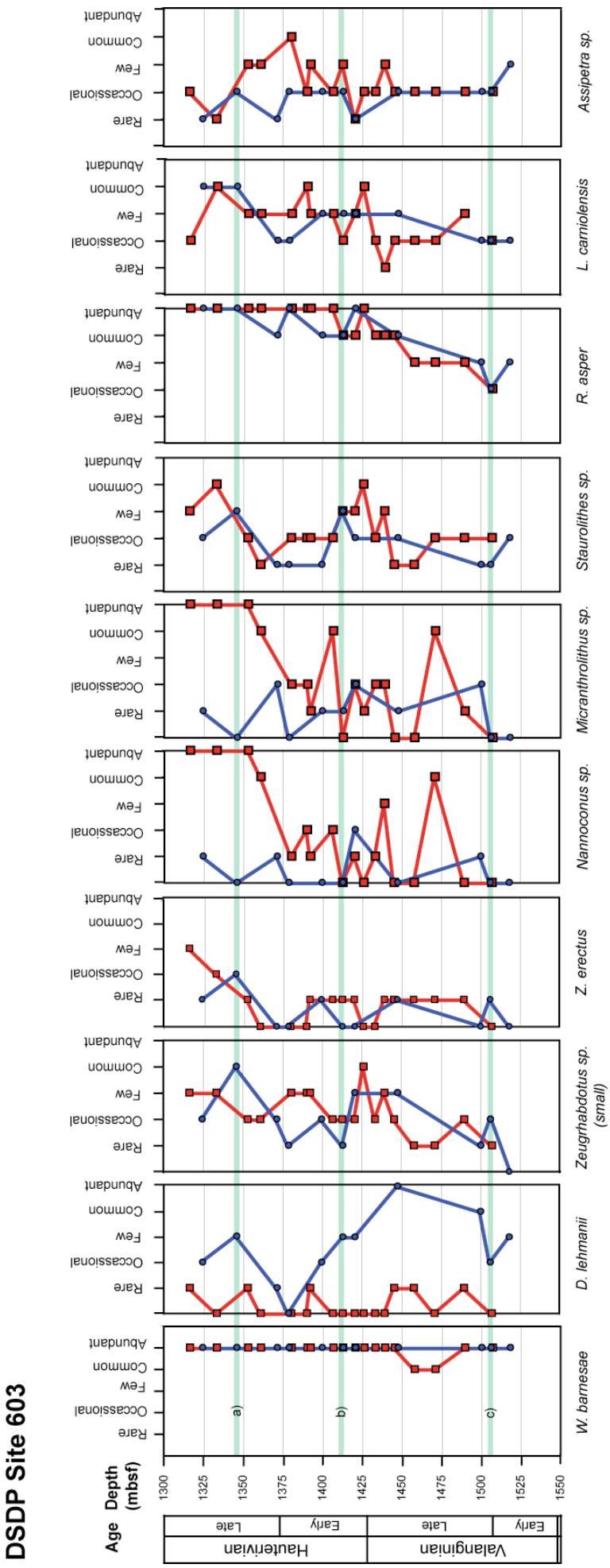

***Figure 52b**. Light microscope observations from all paired laminated marl and homogeneous mudstone samples at Site 603.*

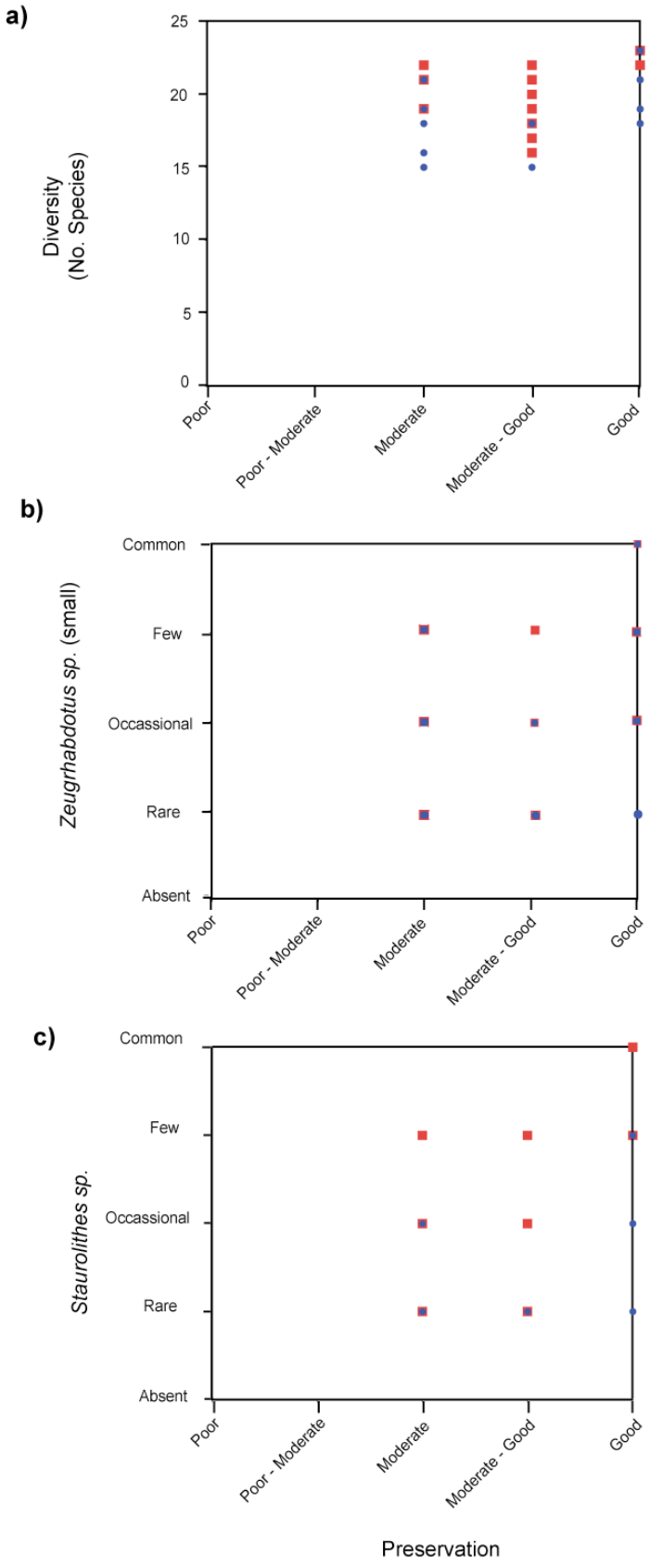

Figure 53. *Cross-plots of a) calcareous nannofossil preservation vs. diversity of assemblage; b) abundance of small* Zeugrhabdotus spp. *vs. preservation; c) abundance of* Staurolithites spp. *vs. preservation, at Site 603. Where* R^2 *values are <0.3 (all plots) the linear regression lines are not shown.*

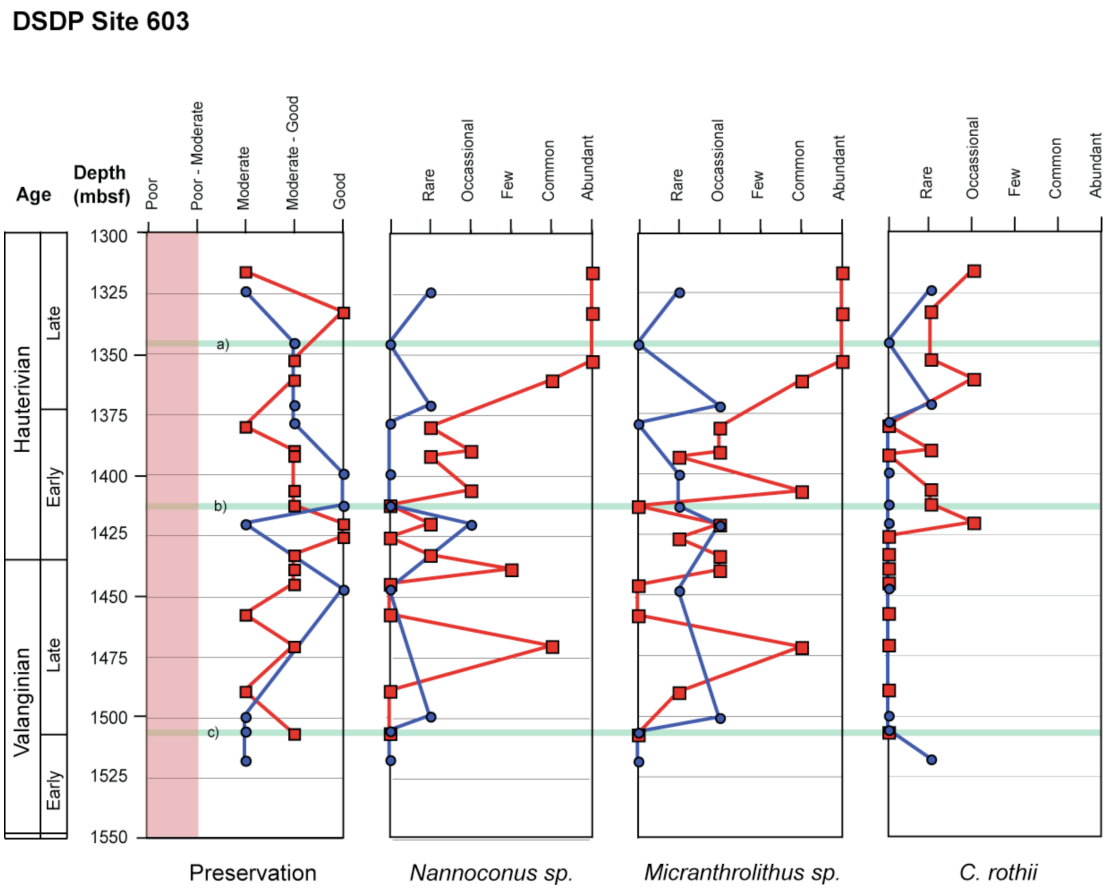

***Figure 54**. Abundance of nannoliths in the Early Cretaceous sediments at Site 603. Poor preservation is shaded in red on "preservation" plot, but all of the samples analysed at this site were deemed to be at least Moderate in their preservation.*

3. 4. 2. 2. SITE 603 GEOCHEMICAL VARIABLES

As for Site 534, the TOC and $CaCO_3$ contents, the bulk-organic carbon-isotope composition ($\delta^{13}C_{org}$), the TEX_{86} ratio, the BIT Index and the GDGT abundance in each sample were determined at Site 603, the results of which are summarised in Table 3. However, the interpretation of geochemical data is more complicated at Site 603, as unlike the analyses at Site 534, the samples were frequently not from the same depth interval in the core, and therefore only broad trends can be discerned from the data.

Lithology	Average $CaCO_3$ %	Average TOC %	Average $\delta^{13}C_{org}$ (‰)	Average TEX_{86}	Average [GDGT] g^{-1}	Average BIT Index
Laminated marl (n = 17)	74.62 (n = 17) [8.6]	1.43 (n = 17) [0.52]	-26.76 (n = 11) [0.67]	0.908 (n = 17) [0.009]	246,000 (n = 17) [206,000]	0.022 (n = 4) [0.022]
Homogeneous mudstone (n = 26)	20.71 (n = 26) [6.83]	1.40 (n = 26) [0.24]	-24.81 (n = 18) [0.67]	0.871 (n = 26) [0.021]	68,000 (n = 26) [62,000]	0.056 (n = 14) [0.056]
T-test value	17.7 (2.70)	0.0369 (2.70)	8.19 (2.75)	5.44 (2.70)	2.88 (2.70)	1.93 (2.92)
P value	<0.0001	0.9707	<0.0001	<0.0001	0.0062	0.071

***Table 3**. Summary of geochemical results from DSDP Site 603. n = the number of analyses in each category, as not all samples yielded data for each geochemical parameter. Square brackets represent the standard deviation. GDGT values are shown to 3 significant figures. Round brackets indicate the unpaired, two-tailed T-test threshold at the P value = 0.01 level, for the relevant degrees of freedom.*

TOC % and $CaCO_3$ %

The trends in $CaCO_3$ content at Site 603 are very similar to those seen at Site 534, with the marls having much higher carbonate content compared to the mudstones, which is statistically significant at greater than the 99% probability level (Table 3, Figure 55). The average TOC content is almost exactly the same (~1.4 %) between the two lithologies with no statistical difference between the two (Table 3, Figure 55).

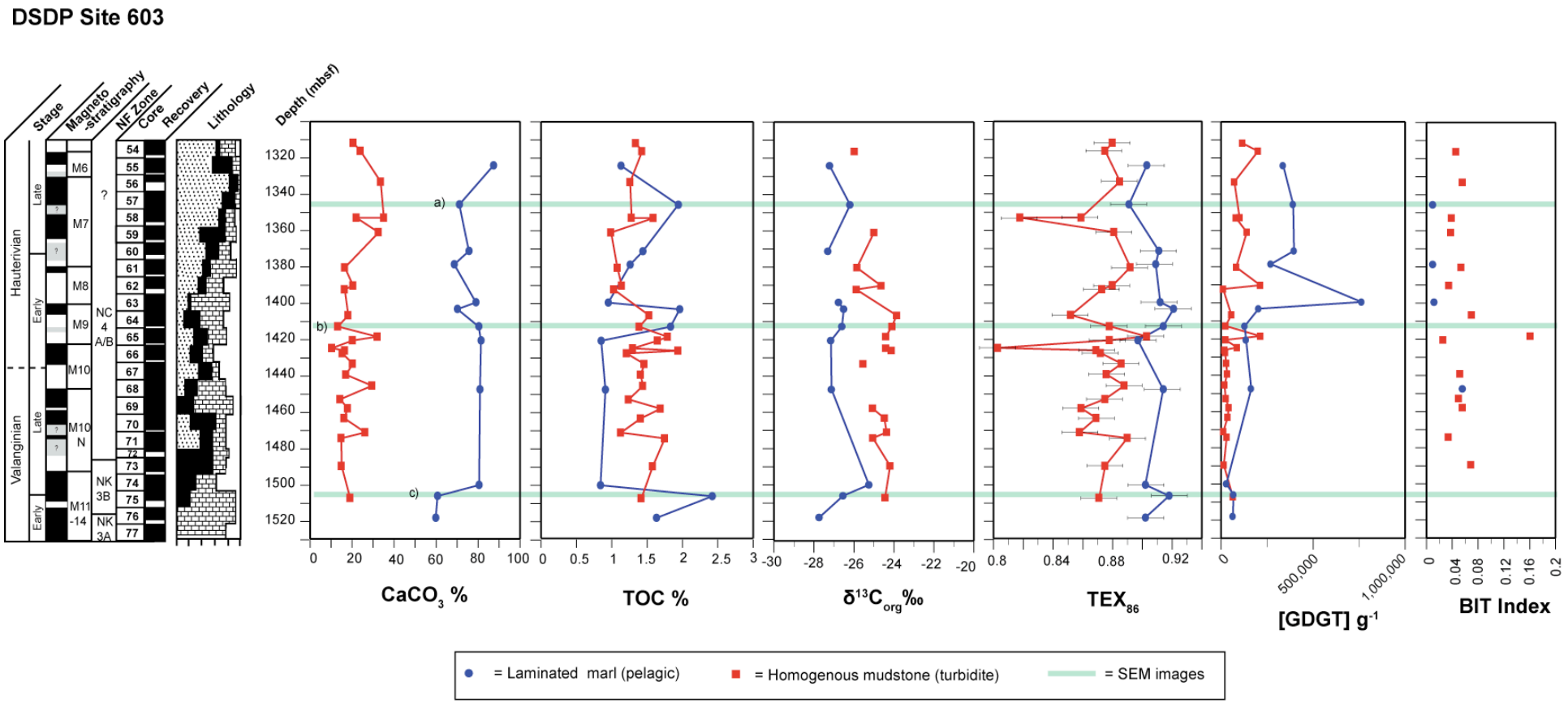

Figure 55 *.Geochemical results from the earliest Cretaceous of DSDP Site 603, showing $CaCO_3$ and TOC contents, $\delta^{13}C_{org}$ trends, TEX_{86} values, GDGT abundances and BIT Index values in each sample. In the TEX_{86} plot, the error bars denote the ±0.012 error seen in the long-term internal standard.*

$\delta^{13}C_{org}$ data

The bulk organic carbon-isotope record ($\delta^{13}C_{org}$) shows a consistent offset between the two lithologies much more clearly than the TOC record, with the homogeneous mudstones consistently having higher (more positive) values than the laminated marls (Figure 55). This is reflected in the ~2 ‰ difference in the average values between the two lithologies, which is far above the reproducibility of the standards of ±0.1 ‰, and is statistically significant according to the P value of <0.0001 (Table 3). Covariance is difficult to ascertain due to the lack of depth paring, but there does appear to be a broad covariance between the difference lithologies throughout the section, where relatively more positive $\delta^{13}C_{org}$ values in one lithology are accompanied by more positive values in nearby samples of the other lithology (Figure 55).

GDGT abundances, TEX_{86} ratios and maturation

In a very similar pattern to that observed at Site 534, the TEX_{86} ratios in the laminated marls, with average values of 0.908, and those in the homogeneous mudstones, with average values of 0.871, are offset on average by 0.037. This is three times the analytical error of 0.012 and corresponds to a temperature difference of ~1.2 ºC at these TEX_{86} ranges using the TEX_{86}^{H} (Kim *et al*., 2010) calibration, and ~0.8 ºC using the less sensitive reciprocal calibration (Kim *et al*., 2010, after Liu *et al*., 2009). The difference between the two lithologies in terms of TEX_{86} is certainly statistically significant with a P value of <0.0001 (Table 3). Although the overall difference in the two lithologies is significant, it is difficult to determine whether the individual data points are within error of one another, as the samples are only rarely depth matched (Figure 55). In the few occasions where two samples of different lithology are closely spaced, the trends are somewhat unclear, e.g. a homogeneous mudstone at 1507.05 mbsf, and a laminated marl at 1505.99 mbsf (labelled "c" on Figure 55), have a difference in TEX_{86} of 0.047 and are therefore significantly different, whereas as a pair at ~1420.40 mbsf have a difference in TEX_{86} values of only 0.019 and are therefore within error (1 standard devaition) of one another.

There is also a difference in TEX_{86} variability between the two lithologies, with the homogeneous mudstones being much more variable (standard deviation of 0.021) and the laminated marls having a more invariant record (standard deviation of 0.009) (Table 3, Figure 55). However, this variability may also be affected by the fact that there are 1.5 times more homogeneous mudstone data points, than laminated marl data points (Figure 55).

Similar to Site 534, a difference in GDGT abundance was observed between the two lithologies, with the laminated marls having higher abundances of GDGTs per gram of sediment extracted, normalised to a 100µl dilution ([GDGT g^{-1}]), than the corresponding homogeneous mudstones, above 1500 mbsf (Figure 55). This is reflected in the statistically significant difference in average GDGT abundance between the two lithologies, with the laminated marls having more than 3.5 times the abundances seen in the transported sediments (Table 3). Below 1500 mbsf the GDGT abundances in all samples are very low, regardless of lithology, which eliminates any difference between the mudstones and marls. No clear covariance in GDGT abundances between the lithologies in each pair is noted.

Similar to the results from Site 534, all six samples from Site 603 (1380 – 1560 mbsf) analysed for their hopane index were found to be below 0.5, and therefore were thermally immature (R. Pancost, *pers comm.*; Littler *et al*., 2011).

BIT Index

Although the abundances of branched GDGTs is very low at Site 603, it was possible to generate more BIT Index data than at Site 534, including 14 homogeneous mudstone and four laminated marl samples (Table 3). The difference in BIT Index between the two lithologies is demonstrated by an average value of 0.022 in the laminated marls and 0.056 in the mudstones (Table 3), with a trend for higher values in the mudstones observed above 1410 mbsf in the core (Figure 55). However this average difference in BIT Index between the two lithologies is not statistically significant at the 0.05 level, with a calculated P value of 0.071 (Table 3).

Geochemical cross-plots

As at Site 534, there is no observed relationship between TEX_{86} values and any of the geochemical parameters at Site 603 (Figure 56). There is a weak negative relationship between GDGT abundance and $\delta^{13}C_{org}$ in the mudstones ($r^2 = 0.391$), but no relationship between any of the other variables (Figure 56).

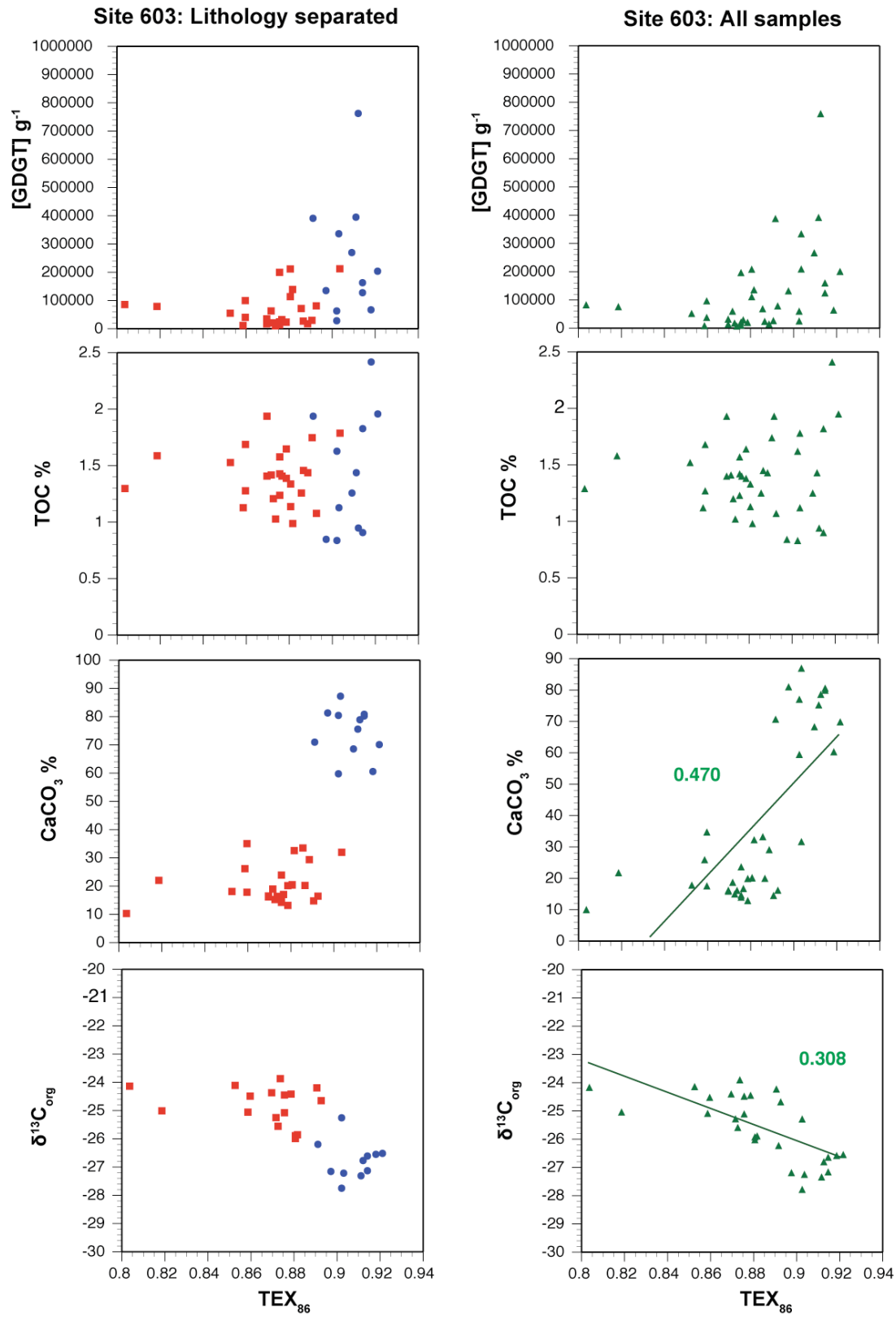

Figure 56a. *Cross-plots to show the relationships between TEX_{86} and other geochemical variables such as [GDGT], TOC%, $CaCO_3$% and $\delta^{13}C_{org}$. Where the R^2 value is <0.3, no regression line is shown.*

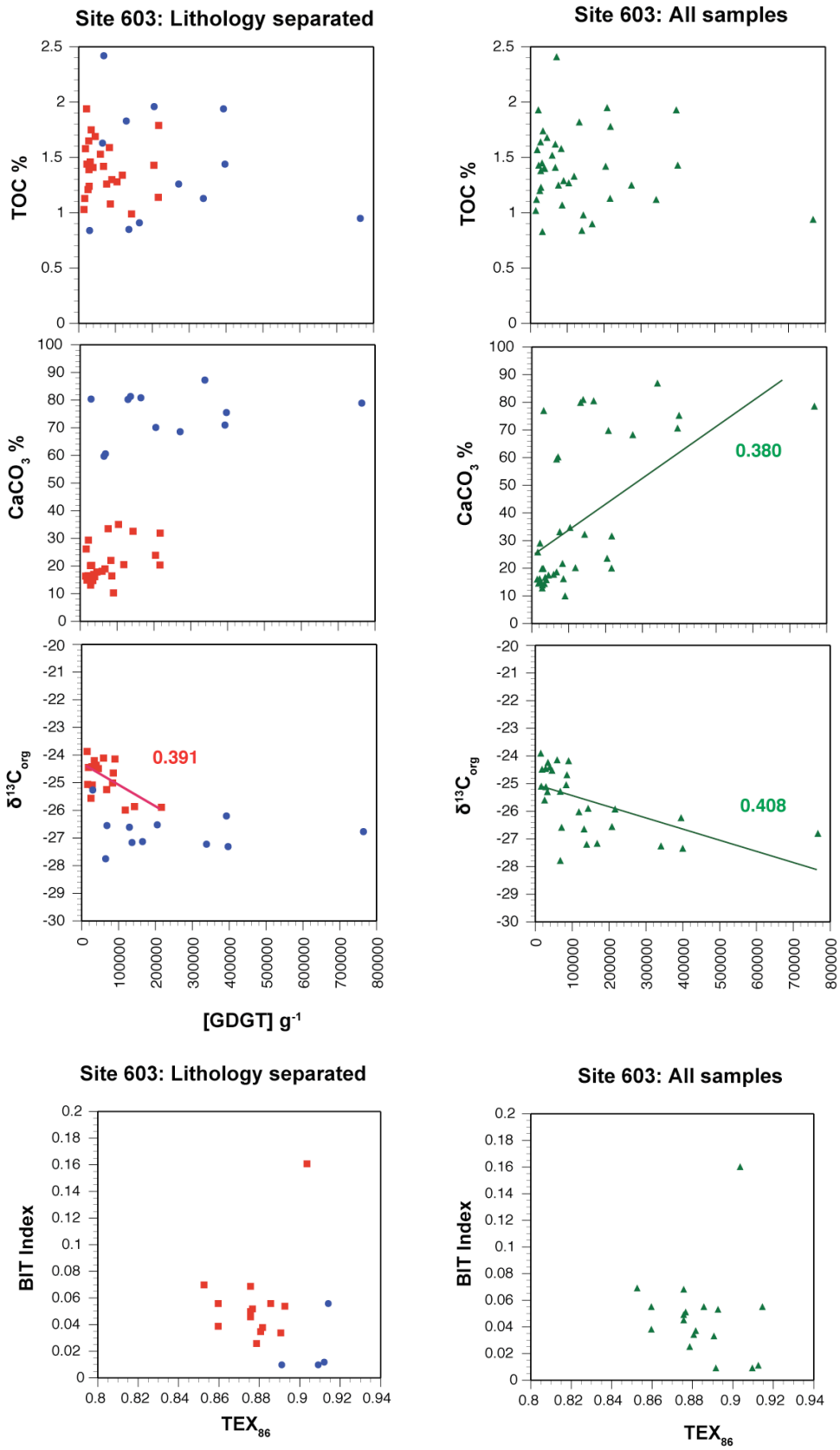

Figure 56b. *Cross-plots to show the relationships between and GDGT and other geochemical variables such as TOC%, $CaCO_3$% and $\delta^{13}C_{org}$, and between the BIT Index and TEX_{86} values. Where the R^2 value is <0.3, no regression line is shown.*

3. 5. DISCUSSION

3. 5. 1. A DIFFERENT ORIGIN FOR THE TWO LITHOLOGIES

It has been proposed in previous studies that the laminated marls and the homogeneous mudstones at Sites 534 and 603 have different depositional origins, with the former considered to be pelagic sediments and the latter to be transported sediments from the shelf (Sheridan *et al.,* 1983; Robertson & Bliefnick, 1983; Robertson, 1984; van Hinte *et al.,* 1987; Summerhayes, 1987; Dean & Arthur 1987; Covington & Wise 1987; Applegate *et al*., 1989). Although these previous interpretations used similar sedimentological, palaeontological and geochemical techniques to this study, it was felt necessary to confirm the different origins for the two lithologies in the same samples as the TEX_{86} data was taken from, as this is crucial for the subsequent interpretation of the TEX_{86} data.

From the new data, both Sites 534 and 603 display a clear difference between the laminated marls and the homogeneous mudstones, in terms of sedimentary constituents and geochemistry, and to a lesser extent calcareous nannofossil assemblages, which strongly suggests a different depositional origin for the two lithologies (Figures 40–43, 45, 48–52, 54).

Laminated marls

The laminated marls at both Sites 534 and 603 are predominantly composed of whole and broken calcareous nannofossils, with minor clay, which gives these marls a high average $CaCO_3$ content of ~75% (Table 2, 3; e.g. Sheridan *et al.,* 1983; Robertson & Bliefnick, 1983; Robertson, 1984; van Hinte *et al.,* 1987). This, coupled with the moderate–good preservation of the nannofossils observed in many samples in this study and the general lack of shallow-water neritic taxa, supports a deep open-marine setting above the calcite compensation depth (CCD) during the Early Cretaceous (Figure 43a, 52a). Previous thin-section observation has revealed that; "Individual laminations are typically seen to comprise numerous minute flecks of translucent brownish organic matter, plus occasional pyrite and dolomite in a micritic matrix…In some cases the organic matter is seen to be associated with relative enrichment of mica and fine quartzose silt. Radiolarian shells may either follow individual fine laminations or may be scattered randomly." (Robertson, 1984). The

difference between nannofossil preservation between these layers can be seen in the SEM images from sample 534A-69-05, 34 cm (1145.34 mbsf), where the very well-preserved delicate taxa in the coccolith-rich layer contrast with the less-well preserved and less diverse assemblage in the clay-rich layers (Figure 42b). Laminations are clearly visible in hand-specimen and in thin-section, however, the origin of these laminations at both Sites 534 and 603 and in the western North Atlantic more broadly, is less obvious.

As there is little evidence of either major dissolution of calcareous nannofossils in the clay-rich lamellae, or major secondary overgrowth in the carbonate-rich lamellae, pressure solution and a secondary diagenetic origin for the laminated marls can be largely discounted (Figures 41, 42, 49, 50, 51). This primary lamination could theoretically be the result of either cyclic changes in plankton and /or clay input, or be due to the action of bottom currents (Robertson, 1984). The laminations do not appear to be the result of current activity, as they are laterally continuous within the core and there is little evidence of ripples, scour marks, or cross-lamination which one would normally associate with such deposits (Robertson and Bliefnick, 1983; Robertson, 1984). It is likely, therefore, that the laminations are the result of cyclic changes in the input of either the calcareous nannoplankton, which make up the carbonate-rich laminae, or the siliciclastics, which compose the carbonate-poor layers. Much of the organic matter in the clay-rich lamellae is thought to be of terrestrial origin based on palynological analysis (Habib 1979), so it is concieveable that cyclic pulses of terrestrially-derived material periodically washed out into the deep sea and diluted the background carbonate sedimentation (Robertson, 1984). However, it is also possible that periodic increases in phytoplankton productivity in the western North Atlantic during the Early Cretaceous, possibly related to changes in circulation and upwelling, lead to increased deposition of coccoliths, which subsequently formed the carbonate-rich lamellae. This last explanation is favoured by both Robertson and Bliefnick (1983) and Robertson (1984), and is supported by the high radiolarian content of these marls, which may be suggestive of relatively fertile conditions.

Regardless of the initial origin of the lamination, the fact that the lamination is preserved in the sediment suggests exclusion of bioturbating benthos due to dysoxic conditions. This could indicate either extensive dysoxic bottom-water in the basin, or merely dysoxic conditions at the sediment water interface due to decomposition of

organic-matter in the sediments, combined with sluggish bottom-water circulation (e.g. Damaison & Moore, 1980; Robertson & Bliefnick, 1983; Robertson, 1984; van Hinte *et al.,* 1987; Summerhayes, 1987).

The calcareous nannofossil assemblages in the laminated marl, as described in this chapter, support a pelagic origin for this Early Cretaceous facies, with relatively high diversity. However, the assemblage is dominanted by the cosmopolitan *Watznaueria* genus, particularly *W. barnesiae,* which is not particularly diagnostic of any one despositional environment (Figures 43, 52); (e.g. Mutterlose 1991; Erba 1991; 1992a; Williams & Bralower, 1995; Herrle, 2003, Herrle *et al*., 2003; Mutterlose & Kessels, 2000). It is interesting to note that *D. lehmanii* is much more common in the marls than the mudstones, and that a prominent peak in abundance occurs during the Valanginian at both sites. This species has previously been associated with high fertility conditions (e.g. Erba *et al*., 2004), which combined with the relatively high radiolarian content at both Sites 534 and 603, suggests a fertile Valanginian proto-North Atlantic (Robertson, 1984).

The abundance and distribution of nannoliths in the laminated marls is not the same at Site 534 and 603 (Figures 48, 45, 48, 54). At 534 the abundance of *Nannoconus* spp*.,* and *Micrantholithus* spp. where present, ranges between Absent to Few, but no coherent trends overall are identified between the two lithologies. However, at Site 603 *Nannoconus* spp. are generally absent in the marls, while *Micrantholithus* spp. are found rarely to occasionally, and *C. rothii* is very rare overall. The near absence of nannoliths in the marls at Site 603, and the higher abundance in the mudstones, tentatively supports a pelagic origin for the marls and a more neritic origin for the mudstones (e.g. Covington & Wise, 1987; Applegate *et al*., 1989).

At Site 534 the marls have a lower TOC content than the mudstones (Table 2; Figure 46a), which could be the result of a greater addition of terrestrial material to the mudstones relative to the marine organic-matter dominated marls (Table 2). The type of organic-matter in the Blake Bahama Formation sediments at both Sites 534 and 604, has previously been characterised with Rock Eval pyrolysis techniques, which suggests a mixture of marine and terrestrial organic-matter in both lithologies (Figure 57; e.g. Katz 1983; Dean & Arthur 1987; Meyers, 1987; Herbin *et al*., 1987). However, lithologically-separated data from Site 603 suggests that the organic-matter in the mudstones has a more terrestrial affinity than the organic-matter in the

laminated marls (Dean & Arthur 1987). The new data from 534 (for which no OI value can be determined) also appears to show similar trends, with both lithologies being characterised by a mixture of marine (Type II) and terrestrial (Type III) organic-matter, but the organic-matter in the mudstones having a slightly stronger terrestrial affinity than the marls (Figures 46b, 58; e.g. Katz 1983; Dean & Arthur 1987; Meyers, 1987; Herbin *et al*., 1987). The average bulk-organic carbon-isotope value in the marls at both sites is ~27 ‰, which suggests a strong marine influence in these sediments, compared to somewhat heavier values in the mudstones (Tables 2, 3; Figures 46a, 55).

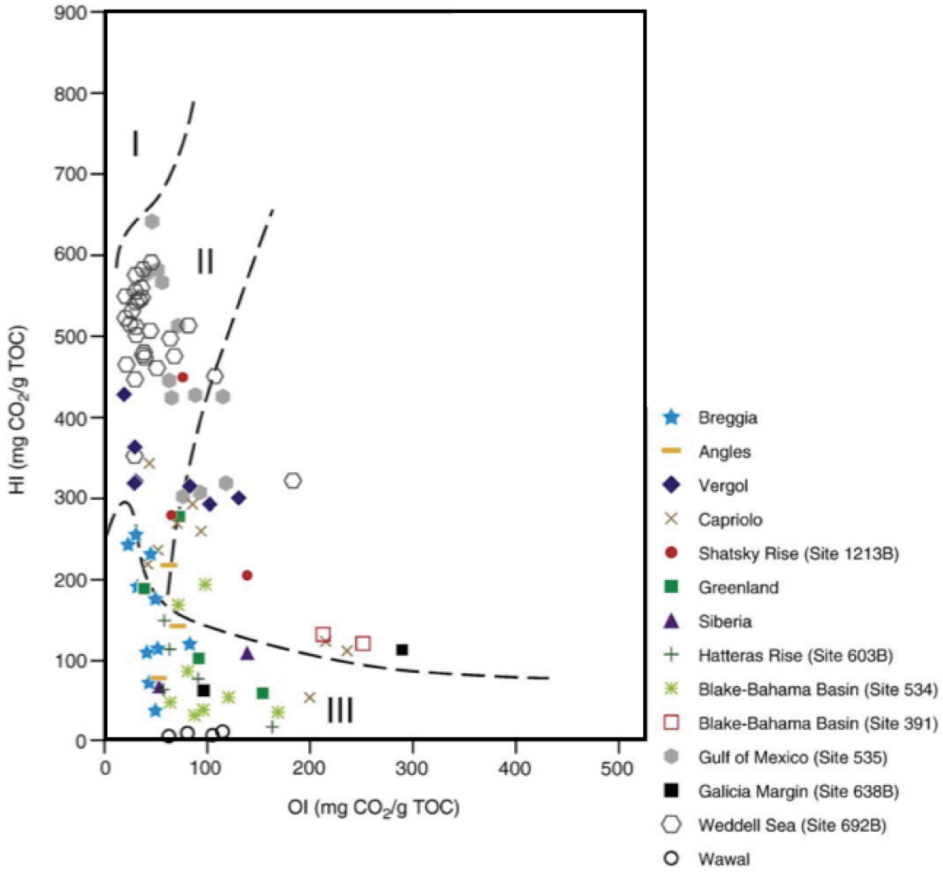

Figure 57*. Modified Van Krevelen diagram showing a compilation of Rock Eval pyrolysis data from Valanginian sections, compiled by Westermann et al. (2010). Site 603 data from Meyers, (1987) and Herbin et al. (1987); Site 534 data from Katz (1983).*

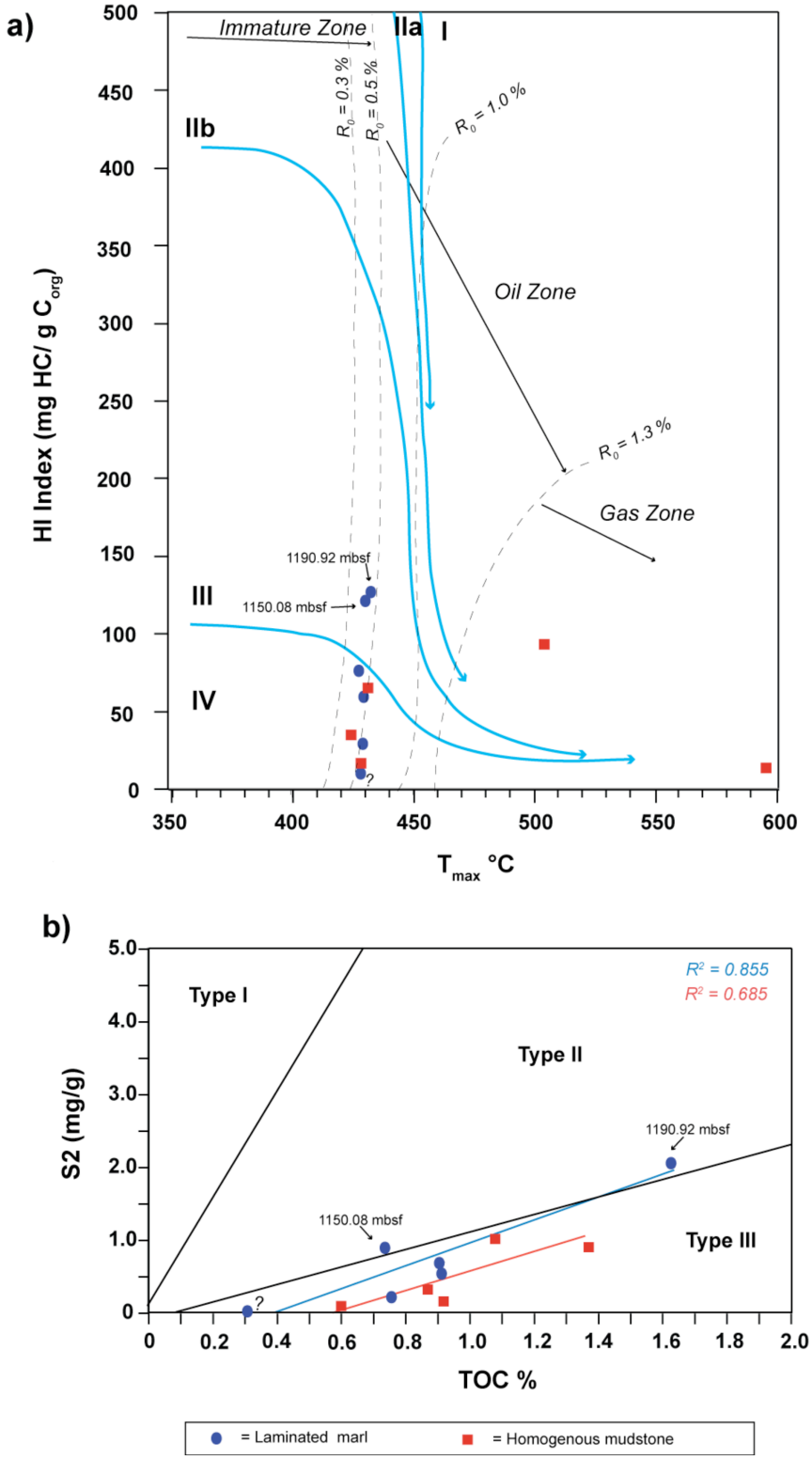

Figure 58. *Rock Eval pyrolysis data for 11 of the Site 534 samples. Panel* ***(a)*** *modified Van Krevelen diagram after Delvaux et al. (1990) showing Tmax against the Hydrogen Index. I = marine organic matter, II = mixed marine and terrestrial organic matter, III = terrestrial organic matter, IV = inert terrestrial organic matter;* ***(b)*** *crossplot after Langford and Blanc-Valleron, (1990) showing wt% TOC against S2, which is the mass of hydrocarbons released during thermal cracking of sedimentary kerogen.*

Homogeneous mudstones

The homogeneous mudstones are dominated by clay, fine siliciclastics and opaque minerals, and are dominated by smectite with minor chlorite and palygorskite (Robertson & Bliefnick, 1983; van Hinte *et al.,* 1987). Small pyrite framboids are relatively common in the mudstones, and often occur in clusters, indicating reducing conditions and anoxia within the sediments, probably related to the greater proportion of organic-matter in the mudstones, which is known to facilitate pyrite formation (e.g. Robertson & Bliefnick, 1983; Wignall *et al*., 2005). Nannofossils only constitute a minor part of the lithology and $CaCO_3$ contents average 20–25% at both sites (Tables 2, 3; Figure 46a, 55). The higher proportion of clay and siliciclastics alone suggests a more proximal setting for the initial deposition of the homogeneous mudstones, but clay-rich layers can also occasionally be the result of dissolution events (e.g. the Palaeocene Eocene Thermal Maximum horizon in the Early Eocene; e.g. Zachos *et al*., 2005), which must be considered as both Sites 534 and 603 were deposited close to the CCD (~3500 m; Sheridan *et al.,* 1983; Robertson & Bliefnick, 1983; van Hinte *et al.,* 1987). However, when the often Moderate–Good preservation of the calcareous nannofossils in these mudstone horizons is considered, this notion can quickly be dismissed (Figures 40, 43a, 48, 52a).

The mudstone beds vary in thickness from <1 cm, to >20 cm, and where the core is suitably well-preserved, sharp contacts between the intercalated mudstones and the underlying carbonates are common, with occasional scour marls suggesting energetic and instantaneous emplacement (Figure 39; Robertson & Bliefnick, 1983; Robertson, 1984; van Hinte *et al.,* 1987). Occasional normal grading (fining upwards) is seen in the base of the thicker beds; however, the mudstones are commonly homogeneous and lack the laminations that are characteristic of the pelagic marls (Figure 39). This suggests turbulent deposition or very active bioturbation, of which the former is most likely considering the sedimentological evidence for energetic lateral emplacement given above (Figure 39; Robertson & Bliefnick, 1983; Robertson, 1984; van Hinte *et al.,* 1987). The general lack of obvious bioturbation structures, except for minor *Chondrites* near the top of some of the mudstone beds, suggests generally dysoxic conditions similar to those present when the intercalated laminated marls were deposited (e.g. Robertson & Bliefnick, 1983). However, the homogeneous nature of the deposits could, conversely, suggest

intense bioturbation of the sediment, which seems unlikely considering the normal grading which is occasionally preserved at the base of these beds.

The mudstones overall are characterised by a rich diversity of calcareous nannofossils, which are generally moderately–well-preserved, with occasional very good preservation of small and dissolution-susceptible taxa (Figures 40, 43a, 48, 52a). Most diagnostic are the abundance of the nannoliths, such as *Nannoconus* spp.*, Micrantholithus* spp. and *Conusphaera rothii,* which at Site 603 appear to be more common in the mudstones than the marls (Figures 48, 52b), although due to the high temporal varience the mean values are within error of one another (Figure 40). These three taxa have all been associated with a thermophilic and shelf-dwelling existence, and therefore should be more abundant in sediment deposited in a proximal environment than in a fully pelagic setting in the proto-North Atlantic (e.g. Applegate *et al*., 1989; Erba, 1994; Erba, 1987, Mutterlose, 1991, Erba *et al*., 1992, Herrle *et al*., 2003a). This general trend is demonstrated by the high abundance of nannoconids in the more marginal western Tethys, where they can constitute up to 40% of the assemblage, and the generally much lower occurrence in the more open-ocean proto-North Atlantic sites (e.g. Covington & Wise, 1987; Applegate *et al*., 1989; Channel *et al*., 1993). In support of a shelf origin for the mudstones at Site 534, rare *C. rothii* occur in three mudstones samples but only in one marl sample, thus also tentatively supporting a shelf-origin for the mudstones at this site (Figures 45). The mean abundances of all other calcareous nannofossil taxa, except for *D. lehmanii,* are within error of one another in both the laminated marl and homogeneous mudstones halves of the pairs, and therefore are not useful in distinguishing the two lithologies (Figures 40, 43b, 48, 52b).

As discussed above, the higher TOC in the mudstones relative to the marls at Site 534 (Tables 2, 3; Figures 46a, 55) is likely to be due to the addition of extra terrestrial matter in the former. This is supported by the limited pyrolysis data (Table 2, Figure 46b; Katz, 1983; Dean & Arthur 1987), palynology (Habib, 1987), and by the fact that the bulk-organic carbon-isotope values in the mudstones average -25 ‰, at least 1.5 ‰ lighter than their $CaCO_3$-rich counterparts on average at both sites (Tables 2, 3; Figure 46a, 55). This range in carbon-isotope values is similar to the reported $\delta^{13}C_{org}$ values of pre-Neogene terrestrial organic-matter (~-20 to ~-26 ‰), which is frequently heavier than contemporaneous samples dominated by marine kerogen (~-24 – -29 ‰); (Tyson, 1995; Figure 59).

The BIT Index evidence from Sites 534 and 603 is rather scant, due to the very low abundance of branched GDGTs in all samples irrespective of lithology, which alone suggests minimal soil-based terrestrial input for all Berriasian–Hauterivian sediments studied (Table 2, 3; Figure 52a, 43a). However, from the limited data available generally higher BIT Index values are noted in the homogeneous mudstones relative to the laminated marls (Table 2, 3; Figure 52a, 43a). These trends suggest a higher terrestrial component in the mudstones *vs*. the marls, consistent with the results from $^{13}C_{org}$ data, although they do suggest that the majority of the organic matter in both lithologies is of marine origin, contrary to the tentative Rock Eval pyrolysis data from Site 534, which suggests a dominantly terrestrial origin for the organic-matter in both lithologies (Figure 58).

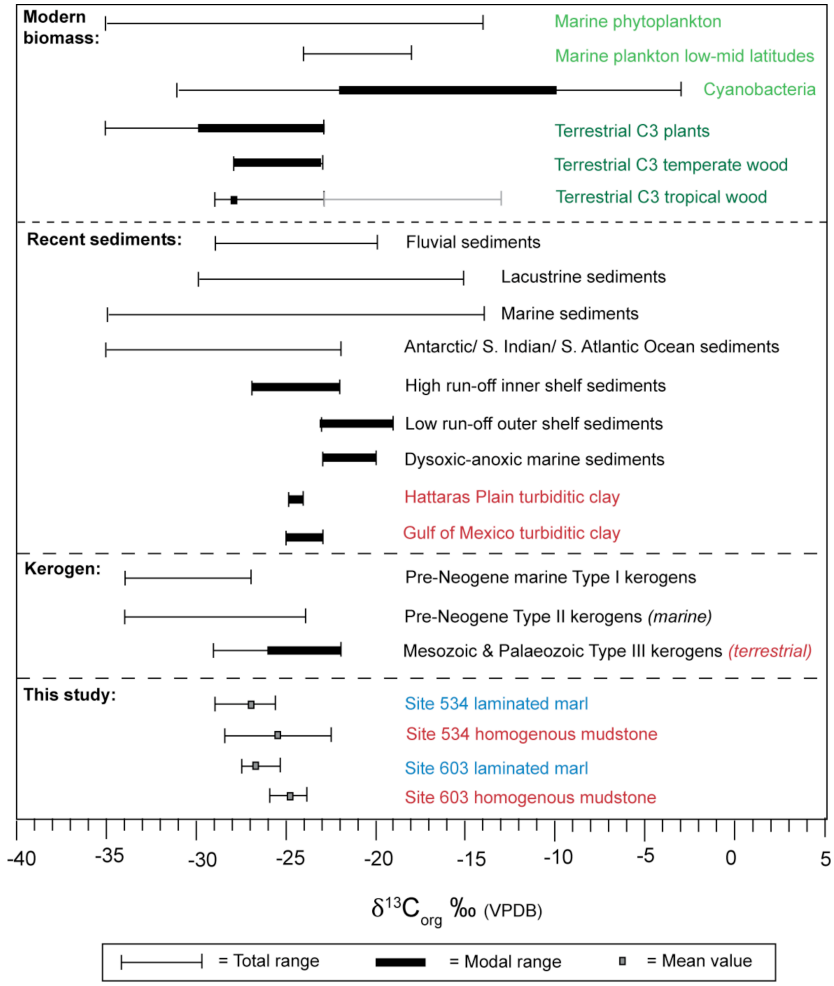

Figure 59. *Carbon-isotope ranges for modern biomass and sediments, and pre-Neogene kerogen, compared to the isotopic ranges seen in the bulk organic matter at Sites 534 and 603 (from various sources, compiled by Tyson (1995)).*

Pelagic vs. transported sediments

In conclusion, sedimentological, geochemical and some palaeontological data strongly suggest that the laminated marls and the homogeneous claystones have different primary depositional origins, with the laminated marls likely being deposited *in situ* in a dysoxic, open-ocean setting, and the homogeneous marls being transported from the shelf regions. These findings are wholly in agreement with earlier studies at these sites based on sedimentology and palaeontology (e.g. Robertson & Bliefnick, 1983; Robertson, 1984; Applegate *et al*., 1989, Covington & Wise, 1987), and confirm that the differences in TEX_{86} are associated with different depositional styles. However, the mechanism for transport of these fine mudstones into the deep-sea from the shelf is not entirely clear, as they do not represent "classic" Bouma sequence coarse siliciclastic turbidites, in the same way as the graded sandstone deposits at Sites 534 and 603 clearly do (e.g. Robertson & Bliefnick, 1983). The coarser sandstones were likely to have been delivered from the shelf to the deep-sea though turbidites funnelled down submarine canyons, and therefore probably represent geologically instantaneous events (Robertson & Bliefnick, 1983; Figure 60). This is especially clear at Site 603 where the sandstones are thought to represent the edge of a large submarine fan (van Hinte *et al*., 1987). The dark grey claystones, however, have a completely separate geometry and occurrence from the coarser sandstone bodies and may therefore have a different transport path (Figure 60).

It may be that the finer cays and silts were deposited on the upper continental rise within an expanded oxygen-minimum zone (thus enhancing their organic-matter preservation potential), before being caught up in downward-slope processes such as a high-density, non-turbulent turbidity currents, leading to final deposition in the deep-sea as "homogenites" (e.g. Robertson & Bliefnick, 1983; Robertson, 1984; McCave & Jones, 1988). Such ungraded mudstone deposits, with thicknesses up to 15m, are seen in recent deposits in the Madeira Abyssal Plain (MAP) region of the North Atlantic (McCave & Jones, 1988).

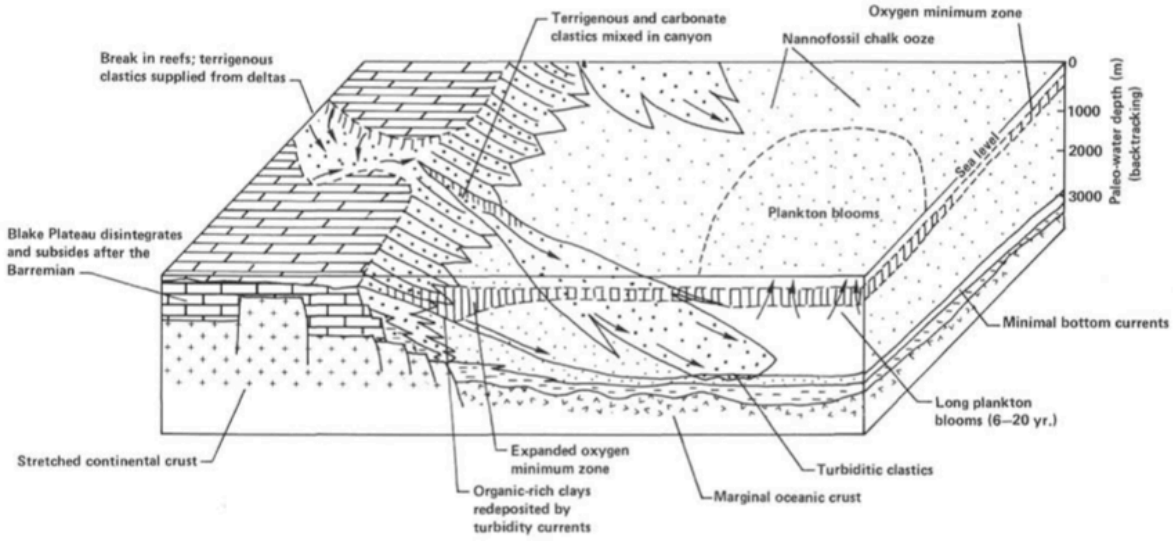

Figure 60. *Block model showing likely depositional processes in the western North Atlantic in the Hauterivian–Barremian, taken from Robertson & Bliefnick (1983).*

3. 5. 2. WHAT IS CAUSING THE LITHOLOGICAL OFFSET IN THE TEX_{86} RATIO?

There is no clear relationship between TEX_{86}, GDGT abundances and any of the geochemical parameters such as TOC or $\delta^{13}C_{org}$ at either of the sites, (Figure 47, 56). First and foremost this suggests that TEX_{86} ratios in these sediments, irrespective of lithology, are dominantly controlled by SST and not by other variables, which should give confidence in their use for palaeotemperature reconstruction. However, average differences of between ~0.02 and ~0.04 in TEX_{86} ratios are observed between the autochthonous laminated marls and the transported homogeneous claystones at both Sites 534 and 603 (Tables 2, 3; Figures 46a, 55). Although this offset in TEX_{86} is small, equating to just ~0.8 ºC at Site 534 and 1.2ºC at Site 603 (TEX_{86}^{H} calibration; Kim *et al*., 2010), this difference is significant, being at least twice the analytical error in both cases. At Site 534, where the depth pairing of samples is most robust, it is clear that although some of the individual pairs lie within error of one another, there is not a single occasion in the ~10 myr study interval where a homogeneous mudstone yields a warmer SST estimate than the corresponding marl (Figure 46a). Similarly, although the poorer depth paring at Site 603 precludes such detailed comparison, the laminated marls clearly yield

consistently higher TEX_{86} values and therefore warmer SST estimates than the transported mudstones throughout the Valanginian–Hauterivian (Figure 55). The greater variability in the TEX_{86} values in the homogeneous mudstones relative to the marls is also noted, particularly at Site 603 (Figures 46a, 55). This is important, because if the data at both sites were plotted without lithological separation, the apparent variation in SST would be far greater during the Berriasian–Hauterivian than is suggested by examining the pelagic sediments in isolation. The difference in the GDGT abundance between the two lithologies is also noted, with the pelagic marls almost always having higher concentrations than the homogeneous mudstones at both sites (Table 2, 3; Figures 46a, 55). The key question therefore is, what is causing this offset in both the TEX_{86} ratios and the GDGT abundance?

The TEX_{86} ratio is based on the distribution of GDGT molecules found within the sediment, which is thought to reflect a surface-ocean temperature signal derived from Crenarchaeota living in the shallow regions of the ocean (e.g. Schouten *et al*., 2002; Kim *et al*., 2008; 2010). However, as discussed previously (Section 1-6) there are other complex variables that can affect this ratio in a sediment sample besides the SST of the seawater in which the Crenarchaeota live. These variables can broadly be divided into two categories: primary oceanographic or biological variations that occur in the water column; and post depositional, secondary diagenetic effects such as oxic degradation of the GDGTs.

These variables can be summed up as three hypotheses to explain the observed differences in TEX_{86} and GDGT concentrations between the pelagic and transported facies at Sites 534 and 603:

(1) The TEX_{86} ratios are genuinely recording a difference in SST between the two areas of ocean that the crenarchaeotal GDGTs are sourced from (e.g. the shelf vs. the deep sea);

(2) The difference in TEX_{86} values does not represent true SST variation and is being skewed by different populations of Crenarchaeota that inhabit the open ocean and the shelf regions, which have different responses to SST;

(3) The TEX_{86} values of one or both of the lithologies has been influenced by secondary diagenesis, probably related to oxic degradation, which has altered the primary GDGT and SST signal, and therefore the difference is unrelated to either primary SST or biological differences.

3. 5. 2. 1. A GENUINE DIFFERENCE IN SSTS OR THE EFFECTS OF UPWELLING?

As discussed above, the mudstones at Sites 534 and 603 represent deposition by turbidites, bringing sediment and organic matter into the open-ocean from the shelf regions, while the laminated marls represent *in situ* pelagic sedimentation. The GDGTs used to reconstruct the TEX_{86} proxy are contained within the organic matter, so it is reasonable to expect a different distribution of GDGTs in the mudstones and the marls, due to the different provenance of the bulk-organic matter in each lithology. It is possible that the shelf regions had different average annual SSTs to the open ocean, as is seen in the modern oceans where seasonal coastal upwelling of deeper waters along some coastlines leads to cooler temperatures at the surface (e.g. offshore western North America, offshore southwest Africa; Figure 23; Bakun, 1990).

Some coastal upwelling is semi-permanent, such as that off the coast of Peru and southwest Africa, while in other regions the upwelling is more seasonal, and in the case of western North America is strongest during the spring-summer months, April–July (e.g. Bakun, 1990). The areas of the strongest coastal upwelling in the modern ocean are often concentrated on the western boundaries of continents, (Figure 61a). However, somewhat cooler waters are found today in the modern western North Atlantic compared to the eastern side of the basin, largely due to the action of the North Atlantic Gyre and the Gulf Stream surface currents bringing warm water from the Caribbean region to Western Europe (Figure 61b). As Sites 534 and 603 occupy the western side of the North Atlantic basin, and would also have done so in the earliest Cretaceous, is there any reason to suspect that upwelling or cooler waters might have occurred in the western proto-North Atlantic?

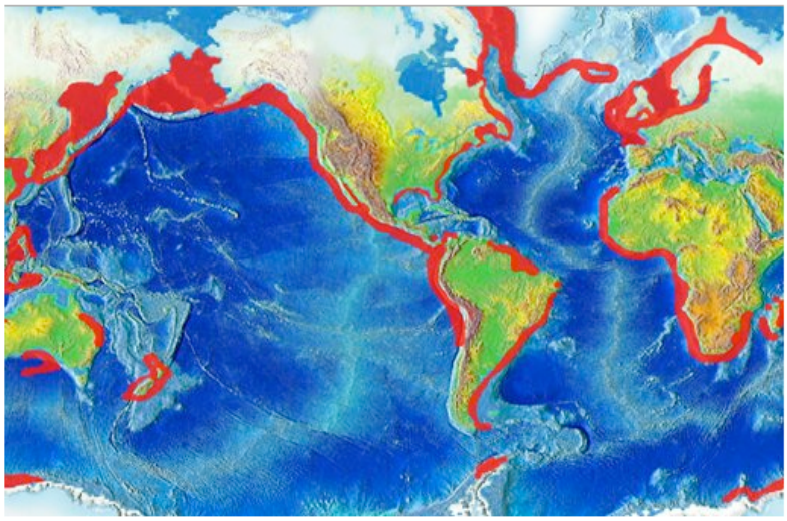

***Figure 61a**. Modern areas of major upwelling, both seasonal and permanent, indicated in red (http://oceanservice.noaa.gov).*

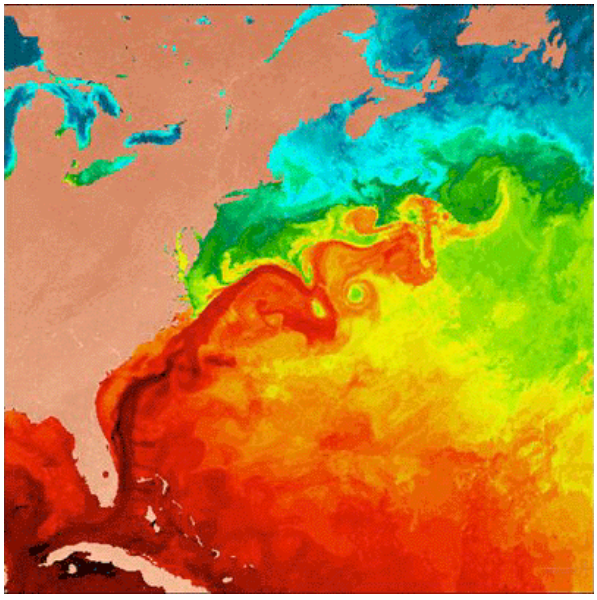

***Figure 61b**. Modern variation in SSTs in the N. Atlantic, showing the action of the Gulf Stream transporting warm water (red colours) from the lower latitudes of the western N. Atlantic to the eastern N. Atlantic (http://seacoos.org).*

In modern oceans, high abundances of radiolarians (>30%) in surface pelagic sediments are only round in areas associated with enhanced fertility, such as the equatorial Pacific and the high-latitude Southern Ocean (e.g. De Wever *et al*., 2001). This modern association has lead to an assumption that an enhanced radiolarian content in Mesozoic sediments is indicative of productive waters at the time of

deposition (e.g. Erba, 1992; Muttoni *et al*., 2005). Therefore, the relatively high (Common to Abundant) radiolarian content in the pelagic marls at both Sites 534 and 603, indicates a generally fertile western proto-North Atlantic, probably primarily a result of high riverine input from the surrounding continents delivering nutrients to the basin, and perhaps a component of upwelling of deeper nutrient-rich waters in some parts of the ocean (Sheridan *et al.,* 1983; van Hinte *et al.,* 1987; Robertson & Bliefnick, 1983; Robertson, 1984). The calcareous nannofossil/ clay laminations in the marls probably represent periodic increase in phytoplankton productivity, perhaps related to episodes of upwelling or changes in surface ocean circulation in the proto-North Atlantic (Robertson & Bliefnick, 1983; Robertson, 1984). Calcareous nannofossil assemblages also indicate an increase in ocean fertility at the Berriasian–Valanginian boundary at both Sites, which persisted into the Valanginian–Hauterivian (Bornemann *et al*., 2008). That the earliest Cretaceous proto-North Atlantic in general was relatively fertile is clear, but is there any evidence for coastal upwelling in the western proto-North Atlantic in particular, which might have lead to a temperature difference between the shelf and the deep sea?

In the Early Cretaceous the proto-North Atlantic was much smaller and probably had only shallow to mid-bathyal connections to the Pacific (Panthalassa) to the west, and a somewhat deeper connection to the Tethyan Ocean to the east (e.g. Robertson & Bliefnick, 1983; Summerhayes 1987; Puceat *et al*., 2005). Modelling evidence suggests that despite the apparently restricted nature of the basin, a weak western boundary current, similar to the modern day Gulf Stream, existed in the proto-North Atlantic as early as the Late Jurassic Kimmeridgian stage, which increased in strength during the Early-mid-Cretaceous (Handoh *et al*., 2003). However, results of modelling studies based on wind stress fields predicated by general circulation models, suggests upwelling was more likely on the eastern side of the basin rather than in the west during the Late Jurassic–Early Cretaceous (Parrish & Curtis 1982; Handoh *et al*., 2003; Figure 62). This is also supported by the increased marine organic-matter content of lower Cretaceous sediments on the eastern side of the North Atlantic, suggesting higher marine productivity relative to the western side, which is attributed to enhanced upwelling on this side of the basin (Summerhayes, 1987).

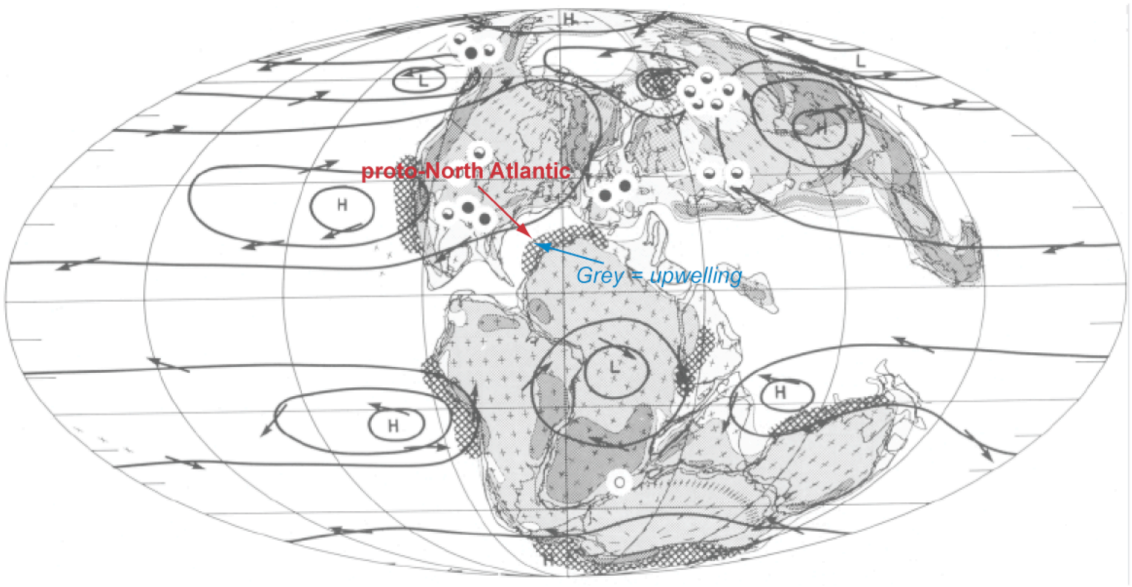

***Figure 62a**. Late Jurassic (Volgian) reconstruction of ocean circulation and upwelling (cross-hatched area). (Parrish & Curtis, 1982).*

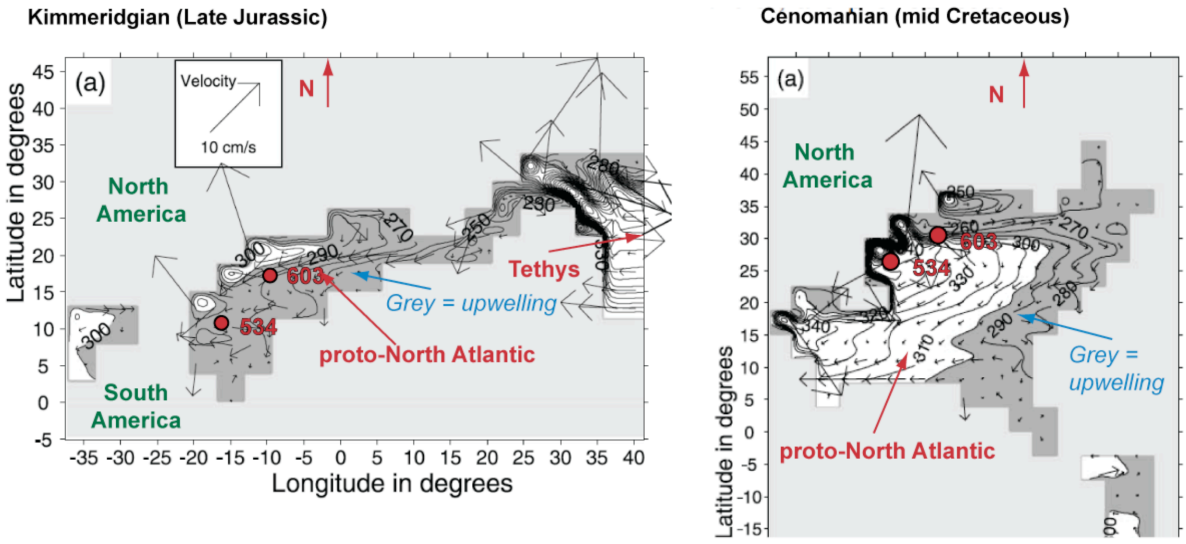

***Figure 62b**. Late Jurassic and mid Cretaceous reconstructions of upwelling in the North Atlantic, from Handoh et al. (2003). No Berriasian-Barremian aged simulation was carried out in this study.*

It is therefore possible there was sufficient upwelling on the western side of the basin to cause a minor SST difference between the shelf and the deep-sea. However, if the difference in TEX_{86}-derived SSTs between the shelf and open ocean

sediments was purely a function of genuine SST variation, why is there a difference in GDGT abundance between the marls and the mudstones? (Tables 2, 3; Figures 46a, 55). Surely if the only parameter that was changing between the two regions was SST, the GDGT abundances would be expected to be roughly equal between the two lithologies, or perhaps even higher in the mudstones which have higher TOC contents and were likely deposited in the anoxic region of the shelf, which favours better preservation.

Another important point to consider in terms of the biological basis for the TEX_{86} proxy is that should there be a component of upwelling in the shelf region, in addition to lowering the SSTs, the upwelling water would also bring Crenarchaeota from the deeper waters of the thermocline to the surface. The distribution of the GDGTs within this deeper water mass may faithfully record *in situ* temperature of the cooler water of the thermocline where they were synthesised, which would then likely be scavenged in the photic zone and exported to the sediment, thus potentially biasing the TEX_{86} "SST" reconstruction. This phenomenon of cooler than expected SST estimates has been observed in the modern Santa Barbara Basin by Huguet *et al*. (2007), but not in the Arabian Sea (Wuchter *et al*., 2005; 2006b), which both experience strong seasonal upwelling. However, in the absence of any detailed evidence for strong upwelling in the coastal regions, it is impossible to better constrain this variable at present.

Could genuine temporal climate variability be responsible for the offset in TEX_{86}-derived SST between the mudstones and the marls? Although cyclic alternations in Early Cretaceous climate, similar to glacial-interglacial type alternations in the Pleistocene, have previously been proposed on the basis of oxygen-isotopes and Sr/Ca ratios in marine sediments (e.g. Stoll & Schrag, 1996), these fluctuations have principally been recorded in pelagic marl-limestone couplets, not marl-mudstone couplets. Importantly, many of these supposed cyclic variations have been shown to be artefacts of diagenetic alteration of geochemical signals in deep-sea sediments (e.g. Frank *et al*., 1999), and therefore cannot be invoked as the origin of the TEX_{86} SST offset. Could the emplacement of the mudstone turbidites themselves be paced by orital forcing? It is possible that there is a cyclicity in the deposition of the mudstones, driven by cyclic changes in climate and sediment supply to the shelf, but both the relative spacing and the absolute time that elapsed between each successive turbidite is difficult to determine. This is primarily due to

incomplete core-recovery and the large uncertainties that remain in the age models at both sites (Section 2-1-4). Regardelss, as the mudstones and the marls have been shown to originate in different parts of the ocean (see above), it would be difficult to deconvolve the temporal signal from the spatial one.

Therefore on the balance of available evidence, neither upwelling-related differences in SST nor genuine climatic variability, seems able to explain the differences in TEX_{86} observed between the shelf and open-ocean SSTs at Sites 534 or 603, although such spatial differences in SST are difficult to rule out completely considering the paucity of the modelling and proxy data for the earliest Cretaceous (e.g. Handoh *et al*., 2003).

3. 5. 2. 2. BIOLOGICAL EFFECTS ON TEX_{86} SST ESTIMATES

A change in the population of GDGT-producing organisms in the water column (principally the Group 1.1 Crenarchaeota) could potentially influence the TEX_{86} ratio, as they may have a different response to temperature with regards to the distribution of their membrane GDGTs for a given SST. Even if the surface-water temperatures in the two source regions were identical, it is possible that coastal or shelf regions harboured different populations of Crenarchaeota with different responses to ambient temperature to the open-ocean regions, meaning that transported shelf sediments containing exotic GDGTs may not yield the same TEX_{86} value as the surrounding pelagic facies. Indeed, Turich *et al*. (2007) suggested that changes in TEX_{86} values were affected by issues such as changes in archaeal community structure due to nutrient availability, and that different regions of the world oceans were characterised by different populations. A marine epipelagic (<100m) group, a marine mesopelagic (200–1500 m) and a marine upwelling group of GDGT-producing crenarchaeaota were recognised, suggesting that different populations of these organisms could indeed inhabit the open-ocean and an upwelling-prone shelf (Turich *et al*., 2007). However, this finding was disputed by Schouten *et al*. (2008a) and no such genetic or geochemical divide between coastal marine and deep-sea populations of Crenarchaeota has been documented in other studies, with the exception of the Red Sea where a different subset of Crenarchaeota

are thought to dwell due to the elevated salinity conditions there (e.g. De Long, 1992; Kim *et al*., 2008). Additionally, the basis for different crenarchaeotal assemblages in the shelf and the deep appears to rest upon the existence of an upwelling regime in the shelf regions which, as discussed above, has not been clearly demonstrated for the western proto-North Atlantic in the earliest Cretaceous. Any difference in crenarchaeotal populations would also have to have a biological basis, i.e. there must be differences in key parameters such as nutrient availability, or competition from other organisms for resources for different populations to favour different marine regions.

Even if the pelagic Crenarchaeota can be assumed to be relatively cosmopolitan, and endemic coastal populations in the Early Cretaceous did not exist, the issue of *in situ* production of GDGTs in the sediments can also not be ignored. It is possible that different degrees of deep-biosphere archaeal activity, and therefore sedimentary GDGT production, occurred during deposition of the different lithologies (e.g. Turich *et al*., 2007; Shah *et al*., 2008). Elevated *in situ* production of GDGTs may have occurred on the anoxic shelf during the initial deposition of the mudstones, which may have subtly altered the original pelagic GDGT ratios. If such differential sedimentary GDGT production did occur it is likely to have been during this shelf deposition, rather than after the mudstones had been redeposited in the open-ocean, as it is difficult to imagine how different populations of archaea could be come established in such a short window of time. However, the greater abundance of GDGTs in the marls relative to the mudstone would not seem to fit with the notion of greater *in situ* sedimentary production in the mudstones due to anoxia on the shelf, as this would be expected to increase, not reduce, the abundance of GDGTs in the mudstones through additional archaeal activity (Figure 46b, 55). Why greater *in situ* sedimentary production of GDGTs should occur in the deep waters of the pelagic zone within the carbonate-rich marls is also unclear.

Unfortunately, there is no way at present of independently determining whether the GDGTs which dominate the earliest Cretaceous marls and mudstones, were synthesised by different populations of organisms, either in the water column or in the sediment. Although in recent and Holocene-Pleistocene sediments it may be possible to use DNA or ^{14}C to distinguish between water column or sedimentary GDGT production (e.g. Inagaki *et al*., 2006; Biddle *et al*., 2006; Shah *et al*., 2008), this is clearly not possible for sediments of Early Cretaceous age. Therefore

speculation based on the relative distribution of the GDGTs between the two sediments, the abundance of these molecules and their relationship to other parameters such as TOC % and $\delta^{13}C_{org}$ is the only option remaining.

3. 5. 2. 2. DEGRADATION AND DIAGENESIS

A final option to explain the offset in the TEX_{86} ratios and GDGT abundances between the laminated marls and the transported mudstones, is the effects of differential secondary alteration of the GDGT distribution due to diagenesis. Excessive thermal maturation has been shown to change the distribution of the GDGTs and therefore the TEX_{86} ratio in laboratory pyrolysis experiments, leading to the recommendation that overly mature sediments be avoided in palaeoclimate reconstructions (Schouten *et al*., 2004). However, despite the earliest Cretaceous sediments being subjected to great burial depths in the modern of >950 mbsf at Site 534 and > 1320 mbsf at Site 603, there is no systematic change in the TEX_{86} ratio with increasing depth in the core, as would be expected with increasing maturation (Figures 46a, 55). Additionally, the hopane index at both sites showed no evidence for overmaturation at either site (Sections 3-4-1-2 and 3-4-2-2). These data did not reveal any systematic changes in maturation with depth, nor any values over the maturation threshold for reliable TEX_{86} SST reconstruction, as suggested in Schouten *et al*. (2004). Additionally, if any maturation effects had occurred there is no reason to suspect that the maturation of the organic matter in the homogeneous mudstones would be any more advanced than that in the adjacent laminated marls, as both would have been buried to the same depth. Therefore maturation cannot be responsible for the differences in TEX_{86} between the two lithologies.

The effects of oxic degradation on the TEX_{86} ratio are less clear. It has been reported that oxic degradation has no tangible effect on the TEX_{86} ratio in the natural marine environment (Schouten *et al*., 2004; Kim *et al*., 2008b). Schouten *et al*. (2004) examined five different sediment samples pairs of the same age from two Pleistocene-age Indian Ocean cores, which had experienced different degrees of oxic degradation due to their position relative to the oxygen-minimum zone. No systematic difference was noted between the two cores in terms of GDGT distribution, leading the authors to conclude that oxic degradation does not affect the TEX_{86} ratio, but will reduce the total abundance of GDGTs. Similar results were

produced by Kim *et al*. (2008b) who placed sediment in an oxidising marine environment for one year under controlled conditions, and detected no effect on the TEX_{86} ratio compared to the control, but did see a reduction in the abundance of all GDGTs in the oxidised sample. Contrary to these findings, a study into the effects of different degrees of oxic degradation within North Atlantic Neogene turbidites sequences concluded that oxic degradation can effect the TEX_{86} ratio (Huguet *et al*., 2009). While the TEX_{86} ratio increased in one Pleistocene turbidite with increasing oxidation, in other Pliocene turbidites the TEX_{86} ratio was frequently significantly reduced in the more oxidised portions (Huguet *et al*., 2009). No explanation was given for this difference in trend between the two ages of turbiditic deposit by Huguet *et al*. (2009).

The pattern of decreasing GDGT abundance seen in all of the studies (Schouten *et al*., 2004; Kim *et al*., 2008b; Huguet *et al*., 2009) and the decreased TEX_{86} ratios seen in the Huguet *et al*. (2009) study, would seem to agree with the earliest Cretaceous data from Sites 534 and 603, where the mudstones consistently have both lower GDGT abundances and SST estimates relative to the laminated marls (Table 2, 3; Figure, 46a, 55). But why would the mudstones have experienced a greater degree of oxic degradation relative to the marls? The marls are thought to have been deposited in a dysoxic envroment, with minimal bottom currents and disturbance by marine benthos, which would seem conducive to good preservation of the organic matter (e.g. Robertson & Bleifnick, 1983; Robertson, 1984). If the organic-matter in the marls is predominantly of marine origin, as suggested by Rock Eval and carbon isotope data (see above), this would be expected to produce relatively strong GDGT abundances and reliable TEX_{86} SST reconstructions. Additionally, the good preservation of the coccoliths in many of the laminations in the marls suggest the possibility of rapid biopackaging due to scavenging, thus reducing the time that the GDGTs would have been exposed to oxic conditions near the surface. All of these factors would perhaps lead to the marls having a relatively high-quality TEX_{86} signal.

In contrast, the homogeneous mudstones have a considerable terrigenous component and were probably initially deposited in the oxygen-minimum zone of the continental shelf. This inferred low-oxygen environment should have been conducive to good preservation of the organic-matter within the sediment. However, the mudstones must then have been transported down from the shelves and into the deep

sea, most probably passing through oxic waters on their descent into the deeper dysoxic ocean (Figure 60). The exact mechanisms for this transport are unclear, but, by analogy to modern MAP homogenites and considering the thickness of the Cretaceous deposits, it is likely that the journey from the shelf to the deep water was initiated by a slump or debris flow, and was probably completed within a timeframe of days to weeks (McCave & Jones 1988; Jones *et al*., 1992). While it is possible that these fine-grained deposits had a longer transport time than contemporaneous coarser-grained sandstone turbidites, which were likely funnelled down submarine canyons, it is difficult to envisage how this model would allow sufficient time for degradation of GDGTs and the skewing of the TEX_{86} ratio to occur in the mudstones, prior to desposition. The exact time-frame needed for substantial oxic degradation to affect the TEX_{86} ratio is unclear from the current studies, but would probably have to be on the order of at least several months to years before any substantial differences were observed (e.g. Kim *et al*., 2009). The lack of obvious oxidation fronts at the tops of the Cretaceous homogenite desposits suggests that the deep-sea seafloor was not sufficiently oxic to cause "burn-down" post deposition, as is often seen in recent turbidites from the North Atlantic (e.g. Wilson *et al*., 1986; Thomson *et al*., 1987). Regardeless, if such deep-sea oxidation was the cause of GDGT degradation in the mudstones, surely this would also have effected the GDGT content of the pelagic marls, and therefore cannot be the origin of the offset in TEX_{86} and GDGT concentration between the two lithologies.

3. 6. CONCLUSIONS

An offset in TEX_{86} ratios is noted between autochthonous pelagic marls, presumably deposited under dysoxic conditions in an open marine environment, and adjacent homogeneous carbonaceous claystones, which have been shown to have a transported origin from the continental shelf. The difference between the two lithologies can be seen in the higher $CaCO_3$ and lower TOC content of the laminated marls relative to the homogeneous claystones; the lighter $\delta^{13}C_{org}$ values in the laminated marls; and the higher proportion of shelf-dwelling calcareous nannofossils associated with the mudstones, which were presumably transported to the deep ocean entrained in turbidity currents. The GDGT content of the two lithologies also varies,

with a much higher abundance of GDGTs in the laminated marls, *vs*. the transported claystones. The TEX_{86} ratio is consistently higher in the pelagic marls than in the homogeneous claystones, which translates to an SST offset of ~1 °C using the TEX_{86}^{H} equation (Kim *et al*., 2010). This offset may appear small, but any variation introduced by lithology could be misinterpreted as genuine and significant SST variation in the proto-North Atlantic when the genuine SST was rather invariant. This finding suggests that only the pelagic marls, with a proven autothonous origin, should be used in subsequent palaeoclimatic reconstructions at these sites.

It is possible that this offset in TEX_{86} represents genuine SST variation, or the effects of upwelling or differences in crenarchaeaotal community structure on GDGT distribution, or that secondary oxic degradation is the cause of the offset. On the stength of the available evidence it is impossible to separate these three phenomena, and it may be that the offset in TEX_{86} and GDGT concentration represents some combination of primary and secondary factors. The results of this study do not undermine the use of the TEX_{86} proxy in general, as the observed differences in SST are very small, but rather suggest that where possible SST reconstructions are based on consistent lithologies within a core to minimise erroneous interpretations of temperature fluctuation where none exist.

CHAPTER 4. SEA-SURFACE TEMPERATURES IN THE EARLIEST CRETACEOUS

4. 1. AIMS

The earliest Cretaceous (Berriasian – Barremian; 145 – 125 Ma) has frequently been characterized as a relatively cool period within the Cretaceous greenhouse; based on sedimentological, palaeontological and geochemical evidence. However in most cases this "coolhouse" evidence does not have a unique interpretation, and could be the result of palaeoceanographic variables unrelated to temperature fluctuations. The variable, but generally high, pCO_2 estimates for this interval are also at odds with the prolonged coolhouse theory, as climate models suggest that temperatures should be higher than suggested by the proxy evidence for the given range of pCO_2 values. Sea-surface temperatures (SSTs) have been estimated from oxygen-isotope and Mg/Ca ratios of calcium carbonate belemnite fossils, but this approach is complicated by unknown seawater chemistry and unconstrained hydrological-cycle effects on these values. These studies are also complicated because belemnites are likely to have inhabited thermocline or deeper depths in the ocean, and so their geochemical signals are unlikely to reflect true SST estimates. Therefore, there is a need for SST estimates that are independent of initial seawater chemistry that can be used to reconstruct the general climatic mode of the earliest Cretaceous. The aim of this chapter is to present new SST data from the Berriasian–Barremian interval from globally distributed deep-sea marine sediments, and to use these temperature estimates to comment on both long-term temperature trends at each location as well as estimated meridional temperature gradients. This chapter expands on data first published in Littler *et al*., (2011), Nature Geoscience, 20th February 2011.

4. 2. INTRODUCTION

As discussed in Chapter 1, the Cretaceous is universally considered to have been a warm and equable world compared to the modern, characterised by high-latitude occurrences of thermophilic taxa such as breadfruit trees (e.g. Tarduno *et al*., 1998) and crocodilians (e.g. Markwick, 1998). Although the Late Jurassic–Early

Cretaceous period is widely considered to have been warmer and more equable relative to the modern, this period is often regarded as a time of relatively cool conditions within the Mesozoic, prior to the onset of true Cretaceous "greenhouse" conditions in the mid-Cretaceous (Figure 1; e.g. Hallam 1985; Kemper 1987; Price, 1999; Larson & Erba 1999; Hay, 2008; Jenkyns, 2010). It has been suggested that the Early Cretaceous, Valanginian–Hauterivian stages in particular were characterised by cooler and more variable climates compared to the mid-Cretaceous hothouse (e.g. Price, 1999), although it remains unclear whether these supposed cooler conditions spanned the entire Early Cretaceous period, or were characterised by transient "cold snaps" within a largely greenhouse world, as recently proposed for other periods in the Cretaceous (Voigt *et al*., 2006; Bornemann *et al*., 2008b; Mutterlose *et al*., 2009; Herrle *et al*., 2010).

Proxy evidence for climate instability in the earliest Cretaceous has been put forward from multiple studies, but is largely based on data from the Northern Hemisphere, and in particular the well-studied NW Tethyan region (Figure 63). Many authors regard the Early–mid Valanginian as the first episode of greenhouse climatic conditions in the Cretaceous, based on regional sedimentological evidence and carbon-cycle inferences (e.g. Lini *et al*., 1992; Weissert *et al*., 1998; Erba *et al*., 2004). However, evidence for a discrete warming episode in the Early Valanginian is almost completely lacking (e.g. Erba *et al*., 2004), the sedimentological evidence is equivocal (e.g. Duchamp-Alphonse *et al*., 2011), and basing interpretations of climate solely on carbon-isotope records may not be a safe assumption (Lini *et al*., 1992; Weissert *et al*., 1998). Similarly, evidence for cooler episodes in the Late Valanginian–Hauterivian is often conflicting, and may be the result of processes other than changes in palaeotemperature such as sea level or changing ocean chemistry (e.g. Price & Mutterlose, 2004; McArthur *et al*., 2007a).

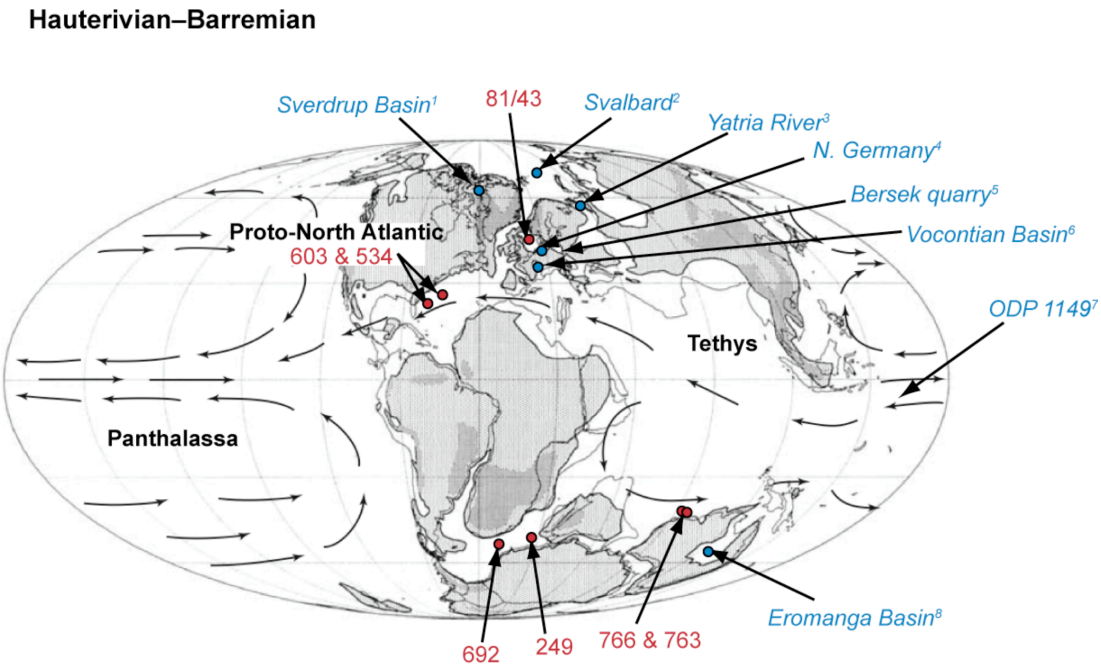

Figure 63. *Palaeographic reconstruction of the Hauterivian–Barremian (taken from Puceat et al., 2005), showing the location of the DSDP, ODP and BGS sites in this study (red), and a selection of other locations where palaeotemperature data has been generated in previous studies (blue). 1= Kemper (1987); 2 = Ditchfield (1997); 3 = Price & Mutterlose, (2004); 4 = Mutterlose et al. (2010); 5 = Price et al. (2011); 6 = McArthur et al. (2007a); 7 = Erba et al. (2004); 8 = Frakes & Francis, (1988); Delurio and Frakes, (1999); Alley & Frakes, (2003).*

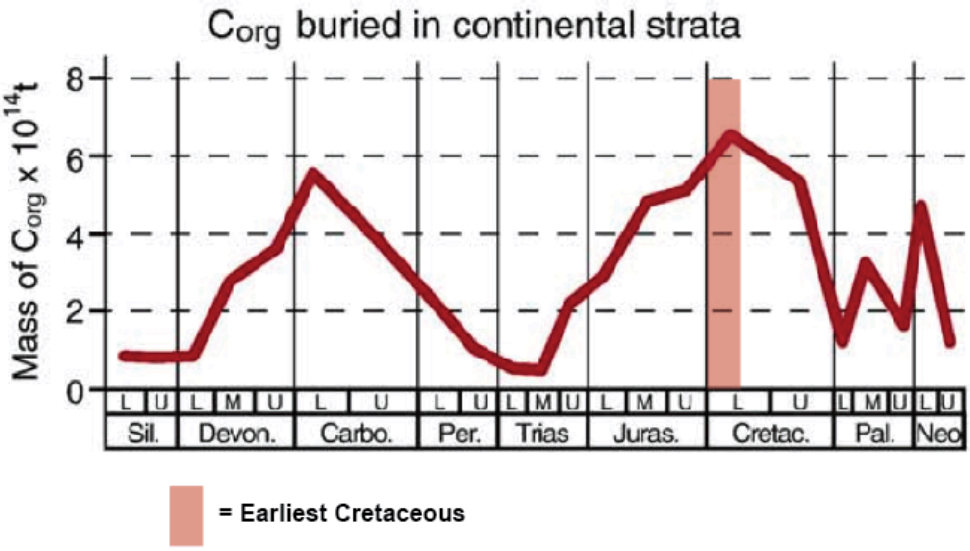

Figure 64. *Estimate of the mass accumulation rates of organic-matter in terrestrial environments during the Phanaerozoic. Adapted from Westermann et al. (2010) after Budyko et al. (1987).*

4. 2. 1. SEDIMENTOLOGICAL EVIDENCE FOR VARIATIONS IN EARLIEST CRETACEOUS CLIMATE

A warm earliest Cretaceous?

The increase in coals relative to evaporites from the Late Jurassic to the Early Cretaceous, has long been recognised and is associated with a general increase in temperature (e.g. Hallam 1984). The widespread deposition of coals, documented in the USA, Russia, China, India, Indonesia, Australia and Canada, makes the Early Cretaceous one of the major periods of coal deposition in Earth's history (Budyko *et al*., 1987; Westermann *et al*., 2010; Figure 64). Such deposits are thought to be indicative of warm, humid conditions in these regions, conducive to lush vegetation growth and the development of waterlogged soils, therefore this increased coal deposition suggests increasingly humid climates during the earliest Cretaceous relative to the Late Jurassic, which could be interpreted as the onset of greenhouse conditions (Figures 64, 65).

Clay mineral composition can also be used as a proxy for changing precipitation patters, which can indicate changes in palaeotemperature (e.g. Ruffell *et al*., 2002). A significant relative increase in kaolinite deposition during the Valanginian and Hauterivian within the NW European Wealden Formation, is taken as evidence for increased humidity in this region relative to the Late Jurassic–Early Berriasian period (Hallam, 1984). In northern England, detailed records of kaolinite *vs.* smectite abundance in the Speeton Clay, document a relative increase in kaolinite abundance from the Ryazanian (Late Berriasian) to the Early Valanginian, suggesting the onset of warm, humid conditions on the continent (e.g. Price *et al*., 2000; Figure 65). This trend is also seen in a similar study in the Vocontian basin, in the NW Tethyan region, where warm and humid conditions are inferred for the mid Valanginian, with a change to more arid and cooler conditions in the Late Valanginian (Duchamp-Alphonse *et al*., 2011; Figure 65). However, the strong influence of sea-level on the Early Valanginian clay-mineral record in this region is highlighted in this study (Duchamp-Alphonse *et al*., 2011).

Evidence for a general increase in precipitation and humidity during the Valanginian can also be found in marginal and deep-water marine records, in the

form of the increased coarse siliciclastic turbidite deposition in the Tethys and proto-North Atlantic, observed during the Valanginian and Hauterivian (Weissert *et al*., 1990; 1998; Figure 65). This general increase in turbidite frequency and coarseness of the sediment within the turbidite packages in the region, has been interpreted as being due to an accelerated hydrological cycle supplying greater quantities of siliciclastic material to the ocean basins, though the action of increased weathering and river discharge (Follmi *et al*., 1994; Weissert *et al*., 1998). A general increase in regional (and global) temperatures is invoked as the cause of this accelerated hydrological cycle (e.g. Weissert *et al*., 1998). Evidence for increased riverine input to marginal ocean basins can also be inferred from phosphorous accumulation rate data, which show a peak in phosphorite deposition in the Valanginian, thought to be due to increased nutrification and subsequent primary productivity in marginal basins (Follmi *et al*., 1994; van de Schootbrugge *et al*., 2003).

A cold snap?

The "coolhouse" theory for the earliest Cretaceous was initially proposed based on sedimentological observations in marine sections, such as the widespread occurrence of deposits thought to be indicative of cool conditions in high palaeolatitudes (e.g. Kemper 1987; Frakes & Francis, 1988; Price, 1999, and references within). As discussed in Chapter 1, these deposits include glendonites, putative ice-rafted debris, dropstones and angular breccias, often interpreted as glacial tills or diamictites. The widespread occurrence of glendonites and dropstones in sediments from Svalbard, Arctic Canada, Australia and Russia, has been used to infer cool temperatures and periods of continental ice-building during the Early Cretaceous (e.g. Frakes & Francis, 1988; Frakes *et al*., 1992; Francis & Frakes 1993; Price, 1999; Figures 1, 65).

Much of the evidence for a cool earliest Cretaceous has come from the high latitudes of the Northern Hemisphere (e.g. Kemper *et al.*, 1987; Kaplan, 1978; Kemper, 1975; Kemper & Schmitz, 1975; Figure 63). As discussed in Chapter 1, glendonites are calcite psuedomorphs of the low-temperature mineral ikaite ($CaCO_3 \cdot 6H_2O$) which, by analogy to modern ikaite deposits, are thought to crystallize at cold bottom-water temperatures between −1.9 to 7°C, in high-alkalinity and phosphate-rich environments (e.g. De Lurio & Frakes, 1999; Selleck *et al*., 2007;

Price & Nunn, 2010). Glendonites have been documented in the Sverdrup Basin of Arctic Canada, including several glendonite-rich horizons from the Lower Valanginian and some isolated occurrences in the Upper Valanginian (Kemper *et al*, 1987; Figure 65). Glendonites and purported dropstones have also be reported from Arctic Russia, where they have been taken as evidence for sub-freezing conditions in the earliest Cretaceous (Epshteyn, 1978; Kaplan, 1978; Chumakov, 1981).

Glendonites and supposed dropstones have also been reported from Berriasian–Valanginian aged sediments from Spitsbergen, where a 30 m-thick glendonite-bearing sequence of purported Late Valanginian age was reported by Price & Nunn, (2010) (Figure 65). However, Rogov & Zakharov (2010) and M. Rogov *pers. comm.* (2011) have asserted these particular glendonite-bearing strata are actually Late Hauterivian in age. Price & Nunn (2010) interpreted the presence of these glendonites, in combination with $\delta^{18}O$ data from belemnites and well-preserved glendonite samples, as evidence for variable temperatures in the earliest Cretaceous, where warm background climates were punctuated by occasional cold periods, ~300 kyr in duration (G. Price, *pers. comm*., 2011).

***Figure 65 (overleaf)**. Sea-level changes and the principal proxy evidence for climatic variation in the earliest Cretaceous (Berriasian – Barremian). Timescale is after Gradstein et al. (2004) with modifications to the Hauterivian-Valanginian boundary after Lugowski et al. (2010). Sea-level curve is after Hardenbol et al. (1998) adjusted to the corrected timescale after McArthur et al. (2007a). Blue bars indicated approximate age of inferred cooler intervals, whereas red bars indicate periods of warmth in each record relative to the cooler periods. Gradients between the two indicate cooling or warming. Yellow bars indicate arid conditions, while green bars indicate more humid conditions. Gradients between the two indicate drying or increasing humidity.*
From left to right, data is sourced from: a = Kemper (1987); b = Price & Nunn (2010); c = Price et al. (2000); d = Duchamp-Alponse et al. (2011); e = Weissert (1990); f = this study (see Methodology Section 2- 1-4); g = Hallam (1984); h = Erba et al. (2004); i =Kessels et al. (2006); j = Mutterlose & Kessels (2002); k = Vakhrameev (1981); l = Podlaha et al. (1998); m = Malkoc & Mutterlose (2010); n = Ditchfield (1997); o = Price & Mutterlose (2004); p = McArthur et al. (2007a); q = Price et al. (2011); r =van de Schootbrugge et al. (2000); s = Puceat et al. (2003); t = Weissert & Erba (2004). Question-marks denote where uncertainties exist in the age model at each site. For glendonite data from Price & Nunn (2010), the bar enclosed by "(?)" symbols denotes the age (mid Valanginian) given in that paper, while the darker bar above it enclosed in "?" symbols denote the age assigned to the same strata by Rogov & Zakharov (2010), and by M. Rovov (pers. comm., 2011) as Late Hauterivian.

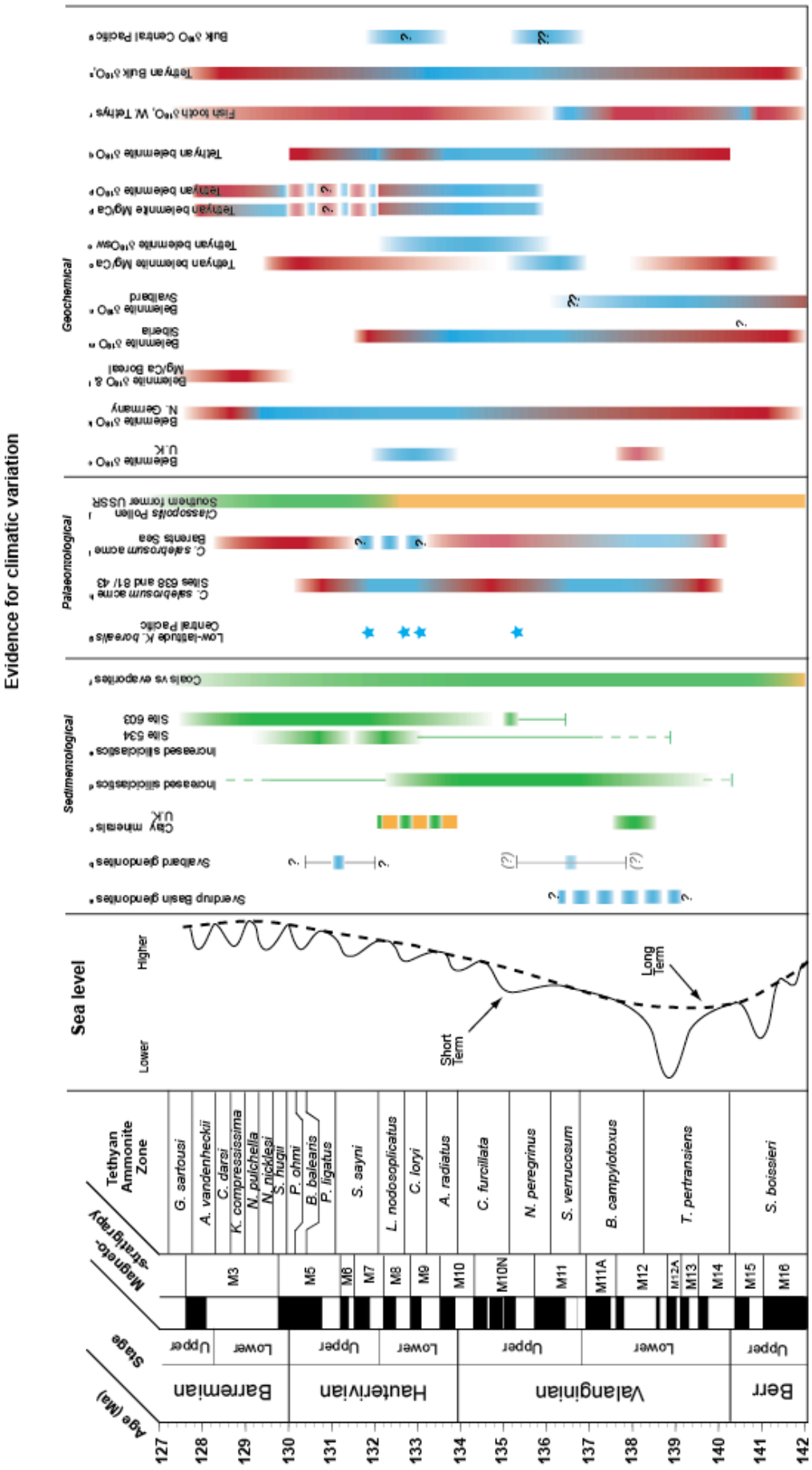
Evidence for climatic variation
Age (Ma)
Stage
Magneto-stratigraphy
Tethyan Ammonite Zone
Berr
Valanginian
Hauterivian
Barremian
Upper
Lower
Upper
Lower
Upper
Lower
M16
M15
M14
M13
M12A
M12
M11A
M11
M10N
M10
M9
M8
M7
M8
M5
M3
S. boissieri
T. pertransiens
B. campylotoxus
S. verrucosum
N. peregrinus
C. furcillata
A. radiatus
C. loryi
L. nodosoplicatus
S. sayni
P. ligatus
B. balearis
P. ohmi
S. hugii
N. nicklesi
K. compressissima
C. darsi
A. vandenheckii
G. sartousi
Sea level
Higher
Lower
Short Term
Long Term
Sedimentological
Svalbard Basin glendonites a
Svalbard glendonites b
Clay minerals c
Increased silicoclastics d
Increased silicoclastics e
Site 534
Site 603
Coals vs evaporites f
Palaeontological
Low-latitude K. borealis g
Central Pacific
C. sabrosum acme h
Sites 638 and 81/ 43
C. sabrosum acme i
Barents Sea
Classopollis Pollen j
Southern former USSR
Geochemical
Belemnite δ18O k
U.K
Belemnite δ18O k
N. Germany
Belemnite δ18O & l
Mg/Ca Boreal
Belemnite δ18O m
Siberia
Belemnite δ18O n
Svalbard
Tethyan belemnite Mg/Ca o
Tethyan belemnite δ18Osw o
Tethyan belemnite Mg/Ca p
Tethyan belemnite δ18O p
Tethyan belemnite δ18O q
Fish tooth δ18O, W. Tethys r
Tethyan Bulk δ18O, r
Bulk δ18O Central Pacific s

In the Southern Hemisphere, evidence for a cool Early Cretaceous is found in the form of glendonites and dropstones from southern Australia (e.g. Frakes & Francis, 1988; Francis & Frakes 1993; Figure 65). Outsized clasts (up to 3 m diameter) within a fine shale matrix of Valanginian–Albian age, were documented in the Eromanga Basin, south Australia, by Frakes & Francis (1988). These "dropstone"-rich sediments were likely deposited at palaeolatitudes of ~65–70 °S, and are interpreted as evidence for at least seasonal periglacial conditions in the high latitudes, if not periodic fully glacial events. Late Aptian glendonites have also been documented within organic-rich mudstones in the Eromanga Basin (~65–70 °S palaeolatitude) by De Lurio & Frakes (1999), who concluded that these deposits are indicative of formation in cool bottom-waters (0 – 5 °C). Purported glacial deposits are also reported from Berriasian–Valanginian sediments of the Northern Flinders ranges, southern Australia, where a 2 m-thick diamictite horizon within a sandstone, siltstone and conglomeratic complex of probable fluvio-lacustrine affinity, is interpreted as a tillite (Alley & Frakes, 2003). The presence of very angular quartz, one putative "frost wedge" structure and one striated pebble is interpreted as suggesting a glacial origin at this relatively high palaeolatitude site (~66 °S).

Evidence for possible cyclic changes in climate in the earliest Cretaceous, has been put forward on the basis of alternating light and dark marl couplets in deep-sea cores from the western North Atlantic (e.g. Dean & Arthur, 1987; Westphal *et al*., 2004). These couplets, with an estimated frequency of between 20 and 100 kyrs, have an enigmatic origin (Westphal *et al*., 2004) but may be the result of chaning primary climatic or oceanographic parameters such as sea-level, precipitation, or temperature, possibly related to Milankovich orbital forcing (Barron *et al*., 1985; Dean & Arthur, 1987). The fluctuating sea level during the Berriasian – Barremian in itself has been taken as evidence for climatic change, in the form of waxing and waning ice-sheets, as some authors maintain that only a glacio-eustatic mechanism is capable of changing eustatic sea level on the rapid 3rd-order scale seen in the Valanginian (e.g. McArthur *et al*., 2007a). The large sea-level fall in the Early Valanginian *T. pertransiens* zone in particular is difficult to explain in the absense of large and dynamic ice sheets (Figure 65; Hardenbol *et al*., 1998; McArthur *et al*., 2007a).

Can these sedimentological proxies be trusted as palaeothermometers? As discussed in Chapter 1, glendonites are considered to have a narrow range of formation temperature, (-1.9 to 7 °C), and for this reason are considered to be indicative of cold bottom-waters and cold or sub-freezing temperatures on the adjacent land (e.g. De Lurio & Frakes, 1999; Selleck *et al*., 2007; Price & Nunn 2010). However, in the modern world ikaite is also known from aquatic environments where the adjacent contintent is decidedly unglaciated, including the Zaire deep-sea fan, offshore Africa (Jansen *et al*., 1987; Zabel & Schulz, 2001), the Gulf of Mexico (Hackworth, 2004), Nankai Trough, off Japan (Stein and Smith, 1985), and Mono lake, California (Council & Bennett, 1993). Although the bottom waters in all of these locations are relatively cool, the presence of ikaite is clearly not indicative of sub-freezing conditions on the adjacent continents, and is probably more heavily influenced by the alkalinity of the water than the temperature of the water (e.g. Rickaby *et al*., 2006). Therefore it is doubtful whether the occurrence of glendonites in earliest Cretaceous sediments, particularly in more organic-rich sediments where phosphate contents may be high, can be said to offer unequivocal evidence of cold snaps (*c.f.* Price & Nunn, 2010)

Dropstones are interpreted as being deposited by rafting continental ice, but could also be the result of vegetation rafting from floating pieces of wood or kelp (Bennett *et al*., 1996; Bennett & Doyle, 1996). Although some large boulders up to 3 m in diameter (e.g. Frakes & Francis 1988), are too large to be explained by this delivery mechanism. There are also arguments for some of the dropstones having a sea-ice rather than a land-ice origin (e.g. Hay, 2008 and references within), which does not necessarily indicate year-round freezing conditions on the continents. Diamictites, which are often interpreted as being of glacial origin, can also have non-glacial origins such as mud-flows (Alley & Frakes, 2003), and may not be indicative of sub-freezing conditions at all.

Cyclicity in deep-sea pelagic sediments is certainly intriguing, but it is difficult to tie these fluctuations to a particular forcing factor such as sea-level, organic-matter supply or productivity, and therefore their origin remains enigmatic (Westphal *et al*., 2004). Certainly some cyclic alternations in lithology in the geological rock-record are forced by orbital parameters, but whether the earliest Cretaceous “rhythmites” are unaltered by diagenesis and represent true changes in climate is uncertain.

In conclusion, the sedimentological evidence for climatic variation in the Early Cretaceous is varied and somewhat contradictory. Widespread coals on the continents suggest that warm and equable climates dominated the earliest Cretaceous, supported by clay-mineral evidence for a warm and humid Early Valanginian. However, equivocal sedimentary evidence in the form of glendonites and dropstones has been put forward to suggest a cooling period in the Valanginian–Hauterivian of indeterminate length, which could also be the result of localised ocean chemistry, or the effect of seasonal ice.

4. 2. 2. PALAEONTOLOGICAL EVIDENCE FOR VARIATIONS IN EARLIEST CRETACEOUS CLIMATE

Several studies have proposed palaeontological (macrofossil and microfossil) evidence for changes in temperature during the earliest Cretaceous (e.g. Mutterlose & Kessels, 2000; Melinte & Mutterlose, 2001; Kessels *et al*., 2006; Erba *et al*., 2004; Figure 65). Such evidence includes sporadic incursions of fauna and flora with a presumed high-latitude affinity into the lower latitudes, which is interpreted in terms of intermittent "cold snaps", and changes in nutrient indicators thought to be related to large-scale changes in climate. Upon examination of the calcareous nannofossil assemblages of marine sections from several mid-high latitude sites in the Barents Sea, Mutterlose & Kessels (2000) concluded that the bipolar distribution of the high-latitude species *Crucibiscutum salebrosum* was strongly suggestive of stable climatic belts during the earliest Cretaceous, and that a relatively steep global latitudinal temperature gradient must have existed (Figure 66). A peak in *C. salebrosum* abundance in the lower latitudes in the Early Valanginian may represent particularly cool-water conditions during that time (Mutterlose & Kessels, 2000; Figure 65).

These findings are broadly supported by the work of Melinte & Mutterlose (2001) who found similar maxima in *C. salebrosum* abundance in a Tethyan section of mid-Valanginian age from Romania. Similarly, calcareous nannofossil assemblages in marine sections in the North and Barents Seas, especially the distribution of *C. salebrosum,* has been used to argue in favour of an Early Valanginian–Hauterivian "moderate ice house" (Mutterlose *et al*., 2003). In

subsequent work, the results of analysing three sites along a palaeolatitudinal transect (17 – 40 ºN) from the Gulf of Mexico, via the North Atlantic, to the North Sea, lead the authors to conclude that the observed changes in earliest Cretaceous calcareous nannofossil assemblages were related to changes in global temperature (Kessels *et al*., (2006). Maxima in *C. salebrosum* abundance at Site BGS 81/43 (North Sea) and ODP Site 638 (Eastern North Atlantic) during two intervals, the Early-Late Valanginian boundary and the Early-Late Hauterivian boundary, have been taken as evidence that these were particularly cool intervals, separated by an intervening warm interval in the Late Valanginian (Kessels *et al*., 2006; Figure 65). In a similar study in the Central Pacific, the presence of another high-latitude calcareous nannofossil species, *Kokia borealis,* at a low-latitude study area, has been taken as indicative of periodic cooling episodes in the Late Valanginian and Hauterivian associated with drawdown of CO_2 (Erba *et al*., 2004; Figure 65).

Changes in calcareous nannofossil fertility indicators have been documented in the Tethys Ocean during the earliest Cretaceous, and have been interpreted as indicating changes in global climate regime, with alternations between warm and cooler conditions (e.g. Melinte & Mutterlose, 2001; Kessels *et al*., 2006; Bornemann *et al*., 2008). The results of a calcareous nannofossil study in the North Atlantic (DSDP Sites 603 and 534), suggest that there is no evidence to support a Late Valanginian cooling event in the western proto-North Atlantic at these sites, but the abundance of fertility indicators did change in the Early Valanginian, which is attributed to increased nutrient input from upwelling (Bornemann *et al*., 2008). Such changes in fertility indicators have also been noted in the Pacific Ocean (Erba *et al*., 2004). Increases in the calcareous nannofossil *Diazomatolithus lehmanii* and the radiolarian species *Pantanellium* during the Valanginian-Hauterivian, have been suggested to be related to changes in fertility, ultimately related to changes in global temperature though an enhanced hydrological cycle and increased weathering feedback (Erba *et al*., 2004).

However, it should be noted that although *C. salebrosum* is almost undoubtedly a high-latitude taxon, it is closely related to the *Biscutum* spp. which are often regarded as high nutrient indicators (e.g. Roth & Krumbach 1986; Erba *et al*., 1992). Therefore, to disintangle whether the high latitude preference of *C. salebrosum* is due to the cooler temperatures at these latitudes, or the likely higher

nutrient conditions, additional information to constrain temperature or nutrient levels is required.

Changes in global temperature have also been inferred from shifts in marine macrofauna. Melinte & Mutterlose (2001) discussed changes in ammonite provincialism in the Boreal and Tethyan realms, in the context of fluctuations in global meridional temperature. They suggested on the basis of previous studies (e.g. Hoedemaker, 1990; Rawson, 1994) that provincialism reached a peak in Berriasian times, when the boundary between the Tethyan and Boreal realms was located at ~60 ºN. Melinte & Mutterlose (2001) attribute the apparent shift of this faunal boundary during the Valanginian Stage, southwards to ~40–45ºN, as being due to a cooler climate during this time relative to the Berriasian.

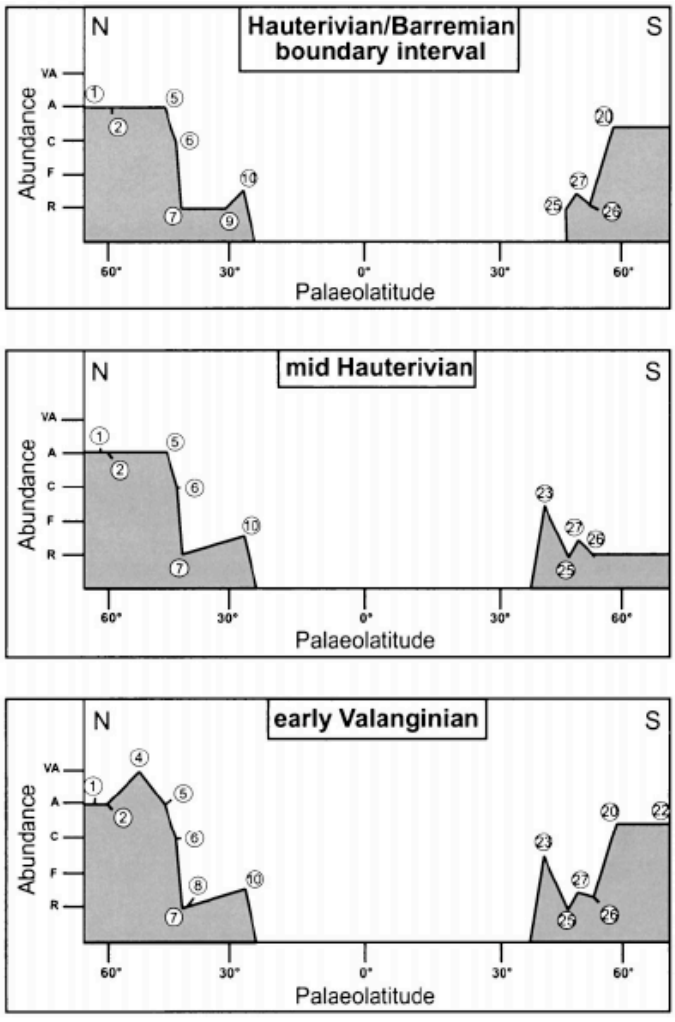

Figure 66. *Changing latitudinal distribution of the calcareous nannofossil C. salebrosum, in the earliest Cretaceous showing its apparent bi-polar distribution. Taken from Mutterlose & Kessels, (2000). R = rare; F = few; C = common; A = abundant; VA = very abundant. Numbers represent specific sites, see Mutterlose & Kessels (2000) for details.*

4. 2. 3. GEOCHEMICAL EVIDENCE FOR VARIATIONS IN EARLIEST CRETACEOUS CLIMATE

Perhaps the most persuasive evidence in support of climate variability in the Berriasian–Barremian comes in the form of the many geochemical studies that have been conducted on bulk sediment and biogenic material of Berriasian–Barremian age (e.g. Podlaha *et al*., 1998; McArthur *et al*., 2007a; Price *et al*. 2000). Changes in the bulk carbonate $\delta^{18}O$ record from the Tethyan (Weissert & Erba, 2004) and Pacific regions (Erba *et al*., 2004), have been used to suggest climate variability in the earliest Cretaceous, both of which suggest a cooling in the Late Valanginian–Early Hauterivian (Figure 65). However, the use of bulk oxygen-isotopes as a palaeothermometer has many uncertainties associated with it, not least the likelihood of diagenetic alteration (e.g. Frank *et al*., 1999), and more persuasive arguments have been made on the basis of single-fossil isotope studies, where such issues are easier to constrain.

The oxygen-isotope composition of belemnites in particular has been used to suggest that transient cool periods, perhaps even severe enough to cause continental glaciations, occurred during the earliest Cretaceous (e.g. McArthur *et al*., 2007a; Price *et al*., 2000). The isotopic values of Early Cretaceous belemnites from Svalbard (~70 ºN palaeolatitude) were examined by Ditchfield, (1997), who concluded that cool temperatures of ~8 ºC, not incompatible with high-latitude ice formation, characterised the Lower–mid Valanginian (Figure 65). These cool values contrast with the appreciably warmer 9–13 ºC estimates for the Mid–Late Jurassic in the same study. A similar decreasing temperature trend from 16 ± 5 ºC in the Berriasian to 10 ± 4 ºC in the Hauterivian was reported by Podlaha *et al*., (1998), based on the $\delta^{18}O$ values of Berriasian–Barremian belemnites in North Germany (Figure 65). Belemnite $\delta^{18}O$ records from Speeton in northeastern England (40–45 ºN palaeolatitude) confirmed this cooling trend, by suggesting that the Early Valanginian was characterised by relatively warm temperatures of 12–15 ºC, while the Early Hauterivian was characterised by cooler temperatures of <9 ºC (Price *et al*., 2000; Figure 65).

The boreal oxygen-isotope studies (Ditchfield, 1997; Podlaha *et al*., 1998; Price *et al*., 2000) all used the equation of Anderson & Arthur (1983) to convert $\delta^{18}O$

to temperature, using estimated values of $\delta^{18}O_{sw}$ of between -1 and -1.2 ‰. This approach comes with many associated uncertainties and errors (see Chapter 1, Section 1-4-3.), particularly the unknown $\delta^{18}O_{sw}$ values in the temperature equation. Price & Mutterlose (2004) attempted to correct for this phenomenon by substituting a range of plausible $\delta^{18}O_{sw}$ values into the temperature equation of Anderson & Arthur (1983), when calculating temperature from $\delta^{18}O$ data of Jurassic–Early Cretaceous Siberian belemnites. Using this approach, Price & Mutterlose (2004) recorded a similar result of decreasing temperatures, from Late Jurassic values of 11–21 ºC to Late Valanginian–Early Hauterivian values of 2–14 ºC (Figure 65). Furthermore they suggested that these cool Late Valanginian–Early Hauterivian temperatures are not inconsistent with the formation of high-latitude ice during this interval. Price & Nunn (2010) also tried to avoid difficulties with unknown $\delta^{18}O_{sw}$ values by using both the ikaite-to-glendonite pseudomorph transition temperature and the $\delta^{18}O$ record of co-occurring belemnites from Svalbard, to argue that cool temperatures of 4 – 7 ºC occurred as a "short cool interlude" in the mid–Late Valanginian (Figure 43-b). However as discussed in Section 3-2-3-1 the age of these deposits may in fact be Late Hauterivian (Rogov & Zakharov, 2010; M. Rogov *pers. comm. 2011*).

A general cooling trend during the earliest Cretaceous was also seen in the Tethyan realm by van de Schootbrugge *et al*., (2000), who examined the $\delta^{18}O$ of belemnites and bulk sediments in the Vocontian Basin, SE France, which was located at ~30–35 ºN in the Early Cretaceous. Van de Schootbrugge *et al*. (2000) estimated that subsurface (of unspecified depth) seawater palaeotemperatures were ~15 ºC in the late Early Valanginian, falling to ~11 ºC in the Late Valanginian and Early Hauterivian, before rising again in the Late Hauterivian to ~12–14 ºC (Figure 65). However, the authors related the cooling event to sea-level rise, on the basis of evidence for opening ocean gateways, which allowed cool nutrient-rich Boreal water into the basin, and not to local or global climatic changes. The poor agreement in the details of this Tethyan record and the Boreal record of Podlaha *et al*., (1998) was noted by the Van de Schootbrugge *et al*. (2000), and put forward as evidence that the cooling mostly represents palaeoceanographic changes and not climatic variation.

In an attempt to circumvent many of the problems with unknown $\delta^{18}O_{sw}$ values, McArthur *et al*. (2007) employed Mg/Ca ratios combined with oxygen-isotope records to examine belemnites from the Berriasian–Hauterivian of SE France

and SE Spain. These authors used the Mg/Ca values to reconstruct palaeotemperatures and then substituted these temperatures into the oxygen-isotope equation of Hays & Grossman (1991) to derive estimates of $\delta^{18}O_{sw}$, which are interpreted in terms of changes in continental ice volume. McArthur *et al*. (2007) concluded that, despite the "noisy" record, the Mg/Ca temperature trend suggests cooling of ~4 ºC in the mid–late Valanginian *Saynoceras verrucosum* ammonite Zone, before returning to warmer temperatures in the mid–Late Hauterivian (Figure 44). Furthermore, McArthur *et al*. (2007) use changes in the calculated $\delta^{18}O_{sw}$ record to argue explicitly that the interval between the *N. peregrinus* and *L. nodosoplicatum* ammonite Zones (Late Valanginian to mid-Hauterivian) was characterised by the presence of variable amounts of polar continental ice, which was initiated once a threshold in temperature had been passed. A similar combined multiproxy approach has also recently been applied to Tethyan belemnites from Hungary (~35 ºN palaeolatitude) by Price *et al*. (2011). These authors discerned a warming trend from the Late Valanginian (16–29 ºC) to the Late Barremian (16–35 ºC) in both Mg/Ca and $\delta^{18}O$ records, despite the highly scattered and species-specific nature of the dataset, which is particularly incoherent in the Late Hauterivian (Figure 65).

Oxygen-isotope records from organisms other than belemnites have also been used to study Early Cretaceous climate, the results of which broadly agree with the belemnite studies (Figure 65). Fluctuations in the $\delta^{18}O$ record of phosphatic fish teeth from subtropical western Tethyan sections were converted to temperature after Kolodny *et al*. (1983), and suggest that a reasonably warm Early Valanginian was followed by a prominent cooling event in the earliest Late Valanginian *Saynoceras verrucosum* ammonite Zone, where minimum temperatures of 13 – 14 ºC were reached (Pucéat *et al*., 2003; Figure 65). Pucéat *et al*. (2003) argue on the basis of complementary Neodymium isotope data, that these changes in $\delta^{18}O$ reflect global climatic events rather than changes in palaeoceanography.

4. 2. 4. EARLIEST CRETACEOUS *p*CO_2 ESTIMATES

Although most workers accept that CO_2 is responsible for regulating long-term changes in global climate, some workers (e.g. Veizer *et al*., 2000) have argued otherwise, partly on the basis of Early Cretaceous SST and CO_2 data. Veizer *et al*., (2000) compared the SST estimates generated from a large oxygen-isotope dataset with those of an energy balance model based on *p*CO_2 estimates, and concluded that there was a mismatch between these two records in the Mesozoic, particularly during the Late Jurassic–Early Cretaceous "ice house". While the oxygen-isotope record, suggest SSTs in the tropics were 1–2 ºC cooler than the modern in the Early Cretaceous, the energy balance model suggests tropical SST anomalies of +5 ±1 ºC relative to the modern. Veizer *et al*., (2000) use this mismatch to suggest that at times during the Phanaerozoic climate and atmospheric CO_2 concentrations were decoupled, which stands at odds with other studies which assert that CO_2 has been the forcing factor behind major climate fluctuations for much of the Phanaerozoic (e.g. Royer *et al.,* 2004, 2006, 2007).

Estimates of *p*CO_2 can be based on either direct proxy data such as stomatal indices and carbon-isotope values from palaeosols, or on indirect studies, which use carbon-cycle models such as GEOCARB. Royer (2006) compiled *p*CO_2 proxy records for the Ordovician to Neogene period and compared them to existing palaeotemperature records and model outputs, in an attempt to constrain "thresholds" of CO_2 concentration for the initiation of glaciations over the Phanerozoic (Figure 46). While *p*CO_2 estimates based on palaeosols suggest values of 1000 – 2300 ppm, in the earliest Cretaceous (3.5 – 8.5 x pre-industrial atmospheric levels PAL; ~270 ppm), stomatal indices suggest broader estimates of 600 – 3200 ppm (2 – 6.5 x PAL). In more detail, the stomatal record, based on data from Retallack (2001), Haworth *et al*. (2005) and Beerling & Royer (2002), show a drop in *p*CO_2 estimates from ~3200 ppm (12 x PAL) in the Berriasian, to values of ~650 – 1800 ppm (2 – 6.5 x PAL) in the Valanginian–Hauterivian, before stabilising at ~550 – 650 ppm (~2 – 2.5 x PAL) in the Late Hauterivian–Barremian. The more sparse palaeosol data, based on data from Platt (1989) and Lee (1999), show a different trend and gives estimates of ~2100 ppm (7.5 x PAL) in the Berriasian rising to ~2300 ppm, (8.5 x PAL) in the Early Hauterivian. Robinson *et al*. (2002) also produced *p*CO_2 estimates for the Early Barremian based on the carbon-isotopic record of soil calcretes from the

Wealden of southern England, of ~560 ppm, (~2 x PAL), which are a good match to the Late Hauterivian stomatal indice estimate of ~2 – 2.5 x PAL from the same sections (Haworth *et al*., 2005).

The long-term trends in the Early Cretaceous pCO_2 record can also be seen in the output of Phanerozoic carbon-cycle models such as GEOCARB and GEOCARBSULF. For instance, the model output of GEOCARB III (Berner & Kothavala, 2001) yields broad values of 500 – 3300 ppm (<2 – 12 x PAL) for the entire Berriasian–Barremian interval, which encompass the full range of the proxy estimates given above. This model generally suggests a fall in pCO_2 from ~8 x PAL in the Berriasian to 6.5 x PAL in the Barremian, which is quite different to the output of an earlier model GEOCARB II, that suggested relatively invariant pCO_2 estimates of ~3.5 x PAL across the same interval (Berner, 1994). Tajika *et al*., (1999) modelled the carbon cycle of the Cretaceous and determined that a peak in pCO_2 levels of ~5.5 x PAL occurred at the Berriasian–Valanginian boundary, which rapidly fell to ~3 x PAL in the Late Valanginian-Early Hauterivian, before recovering to ~4 x PAL by the close of the Barremian. This fall in CO_2 from the Berriasian to the Hauterivian broadly matches the Berner & Kothavala (2001) model, but not the Wallmann *et al*. (2001) simulation, which suggests generally invariant PCO_2 levels of ~2 – 2.5 x PAL in the earliest Cretaceous before a sharp rise in the Late Barremian.

In conclusion, the pCO_2 of the earliest Cretaceous is not well constrained, with estimates ranging from <2 – 12 x PAL (~500 to 3300 ppm, Figure 46). The general consensus in both the proxy and modelling data is that CO_2 was at least twice the pre-industrial level of the Holocene, and probably not more than 6 x PAL for extended periods of time, except for the Berriasian when it may have been much higher. There is evidence for variation within the earliest Cretaceous, with some models predicting a drop from the Berriasian into the Hauterivian, which appears to also be supported by some pCO_2 proxy data. Such a drop in pCO_2 would not be inconsistent with the hypothesised cooling in the late Valanginian and Early Hauterivian suggested by some proxy data (Section 4-2-3), however there is no pCO_2 proxy or modelling evidence to support an Early Valanginian onset of greenhouse conditions.

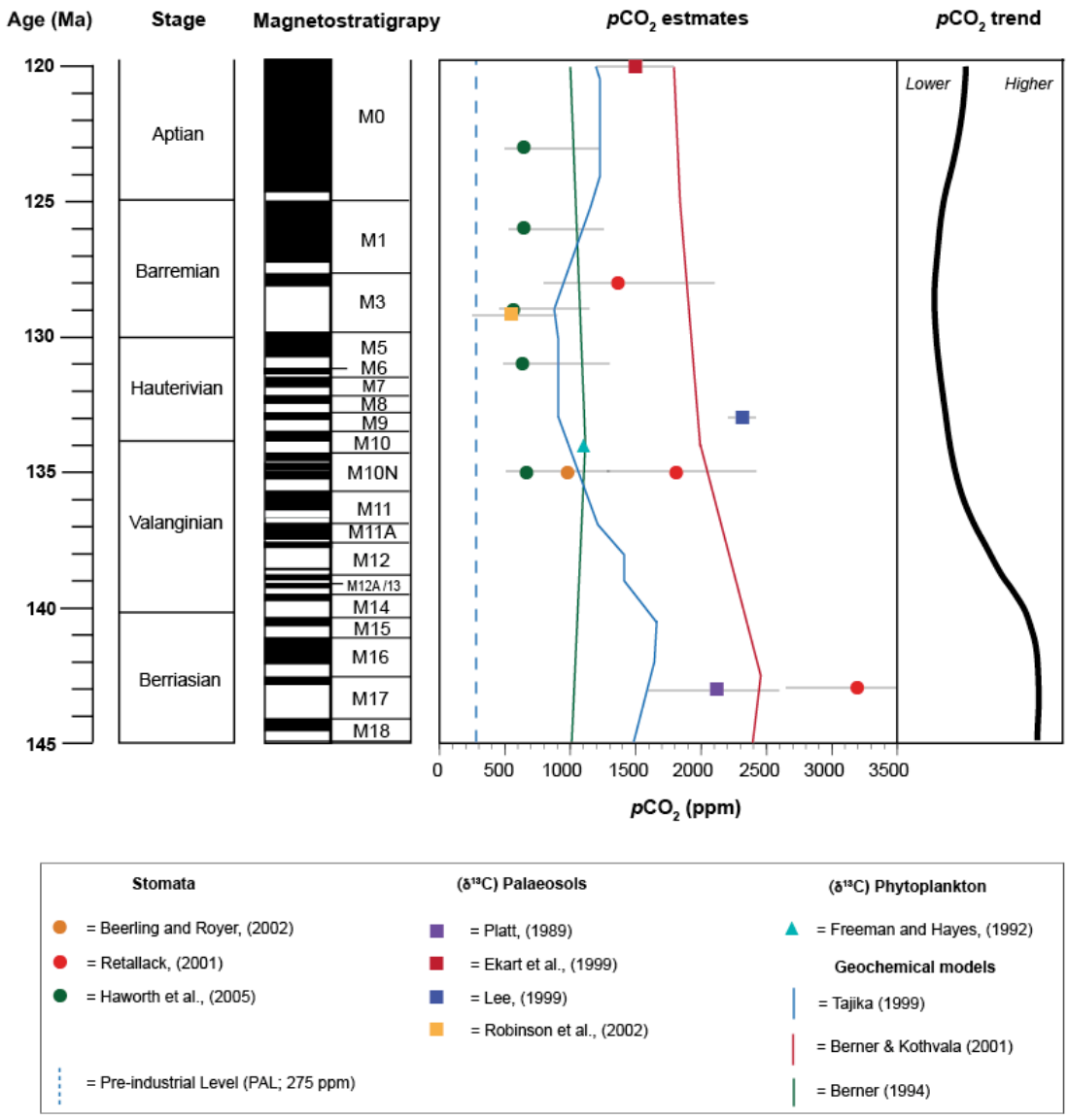

Figure 67. *Estimates of pCO_2 in the Early Cretaceous based on both proxy data and geochemical modelling results. Adapted from Royer et al. (2006) and Haworth et al. (2005). Black pCO_2 trend line is best fit line of all proxy and modelling data drawn by eye.*

4. 3. METHODOLOGY AND SAMPLED SITES

Nine deep-sea drilling sites were sampled in this study; two in the western North Atlantic (DSDP 534 and 603), one in the eastern North Atlantic (DSDP 416), three in the southeastern Indian Ocean (ODP 763, 765 and 766), one in the southwestern Indian Ocean (DSDP 249), one in the Weddell Sea (ODP 692) and one in the North Sea (BGS 81/43), (Section 2-1; Figures 31, 32). Based on the conclusions of the lithology study in Chapter 3, only sediments which had a clear autochthonous pelagic origin (laminated marls) were considered from the low-latitude sites (DSDP 534 and 603) in this study, while an assortment of predominantly hemipelagic sediments were analysed from the other seven sites, as true pelagic sediments were not present. The general methodology for determination of TEX_{86}, BIT Index, carbon-isotope, TOC% and CaCO3% values is outlined in detail in Chapter 2 (Section 2-1.) Of the 38 samples from Site 534 which were successful for TEX_{86} analysis, 26 (68 %) were rerun at least twice to check reproducibility, which was ± 0.006. Two samples at Site 603 were rerun twice, with an average reproducibility of ± 0.02, and two samples at Site 766 were rerun twice with an average reproducibility of ± 0.01.

4. 4. RESULTS

4. 4. 1. OVERVIEW

Of the nine marine sections sampled in this study, six yielded TEX_{86} data, while the other three sites were effectively barren of GDGTs. In total 94 TEX_{86} data points and 47 BIT Index points were generated for this study, out of the 148 samples that were analysed (64 % success rate overall for TEX_{86}). Additionally, new $\delta^{13}C_{org}$ records were generated at two of the sampled sites (see Table 2) and some additional Hauterivian and Barremian $\delta^{13}C_{carb}$ data were added to existing dataset at Sites 534 and 603.

Site	Palaeo-latitude	TEX_{86} data?	BIT Index data?	Carbonate carbon-isotope data?	Organic carbon-isotope data?
249	~61 °S	Yes (7/ 9)	Yes (7/ 9)	No	No
416	~20 °N?	No (0 / 9)	No (0 / 9)	Yes (9)	No
534	~15 °N	Yes (38/ 49)	Yes (11/ 49)	Yes (Bornemann *et al*., 2008, + 8 new data points)	*Yes*
603	~20 °N	Yes (17 / 30)	Yes (4/ 30)	Yes (Bornemann *et al*., 2008, + 10 new data points)	*Yes*
692	~59 °S	Yes (12/ 12)	Yes (7/ 12)	No	Yes (11)
763	~53 °S	Yes (1/2)	Yes (1/ 2)	No	No
765	~50 °S	No (0/ 5)	No (0/ 5)	No	No
766	~53 °S	Yes (19/ 24)	Yes (17/ 24)	No	Yes (24)
81/43	~40 °N	No (0/ 8)	No (0/ 8)	No	No
Total	/	**(94 data points/ 148 samples analysed)**	**(47 data points / 148 samples analysed)**	**27**	***35***

Table 4: *Summary of geochemical data collected at each site. The organic carbon-isotope data for Sites 534 and 603 are presented in detail in Chapter 5, and therefore are shown in italics in this table and no numbers are shown. Bracketed numbers in TEX_{86} column represent the number of successful data points compared to the number of samples analysed.*

Site	Palaeo-latitude	Av TEX86	Min TEX86	Max TEX86	Av Temp ºC (TEX_{86}^{H})	Av Temp ºC (1/ TEX_{86})	Temp Range (TEX_{86}^{H})	Av BIT Index	Average [GDGT] g^{-1}	Av TOC %	Av CaCO3 %
249*	~61 ºS	0.605	0.586	0.671	23.6	22.9	4.1	0.076	1,730,860	0.92	1
416	~20 ºN?	/	/	/	/	/	/	/	/	/	/
534	~15 ºN	0.92	0.899	0.94	36.1	33.7	1.4	0.021	507,978	0.88	61.45
603	~20 ºN	0.903	0.869	0.921	35.6	33.3	1.8	0.022	186,416	1.41	69.35
692	~59 ºS	0.714	0.68	0.75	28.6	27.7	2.8	0.022	1,819,855	8.13	30.17
763**	~53 ºS	0.61	/	/	23.9	23.2	/	0.126	32,564	/	/
765	~50 ºS	/	/	/	/	/	/	/	/	/	/
766	~53 ºS	0.657	0.632	0.71	26.1	25.4	3.4	0.038	201,983	0.64	3.37
81/43	~40 ºN	*0.687*	*0.634*	*0.728*	*27.4*	*26.6*	*3.0*	/	*12, 955*	/	/

Table 5: *Summary of early Cretaceous TEX_{86}, BIT Index, percent carbonate (CaCO3 %) and percent Total Organic Matter (TOC %) data. *Only Neocomian data considered; **Data from 763 is very tentative and only represented by one late Berriasian data point. Data from Site 81/43 should be regarded as a general indicator of temperature only.*

4. 4. 1. DSDP Site 534

The carbon-isotope data for DSDP Hole 534A was taken from Bornemann *et al*. (2008) supplemented with eight new Hauterivian and Early Barremian data points from this study (Figure 68). Site 534 was one of the two low-latitude, western North Atlantic sites to yield TEX_{86} and BIT Index data. Of the 49 Late Berriasian- Early Barremian laminated marl samples analysed in this study, 38 yielded TEX_{86} data reliable enough to convert to SST estimates (Table 4 and Figure 68). The average abundance of GDGTs is 508,000g^{-1} (abundance of GDGTs 1, 2, 3, and 4' per gram of sediment, normalised to a 100 μl injection volume) throughout the section. There is no correlation ($r^2 = 0.0003$) between TEX_{86} values and GDGT abundance.

As the sampled lithology was selected to be "laminated marl" throughout, it is not surprising that all of the samples displayed similar $CaCO_3$ % and TOC% contents, although there was some local variation (Figure 68). The average $CaCO_3$ content overall was quite high at 61.5 %, while the average TOC content was quite low at only 0.9 %. The Early Valanginian (1200 to 1240 mbsf) was characterized by low TOC contents of ~0.4 – 1 %, while highest TOC values (~1.6 %) were observed between 1190 and 1200 mbsf, coincident with the start of the peak of the $\delta^{13}C_{carb}$ positive excursion in the mid Valanginian. The Late Valanginian (1120 to 1200 mbsf) was characterized by variable TOC contents of 0.2 – 1.4 %, which progressed to consistently low values of 0.4 – 0.7 % in the Early Hauterivian, before increasing again to values of 0.9 to 2.1 % in the Late Hauterivian and Early Barremian.

Where it was possible to calculate the BIT Indices, they are uniformly very low and average only 0.021 (Table 5 and Figure 68). A small range encompassing minimum and maximum values of 0.006 and 0.046 respectively was observed. These values indicate terrestrial GDGT input was minimal in all pelagic marls sampled in this study, and therefore that the SST reconstructions based on the TEX_{86} values are robust in terms of terrestrial contamination.

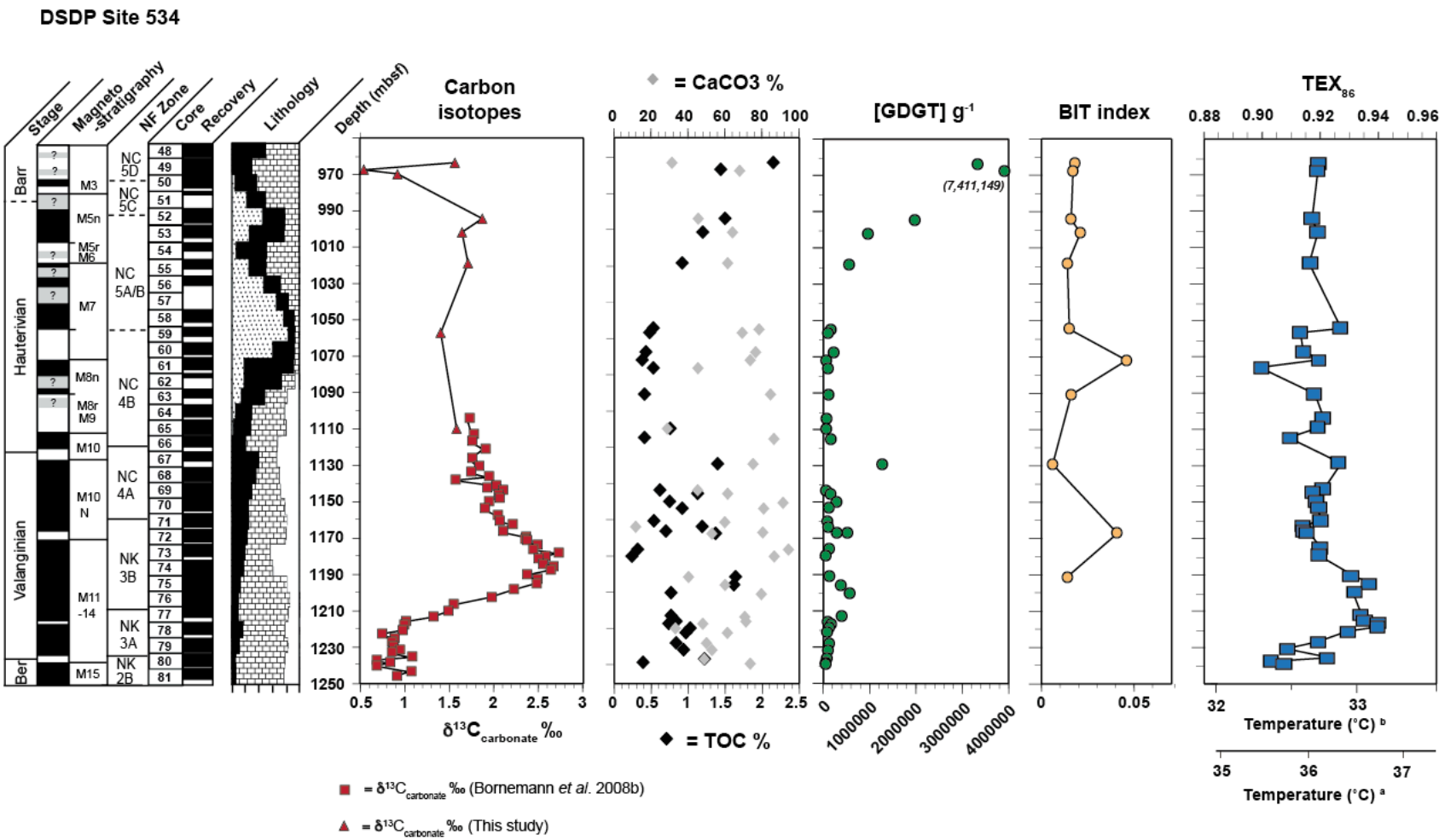

Figure 68. *Carbonate carbon isotope, Total Organic Carbon content (TOC %), calcium carbonate content ($CaCO_3$%), GDGT abundance, BIT Index and TEX_{86} / SST data for DSDP Hole 534A. $CaCO_3$ and TOC% are weight percent measurements. Lithology is the same as for Figure 33a.*

The TEX_{86} values for this site across the entire Berriasian-Barremian are very high and average 0.920 (Table 5 and Figure 68). Minimum values of 0.899 in the Early Hauterivian and maximum values of 0.940 in the Early Valanginian lead to a small total range in TEX_{86} values of only 0.041. When converted to SST using the Kim *et al*. (2010) TEX_{86}^{H} calibration (hereafter referred to as the "logarithmic calibration"), this equates to average temperatures of 36.1 ºC, with minimum and maximum temperatures of 35.4 ºC and 36.8 ºC respectively. When using the less sensitive reciprocal calibration after Liu *et al*. (2009) (1/ TEX_{86}; hereafter referred to as the "reciprocal calibration") these values translate as 33.7 ºC, 33.3 ºC and 34.2 ºC respectively. The general trend is for very stable temperatures across the entire 12 Myr study interval, as the small range in SSTs demonstrates, but a small warming pulse ~0.04 in magnitude could tentatively be discerned between 1200 and 1240 mbsf (~137 to 140 Ma), in the Early Valanginian (Figure 68).

There is only a very weak positive correlation between GDGT abundance and TOC%, (r^2 = 0.238), and no correlation between GDGT abundance and $CaCO_3$% (r^2 = 0.003). There is also no correlation between TOC % and TEX_{86} values (r^2 = 0.071), nor is there any correlation between $CaCO_3$ % and TEX_{86} values (r^2 = 0.005), indicating that minor variations in organic matter content or calcium carbonate content within the laminated marl lithology is not a controlling factor on the reconstructed SST at this site.

4. 4. 2. DSDP SITE 603

The carbon-isotope data for DSDP Hole 603B was taken from Bornemann *et al*. (2008) supplemented with 10 new Hauterivian and Early Barremian data points from this study (Table 3, Figure 69). The TOC% and $CaCO_3$% records for the laminated marls show little variation (Figure 69). The average $CaCO_3$ content overall is 69.4 %. The average TOC content is 1.4 %, which is distinctly higher than the values seen at Site 534. There are relatively modest TOC values of ~1.3 to 1.4 % in the Late Berriasian section, which rise to ~0.9 to 1.7 %, in the Early Valanginian, and culminated in a TOC spike of 2.4% in the mid Valanginian, coincident with the peak in the $\delta^{13}C_{carb}$ positive excursion.. A later maxima in TOC content of ~1.8 to 2.0 % is seen in the Early Hauterivian.

The abundance of Branched GDGTs at Site 603 was even lower than at Site 534, and therefore it was only possible to quantify the BIT index for 4 of the 17 samples that yielded usable TEX_{86} data. All of these values were extremely low, averaging 0.022, which coupled with the very low abundance of the branched GDGTs overall, suggests an insignificant terrestrial GDGT component to the organic matter at this site, and that the TEX_{86} SST estimates have therefore not been biased by terrestrial contamination (Table 5, Figure 69).

Site 603B was the second of the two low-latitude, western North Atlantic sites to yield TEX_{86} data in this study. Of the 30 Late Berriasian – Late Hauterivian laminated marl samples analysed in this study, only 17 yielded TEX_{86} data reliable enough to convert to SST estimates (Table 5, Figure 69). This poor success rate of only 56 % was predominantly due to the very low GDGT abundances observed throughout the hole, which were particularly poor in the deeper cores below 1545 mbsf. The average GDGT abundance, was 186,000 g^{-1}, which is slightly more than a third of the average GDGT abundances seen at Site 534. There is no correlation between GDGT abundance and TEX_{86} value ($r^2 = 0.083$).

The TEX_{86} values for this site across the entire Berriasian to Late Hauterivian at Site 603 are very high and average 0.903, (~35.6 ºC using the logarithmic calibration), which is ~0.02 less than at Site 534 (Table 5 Figure 69). Although the Site 603 TEX_{86} record suggests relatively invariant SSTs from the Berriasian to the Barremian (~0.05 total range in TEX_{86} values), minimum values of 0.869 are observed in the earliest Valanginian and there are two temperature "maxima" in the mid-Valanginian and Early Hauterivian with values of 0.918 and 0.921 respectively. When converted to SST using the logarithmic calibration, these SST minima and maxima equates to temperatures of 34.4 ºC and 36.2 ºC respectively, which is a temperature difference of only 1.8 ºC. When using the less sensitive reciprocal calibration, the difference between the maxima and minima decreases to 1.3 ºC.

There is no correlation between GDGT abundance and TOC% ($r^2 = 0.015$), and only a very weak positive correlation between GDGT abundance and $CaCO_3$ % ($r^2 = 0.261$). Similar to the results from Site 534, no correlation is observed between TOC % and TEX_{86} values ($r^2 = 0.014$).

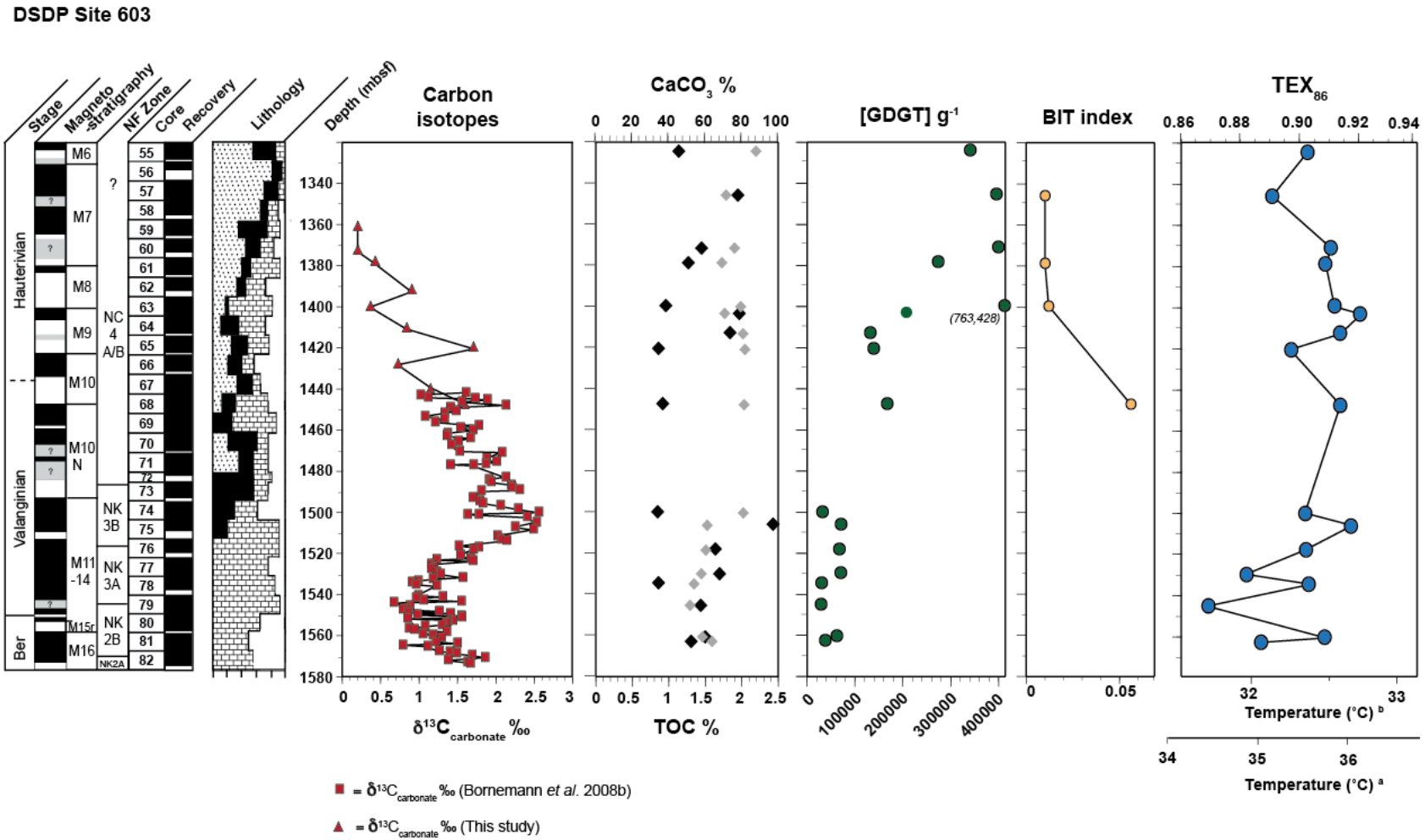

Figure 69. *Carbonate carbon isotope, Total Organic Carbon content (TOC %), calcium carbonate content ($CaCO_3$%), GDGT abundance, BIT Index and TEX_{86} / SST data for DSDP Hole 603B. $CaCO_3$ and TOC% are weight percent measurements. Lithology is the same as for Figure 33b.*

4. 4. 3. DSDP SITE 766

A new bulk –organic matter carbon-isotope record ($\delta^{13}C_{org}$) was generated at ODP Site 766 in order to further constrain the age model (Figure 70). There is no evidence for a positive excursion associated with the mid Valanginian CIE in the lower part of the core (410 – 460 mbsf), supporting the Late Valanginian age assignment suggested by bio- and magnetostratigraphy. The relatively steady $\delta^{13}C_{org}$ values observed between 410 and 310 mbsf support a Hauterivian age interpretation for these sediments, while the drift to more positive $\delta^{13}C_{org}$ values between 310 and 240 mbsf mirrors a similar rise seen in Late Hauterivian-Early Barremian sediments in other carbonate Tethyan records (e.g. the Cismon Core record, Erba *et al*., 1999), supporting a similar age assignment at Site 766.

The $CaCO_3$ content throughout the Neocomian sediments at Site 766 is uniformly low and does not rise above 10%, with an average value of only 3.4 %, consistent with the dominant siliciclastic sediments at this location. The average TOC content at Site 766 is very low at only 0.6 % and is more variable than that of the $CaCO_3$ record. A prominent maxima in TOC% of ~0.9 – 1.0 % in the Late Valanginian against a background of 0.3 – 0.6 % values, occurs prior to the maxima in TEX_{86} SSTs in the earliest Hauterivian.

It was possibly to quantify the BIT index for 17 of the 19 successful TEX_{86} samples, which yielded average values of 0.038 (Table 5, Figure 70). This value is nearly twice that seen at Sites 534 or 693, and suggests slightly higher input of terrestrial GDGTs to this hemipelagic site, consistent with results from Rock Eval analysis that suggest a dominantly terrestrial source for the organic matter at Site 766 (Ludden *et al*., 1990b). BIT Index values are relatively constant throughout the studied interval, but begin to steadily increase in the latest Hauterivian to earliest Barremian, mirrored by an increase in TEX_{86} values and $\delta^{13}C_{org}$; however, there is no overall correlation between TEX_{86} and BIT Index at Site 766, ($r^2 = 0.047$) (Figure 70).

Site 766 was the only one of the three southeastern Indian Ocean Sites sampled to yield TEX_{86} and BIT Index data in this study, although one data point was also obtained from Site 763 (see Section 4-4-7). Of the 24 Late Valanginian – Early Barremian mixed siliclastic samples analysed in this study, 19 yielded TEX_{86}

data reliable enough to convert to SST estimates (Table 5; Figure 70). The average GDGT abundance observed throughout the hole was 202,000, which is less than half the abundances seen at Site 534, and only slightly more than the average abundances seen at Site 603.

The TEX_{86} record at Site 766 shows significant variation over the course of the Valanginian to Barremian (Figure 70). These trends can be interpreted in terms of both changes in SST as well as some influence from changing lithology, as unfortunately due to the nature of the hemipelagic sediments, it was not possible to select nannofossil-rich laminated marls for direct comparison with the low-latitude sites. The average TEX_{86} value at this site is 0.657, which translates as 26.1 ºC using the logarithmic calibration, and slightly cooler temperatures of 25.4 ºC using the reciprocal calibration (Table 5, Figure 70). A cooling trend, 1.4 ºC in magnitude regardless of calibration, is seen in the Late Valanginian, which culminates in a minimum value of 0.632 (25.0 º C, logarithmic calibration) in the latest Valanginian. A sharp excursion to more positive values of 0.710 (28.4 ºC, logarithmic calibration) occurs in the earliest Hauterivian, which then decays back to lower values of 0.640 – 0.660 (25.5 – 26 ºC) in the mid Hauterivian, before rising once again in the earliest Barremian to ~0.690 (27.6 ºC). The total range in SST is 0.078, which corresponds to 3.4 ºC of temperature variation using the reciprocal calibration.

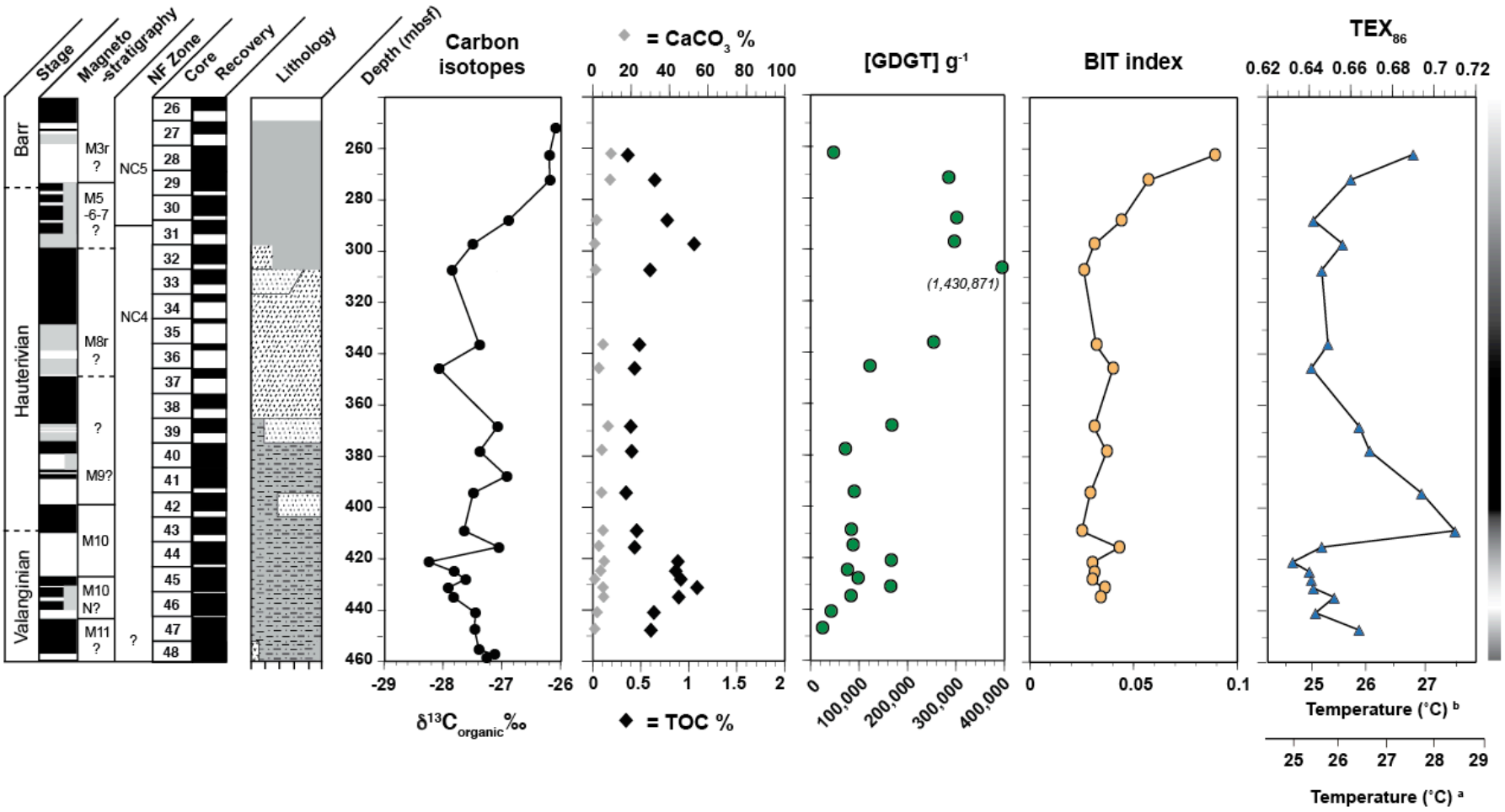

Figure 70. *Carbonate carbon isotope, Total Organic Carbon content (TOC %), calcium carbonate content ($CaCO_3$%), GDGT abundance, BIT Index and TEX_{86} / SST data for ODP Hole 766A. $CaCO_3$ and TOC% are weight percent measurements. Lithology is the same as for Figure 33c.*

4. 4. 4. ODP SITE 692

Bulk organic carbon-isotope ($\delta^{13}C_{org}$) data were generated for ODP Site 692 in an attempt to constrain the age assignment more tightly than the "Valanginian-Hauterivian" estimates provided by the biostratigraphy (Section 2-1-4., Figure 71). The average value is ~-30.5 ‰ and there is some variation in the record, with a range of values from 29 to 31.5 ‰. Although there are no distinctive excursions in the CIE record that can be tied convincingly to any particular time period, the generally light values could be interpreted as suggesting either an Early Valanginian or mid-Late Hauterivian age.

The $CaCO_3$ content is quite variable at Site 692, ranging from 4.4 % in the lower part of the Section to a high of 70.0 % in one sample from 70 mbsf, with an average value of 30.0 % overall. The TOC record is more remarkable, and shows that the Valanginian-Hauterivian sediments are heavily enriched in organic-matter rich with an average value of 8.1 % (Table 5, Figure 71). There is variation in the TOC % record with time, with values ranging from 3.8% in the lower part of the section, to extraordinary highs of 16.2 % near the top of the section. There is also an interesting covariance between TOC% and GDGT concentration in the upper part of the section, with higher TOC values generally being accompanied by more abundant GDGTs ($r^2 = 0.680$).

The BIT Index could be determined at 7 out of the 12 samples, and averaged 0.022 (Table 5, Figure 71). This finding lends confidence to the assumption that the SST reconstructions using the TEX_{86} proxy have not been unduly biased by terrestrial contamination, despite its marginal hemipelagic setting. All of the 12 samples that were analysed for TEX_{86} at this site yielded TEX_{86} data (Table 5, Figure 71).

The GDGT abundances were generally high throughout and averaged 1,820,000. TEX_{86} values average 0.714, which corresponds to 28.6 ºC or 27.7 ºC when using the logarithmic and reciprocal calibrations respectively (Table 5, Figure 71). The TEX_{86} record at Site 692 shows some variability with time, in particular a coherent cooling and subsequent warming event in the centre of the section of unknown age and duration. Maximum values of ~0.750 (29 – 30 ºC) are seen at the base and at top of the core, while cooler minimum values of ~0.680 (26 – 27 ºC) are seen in the centre of the section (Figure 71). There is no correlation between TEX_{86} and TOC % ($r^2 = 0.05$), nor between $CaCO_3$ and any of the organic variables.

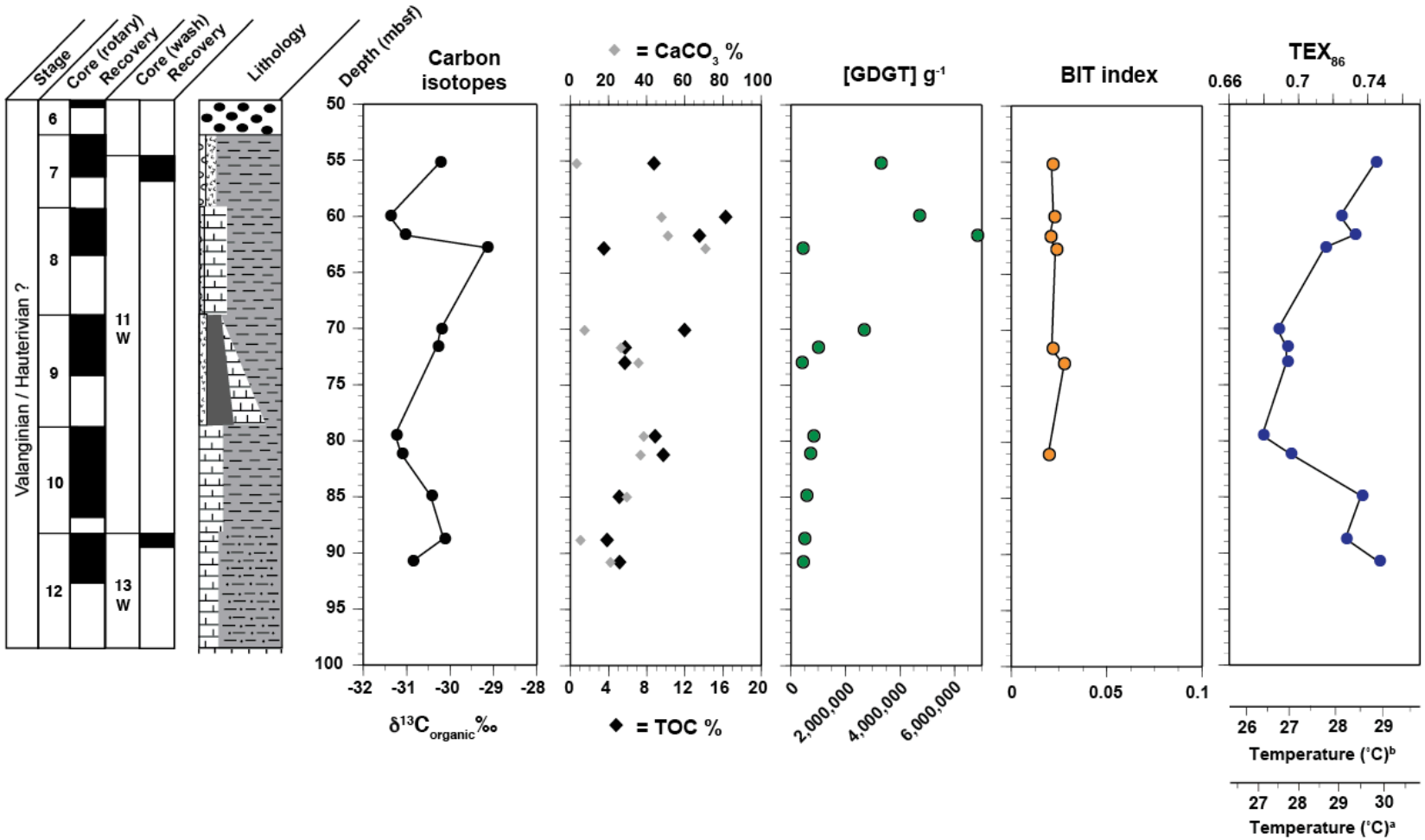

Figure 71. *Carbonate carbon isotope, Total Organic Carbon content (TOC %), calcium carbonate content ($CaCO_3$%), GDGT abundance, BIT Index and TEX_{86} / SST data for ODP Hole 692B. $CaCO_3$ and TOC% are weight percent measurements. Lithology is the same as for Figure 33d.*

4. 4. 5. DSDP SITE 249

The age control at DSDP Site 249 in the southwestern Indian Ocean is not well constrained, and Cores 25 to 32 can only be resolved to a tentative "Neocomian" (Berriasian to Hauterivian) age bracket, while Core 24 is likely Aptian/Albian in age. This is due to the poor recovery associated with spot-coring at this site. No carbon-isotope data are available or was generated for this site.

The $CaCO_3$ content is uniformly low throughout the section, consistent with the siliciclastic-dominated hemipelagic setting, with average values of only ~1 % (Table 5, Figure 72). The TOC content is also fairly invariant, fluctuating between 0.4 % and 1.4 % with average Neocomian values of 0.92 %.

The BIT Index is consistently low with a Neocomian average of 0.076, however, this value is still twice as high as the DSDP Site 766 values and more than three times as high as the low-latitude values (Table 5, Figure 72). This indicates a greater input of terrestrial GDGTs to this site than at the pelagic North Atlantic sites, or the other hemipelagic sites in the Weddell Sea and southeasten Indian Ocean, but it is still far below the 0.3 BIT Index threshold above which palaeotemperature estimates may become suspect.

Of the nine samples analysed, seven returned usable TEX_{86} data, with a generally strong GDGT signal throughout. The average GDGT abundance was 2,050,000 g^{-1} for all the data, or slightly lower at 1,730,000 g^{-1} if only the Neocomian data are considered, which is on a par with the signal from the very TOC-rich samples from Site 692 (Table 5, Figure 72). There is no correlation between GDGT abundance and TEX_{86} value (r^2 = 0.068) in the Neocomian sediments. There is a large range in TEX_{86} values and therefore SST estimates at this site, which is probably an artifact of the large age-range represented by Cores 24 to 32. The average value of the Neocomian sediments is 0.605, which correspond to SSTs of 23.6 ºC using the logarithmic calibration, or 22.9 ºC using the reciprocal calibration (Table 5, Figure 72). There is a very weak positive relationship between TOC% and GDGT abundance throughout (r^2 = 0.301), but no relationship between $CaCO_3$ % and GDGT abundance (r^2 = 0.002), although conclusions based on such a small dataset (n= 6) should be treated with caution. There are only very weak relationships between both TOC and TEX_{86} (negative; r^2 = 0.265), and between $CaCO_3$ % and TEX_{86} (positive; r^2 = 0.356), but again these are likely to be artifacts of the small sample size.

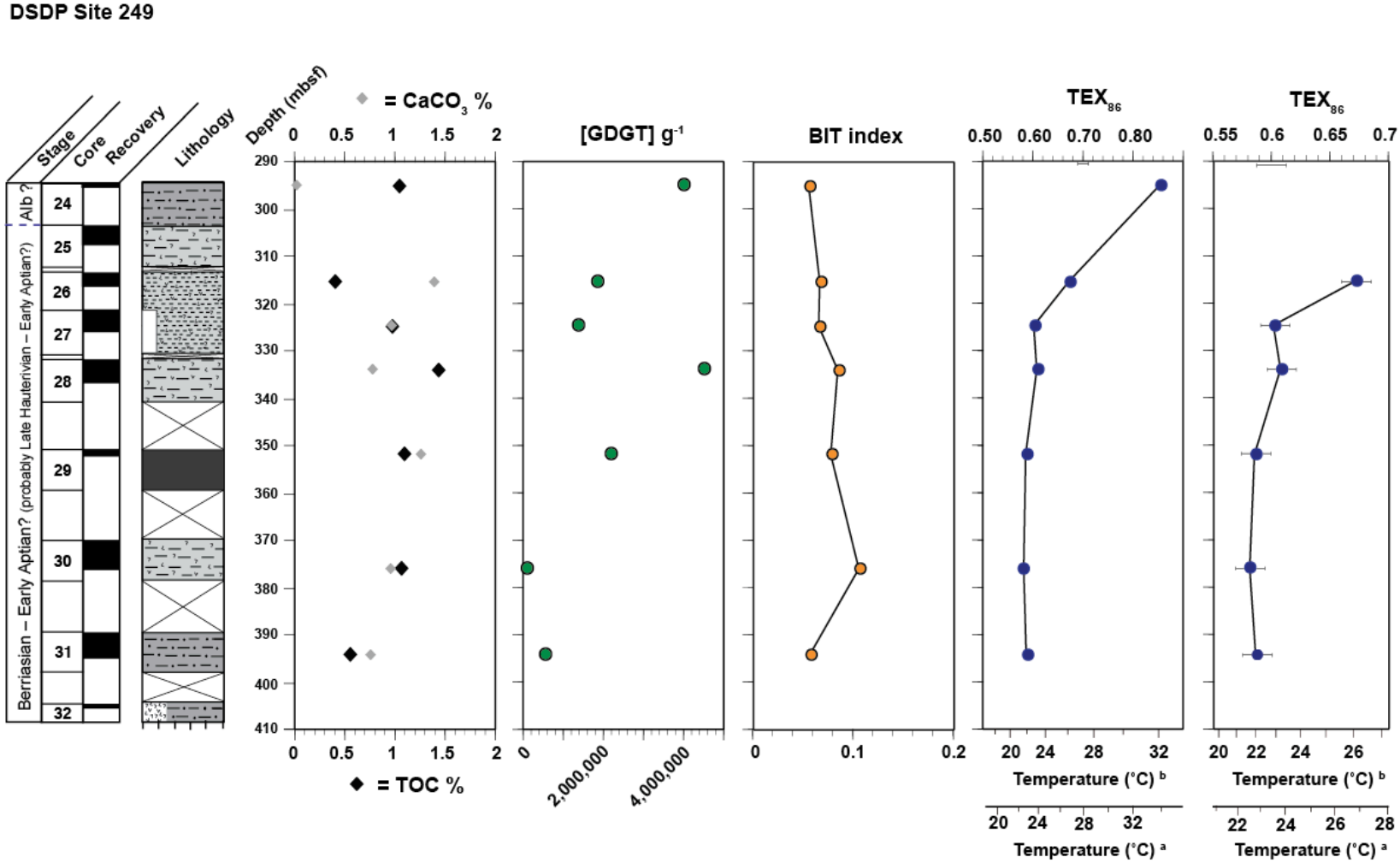

Figure 72. *Carbonate carbon isotope, Total Organic Carbon content (TOC %), calcium carbonate content ($CaCO_3$%), GDGT abundance, BIT Index and TEX_{86} / SST data for DSDP Hole 249. $CaCO_3$ and TOC% are weight percent measurements. Lithology is the same as for Figure 33e. Final panel on right is the same TEX_{86} data presented at a different scale for clarity.*

4. 4. 6. ODP SITE 763

Site 763 lies close to Site 766 on the central Exmouth Plateau, but is located in water depths of only ~1.3 km, compared to nearly 4 km at Site 766. Two pilot samples of Late Berriasian–Early Valanginian age were analysed for TEX_{86}, and initially both failed to yield sufficient GDGTs for integration and further analysis of the site was abandoned. However, subsequent reanalysis of the samples at a much higher concentration yielded a positive TEX_{86} result for one Late Berriasian sample. The abundance of GDGTs per gram in this sample was quite low at 32,600, but the absolute abundance of GDGTs in the sample-run was sufficient to suggest that the result is reliable. The TEX_{86} value from this one sample was 0.610, which corresponds to SSTs of 23.9 ºC using the logarithmic calibration and the very similar value of 23.2 ºC using the reciprocal assumption (Table 5, Figure 73).

Interestingly, the BIT Index for this sample is 0.126, which is by far the highest value seen at any of the sites, pelagic or hemipelagic in nature, and which suggests a not insignificant contribution of terrestrial Branched GDGTs. This is consistent with the findings of the biostratigraphic studies conducted at this site, which concluded that the regional Barrow Group, which this sample corresponds to in terms of age and lithology, is only "partially marine" and was certainly deposited in a marginal marine environment (e.g. Bralower & Siesser 1992). As previously noted however, a BIT Index <0.3 is not considered problematic with regards to absolute SST reconstruction.

4. 4. 7. DSDP SITE 416

Low-resolution carbonate carbon-isotope ($\delta^{13}C_{carb}$) data was generated at Site 416 (Appendix Table 3). However, the record was dominated by very negative $\delta^{13}C$ values averaging -2.0 ‰, with large swings in both carbon and oxygen isotopes indicative of a diagenetic origin for the isotopic signals (Appendix Table 5).

Of the 9 samples that were analysed from DSDP Site 416 in the eastern North Atlantic, none returned a usable TEX_{86} value, due to an almost complete absence of GDGTs in these turbiditic samples. On one hand this is surprising, as the TOC content reported in the Site 416 Initial Report (Lancelot *et al.*, 1980) for the

Neocomian sediments, is on the order of 0.6%, which is higher than many of the samples which returned successful TEX_{86} results in the pelagic sediments at DSDP Sites 534 and 603. However, when the nature of the sediment is considered, which was often a reddish brown colour indicative of oxidative conditions, and the style of deposition in thick turbidite deposits, the poor preservation of the GDGTs is perhaps less surprising.

4. 4. 8. ODP SITE 765

No isotope or TOC/ $CaCO_3$ % data were generated for ODP Site 765. Five samples of Barremian to Berriasian/Valanginian in age were analysed for TEX_{86}, however, none of these samples returned a positive result. This was due to abundances of GDGTs that were, presumably, below detection limits in all cases except for the shallowest sample, where GDGT peaks were detected in the spectra but were too small to integrate. This is likely due to the deep-water setting of this site, currently at 5717 m, and the subsequent low TOC contents observed throughout this section, as published in the initial report (Ludden *et al*., 1990a).

4. 4. 9. BGS SITE 81/ 43

No isotope or TOC/ $CaCO_3$ % data were generated for BGS site 81/43. A selection of 8 samples of Valanginian to Hauterivian age were analysed for TEX_{86}, to extend the latitudinal range of the TEX_{86} study into the boreal realm of the Northern Hemisphere, however none of these analyses were judged to be have produced reliable SST estimates. GDGTs were present all samples but abundances were very low and generally below integration limits. This could be due to low original concentrations of GDGTs in the sediments, or subsequent post-depositional or post-sampling degradation of the lipids. It should be noted however, that if the GDGT total abundance limit of 100,000 is ignored, and three of the strongest GDGT spectra samples are converted to TEX_{86} values regardless of the inherent uncertainties, very tentative SST estimates can be calculated (Table 5). In this case, average SSTs for the Late Berriasian–Early Barremian are 27.4 ºC overall (logarithmic calibration), with cooler temperatures in the Early Valanginian of 25.0 ºC which peak at 29.2 ºC

in the Latest Hauterivian. However, these SSTs are not considered reliable, and should be regarded as general indicators of temperature range only.

4. 4. 10. TOC AND CaCO3 % ALL SITES

TOC and $CaCO_3$ contents varied between the sites depending on their oceanographic setting and sampled lithology (Figures 47–51). At the low-latitude proto-North Atlantic Sites, 534 and 603, the TOC and $CaCO_3$ records are largely invariant due to lithology selection for "laminated marls" throughout. The average $CaCO_3$ content at both sites is high (>60 %) which reflects the large calcareous nannofossil component of the marls at both locations (Table 3). The TOC content was relatively low at Site 534 and averaged just 0.88 %, while the value at Site 603 was distinctly higher averaging 1.41 %. There was some variability in the TOC% record, for example at both sites there is a small but significant increase in TOC% coincident with the base of the peak $\delta^{13}C_{carb}$ positive excursion in the mid-Valanginian (Figures 47 and 48).

The $CaCO_3$ content at the mid-latitude sites is much lower than at the low-latitude sites and generally does not rise above 10%, consistent with the hemipelagic settings and siliciclastic nature of the sediments, with the exception of Site 692 which had a higher average carbonate content (Table 3; Figures 49–51). The TOC contents in the hemipelagic sediments are much more variable, ranging from lows of 0.34 % at Site 766 to highs of >16 % and average value of 8.13 % at Site 692, which demonstrates that the Valanginian – Hauterivian sediments at the latter site are heavily enriched in organic-matter, likely due to the restricted nature of the basin.

Importantly there is no correlation between $CaCO_3$% and TOC% with either TEX_{86} value or GDGT abundance at any of the sites (correlation below $r^2 = 0.3$), suggesting that lithology is not playing an important role in determining SST trends within the sites. One exception to this rule is the significant correlation between TOC% and GDGT concentration seen at Site 692 in the upper part of the section, where higher TOC values are often accompanied by more abundant GDGTs (correlation coefficient of all 692 data GDGT and TOC% = 0.680). However, importantly this covariance does not have an effect on the TEX_{86} values, as there is no correlation between TEX_{86} and TOC % ($r^2 = 0.05$).

4. 4. 11. GDGT CONCENTRATIONS ALL SITES

GDGT abundances varied markedly between the different sites (Table 5), which led to varying levels of success with regards to TEX_{86} analysis. Highest values were seen in the organic-matter rich sediments from Site 692 (average of 1,820,000 g^{-1}), which contained nearly 10x the average abundances seen in the weakest site, DSDP Site 603, where only 57 % of the samples were successfully analysed for TEX_{86}. Both Site 534 and Site 766 had consistently higher GDGT abundances than Site 603, despite having much lower TOC % values. The finding that the site with the highest organic-matter content had the highest GDGT abundance is perhaps not surprising. However, the fact that Site 603 had the lowest GDGT signal, despite having relatively high average TOC contents, suggests that raw TOC % alone is not a good predictor for GDGT abundance.

At all sampled sites where more than one data point was obtained, both pelagic and hemipelagic, there is a trend for higher GDGT abundances in the shallower samples *vs*. the deeper samples (Figures 47–51). This trend is independent of factors such as TOC or $CaCO_3$ content *within* each site, which show no correlation ($r^2 < 0.3$) to GDGT abundances.

4. 4. 12. BIT INDICES ALL SITES

The higher BIT Indices seen at three of the hemipelagic mid-latitude sites (Sites 766, 763 and 249), compared to the pelagic low-latitude sites (Sites 534 and 603), suggests that the BIT Index is generally reflecting a relatively higher terrestrial input at these sites during the earliest Cretaceous. However, BIT Indices at all of the studied sites, both pelagic and hemipelagic, were far below the recommended threshold of 0.3 (Weijers *et al*., (2006b), lending confidence to the notion that the TEX_{86} palaeotemperature reconstructions have not been unduly influenced by terrestrial GDGT contamination at any of the studied sites. Importantly, there was no covariation noted between BIT Indices and TEX_{86} values, nor between BIT indices and GDGT contents at any of the sites, further suggesting that terrestrial GDGTs have not influenced the SST reconstructions in this study.

4. 4. 13. TEX_{86} SST ESTIMATES ALL SITES

The reconstructed average annual SSTs at both of the low-latitude proto-North Atlantic sites are very warm, ranging between 33–37 ºC depending on calibration (Table 5; Figures 68, 69). Temperatures at Site 603 appear slightly cooler than at Site 534 throughout the Berriasian–Valanginian, however this difference of ~0.4 ºC (logarithmic equation) between the sites is only slightly above the analytical error of ±0.01 (~0.25 ºC) and so probably cannot be regarded as statistically significant (Figure 73). The average reconstructed SSTs at the four mid-latitude sites that yielded TEX_{86} data were also very warm, ranging between ~23 – 29 ºC (Figures 70 – 72). The average SST estimates at Site 766 are 25.4 – 26.1 ºC depending on calibration, which is very warm considering the palaeolatitude estimate of ~53 ºS, but still considerably lower than those seen at Sites 603 and 534 (Table 5; Figures70, 73). The SST estimate of 23.9 ºC (logarithmic calibration) for the Late Berriasian data point at Site 763, is similar to the other mid-latitude values seen in the Indian Ocean and Weddell Sea, however, compared to the lowest SST seen at nearby Site 766 in the latest Valanginian of 26.4 ºC, this value is significantly cooler (Figure 73). The average SST estimates at Site 692 (28.6 ºC, logarithmic calibration) also suggest very warm temperatures with respect to the modern at equivalent latitudes (~59º), but is slightly warmer than the ~26 ºC seen at Site 766. However, the age control is not as robust at Site 692 as for the other sites so direct comparison is difficult (Table 5; Figures 71, 73). The Neocomian SSTs at Site 249 are the coolest seen at any of the studied sites (range of 21 –27 ºC depending on calibration), although the poor age control at this site hampers accurate comparison with the other SST records (Table 5; Figures 72, 73).

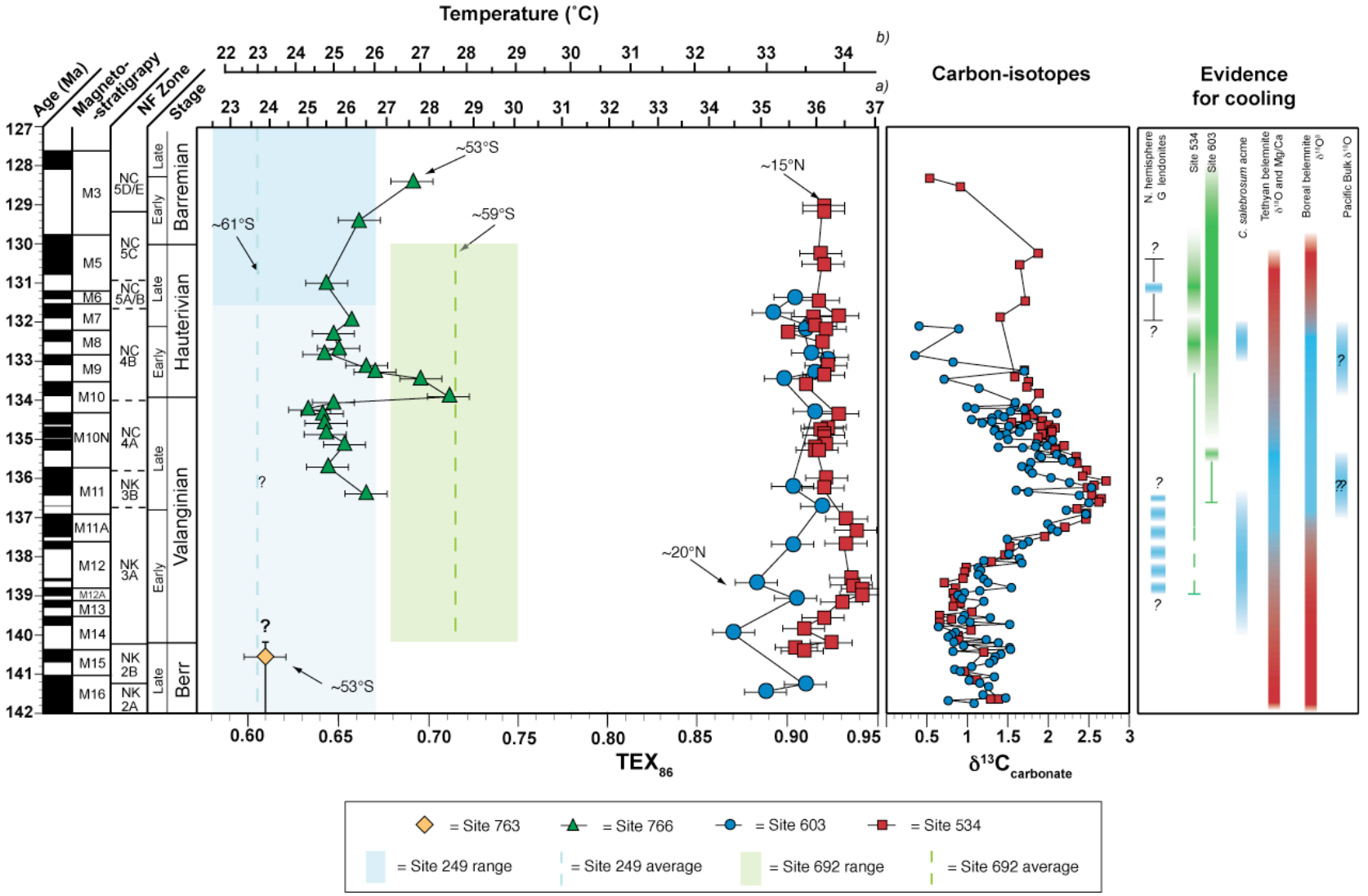

Figure 73. *All TEX86 data from Sites 534, 603, 766 and 763 on a common age model based on magnetostratigraphy and biostratigraphy. Due to major uncertainties in the age model at Sites 249 and 692, the TEX86 data are plotted as a range and an average value for each site. A selection of other temperature indicators is also plotted for comparison (see Figure 66 and Section 4.2 for*

4. 4. 14. TEX_{86} SST VARIABILITY ALL SITES

At both the low-latitude proto-North Atlantic sites the trend is for very stable temperatures across the entire 12 Myr study interval, as the small total range in temperatures demonstrates (1.4 – 1.8 ºC). However, at Site 534 there is a small (<1 ºC) discrete "warming pulse" between 1200 and 1240 mbsf which is Early Valanginian in age (~137 to 140 Ma), although the magnitude of this increase in (~0.04) is only slightly above analytical error of ±0.01 and so may not be statistically significant (Figures 68, 73). Similar but less coherent variability is seen in the Late Berriasian–Early Valanginian at Site 603, and a small shift (~1.7 ºC) to cooler SSTs from the Berriasian–Valanginian boundary to the mid-Valanginian may be discernable (Figures 69, 73).

The higher-latitude sites display more variability in SSTs, as seen in the larger total range of temperatures at Sites 766, 692 and 249 (Table 5; Figures 70–73), which is probably attributable to both genuinely higher SST variability at these latitudes, and the effects of minor lithological differences in the hemipelagic sediments. For example, at Site 766 the total range in SSTs from the Late Valanginian to the Early Barremian is quite high compared with the low-latitude sites (range of 3.4 ºC), showing a cooling trend of 1.4 ºC in the Late Valanginian followed by a prominent warming event of 3.4 ºC just above the Valanginian-Hauterivian boundary (logarithmic calibration; Figures 70, 73). The TEX_{86} record at Site 692 also shows some variability, in particular a coherent minor cooling and subsequent warming event in the centre of the section, with a magnitude of 2.8 ºC (logarithmic calibration; Figure 71). Unfortunately, neither the age nor the duration of this cooling event can be determined, as the Early Cretaceous part of the core can only be constrained to a likely "Valanginian- Hauterivian" age. Site 249 exhibits the largest range in palaeotemperatures of all the sites (4.3 ºC), which may, in part, be due to the large age-range this core likely represents (Neocomian or Early Aptian to possibly Albian), combined with a more variable higher latitude climate than the low-latitude proto-North Atlantic sites (Figures 72, 73).

4. 5. DISCUSSION

4. 5. 1. A WARM AND STABLE EARLIEST CRETACEOUS?

4. 5. 1. 1. ELEVATED TEMPERATURES AT ALL LATITUDES ?

The earliest Cretaceous TEX_{86} dataset suggests that SSTs were greatly elevated with respect to the modern at a range of palaeolatitudes, from the low-latitudes to the upper mid-latitudes (15 – 60º). As the choice of TEX_{86} calibration will undoubtedly influence the SST reconstruction, particularly in the lower latitudes, it is prudent to first consider the raw TEX_{86} values when comparing to the modern. When all the average earliest Cretaceous TEX_{86} values (Table 5) are plotted against the modern calibration set, it is clear that the Cretaceous values at all latitudes are far in excess of those seen in the modern (Figure 74). The tropical TEX_{86} values far exceed any seen in the modern world, and the higher latitude samples (50–60º latitude) values of >0.600 are only found at < 30º absolute latitude in the modern world (Kim *et al*., 2010). The excellent agreement between Sites 534 and 603 in terms of TEX_{86} and the relatively good agreement between the various higher latitude sites despite the differences in longitude, should give confidence that the earliest Cretaceous TEX_{86} values are indeed reflecting latitudinal temperature gradients (Figure 74).

The low-latitudes

Modern average annual SSTs in the tropics (0 – 20º) ranges between ~19 and 29 ºC, with most non-upwelling regions being characterized by temperatures > 25 ºC (Figure 74, 75; Locarini *et al*., 2006). Regardless of calibration, even using the less sensitive reciprocal calibration the average SST at Site 534 (~15º palaeolatitude) is ~34 ºC, which is 5 ºC warmer than the warmest average annual SSTs seen at that latitude in the modern (Figure 74). If the logarithmic assumption is used then the earliest Cretaceous SST estimate at 15º is ~36 ºC, some 7 ºC warmer than the warmest modern equivalent. The SST estimates from Site 603, located slightly farther north at a palaeolatitude of ~20 ºN, also suggest very warm tropical temperatures, only slightly lower than those seen at Site 534 (Figure 74). These

results strongly suggest very warm conditions in the earliest Cretaceous tropical regions.

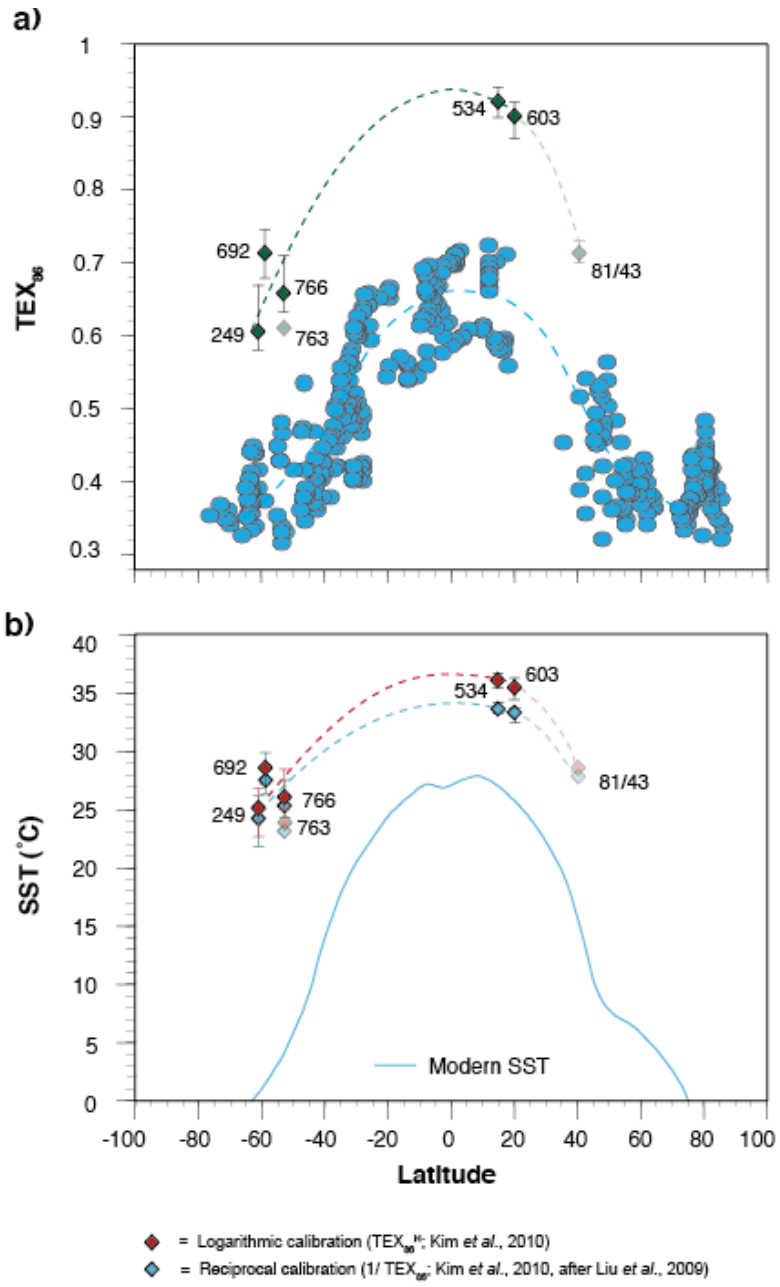

Figure 74. *a) All earliest Cretaceous average TEX_{86} plotted against latitude and compared to modern calibration set (Kim et al., 2010) minus the Red Sea data. b) TEX_{86} SST estimates (both calibrations) plotted against latitude and compared to modern SST gradient (Shea et al., 1992; Locarini et al., 2006). Error bars represent the total range of SSTs seen at each site. Translucent earliest Cretaceous data points are to be considered as tentative, especially data from BGS Site 81/43 which is probably not reliable. Bars indicate range of TEX_{86} values at each site.*

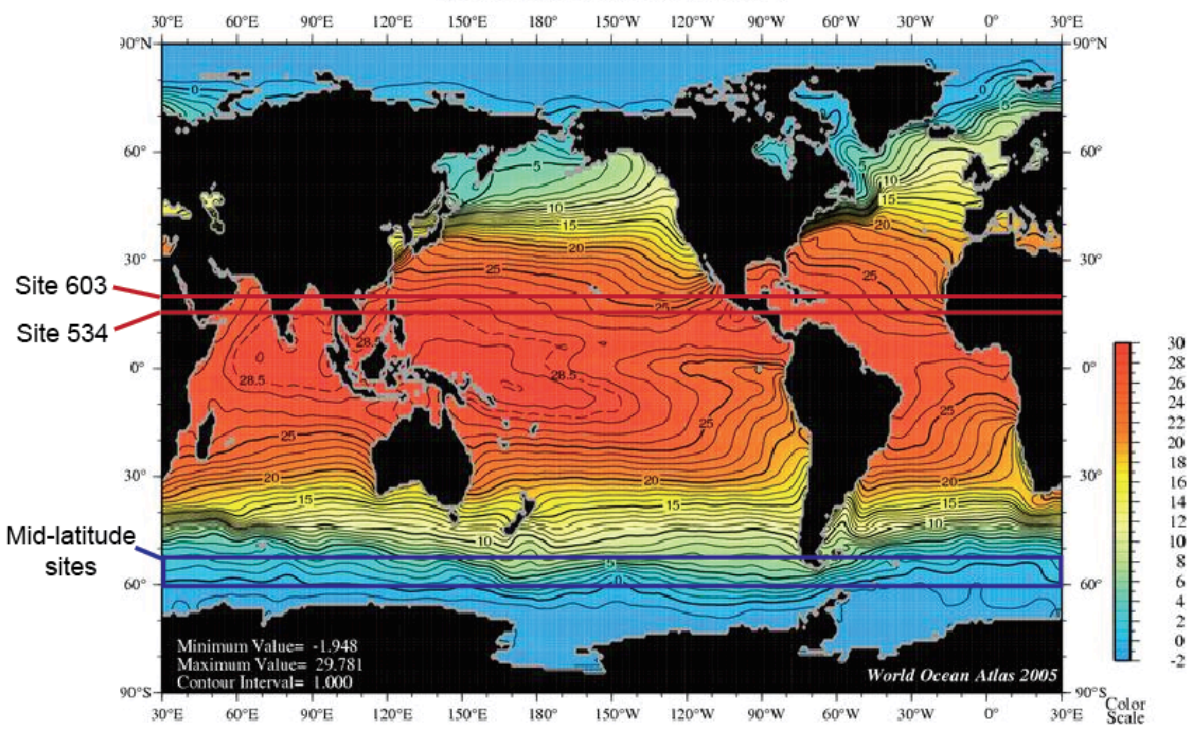

***Figure 75**. Modern average annual sea-surface temperatures showing great longitudinal variation, (Locarini et al., 2006), with palaeolatitudes of Early Cretaceous sites (Site 534 = ~15°N, Site 602 =~20 °N, Sites 766, 763, 249 and 692 = 53 to 61 °S) shown as coloured lines.*

Although the earliest Cretaceous SSTs at Sites 534 and 603 clearly demonstrate elevated temperatures in the low-latitudes with respect to the modern, there are some palaeoceanographic reasons why the palaeo-North Atlantic might be expected to have both higher temperatures than a larger marine body at an equivalent latitude. The palaeo-North Atlantic in the Late Jurassic–Early Cretaceous was considerably smaller and narrower than the present day North Atlantic and is likely to have had a correspondingly more restricted circulation regime (Figure 76; Ager 1975; Sheridan *et al*., 1983; Puceat *et al*., 2005). During the Late Jurassic it is likely that the proto-North Atlantic was still a rather narrow seaway, with shallow connections to the Western Tethys in the straits between Africa and southern Europe, narrow connections to the boreal realm and the Arctic Ocean to the north, and limited if any connection to Panthalassa (the modern Pacific Ocean) at its western extremity (Ager 1975; Sheridan *et al*., 1983; Figure 76). However, it is thought that by the earliest Cretaceous the continued rifting of Pangaea had made the proto-North Atlantic more open and unrestricted, with stronger and deeper connections to the Western Tethys and a likely connection to Panthalassa via the westward flowing

Tethyan Circumglobal Current (TCC) through Central America, (Figure 76; Puceat *et al*., 2005). Additionally, as sea-levels rose through the Valanginian and Hauterivian it is likely that the proto-North Atlantic became even less restricted with increased connectivity to the World oceans through newly opened oceanic gateways (e.g. Hardenbol *et al*., 1998; Mutterlose *et al*., 2003, Melinte & Mutterlose 2001; Figure 65).

Both sedimentological and palaeontological data support a normal open marine depositional environment during the Berriasian–Barremian for Sites 534 and 603 in the western proto-North Atlantic, and at many other Atlantic sites of this age (e.g. Robertson & Bliefnick, 1983; Sheridan *et al*., 1983; Robertson, 1984; van Hinte *et al.,* 1987). Such evidence includes the widespread deposition of pelagic carbonate facies dominated by calcareous nannofossils (e.g. Sites 534, 535 and 603), a lack of organic-matter enriched facies, which might be expected in an oxygen-poor restricted basin (e.g. Site 692), and the presence of open marine fauna such as ammonites and belemnites. However, the proto-North Atlantic is still likely to have had more restricted and sluggish deep-water circulation than a larger ocean at comparable latitudes, as evidenced by the common occurrence of laminated and unbioturbated carbonate facies at localities such as Sites 534 and 603 which suggest periodically dysoxic bottom water (Robertson & Bliefnick, 1983; Robertson, 1984; Puceat *et al*., 2005).

The closest suitable analogy for the proto-North Atlantic in the earliest Cretaceous may be the modern Mediterranean Sea, which is a partially restricted low-latitude basin with limited connectivity to the World Oceans. However, the Early Cretaceous proto-North Atlantic is not thought to have been as restricted as the modern Mediterranean, which only maintains a connection to the modern Atlantic Ocean through the narrow Straits of Gibraltar (Puceat *et al*., 2005). Regardless, even if circulation was somewhat restricted relative to the modern, average SSTs in the modern day Mediterranean Sea are warmer by only 1 – 2°C, relative to the eastern Atlantic Ocean at equivalent latitudes (Locarini *et al*., 2006), and therefore cannot fully explain SSTs >5 ºC warmer relative to the modern at Sites 534 and 603 (Figure 75). However, the potential effect of salinity on the TEX_{86} proxy in such a restricted basin should also be considered, as even though no salinity effect is seen in "normal" marine conditions (e.g. Wuchter *et al*., 2004), in the modern Red Sea where salinity levels average 40 psu, the TEX_{86} values do not match the global calibration (Kim *et*

al., 2008). There are no estimates for proto-North Atlantic salinity in the earliest Cretaceous, but Albian modelled estimates suggest normal marine salinities of only ~36 psu (Poulsen *et al*., 2001). Higher salinities than this in the modern Mediterranean Sea of 37–39 psu, do not show any deviation from the open ocean TEX_{86} values at equivalent latitudes (Kim *et al*., 2008, 2010).

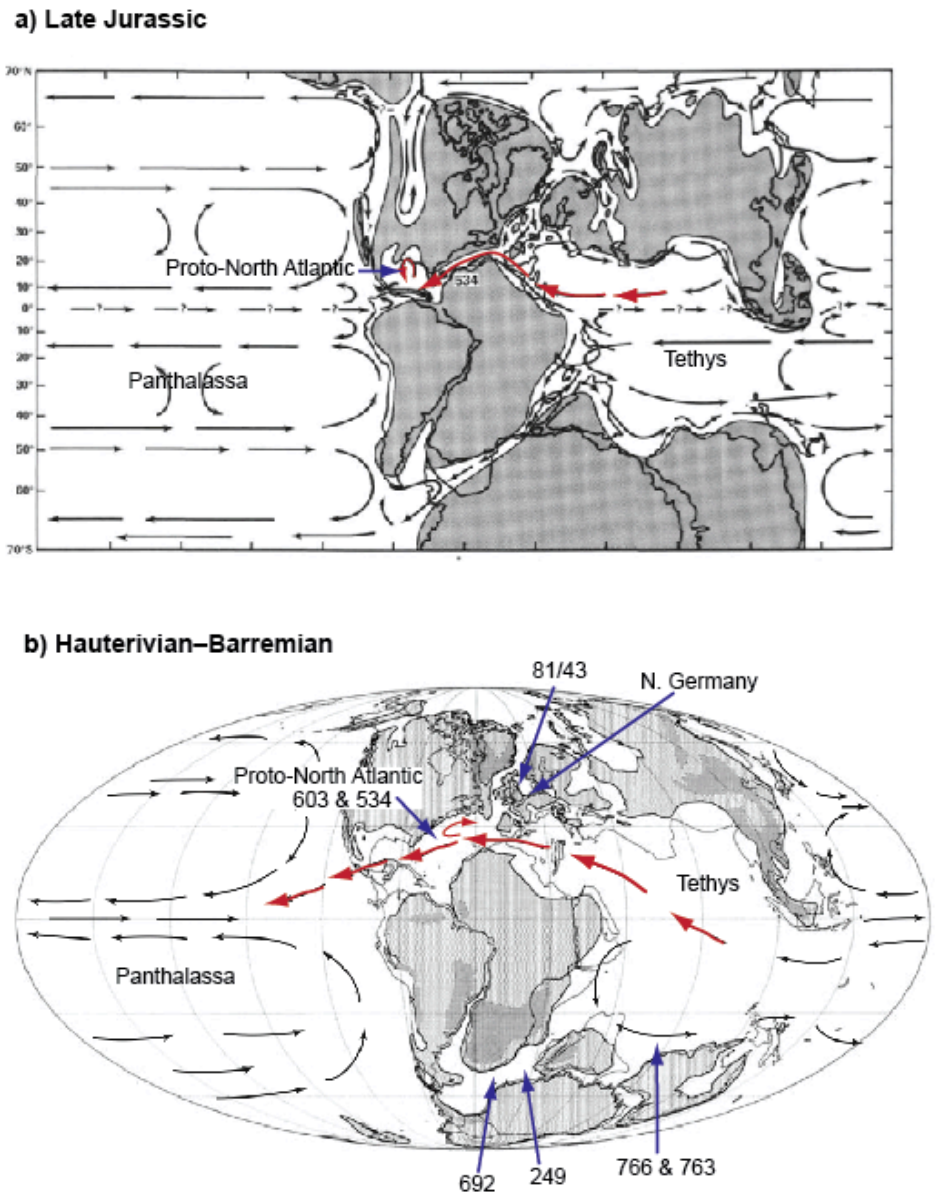

Figure 76. *Surface currents and palaeogeography, (a) the Late Jurassic (adapted from Sheridan et al., 1983); (b) the Early Cretaceous (Hauterivian–Barremian) adapted from Puceat et al., (2005). The TCC (red line) can be seen moving water from the Tethys into the North Atlantic, and beyond into the Panthalassic ocean in the Early Cretaceous, but not in the Late Jurassic.*

THE HIGHER LATITUDES

The higher latitude data (53 – 61 ºS) from Sites 766, 763, 692 and 249 also suggest greatly elevated SSTs with respect to the modern, with a total range in temperature from 22–29 °C (both calibrations; Figure 74). Modern annual average SSTs at these latitudes in the Southern Hemisphere range between -1 – 8 ºC, which are considerably cooler than the ~23 – 29 ºC SSTs suggested from the earliest Cretaceous mid-latitude SST estimates (Figures 75; Locarini *et al*., 2006). Combined with the complementary low-latitude data, these very warm average SSTs suggests a globally warm earliest Cretaceous period, which is not inconsistent with the hypothesised long-term evolution from cooler Late Jurassic temperatures (for which there is no available TEX_{86} data) to warmer and more humid conditions in the Early Cretaceous, as suggested by the prevalence of earliest Cretaceous coal deposits in many regions (e.g. Hallam 1984; 1985; Frakes *et al*. 1992).

The very warm temperatures at the higher latitudes, which are on the order of 20 °C warmer than the modern equivalent, cannot be explained purely by the oceanographic settings of the studied sites, although it is true that all of the sites (763, 766, 249, 692 and 81/43) occupied relatively marginal marine positions during the earliest Cretaceous, with variable levels of dysoxia and restriction in each case (Figure 76b). However, the sampling of such hemipelagic and potentially restricted sites is unavoidable, as no truly open marine pelagic sediments of this age have been recovered, or are likely to be recovered, from the higher latitudes of the Southern Hemisphere, due to a paucity of surviving oceanic crust of this age.

The Neocomian sediments at both Sites 766 and 249 are dominated by siliciclastic and volcanoclastic turbiditic sediments, thought to have been deposited in partially restricted, marginal settings, with strong terrestrial influences (Simpson *et al.,* 1974; Haq *et al*., 1990; Ludden *et al.,* 1990b). This conclusion is based on sedimentological inferences, benthic foraminiferal assemblages, the TOC and reduced iron content of the sediments, and Rock Eval analysis of the organic matter. It does not appear that lithology has a strong influence on TEX_{86} reconstructions in these higher latitude sites overall, however, there is an interesting covariance between magnetic susceptibility and TEX_{86} at Site 766, which may be significant in terms of the SST variability at that site (Figure 76). The increase in volcaniclastics at

the Hauterivian boundary appears to be accompanied by a spike in SSTs, but thereafter the temperatures decrease sharply even though the magnetic susceptibility remains high. This is not accompanied by any change in the BIT index or TOC content and is therefore inexplicable at present (Figure 71).

Site 692 is likely to have been the most restricted of the sites, with permanent dysoxic bottom-water conditions and occasional anoxia, as evidenced by the extraordinarily high TOC content, frequent laminations and limited evidence for marine benthos (Barker *et al*., 1988; Mutterlose 1990; O'Connell, 1990). Oceanographically it is likely that these semi-restricted conditions had some effect on the local SST conditions, which would perhaps be expected to be slightly warmer than open-ocean conditions where circulation was more vigorous. However, no modern analogies to these greenhouse world, higher latitude (~60°) enclosed basins exist, as basins in the modern World at such latitudes are much shallower than the 500–1000 m estimated for the Cretaceous basins and are uniformly cool and seasonally freezing (e.g. the Baltic Sea, Hudson Bay; Figure 75).

Importantly, in the context of the TEX_{86} proxy, the likely strong terrestrial influence at these marginal sites means that it is very important to constrain the terrestrial input of GDGTs to give confidence in the SST reconstructions. In all cases the BIT Index was far below the 0.3 threshold, and in most cases does not exceed 0.1 (Table 5, Section 4-4-12), suggesting that although there may be a large terrestrial component to the organic matter, the TEX_{86} proxy has not been affected. An additional complication at Site 692 may be the influence of sustained upwelling on the TEX_{86} signal itself, which is thought to have been common during the Valanginian–Hauterivian in this basin, on the basis of the high radiolarian and organic-matter content of the sediments (O'Connell, 1990). TEX_{86} is known to have a more complex relationship to temperature in modern dysoxic, upwelling regimes such as the Santa Barbara Basin or in organic-rich basins (e.g. Menzel *et al*., 2006; Huguet *et al*., 2007; Shah *et al*., 2008; Section 1-4-5), which may partially explain the slightly warmer SST estimates at this site relative to those from Site 766, despite the latter site being 6° of latitude further north in the Early Cretaceous.

The potential effect of seasonality on the TEX_{86} proxy at higher latitudes (e.g. the mid-latitude sites in this study) must also be considered. As discussed in Chapter 1, although the TEX_{86} core-top calibration-set correlates best with mean annual SST,

individual modern studies have demonstrated that strongly seasonal settings can modulate both the abundance of Crenarchaeota in the seawater and therefore potentially the TEX_{86} proxy and SST reconstruction (e.g. Murray *et al*., 1998; Church *et al*., 2003; Herfort *et al*., 2006). In modern high-latitude settings, GDGT production is highest in the winter-spring months, but GDGT flux to the sediments may be highest in the summer due to scavenging. Therefore it is possible that the SST reconstructions in the higher latitude earliest Cretaceous sites may not reflect mean annual average SST values and may instead either be skewed towards winter or summer temperatures (e.g. Church *et al*., 2003; Herfort *et al*., 2006; Wuchter *et al*., 2006b).

However, these calibration observations may not be applicable in the Cretaceous world. Firstly, the evidence for seasonality effects on TEX_{86} in the high-latitudes is based on observations in the modern (icehouse) world, where temperature extremes are encountered in the high-latitudes. The Cretaceous world has been shown from numerous lines of evidence to be warmer and more equable (e.g. Herman & Spicer, 1996; Skelton, 2003), so perhaps seasonality, and therefore differences between low- and higher-latitude TEX_{86} calibrations, might be expected to be less in a greenhouse scenario. Secondly, the earliest Cretaceous sites occupy only a mid-latitude palaeolatitude (53–61ºS), rather than the true high-latitudes (>65º), which would be more strongly affected by seasonal differences in variables such as light levels. In a greenhouse world, temperatures would be expected to be more equable, therefore seasonality extremes would not be expected at a latitude of only ~60 ºS. Thirdly, modern studies in the North Sea at a palaeolatitude of ~53 N suggest that TEX_{86} temperatures are skewed towards winter temperatures, in which case the SST reconstructions for the early Cretaceous at Site 766 can be regarded as minimum estimates for mean annual SST.

Lastly, the relatively good agreement between the three higher-latitude sites in terms of absolute temperature estimates, over a wide range of longitude, suggests that local conditions related to seasonality have not unduly modulated the SST signal (Figure 74). However, as a precaution it may be prudent to follow the example of Sluijs *et al*., (2006), who interpreted their very warm, high-latitude Eocene (greenhouse world) TEX_{86} record as probably representing summer-skewed values, for similar reasons to the ones discussed here. Regardless, even in the somewhat unlikely event of a slight summer bias in the TEX_{86} data, this would not be enough to

explain SSTs elevated by >20 ºC relative to the modern (Figures 70, 71, 72, 74). Furthermore, the fact that SSTs in the low-latitude sites are elevated, despite little evidence for low-latitude biasing of GDGT production or TEX_{86} values in open ocean in the modern World, lends confidence that global temperatures were likely to be genuinely elevated at all latitudes in the earliest Cretaceous, with respect to the modern (e.g Karner *et al*., 2001).

In conclusion, although the high TEX_{86} SST estimates at Sites 763, 766, 249 and 692 may reflect a minor influence from the marginal setting of these basins, or from limited seasonality effects on the TEX_{86} proxy, these factors cannot entirely explain the ~20–23 °C higher average temperatures relative to the modern at equivalent latitudes. The remainder of the temperature difference must be due to genuinely warmer global climates, as evidenced by increased SSTs at a range of latitudes.

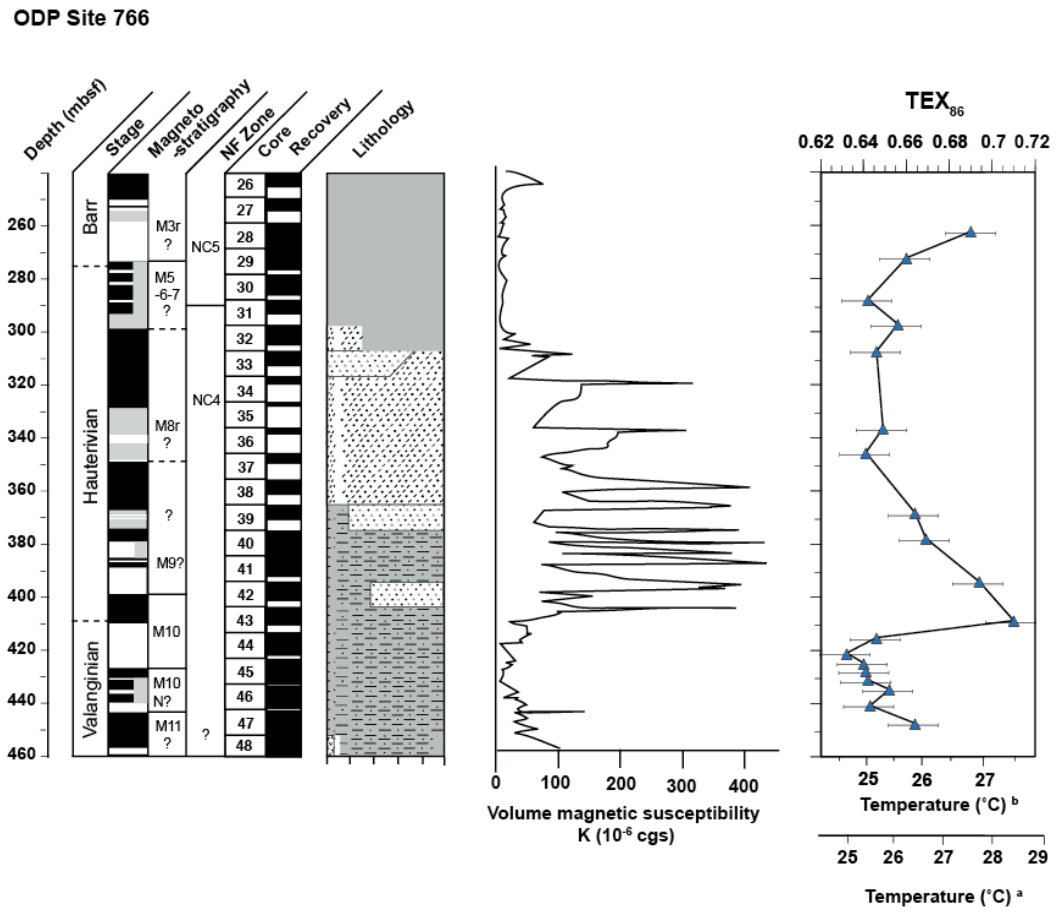

***Figure** 77. SST variation at Site 766 compared to the changes in lithology with time, showing the increased volcaniclastic input in the Hauterivian with respect to the Valanginian.*

4. 5. 1. 2. EARLIEST CRETACEOUS MERIDIONAL SST GRADIENTS

As absolute SST records of Valanginian–Hauterivian age have been produced from a range of latitudes in this study, it is possible to construct tentative meridional SST gradients based on this data. As three sites (534, 603 and 766) have well-constrained SST data of Hauterivian age, and this stage gives the most complete latitudinal coverage. If absolute temperatures are calculated, then numerical gradients can be determined between average Hauterivian values (Table 6a; Figure 78).

Site	Palaeolatitude	Average Hauterivian TEX_{86}	Average Hauterivian SST ºC (TEX_{86}^{H})	Average Hauterivian SST ºC ($1/TEX_{86}$)
534	~15 ºN	0.916	36.0	33.6
603	~20 ºN	0.907	35.7	33.5
766	~53 ºS	0.663	26.4	25.7

Table 6a. *Average Hauterivian TEX_{86} data and SST estimates from Sites 534, 603 and 766.*

Sites	Absolute Latitudes	Latitude difference	Hauterivian Gradient ºC/ ºLat (TEX_{86}^{H})	Hauterivian Gradient ºC/ ºLat ($1/TEX_{86}$)	Modern N. H. Gradient ºC/ ºLat	Modern S. H. Gradient ºC/ ºLat
534 – 603	15 º – 20º	5º	0.06	0.02	0.22	0.30
603– 766	20 º – 53º	33º	0.28	0.24	0.57	0.62
534– 766	15 º – 53º	38º	0.25	0.21	0.52	0.57
534– N. G	15 º – 33º	18º	0.47	0.38	0.36	0.37
603– N. G	20 º – 33º	13º	0.63	0.52	0.41	0.41

Table 6b. *Average Hauterivian gradients from Sites 534, 603 and 766, compared to modern gradients at equivalent latitudes. N. G. = Early Barremian data from northern Germany after Mutterlose et al. (2010).*

Between 15º and 53º latitude (Sites 534 and 766) average SST gradients for the Hauterivian are between ~0.25 ºC / º latitude using the logarithmic calibration

(TEX_{86}^{H}) and ~0.21 ºC / º latitude when using the reciprocal calibration ($1/TEX_{86}$) (Figure 78; Table 6b). This contrasts with a considerably steeper modern average gradient of ~0.52 ºC/ ºlat in the Northern Hemisphere and ~0.57 ºC / ºlat in the Southern Hemisphere for the same latitudinal range (Shea *et al*., 1992; Locarini *et al*., 2006; Figure 78b; Table 6b). The Hauterivian gradient between 15º and 53º latitude is approximately half that of the modern gradient in the Southern Hemisphere, regardless of calibration, with the low-latitude gradient between 15 and 20º being reduced to almost 0 (Table 6b; Figure 78). This represents a significant increase in meridional heat-transfer from the equator to the poles in order to sustain the observed flattened global SST gradient in the Hauterivian (e.g. Barron, 1983; Poulsen *et al*., 2003). This suggests that not only were global temperatures warmer than the modern in the earliest Cretaceous, but they were also much more equable, a concept which has long been suggested for the Cretaceous (Frakes 1975; Barron, 1983; Hallam 1985; Skelton, 2003).

The elevated temperatures at mid-latitudes in the Hauterivian data are also broadly in line with other recently published Early Barremian TEX_{86} data from northern Germany, which suggest that at a palaeolatitude of ~33 ºN, average TEX_{86} values were 0.690 (SST of ~26.8 – 27.5 ºC; logarithmic and reciprocal calibrations respectively) (Figure 78). Although these data are from younger strata than the Hauterivian data in this study, extrapolation of the Hauterivian gradient into the Northern Hemisphere using the Barremian study would suggest a sudden steepening of the SST gradient between 20 ºN (Site 603) and 33 ºN (northern Germany) to 0.63 ºC/ ºlat (logarithmic) or 0.52 ºC/ ºlat (reciprocal) (Table 6b). These gradient estimates are much steeper than modern gradients at this latitude (0.41 ºC/ ºlat) and are therefore probably unrealistic, as one would expect gradients in a greenhouse World to be somewhat flatter than the modern icehouse at these latitudes. If one extrapolates the gradients determined between 20º and 53º latitude using the Hauterivian data and both calibrations (0.28 and 0.24 ºC/ ºlat respectively), to the northern German site and try to predict the *expected* SSTs there, the logarithmic calculation predicts SSTs of 32.6 ºC and the reciprocal calibration predicts SSTs of 30.4 ºC (Figure 78b). These predicted values are 5.1 ºC and 3.6 ºC warmer than the actual data from Germany depending on calibration (Table 6b).

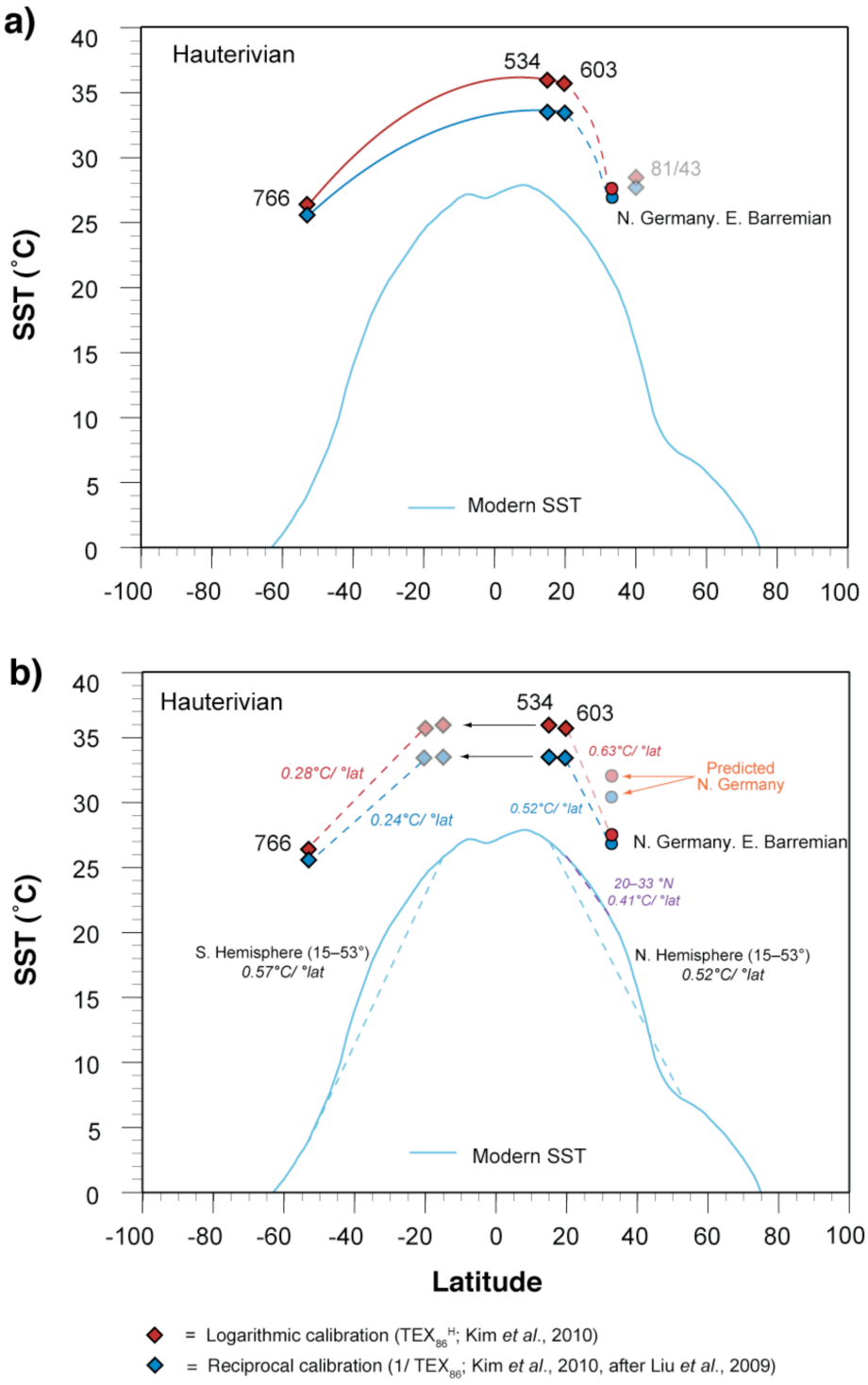

Figure 78. *a) Average Hauterivian SST estimates for Sites 534, 603 and 766 (diamonds; both calibrations) plotted against latitude and compared to modern SST gradient (Shea et al., 1992) and Early Barremian data (circles; Mutterlose et al., 2010). b) Comparison of SST gradient estimates for the Hauterivian (both calibrations) between 20 and 53°, compared to modern SST gradients in the Northern and Southern Hemispheres (Shea et al., 1992). Northern Hemisphere low-latitude data from Sites 534 and 603 has been "reflected" into the Southern Hemisphere at equivalent latitudes. Site 81/43 data is very tentative and is shown only for comparison.*

Apart from the obvious errors in temperature calibration of TEX_{86} ratios discussed in Chapters 1 and 2, one explanation for the mismatch may be geographic variability in the SST signal between the low-latitude sites (534 and 603) and the northwest German Basin, due to differences in regional climate or circulation (Figure 78b). It is also possible that a global cooling event occurred between the Hauterivian and the Early Barremian, rendering the two records incompatible, although there is no evidence of this in the upper part of the 534 or 766 SST records, which if anything suggest a warming trend (Figure 73). Another explanation is that there may be different populations of Crenarchaeota living in the marginal, semi-restricted, organic-matter rich Boreal basin, with a slightly different relationship to temperature than the open-ocean organisms, thereby leading to cooler SST estimates in the German sections. Such differences in crenarchaeotal population structure and GDGT distribution have been noted in the modern and in Pliocene sapropels (e.g. Menzel *et al*., 2006; Huguet *et al*., 2007; Shah *et al*., 2008). However, this argument might also suggest the SST results from the restricted basin at Site 692 may be too cool for the same reasons, which if anything, are slightly warmer than the predicted temperature for that palaeolatitude (~61 ºS). It is interesting to note that the very weak Late Hauterivian sample from Site 81/43 at ~40 ºN, suggests tentative SSTs of 28.3 – 29.2 ºC depending on calibration, which are up to 2 ºC warmer than the SST estimates from the north German Basin, despite being ~7º further north (Figure 78a). This may lend weight to the suggestion that unique oceanographic or biological conditions in the semi-restricted German Basin are the source of the somewhat cooler temperature estimates there.

4. 5. 2. Comparison of early Cretaceous TEX_{86} data with other SST proxies

As discussed previously, the Late Valanginian–Early Hauterivian has frequently been described as a "coolhouse" interval, on the basis of numerous sedimentological, palaeontological and geochemical studies (e.g. Frakes *et al*. 1992; Price, 1999; McArthur *et al*., 2007a; Figure 65). Furthermore, it has been suggested that the onset of greenhouse conditions occurred in the Early Valanginian, marking the end of the Late Jurassic cool and arid period, based on carbon-cycle perturbations

(e.g. Weissert *et al*., 1998; Erba *et al*., 2004). If these previous data are correct, the new TEX_{86} SST estimates from a range of palaeolatitudes would be expected to show: (a) cooler temperatures in the Valanginian and Hauterivian relative to the Late Berriasian and Early Barremian; (b) climate variability at a range of palaeolatitudes related to putative ice-building events in the Valanginian and Hauterivian; (c) a significant peak in temperatures in the Early Valanginian. However, no such SST trends are seen in the TEX_{86} data (Figure 73) and the Hauterivian SST gradients suggest a generally warm and equable earliest Cretaceous at odds with the prolonged coolhouse theory (Figure 73). There is certainly some variation in temperature in the higher latitude sites in the earliest Cretaceous, particularly Sites 766 and 249. However the overall pattern is for long-term warmth and stability across the entire ~13 Myr study interval, particularly the long-term records from the proto-North Atlantic which have a very small range in SSTs from the Late Berriasian to the Early Barremian (~1.5 – 2 ºC range) (Figures 70, 71, 72). The disparity between the new TEX_{86} records and the other SST proxies will be explored in detail below.

4. 5. 2. 1. TEX_{86} *VS.* OTHER SST PROXIES IN THE LOW-LATITUDES

The warm and relatively invariant temperatures suggested by TEX_{86} data at the North Atlantic sites, are perhaps at odds with other proxy evidence that suggests significant temperature variation in the proto-North Atlantic and western Tethyan regions (Section 4-2). Increased siliciclastic input in these regions, particularly at Sites 534 and 603, has been used to suggest the onset of warm and humid conditions in the Early Valanginian, but this is not evident in the TEX_{86} record at either of these sites (e.g. Weissert, 1990; Follmi *et al*., 1994; Weissert *et al*., 1998; Figures 68, 69, 73). Interestingly however, a small warming pulse of <1 ºC seen in the Early Valanginian TEX_{86} record occurs just prior to the increased input of claystone turbidites at this Site (~137 to 140 Ma) (Figure 79), which Weissert (1990) and Weissert *et al*. (1998) took as evidence for increasing humidity at this time. However, in addition to the fact that this "warming event" is only slightly above analytical error and therefore may not be significant, there is no increase in TEX_{86} SSTs at Site 534 and 603 during the Early Hauterivian, which one might expect to be associated with the much larger influx of coarse siliciclastics at both basins seen at

this time (Figures 68, 69). This suggests that perhaps a global increase in temperatures is not the root cause of the Tethyan siliciclastic input.

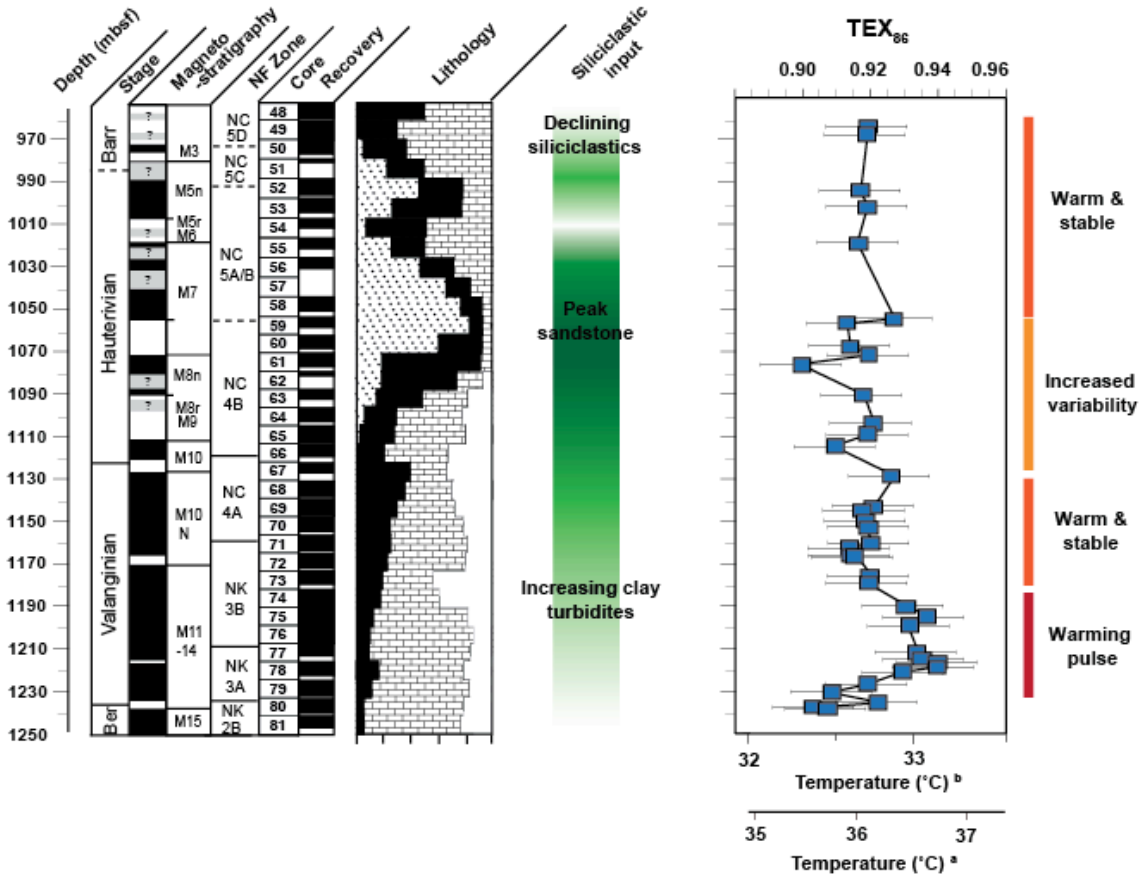

Figure 79. *Minor SST variation at Site 534 compared to the changes in lithology with time, showing the varying siliciclastic input at this site.*

As sea-levels were rising throughout the mid-Valanginian to Early Barremian (Figure 65; Hardenbol *et al*., 1998) a drop in sea-level cannot be responsible for this siliciclastic pulse. The largest drop in sea level occurred during the Early Valanginian, long before the onset of supposed cooling conditions or increased siliciclastics (Figure 65). Local tectonic uplift could certainly be responsible for the increase in coarse siliciclastic input in one basin or region, but the Valanginian–Hauterivian sandstone pulse can be seen from the western Tethys (e.g. Tunisia, Morocco, Siciliy) to the eastern and western North Atlantic (e.g. Sites 638, 534, 603) (Weissert, 1990), which makes such an origin unlikely. Alternatively, is it possible that while the SSTs in the western North Atlantic remained virtually unchanged throughout the Valanginian–Early Hauterivian, the humidity and precipitation on the

nearby continents increased enough to cause a larger volume of runoff and siliciclastic input into the Tethys? It is plausible that as the proto-North Atlantic continued to open during the Valanginian, and as sea levels rose (Figure 65), a reorganisation of ocean and atmospheric circulation occurred which drew moister air over eastern North America and the western Tethyan region. Such a change is not beyond the bounds of the known palaeoceanography of the region (Figure 76).

Indeed Bornemann *et al*. (2008), upon examining the calcareous nannonfossil assemblages from Sites 534 and 603, identified an increase in nutrification at the Berriasian–Valanginian boundary that persisted into the Valanginian, which they attributed to increased upwelling in the proto-North Atlantic. Bornemann *et al.* (2008) hypothesised that such an increase in upwelling could have been caused by rising sea-levels and changing palaeogeography during that time, which could be used to argue that as regional ocean circulation evolved, so too did the coupled atmospheric circulation (e.g. Parrish, 1993). The effects of opening oceanographic gateways on climate are not unknown and have been shown to be important in the mid Cretaceous supergreenhouse with regards to the opening of the South Atlantic (e.g. Poulsen *et al*., 2003).

Therefore, perhaps the disparity between sedimentological evidence for low-latitude climatic variation and the TEX_{86} evidence for low-latitude climatic stability, can largely be reconciled if evolving ocean and atmospheric circulation due to the widening North Atlantic is invoked. Perhaps large changes in temperature are not required in order to enact large changes in sedimentation regimes, and that changing regional patterns of precipitation are more important in triggering increased siliciclastic input.

Palaeontological evidence for variation in earliest Cretaceous SSTs has been suggested, which must also be reconciled with the relatively invariant low-latitude TEX_{86} records. Southward movement of the faunal divide between the Boreal and Tethyan realms seen in ammonite distributions has been suggested as evidence for cooling in the Valanginian (e.g. Melinte & Mutterlose, 2001). However, Mutterlose *et al*. (2003) dispute this inferred southward movement of the boundary, and instead suggested it remained roughly constant at ~30 ºN during most of the Early Cretaceous, perhaps interpretable as inferring temperature stability. Regardless, even if these changes in macrofauna distribution in the Valanginian are real, they could also be the result of the well-documented rise in sea-level that occurred during this

interval, which may have opened oceanic gateways and allowed the exchange of biota from one realm to another (Hardenbol *et al*., 1998; Melinte & Mutterlose, 2001; Figure 65). This view is supported by the observation that the exchange in fauna at this time was multi-directional, with Tethyan fauna also appearing in Boreal latitudes, and that therefore these changes to faunal assemblages are probably not controlled solely by global temperature variations (Mutterlose *et al*., 2003).

In the proto-North Atlantic, Tethyan and Boreal regions, data from both Kessels *et al*. (2006) and Mutterlose & Kessels (2004) suggest two cooling phases in the Early–mid Valanginian and the Early Hauterivian due to incursions of *C. salebrosum* into the lower latitudes (Figure 66). Erba *et al*. (2004) also documented an incursion of the high-latitude taxa *K. borealis* into the low-latitude Pacific in the Early Hauterivian, which they too attributed to cooling. However, such cooling episodes are not observed in the low-latitude TEX_{86} record from Sites 534 or 603 (Figure 73). Kessels *et al*. (2006) stated that sea-level rises alone could not be the cause of these changes in nannofossil assemblage as only one species was seen to migrate, and not a homogenisation of the entire assemblage. However work by Melinte & Mutterlose (2001) on boreal nannofossils from Romania, explicitly highlight the importance of sea-level in modifying the distribution of marine fauna through the opening and closing of ocean gateways. The view that calcareous nannofossil provincialism is due more to land barriers and sea level than temperature gradients, has also been proposed by Applegate *et al*., (1989).

Additionally, if ocean circulation patterns were evolving throughout the Valanginian–Hauterivian as suggested above (Figure 76), this could also have an effect on the distribution of calcareous nannofossil species independent of temperatures. Increases in fertility indicators at the Central Pacific site in the Late Valanginian and Early Hauterivian, coincident with the influx of *K. borealis*, suggest an increase in ocean upwelling, so ocean circulation patterns may indeed have changed during this interval (Erba *et al*., 2004).

Thus the apparent conflict between palaeontological evidence for low-latitude climatic variation and the TEX_{86} evidence for low-latitude climatic stability, can largely be reconciled if changes in sea-level and ocean circulation are invoked to explain the changes seen in palaeontological trends. However, it is of course possible that a small component of temperature control exists in the calcareous nannofossil

distribution during the earliest Cretaceous, perhaps at a frequency below the temporal resolution or analytical error of the low-latitude TEX_{86} records.

There is no obvious correlation between oxygen-isotope and Mg/Ca records from the Tethyan or Central Pacific region, and the new TEX_{86} records from the proto-North Atlantic (Figures 65, 73). Most of the geochemical records suggest a cooling phase in the Late Valanginian–Early Hauterivian, while the TEX_{86} records suggest long-term stability (e.g. McArthur *et al*., 2007a; van de Schootbrugge *et al*., 2000; Price *et al*., 2011; Figure 65). This disparity may be due to a number of factors, including misinterpretation of $\delta^{18}O$ and Mg/Ca records as reflecting temperature changes, differences in using an integrated bulk geochemical proxy (TEX_{86}) *vs*. single specimen geochemical proxies (Mg/Ca and $\delta^{18}O$ of belemnites), and differences in temporal resolution of the two approaches.

In terms of integrated bulk geochemical proxies other than TEX_{86}, as discussed earlier, it is unlikely that the low-latitude bulk oxygen-isotope records put forward to suggest cooling in the Valanginian are reliable (Erba *et al*., 2004; Weisert & Erba, 2004). The record from the Central Pacific is low resolution (17 data points) and shows very little coherent variation, the magnitude of the change in $\delta^{18}O$ is very small, and the values are probably subject to unconstrained diagenetic alteration (Frank *et al*., 1999; Erba *et al*., 2004). Similarly the Tethyan composite bulk $\delta^{18}O$ record, which purports to show cooling in the Late Valanginian, is probably not reliable, due to differential diagenesis and the effects of compiling data from multiple sections and inferring trends between sections (Weissert & Erba, 2004). The TEX_{86} records by contrast are relatively high resolution, and individual records in the low-latitudes span up to 12 Myr of time, reducing the effects of intra-site comparison errors (Figures 68, 69, 73).

The discrepancy between the new earliest Cretaceous TEX_{86} records, and oxygen-isotope and Mg/Ca records from single organisms, requires more exploration however. Absolute SST estimates based on oxygen-isotopes from belemnites are inherently error-prone and could be the result of inaccurate assumptions for the $\delta^{18}O_{sw}$ of an ice-free world, or other biological issues such as failing to account for the likely sub-surface depth habit of belemnites (e.g. Anderson *et al*., 1994; van de Schootbrugge *et al*., 2000; Price & Mutterlose, 2004; Dutton et al., 2007). Even if absolute temperatures are disregarded however, temporal shifts in belemnite $\delta^{18}O$

records could be due to other factors such as changing salinity caused by evolving precipitation regimes and ocean circulation, or migration of belemnites from a different, warmer or cooler, region of the ocean (e.g. Price *et al*., 2011).

Although using Mg/Ca ratios in conjunction with $\delta^{18}O$ values has been employed to circumvent some of these problems with using $\delta^{18}O$ alone, certain assumptions must also be made, such as a constant Mg/Ca ratio in the oceans with time, which may not hold true over timescales > 1 Myr (e.g. Lea, 2003). The response of belemnites to changing SST is unknown, as are the specific vital effects associated with thsis genera in terms of Mg/Ca incorporation. Complications in reconciling Mg/Ca ratios and SSTs in modern calibration studies of molluscs have also been reported, suggesting Mg/Ca may not always be a faithful recorder of temperature in larger marine organisms (van der Putten *et al*., 1999). TEX_{86} on the other hand, has been shown both in culture studies and global core-top calibrations, to be an accurate recorder of the *in situ* seawater temperature (e.g. Wuchter *et al*., 2004; Kim *et al*., 2008).

Different interpretations of similar data trends in the earliest Cretaceous are also noted. For example, while McArthur *et al*. (2007a) attributed the fall in $\delta^{18}O_{sw}$ and Mg/Ca in Tethyan belemnites as representing a cooling climatic signal, van de Schootbrugge *et al*. (2000) interpreted the very similar trends in their $\delta^{18}O$ record in the context of the rising sea-levels seen through the Valanginian, which they hypothesised introduced cool boreal water into the Tethyan realm, independent of global temperature (Figure 65). Thus, such regional variations in $\delta^{18}O_{sw}$ and Mg/Ca in the western Tethys are not necessarily to be interpreted in terms of global palaeotemperature variations. Additionally, in many geochemical studies, the Mg/Ca and $\delta^{18}O$ belemnite records consist of highly scattered data, which hinders unique interpretation of the purported warming or cooling trends in each record (e,g, McArthur *et al*., 2007a; Price *et al*., 2011).

So it appears that much of the conflict between existing proxy evidence, encompassing sedimentological, palaeontological and geochemical data, and the TEX_{86} data in the low-latitudes can, in part, be explained by changes in sea-level, ocean circulation and palaeogeography, but what of the higher latitudes?

4. 5. 2. 2. TEX_{86} *VS.* OTHER SST PROXIES IN THE HIGHER LATITUDES

As detailed previously (Figure 65), evidence has been put forward to suggest that there were intermittent "cold snaps" in the Late Valanginian–Early Hauterivian, against a backdrop of generally cooler conditions relative to the Berriasian and Barremian. Much of the sedimentological and geochemical evidence for this supposition has come from the higher-latitudes (>50 ºN palaeolatitude) (e.g. Kemper *et al*., 1987; Podlaha *et al*., 1998; Price *et al*., 2000; Price & Mutterlose, 2004; Figure 42). Unfortunately, it is difficult to directly compare existing proxy evidence from the high-latitudes to the new TEX_{86} data, as none of the sampled sites were deposited above a palaeolatitude of 61 ºS (Table 4). Secondly, the age control on the mid-latitude sites sampled in this study is not as robust as for the proto-North Atlantic sites, making comparison difficult, and the only well-constrained site (Site 766) is no older than the Late Valanginian (Figures 70–72). Additionally, age control at many of the sections examined in previous studies also appear poorly constrained in terms of age, hindering comparison further (e.g. Price & Nunn, 2010). Despite these shortcomings, it is possible to comment on both the absolute temperatures and the greater variability seen at these sites, which suggests that, (1) the upper mid-latitudes were very warm with respect to the modern during the Valanginian–Hauterivian, which is incompatible with an overarching "coolhouse" hypothesis; and (2) that the greater temperature variability seen at these higher latitude sites is perhaps indicative of a more responsive climate to short-term perturbations at these latitudes.

Sedimentological evidence for cool high-latitudes centers on the presence of glendonites and purported dropstones in regions such as Svalbard, Arctic Canada and Australia (e.g. Kemper *et al*., 1987; Frakes & Francis 1988; Figure 42, 44). However, as discussed previously, doubt has been cast on the merits of using "dropstones" as indicators of sub-freezing conditions, as other non-glacial mechanisms for the delivery of outsized clasts to marine basins have been suggested (Bennett *et al*., 1996; Bennett & Doyle, 1996). If the outsized clasts are indeed dropstones, then it may be that they represent the action of seasonal ice-rafting due to high latitude (<65º) winter darkness, rather than persistent freezing conditions. In the case of purported high-latitude tillites or diamictites, a glacial origin is not always obvious as there are alternative non-glacial mechanisms such as debris flows

where glacial conditions need not be invoked. In the case of the Australian "tillite" reported by Alley & Frakes, (2003), the authors themselves conceded that it likely represents the result of a small, and perhaps transient, body of ice, which would not be incompatible with the ~66 ºS palaeolatitude. The generally very warm upper mid-latitudes (~60º) suggested by the annual average TEX_{86} SST values, do not of course preclude the existence of small, potentially high-altitude, ice bodies in the high latitudes. Indeed in the modern world large glaciers exist on the west coast of the South Island of New Zealand, which originate at altitudes of ~2300 m and flow almost to sea level, despite relatively warm annual average SSTs in that region of ~15 ºC (Figure 75). However, if the earliest Cretaceous gradients calculated between 15º and 53º are extrapolated to the poles, the existence of significant ice-caps even in the high latitudes becomes doubtful (Figure 78).

The fact that glendonites are not necessarily indicative of sub-freezing conditions has already been addressed previously, and it may be that they simply represent relatively cool, phosphate rich bottom waters, which do not reflect glacial conditions on the continents. Additionally, the majority of reported glendonites are from the high latitudes of the northern hemisphere (>65º N), where seasonal darkness and cooler temperatures might be expected to generate seasonally cool bottom waters (e.g. Kaplan 1978; Kemper, 1987; Price & Nunn 2010). It is possible that during the earliest Cretaceous, high-latitude sea-water temperatures were cool enough to allow the formation of ikiaite in the winter, but considerably warmer in the summer months, leading to a warmer annual average SST value than suggested by the glendonites.

Variations in clay mineral assemblage in the boreal Northern Hemisphere has been put forward as evidence for climatic variation (e.g. Hallam, 1984; Muttelose & Kessels, 2000; Price *et al*., 2000). However, the well-documented increase in kaolinite deposition during the Valanginian and Hauterivian within the NW European Wealden Formation could also be the result of changes in local climate, caused by uplift of the Anglo-Brabant Massif, and not to large-scale reorganization of global climate (Sladen & Batten, 1984). Such regional changes in the Boreal realm may not be related to global climate variation, and so would not be expected to be recorded in SST records from either the low-latitude proto-North Atlantic or the higher latitude Southern Hemisphere sites.

Variations in oxygen-isotope values from higher-latitude belemnites has been suggested as representing significant high-latitude temperature variation, which is not supported by the low-latitude or the majority of the higher-latitude TEX_{86} data (Figures 68 –73). Oxygen-isotope data from belemnites collected from regions such as Siberia, Svalbard and northern Germany, exists and purports to show a broad cooling trend in the Late Valanginian–Early Hauterivian, (e.g. Podlaha *et al*., 1998; Price *et al*., 2000, Price & Mutterlose, 2004; Price & Nunn, 2010; Figure 65), which is not observed in the continuous SST records at mid-latitude Site 766 (Figure 70, 73). Although a minor cooling trend of 1.4 ºC is seen in the latest Valanginian at Site 766, this small change in temperature is not of the same magnitude as the dramatic cooling suggested by oxygen-isotopes (e.g. Price *et al*., 2000, Price & Mutterlose, 2004; Figure 70). It is, of course, unfortunate that SST records at this site do not extend beyond the late Valanginian, which would aid in the interpretation of temperature at this latitude. There is variability seen in the SST records at Sites 692 and 249, particularly a 3 ºC cooling event at Site 692, but the lack of suitable age control means it is impossible to correlate this event with cooling observed in oxygen-isotope records (Figure 71).

There are reasons why the higher-latitude $\delta^{18}O$ records may not be accurately representing changes in global SST, including those related to changes in sea-level and ocean circulation, as previously discussed. An additional consideration in the high-latitudes is the determination of $\delta^{18}O_{sw}$ for the generation of palaeotemperature estimates, which, already complicated by the assumption of ~-1‰ $\delta^{18}O_{sw}$ in a "ice free world", becomes ever more poorly constrained with increasing latitude due to the greater effects of precipitation and salinity variations in these regions (e.g. Zachos *et al*., 1994; Price & Mutterlose, 2004; LeGrande & Schmidt, 2006).

It is also possible however, that even if the purported cooling in the Late Valanginian–Early Hauterivian was real, and not an artefact of local changing sea-levels and circulation, that it may have affected the Northern Hemisphere to a greater extent than the Southern Hemisphere. The mid-latitude TEX_{86} data is primarily from the Southern Hemisphere (Sites 692, 249, 766 and 763) with the only Northern Hemisphere data being very tentative (Site 81/43) or from a slightly later time period (Barremian of northern Germany; Mutterlose *et al*., 2010). The oxygen-isotope data, by contrast, comes exclusively from the Northern Hemisphere, therefore "global"

SST changes are inferred solely on the basis of Northern Hemisphere information combined with Southern Hemisphere sedimentological inferences which may not be correct (see above) (Figure 63; Podlaha *et al*., 1998; Price *et al*., 2000, Price & Mutterlose, 2004; Price & Nunn, 2010). This highlights the possibility that these temperature variations, if real, were regional rather than global, or that the Southern Hemisphere was somehow buffered from these large changes in temperature. In support of this, the calculated Hauterivian gradients, although tentative, do suggest that the gradient in the Northern Hemisphere may have been steeper than the Southern Hemisphere gradient, although more data would be needed to confirm this trend (Figure 78). It is possible for the Northern Hemisphere to experience cooling while the Southern Hemisphere does not, as exemplified by the "Little Ice Age" of the Late Holocene, however the feasibility of longer term (>1 Myr) imbalances in global thermal gradients, particular in a greenhouse world, is unknown (e.g. Kreutz *et al*., 1997).

In conclusion, it seems that the Valanginian–Hauterivian period was not characterized by a prolonged global "coolhouse" climate as previously suggested (e.g. Price 1999), but rather by a generally warm and humid climate punctuated by occasional cold snaps at high-latitudes, and that evidence put forward to propose low-latitude cooling is in fact related to changes in sea-level, regional tectonics, or regional climatic variations. There may have been relatively longer term cooling episodes in the higher latitudes during the Valanginian-Hauterivian, as typified by the cooling and subsequent warming pulse of uncertain duration seen at Site 692 (Figure 71), or shorter term, more abrupt changes in temperature as seen in the earliest Hauterivian at Site 766 (Figure 70, 73), which were not large enough to effect the more stable open-ocean tropical regions (Figures 68, 69, 73). It may be that very sharp and short-lived global cooling episodes on the scale of kyr, did occur, and they remain below the resolution of this study, however the average resolution of 1 sample per ~300 kyr at Site 534 makes the likelihood of major undetected SST excursions in the tropics somewhat remote.

4. 5. 3. COMPARISON WITH MID-CRETACEOUS AND EOCENE GRADIENTS

Although noting that both absolute temperatures and gradients in the earliest Cretaceous were different from the modern is important, comparison of a likely "greenhouse" (or possible "coolhouse") interval with the modern "icehouse" will not shed light on the relative temperature of the earliest Cretaceous within the greenhouse world. If the earliest Cretaceous TEX_{86} SST records are viewed in the context of the longer-term Mesozoic and Palaeogene TEX_{86} SST records, it can be seen that there is little evidence for the 'coolhouse' Early Cretaceous (Figure 80).

It is immediately obvious that the TEX_{86} data are somewhat temporally limited, being mostly restricted to Cretaceous OAEs and Palaeogene hyperthermals, and in this sense the Early Cretaceous data are unique in representing a long-term, "background" record of tropical SSTs (Figure 80). Secondly, despite the paucity of data, it is clear that tropical SSTs in the earliest Cretaceous were very similar to those of the Cenomanian and Turonian periods, which are often regarded as times of peak Cretaceous global warmth. This finding suggests that far from having a predominantly cool climate, the tropics of the earliest Cretaceous were, on average, as warm as the "supergreenhouse" tropics of the mid Cretaceous, regardless of calibration.

If the raw TEX_{86} values of the Hauterivian tropics (Sites 534 and 603; 0.907 – 0.916) are compared to the average Cenomanian–Turonian tropical values, of 0.915 or the Cenomanian average tropical value of 0.899 (Forster *et al*., 2007; Sites 1260 and 367 respectively), the close similarity between the datasets becomes obvious. After peak temperatures in the Turonian, temperatures drop somewhat, reaching minimum average values in the Santonian at Site 1259 with values of 0.899 (35.4 ºC, TEX_{86}^{H}) (Bornemann *et al*., 2008b). There are no tropical data throughout the remainder of the Cretaceous, although mid-latitude (22–24 ºN) SSTs of 0.761–0.865 (30.5–34.6 ºC, TEX_{86}^{H}) suggests very warm conditions in the Early Albian associated with OAE1b (Wagner *et al*., 2008; Figure 80). The Late Cretaceous is marked by only one average data point, the high-latitude Alpha Ridge data from the Arctic, which with average TEX_{86} values of 0.510 suggests very warm SSTs in the region of 18.8 ºC, (TEX_{86}^{H} calibration), and by extrapolation, very warm climates at all latitudes (Jenkyns *et al*., 2004; Figure 80).

Much more data are available for the Palaeocene and Eocene, as the hyperthermal events in the Early Eocene have been the target of repeated studies at a range of latitudes (e.g. Bijl *et al*., 2009; Hollis *et al*., 2009; Zachos *et al*., 2006; Figure 80). The Early Eocene in particular (~56- 48 Ma) is worthy of comparison to the earliest Cretaceous data, as it is regarded as one of the warmest periods in the Cenozoic, and therefore if the coolhouse earliest Cretaceous theory is correct, should be considerably warmer than the Hauterivian. However, the TEX_{86} evidence indicates high background tropical SSTs of ~33 ºC, (~32 ºC with the reciprocal calibration), which are comparable to the earliest Cretaceous estimates from Sites 534 and 603 (Pearson *et al*., 2007). Background mid-latitude temperatures were also very warm (Zachos *et al*., 2006), as were those found at latitudes of ~55–65 ºS on the East Tasman Plateau (Bijl *et al*., 2009) and New Zealand (Hollis *et al*., 2009); and were even found to be greatly elevated in the high Arctic where SSTs in excess of 21 ºC were reported (Sluijs *et al*., 2006, 2009) (Figure 59). Interestingly, high-latitude temperatures cool gradually during the Middle and Late Eocene (Bijl *et al*., 2009), while low-latitude temperatures appear to remain largely invariant (Pearson *et al*., 2007). This is similar to the SST records from the early Cretaceous, and suggests that perhaps stable low-latitudes and more variable higher latitudes are a persistent feature of greenhouse worlds.

As discussed above, the Hauterivian gradients within the earliest Cretaceous show a significant flattening of the latitudinal SST gradient with respect to the modern, with the tropics being on average ~5 ºC warmer and the higher latitudes being ~20 ºC warmer (Figure 81). Similarly, the tropics during the mid-Cretaceous are clearly much warmer than the modern, and on a par with earliest Cretaceous values, but no higher-latitude TEX_{86} data exist to determine the gradient beyond 30ºN. However, if the extremely flat gradient seen between ~2 ºN and 30 ºN were to be extrapolated to the poles, it is likely that they were very warm indeed, and probably in excess of temperatures seen in the earliest Cretaceous higher latitudes (Figure 81). The likely flatter gradient in the mid-Cretaceous is supported by the virtually indistinguishable mid-latitude temperatures compared to the tropics, which contrasts with the earliest Cretaceous data where there is still considerable SST difference between the tropics and the mid-latitudes of the Northern and Southern Hemispheres (Mutterlose *et al*., 2010; Figure 81).

Similar comparisons can be drawn between the Early Eocene and Hauterivian gradients. While extrapolation of the Early Eocene data at 20 ºS and 35 ºN suggests warm tropics relative to the modern, they do not appear as warm as the low-latitudes of the earliest Cretaceous (Zachos *et al*., 2006; Pearson *et al*., 2007; Figure 81). In contrast, Early Eocene mid-latitude temperatures in both the Northern and Southern Hemisphere may have been slightly warmer than equivalent earliest Cretaceous palaeolatitudes, which would imply that the earliest Cretaceous had a steeper SST gradient than the Early Eocene between the low and mid-latitudes (Zachos *et al*., 2006; Bijl *et al*., 2009; Hollis *et al*., 2009; Figure 81). This flattened gradient in the Early Eocene can be seen to lessen during the Middle Eocene as the higher-latitudes cooled to a greater degree than the tropics (Pearson *et al*., 2007; Bijl *et al*., 2009).

In conclusion, the relatively close agreement between the Early Eocene, Cenomanian–Turonian and earliest Cretaceous SSTs, is a strong indication that the Early Cretaceous was, overall, not an unusually cool interval within the late Mesozoic – early Cenozoic greenhouse period, and in fact was on a par with the mid-Cretaceous "supergreenhouse" in terms of tropical temperature. The SST gradients appear to be steeper than both the Cenomanian–Turonian, which may have been extremely equable, and the Early Eocene, although much more data would be needed to confirm these trends.

Figure 80 (overleaf). *Overview of all Cretaceous and Palaeogene TEX_{86} SST estimates, separated into ~20º degree latitude bins, with major oceanographic and climatic events shown as grey bars. All TEX_{86} data have been recalibrated using the TEX_{86}^{H} logarithmic calibration of Kim et al. (2010). OAE = oceanic anoxic event; PETM = Palaeocene Eocene Thermal Maximum; ETM2= Eocene Thermal Maximum -2; EECO = Early Eocene Climatic Optimum; MECO = Middle Eocene Climatic Optimum; EOT = Eocene Oligocene Transition. Data are taken from various papers: N. Germany = Mutterlose et al. (2010); Site 463 = Schouten et al. (2003); Site 1207 = Dumitrescu et al. (2006); Site 1049 = Wagner et al. (2008); Schouten et al. (2003); 545 = Wagner et al. (2008); Site 1260 = Forster et al. (2007); Site 367 = Forster et al. (2007) & Schouten et al. (2003); Site 1259 = Bornemann et al. (2008b); Site 1276 = Sininnghe Damsté et al. (2010); Alpha Ridge = Jenkyns et al. (2004); Site 511 & Site 693 = Jenkyns et al. (2011); Site 1072 = Bijl et al., (2009), North America = Zachos et al. (2004); N. Z = New Zealand, Hollis et al. (2009), Burgess et al., (2008); Lomonoszov Ridge = Sluijs et al., (2006, 2009); TDP = Tanzania, Pearson et al., (2007); Sites 511, 277, 925 and 929 = Liu et al., (2009).*

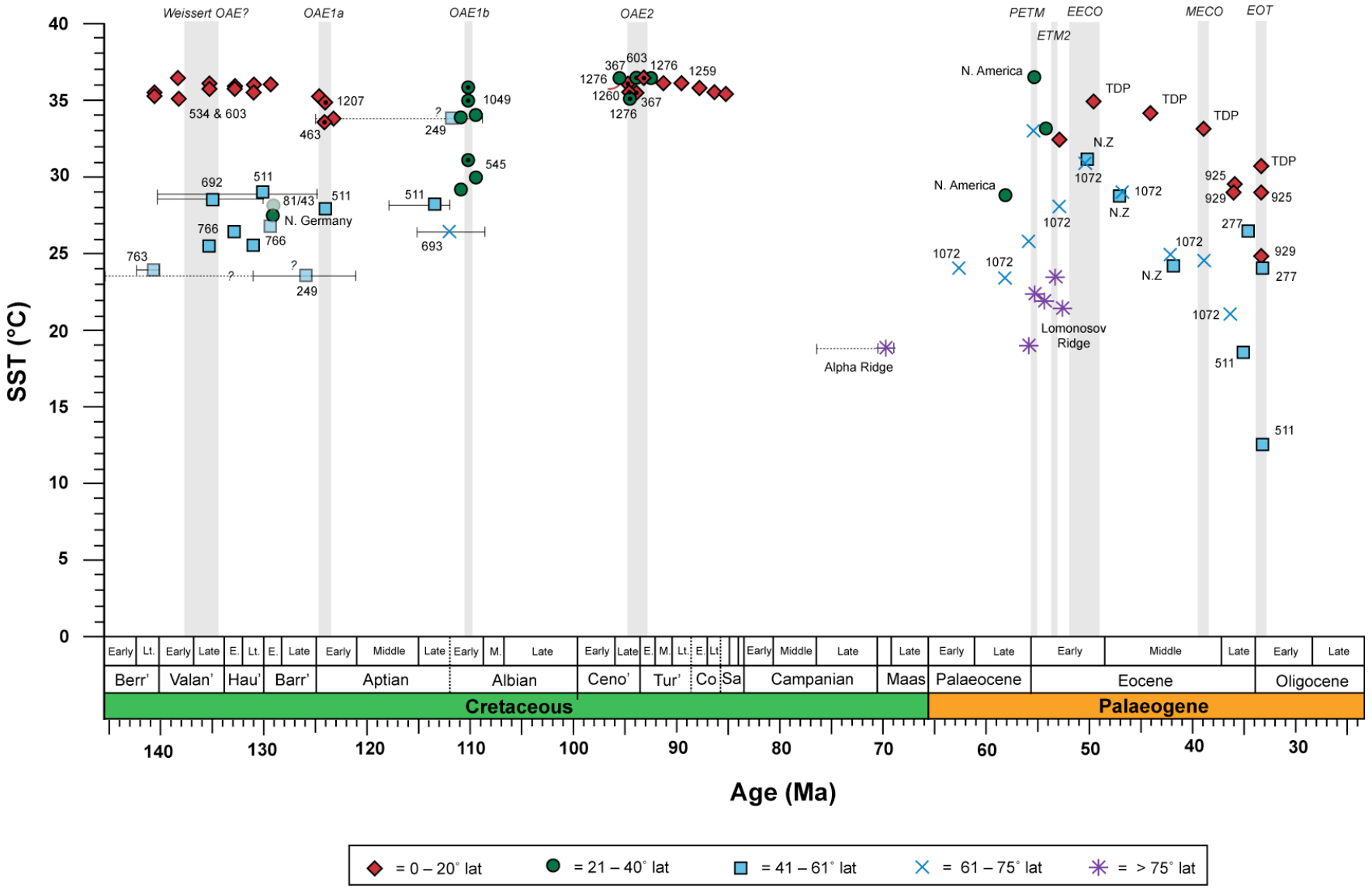
Weissert OAE?
OAE1a
OAE1b
OAE2
PETM
EECO
ETM2
MECO
EOT
SST (°C)
Age (Ma)
534 & 603
1207
463
1049
249
545
511
692
81/43
N. Germany
766
763
693
367
603
1276
1259
1260
N. America
TDP
N.Z
1072
925
929
277
Alpha Ridge
Lomonosov Ridge
Berr'
Valan'
Hau'
Barr'
Aptian
Albian
Ceno'
Tur'
Co
Sa
Campanian
Maas
Palaeocene
Eocene
Oligocene
Cretaceous
Palaeogene
= 0 – 20° lat
= 21 – 40° lat
= 41 – 61° lat
= 61 – 75° lat
= > 75° lat

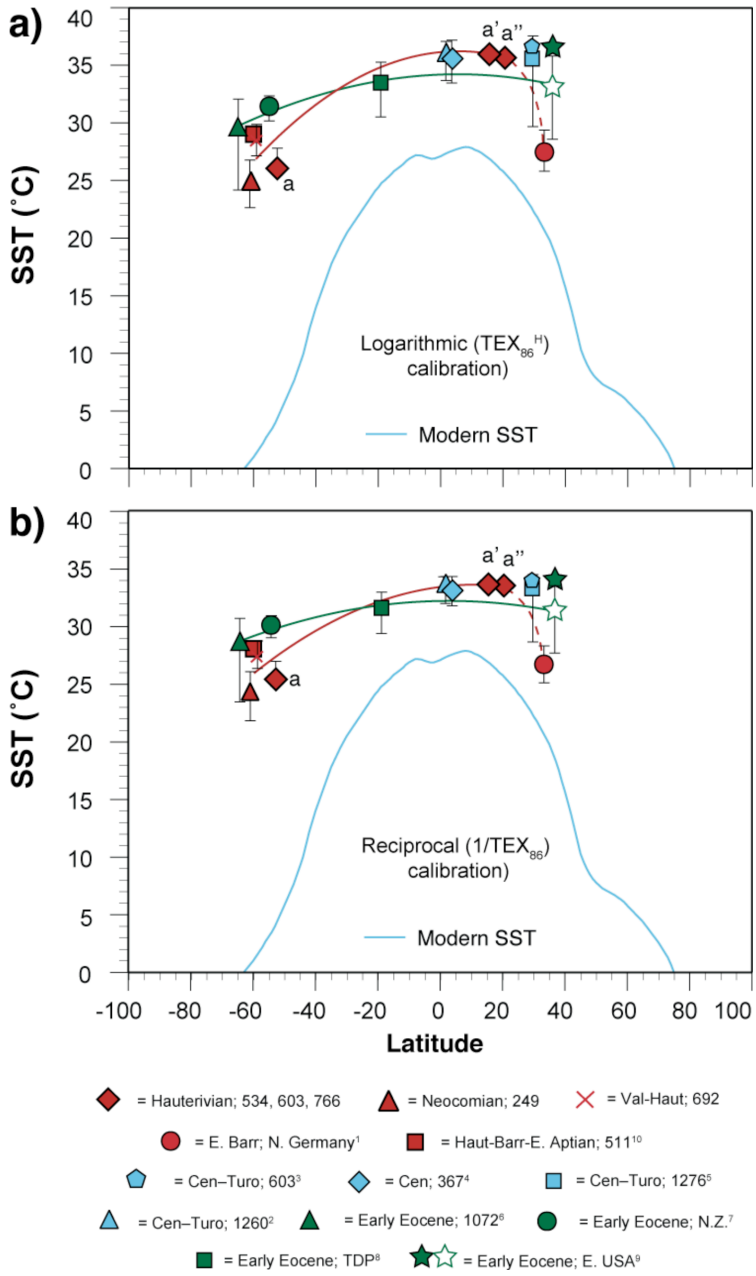

Figure 81. *Comparison of Early Cretaceous meridional temperature gradients with the modern, the mid Cretaceous and the Early Eocene.* ***a****) Hauterivian SSTs (red symbols; a, a' and a") compared to, Valanginian–Hauterivian SSTs (Site 692), Neocomian (Site 249), Early Barremian (red circle), Late Cretaceous (blue symbols), and Early Eocene (green symbols) average* TEX_{86} *SST estimates, recalibrated according to logarithmic equation (*$TEX_{86}H$*). 1 = Early Barremian, NW Germany (Mutterlose et al., 2010); 2 = Site 1260, Cenomanian–Turonian (Forster et al., 2007); 3 = Site 603, Cenomanian–Turonian (Schouten et al., 2003); Site 367, Cenomanian (Forster et al., 2007), 6 = Early Eocene, East Tasman Plateau (Bijl et al., 2009), 7 = Early Eocene, New Zealand (Hollis et al., 2009), 8 = Early Eocene, Tanzania (Pearson et al., 2007), 9 = Early Eocene, New Jersey (Zachos et al., 2004; peak Paleocene Eocene Thermal Maximum SST is shown as open star).* ***b****) As for a but all data recalibrated after reciprocal equation (*$1/TEX_{86}$*). Error bars indicate the total range of values in each dataset.*

4. 5. 4. CLIMATE SENSITIVITY TO pCO_2

In theory the new temperature record for the earliest Cretaceous should be very useful in commenting upon the climate sensitivity to atmospheric CO_2 levels (e.g. Royer *et al*., 2007). However, as demonstrated in Section 4-2-4, the estimates of Early Cretaceous pCO_2 vary wildly depending on the proxy or model used (e.g. Royer, 2006; Figure 67). While it is accepted on the basis of all proxy and modeling evidence that the Early Cretaceous had higher pCO_2 levels than the modern, of at least 2x PAL (~560 ppm), (Retallack, 2001; Berner & Kothavala, 2001; Beerling & Royer, 2002; Robinson *et al*., 2002; Haworth *et al*., 2005;), the upper estimates put pCO_2 at up to ~3200 ppm (12 x PAL) (Beerling & Royer, 2002), which is a huge range of uncertainty. The TEX_{86} record suggests tropical temperatures 5 – 7 ºC degrees warmer than the present, which is almost exactly the magnitude of the temperature anomaly predicted by the energy model proposed by Veizer *et al*., (2000) of +5 ±1 ºC. This concordance strongly suggests that the energy balance model based on pCO_2 proxy data is broadly correct and the reconstructions based on the oxygen-isotope data compilation are erroneous. The errors associated with oxygen-isotope analysis, as discussed above, may go some way to explaining why the $\delta^{18}O$ data may have consistently underestimate SSTs in the Late Jurassic–Early Cretaceous.

These very warm SST estimates at a range of palaeolatitudes, coupled with the lower estimates of pCO_2 for the earliest Cretaceous of ~2x PAL, would suggest a very high sensitivity to atmospheric CO_2 concentrations, which perhaps we should find concerning in the context of ongoing anthropogenic activities (e.g. Robinson *et al*., 2002; Haworth *et al*., 2005). However if the upper limit of ~3200 ppm for the Early Berriasian is correct, then this suggests very low sensitivity of the climate system to pCO_2, or perhaps a non-linear response to rising pCO_2 once a certain threshold is reached (Beerling & Royer, 2002). Royer *et al*. (2007) attempted to constrain the climate sensitivity of the Phanerozoic based on a large proxy database, and determined that "a weak radiative forcing by carbon dioxide is highly unlikely on multi-million-year timescale", and that a sensitivity > 1.5 ºC per doubling of the pCO_2 concentration has probably been a constant feature of the Earth's climate system over the past 420 million years. As most estimates for the Late Berriasian to

Early Barremian lie between 2000 and 550 ppm, perhaps an "intermediate" sensitivity to pCO_2 can be inferred.

In terms of the relationship between pCO_2, and the temperature record, the general fall in pCO_2 between the Berriasian and Early Barremian predicted by the modelling of Berner & Kothavala (2001) or Tajika *et al*. (1999), or the stomatal index evidence of Beerling & Royer (2002), would agree with much of the other sedimentological, palaeontological and geochemical evidence which suggest a drop in SSTs across the same period, but is not supported by the relatively invariant low-latitude TEX_{86} data. There is not correlation observed between the TEX_{86} SST record and any of the pCO_2 reconstructions. However, the temporal resolution of the pCO_2 proxy records is extremely low and the difference between all of the suggested pCO_2 concentrations is so great, that no robust relationship can be determined at present between the two variables in the Early Cretaceous, and more accurate pCO_2 data are needed before more robust inferences can be made.

4. 6. CONCLUSIONS

It can be seen that the TEX_{86} palaeotemperature proxy can be used with confidence to determine SSTs in the earliest Cretaceous, extending the known use of this technique back by a further 10 Myr. The absolute temperatures, regardless of calibration, in the low-latitude palaeo-North Atlantic (Sites 534 and 603) are elevated by at least 5 ºC with respect to the modern tropics throughout the entire Late Berriasian to Early Barremian period, in line with the predictions of an energy balance model based on pCO_2 concentrations. Despite poorer age constraint, the Valanginian – Hauterivian period in the higher mid-latitudes (Sites 766, 692 and 249) also appear to be characterized by greatly elevated temperatures, which are at least 16 ºC warmer than modern SSTs at equivalent latitudes, and generally in excess of 20 ºC warmer than the modern values. Comparing average Hauterivian SSTs from different latitudes allows tentative meridional SST gradients to be constructed, which suggest a gradient of ~0.20 – 0.25 ºC/º lat between 15º and 53º, and contrasts with a modern average gradient of ~0.5 ºC/º lat in the Northern Hemisphere and ~0.6 ºC/º

lat in the Southern Hemisphere for the same latitudinal range. This suggests warmer global temperatures and a significantly flatter SST gradient from the equator to the poles than exists in the modern world, although more truly high-latitude data (>65º) would be desirable to constrain the gradient in the polar regions.

Interestingly these very warm earliest Cretaceous tropical SST estimates are not dissimilar from TEX_{86}-based SST estimates from the "super greenhouse" of the mid-Cretaceous, nor from the elevated Cenozoic temperatures of the Early Eocene, suggesting that contrary to the many other proxy studies, the earliest Cretaceous was not a particularly cool interval within the Mesozoic – Palaeogene greenhouse. The tentative gradient data from each time-slice suggests the Early Cretaceous had somewhat steeper SST gradients than either the mid Cretaceous or the Early Eocene, but more data are required to confirm these inferences.

In addition to the high average temperatures, the great stability of the SST records at both Sites 603 and 534 over >13 Myr further reinforces the assertion that the earliest Cretaceous was generally characterized by a warm and stable climate, despite large purported changes in palaeotemperatures suggested by sedimentological, palaeontological and other geochemical evidence. However, it may be that the tropics were less responsive to regional climate change than the higher latitudes, which is demonstrated by the greater variability in temperature exhibited at the mid-latitude sites. The very warm global temperatures suggested by the TEX_{86} data may provide interesting insights into climate sensitivity to pCO_2 levels in a greenhouse world, but higher resolution and better constrained pCO_2 records are needed to fulfill this potential.

CHAPTER 5. ORGANIC CARBON-ISOTOPE RECORDS FROM THE WESTERN PROTO-NORTH ATLANTIC

5. 1. AIMS

During the earliest Cretaceous, a global perturbation to the carbon-cycle occurred, known as the "Valanginian positive carbon-isotope event" or the "Weissert OAE". This prominent event, which was marked by a positive carbon-isotope excursion (CIE) of magnitude ~+1.5‰ in carbonate and ~+1.5 to 5 ‰ in organic-matter records, has been documented from many sections around the world, including Tethyan, North Atlantic and Central Pacific regions. The aim of this chapter is to explore the dynamics of the carbon-cycle during the earliest Cretaceous, with particular focus on the Valanginian CIE, using new data from western North Atlantic DSDP Sites 534 and 603. Existing bulk-carbonate ($\delta^{13}C_{carb}$) and new bulk-organic ($\delta^{13}C_{org}$) records will be compared to ascertain the extent and effect of the CIE in the western proto-North Atlantic, and to determine whether there are any lead and lag times in expression of the excursion between the two carbon reservoirs. The effects of the Valanginian CIE on both marine and terrestrial organic-matter will be investigated, by determining the carbon-isotope record from co-occurring pelagic and turbiditic samples from Sites 603 and 534. Additionally, depth-paired $\delta^{13}C_{org}$ and $\delta^{13}C_{carb}$ records will be used to generate delta-delta ^{13}C ($\Delta^{13}C$) records, which can be interpreted in the context of changing pCO_2 through the Valanginian–Hauterivian. Finally, the $\delta^{13}C$ and $\Delta^{13}C$ records, combined with the new TEX_{86} temperature records described in Chapter 4, will be used to comment on the utility of the existing mechanisms put forward to explain the origins of the Valanginian CIE.

5. 2. INTRODUCTION

5. 2. 1. THE VALANGINIAN CARBON-ISOTOPE EVENT

A GLOBAL EVENT?

The Early Cretaceous is punctuated by several large perturbations to the carbon-cycle, which are recorded in marine and terrestrial sediments as both positive

and negative carbon-isotope excursions (CIEs), related to variations in the partitioning of carbon between the organic and inorganic reservoirs (e.g. Weissert, 1989; Section 1- 2; Figure 82). These perturbations have been associated with major climatic and palaeontological events such as carbonate platform drowning, calcification crises and oceanic anoxic events (OAEs) (e.g. Weissert *et al*., 1998, Leckie *et al*., 2002, Erba *et al*., 2004; Weissert & Erba 2004).

During the earliest Cretaceous (Berriasian–Barremian) a large perturbation to the carbon-cycle is recorded in the form of a prominent positive CIE, which peaked during the mid-Valanginian (~137 Ma; e.g. Lini *et al*., 1992; Weissert *et al*., 1998; Erba *et al*., 2004). Relatively positive carbon-isotope values in bulk-carbonate ($\delta^{13}C_{carb}$) have been recorded from Valanginian age sediments in the Gulf of Mexico, DSDP Site 535 (Cottillon & Rio, 1984), the North Atlantic (Site 534: Robertson & Bleifnick, 1983), the central Pacific (Site 167: Coplen & Schlanger, 1973; Douglas & Savin, 1973) and the Southern Alps of northern Italy (Lini *et al*., 1992; Channell *et al*. 1993) (Figure 83, 84). The occurrence of the positive carbon-isotope perturbation at many geographically-disparate locations suggests the event was of at least regional importance, and it was named the "Valanginian carbon isotope event" by Lini *et al*. (1992). Additional detailed bulk-carbonate $\delta^{13}C$ records have since been generated for the NW Tethyan (e.g. Follmi *et al*., 1994; Hennig *et al*., 1999; Fozy *et al*., 2010; A. Kujau *et al., pers comm. 2011*) and proto-North Atlantic (Bornemann *et al*., 2008a) regions, with other studies demonstrating the presence of the excursion in Mexico (Adatte *et al*., 2001) and the central Pacific (Erba *et al*., 2004; Figure 66).

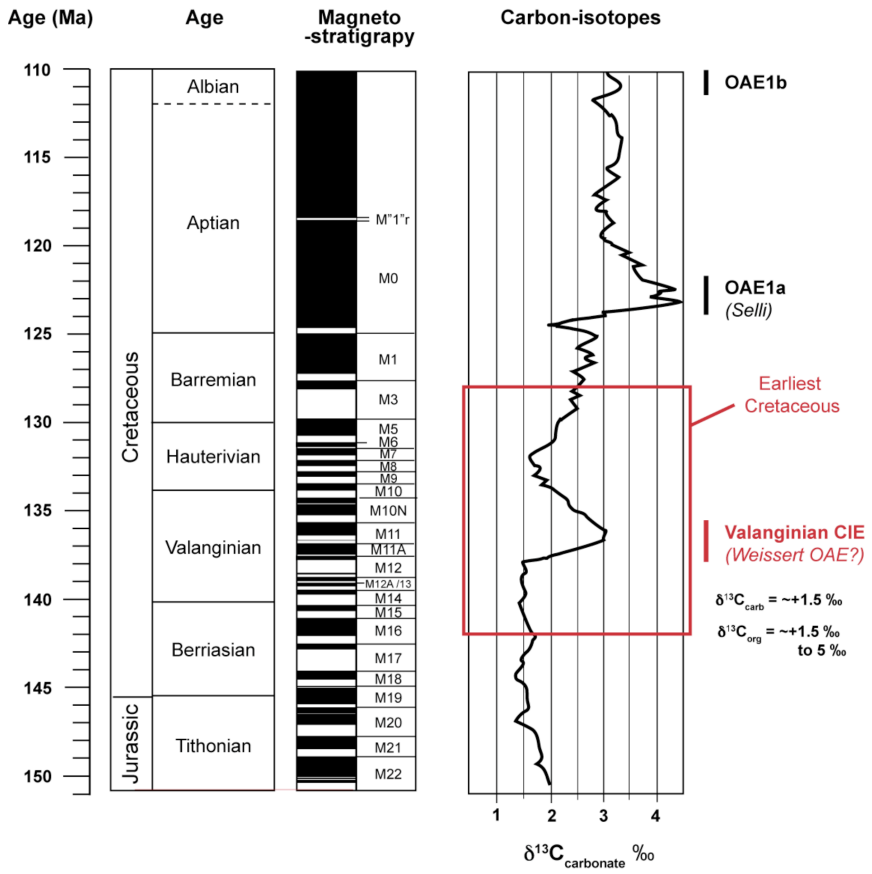

Figure 82. *Late Jurassic-Early Cretaceous composite carbon-isotope records. Adapted from Weissert et al. (1998) and Leckie et al. (2002).*

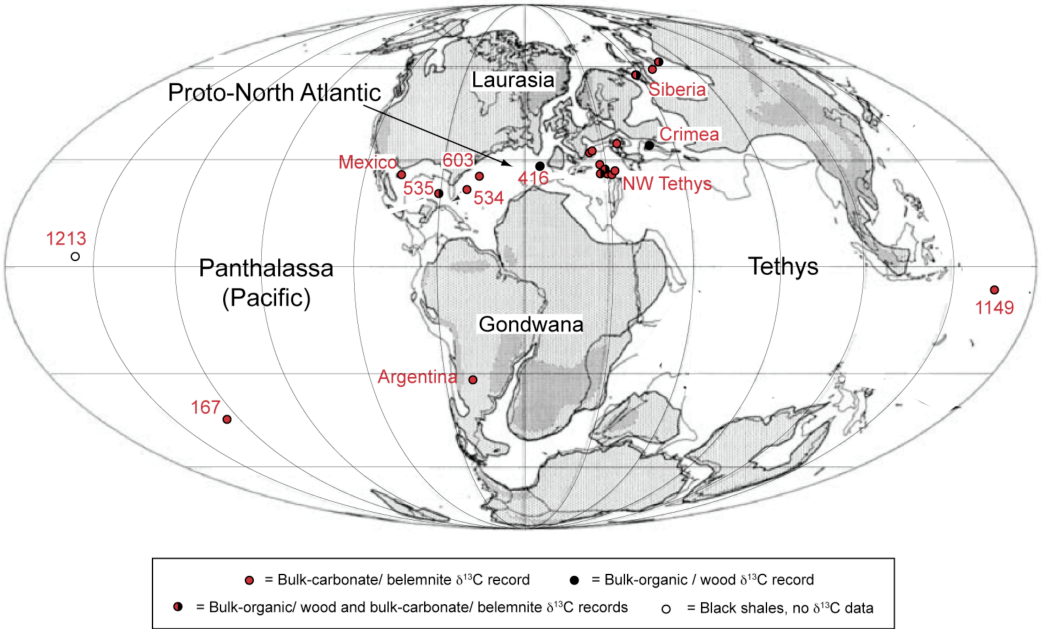

Figure 83. *World map (Valanginian–Hauterivian reconstruction) showing the location of significant sites where the Valanginian CIE, or the occurrence of organic-rich shales tentatively associated with the CIE, have been documented. Map modified after Puceat et al. (2005). Numbers represent DSDP/ ODP sites. See text for details of individual studies.*

In addition to the bulk-carbonate records, $\delta^{13}C$ records generated from carbonate macrofossils also show a trend for more positive values in the mid–Late Valanginian, albeit with far more "noise" than the contemporaneous bulk $\delta^{13}C_{carb}$ records. Studies from the Vocontian Basin in the western Tethys identified the peak positive $\delta^{13}C$ excursion in belemnite calcite during the *Saynoceras verrucosum* ammonite Zone and magnetochron M11, which broadly matches the age of the peak excursion seen in bulk carbonate Tethyan sections (Van de Schootbrugge *et al*., 2000; Lini *et al*., 1992; McArthur *et al*., 2007; Figure 84). This trend is echoed in Boreal belemnite records from several sites in northern Siberia, where the peak in $\delta^{13}C$ values is seen to occur in the mid-Late Valanginian, in strata that are age-equivalent to the *Saynoceras verrucosum – Neocomites peregrinus* ammonite Zones (Price & Mutterlose 2004; Nunn *et al*., 2010). $\delta^{13}C$ records taken from oyster shells from western-central Argentina, also show mid-Valanginian positive $\delta^{13}C$ values, broadly coincident with the Tethyan Valanginian CIE (Aguirre-Urreta *et al*., 2008), further extending the geographical extent of this event (Figure 83).

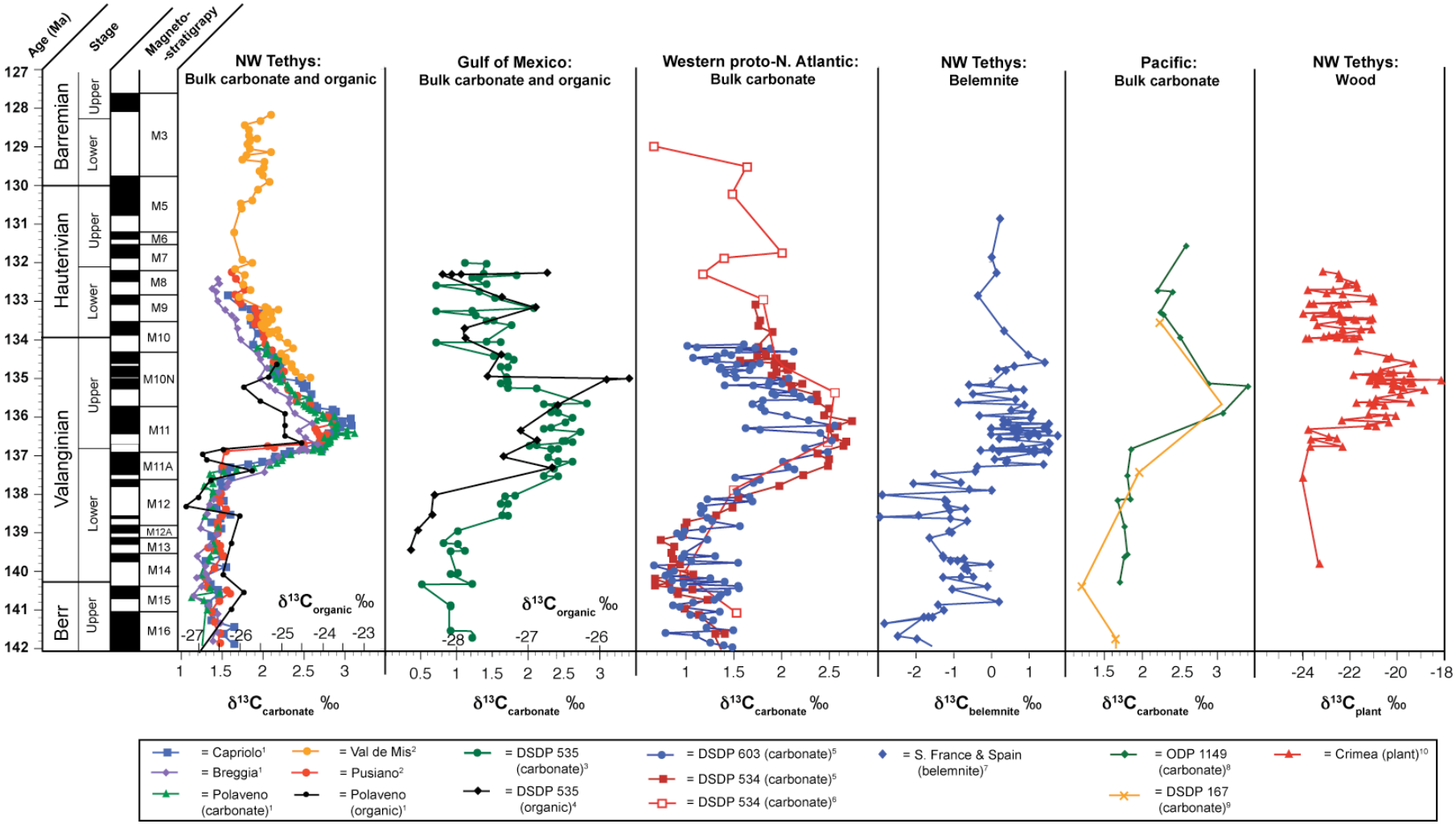

Figure 84. *Selected carbon-isotope records from the NW Tethys, western North Atlantic and the central Pacific. 1 = Lini et al. (1992); 2 = Channell et al. (1993); 3 = Cotillon & Rio, (1984); 4 = Patton et al. (1984;) 5 = Bornemann et al., (2008a); 6 = Robertson & Bliefnick, (1983), 7 = McArthur et al., (2007); 8 = Erba et al. (2004); 9 = Douglas & Savin, (1973); 10 = Grocke et al. (2005). Tethyan and North Atlantic age models are based on integrated magnetostratigraphy, and biostratigraphy, Gulf of Mexico and Central Pacific models are based on calcareous nannofossil data alone. Age of the belemnite record and wood record are based on Tethyan and Boreal ammonite zonation respectively.*

The Valanginian CIE has also been identified in bulk organic carbon-isotope ($\delta^{13}C_{org}$) records, in several sections from the western Tethys (Lini *et al*., 1992; Figures 83, 84), the Gulf of Mexico (Patton *et al*., 1984; Figure 84) and the eastern North Atlantic (Wortmann & Weissert, 2000). The magnitude of the excursion in bulk -organic matter ranges from ~1.5‰ (Lini *et al*., 1992; Wortmann & Weissert, 2000) to ~3‰ (Patton *et al*., 1984), and is generally larger in magnitude than the bulk-carbonate excursion. Importantly, the Valanginian CIE has also been documented in wood records from the NW Tethys (Crimea; Grocke *et al*., 2005) and two sites in northern Siberia (Nunn *et al*., 2010). The magnitude of the isotope excursion in the Crimean plant material is on the order of ~+5 ‰, while in the Siberian sections it is much smaller at only ~+2 ‰ (Grocke *et al*., 2005; Nunn *et al*., 2010). As plants obtain their carbon through assimilation of atmospheric CO_2, the presence of the excursion in terrestrial wood strongly suggests that the Valanginian CIE affected the entire ocean-atmospheric carbon reservoir, and therefore that the event was of truly global significance (Grocke *et al*., 2005).

MECHANISTIC ORIGINS OF THE CIE

Although the global nature of the Valanginian CIE has been established by the presence of the positive excursion in many different sites around the world, and in a variety of geological materials, the underlying mechanism to explain the origin of the perturbation remains somewhat controversial. The common model used to explain the excursion, set out by Weissert (1989) and subsequently expanded by Lini *et al*. (1992), requires a major change in climate, specifically the onset of greenhouse conditions in the mid-Valanginian following the relatively cooler conditions of the Late Jurassic and Berriasian. Increased volcanic activity in the Paraná-Etendeka large igneous province (LIP) in southern Gondwana is blamed for a transient increase in pCO_2 during the mid Valanginian, which is hypothesised to have led to higher global temperatures (Lini *et al*., 1992; Weissert *et al*., 1998). This supposed increase in mean temperature could have triggered a more humid climate in the Tethyan region, which would have led to increased run-off and subsequent nutrification of the marine margins by rivers, facilitating a change from oligotrophic to eutrophic conditions and a concurrent increase in marine productivity (e.g. Lini *et al*., 1992). According to this model, the excess marine organic matter generated

would have been buried in organic-rich sedimentary deposits in the ocean, driving the carbon-isotopic composition of the ocean and atmosphere to heavier values (e.g. Lini *et al*. 1992; Weissert *et al*. 1998). This hypothesised sequence of events, combined with the similarity of disparate isotopic records and the apparently widespread deposition of organic-rich strata, led Erba *et al*. (2004) to suggest that the Valanginian CIE actually represented the first Cretaceous OAE, which they named the "Weissert OAE" in recognition of Helmut Weissert's many years of work on the earliest Cretaceous.

The original theory, of increased temperatures triggering increased organic-matter burial in the marine realm, has proven attractive, and the majority of the subsequent studies investigating the Valanginian CIE have tended to agree with its basic tenets (e.g. Channell *et al*., 1993; Follmi *et al*., 1994; Weissert *et al*., 1998; Hennig *et al*., 1999; Wortmann & Weissert 2000; van de Schootbrugge *et al*., 2003; Erba *et al*., 2004; Grocke *et al*., 2005; Kuhn *et al*., 2005; Duchamp-Alphonse *et al*., 2011). However, as attractive as this simple model may be, the evidence for the Valanginian greenhouse theory, beyond interpretation of the carbon-isotope curves themselves, is somewhat contradictory. While trace-element and sedimentological data supports the theory for increased run-off and nutrification on the Tethyan margins (e.g. Weissert, 1990; Follmi *et al*., 1994; van de Schootbrugge *et al*., 2003; Duchamp-Alphonse *et al*., 2011), the evidence for discrete organic-carbon-rich beds, analogous to the major OAEs of the mid-Cretaceous, is limited (Bersezio *et al*., 2002; Bralower *et al*., 2002; Reboulet *et al*., 2003). Proxy evidence for the required discrete pulse of warming during the Valanginian is virtually non-existent, while the evidence for a relatively cool period in the Late-Valanginian-Early Hauterivian is more convincing, although still not without regional variations in palaeotemperature trends (e.g. Kemper, 1987; Price, 1999; Erba *et al*., 2004; McArthur *et al*., 2007; Kessels *et al*., 2006; Littler *et al*., 2011; see Chapter 4). Disparities between the model and some of the proxy evidence has led some authors to speculate that the Valanginian does not represent an OAE at all, but rather the consequence of a generally warm and humid climate in the earliest Cretaceous leading to excessive coal deposition on the continents with minor increases in organic-matter storage on the marine margins (e.g. Westermann *et al*., 2010). As a key tenet of the original greenhouse model rests on increased pCO_2 during the early Valanginian, supposedly triggered by volcanic degassing, it would be desirable to be able to constrain relative

fluctuations in pCO_2 during the Valanginian–Hauterivian in order to attempt to reconcile the differences between the various conceptual models.

5. 2. 2. USING $\Delta^{13}C$ TO RECONSTRUCT pCO_2

Constraining the relative timing of $\delta^{13}C_{carb}$ and $\delta^{13}C_{org}$ excursions in the Valanginian–Hauterivian is important, as any offsets between the bulk-carbonate and bulk-organic matter reservoirs could be significant for interpreting carbon-cycling. Offsets would imply non-synchronous responses in the surface ocean carbonate and organic-matter pools to the carbon-isotope perturbation, possibly related to changing pCO_2.

While changes in marine bulk-carbonate $\delta^{13}C$ values are largely controlled by changes in the surface-ocean carbon-isotope reservoir, marine bulk-organic matter $\delta^{13}C$ is also affected by other factors such as the partial pressure of dissolved CO_2 in the surface ocean (e.g. Arthur *et al*., 1985; Dean *et al*., 1986; Freeman & Hayes, 1992; Lini *et al*., 1992). The degree to which marine algae isotopically fractionate carbon during photosynthesis (εp) increases with increasing CO_2 availability, (and other factors such as PO_4 content) and therefore is directly related to the pCO_2 in the surface-ocean and hence the atmosphere (e.g. Arthur *et al*., 1985; Dean *et al*., 1986). Therefore, if the source organic-matter in a sediment sample can be assumed to be dominantly marine, and both the $\delta^{13}C_{carb}$ and $\delta^{13}C_{org}$ values from the same samples are known, the difference between these two can be used to reconstruct changes in pCO_2 with time (e.g. Arthur *et al*., 1985; Freeman & Hayes, 1992; Kump & Arthur 1999; Kuypers *et al*., 2004). Using bulk-carbonate and bulk organic $\delta^{13}C$ values from the same samples, the "delta-delta ^{13}C" ($\Delta^{13}C = \delta^{13}C_{carb} - \delta^{13}C_{org}$) record can be reconstructed, which has previously been used as a proxy for changing pCO_2 in the Cretaceous (e.g. Lini *et al*., 1992; Kump & Arthur, 1999; Grocke *et al*., 2005; Jarvis *et al*., 2011). It is not possible to reconstruct absolute pCO_2 values using this method, and only relative trends can be inferred, as the reconstruction of absolute pCO_2 levels requires the presence of alkenones and well-constrained estimates of PO_4^{3-} (e.g. Pagani *et al*., 1999), neither of which exist in Early Cretaceous sediments.

Although a lag between $\delta^{13}C_{org}$ and $\delta^{13}C_{carb}$ trends has previously been suggested for the Valanginian CIE (Patton *et al*., 1984; Cotillon & Rio, 1984), there are very few existing bulk-organic $\delta^{13}C$ records that are paired with corresponding bulk-carbonate records from the same samples. This is required to construct reliable $\Delta^{13}C$ estimates. Only three published sections have both $\delta^{13}C_{org}$ and $\delta^{13}C_{carb}$ data, in the western North Atlantic and southern Europe, (Patton *et al*., 1984; Cotillon & Rio, 1984; Lini *et al*., 1992) although other paired Tethyan records are being prepared from the Polish and Vocontian Basins (A. Kujau *pers comm.* 2011). The $\delta^{13}C_{org}$ record from Site 535 in the Gulf of Mexico is relatively low-resolution across the CIE onset and the measurements are not from the same samples, meaning the record is not sufficient to ascertain if the apparent lag between $\delta^{13}C_{carb}$ and $\delta^{13}C_{org}$ during the onset phase of the CIE is real or an artefact of sampling (Patton *et al*., 1987; Cotillon & Rio, 1987). However, new unpublished high-resolution records at Site 535 do not suggest the existence of a genuine lag between the bulk-carbonate and the bulk-organic matter reservoirs during the onset of the CIE (J. Rosling, UCL, u*npublished MSc Dissertation, 2010, UCL*). The $\delta^{13}C_{carb}$ and $\delta^{13}C_{org}$ records from the NW Tethyan sections at Polaveno and Rio Corna are from the same samples, but the organic records are of a much lower resolution compared to the carbonate samples (Lini *et al*., 1992). The records from Rio Corna also miss the important CIE onset phase, making determination of lead and lag times across the excursion difficult (Lini *et al*., 1992).

Using a similar reasoning to that employed in the study of marine bulk-organic and bulk carbonate $\Delta^{13}C$ records, Grocke *et al*. (2005) attempted to use the difference between the $\delta^{13}C$ record of wood from the Crimea and bulk carbonate $\delta^{13}C$ records from Southern Europe, to reconstruct $\Delta^{13}C$ and pCO_2 across the Valanginian CIE. This method is predicated on the theory that the amount of photosynthetic fractionation imposed by plants on carbon, is related to the pCO_2 of the atmosphere in a similar manner to the relationship between dissolved pCO_2 and $\delta^{13}C$ in marine algae (e.g. Hasegawa *et al*., 2003; Grocke *et al*., 2005, and references within). Using this method Grocke *et al*. (2005) estimated a ~40% drop in pCO_2 between the onset and peak of the CIE occurred during the Valanginian. However, the relationship between $\delta^{13}C_{plant}$ and pCO_2 may not be as straightforward as that found in marine photosynthetic organisms, as fossil higher plant material will often

contain a mixture of different genera, each of which may have a different $\delta^{13}C_{plant}$ values due to variations in photosynthetic pathways, or within-plant isotopic variation (e.g. Robinson & Hesselbo, 2004). This fact, combined with the large uncertainties in correlating the age models between the Crimea and southern Europe, complicate the interpretation of the $\Delta^{13}C$ records from the Crimea.

At DSDP Sites 534 and 603 in the western North Atlantic, two high-resolution bulk carbonate carbon-isotope record ($\delta^{13}C_{carb}$) have recently been generated, both of which clearly show the CIE onset, peak and recovery period and place the peak of the event in the mid–Late Valanginian (Bornemann *et al*., 2008a; Figures 84, 85). Both of these sites therefore provide an excellent opportunity to compare the responses of the carbonate and organic carbon reservoirs to the Valanginian perturbation. However, there are currently no bulk-organic data from Site 534, and the existing data for Site 603 is very low-resolution and not optimally spaced to capture the CIE, and therefore, not suitable for comparison with the new high-resolution $\delta^{13}C_{carb}$ records (Dean & Arthur 1987; Dunham, 1987; Figure 85). Existing $\delta^{13}C_{org}$ data from Site 603 also suggest a minor lithological effect on the carbon-isotopic values, with the dark grey homogeneous mudstones consistently having heavier values than co-occurring laminated marls and limestones, which contributes to the scatter (Figure 85). Such an offset between the marls and the mudstones, is also seen in the $\delta^{13}C_{org}$ data presented in Chapter 3. Therefore there is a clear need for lithologically-separated, Berriasian–Valanginian $\delta^{13}C_{org}$ records from both Sites 534 and 603, to further constrain the expression of the Valanginian CIE in the western proto-North Atlantic, and to allow effective comparison with the new bulk carbonate records.

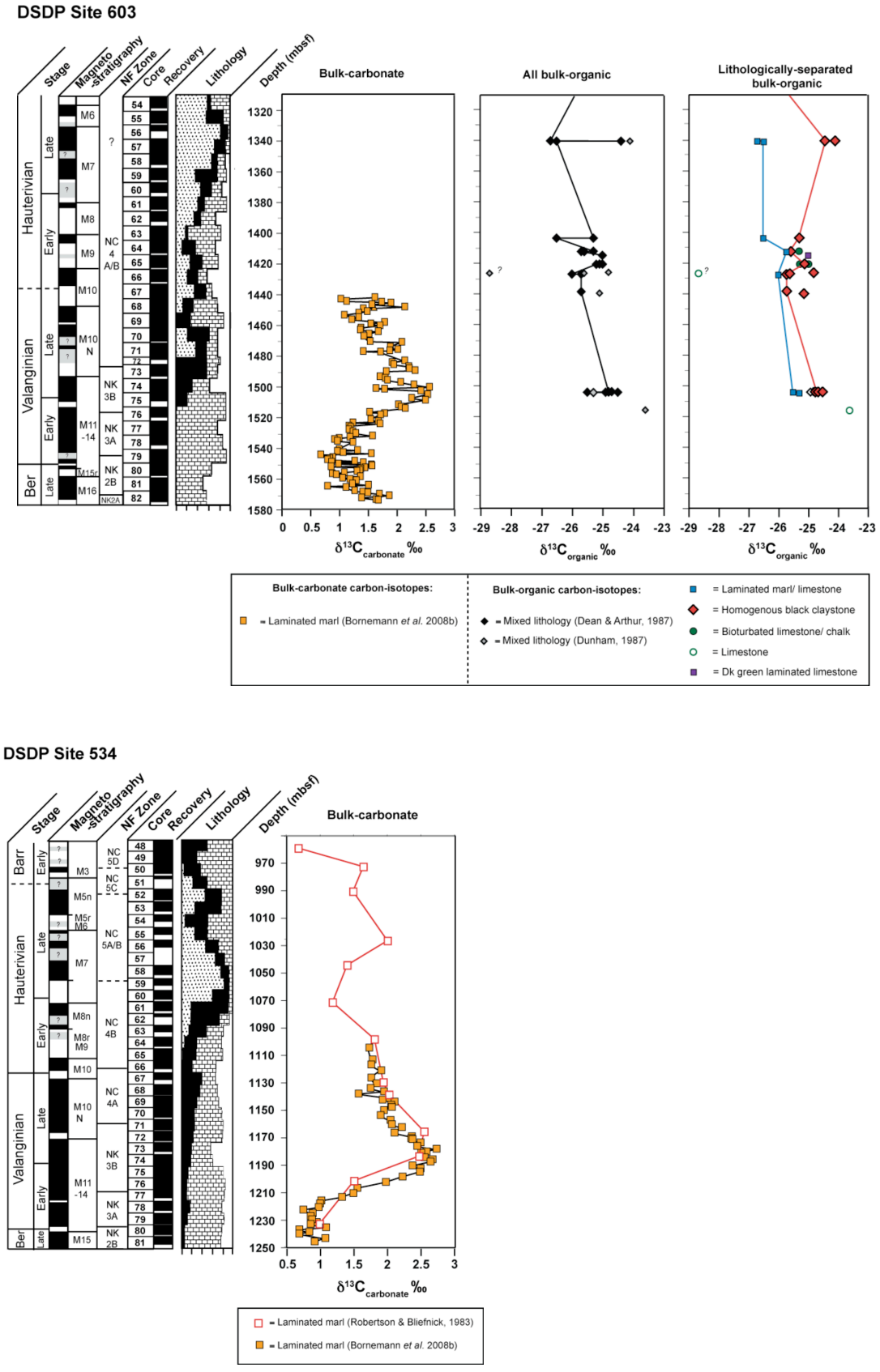

Figure 85. *Existing carbon-isotope data from DSDP Site 603 (top) and DSDP Site 534 (below). No published bulk organic-matter carbon-isotope data are currently available at Site 534.*

5. 3. METHODS AND MATERIALS

The modern location of Sites 534 and 603 in the western North Atlantic, and the age models used to tie them to relative and absolute time, are discussed in Chapter 2. The sedimentological, palaeontological, and geochemical basis for the separation of the lithologies into laminated marls and bioturbated chalks (pelagic) and homogeneous mudstones (transported) has been established in detail in Chapter 3 and follows the lithological divisions after Robertson & Bliefnick (1983).

At DSDP Site 603, 29 bioturbated chalk and 29 laminated marl samples were taken from cores 58 to 82, from a similar depth to one another, and analysed to determine their bulk-carbonate $\delta^{13}C_{carb}$ and $\delta^{18}O_{carb}$ values. At Site 603, 68 samples of Late Berriasian–Late Hauterivian age (Core 54 to 82; 1324 to 1573 mbsf) were analysed to determine their bulk organic carbon-isotope values, including 38 laminated marls and 30 homogeneous mudstone samples. Additionally, 30 discrete samples of Early Valanginian–Late Hauterivian age wood, taken from Cores 58 to 77 (1350 to 1529 mbsf) were analysed for $\delta^{13}C$ by Dr Stuart Robinson. At Site 603, there are 19 $\delta^{13}C_{org}$ samples that also have paired $\delta^{13}C_{carb}$ data, from which $\Delta^{13}C$ values ($\delta^{13}C_{carb}$ - $\delta^{13}C_{org}$) have been calculated. Using new $\delta^{13}C_{org}$ data and $\delta^{13}C_{carb}$ data points from Bornemann *et al*. (2008a) a further 11 $\Delta^{13}C$ values have also been calculated.

At DSDP Site 534, 71 samples of Late Berriasian–Early Barremian age (Core 49 to 84; 964 to 1274 mbsf) were analysed to determine their $\delta^{13}C_{org}$ values, including 47 laminated marls and 29 homogeneous mudstone samples. At Site 534, 19 of the laminated marl samples also have bulk-carbonate $\delta^{13}C$ values, allowing $\Delta^{13}C$ values to be determined. Using new $\delta^{13}C_{org}$ data and $\delta^{13}C_{carb}$ data points from Bornemann *et al*. (2008a) a further 20 $\Delta^{13}C$ values have also been calculated.

Methods for generating $\delta^{13}C_{org}$ and $\delta^{13}C_{carb}$ data are outlined in detail in Chapter 2, Section 2-2-3-1. and 2-2-3-2 respectively. The uncertainty of standards is generally better than 0.1‰, however the reproducibility of samples is often higher than this. At Site 534, 14 $\delta^{13}C_{org}$ samples were rerun at least twice, (thirteen laminated marls and one homogeneous mudstone) with an average range from different analysis of the same sample of 0.20 ‰; however, some samples had differences of up to 0.36 ‰ between runs on the same sample. At Site 603, six

samples, (four laminated marls, four homogeneous mudstones) were re-run twice, yielding an average range of 0.31 ‰ between runs on the same sample.

5. 4. RESULTS

5. 4. 1. BULK-CARBONATE CARBON-ISOTOPES

In order to assess the suitability of different lithologies for reconstructing the $\delta^{13}C_{carb}$ record of the surface ocean in the western proto-North Atlantic, a small study examined the differences between carbon and oxygen isotopes in two different lithologies at Site 603. An offset in $\delta^{13}C_{carb}$ carbon-isotopes between these co-occurring laminated marls and bioturbated limestones is observed, which spans the entire Berriasian–Hauterivian interval (Figure 86). The isotopic offset between the two lithologies is clear and consistent, with the laminated marls consistently having heavier $\delta^{13}C_{carb}$ values than the chalks by ~0.5 ‰ in the Berriasian–Valanginian, rising to a >1‰ offset in the Hauterivian (Figure 86). The timing of the onset of the excursion during the Early Valanginian, and the attainment of peak values in the mid Valanginian, is identical in both lithologies despite the offset in absolute values (Figure 86). There is also an offset noted between the chalk and the marl in oxygen-isotopes, with the chalk once again having consistently lighter $\delta^{18}O_{carb}$ values, between 0.3 to >3‰ lighter than the marls (Figure 86). Although the data show some scatter, a general decreasing trend can perhaps be discerned in both lithologies from the Berriasian to the Late Valanginian, which then reverses to a moderate positive trend during the Early Hauterivian (Figure 86).

At both Sites 534 and 603, the new low-resolution bulk-carbonate $\delta^{13}C$ records from the laminated marls, follow the existing Berriasian–Valanginian higher-resolution $\delta^{13}C_{carb}$ records closely, with both clearly demonstrating the presence of the Valanginian positive CIE in the western proto-North Atlantic during the mid-Valanginian (Figures 86, 87, 88; Bornemann *et al*., 2008a). At Site 534 however, there is a slight tendency for the new $\delta^{13}C_{carb}$ values to be approximately ~0.4 ‰ heavier than the existing record in the Early Valanginian pre-CIE interval, and ~0.3‰ heavier at the peak of the excursion (Figure 87; Bornemann *et al*.,

2008a). This is likely due to minor analytical error and/or scatter in the $\delta^{13}C_{carb}$ data and is not thought to be significant.

At Site 534 a minor fall in $\delta^{13}C_{carb}$ values from the Late Berriasian–Early Valanginian, of ~0.5 ‰, is observed in both the new and existing records, which is also visible at Site 603 (Figures 87, 88). A sharp rise in $\delta^{13}C_{carb}$ values at both sites occurs in the middle of the Early Valanginian during the CIE onset, which peaks at maximum values of 2.7 to 3.0 ‰ in the earliest Late Valanginian (Figures 87, 88). At both sites the data suggests falling $\delta^{13}C_{carb}$ values from the Late Valanginian into the Early Hauterivian during the recovery interval, with the Site 534 data further suggesting relatively stable Late Hauterivian values and a possible sharp negative excursion of ~1.3 ‰ in the Early Barremian (Figures 87, 88). At Site 603, laminated marl $\delta^{13}C_{carb}$ records from both published data (Bornemann *et al*., 2008a) and this study appear to show a more variable signal than concurrent records from Site 534 (Figures 87, 88; Bornemann *et al*., 2008a). As all the samples from Site 603 were selected to represent pelagic laminated marls (see Chapter 3), simple lithological changes cannot be used to explain the variability present at Site 603 but absent at Site 534 (Bornemann *et al*., 2008a).

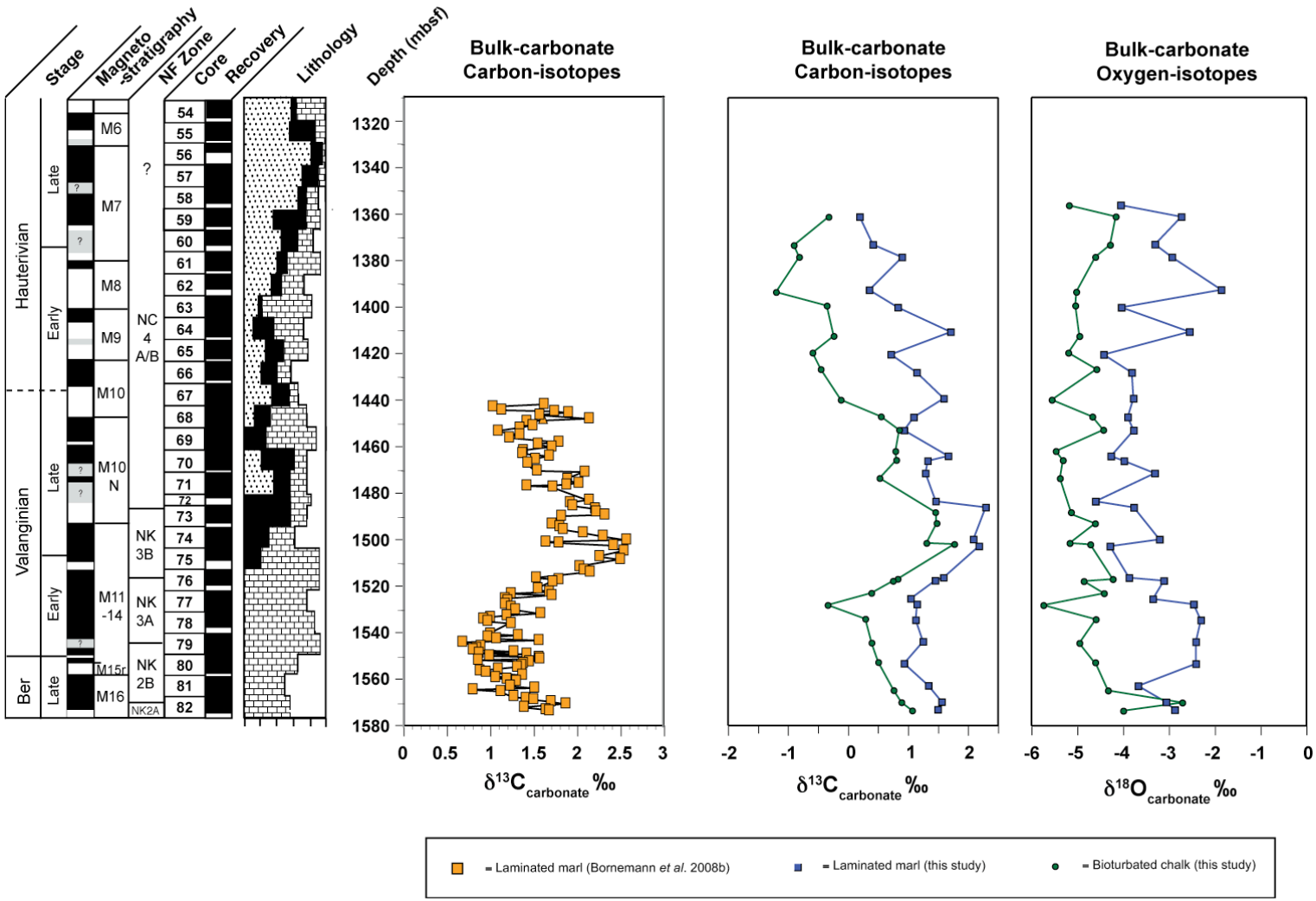

Figure 86. *Lithologically -separated bulk-carbonate carbon-isotope records from DSDP Site 603.*

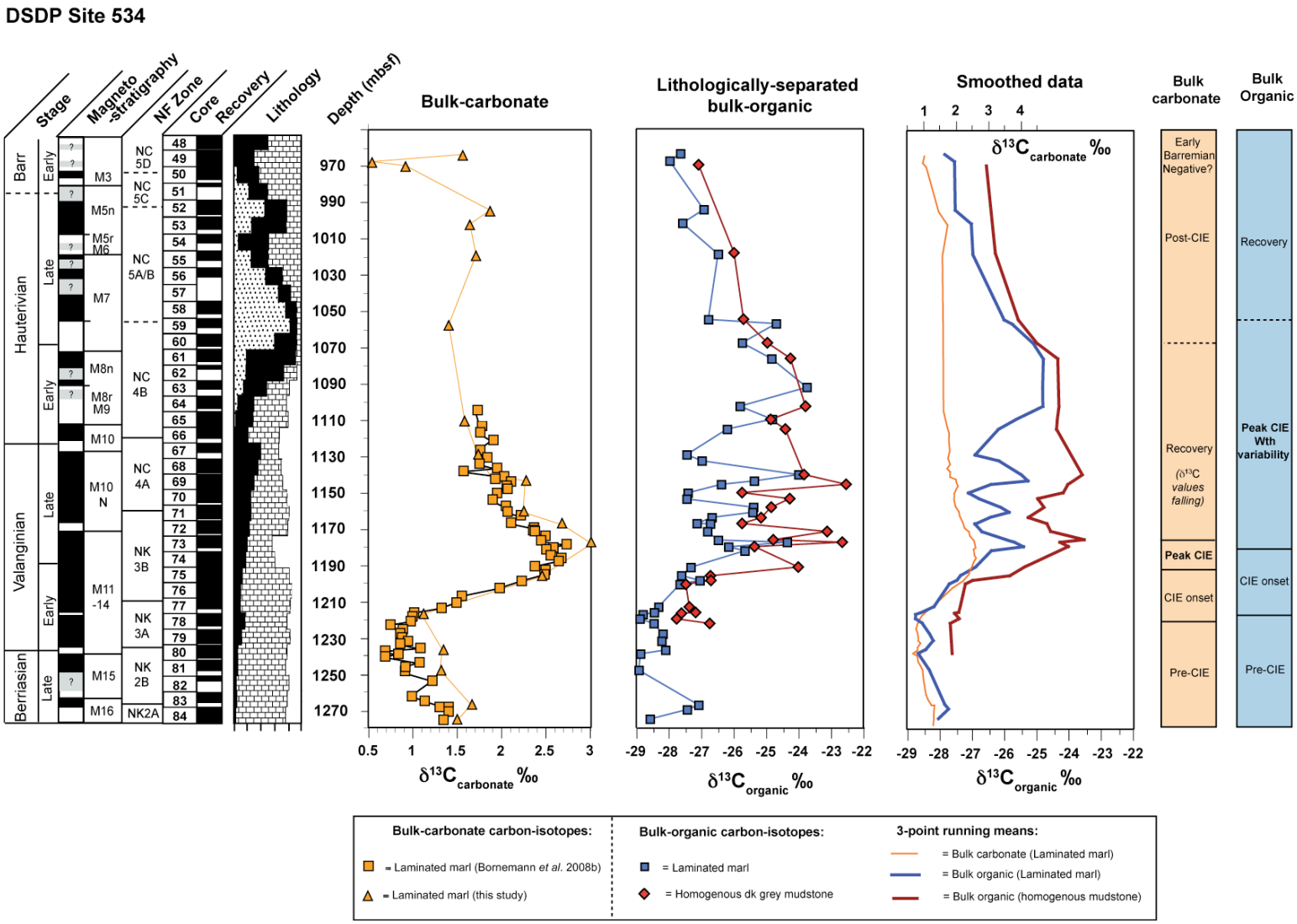

Figure 87. *Bulk-carbonate and bulk-organic matter records from DSDP Site 534.*

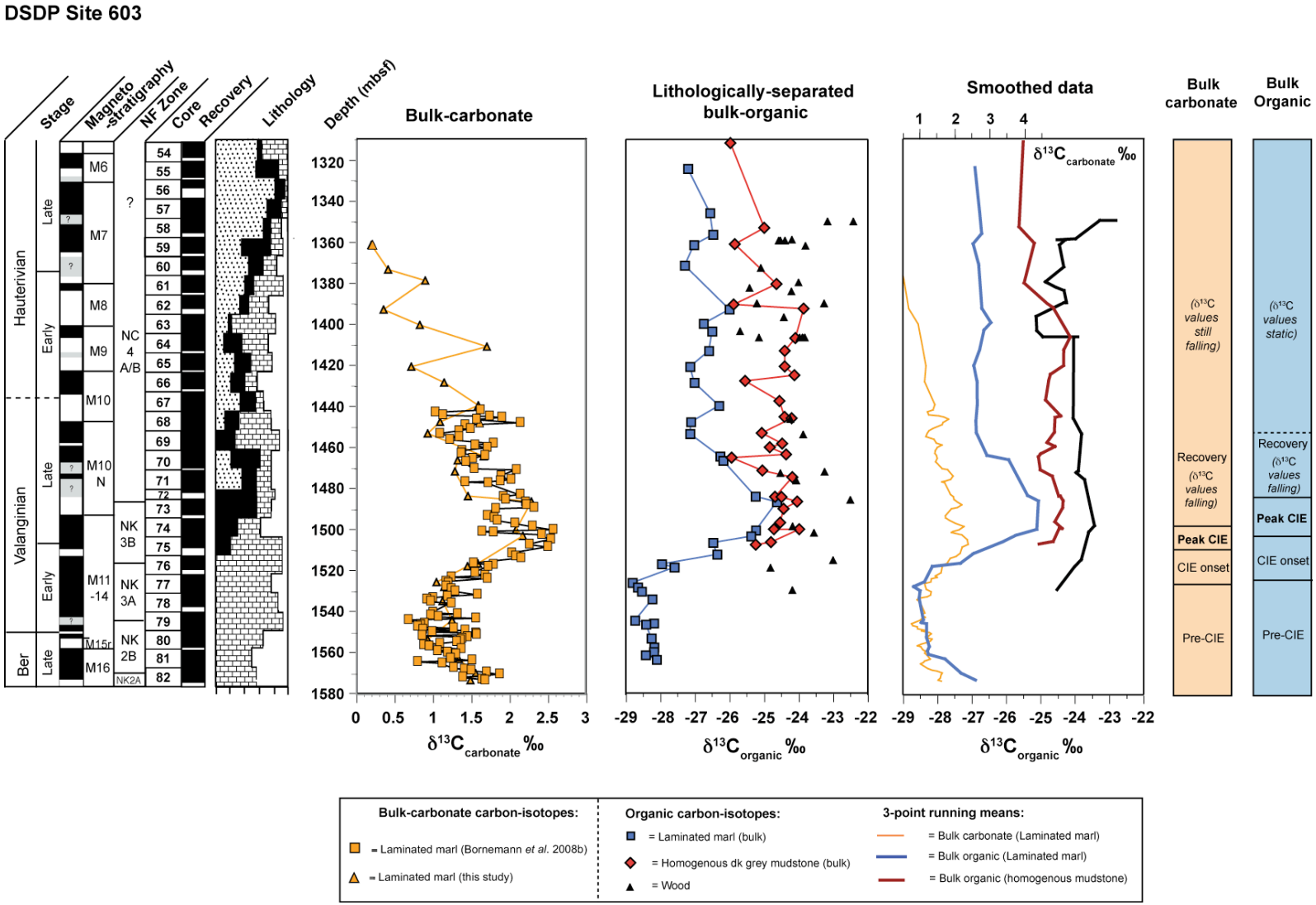

Figure 88. *Bulk-carbonate and bulk-organic matter records from DSDP Site 603.*

5. 4. 2. BULK-ORGANIC VS. BULK CARBONATE CARBON-ISOTOPES

The Valanginian positive CIE can be identified in the bulk-organic $\delta^{13}C$ record from the laminated marls at both Sites 534 and 604, although both the magnitude and timing of the excursion differs from that seen in the corresponding bulk-carbonate records (Figures 87, 88). At Site 534 the $\delta^{13}C_{org}$ record from the laminated marls ("$\delta^{13}C_{org}$ (marl)") record is somewhat noisy in the Late-Valanginian–Early Hauterivian, and features several sharp alternations between more positive and negative values (Figure 87). At Site 603 the $\delta^{13}C_{org}$ (marl) record is somewhat less noisy than that seen at Site 534, and the excursion and recovery period are more sharply defined (Figure 88). At both sites there is good agreement between the $\delta^{13}C_{carb}$ and $\delta^{13}C_{org}$ (marl) records in the Late Berriasian–mid-Early Valanginian, prior to the onset of the CIE. Both the $\delta^{13}C_{carb}$ and $\delta^{13}C_{org}$ (marl) records show a synchronous negative trend, with a fall of ~0.7 % in the $\delta^{13}C_{carb}$ record matched by a fall of ~1.2 % in the $\delta^{13}C_{org}$ (marl) record (Figures 87, 88).

However, despite the overall good agreement between the $\delta^{13}C_{carb}$ and $\delta^{13}C_{org}$ (marl) records in the earliest Cretaceous, lags between the $\delta^{13}C_{carb}$ and the $\delta^{13}C_{org}$ (marl) record do exist in the timing of the subsequent positive CIE. At Site 603, the initial shift to more positive values at the start of the CIE is virtually synchronous between the $\delta^{13}C_{carb}$ and $\delta^{13}C_{org}$ (marl) records, but occurs slightly later in the $\delta^{13}C_{org}$ record than the $\delta^{13}C_{carb}$ record at Site 534 (Figures 87, 88). There is also a lag in the timing of the onset and duration of peak $\delta^{13}C$ values between the $\delta^{13}C_{carb}$ and the $\delta^{13}C_{org}$ (marl) records at both sites (Figures 87, 88). At Site 534, the first peak value of -24.5 ‰ is reached in the earliest Late Valanginian, in the upper part of the NK3B Subzone, which is concurrent with the *end* of the peak values in the bulk-carbonate record (Figure 87). Similarly at Site 603, peak values of -24.5– -25.2 ‰ are reached in the earliest Late Valanginian, slightly later than the peak values seen in the carbonate record (Figure 88).

There is also a considerable lag in the CIE recovery period, where the relatively stable decay of $\delta^{13}C$ values to more negative values seen in the $\delta^{13}C_{carb}$ record in the Late Valanginian–Hauterivian, contrasts with more variable and positive trends in the $\delta^{13}C_{org}$ (marl) record (Figures 87, 88). At Site 534, peak $\delta^{13}C_{org}$

(marl) values of ~-24.5 ‰ are followed by a fall in values back to -27 ‰, broadly in-step with the recovery in the bulk-carbonate values (Figure 87). However, values do not remain as relatively negative as they do in the $\delta^{13}C_{carb}$ record and the remainder of the Late Valanginian features several alternations between more positive and negative values, which eventually return to pre-excursion values of ~-28 ‰ in the Early Barremian (Figure 87). At Site 603, there is far less variation in the $\delta^{13}C_{org}$ (marl) record during the recovery period, with a coherent fall to more negative values seen in the latest Late Valanginian, which then remains relatively negative at ~-26 to -27.5 ‰ for the remainder of the Hauterivian (Figure 87, 88).

In addition to the laminated marl record, the $\delta^{13}C_{org}$ of co-occurring turbiditic mudstones was also determined at both sites where possible, to examine the effect of lithology on the carbon-isotope signal. At Site 534, the fluctuations in the $\delta^{13}C_{org}$ (marl) record detailed above are virtually synchronous with changes in the homogeneous mudstone $\delta^{13}C_{org}$ record ("$\delta^{13}C_{org}$ (mudstone)") record, albeit with a consistently heavier values of ~0.4 –1.7 ‰ relative to the marl record (Figure 87). The same pattern of heavier $\delta^{13}C_{org}$ (mudstone) values relative to the $\delta^{13}C_{org}$ (marl) values is also observed at Site 603, however there is less synchroneity between the mudstone and marl records than that observed at Site 534 (Figure 87, 88). The $\delta^{13}C_{org}$ (mudstone) record also only extends from the Late Valanginian onwards at Site 603, meaning there is little available information for the pre-excursion or onset phase of the CIE (Figure 88). Similar to Site 534, the $\delta^{13}C_{org}$ (mudstone) values are consistently heavier than those of the pelagic marls by ~0.2 – 2 ‰, with values fluctuating between ~-24 and -26 ‰ throughout the Valanginian–Hauterivian (Figure 88). No coherent trends are seen from the Late Valanginian to the Late Hauterivian at Site 603 in the $\delta^{13}C_{org}$ (mudstone) record, in contrast to the trends seen in both the $\delta^{13}C_{org}$ (marl) and $\delta^{13}C_{carb}$ records, which suggests a return to more negative values in the Late Valanginian–Hauterivian (Figure 88). However by the mid-Hauterivian, slightly more negative values are observed in the $\delta^{13}C_{org}$ (mudstone) record, suggesting that the CIE recovery period may also be visible in this lithology (Figure 88).

5. 4. 3. WOOD CARBON-ISOTOPES

Dr S. Robinson has analysed 30 wood samples of Early Valanginian–Late Hauterivian age at Site 603, and has supplied the unpublished $\delta^{13}C$ values, (Figure 88). The $\delta^{13}C_{wood}$ values range from ~ -22.5 to -25.5 ‰, and are normally at least 1 ‰ heavier than the laminated marls from a similar depth, and either comparable to, or slightly heavier than the homogeneous mudstone values (~-24 to - 26 ‰) (Figure 88). Unfortunately no wood samples were recovered prior to the onset of the CIE at Site 603, and the data are highly scattered with a range of ~3 ‰, meaning it is difficult to ascertain whether the carbon-isotope excursion is recorded in this material in the western proto-North Atlantic (Figure 88). However, there may be a tentative trend to more positive values in the lowermost wood samples, coincident with the earliest part of the CIE in the laminated marl record (Figure 88).

5. 4. 4. DELTA-DELTA CARBON-ISOTOPES

$\Delta^{13}C$ has been determined from multiple laminated marl samples at both Sites 534 and 603 (Figures 89, 90). The greater amplitude of the bulk organic record at both sites 534 and 603, mean the resulting $\Delta^{13}C$ record is largely controlled by fluctuations in the $\delta^{13}C_{org}$ record. At Site 534, $\Delta^{13}C$ values of ~28.5 – 30 ‰ characterise the Berriasian–earliest Valanginian, which are followed by a general fall in values through the Valanginian, reaching the lowest values of ~26.5 ‰ in the mid-Hauterivian (Figure 89). However, the large variability in the bulk-organic record during the Late Valanginian at Site 534 generates considerable variability in the $\Delta^{13}C$ values, with values fluctuating between 27.5 and 29.5 ‰ (Figure 89). At Site 534, $\Delta^{13}C$ values then increase back to values of 28.5 – 29 ‰ during the Late Hauterivian–Early Barremian. At Site 603, the Late Berriasian–mid Early Valanginian pre-CIE period is characterised by a rise in $\Delta^{13}C$ values of ~1.5‰, from ~ 28.5 ‰ to 30 ‰ (Figure 90). During the CIE onset period at Site 603, the $\Delta^{13}C$ values fall sharply to minimum values of ~27 ‰ in the mid-Late Valanginian. As the recovery to more negative values in the organic matter record begins, the $\Delta^{13}C$ values rise again, peaking at ~ 28 ‰, before falling back to ~27 ‰ again in the Late Hauterivian (Figure 90).

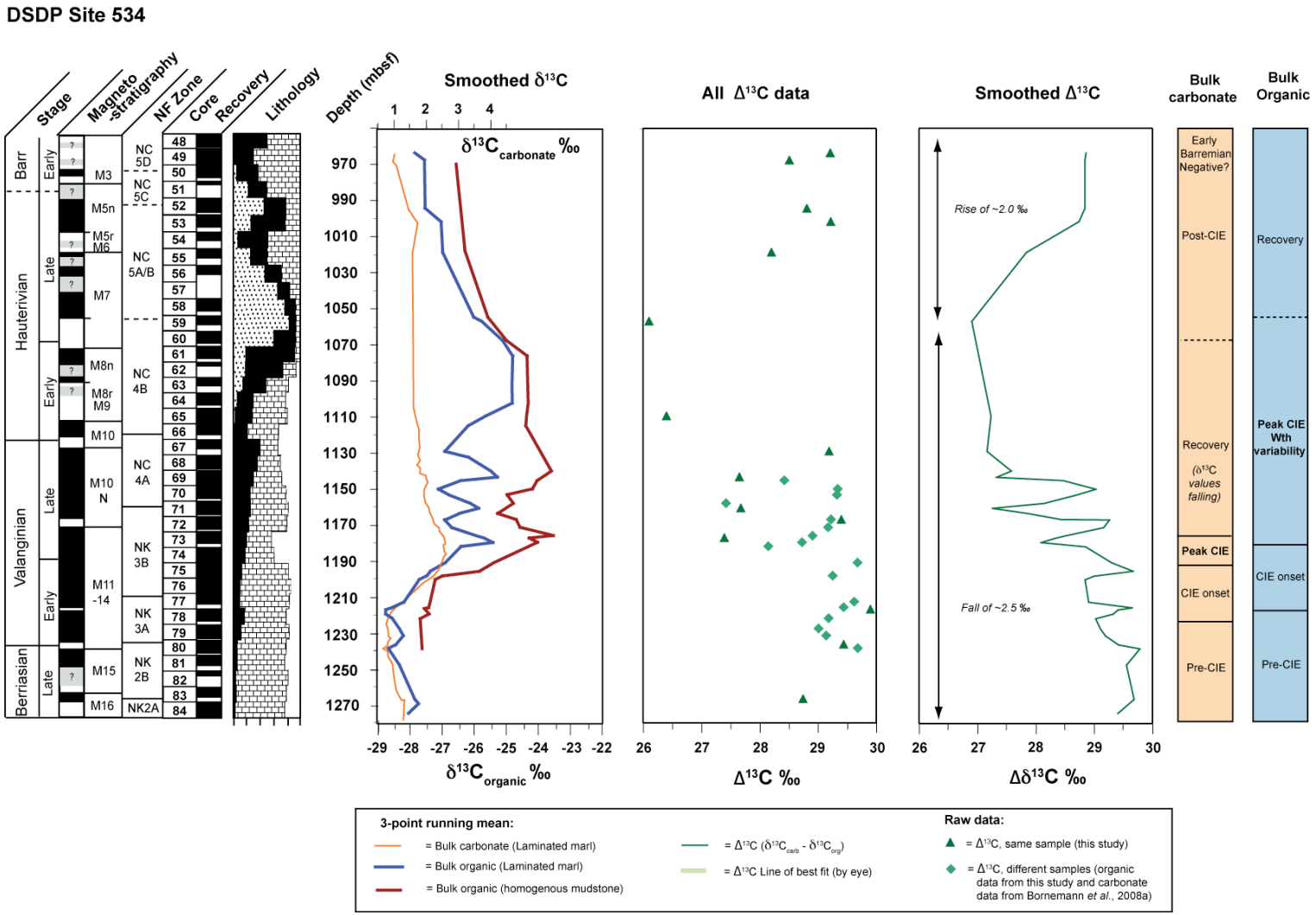

Figure 89. *Delta-delta records from DSDP Site 534.*

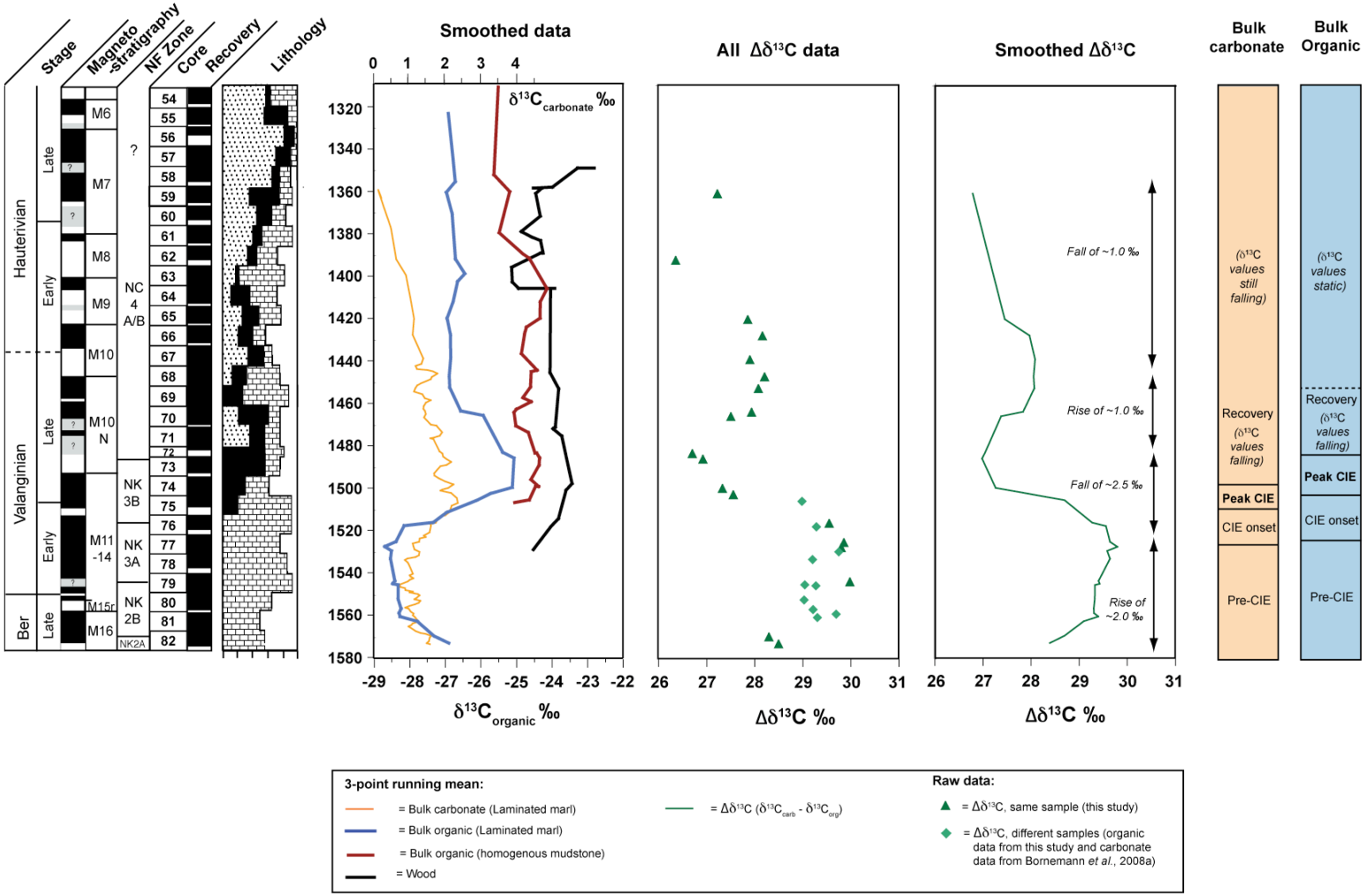

Figure 90. *Delta-delta records from DSDP Sites 603.*

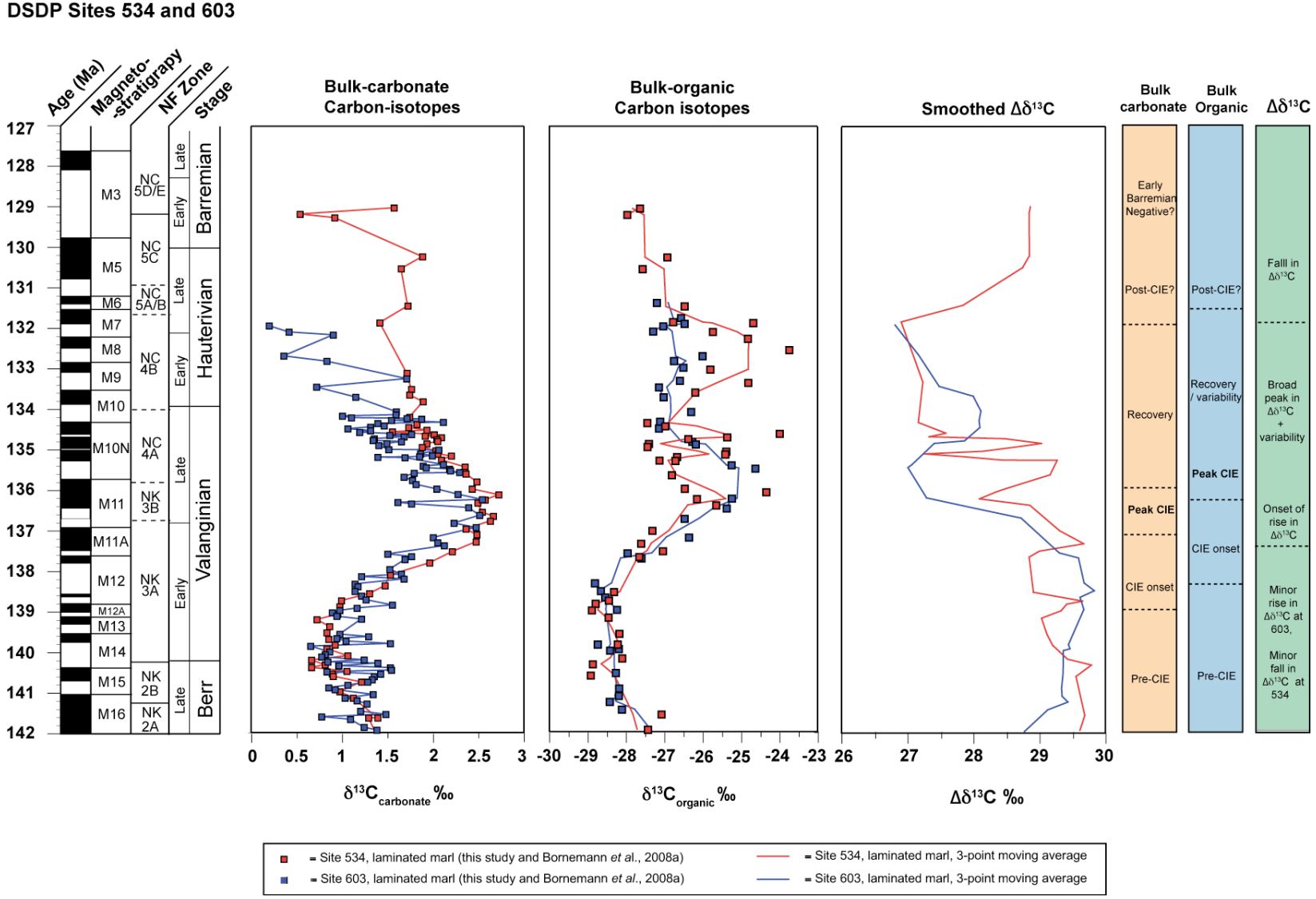

Figure 91. *Bulk-carbonate and bulk-organic matter records from DSDP Sites 534 and 603 and the calculated $\Delta^{13}C$ records from both sites.*

5. 5. DISCUSSION

5. 5. 1. THE VALANGINIAN CIE IN THE WESTERN PROTO-NORTH ATLANTIC

Bulk-carbonate records

The Valanginian CIE is present in the new bulk-carbonate records from both Sites 534 and 603, in good agreement with the existing $\delta^{13}C_{carb}$ records from these sites (Figure 87, 88, 91; Robertson & Bliefnick 1983; Bornemann *et al*., 2008a). The offset observed in $\delta^{13}C_{carb}$ and $\delta^{13}C_{org}$ between the chalk and the laminated marl lithologies (Figure 86), are consistent with earlier observations by Frank *et al*. (1999), and are attributed to alteration of the isotopic ratios during diagenesis. The chalks at both Sites 534 and 603 are heavily bioturbated, and are thought to have been lithified and cemented earlier in their diagenetic history than the laminated marls, as evidenced by the existence of spherical radiolarian moulds in the chalks compared to the more flattened radiolarians in the marls (e.g. Robertson & Bliefnick 1983). The deposition of secondary calcite overgrowths on the calcareous nannofossils in the chalks has also been documented in SEM images taken by Robertson & Bliefnick (1983), which compare with relatively little overgrowth seen in the laminated marls in this study (Figures 41, 42b, 49). This cementation would have introduced secondary-calcite precipitated from interstitial waters, with depleted carbon and oxygen isotopic values, thus altering the chalks to preferentially lighter values than the less well-cemented marls (Frank *et al*., 1999; Figure 92). This effect is thought to be much more pronounced in the oxygen-isotope system than in the carbon-isotope system, as the $\delta^{13}C$ of carbonates is generally more difficult to disturb through diagenesis (e.g. Frank *et al*., 1999). Therefore the alternation in $\delta^{18}O$ between the chalks and the marls cannot be used to reconstruct primary temporal shifts (Frank *et al*. 1999; c.f. Stoll & Schrag 1996).

The Valanginian CIE is visible in both lithologies at Site 603, suggesting that the primary $\delta^{13}C$ values have not been overprinted in the chalks to such a large extent as to completely destroy the long-term signal of global carbon-cycling (Figure 86). However, results from Site 603 confirm the need for lithologically-separated $\delta^{13}C$ records, to reduce the amount of "noise" in the resultant data when making

qualitative and quantitative comparisons between different types of data (e.g. $\delta^{13}C_{org}$ and $\delta^{13}C_{carb}$) and different sites. The results of this study suggest that only the laminated marls at Site 603, and by extension Site 534, should be used for comparison with the $\delta^{13}C_{org}$ data, and for the generation of $\Delta^{13}C$ records at each site.

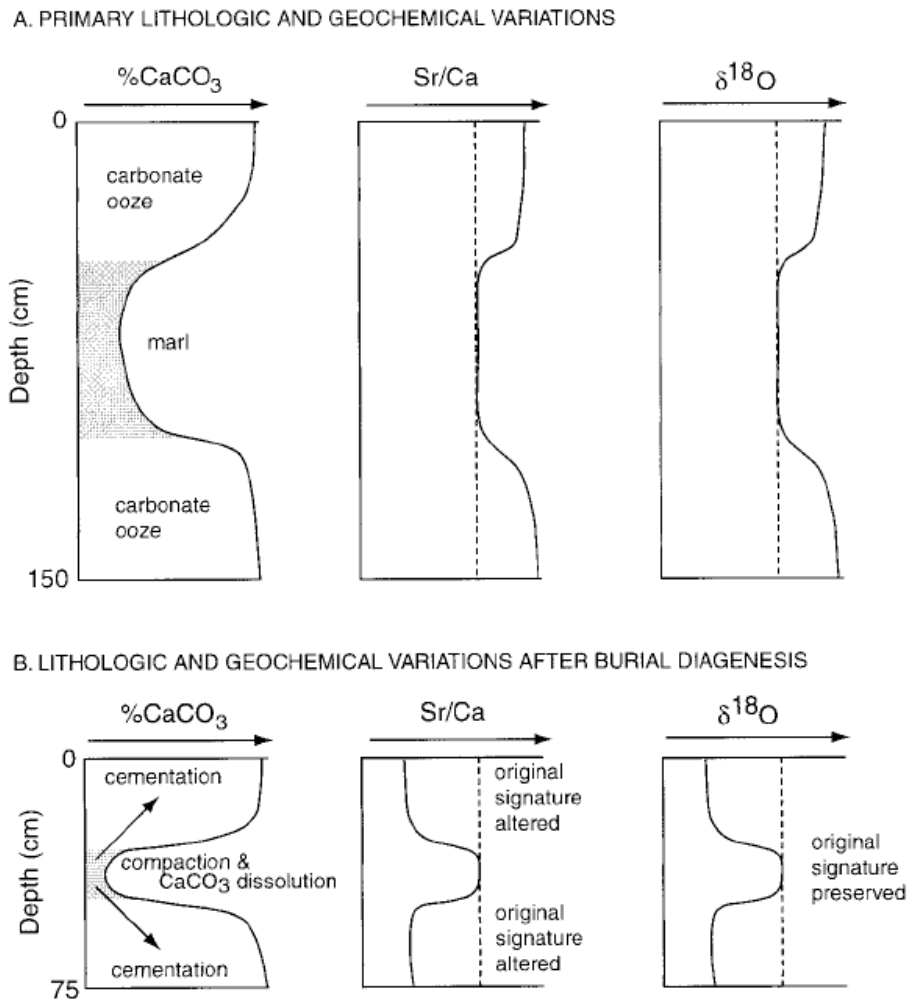

Figure 92. *Model taken from Frank et al. (1999) to illustrate the skewing of the primary $\delta^{18}O$ values (A) by diagenetic addition of secondary cement (B). A similar principle can apply to the diagenetic alteration of the $\delta^{13}C$ signal in sediments, although this effect will be less pronounced than for $\delta^{18}O$.*

The CIE in bulk-organic records

As with the $\delta^{13}C_{carb}$ records, the onset, peak and subsequent recovery period associated with the Valanginian CIE is present in the new bulk-organic carbon-isotope records from both Sites 534 and 603. This is the first time the perturbation has been documented in organic-matter from the western proto-North Atlantic, outside of the Gulf of Mexico (Cotillon & Rio, 1984; Patton *et al*., 1984; Figures 87, 88, 91). The sharp positive excursion in bulk-organic matter in the laminated marl record, has a maximum amplitude of ~4.5 ‰ at both sites, followed by a more gradual decay back to more negative values, ~3 ‰ in magnitude (Figures 87, 88, 91). At Sites 534 and 603 the CIE is observed in the $\delta^{13}C_{org}$ records in both the pelagic marls and the turbiditic mudstones, the latter of which have been shown to contain a significant terrigenous organic-matter component, including fragments of higher plants and pollen (e.g. Habib 1983; Robertson & Bliefnick, 1983; Dean & Arthur 1987; see Chapter 3). The higher proportion of terrigenous organic-matter in the homogeneous mudstones is further supported at Site 603 by the wood $\delta^{13}C$ values, which are only slightly heavier than the mudstones but significantly heavier than the laminated marls (Figure 88). The fact that the Valanginian CIE is present in the $\delta^{13}C_{org}$ records from transported mudstones, as well as in the pelagic marl $\delta^{13}C_{org}$ records at Site 534, suggests that the terrestrial organic-matter sourced from the shelf was also perturbed by the CIE. This can be used to suggest, as previously shown in wood records from the Crimea and Siberia, that the Valanginian CIE also affected the atmospheric carbon reservoir (Grocke *et al*., 2005; Nunn *et al*., 2010).

Bulk-organic vs. bulk-carbonate records

On the basis of the data presented here and in Chapter 3, the laminated marls represent the most pelagic sediments at Sites 534 and 603, with the least amount of diagenesis. Consequently, the $\delta^{13}C$ of these sediments is thought to best approximate to the $\delta^{13}C$ values of seawater and marine organic-matter and only data from these sediments will be considered in the forthcoming discussion.

Importantly, there is a broad similarity between the pelagic marl $\delta^{13}C_{org}$ records and $\delta^{13}C_{carb}$ records at both Sites 534 and 603, prior to the CIE and during

the onset, demonstrating coupling between the marine carbonate and organic-matter carbon reservoirs in the Early Valanginian (Figures 87, 88, 91, 93). This is perhaps to be expected, as both materials should primarily be sampling the surface ocean carbon-isotope reservoir. Indeed, good agreement between the records is seen in the Late Berriasian–mid Early Valanginian at both sites, where the bulk-carbonate and the bulk-organic records show a synchronous negative trend, falling from ~-27.5 to ~-28.5 ‰ in the $\delta^{13}C_{org}$ record and from ~1.4 to ~0.8 ‰ in the $\delta^{13}C_{carb}$ record (Figures 87, 88, 91, 93).

However, despite the overall good agreement between the bulk carbonate and bulk-organic records at Site 534 and 603, lag times between the $\delta^{13}C_{carb}$ and the $\delta^{13}C_{org}$ record do exist in the timing and duration of the subsequent positive CIE. As reviewed in Section 5-2-2, previous work has suggested the existence of a lag between the organic and carbonate carbon reservoirs during the Valanginian CIE onset and peak intervals (Figure 93; Cotillon & Rio 1984; Patton *et al*., 1984; Lini *et al*., 1992). It is however possible that such a lag is merely an artefact of the lower resolution $\delta^{13}C_{org}$ data in the NW Tethyan (Polaveno section) and western North Atlantic (DSDP Site 535) relative to the $\delta^{13}C_{carb}$ data (Cotillon & Rio 1984; Patton *et al*., 1984; Lini *et al*., 1992). This theory would seem to be born out by the apparent lack of a significant lag seen in new high-resolution data from the CIE onset phase at Site 535 (Figure 93; J. Rosling*, UCL unpublished MSc Dissertation, 2010*). Indeed, while a small lag in the onset of the positive CIE is observed at Site 534, at Site 603 the initial shift to more positive values is virtually synchronous between the $\delta^{13}C_{carb}$ and $\delta^{13}C_{org}$ records (Figure 93). This minor lag at Site 534 may be an artefact of poor resolution across this interval, or may suggest a slightly delayed response in the organic-matter reservoir with respect to the carbonate reservoir, which may be a consequence of changing marine organic-matter type, or pCO_2 fluctuations (see below).

There is a much more significant lag between the organic and inorganic carbon reservoirs in the timing and length of the peak Valanginian CIE. Although comparison of the duration of the CIE peak and recovery between the two sites is complicated by uncertainties in the age models, particularly in the assignment of absolute ages, the offsets between $\delta^{13}C_{carb}$ and $\delta^{13}C_{org}$ records at each site are comparable. At both Sites 534 and 603, the peak $\delta^{13}C_{carb}$ values are reached between

~136.8 –137 Ma, and last for ~800 kyrs before rapidly decaying back to more negative values (Figures 87, 88, 91, 93). The $\delta^{13}C_{org}$ records however, do not reach peak values until ~136–136.4 Ma at either site and range in duration from 1.2 Myr at Site 603, to ~3.8 Myr at Site 534 (Figure 87, 88, 91, 93). The relatively stable $\delta^{13}C_{org}$ (marl) record at Site 603 gives confidence in the extended duration of the peak CIE at this site, but the greater variability in the $\delta^{13}C_{org}$ (marl) record at Site 534 record makes quantification of "peak" *vs*. "recovery" intervals difficult (Figures 87, 88, 91, 93).

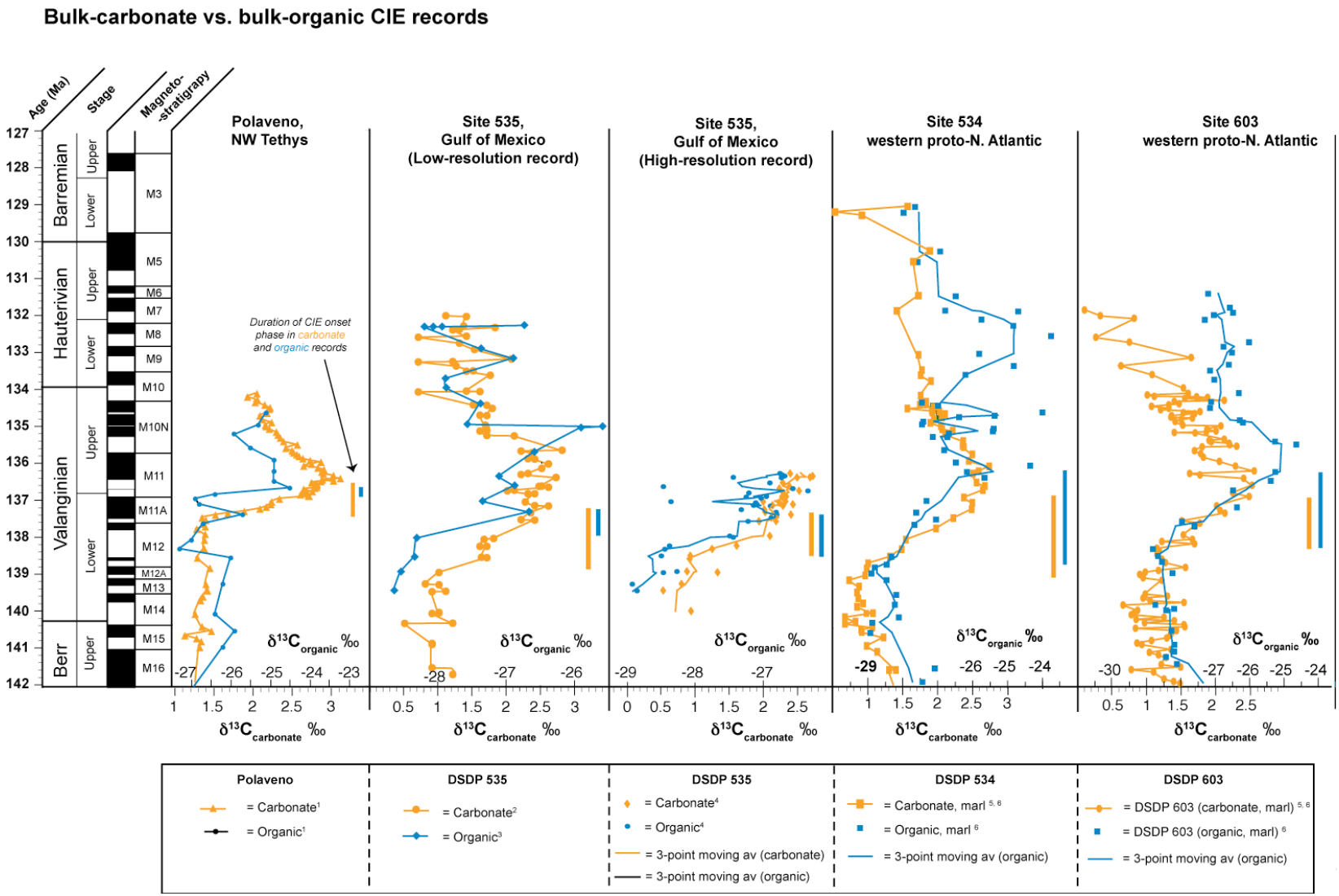

Figure 93. *Comparison of bulk-carbonate and bulk-organic matter records from Polaveno (1 = Lini et al., 1992), DSDP 535 (2 = Cotillon & Rio 1984, 3 = Patton et al., 1984; 4 = J. Rosling, unpublished thesis, UCL, 2010), Site 534 and 603 (5 = Bornemann et al., 2008a; 6 = this study).*

It may be that the CIE in the organic-matter record at Site 534 is complicated and extended in duration by increased terrestrial organic-matter contamination in the marls, shifting the bulk organic composition to heavier values (Figure 87, 88, 91, 93). Regardless of this, is clear from Site 603 that the duration of the CIE peak and recovery expressed in organic matter was longer than the equivalent CIE interval expressed in the bulk carbonate. How can this be explained?

$\Delta^{13}C$ records and pCO_2

$\delta^{13}C_{carb}$ records can largely be interpreted in terms of changes in surface-ocean carbon reservoir, driven by local productivity, circulation and changes in the isotopic composition of the whole global carbon reservoir. When multiple records from widespread geographic areas show the same temporal trends, the last of these is assumed to be dominant. In addition to the factors effecting $\delta^{13}C_{carb}$, $\delta^{13}C_{org}$ record can also be influenced by: (1) changing contributions of marine and terrestrial organic matter to the sediments; (2) changing fractionation of carbon-isotopes during photosynthesis by organisms related to changes in pCO_2 (e.g. Arthur *et al*., 1985; Dean *et al*., 1986; Freeman & Hayes, 1992). The presence of the Valanginian CIE in the organic-matter record at both Sites 534 and 603, virtually synchronous with the CIE in the bulk-carbonate record, strongly suggests that the $\delta^{13}C_{org}$ record is influenced by changes in surface ocean carbon reservoir (Figures 87, 88, 91). However, the lag between the $\delta^{13}C_{carb}$ and $\delta^{13}C_{org}$ records, particularly in the CIE recovery period in the Late Valanginian–Early Hauterivian, suggests that other factors must also be influencing the $\delta^{13}C_{org}$ values.

It is possible that some of the variations in $\delta^{13}C_{org}$, particularly at Site 534, are caused by fluctuating contributions of terrestrial and marine organic matter, which have distinct isotopic compositions, although the effects of this should largely have been negated by the lithological separation of the marine-dominated pelagic marls and the terrestrial-dominated homogeneous mudstones. However, this cannot be excluded as a possibility without detailed Rock Eval pyrolysis data from every sample in the study to determine the organic matter characteristics.

As discussed in Section 5-2-2, $\Delta^{13}C$ values, requiring paired $\delta^{13}C_{carb}$ and $\delta^{13}C_{org}$ data from the same samples, have previously been used to reconstruct relative changes in pCO_2 of the atmosphere (e.g. Freeman & Hayes, 1992; Kump & Arthur 1999; Jarvis *et al*., 2011). If the same approach is applied to the laminated marls at Site 534 and 603, interesting trends in pCO_2 across the Valanginian CIE can be inferred. At both sites, $\Delta^{13}C$ values in the Late Berriasian–earliest Valanginian are relatively constant, with perhaps a minor positive trend seen at Site 603 (Figure 89, 90, 91). However, from the late Early Valanginian to the Late Valanginian–Early Hauterivian, a generally negative trend in $\Delta^{13}C$ is observed at both sites, where pre-CIE values of ~29 to ~30 ‰ fall to post-CIE minimum values of ~27 ‰ (Figure 89, 90, 91). This suggests a decrease in $\Delta^{13}C$ across the excursion of ~ 2.5 ‰, which if interpreted purely in terms of changing pCO_2, suggests a drop in pCO_2 across the positive CIE. Additionally, the rise in $\Delta^{13}C$ from the mid-Hauterivian to the Early Barremian of ~2 ‰ observed at Site 534, could be interpreted in terms of a rise in pCO_2 (Figure 89, 90, 91).

Existing proxy and modelling data give a wide-range of absolute pCO_2 estimates (600 –2300 ppmv) across the Berriasian–Barremian interval, but the general trend is for decreasing pCO_2 levels from the Late Berriasian to Early Hauterivian, which stabilize in the Late Hauterivian and begin to increase again in the Barremian (see Chapter 4 for more details; Figure 94). This is broadly in agreement with the trends estimated from the $\Delta^{13}C$ data (Figure 94). Additionally, estimates of pCO_2 constructed using $\Delta^{13}C$ records from terrestrial land plants also suggest a drop in pCO_2 from the pre- to peak-CIE interval (Grocke *et al*., 2005), consistent with the observations from this study. Together, these data suggests that a Late Valanginian drawdown in pCO_2 is a real feature of Early Cretaceous carbon cycling (Figure 94).

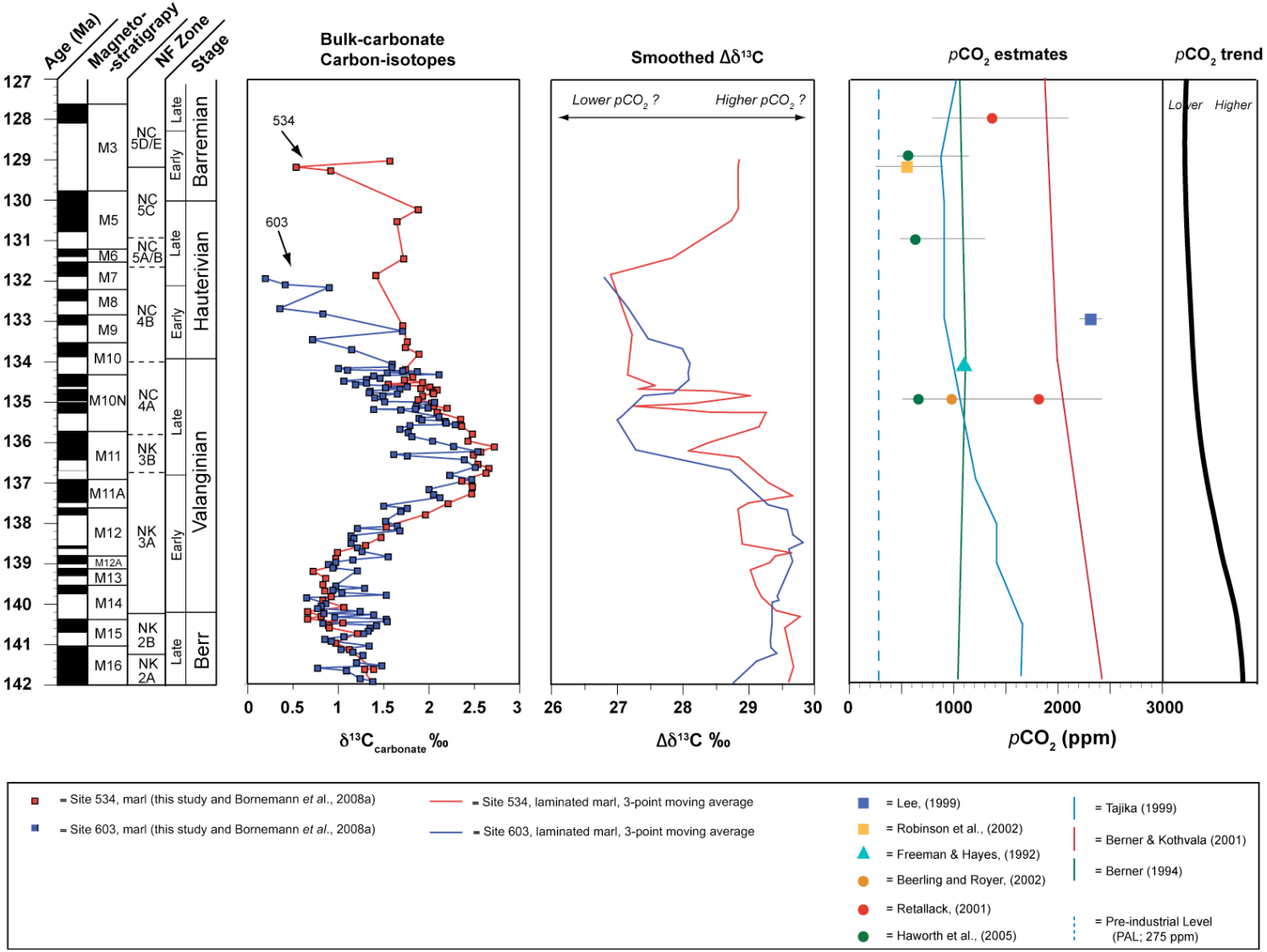

Figure 94. *Comparison of pCO_2 estimates from $\Delta^{13}C$ trends, with other published pCO_2 estimates from proxy and modelling-based studies. Thick black line represents best line of fit for the proxy/modeling data, by eye.*

5. 5. 2. ADEQUATE MECHANISMS TO EXPLAIN THE VALANGINIAN CIE?

The Valanginian CIE is often explained through a conceptual model similar to those used to explain other Mesozoic positive CIEs and OAEs (Figure 95; e.g. Weissert, 1989; Menegatti *et al*., 1998; Leckie *et al*., 2002; Jenkyns, 1999, 2003, 2010). Although a sequence of events involving continental weathering, nutrification and organic-matter burial are invoked as the cause of the CIE, the mechanism ultimately hinges on the hypothesised increase in global temperatures in the Early Valanginian, thought to be related to volcanism in the Paraná-Etendeka LIP (e.g. Lini *et al*., 1992; Weissert *et al*., 1998; Erba *et al*., 2004, Figure 95). This greenhouse climate mechanism for the origin of the perturbation, potentially explains the Valanginian CIE and many of the associated phenomena, including increased siliciclastics in the NW Tethys, the occurrence of organic-rich sediments in certain locations and evidence for elevated nutrients in the surface oceans (Figure 95). However, this theory needs to satisfy two major requirements in order to for the mechanism to operate: (1) that the volcanism in the Paraná-Etendeka LIP occurred prior to the onset of the CIE (i.e. < ~138 Ma); (2) that the supposed increase in volcanogenic CO_2 actually triggered increased global temperatures, which could in turn trigger increased continental weathering and nutrification.

Evidence for volcanism and volcanogenic CO_2 release

During the earliest Cretaceous there were two active large igneous provinces (LIPs); the relatively small Etendeka LIP, centred in modern-day Namibia, and the larger Paraná LIP, in modern day eastern South America, with a combined preserved extent of ~1.5 x10^6 – 2.3 x10^6 km^3 (Stewart *et al*., 1996; Peate, 1997; Gladczenko *et al*., 1997; Jerram & Widdowson 2005). Dating of the Paraná-Etendeka LIP has proved problematic and has generally been quite poorly constrained (e.g. Stewart *et al*., 1996; de Assis Janasi *et al*., 2010; Thiede & Vasconcelos *et al*., 2010). Although until recently the duration of the eruptive activity was thought to span from ~138 Ma – 127 Ma (mid Early Valanginian–mid Barremian) (e.g. Stewart *et al*., 1996; Figure 96), more recent U-Pb and improved ^{30}Ar-^{49}Ar ages suggest that the main phase of the activity occurred in a very short window of time (~1.2 Ma) at ~ 134.6 ± 0.6 Ma

(de Assis Janasi *et al*., 2010; Thiede & Vasconcelos *et al*., 2010; Figure 96). This short pulse of activity would have generated large eruption rates of ~2 km^3 $yr^{-1,}$ which would have led to high CO_2 effusion rates of ~0.3 Gt CO_2 yr^{-1}. Such a rate may be capable of producing significant changes in pCO_2 and perhaps climate, However, using the current absolute age scale after Gradstein *et al*. (2004) and McArthur *et al*. (2007a) the peak eruption of the Paraná-Etendeka LIP is dated as latest Valanginian, far too late to be the trigger for the positive CIE in the Early Valanginian (at ~138 ma) (Figure 96). Although this casts doubt on the Paraná-Etendeka LIP as the CIE trigger, it should be noted that the Early Cretaceous timescale is not well-constrained due to the paucity of radiometrically dated tie-points and, as such, the absolute age of the Valanginian CIE is still extremely uncertain.

A further difficulty for the volcanic model is that the $\Delta^{13}C$ and $\delta^{13}C$ records from Sites 534 and 603 do not support a large and sudden injection of volcanogenic CO_2 during the Early Valanginian, although the trend to slightly more negative values in both the carbonate and bulk organic matter record points towards a steady increase in isotopically light carbon from an unknown source, or increased sequestration of ^{13}C (Figures 87, 88, 91). As noted above, the general negative trend in $\Delta^{13}C$ suggests decreasing pCO_2 during the Valanginian–Hauterivian, inconsistent with a large input of volcanogenic CO_2 (Figure 94). It is interesting to note however, that the pulse in volcanic activity in the Parana-Etendeka LIP in the revised age models at ~134.6 Ma, is broadly coincident with a peak in the $\Delta^{13}C$ values, and therefore $pCO_{2,}$ during the CIE recovery period at Site 603 (Figure 90).

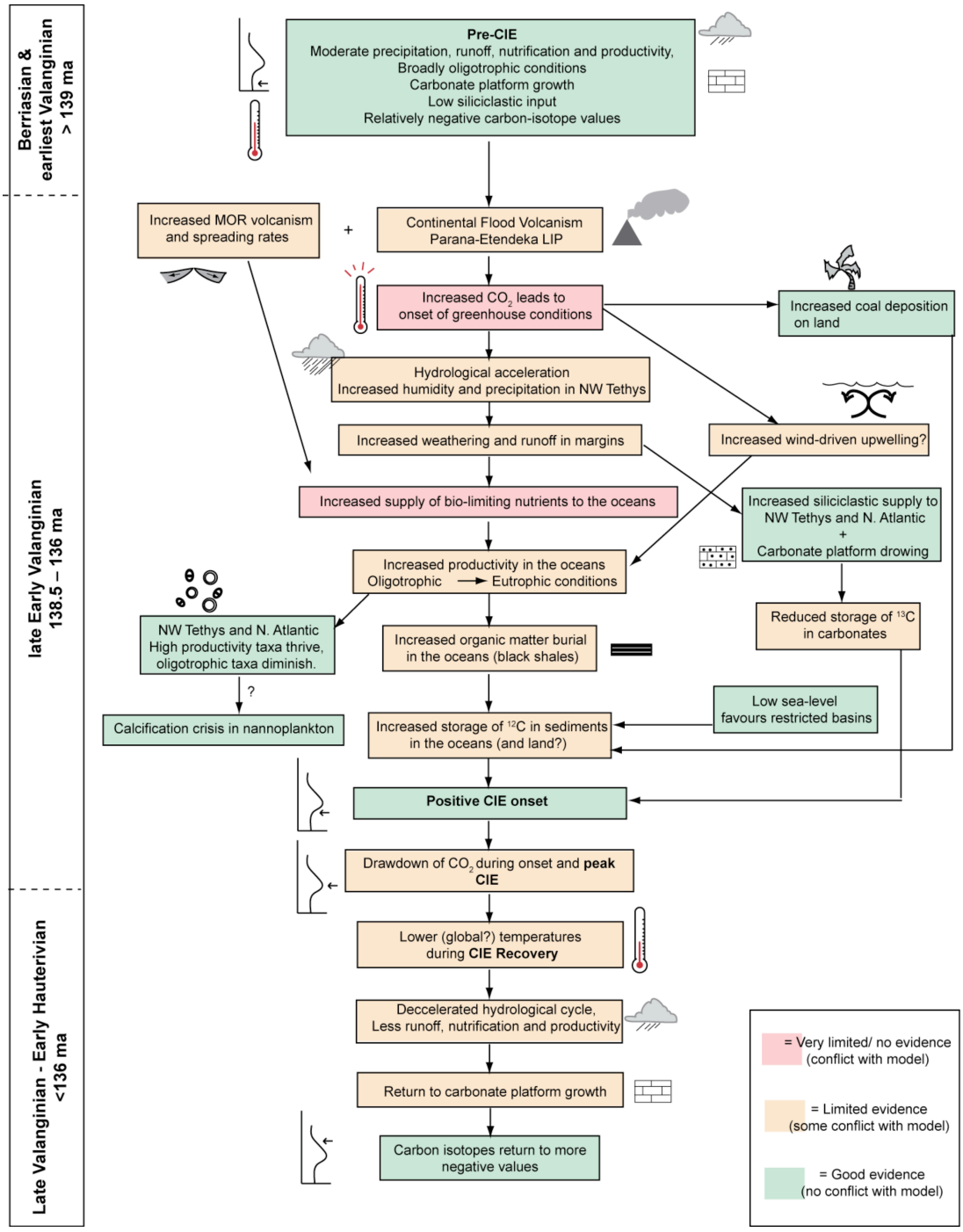

Figure 95. *Diagram to show the conceptual model put forward to explain the Valanginian CIE. Based on the original model after Lini et al. (1992) and Weissert et al. (1998), with modifications after Westermann et al. (2010).*

Evidence for the onset of greenhouse conditions?

If LIP volcanism cannot be regarded as the CIE trigger, is there at least evidence for the increased global temperatures hypothesised to have existed in the Early Valanginian, thought to be responsible for increased continental weathering (Figure 95)? As discussed in Chapter 4, there is much conflicting palaeotemperature evidence for the Early Cretaceous, spanning sedimentological, palaeontological and geochemical proxies (e.g. Kemper 1987; Price, 1999; Mutterlose & Kessels, 2000; Price *et al*., 2000; Erba *et al*., 2004; McArthur *et al*., 2007, Brassell *et al*., 2009; Price & Nunn, 2010; Duchamp-Alphonse *et al*., 2011; Littler *et al*., 2011). Although many palaeoclimatic studies have been conducted on sediments of earliest Cretaceous age, there is virtually no evidence for a discrete warming pulse in the Early Valanginian that could have triggered the Valanginian CIE (e.g. Erba *et al*., 2004; McArthur *et al*., 2007a; Chapter 4). Although increased global coal *vs.* evaporite deposition and a shift away from more aridity-tolerant taxa demonstrate a generally warm and humid earliest Cretaceous, relative to the widespread aridity of the Late Jurassic (e.g. Vajhrameev 1981; Hallam 1984, Westermann *et al*., 2010;), the evidence for a pulse of particularly warm and humid climates in the Early Valanginian remains elusive.

Clay mineral evidence from the Vocontian Basin has recently been put forward in support of the greenhouse theory, but by the authors own admission, much of the Early Valanginian signal is likely controlled by sea-level in this basin and therefore cannot yield information about pre-CIE palaeotemperatures (Duchamp-Alphonse *et al*., 2011). Siliciclastic deposition has been shown to have increased from the Valanginian onwards in the NW Tethys, but the main pulse of increased siliciclastics in the western proto-North Atlantic (Sites 534 and 603) occurs in the Hauterivian and therefore cannot be used as evidence for increased continental weathering prior to the CIE (Follmi *et al*., 1994; Weissert *et al*., 1998; Chapter 4). Palaeontological and geochemical evidence certainly suggests changes in surface-ocean fertility in the NW Tethys and proto-North Atlantic during the Early Valanginian, which have been associated with changes in palaeotemperature, continental weathering and nutrient input (e.g. Mutterlose & Kessels 2000; Bersezio *et al*., 2002; Erba & Tremolada, 2004; van de Schootbrugge *et al*., 2003; Duchamp-Alphonse *et al*., 2011; Figure 96). Indeed the calcareous nannofossil records from

Sites 534 and 603, presented in Chapter 3, show an increase in the abundance of *D. lehmanii* in the Early–Late Valanginian, which has been suggested to represent increased fertility in the NW Tethys and Pacific in previous studies (Bersezio *et al*., 2002; Erba & Tremolada 2004, Erba et al., 2004). However, many of these changes could equally be the result of changing sea-level and evolving circulation and upwelling patterns in these regions and may not reflect changes in palaeotemperature (See Chapter 4). The new Berriasian–Barremian TEX_{86}-derived SST records presented in Chapter 4 suggest warm and equable climates overall but no strong evidence for elevated tropical temperatures in the Early Valanginian with respect to the supposedly cooler Hauterivian (Chapter 4, Littler *et al*., 2011). A very small warming pulse of ~0.5 ºC is noted in the Early Valanginian, NK3b Subzone, at Site 534, but this seems unlikely to be large enough to indicate major climate change prior to the positive CIE (Chapter 4, Figure 79).

In conclusion, while the evidence for a warm and equable Berriasian–Valanginian is strong, there is little evidence to support a discrete warming pulse in the early Valanginian prior to the CIE, and thus it seems unlikely that this event marks "the onset of greenhouse conditions in the Cretaceous" (Lini *et al*., 1992), as such conditions were already established (see Chapter 4).

Alternatives to the greenhouse onset model?

Other mechanisms have been put forward to explain CIEs and OAEs which are largely independent of temperature changes, such as the model for increased nutrient supply and productivity due to the input of volcanogenic sulphate, which has been suggested for OAE-2 (Adams *et al*., 2010). However, this model would still require a volcanic trigger prior to the positive CIE, which as discussed above, may not exist during the Early Valanginian. Direct nutrification of oceans by submarine eruption and hydrothermal alternation of basalt has also been proposed as a mechanism by which OAEs can be initiated in the Early Cretaceous (Larson & Erba 1999; Leckie *et al*., 2002), although the evidence for such activity in the Valanginian is limited. It has recently been proposed that the Valanginian CIE is not an OAE-like event, and instead represents a period of extensive coal formation on the continents and some organic-matter burial on the continental margins (Westermann *et al*.,

2010). In this model, there is less need for a discrete pulse of vocanogenically-induced warming in the Early Valanginian. Burial of organic carbon in continental and marginal marine basins could have been enhanced by the generally warm and equable conditions on land and increasing isolation of marginal basins due to a sharp fall in sea-level. Carbon-isotope values could also have been driven to more positive values by a decrease in the abundance of carbonate platforms that lock away ^{13}C (Follmi *et al*., 1994; Weissert *et al*., 1998; Westermann *et al*., 2010; Figure 96).

There is no evidence for a single widespread marine black shale event during in the Valanginian, in contrast to the major OAEs of the mid-Cretaceous. Geographically-restricted and, in many cases, thin organic-rich levels occur in the NW Tethys and proto-North Atlantic (e.g. Summerhayes 1987; Reboulet *et al*., 2003; Bersezio *et al*., 2002), Central Pacific (Bralower *et al*., 2002), and Arctic (Dypvik, 1985; Hvoslef *et al*. 1986) (Figure 96). In constrast, the evidence for widespread coal deposition is compelling, as is the evidence for anoxic conditions and enhanced organic-matter burial in restricted basins such as the Weddell Sea (Figure 96; Barker *et al*., 1988; O'Connell, 1990).

The sea-level low in the early Valanginian *Tirnovella pertransiens* Zone (~139 Ma) represents one of the largest 2nd -order sea-level falls in the Mesozoic (Hardenbol *et al*., 1998). Setting aside the nature of the mechanism that may have led to the sea-level fall itself, the relative decrease in sea-level is clearly observed in the Tethyan region and beyond, and would certainly have contributed to the isolation and restriction of basins in the Boreal and southern Tethyan realms. These isolated basins would have been more likely to accumulate and sequester organic matter, as is seen in the Valanginian-Hauterivian sediments at Sites 692 (Chapters 2 and 4; Barker *et al*., 1988; O'Connell, 1990; Westermann *et al*., 2010).

In this model, the burial of excess organic matter in both continental and the marginal marine basins would have led to the drawdown of CO_2 in the mid-Valanginian during the peak CIE, which may explain the decrease seen in the $\Delta^{13}C$ records from Sites 534 and 603 (Figures 89, 90, 91) and the downward trends recorded by other CO_2 proxies and models (Figure 94). This hypothesised drawdown of CO_2 has been widely suggested to have caused a global cooling event in the Late Valanginian–Early Hauterivian, as suggested by sedimentological (e.g. glendonites) palaeontological (e.g. calcareous nannofossils) and geochemical (e.g. oxygen-isotopes and Mg/Ca) records (e.g. Kemper 1987; Mutterlose & Kessels, 2000; Price

et al., 2000; Price & Mutterlose, 2004; McArthur *et al*., 2007a; Price & Nunn, 2010; Duchamp-Alphonse *et al*., 2011). However, as detailed in Chapter 4, many of these proxies which purport to yield information about palaeotemperature are likely to also be affected by other variables, such as sea-level or changing ocean chemistry, and therefore cannot necessarily be regarded as reliable SST proxies. Futhermore the detailed new TEX_{86}-derived SST records from the palaeo-North Atlantic and the available information from the Southern Hemisphere, show no evidence for cooling at this time (Chapter 4; Littler *et al*., 2011). Additionally, even if a degree of temperature control does exist in the oxygen-isotope or palaeontological records, the majority of these studies are focused in the NW Tethyan or northern Boreal regions and therefore may represent more of a regional than a global record of palaeotemperature (e.g. Figure 63).

Even though a period of cooling during the Late Valanginian would fit the observations of decreasing pCO_2 seen in this study and others, and is parsimonious with the modified mechanism put forward to explain the CIE (Westermann *et al*., 2010), it cannot be verified on the basis of the existing palaeotemperature records, and according to the latest low-latitude TEX_{86}-derived SST estimates, did not occur (Littler *et al*., 2011; Chapter 4). However, the tropical latitudes might be expected to be more resistant to climate change than the higher latitudes, which at present do not have sufficient TEX_{86} data in the Valanginian to definitively rule out a transient cooling event. This pattern of relatively stable tropical temperatures and more variable higher latitudes, suggested by the TEX_{86}-derived SST estimates, is reminiscent of the Eocene, where tropical SSTS remained relatively invariant (Pearson *et al*., 2007), while higher latitude SSTs showed a gradual decline (Bijl *et al*., 2009) in response to falling pCO_2 (e.g. Doria *et al*., 2011).

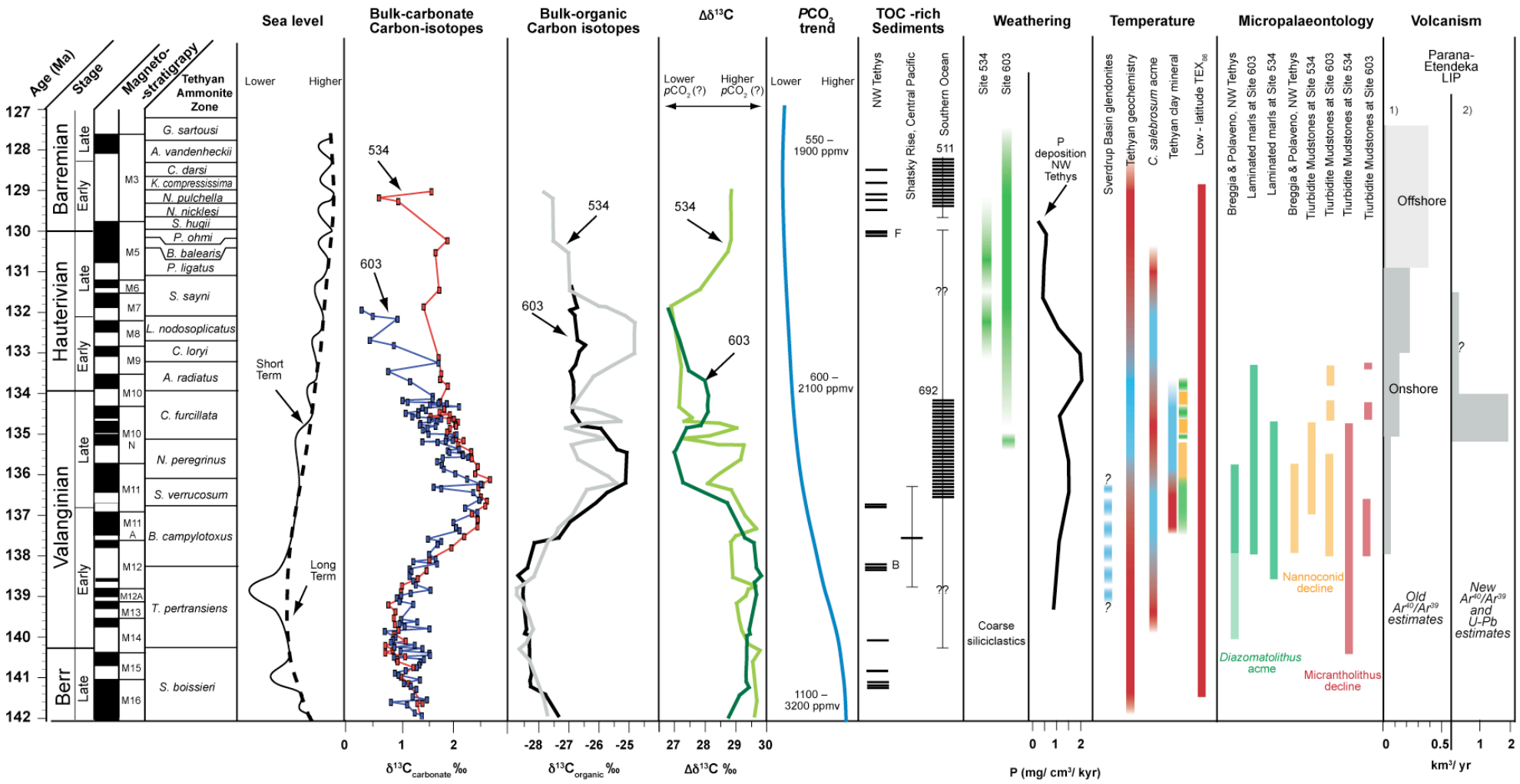

Figure 96. *Comparison of new carbon-isotope and $\Delta^{13}C$ data from Sites 534 and 603 with published pCO_2 data (see Chapter 4), the location of black shales (Reboulet et al., 2003; Bersezio et al., 2002; Barker et al., 1988); the increase in coarse siliciclstics seen at Site 534 and 603; phosphorous accumulation rates in the NW Tethys (van de Schootbrugge et al., 2003); palaeotemperature trends (see Chapter 4); calcareous nannofossil trends (this study and Bersezio et al., 2002); Parana-Etendeka eruption rates (1= Stewart et al., 1996; 2 = Thiede & Vasconcelos et al., 2010).*

5. 6. CONCLUSIONS

The Valanginian CIE is clearly visible in the new organic matter records at both Sites 534 and 603, which complements the existing bulk-carbonate records from these cores and this region. The presence of the excursion in both marine-dominated laminated marls and terrestrially-dominated homogeneous marls suggests that the CIE affected the terrestrial organic matter reservoir via the atmosphere, as well as the surface ocean carbon reservoir. A minor lag in the onset of the CIE between the bulk carbonate and bulk organic-matter records is identified at Site 534, but not at 603, but the $\delta^{13}C_{org}$ and $\delta^{13}C_{org}$ records are synchronous overall in the Late Berriasian–Early Valanginian. A larger lag exists in the expression of the peak and recovery phases of the CIE between the two reservoirs and may represent changes in either organic-matter provenance or atmospheric pCO_2. The $\Delta^{13}C$ records can be used to construct relative pCO_2 trends from Sites 534 and 603, with both records suggesting a substantial decrease in pCO_2 from the Berriasian–Early Valanginian to the Early Hauterivian.

The age estimates for the Parana-Etendeka LIP activity precludes volcanogenic CO_2 from this province from being the trigger for the Valanginian CIE, as the main phase is now thought to be in the Hauterivian (~134 Ma). However this conclusion is predicated on the assumption that the current age models tying magneto- and biostratigraphy to absolute time are robust. The declining pCO_2 estimates, determined from $\Delta^{13}C$ records from Sites 534 and 603 also do not support volcanic CO_2 as the CIE trigger mechanism. The general lack of evidence for a discrete warming pulse in the Early Valanginian, combined with the scant evidence for black shales in the open oceans, suggests the Valanginian CIE was not a true OAE. Alternative mechanisms involving excess burial of organic matter on the continents and in the restricted oceans margin basins during the sea-level low stand, coupled with decreasing storage of ^{13}C in platform carbonates, are more consistent with the current data. This mechanism is not incompatible with the evidence for increased nutrification and productivity in the NW Tethys, and would also explain the apparent drawdown of CO_2 and associated cooling in the Late Valanginian–Early Hauterivian observed in this study and others.

CHAPTER 6. CONCLUSIONS AND FUTURE WORK

As global climate and carbon-cycling were likely to have been intimately linked during the earliest Cretaceous, an integrated multi-proxy approach utilising palaeotemperature proxies and carbon-isotope analysis would be expected to yield the most comprehensive overview of this period. The work in this thesis combines organic-geochemistry, stable-isotope geochemistry and micropalaeontology in an attempt to understand the evolving climate and carbon-cycle during the Late Berriasian–Early Barremian, from a more global, rather than a purely regional, perspective.

The TEX_{86} calibration study from the proto-North Atlantic sites demonstrates that this organic palaeothemometer technique can be applied to sediments of earliest Cretaceous age with great success, adding another tool for palaeoclimatic reconstruction of this time period. However, the results of the lithology-separation study do highlight that for robust palaeoclimatic reconstructions, the provenance and organic-matter composition of the host sediment must be taken into consideration when using TEX_{86}. The fact that it is currently impossible to constrain whether primary or secondary factors are responsible for the observed small offset in SST between the pelagic and transported sediments, highlights the need for further calibration studies in both the modern ocean and other ancient sediments. However, the relatively small offset in the SST estimates between the different lithologies, gives confidence that even when the source-organism ecology or degree of oxic degradation cannot be independently determined in ancient sediments, the overall temporal trends in SST should not be unduly obscured.

The TEX_{86} SST estimates from the proto-North Atlantic and elsewhere demonstrate the warm and stable nature of Late Berriasian–Early Barremian temperatures in the low-latitudes, which stands in contrast to many previous studies suggesting a relatively cool and variable earliest Cretaceous. It may be that these earlier palaeotemperature proxy studies, which are overwhelmingly concentrated in the Northern Hemisphere and largely in the well-exposed NW Tethyan region, are recording genuine regional or seasonal temperature fluctuations. However, the interpretation of some of these records as global palaeotemperature signals, is open

to debate, and other factors such as changing sea-level may exert a stronger influence than is currently recognised. In this study, the sampling and analysis of multiple sites spanning ~40ºN to ~60ºS, allows tentative global SST gradients to be generated, which suggest that far from being a variable "coolhouse" world within the Mesozoic, earliest Cretaceous global temperatures were on a par with the greenhouse worlds of the mid-Cretaceous and Early Eocene. There may of course be a component of longitudinal variation in the SST gradients, as exemplified by the range of temperatures seen in the higher latitude sites, but this alone cannot explain the flattened meridional gradient observed between the proto-North Atlantic and the three individual mid-latitude sites. There may also be a component of lithological modulation on the SST estimates, particularly in the hemipelagic higher latitude sites, but as demonstrated by the TEX_{86} calibration study in Chapter 3 of this thesis, such effects are likely to be minor (<1 ºC).

The generally invariant temperatures seen in the low-latitude earliest Cretaceous TEX_{86} SST records, compared to the more variable mid-latitude SSTs, are reminiscent of similar temperature records from the Eocene. Such records suggest long-term stability in the Eocene tropics, while SSTs at latitudes of ~65 ºS show considerable variability and a long-term decrease in temperature, likely related to decreasing pCO_2. It is conceivable therefore, that in greenhouse worlds in general, the low-latitudes are less sensitive to fluctuations in pCO_2 and subsequent climatic perturbations than the higher latitudes, and that a greater magnitude of forcing is required to influence SSTs in these regions.

The new early Cretaceous SST records can be used to comment on climatic conditions before, during and after the Valanginian CIE, and to place constraints on the mechanisms behind the onset of the carbon-cycle perturbation. The global nature of the CIE is undeniable, having previously being identified in sections from the NW Tethys, proto-North Atlantic, Boreal region and western South America. Indeed the new bulk-organic carbon-isotope records from the western proto-North Atlantic reinforce the concept of a global event, which perturbed the bulk-organic as well as the bulk-carbonate carbon reservoir. The evidence for the global distribution of marine black shales is somewhat limited, questioning the "OAE" interpretation of the CIE, but there is no doubt that enhanced organic-matter deposition did occur in several marginal basins during the earliest Cretaceous. The increased deposition of coal on the continents is also well supported by sedimentary evidence, suggesting a

further sink for light carbon in the terrestrial realm. However, the trigger mechanism for the initiation of increased organic-matter deposition remains elusive.

From the TEX_{86} SST evidence, the lack of an identifiable pulse of increased temperatures in the Early Valanginian prior to the CIE, suggests that the sudden onset of greenhouse conditions linked to massive volcanism was not responsible for the onset of the perturbation. The well-documented increase in ocean fertility in the NW Tethys and the proto North Atlantic in the Valanginian, derived from trace-metal geochemistry, clay mineralogy and calcareous nannofossil studies, do suggest increased precipitation in the NW Tethyan realm, which have been linked to increased temperatures. However, such changes in the location and intensity of precipitation belts can also be influenced by changes in ocean circulation and palaeogeography, which are known to have been continually evolving throughout the Early Cretaceous.

Combined with the lack of SST evidence for warming, the apparent lack of synchroneity between volcanic activity in the Parana-Etendeka and the onset and peak of the CIE casts doubt on the greenhouse climate mechanism as the trigger. Assuming current age models are correct, the peak LIP activity appears to have occurred in the Hauterivian, long after the initiation of the CIE in the Valanginian. Relative pCO_2 trends generated from the paired bulk-organic and bulk-carbonate records from the proto-North Atlantic in this study, show no evidence for the peak in pCO_2 in the Early Cretaceous needed for the initiation of greenhouse warming. Instead such trends suggest a declining trend in pCO_2 from the Late Berriasian to the Hauterivian, which is concordant with previous estimates from other pCO_2 proxies such as stomatal indices and calcrete carbon-isotope studies, and the results of modelling exercises. Such a drawdown in pCO_2 is likely to be attributable to the burial of excess organic-matter during the onset phase of the CIE, in both marginal marine and continental strata. The promotion of anoxic basins as sites of organic -matter deposition is likely to have been facilitated by the pronounced sea-level low-stand documented in the earliest Valanginian.

Although a reduction in pCO_2 may be expected to cause climatic cooling in the Late Valanginian–early Hauterivian, no convincing evidence for a low-latitude reduction in temperature is seen in the TEX_{86}-derived SST records generated so far. Other proxy evidence put forward to suggest cooling at this time is equivocal, and may equally be explained by changes in sea-level or ocean chemistry. It is possible

that an element of regional cooling occurred in the NW Tethyan region at this time, and that the lower-latitude western proto-North Atlantic was more resistant to such transient changes in temperature. Such an interpretation would not be at odds with the evidence put forward for a generally warm and equable earliest Cretaceous, nor would it contradict the revised model put forward to explain the origins of the Valanginian CIE though increased deposition of organic matter in marginal ocean basin and continental strata.

Future work

Despite the substantial progress made in both the application of the TEX_{86} proxy in the Early Cretaceous, and in the understanding of Berriasian–Barremian climate and carbon-cycling, there are still questions which remain unanswered and future work to conduct.

The TEX_{86} proxy

The TEX_{86} palaeotemperature proxy is still a relatively recent innovation in palaeoclimate quantification, and while the basic tenets of the proxy have already been established by modern calibration and empirical studies in the field and laboratory, more work is certainly needed to refine the subtleties of the technique. In particular, much is still unknown about the life habits and ecological role of modern Archaea in both the pelagic and sedimentary environment. Until more information is available regarding archael community structures in the shelf and deep sea, and the effect of *in situ* deep water and sedimentary GDGT production on TEX_{86} values, temporal and spatial variations observed in the TEX_{86} records of ancient sediments will retain a degree of uncertainty. With regards to the use of TEX_{86} in the Cretaceous and other greenhouse worlds, further mesocosm studies, which examine the effect of elevated temperatures on the TEX_{86} proxy, must be undertaken, to constrain which of the SST calibration models is best suited to palaeotemperature reconstruction at >27 ºC. Further studies examining modern and recent turbidites, and comparison of these results to other ancient transported sediments, may illuminate the long-term effect of oxic degradation on GDGT abundance and distribution in the oceans.

Palaeoclimate reconstruction in the Early Cretaceous

While the new TEX_{86} records from the tropics and upper mid-latitudes provide much needed long-term, and geographically widespread palaeoclimate data for the Late Berriasian–Early Barremian, there is still far more to be done in terms of constraining palaeotemperatures in the Neocomian. More marine sediments, from a greater array of palaeolatitudes, must be analysed for TEX_{86}, to determine if the SST gradients calculated in this thesis are robust. In particular, more data are needed from the Pacific to determine if the elevated (and possibly relatively insensitive) temperatures seen in the proto-North Atlantic can partly be attributed to the more enclosed nature of this ocean basin during the earliest Cretaceous. TEX_{86}-derived SST records from Site 535 in the Gulf of Mexico, which is similar in lithology and latitude to Sites 534 and 603 analysed in this thesis, may add further weight to the argument for globally elevated temperatures at this time. Further studies incorporating multiple palaeotemperature proxies from the same sections, such as the Barremian oxygen-isotope and TEX_{86}, study from the German Basin, are needed to calibrate the SST signals more precisely in the Mesozoic.

Carbon-cycle perturbations in the earliest Cretaceous

Further work is needed to constrain the apparent lag between bulk-carbonate carbon isotopes and concurrent records from bulk organic-matter records, during the CIE recovery period. This is important, as the fall in the pCO_2 recorded by the $\Delta^{13}C$ records at Site 534 and 603 is predicated on the assumption that the terrestrial vs. marine organic matter composition did not change appreciably throughout the section, within the laminated marl lithology. Compound-specific carbon-isotope work, which isolates individual fossil biomarkers that can be tied to specific types of organisms, would allow more certain interpretations about pCO_2 to be made. In general, more paired bulk-organic and bulk-carbonate carbon-isotope studies from other sections in the NW Tethys and beyond are needed, to determine if the changes in pCO_2 are globally reproducible, and to further constrain the mechanisms behind the Valanginian CIE.

REFERENCES

Adams, D. D., Hurtgen, M.T. & Sageman, B.B. Volcanic triggering of a biogeochemical cascade during Oceanic Anoxic Event 2. *Nature Geoscience* **3**, 201–204 (2010)

Ager, D. V. The Jurassic world ocean (with special reference to the North Atlantic). *In Jurassic Northern North Sea Symposium, Norwegian Petroleum Society, Stavanger*, pp. 1–43 (1975)

Alley, N. F. & Frakes, L. A. First known Cretaceous glaciation: Livingston Tillite Member of the Cadna–owie Formation, South Australia. *Australian Journal of Earth Sciences* **50,** 139–144 (2003)

Anderson, T. F. & Arthur, M. A. Stable isotopes of oxygen and carbon and their application to sedimentologic and environmental problems, in Arthur, M. A., *et al*., eds., *Stable isotopes in Sedimentary Geology: Society of Economic Paleontologists and Minerologists Short Course Notes*, **10,** 11–151 (1983)

Anderson, T. F., Popp, B. N., Williams, A. C., Ho, L.-Z., & Hudson, J. D. The stable isotopic records of fossils from the Peterborough Member, Oxford Clay Formation (Jurassic), UK: palaeoenvironmental implications. *Journal of the Geological Society of London* **151**, 125–138 (1994)

Applegate, J. L., Bergen, J. A., Covington, J. M. & Wise, S. W. J. Lower Cretaceous calcareous nannofossils from continental margin drill sites off North Carolina (DSDP LEG 93) and Portugal (ODP LEG 103) A comparison, in Crux, J., and Heck, S.E.V., eds., *Nannofossils and Their Applications*. Ellis Horwood, Chichester, 212–222 (1989)

Arthur, M. A., Dean, W. E. & Claypool, G. E. Anomalous ^{13}C enrichment in modern marine organic carbon. *Nature* **315**, 216–218 (1985)

Barker, P. R, Kennett, J. P., *et al*. Sites 691 and 692. *Proceedings of the Ocean Drilling Program, Initial Reports* **113,** 293–328 (1988)

Barron, E. J., Harrison, C. G. A., Sloan, J. L., Hay, W. W. Paleogeography, 180 million years ago to the present. *Eclogae Geologicae Helvetiae* **74,** 443–470 (1981)

Barron, E. J., Arthur, M. A. & Kauffman, E. G. Cretaceous rhythmic bedding sequences: a plausible link between orbital variations and climate *Earth and Planetary Science Letters* **72**, 327–340 (1985)

Baumgartner, P. O., Bown, P. R, Marcoux, J., Mutterlose, J., Kaminski, M. A., Haig, D. W., McMinn, A. Early Cretaceous Biogeographic and oceanographic synthesis of Leg 123 (off northwestern Australia). *Proceedings of the Ocean Drilling Program, Scientific Results* **123**, 739–758 (1992)

Beerling D. J. & Royer D. L. Fossil plants as indicators of the Phanerozoic global carbon cycle. *Annual Review of Earth and Planetary Sciences* **30**, 527–556 (2002)

Bergen, J.A. Berriasian to early Aptian calcareous nannofossils from the Vocontian trough (SE France) and Deep Sea Drilling site 534: New nannofossil taxa and a summary of low–latitude biostratigraphic events. *Journal of Nannoplankton Research* **16**, 59–69 (1994)

Bennett, M. R., Doyle, P. & Mather, A. E. Dropstones: their origin and significance. *Palaeogeography, Palaeoclimatology, Palaeoecology* **121**, 331–339 (1996)

Bersezio, R., Erba, E., Gorza, M. & Riva, A. Berriasian–Aptian black shales of the Maiolica formation (Lombardian Basin, Southern Alps, Northern Italy): local to global events. *Palaeogeography, Palaeoclimatology, Palaeoecology* **180**, 253–275 (2002)

Berner, R. A. A New Look at the Long–term Carbon Cycle. *GSA Today* **9**, 1–6 (1999)

Berner, R. A. The long–term carbon cycle, fossil fuels and atmospheric composition. *Nature* **426**, 323–326 (2003)

Berner, R. A. & Kothavala, Z. GEOCARB III. A revised model of atmospheric CO_2 over Phanerozoic time. *American Journal of Science* **301**, 182–204 (2001)

Biddle, J. F., Lipp, J. S., Lever, M. A., Lloyd, K. G., Sørensen, K. B., Anderson, R. D., Fredricks, H. F., Elvert, M., Kelly, T. J., Schrag, D. P, Sogin, M. L., Brenchley, J. E., Teske, A., House, C. H. & Hinrichs, K–U. Heterotrophic Archaea dominate sedimentary subsurface ecosystems off Peru. *Proceedings of the National Academy of Science* **103,** 3846–3851 (2006)

Bijl, P. K., Schouten, S., Sluijs, A., Reichart, G-J., Zachos, J. C. & Brinkhuis, H. Early Palaeogene temperature evolution of the southwest Pacific Ocean. *Nature* **461**, 776–779 (2009)

Bornemann, A. & Mutterlose, J. Calcareous nannofossil and $\delta^{13}C$ records from the Early Cretaceous of the western Atlantic Ocean: evidence for enhanced fertilization across the Berriasian–Valanginian transition. *Palaios* **23**, 821–832 (2008a)

Bornemann, A., Norris, R. D., Friedrich, O., Beckmann, B., Schouten, S., Sinninghe Damsté, J. S., Vogel, J., Hofmann, P. & Wagner, T. Isotopic evidence for glaciation during the Cretaceous supergreenhouse. *Science* **319**, 189–192 (2008b)

Bown, P. R. New calcareous nannofossil taxa from the Jurassic/ Cretaceous Boundary interval of Sites 765 and 261, Argo Abyssal Plain. *Proceedings of the Ocean Drilling Program, Initial Reports* **123,** 369–379 (1992)

Bralower, T.J., and Siesser, W.G.,. Cretaceous calcareous nannofossil biostratigraphy of Sites 761, 762, and 763, Exmouth and Wombat Plateaus, northwest Australia. *In* von Rad, U., Haq, B.U., et al., *Proceedings of the Ocean Drilling Program, Scientific Results,* **122**. College Station, TX (Ocean Drilling Program), 529–556 (1992)

Bralower, T. J., Arthur, M. A., Leckie, R. M., Sliter, W. V., Allard, D. J., Schlanger, S. O. Timing and Paleoceanography of Oceanic Dysoxia/Anoxia in the Late Barremian to Early Aptian (Early Cretaceous). *Palaios* **9**, 335–369 (1994)

Bralower, T. J., Premoli Silva, I., Malone, M. J., *et al*. *Proceedings of the Ocean Drilling Program, Initial Reports* **198***:* College Station, TX (Ocean Drilling Program) (2002)

Brenner, W. Dinoflagellate cyst stratigraphy of the Lower Cretaceous sequence at Sites 762 and 763, Exmouth Plateau, northwest Australia. von Rad, U., Haq, B. U., et al. *Proc. ODP, Sci. Results,* 122. College Station, TX (Ocean Drilling Program) (1992)

Bralower, T. J, & Siesser, W. J. Cretaceous calcareous nannofossil biostratigraphy of sites 761, 762, and 763, Exmouth and Wombat Plateaus, Northwest Australia. In: von Rad, U; Haq, BU; et al. (eds.), *Proceedings of the Ocean Drilling Program, Scientific Results,* College Station, TX *(Ocean Drilling Program*) (1992)

Broecker, W. S. The salinity contrast between the Atlantic and Pacific Oceans during glacial time. *Paleoceanography* **4**, 207–212 (1989)

Brassell, S. C., Eglinton, G., Marlowe, I. T., Pflaumann, U., Sarnthein, M. Molecular Stratigraphy – A new tool for climatic assessment. *Nature* **320**, 129–133 (1986)

Brassell, S. C. & Dumitrescu, M. and the ODP Leg 198 Shipboard Scientific Party. Recognition of alkenones in a lower Aptian porcellanite from the west-central Pacific. *Organic Geochemistry* **35**, 181–188 (2004)

Brassell, S. C. Steryl ethers in a Valanginian claystone: Molecular evidence for cooler waters in the central Pacific during the Early Cretaceous? *Palaeogeography, Palaeoclimatology, Palaeoecology* **282**, 45–57 (2009)

Budyko, M. I., Ronov, A. B., Yanshin, A. L. History of the Earth's Atmosphere. Berlin; New York: Springer-Verlag (1987)

Bukry, D. Phytoplankton stratigraphy, offshore East Africa, Deep Sea Drilling Project Leg 25. *Initial Reports of the Deep Sea Drilling Project* **25**, 635–646 (1974)

Cazenave, S., Chapoulie, R. & Villeneuve, G. Cathodoluminescence of synthetic and natural calcite: the effects of manganese and iron on orange emission. *Minerology and Petrology,* **78**, 243–253 (2003)

Cepek, P., Gartner, S. & Cool, T. Mesozoic calcareous nannofossils, Deep Sea Drilling Project Sites 415 and 416, Moroccan Basin. *Initial Reports of the Deep Sea Drilling Project* **50**, 345–351(1980)

Chappe, B., Albrecht, P. & Michaelis. W. Polar lipids of archaebacteria in sediments and petroleum. *Science* **217,** 65–66 (1982)

Church, M. J., DeLong, E. F., Ducklow, H. W., Karner, M. B., Preston, C. M. & Karl, D. M. Abundance and distribution of planktonic *Archaea* and *Bacteria* in the Western Antarctic Peninisula. *Limnology and Oceanography* **48,** 1893–1902 **(**2003)

Conte, M, H., Sicre, M–A., Rühlemann, C., Weber, J.C., Schulte, S., Schulz–Bull, D. & Blanz, T. Global temperature calibration of the alkenone unsaturation index ($U^{K'}_{37}$) in surface waters and comparison with surface sediments. *Geochemistry, Geophysics, Geosystems* **7**, Q02005 (2006)

Coolen, M. J. L., Abbas, B., van Bleiswijk, J., Hopmans, E. C., Kuypers, M. M. M., Wakeham, S. G., Sinninghe Damsté, J. S. Putative ammonia–oxidizing Crenarchaeota in suboxic waters of the Black Sea: a basin–wide ecological study using 16S ribosomal and functional genes and membrane lipids. *Environmental Microbiology* **9**, 1001–1016 (2007)

Coplen T.B. and Schlanger S. O. Oxygen and carbon isotope studies of carbonate sediments from site 167, Magellan Rise, Leg 17, *Initial Reports of the Deep Sea Drilling Project* **17**, 505–509 (1973)

Cotillon P. & Rio M. Cyclic sedimentation in the Cretaceous of DSDP site 535 and 540 (Gulf of Mexico), 534 (central Atlantic) and the Vocontian Basin (France), *Initial Reports of the Deep Sea Drilling Project* **77**, 339–376 (1984)

Council, T. C. & Bennett, P. C. Geochemistry of ikaite formation at Mono Lake, California: Implications for the origin of tufa mounds. *Geology* **21**, 971–974 (1993)

Covington, J. M. & Wise, S. W., Jr. Calcareous nannofossil biostratigraphy of a lower Cretaceous deep–sea fan complex: Deep Sea Drilling Project Leg 93 Site 603, lower continental rise off Cape Hatteras. *Initial Reports of the Deep Sea Drilling Project* **93**, 617–660 (1987)

Craig, H., & Gordon, L. I. Deuterium and oxygen 18 variations in the ocean and marine atmosphere. *In Proc. Conference on Stable Isotopes in Oceanographic Studies and Palaeotemperatures. Spoleto, Italy, Consiglio Nazional delle Richerche, Pisa,* pp. 9-130. Edited by Tongiogi, Lischi & Figli (1965)

Dean, E. D., Arthur, M. A., Claypool, G. E. Depletion of C in Cretaceous marine organic matter: source, diagenetic, or environmental signal? *Marine Geology* **7**, 119–157 (1986)

Dean, W. E., & Arthur, M. A. Inorganic and organic geochemistry of Eocene to Cretaceous Strata recovered from the Lower Continental Rise, North American Basin, Site 603, Deep Sea Drilling Project Leg 93. In, van Hinte, J. E., Wise, S. W., Jr., *et al., Initial Reports of the Deep Sea Drilling Project* 93: Washington (U.S. Govt. Printing Office) (1987)

Dypvik, H. Jurassic and Cretaceous black shales of the Janusfjellet Formation, Svalbard, Norway. *Sedimentary Geology* **41**, 235–248 (1985)

De la Torre, J. R., Walker, C. B., Ingalls, A. E., Konneke, M. & Stahl, D. A. Cultivation of a thermophilic ammonia oxidizing archaeon synthesizing crenarchaeol. *Environmental Microbiology* **10**, 810–818 (2008)

DeLong, E. F. Archaea in coastal marine environments. *Proceedings of the National Accademy of Sciences* **89**, 5685−5689 (1992)

DeLong, E. F., Ying Wu, K., Prezelin, B. B. & Jovine, R. V. M. High abundance of archaea in Antarctic marine picoplankton. *Nature* **371**, 695–697 (1994).

DeLong, E. F., King, L. L., Massana, R., Cittone, H., Murray, A., Schleper, C. & Wakeham, S. G. Dibiphytanyl Ether Lipids in Nonthermophilic Crenarchaeotes. *Applied and Environmental Microbiology* **64***,* 1133–1138 (1998a)

DeLong E. F. Everything in moderation: Archaea as 'non–extremophiles'. *Current Opinion in Genetics & Development* **8**, 649–654 (1998b)

De Lurio, J., & Frakes. L. A. Glendonites as a paleoenvironmental tool: Implications for early Cretaceous high latitude climates in Australia. *Geochimica et Cosmochimica Acta* **63**, 1039–1048 (1999)

Delvaux, D., Martin, H., Leplat, P., Paulet, J. Comparative Rock-Eval pyrolysis as an improved tool for sedimentary organic matter analysis*. Organic Geochemistry* **16***,* 1221–1229 (1990)

De Wever, P., Dumitrica, P. .& Caulet, J. P. *et al.*, Radiolarians in the Sedimentary Record. Gordon and Breach Scientific Publications (2001)

Dickens, G., O'Neil, J. R., Rea, D. K. & Owen, R. M. Dissociation of oceanic methane hydrate as a cause of the carbon isotope excursion at the end of the Paleocene. *Paleoceanography* **10,** 965–971 (1995)

Dickens, G. On the fate of past gas: what happens to methane released from a bacterially mediated gas hydrate capacitor. *Gechemistry, Geophysics, Geosystems* **2,** 2000GC000131 (2001)

Ditchfield, P. W. High northern palaeolatitude Jurassic–Cretaceous palaeotemperature variation: new data from Kong Karls Land, Svalbard**.** *Palaeogeography, Palaeoclimatology, Palaeoecology* **130**, 163–175 (1997)

Doria, G., Royer, D. L., Wolfe, A. P., Declining atmospheric CO_2 during the Late Middle Eocene climate transition. *American Journal of Science* **311**, 63–75 (2011)

Douglas, R.G. and Savin, S.M., 1973. Oxygen and carbon isotope analyses of Cretaceous and Tertiary foraminifera from Central North Pacific. *Initial Reports of the Deep Sea Drilling Project* **17**, pp. 591–605

Duchamp-Alphonse, S., Fiet, N., Adatte, T. & Pagel, M. Climate and sea-level variations along the northwestern Tethyan margin during the Valanginian C-isotope excursion: Mineralogical evidence from the Vocontian Basin (SE France). *Palaeogeography, Palaeoclimatology, Palaeoecology* **302** (2011) 243–254

Dunham, K. W., Meyers, P. A. & Dunham, P. L. Organic geochemical comparison of Cretaceous black shales and adjacent strata from deep sea drilling project Site 603, Outer Hatteras Rise. van Hinte, J. E., Wise, S. W., Jr., et al., Site 603. *Initial Reports of the Deep Sea Drilling Project* **93**. 25–226 (1987)

Dutton, A., Huber, B. T., Lohmann, K. C., and Zinsmeister, W. J. High-resolution stable isotope profiles of a dimitobelid belemnite: implications for paleodepth habitat and late Maastrichtian climate seasonality. *Palaios* **22**, 642–650 (2007)

Elderfield, H & Ganssen, G. Past temperature and ^{18}O of surface ocean waters inferred from foraminiferal Mg/Ca ratios. *Nature* **405**, 442–445 (2000)

Erba E**.,** Channell J. E. T., Claps M., Jones C., Larson R. L., Opdyke B., Premoli Silva I., Riva A., Salvini G., Torricelli S. Integrated streatigraphy of the Cismon Apticore (Southern Alps, Italy): a "reference section" for the Barremian–Aptian interval at low latitudes. *Journal of Foraminiferal Research* **29**, 371–391 (1999)

Erba, E. Middle Cretaceous calcareous nannofossil from the western Pacific (Leg 129): Evidence for palaeoquatorial crossings. In: Larson, R. L., Lancelot, Y., *et al. Proceedings of the Ocean Drilling Program, Scientific Results*, **129**, 189–201 (1992)

Erba, E., Bartolini, A., Larson, R.L. Valanginian Weissert oceanic anoxic event. *Geology* **32**, 149–152 (2004)

Erbacher, J., Huber, B.T., Norris, R.D. & Markey, M. Increased thermohaline stratification as a possible cause for an ocean anoxic event in the Cretaceous period. *Nature* **409**, 325–327 (2001)

Erbacher, J, Friedrich, O, Wilson, P.A., Lehmann, J., Weiss, W. Short–term warming events during the boreal Albian (mid–Cretaceous). *Geology* **39**, 223–226 (2011)

Farrimond, P., Eglinton, G., Brassell, S.C. Geolipids of black shales and claystones in Cretaceous and Jurassic sediment sequences from the North American Basin (Atlantic, DSDP). *North Atlantic palaeoceanography*, 347–360 (1986) Oxford, Blackwell.

Farquhar, G. D., Ehleringer, R. & Hubick, K. T. Carbon isotope discrimination and photosynthesis. *Annual Review of Plant Physiology and Plant Molecular Biology* **40**, 503–37 (1989)

Follmi, K. B., Weissert, H., Bisping, M., Funk, H. Phosphogenesis, carbon–isotope stratigraphy, and carbonate–platform evolution along the Lower Cretaceous northern Tethyan margin. *Geological Society of America Bulletin* **106**, 729– 746 (1994)

Follmi, K. B., Godet, A., Bodin, S. & Linder, P. Interactions between environmental change and shallow water carbonate buildup along the northern Tethyan margin and their impact on the Early Cretaceous carbon isotope record. *Paleoceanography* **21**, PA4211, (2006)

Forster, A., Schouten, S., Moriya, K., Wilson, P. A. & Sinninghe Damsté, J. S. Tropical warming and intermittent cooling during the Cenomanian/Turonian oceanic anoxic event 2: Sea surface temperature records from the equatorial Atlantic. *Paleoceanography* **22**, PA1219, (2007)

Fox. G. E., Magrum, L. J., Balch, W. E., Wolfe, R. S. & Woese, C. R. Classification of methanogenic bacteria by 16S ribosomal RNA characterization. *Proceedings of the National Accademy of Sciences* **74**, 4337–4541 (1977)

Frakes, L. A. *Climates throughout Geologic Time.* Amsterdam, New York: Elsevier Scientific (1979)

Frakes, L.A. & Francis, J.E. A guide to Phanerozoic cold polar climates from high latitude ice rafting in the Cretaceous. *Nature* **333**, 547–549 (1988)

Frakes, L. A., Francis, J. E. & Syktus, J. I. *Climate Modes of the Phanerozoic.* Cambridge University Press (1992)

Frank, T. D., Arthur, M. A. & Dean W. E., Diagenesis of Lower Cretaceous Pelagic Carbonates, North Atlantic: Paleoceanographic Signals Obscured. *Journal of Foraminiferal Research* **29,** 340–351 (1999)

Francis, C. A., Roberts, K. J., Berman, J. M., Santoro. A. E. & Oakley, B. B. Ubiquity and diversity of ammonia–oxidising archaea in water columns and sediments of the ocean. *Proceedings of the National Accademy of Sciences* **102**, 14683–14688 (2005)

Freeman, K. & Hayes, M. Fractionation of carbon isotopes by phytoplankton and estimates of ancient CO_2 levels. *Global Biogeochemical cycles* **6**, 85–198 (1992)

Fuhrman, J. A., McCallum, K. & Davis, A. A. Novel major archaebacterial group from marine plankton. *Nature* **356**, 148–149 (1992)

Fuhrman, J. A., McCallum, K. & Davis, A. A. Phylogenetic Diversity of Subsurface Marine Microbial Communities from the Atlantic and Pacific Oceans. *Applied and Environmental Microbiology* **59** 1294–1302 (1993)

Fuhrman, J. A., and A. A. Davis. Widespread archaea and novel bacteria from the deep sea as shown by 16S rRNA gene sequences. *Marine Ecology Progress Series* **150,** 275–285 (1997)

Gliozzi, A., G. Paoli, M. De Rosa, and A. Gambacorta Effect of isoprenoid cyclization on the transition temperature of lipids in thermophilic archaebacteria. *Biochimica et Biophysica Acta* **735**, 234– 242 (1983)

Gradstein, F. M., Ogg, J., Smith, A. A geologic time scale 2004. Cambridge University Press, Cambridge, UK (2004)

Grant, W. D., Gemmell, R. T. & McGenitym T. J. Halobacteria: The evidence for longevity. *Extremophiles* **2**, 279–287 (1998)

Grocke, D. R., Hesselbo, S.P. & Jenkyns, H. C. Carbon–isotope composition of Lower Cretaceous fossil wood: ocean-atmosphere chemistry and relation to sea-level change. *Geology* **27,** 155 – 158 (1999)

Grocke, D. R., Price G. D., Robinson, S. A., Baraboshkin, E. Y., Mutterlose, J. & Ruffell, A. H. The Upper Valanginian (Early Cretaceous) positive carbon–isotope event recorded in terrestrial plants. *Earth and Planetary Science Letters* **240,** 495 – 509 (2005)

Habib, D. Sedimentary origin of North Atlantic Cretaceous palynofacies, in Deep drilling results in the Atlantic Ocean: continental margins and paleoenvironment. *American Geophysical Union Maurice Ewing Series* **3**, 420–437 (1979)

Habib, D. Sedimentation–rate dependent distribution of organic matter in the North Atlantic Jurassic–Cretaceous. in: Sheridan, R. E., Gradstein, F. M., *et al*., *Initial Reports of the Deep Sea Drilling Project* 76: Washington (U.S. Govt. Printing Office) (1983)

Hackworth, M. S. Carbonate Records of Submarine Hydrocarbon Venting: Northern Gulf of Mexico. *PhD thesis, Louisiana State University* (2004)

Hallam, A. Continental humid and arid zones during the Jurassic and Cretaceous. *Palaeogeography, Palaeoclimatology, Palaeoecology* **47** 195–223 (1984)

Hallam, A. A review of Mesozoic climates. *Journal of the Geological Society* **142**, 433–445 (1985)

Hallam, A. Role of climate in affecting late Jurassic and early Cretaceous sedimentation in the North Atlantic. *Geological Society, London, Special Publications* **21**, 277–281 (1986)

Hallam, S. J., Mincer T., Schleper C., Preston C. M., Roberts K., Richardson P. M., and DeLong D. F. Pathways of carbon assimilation and ammonia oxidation suggested by environmental genomic analyses of marine Crenarchaeota. *PLoS Biology* **4**, e95 (2006)

Handoh, I. C., Bigg, G. R. & Jones, E. J. W. Evolution of upwelling in the Atlantic Ocean basin. Palaeogeography, Palaeoclimatology, Palaeoecology 202, 31–58 (2003)

Haq, B. U., von Rad, U., *et al*. Site 763 *Proceedings of the Ocean Drilling Program, Initial Reports* **122**, 289–352 (1990)

Hardenbol, J., Thierry, J., Farley, M. B., Jacquin, T., Graciansky, P.C. de., & Vail, P. R. Mesozoic–Cenozoic sequence chronostratigraphic framework of European basins. In: Graciansky, P.C. de, Hardenbol J, Jacquin T, Vail PR, Farley MB (eds) Sequence

stratigraphy of European basins. *Society for Sediementary Geology Special Publication* **60**, 1–13 (1998)

Hatzenpichler, R. E. V. Lebedeva, E. Spieck, K. Stoecker, A. Richter, H. Daims, and M. Wagner**.** A moderately thermophilic ammonia–oxidizing crenarchaeote from a hot spring. *Proceedings of the National Accademy of Sciences* **105,** 2134–2139 (2008)

Haworth, M., Hesselbo, S. P., McElwain, J. C., Robonson, S. A. & Brunt, J. W. Mid-Cretaceous pCO_2 based on stomata of the extinct conifer *Pseudofrenelopsis* (Cheirolepidiaceae). *Geology,* **33,** 749–752 (2005)

Hay, W. W. Evolving ideas about the Cretaceous climate and ocean circulation. *Cretaceous Research* **29**, 725–753 (2008)

Hays, P., Grossman, E. L. Oxygen isotopes in meteoric calcite cements as indicators of continental climate. *Geology* **19**, 441–444 (1991)

Hennig, S., Weissert, H. & Bulot, L. C-isotope stratigraphy, a calibration tool between ammonite- and magnetostratigraphy: the Valanginian – Hauterivian transition. *Geologica Carpathica* **50**, 91–96 (1999)

Herbin, J. P., Deroo, G. & Roucaché, J. Organic Geochemistry in the Mesozoic and Cenozoic Formations of Site 534, Leg 76, Blake-Bahama Basin, and Comparison with Site 391, Leg 44. *Initial reports of the Deep Sea Drilling Project* **76,** 481–493 (1983)

Herbin, J. P., Masure, E. & Roucaché, J. Cretaceous Formations from the Lower Continental Rise off Cape Hatteras: Organic Geochemistry, Dinoflagellate Cysts, and the Cenomanian/Turonian Boundary Event at Sites 603 (Leg 93) and 105 (Leg 11). In: van Hinte, J. E., Wise, S. W., Jr., et al., *Deep sea Drilling Project, Scientific results* **93. (**Washington (U.S. Govt. Printing Office) (1987)

Herfort, L., Schouten, S., Boon, J. P. & Damsté, J. S. S. Application of the TEX_{86} temperature proxy to the southern North Sea. *Organic Geochemistry* **37**, 1715–1726 (2006)

Herrle, J. O., Kössler, P. & Bollmann, J. Palaeoceanographic differences of early Late Aptian black shale events in the Vocontian Basin (SE France). *Palaeogeography, Palaeoclimatology, Palaeoecology* **297,** 367–376 (2010)

Herman, A. B. & Spicer, R. A. Palaeobotanical evidence for a warm Cretaceous Arctic Ocean. *Nature* **380**, 330–333 (1996)

Herndl, G. J., T. Reinthaler, E. Teira, H. van Aken, C. Veth, A. Pernthaler, & Pernthaler, J Contribution of Archaea to total prokaryotic production in the deep Atlantic Ocean. *Appl. Environmental Microbiology* **71**, 2303–2309 (2005)

Hesselbo, S. P., Grocke, D. R., Jenkyns, H. C., Bjerrum, C. J., Farrimond, P., Morgans Bell, H. S. & Green, O. R. Massive dissociation of gas hydrate during a Jurassic oceanic anoxic event. *Nature* **406**, 392–395 (2000)

Hesselbo, S. P., Jenkyns, H. C., Duarte, L. V., Oliveira, L. C. V. Carbon–isotope record of the Early Jurassic (Toarcian) Oceanic Anoxic Event from fossil wood and marine carbonate (Lusitanian Basin, Portugal). *Earth and Planetary Science Letters* **253**, 455–470 (2007)

Higgins, J. A. & Schrag, D. P. Beyond methane: Towards a theory for the Paleocene–Eocene Thermal Maximum. *Earth and Planetary Science Letters* **245**, 523–537 (2006)

Hoedemaker, P. J. The Neocomian boundaries of the Tethyan Realm based on the distribution of ammonites. *Cretaceous Research* **11**, 331–342 (1990)

Hoefs, M. J. L., Schouten, S., de Leeuw, J. W., King, L. L. Wakeham, S. G. & Sinninghe Damste, J. S. Ether lipids of planktonic Archaea in the marine water column? *Applied and Environmental Microbiology* **63**, 3090–3095 (1997)

Hollis, C. J. Handley, L., Crouch, E. M., Morgans, H. E. G., Baker, J. A., Creech. J., Collins, K. S., Gibbs, S. J., Huber, M., Schouten, S. & Zachos, J. C. Tropical sea temperatures in the high–latitude South Pacific during the Eocene. *Geology* **37**, 99–102 (2009)

Hopmans, E. C., Weijers, J. W. H., Schefuß, E., Herfort, L., Sinninghe Damsté, J. S. & Schouten, S. A novel proxy for terrestrial organic matter in sediments based on branched and isoprenoid tetraether lipids. *Earth and Planetary Science Letters* **224**, 107–116 (2004)

Howland, J. L. The Surprising Archaea. New York & Oxford: Oxford University Press. (2000)

Hsü, K. J. & Jenkyns, H. C., Editors, Pelagic sediments: on land and under the sea. Special *Publication of the International Assocciation of Sedimentologists* **1**, 1–10. Blackwell Scientific Publications (1974)

Huguet, C., Cartes, J.E., Sinninghe Damsté, J.S., Schouten, S. Decapods. Marine crenarchaeotal membrane lipids in decapods: Implications for the TEX_{86} paleothermometer. *Geochemistry, Geophysics, Geosystems* **7,** Q11010 (2006)

Huguet, C., Schimmelmann, A., Thunell, R., Lourens, L.J., Sinninghe Damsté, J.S. & Schouten, S. A study of the TEX_{86} paleothermometer in the water column and sediments of the Santa Barbara Basin, California. *Paleoceanography* **22** PA3203 (2007).

Huguet, C., de Lange, G–J., Gustafsson, O., Middelburg, J. J., Sinninghe Damsté, J. S., & Schouten, S. Selective preservation of soil organic matter in oxidized marine sediments (Madeira Abyssal Plain). *Geochimica et Cosmochimica Acta* **72**, 6061–6068 (2008).

Huguet, C., Kim, J–H., de Lange, G–J., Sinninghe Damsté, J.S. & Schouten, S. Effects of long term oxic degradation on the UK^{37}, TEX_{86} and BIT organic proxies. *Organic Geochemistry* **40**, 1188–1194 (2009)

Hvoslef, S., Dypvik, H. & Solli, H. A combined sedimentological and organic geochemical study of the Jurassic/Cretaceous Janusfjellet formation (Svalbard), Norway. *Organic Geochemistry* **10**, 101–111 (1986)

Inagaki, F., Nunoura, T., Nakagawa, S., Teske, A., Lever, M., Lauer, A., Suzuki, M., Takai, K., Delwiche, M., Colwell, F. S., Nealson, K, H., Horikoshi, K., D'Hondt, S. & Jørgensen, B. B. Biogeographical distribution and diversity of microbes in methane hydrate–bearing deep marine sediments on the Pacific Ocean Margin. *Proceedings of the National Accademy of Sciences* **103**, 2815–2820 (2006)

Ingalls, A. E., Shah, S. R., Hansman, R. L. Aluwihare, L. I., Santos, G. M., Druffel E. R. M. & Pearson, A. Quantifying archaeal community autotrophy in the mesopelagic ocean using natural radiocarbon. *Proceedings of the National Accademy of Sciences* **103**, 6442–6447 (2006)

IPCC, 2007: Climate Change 2007: Synthesis Report. Contribution of Working Groups I, II and III to the Fourth Assessment Report of the Intergovernmental Panel on Climate Change [Core Writing Team, Pachauri, R.K and Reisinger, A. (eds.)]. IPCC, Geneva, Switzerland, 104 pp.

Jahren, A. H. & Arens, N. C. Methane hydrate dissociation implicated in Aptian OAE events. *Geological Society of America Abstracts with Programs* **30,** 53 (1998)

Janasi, A. V., Freitas, V. A. & Heaman, L. H. The onset of flood basalt volcanism, Northern Paraná Basin, Brazil: A precise U–Pb baddeleyite/zircon age for a Chapecó–type dacite. *Earth and Planetary Science Letters* **302** 147–153 (2011)

Jansen, J. H. F. Woensdregt, C. F. Kooistra M. J. & Van der Gaast, S. J. Ikaite pseudomorphs in the Zaire deep-sea fan: An intermediate between calcite and porous calcite, *Geology* **15** 245–248 (1987)

Jarvis, I., Lignum, J. S., Gröcke, D. R., Jenkyns, H. C., Pearce, M. A. Black shale deposition, atmospheric CO_2 drawdown and cooling during the Cenomanian–Turonian Oceanic Anoxic Event (OAE2). *Palaeoceanography* **26**, PA3201; doi:10.1029/2010PA002081 (2011)

Jenkyns, H. C. Cretaceous anoxic events: from continents to oceans. *Journal of the Geological Society* **137**, 171–188. (1980)

Jenkyns, H. C. Mesozoic anoxic events and palaeoclimate. *Zentralblatt fur Geologie und Palaontologie,* 943–949 (1999)

Jenkyns, H. C. Evidence for rapid climate change in the Mesozoic–Palaeogene greenhouse world. *Philosophical Transactions of the Royal Society of London A* **361**, 1885–1916 (2003)

Jenkyns, H. C. Geochemistry of oceanic anoxic events. *Geochemisty, Geophysics, Geosystems* **11**, Q03004, (2010)

Jenkyns, H. C. & Clayton, C. J. Lower Jurassic epicontinental carbonates and mudstones from England and Wales: chemostratigraphic signals and the early Toarcian anoxic event. *Sedimentology* **44**, 687–706 (1997)

Jenkyns H. C., Forster A., Schouten S., & Sinninghe Damsté J. S. High temperatures in the Late Cretaceous Arctic Ocean. *Nature* **432**, 888–892 (2004)

Jenkyns, H. C., Schouten-Huibers, L., Schouten, S. & Sinninghe Damsté, J. S. Middle Jurassic-Early Cretaceous high-latitude sea-surface temperatures from the Southern Ocean. *Climate of the Past Discussions,* 7, 1339–1361 (2011)

Jones, K. P. N., McCave, I.N. & Weaver, P.P.E. Textural and dispersal patterns of thick mud turbidites from the Madeira Abyssal Plain. *Marine Geology,* **107,** 149–173 (1992)

Kaminski, M. A., Baumgartner, P. O., Bown, P. R., Haig, D. W., McMinn, A., Moran, M. J., Mutterlose, J., Ogg, J. G. Magnetobiostratigraphic synthesis of Leg 123: Sites 765 and 766 (Argo Abyssal Plain and Lower Exmouth Plateau). *Proceedings of the Ocean Drilling Program, Scientific Results*, Vol. **123**, 717–737 (1992)

Kaplan M. E. Calcite pseudomorphosis from theJurassic and Lower Cretaceous deposits of Eastern Siberia. *Soviet Geology and geophysics* **12**, 62–70 (1978)

Karner, M. B., DeLong, E. F. & Karl, D. M. Archaeal dominance in the mesopelagic zone of the Pacific Ocean. *Nature* **409,** 507–510 (2001)

Katz, B. J. Organic Geochemical Character of Some Deep Sea Drilling Project Cores from Legs 76 and 44. *Initial reports of the Deep Sea Drilling Project* **76**: Washington (U.S. Govt. Printing Office) (1983)

Keller, C. E., Hochuli, P. A., Weissert, H., Bernasconi, S. M., Giorgioni, M., Garcia, T. I. A volcanically induced climate warming and floral change preceded the onset of OAE1a (Early Cretaceous). *Palaeogeography, Palaeoclimatology, Palaeoecology* **305**, 43–49 (2011)

Kemper, E. Das Klima der Kreide–Zeit. *Geologisches Jahrbuch* **A96**, 5–185 (1987)

Kessels, K., Mutterlose, J., Michalzik, D. Early Cretaceous (Valanginian–Hauterivian) calcareous nannofossils and isotopes of the northern hemisphere: proxies for the understanding of Cretaceous climate. *Lethaia* **39,** 157–172 (2006)

Kim, J–H., Schouten, S., Hopmans, E.C., Donner, B. & Sinninghe Damsté, J.S. Global sediment core–top calibration of the TEX_{86} paleothermometer in the ocean. *Geochimica et Cosmochimica Acta* **72**, 1154–1173 (2008)

Kim, J–H., Huguet, C., Zonneveld, K.A.F., Versteegh, G.J.M., Roeder, W., Sinninghe Damste, J.S. & Schouten, S. An experimental field study to test the stability of lipids used for the TEX_{86} and U^{K}_{37} palaeothermometers. *Geochimica et Cosmochimica Acta* **73**, 2888–2898 (2009)

Kim, J–H., van der Meer, J., Schouten, S., Helmke, P., Willmott, V., Sangiorgi, F., Koc, N., Hopmans, E.C. & Sinninghe Damsté, J. S. New indices and calibrations derived from the distribution of crenarchaeal isoprenoid tetraether lipids: Implications for past sea surface temperature reconstructions. *Geochimica et Cosmochimica Acta* **74**, 4639–4654 (2010)

Kohnen, M. E. L., Schouten, S., Sinninghe Damsté, J. S., de Leeuw, J. W., Merrit, D. A. & Hayes, J. M. Recognition of palaeobiochemicals by a combined molecular sulfur and isotope geochemical approach. *Science* **256,** 358–362 (1992)

Könneke, M., Bernhard, A.E., de la Torre, J.R., Walker, C.B., Waterbury, J.B. & Stahl, D.A., Isolation of an autotrophic ammonia–oxidizing marine archaeon Nature **437**, 543 – 546 (2005)

Kreutz, K. J., Mayewski, P. A. Meeker, L. D. Twickler, M. S. Whitlow, S. I. Pittalwala, I. I. Bipolar Changes in Atmospheric Circulation During the Little Ice Age. *Science* **277,** 1294–1296 (1997)

Kuhnt, W., Holbourn, A. & Moullade, M. Transient global cooling at the onset of early Aptian oceanic anoxic event (OAE) 1a. *Geology* **39**, 323–326 (2011)

Kump, L. R. & Arthur, M. Interpreting carbon–isotope excursions: carbonates and organic Matter. *Chemical Geology* **161**, 181–198 (1999)

Kuypers M. M. M., Blokker, P., Erbacher, J., Kinkel, H., Pancost, R. D., Schouten,S., Sinninghe Damste, J. S. Massive Expansion of Marine Archaea During a Mid–Cretaceous Oceanic Anoxic Event. *Science* **293**, 92–94 (2001)

Kuypers, M. M. M., Lourens, L. J., Rijpstra, W. R. C., Pancost, R. D., Nijenhuis, I. A., Sinninghe Damsté, J. S. Orbital forcing of organic carbon burial in the proto–North Atlantic during Oceanic Anoxic Event 2, *Earth and Planetary Science Letter*s **228**, 465–482 (2004)

Kvenvolden K. A., A review of the geochemistry of methane in natural gas hydrate. *Organic Geochemistry* **23**, 997–1008 (1995)

Lancelot, Y., Winterer, L., et al. Site 416, in the Moroccan Basin, Deep Sea Drilling Project Leg 50. *Initial Reports of the Deep Sea Drilling Project,* Vol. **50**, 115–301 (1980)

Langford, F. F. & Blanc-Valleron, M. M. Interpreting Rock-Eval Pyrolysis Data Using Graphs of Pyrolizable Hydrocarbons vs. Total Organic Carbon. *AAPG Bulletin* **74** (1990)

Larson, R. L. & Erba, E. Onset of the Mid-Cretaceous greenhouse in the Barremian-Aptian: Igneous events and the biological, sedimentary, and geochemical responses. *Paleoceanography*, **14,** 663–679 (1999)

Lea, D. W., Elemental and Isotopic Proxies of Past Ocean Temperatures. In: K. Turkien (Editor), *Treatise On Geochemistry*. Elsevier. (2003)

Lea, D. W., Pak, D. K., Peterson, L. C. & Hughen, K.A. Synchroneity of Tropical and High–Latitude Atlantic Temperatures over the Last Glacial Termination. *Science* **301**, 1361–1364 (2003)

Lear, C. H. Rosenthal, Y., & Slowey, N. Benthic foraminiferal Mg/Ca-paleothermometry: a revised core-top calibration. *Geochimica et Cosmochimica Acta* **66**, 3375–3387 (2002)

Leckie, R. M., Bralower, T. J. & Cashman, R. Oceanic anoxic events and plankton evolution: Biotic response to tectonic forcing during the mid–Cretaceous. *Paleoceanography* **17**, PA000623, (2002)

LeGrande, A. N. & Schmidt, G. A. Global gridded data set of the oxygen isotopic composition in seawater. *Geophysical Research Letters*, **33** (2006)

Lehmann, M. F., Bernasconi, S. M., Barbieri, A. & McKenzie, J. A. Preservation of organic matter and alteration of its carbon and nitrogen isotope composition during simulated and *in situ* early sedimentary diagenesis. *Geochimica et Cosmochimica Acta* **66**, 3573–3584, (2002)

Lini, A., Weissert, H., Erba, E. The Valanginian carbon isotope event: a first episode of greenhouse climate conditions during the Cretaceous. *Terra Nova* **4**, 374–384 (1992)

Lipp, J. S. & Hinrichs, K–U. Structural diversity and fate of intact polar lipids in marine sediments. *Geochimica et Cosmochimica Acta* **73***,* 6816–6833 (2009)

Littler, K., Robinson, S. A., Bown, P. R., Nederbragt, A. J. & Pancost, R. D. High sea-surface temperatures during the Early Cretaceous Epoch. *Nature Geoscience* **4**, 169–172 (2011)

Liu, Z., Pagani, M., Zinniker, D., DeConto, R., Huber, M., Brinkhuis, H., Shah, S. R., Leckie, M., Pearson, A. Global Cooling During the Eocene–Oligocene Climate Transition. *Science* **323**, 1187–1190 (2009)

Locarnini, R. A., Mishonov, A. V., Antonov, J. I., Boyer, T. P. & Garcia, H. E. *World Ocean Atlas 2005, Volume 1: Temperature.* S. Levitus, Ed. NOAA Atlas NESDIS 61, U.S. Government Printing Office, Washington, D.C., 182 pp (2006)

Ludden, J. N., Gradstein, F. M., *et al*. Site 765. *Proceedings of the Ocean Drilling Program, Initial Reports,* Vol. **123,** 63–267 (1990a)

Ludden, J. N., Gradstein, F. M., *et al*. Site 766. *Proceedings of the Ocean Drilling Program, Initial Reports,* Vol. **123,** 269–352 (1990b)

Lugowski, A., Ogg, J. & Gradstein, F.M. TS–Creator PRO (2005–2010), visualization of enhanced Geologic Time Scale 2004 database (Version 4.2.5; 2010). *http://www.tscreator.org*)

Massana, R., A. E. Murray, C. M. Preston, and E. F. DeLong.. Vertical distribution and phylogenetic characterization of marine planktonic Archaea in the Santa Barbara Channel. *Applied Environmental Microbiology* **63,** 50–56 (1997)

Massana, R., Taylor, L.T., Murray, Wu, K.Y., Jeffrey, W.H. & DeLong, E. E. Vertical distribution and temporal variation of marine planktonic Archaea in the Gerlache Strait, Antarctica, during early spring. *Limnology and Oceanography* **43**, 607– 617 (1998).

Massana R., DeLong, E.F., Pedros–Alio, C. A few cosmopolitan phylotypes dominate planktonic archaeal assemblages in widely different oceanic provinces. *Applied Environmental Microbiology* **66**, 1777–1787 (2000)

Markwick, P. J. Fossil crocodilians as indicators of Late Cretaceous and Cenozoic climates: implications for using palaeontological data in reconstructing palaeoclimate. *Palaeogeography, Palaeoclimatology, Palaeoecology* **137**, 205–271 (1998)

Martens–Habbena, W., Berube, P. M., Urakawa1, H., de la Torre, J. R. & Stahl, D. A. Ammonia oxidation kinetics determine niche separation of nitrifying Archaea and Bacteria. *Nature* **461**, 976–981 (2009)

McArthur, J. M., Janssen, N. M. M., Reboulet, S., Leng, M. J., Thirlwall, M. F., van de Schootbrugge, B. Palaeotemperatures, polar ice–volume, and isotope stratigraphy (Mg/Ca, $\delta^{18}O$, $\delta^{13}C$, $^{87}Sr/^{86}Sr$): The Early Cretaceous (Berriasian, Valanginian, Hauterivian). *Palaeogeography, Palaeoclimatology, Palaeoecology* **248**, 391–430 (2007a)

McArthur, J. M., Doyle, P., Leng, M. J., Reeves, K., Williams, C. T., Garcia–Sanchez, R. & Howarth, R. J. Testing palaeo–environmental proxies in Jurassic belemnites: Mg/Ca, Sr/Ca, Na/Ca, $\delta^{18}O$ and $\delta^{13}C$. *Palaeogeography, Palaeoclimatology, Palaeoecology* **252**, 464–480 (2007b)

McCave, I. N. & Jones, K. P. N. Deposition of ungraded muds from high–density non–turbulent turbidity currents. *Nature* **333**, 250–252 (1988)

Méhay, S., Keller, C. E., Bernasconi, S. M., Weissert, H., Erba, E., Bottini, C. & Hochuli, P. A. A volcanic CO_2 pulse triggered the Cretaceous Oceanic Anoxic Event 1a and a biocalcification crisis. *Geology* **37**, 819–822 (2009)

Melinte, M. & Mutterlose, J. An Early Cretaceous (Valanginian) 'boreal nannoplankton excursion' in sections from Romania. *Marine Micropaleontology* **43**, 1–25 (2001)

Menegatti, A. P, Weissert, H., Brown, R. S., Tyson R. V., Farrimond, P., Strasser, A., Caron. M. High–resolution $\delta^{13}C$ stratigraphy through the Early Aptian "Livello Selli" of the Alpine Tethys. *Paleoceanography* **13**, 530–545, (1998)

Menzel, D., Hopmans, E. C., Schouten, S., Sinninghe Damsté, J. S. Membrane tetraether lipids of planktonic Crenarchaeota in Pliocene sapropels of the eastern Mediterranean Sea. *Palaeogeography, Palaeoclimatology, Palaeoecology* **239** 1–15 (2006)

Meyers, P. A. Sources and deposition of organic matter in Cretaceous passive margin deep-sea sediments: a synthesis of organic geochemical studies from Deep-Sea Drilling Project Site 603, outer Hatteras Rise. *Marine and Petroleum Geology* **6,** (1989)

Milkov, A. V. Global estimates of hydrate-bound gas in marine sediments: How much is really out there? *Earth Science Reviews* **66**, 183–197 (2004)

Mincer, T. J., Church, M. J., Trent Taylor, L., Preston, C., Karl, D. M., & DeLong, E. F. Quantitative distribution of presumptive archaeal and bacterial nitrifiers in Monterey Bay and the North Pacific Subtropical Gyre. *Applied Environmental Microbiology* **9**, 1162–1175 (2007)

Murray, A.E., Preston, C.M., Massana, R., Taylor, L.T., Blakis, A., Wu, K. & DeLong, E.F. Seasonal and spatial variability of bacterial and archaeal assemblages in the coastal waters near Anvers Island, Antarctica, *Applied Environmental Microbiology* **64** 2585–2595 (1998)

Murray, A.E., Blakis, A., Massana, R., Strawzewski, S., Passow, U., Alldredge, A. & DeLong, E.F. A time series assessment of planktonic archaeal variability in the Santa Barbara Channel. *Aquatic Microbial Ecology* **20,** 129–145 (1999)

Mutterlose, J. & Wise, S.W. Lower Cretaceous nannofossil biostratigraphy of ODP Leg 113, Holes 692B and 693A, continental slope off East Antarctica, Weddell Sea. *Proceedings of the Ocean Drilling Program, Scientific Results* **113,** 325–351 (1990)

Mutterlose, J. Lower Cretaceous Nannofossil Biostratigraphy off northwestern Australia. *Proceedings of the Ocean Drilling Program, Scientific Results* **123**, 343–368 (1992)

Mutterlose, J. Hans Brumsack, H., Flogel, S., Hay, W., Klein, C., Langrock, U., Lipinski, M., Ricken, W., Soding, E., Stein, R. & Swientek, O. The Greenland–Norwegian Seaway: A key area for understanding Late Jurassic to Early Cretaceous paleoenvironments. *Paleoceanography* **18,** PA000625 (2003)

Mutterlose. J., Bornemann, A., Herrle, J. The Aptian - Albian cold snap: Evidence for "mid" Cretaceous icehouse interludes. *Neues Jahrbuch für Geologie und Paläontologie – Abhandlungen* **252**, 217-225 (2009)

Mutterlose, J., Malkoc, M., Schouten, S., Sinninghe Damste, J. S. & Forster, A. TEX_{86} and stable $\delta^{18}O$ paleothermometry of early Cretaceous sediments: Implications for belemnite ecology and paleotemperature proxy application. *Earth and Planetary Science Letters* **298**, 286–298 (2010)

Muttoni, G., Erba, E., Kent, D. V. & Bachtadse, V. Mesozoic Alpine facies deposition as a result of past latitudinal plate motion. *Nature* **434,** 59–63 (2005)

Nier A. 0. A redetermination of the relative abundances of the isotopes of carbon, nitrogen, oxygen, argon, and potassium. *Physical Reviews* **77**, 789–793 (1950)

Nürnberg, D., Bijma, J., & Hemleben, C. Assessing the reliability of magnesium in foraminiferal calcite as a proxy for water mass temperatures. *Geochimica et Cosmochimica Acta* **60**, 803–814 (1996)

Nürnberg D. & Müller, A. Paleo–sea surface temperature calculations in the equatorial east Atlantic from Mg/Ca ratios in planktic foraminifera– A comparison to sea surface temperature estimates from Uk37, oxygen isotopes, and foraminiferal transfer function. *Paleoceanography* **15**, 124–134 (2000)

Ocean Drilling Stratigraphic Network (ODNS), Plate Tectonic Reconstruction Service Paleomap project (http://www.odsn.de/odsn/services/paleomap/paleomap.html) (2011)

O'Connell, S.B. Sedimentary facies and depositional environment of the Lower Cretaceous East Antarctic margin: Sites 692 and 693. *Proceedings of the Ocean Drilling Program, Scientific Results* **113,** 71–88 (1990)

Ogg, J.G. Early Cretaceous magnetic polarity time scale and the magnetostratigraphy of deep sea drilling project sites 603 and 534, western central Atlantic. *Initial reports of the deep sea drilling project* **93**, 849–879 (1987)

Ouverney, C. C. & Fuhrman, J. A. Marine Planktonic Archaea take up amino acids. *Applied and Environmental Microbiology* **66**, 4829–4833 (2000)

Pancost, R. D., van Geel, B., Baas, M. & Sinninghe Damsté, J.S. $d^{13}C$ values and radiocarbon dates of microbial biomarkers as tracers for carbon recycling in peat deposits, *Geology* **28,** 663–666 (2000)

Pancost R. D., Hopmans E. C., Sinninghe Damsté J. S. & the MEDINAUT Shipboard Scientific Party. Archaeal lipids in Mediterranean cold seeps: molecular proxies for anaerobic methane oxidation. *Geochimica et Cosmochimica Acta* **65**, 1611–1627 (2001)

Parrish, J. T. Climate of the supercontinent Pangea. *The Journal of Geology* **101**, 215–233 (1993)

Parrish, J. T. & Curtis, R. L. Atmospheric circulation, upwelling, and organic-rich rocks in the Mesozoic and Cenozoic eras. *Palaeogeography, Palaeoclimatology, Palaeoecology* **40**, 3166 (1982)

Patton, J. W., Choquette, P. W., Guennel, G.K., Kaltenback, A. J. & Moore, A. Organic geochemistry and sedimentology of Lower to mid–Cretaceous deep–sea carbonates, Sites 535 and 540, Leg 771. *Initial reports of the deep sea drilling project* **77**, 339–376 (1984)

Pearson, P. N. Ditchfield, P. W., Singano, J., Harcourt–Brown, K.G., Nicholas, C.J., Olsson, R. K., Shackleton, N. J. & Hall, M. A. Warm tropical sea surface temperatures in the Late Cretaceous and Eocene epochs. *Nature* **413**, 481–470 (2001)

Pearson, A., McNichol, A. P., Benitez–Nelson, B. C., Hayes, J. M. & Eglinton, T. I. Origins of lipid biomarkers in Santa Monica Basin surface sediment: A case study using compound–specific D14C analysis. *Geochimica et Cosmochimica Acta* **65**, 3123–3137 (2001)

Pearson, A., Huang, Z., Ingalls, A.E., Romanek, C.S., Wiegel, J., Freeman, K.H., Smittenberg, R.H., Zhang, C.L., Nonmarine crenarchaeol in Nevada hot springs. *Applied and Environmental Microbiology* **70**, 5229–5237 (2004)

Pearson, P. N. van Dongen, B. E., Nicholas, C. J., Pancost, R. D., Schouten, S., Singano, J. M. & Wade, B. S. Stable warm tropical climate through the Eocene Epoch. *Geology* **35**, 211–214 (2007)

Pitcher, A., Schouten, S. & Sinninghe Damsté, J. S. In Situ production of Crenarchaeol in two California hot springs. *Applied and Environmental Microbiology* **75**, 4443–4451 (2009)

Pitcher A. S., Rychlik N., Hopmans E. C., Spieck E., Rijpstra W. I. C., Ossebaar J., Schouten S., Wagner M. and Sinninghe Damsté, J.S. Crenarchaeol and its regioisomer dominate the membrane lipids of 2 "Candidatus Nitrososphaera gargensis" a thermophilic Group I.1b Crenarchaeote. *ISME Journal* **4**, 542–552 (2010)

Podlaha, O. G., Mutterlose, J. & Veizer, J. Preservation of $\delta^{18}O$ and $\delta^{13}C$ in belemnite rostra from the Jurassic/ Early Cretaceous successions. *American Journal of Science* **298**, 324–347 (1998)

Poulsen, C. J., Gendaszek, A. S. & Jacob, R. L. Did the rifting of the Atlantic Ocean cause the Cretaceous thermal maximum? *Geology* **31**, 115–118 (2003)

Powers, L. A., Werne, J. P., Johnson, T.C., Hopmans, E. C., Damsté, J. S. S., Schouten, S. Crenarchaeotal membrane lipids in lake sediments: A new paleotemperature proxy continental paleoclimate reconstruction? *Geology* **32**, 613–616 (2004)

Price, G.D., The evidence and implications of polar ice during the Mesozoic. *Earth Science Reviews* **48**, 183–210 (1999)

Price, G.D. & Sellwood, B.W. 'Warm' palaeotemperatures from high Late Jurassic palaeolatitudes (Falkland Plateau): Ecological, environmental or diagenetic controls? *Palaeogeography, Palaeoclimatology, Palaeoecol*ogy **129**, 315–327 (1997)

Price, G. D., Ruffell, A. H., Jones, C.E., Kalin, R. M., Mutterlose, J. Isotopic evidence for temperature variation during the early Cretaceous (late Ryazanian–mid–Hauterivian). *Journal of the Geological Society of London* **157**, 335–343 (2000)

Price, G. D, Mutterlose, J. Isotopic signals from late Jurassic–early Cretaceous (Volgian–Valanginian) sub–Arctic belemnites, Yatria River, Western Siberia. *Journal of the Geological Society of London* **161**, 959–968 (2004)

Price, G. D., Wilkinson, D., Hart, M. B. Page, K. N. & Grimes, S. T. Isotopic analysis of coexisting Late Jurassic fish otoliths and molluscs: Implications for upper-ocean water temperature estimates. *Geology* **37,** 215–218 (2009)

Price, G.D. & Nunn, E.V. Valanginian isotope variation in glendonites and belemnites from Arctic Svalbard: Transient glacial temperatures during the Cretaceous greenhouse. *Geology* **38**, 251–254 (2010)

Price, G.D., Főzy, I., Janssen, N.M.M. Pálfy, J. Late Valanginian–Barremian (Early Cretaceous) palaeotemperatures inferred from belemnite stable isotope and Mg/Ca ratios from Bersek Quarry (Gerecse Mountains,Transdanubian Range, Hungary) *Palaeogeography, Palaeoclimatology, Palaeoecol*ogy **305***,* 1–9 (2011)

Rawson, P. F. Sea level changes and their influences on ammonite biogeography in the European Early Cretaceous. *Palaeopelagos Special Publication* **1**, 317–326 (1994)

Reboulet, S., Klein, J., Barraga´n, R., Company, M., Arreola, C. G., Lukeneder, A., Raisossadat, S. N., Sandoval, J., Ottilia Szives, Tavera, J. M., Vasˇı´cˇek, Z. & Vermeulen, J. Report on the 3rd International Meeting of the IUGS Lower Cretaceous Ammonite Working Group, the ‘‘Kilian Group’’ (Vienna, Austria, 15th April 2008). *Cretaceous Research* **30,** 496–502 (2009)

Retallack, G. J., A 300–million–year record of atmospheric carbon dioxide from fossil plant cuticles. *Nature* **411**, 287–290 (2001)

Rickaby, R. E. M. Shaw, S. Bennitt, G. Kennedy, H., Zabel, M. & Lennie, A. Potential of ikaite to record the evolution of oceanic $\delta^{18}O$. *Geology* **34**, 497–500 (2006)

Robertson, A. H. F., Bliefnick, D. M. Sedimentology and origin of Lower Cretaceous pelagic carbonates and deposited clastics, Blake–Bahama formation, Deep Sea Drilling Project Site 534, Western Equatorial Atlantic. *Initial Reports of the Deep Sea Drilling Project* **76**, 795–828 (1983)

Robertson, A. H. F. Origin of varve-type lamination, graded claystones and limestone-shale 'couplets' in the lower Cretaceous of the western North Atlantic. Geological Society, London, Special Publications 15, 437–452 (1984)

Robinson, S. A., Andrews, J., Hesselbo, S., Radley, J. D., Dennis, P. F., Harding, I., Allen, P. Atmospheric pCO2 and depositional environment from stable–isotope geochemistry of calcrete nodules (Barremian, Lower Cretaceous, Wealden Beds, England. *Journal of the Geological Society of London* **159**, 215–224 (2002)

Robinson, S. A. & Hesselbo, S. P. Fossil-wood carbon-isotope stratigraphy of the non-marine Wealden Group (Lower Cretaceous, southern England). *Journal of the Geological Society of London* **161**, 133–145 (2004)

Robinson, S. A., Clarke, L. J., Nederbragt, A., Wood, I. G. Mid–Cretaceous oceanic anoxic events in the Pacific Ocean revealed by carbon–isotope stratigraphy of the Calera Limestone, California, USA. *Bulletin of the Geological Society of America* **120,** 1416–1426 (2008)

Rogov, M. A. & Zakharov, V. A. Jurassic and Lower Cretaceous glendonite occurrences and their implication for Arctic paleoclimate reconstructions and stratigraphy. *Earth Science Frontiers* **17** (2010)

Roth, P. H. & Bowdler, J. L. Middle Cretaceous calcareous nannoplankton biogeography of the Atlantic Ocean. *SEPM Special Publication* **32,** 517–546 (1981)

Roth, P. H. Mesozoic palaeoceanography of the North Atlantic and Tethys Oceans. *Geological Society of London Special Publication* **21**, 299-320 (1986)

Royer, D. L., Berner, R. A., Montanez, I. P., Tabor, N. J. & Beerling, D. J. CO_2 as a primary driver of Phanerozoic climate. *GSA Today* **14**, 4–10 (2004)

Royer, D. L. CO_2–forced climate thresholds during the Phanerozoic. *Geochimica et Cosmochimica Acta* **70**, 5665–5675 (2006)

Royer, D. L., Berner, R. A. & Park, J. Climate sensitivity constrained by CO_2 concentrations over the past 420 million years. *Nature* **446**, 530–532 (2007)

Schouten S., Hopmans, E.C., Pancost, R.D. & Sinninghe Damsté, J.S. Widespread occurrence of structurally diverse tetraether membrane lipids: Evidence for the ubiquitous presence of low–temperature relatives of hyperthermophiles. *Proceedings of the National Accademy of Science* **97**, 14421–14426 (2000)

Schouten, S., Hopmans, E. C., Schefuß, E., Sinninghe Damsté, J. S., Distributional variations in marine crenarchaeotal membrane lipids: a new tool for reconstructing ancient sea water temperatures? *Earth and Planetary Science Letters* **204**, 265–274 (2002)

Schouten, S., Hopmans, E. C., Forser, A., van Breugel, Y., Kuypers, M. M. M. & Sinninghe Damsté, J. S. Extremely high sea–surface temperatures at low latitudes during the middle Cretaceous as revealed by archaeal membrane lipids. *Geology* **31**, 1069–1072 (2003)

Schouten, S., Hopmans, E.C. & Sinninghe Damsté, J.S. The effect of maturity and depositional redox conditions on archaeal tetraether lipid palaeothermometry. *Organic Geochemistry* **35,** 567–571 (2004)

Schouten S., van der Meer M. T. J., Hopmans E. C., Rijpstra W. I. C., Reysenbach A. L., Ward D. M. and Sinninghe Damsté, J. S. Archaeal and bacterial glycerol dialkyl glycerol tetraether lipids in hot springs of Yellowstone National Park. *Applied Environmental Microbiology* **73**, 6181–6191 (2007a)

Schouten S., Forster, A., Panoto, E. F. & Sinninghe Damsté, J. S. Towards calibration of the TEX_{86} palaeothermometer for tropical sea surface temperatures in ancient greenhouse worlds. *Organic Geochemistry* **38**, 1537– 1546 (2007)

Schouten, S., Huguet, C., Hopmans, EC., Kienhuis, M.V.M., Sinninghe Damsté, J.S. Analytical Methodology for TEX_{86} Paleothermometry by High–Performance Liquid Chromatography/Atmospheric Pressure Chemical Ionization–Mass Spectrometry. *Analytical Chemistry* **79**, 2940–2944 (2007)

Schouten, S., van der Meer, M. T. J., Hopmans, E. C. and Damsté, J. S. S. "Comment on "Lipids of marine Archaea: Patterns and provenance in the water column and sediments" by Turich et al. (2007)." *Geochimica et Cosmochimica Acta* **72**, 5342–5346 (2008a).

Schouten S., Hopmans E. C., Baas M., Boumann H., Standfest S., Konneke M., Stahl D. A. and Sinninghe Damsté J. S. Intact membrane lipids of ‘‘*Candidatus Nitrosopumilus maritimus*,” a cultivated representative of the cosmopolitan mesophilic group I crenarchaeota. *Applied Environmental Microbiology* **74**, 2433–2440 (2008b)

Schouten, S., Hopmans, E. C., van der Meer, J., Mets, A, Bard, E., Bianchi, T. S., Diefendorf, A., Escala, M., Freeman, K., Furukawa, Y., Huguet, C., Ingalls, A., Ménot–Combes, G., Nederbragt, A. J., Oba, M., Pearson, E. J., Rosell–Melé, A., Schaeffer, P., Shah, S., Shanahan, T. M., Shanahan, T. M., Smith, R.W., Smittenberg, R., Talbot, H. M., Uchida, M., Van Mooy, B. A. S., Yamamoto, M., Zhang, Z. & Sinninghe Damsté, J. S. An interlaboratory study of TEX_{86} and BIT analysis using high–performance liquid chromatography – mass spectrometry. *Geochemistry, Geophysics, Geosystems* **10,** (2009)

Scholle, P. A. & Arthur, M. A. Carbon isotope fluctuations in Cretaceous pelagic limestones: potential stratigraphic and petroleum exploration tool. *American Association of Petroleum Geologists Bulletin* **64**, 67–87 (1980)

Schleper, C., Jurgens, G. & Jonuscheit, M. Genomic studies of uncultivated archaea. *Nature Reviews in Microbiology* **3**, 479–488 (2005).

Schleper, C. & Nicol, G.W. Ammonia–oxidising archaea – physiology, ecology and evolution. *Advances in Microbial Physiology* **57**, C, 1–41 (2010)

Selleck, B. W., Carr, P. F. & Jones, B. G. A Review and Synthesis of Glendonites (Pseudomorphs after Ikaite) with New Data: Assessing Applicability as Recorders of Ancient Coldwater Conditions. *Journal of Sedimentary Research* **77**, 980-991 (2007)

Shackleton, N. Oxygen isotope analyses and Pleistocene temperatures re–assessed. *Nature* **215,** 15–17 (1967)

Shackleton, A. J & Kennett, J. P. Paleotemperature history of the Cenozoic and the initiation of Antarctic glaciation: oxygen and carbon analyses in DSDP sites 277, 279 and 281. In: J.P. Kennett and R.E. Houtz *et al.*, Editors, *Initial Reports of the Deep Sea Drilling Programs* **29**, U.S. Gov. Print. Off., Washington, DC (1975), pp. 743–755.

Shah S. R., Mollenhauer, G., Ohkouchi, N., Eglinton, T. I. and Pearson, A. Origins of archaeal tetraether lipids in sediments: Insights from radiocarbon analysis. *Geochimica et Cosmochimica Acta* **72**, 4577–4594 (2008)

Sheridan, R. E., Gradstein, F. M., *et al*. Site 534. *Initial Reports of the Deep Sea Drilling Project* **76**, 141–340 (1983)

Shevenell, A. E., Ingalls, A. E., Domack, E. W. & Kelly, C. Holocene Southern Ocean surface temperature variability west of the Antarctic Peninsula. *Nature* **470**, 250–254 (2011)

Simpson, E. S. W., Schlich, R., *et al*. Site 249. *Initial Reports of the Deep Sea Drilling Project* **25**, 287–346 (1974)

Sinninghe Damsté, J. S., van Bentum, E. C., Reichart, G–J., Pross, J., Schouten, S. A CO_2 decrease–driven cooling and increased latitudinal temperature gradient during the mid–Cretaceous Oceanic Anoxic Event 2. *Earth and Planetary Science Letters* **293**, 97–103 (2010)

Sinninghe Damsté, J.S., Hopmans, E.C., Pancost, R.D., Schouten, S. & Geenevasen, J.A.J. Newly discovered non–isoprenoid dialkyl diglycerol tetraether lipids in sediments, *Journal of the Chemical Society, Chemistry Communications* **17,** 1683–1684 (2000)

Sinninghe Damsté, J. S. Schouten, S., Hopmans, E. C., van Duin, A. C. T. & Geenevasen J. A. Crenarchaeol: the characteristic core glycerol dibiphytanyl glycerol tetraether membrane lipid of cosmopolitan pelagic crenarchaeota. *Journal of Lipid Research* **43**, 1641–1651 (2002a)

Sinninghe Damsté J. S., Rijpstra, W. I. C., Hopmans, E. C., Schouten, S., Wakeham, S. G. Prahl, F. G. Distribution of intact core ether lipids of planktonic crenarchaeota in the Arabian sea water column. *Applied Environmental Microbiology* **68**, 2997–3002 (2002b)

Sinninghe Damsté, J. S., van Bentum, E. C., Reichart, G–J., Pross, J. & Schouten, S. A CO_2 decrease–driven cooling and increased latitudinal temperature gradient during the mid–Cretaceous Oceanic Anoxic Event 2. *Earth and Planetary Science Letters* **293,** 97–103 (2010)

Shea, D. J., Trenberth, K. E. & Reynolds, R. W. A global monthly sea surface temperature climatology. *Journal of Climate* **5**, 987–1001 (1992)

Skelton, P. W, Spicer, R. A., Kelley, S.P. & Gilmour, I. The Cretaceous World. (Ed. Skelton, P.W) Cambridge University Press, pp. 9–360 (2003)

Sladen, C. P. & Batten, D. J. Source–area environments of late Jurassic and early Cretaceous sediments in Southeast England. Proceedings of the Geologists' Association 95, Issue 2, 149–163 (1984)

Smith, A. G., Smith, D. G., Funnell, B.M. Atlas of Mesozoic and Cenozoic Coastlines, Cambridge University Press, Cambridge, pp. 99 (1994)

Sorensen, K. B. & Teske, A. Stratified Communities of Active Archaea in Deep Marine Subsurface Sediments. *Applied and Environmental Microbiology* **72**, No. 7, 4596–4603 (2006)

Stein, C. L. & Smith, A. J. Authigenic carbonate nodules in the Nankai Trough, Site 583. *Initial reports of the Deep Sea Drilling Project* **87**, 659–668 (1985)

Stoll, H. M. & Schrag, D. P. Evidence for Glacial Control of Rapid Sea Level Changes in the Early Cretaceous. *Science* **272**, 1771–1774 (1996)

Sturt, H. F., Summons, R. E., Smith, K., Elvert, M. & Hinrichs, K.–U. Intact polar membrane lipids in prokaryotes and sediments deciphered by high–performance liquid chromatography/electrospray ionization multistage mass spectrometry – New biomarkers for biogeochemistry and microbial ecology. *Rapid Communication in Mass Spectrometry* **18,** 617–628 (2004)

Summerhayes, C. P. Organic-rich Cretaceous sediments from the North Atlantic. *Geological Society, London, Special Publications* **26**, 301–316 (1987)

Svensen, H., Planke, S., Chevallier, L., Malthe-Sørenssen, A., Corfu, F., & Jamtveita, B. Hydrothermal venting of greenhouse gases triggering Early Jurassic global warming. *Earth and Planetary Science Letters* **256,** 554–566 (2007)

Tajika, E. Climate change during the last 150 million years: reconstruction from a carbon cycle model. *Earth and Planetary Science Letters* **160**, 695–707 (1998)

Tajika, E. Carbon cycle and climate change during the Cretaceous inferred from a biogeochemical carbon-cycle model. *The Island Arc* **8**, 293–303 (1999)

Tarduno, J. A. Brinkman, D. B. Renne, P. R. Cottrell, R. D. Scher H. & Castillo P. Evidence for extreme climatic warmth from Late Cretaceous Arctic vertebrates. *Science* **282,** 2241–2244 (1998)

Theroux, S., D'Andrea, W. J., Toney, J., Amaral–Zettler, L. & Huang, Y., Phylogenetic diversity and evolutionary relatedness of alkenone–producing haptophyte algae in lakes: Implications for continental paleotemperature reconstructions. *Earth and Planetary Science Letters* **300**, 311–320, (2010)

Thomson, J., Colley, S., Higgs, N. C., Hydes, D. J., and Wilson, T. R. S. Geochemical oxidation fronts in NE Atlantic distal turbidites and their effects in the sedimentary record. *Geological Society, London, Special Publications* **31**, 167–177 (1987)

Treusch, A. H., Leininger, S., Kletzin, A., Schuster, S. C., Klenk, H. P. & Schleper, C. Novel genes for nitrite reductase and Amo–related proteins indicate a role of uncultivated

mesophilic crenarchaeota in nitrogen cycling. *Environmental Microbiology* **7**, 1985–1995 (2005)

Turich, C., Freeman, K. H., Bruns, M. A., Conte, M., Jones, A. D. & Wakeham, S. G. Lipids of marine Archaea: Patterns and provenance in the water– column and sediments. *Geochimica et Cosmochimica Acta* **71,** 3272–3291 (2007)

Turich, C., Freeman, K. H., Jones, A. D., Bruns, M. A., Conte, M. and Wakeham, S. G. "Reply to the Comment by S. Schouten, M. van der Meer, E. Hopmans, and JS Sinninghe Damsté on "Lipids of marine Archaea: Patterns and provenance in the water column. *Geochimica et Cosmochimica Acta* **72**, 5347–5349 (2008)

Uda, I., Sugai, A., Itoh Y. H. & Itoh, T. Variation in molecular species of polar lipids from Thermoplasma acidophilum depends on growth temperature, *Lipids* **36,** 103–105 (2001)

van de Schootbrugge, B., Follmi, K., Bulot, L. G. & Burns, S. J. Paleoceanographic changes during the early Cretaceous (Valanginian–Hauterivian) : evidence from oxygen and carbon stable isotopes. *Earth and Planetary Science Letters* **181**, 15–31 (2000)

van de Schootbrugge, B., Kuhn, O., Adatte, T., Steinmann, P. & Follmi, K. Decoupling of P- and Corg-burial following Early Cretaceous (Valanginian–Hauterivian) platform drowning along the NW Tethyan margin. *Palaeogeography, Palaeoclimatology, Palaeoecology* **199** 315–33 (2003)

Vander Putten, E., Dehairs, F., André, L., Baeyens, W. Quantitative in situ microanalysis of minor and trace elements in biogenic calcite using infrared laser ablation-inductively coupled plasma mass spectrometry: a critical evaluation. *Analytica Chimica Acta* **378,** 261–272 (1999)

van Hinte, J. E., Wise, S. W., Jr., *et al*., Site 603. *Initial Reports of the Deep Sea Drilling Project* **93**. 25–226 (1987)

Veizer, J., Godderis, Y. & Francois, L. M. Evidence for decoupling of atmospheric CO_2 and global climate during the Phanerozoic Eon. *Nature* **408**, 698–701 (2000)

Venter, J. C., Remington, K., Heidelberg, J. F., Halpern, A. L., Rusch, D., Eisen, J. A., Wu, D., Paulsen, I., Nelson, K. E., Nelson, W. Environmental Genome Shotgun Sequencing of the Sargasso Sea. *Science* **304**, 66–74. (2004)

Vetriani C., Reysenbach A. L. and Dore J. Recovery and phylogenetic analysis of archaeal rRNA sequences from continental shelf sediments. *FEMS Microbiology Letters* **161**, 83–88 (1998)

Voigt, S., Gale, A. S., Voigt, T. Sea–level change, carbon cycling and palaeoclimate during the Late Cenomanian of northwest Europe; an integrated palaeoenvironmental analysis. *Cretaceous Research* **27** 836–858 (2006)

Wagner, T., Herrle, J. O., Sinninghe Damsté, J. S., Schouten, S., Stüsser, I. & Hofmann, P. Rapid warming and salinity changes of Cretaceous surface waters in the subtropical North Atlantic. *Geology* **36**, 203–206 (2008)

Wakeham S.G., Lewis, C.A Hopmans, E.C. Schouten, S.. Sinninghe Damsté, J.S. Archaea mediate anaerobic oxidation of methane in deep euxinic waters of the Black Sea. *Geochim. Cosmochim. Acta*, **67**, 1359–1374 (2003)

Wallmann, K. Controls on the Cretaceous and Cenozoic evolution of seawater composition, atmospheric CO_2 and climate. *Geochimica et Cosmochimica Acta* **65**, 3005–3025 (2001)

Weijers, J. W. H., Schouten, S., Hopmans, E.C., Geenevasen, J.A.J., David, O.R.P., Coleman, J.M., Pancost, R.D. & Sinninghe Damsté, J.S., Membrane lipids of mesophilic anaerobic bacteria thriving in peats have typical archaeal traits. *Environmental Microbiology* **8**, 648–657 (2006a)

Weijers, J. W. H., Schouten, S., Spaargaren, O. C. & Sinninghe Damsté, J. S. Occurrence and distribution of tetraether membrane lipids in soils: Implications for the use of the TEX_{86} proxy and the BIT index. *Organic Geochemistry* **37**, 1680–1693 (2006b)

Weijers, J. W. H., Wiesenberg, G. L. B., Bol, R., Hopmans, E. C., Pancost, R. D. Carbon isotopic composition of branched tetraether membrane lipids in soils suggest a rapid turnover and a heterotrophic life style of their source organism(s). *Biogeosciences* **7,** 2959 – 2973 (2010)

Weissert, H. C–isotope stratigraphy, a monitor of palaeoenvironmental change: A case study from the Early Cretaceous. *Surveys in Geophysics* **10**, 1–61, (1989)

Weissert, H. Siliciclastics in the Early Cretaceous Tethys and North Atlantic Oceans: documents of periodic greenhouse climate conditions. *Memoirs Società Geologica Italiana* **44**, 59–69 (1990)

Weissert, H., Lini, A., Föllmi, K.B., Kuhn, O. Correlation of Early Cretaceous carbon isotope stratigraphy and platform drowning events: a possible link? *Palaeogeography, Palaeoclimatology, Palaeoecology* **137**, 189–203 (1998)

Weissert, H. & Erba, E. Volcanism, CO_2 and palaeoclimate: a Late Jurassic–Early Cretaceous carbon and oxygen isotope record. *Journal of the Geological Society* **161**, 695-702 (2004)

Westermann, S., Föllmi, K. B., Adatte, T., Matera, V., Schnyder, J., Fleitmann, D., Fiet, N., Ploch, I., Duchamp-Alphonse, S. The Valanginian $\delta^{13}C$ excursion may not be an expression of a global oceanic anoxic event. *Earth and Planetary Science Letters **290**,* 118–131 (2010)

Westphal, H., Munnecke, A., Pross, J., & Herrle, J. O. Multiproxy approach to understanding the origin of Cretaceous pelagic limestone–marl alternations (DSDP Site 391, Blake–Bahama Basin). *Sedimentology* **51**, 109–126 (2004)

Wignall, P. B., Newton, R. & Brookfield, M. E. Pyrite framboid evidence for oxygen-poor deposition during the Permian–Triassic crisis in Kashmir. P*alaeogeography, Palaeoclimatology, Palaeoecology* **216**, 183–188 (2005)

Williams, S. N., Schaeffer, S., Calvachev, M. L. Global carbon dioxide emission to the atmosphere by volcanoes. *Geochimica et Cosmochimica Acta* **56**, 1765–1770 (1992)

Wilson. T. R. S., Thomson, J., Hydes, D. J., Colley, S., Culkin, F. & Sorensen, J. Oxidation Fronts in Pelagic Sediments: Diagenetic Formation of Metal-Rich Layers. *Science* **232**, 972–975 (1986)

World Ocean Atlas 1998, On–line version at *www.nodc.noaa.gov/OC5/WOA98F/,* National Oceanographic Data Center Internal Report 16, Silver Spring (1999)

Wuchter, C., Schouten, S., Boschker, H. T. S. & Sinnighe Damsté, J. S. Bicarbonate uptake by marine Crenarchaeota. *FEMS Microbiological Letters* **219,** 203–207 (2003)

Wuchter, C., S. Schouten, M. J. L. Coolen, & Sinninghe Damsté, J. S. Temperature dependent variation in the distribution of tetraether membrane lipids of marine Crenarchaeota: Implications for TEX86 paleothermometry. *Paleoceanography* **19**, PA4028, (2004)

Wuchter, C., Schouten, S., Wakeham, S.G. & Sinninghe Damsté, J.S. Temporal and spatial variation in tetraether membrane lipids of marine Crenarchaeota in particulate organic matter: Implications for TEX_{86} paleothermometry. *Paleoceanography* **20**, PA3013, (2005).

Wuchter, C., Abbas, B., Coolen, M. J. L., Herfort, L., van Bleijswijk, J., Timmers, P., Strous, M., Teira, E., Herndl, G. J., Middelburg, J. J., Schouten, S., & S. Sinninghe Damsté, J. Archaeal nitrification in the ocean. *Proceedings of the National Accademy of Science* **103**, 12317–12322 (2006a)

Wuchter C., Schouten S., Wakeham S. G. & Sinninghe Damsté J. S. Archaeal tetraether membrane lipid fluxes in the northeastern Pacific and the Arabian Sea: implications for TEX_{86} paleothermometry. *Paleoceanography* **21**, PA4208 (2006b)

Zabel, M., Schulz, H. D. Importance of submarine landslides for non-steady state conditions in pore water systems; lower Zaire (Congo) deep-sea fan. *Marine Geology* **176**, p. 87–99 (2001)

Zachos, J. C., Stott, L. D., & Lohmann, K. C. Evolution of early Cenozoic marine temperatures. *Paleoceanography* **9,** 353–387 (1994)

Zachos, J. C., Schouten, S., Bohaty, S., Quattlebaum, T., Sluijs, A., Brinkhuis, H., Gibbs, S. J. & Bralower, T. J. Extreme warming of mid–latitude coastal ocean during the Paleocene–Eocene Thermal Maximum: Inferences from TEX_{86} and isotope data. *Geology* **34**, 737–740 (2006)

Zachos, J. C. McCarren, H., Murphy, B., Röhl, U. & Westerhold, T. Tempo and scale of Late Paleocene and Early Eocene carbon isotope cycles: Implications for the origin of hyperthermals. *Earth and Planetary Science Letters* **299**, 242–249 (2010)

Zeng, X., Birrien, J.–L., Fouquet, Y., Cherkashov, G., Jebbar, M., Querellou, J., Oger, P., Cambon–Bonavita, M.–A., Xiao, X. & Prieur, D. Pyrococcus CH1, an obligate piezophilic hyperthermophile: Extending the upper pressure–temperature limits for life. *ISME Journal* **3**, 873–876 (2009)

Zhang, C. L., Ye, Q., Huang, Z., Li, W–J., Chen, J., Song, Z., Zhao, W., Bagwell, C., Inskeep, W.P., Ross, C., Gao, L., Wiegel, J., Romanek, C.S., Shock, E.L., & Hedlund. B.P. global occurrence of archaeal *amoA* Genes in terrestrial hot springs. *Applied Environmental Microbiology* **74,** 6417–6426 (2008)

Zhang, Y., Sintes, E., Chen, M. N., Dai, M. H., Jiao, N. Z. & Herndl, G. J. Role of mesoscale cyclonic eddies in the distribution and activity of Archaea and Bacteria in the South China Sea. *Aquatic Microbial Ecology* **56,** 65–79 (2009)

APPENDICES

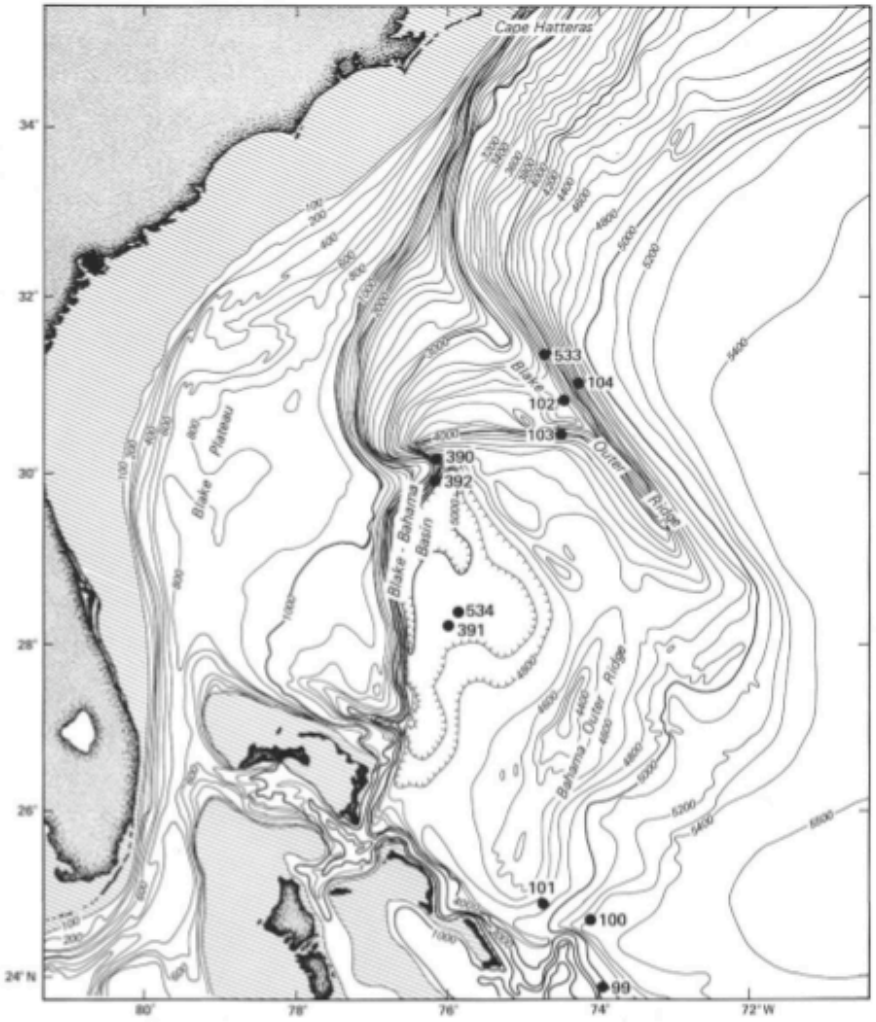

***Appendix Figure 1**. DSDP Site 534 bathymetry*

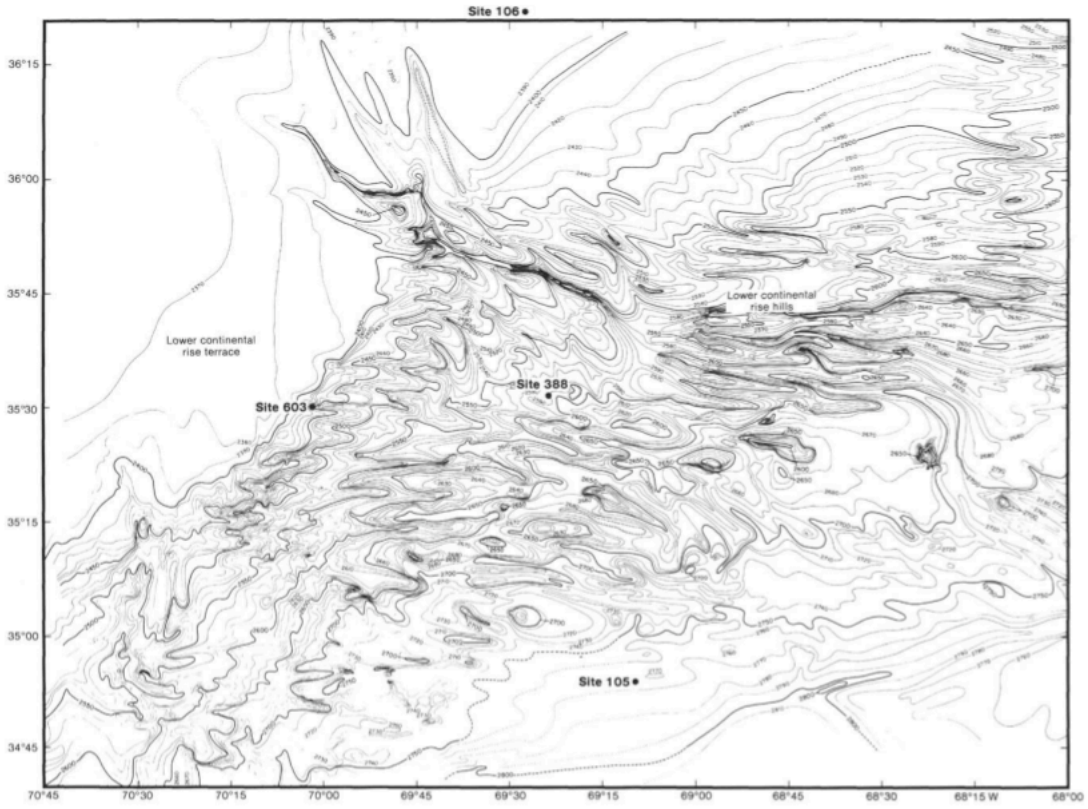

Appendix Figure 2. *DSDP Site 603 bathymetry.*

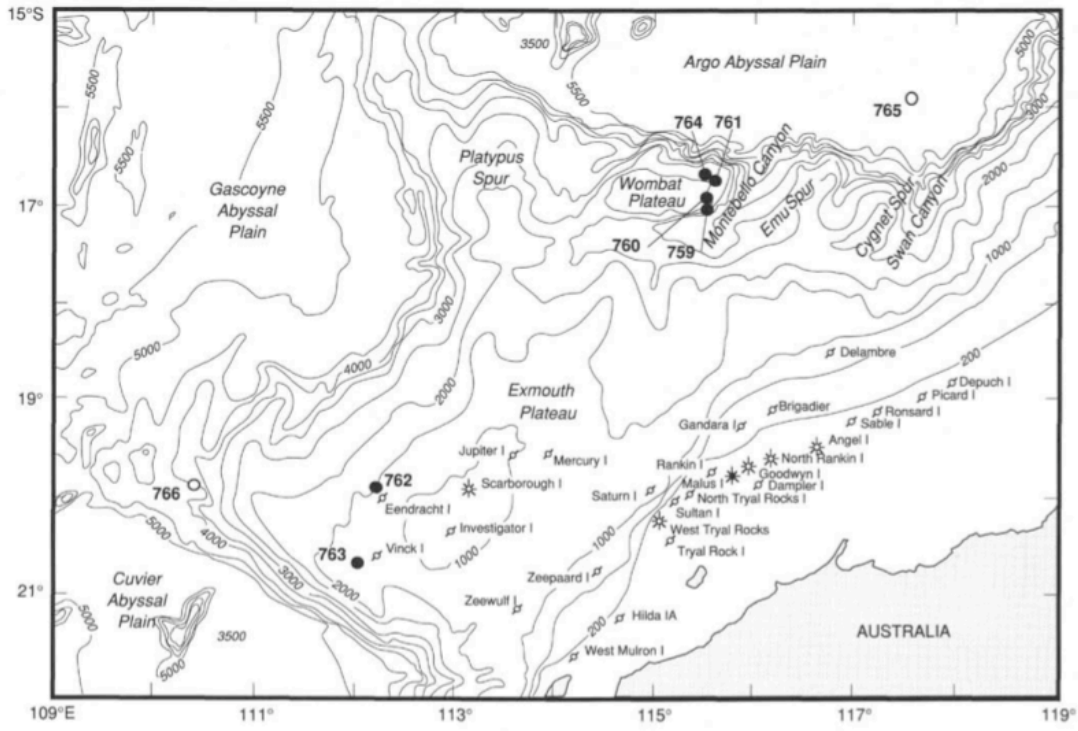

Appendix Figure 3. *Bathymetry at ODP Sites 763, 765 and 766.*

Magnetostratigraphic Event	Age (Ma)	Depth at 534A (mbsf)	Depth at 603B (mbsf)	Depth at 766A (mbsf)
M3r	129.765	982.66		276
M5n	130.798	1008.90		
M5r	131.411	1317.65	1317.65	
M6r	131.558	1020.57	1330.00	
M7n	131.849	1056.66		
M7r	132.197	1073.31	1380.00	300
M8n	132.518	1092.00	1383.35	
M8r	132.825		1401.00	349
M9n	133.14		1406.00	370
M9r	133.498	1112.93	1422.63	400
M10n	133.87	1122.56	1433.00	408.5
M10r	134.297	1127.57	1447.25	425
M10Nn	135.28	1167.41		437
M10Nr	135.685	1171.96	1493.54	441
M14r	140.361	1239.00		
M15r	141.048	1263.21		
M16n	142.061	1269.84		

Appendix Table 1. *Magnetostratigraphic tie points for Sites 534, 603 and 766. Age and depth refer to the base of the magnetochron in question. Absolute ages after Gradstein et al. (2004), with modifications to the Valanginian–Hauterivian boundary after McArthur et al. (2007a).*

Hole 534A, Core:	Lithology	Depth (mbsf)	Age (stage)	[GDGT] g^{-1}	TEX_{86}	SST (°C)1	SST (°C)2	BIT Index	TOC %	$CaCO_3$ %	$\delta^{13}C_{org}$ ‰
55-01-61	Homogeneous mudstone	1018.11	Late Hauterivian	13879	0.893	35.2	33.1		0.49	32.91	-25.99
59-01-121	Homogeneous mudstone	1054.71	Late Hauterivian	20178	0.889	35.1	33.0	0.094	0.74	44.17	-25.70
60-04-63	Homogeneous mudstone	1067.63	Late Hauterivian	119274	0.894	35.3	33.1		1.04	28.09	-24.96
64-03-102	Homogeneous mudstone	1102.47	Early Hauterivian	6973	0.890	35.1	33.0		1.63	12.21	-23.78
65-06-03	Homogeneous mudstone	1115.03	Early Hauterivian	32935	0.900	35.5	33.3		0.86	22.63	-24.41
69-05-35	Homogeneous mudstone	1145.35	Late Valanginian	10820	0.869	34.4	32.5		2.64	9.96	-22.53
70-02-49	Homogeneous mudstone	1149.99	Late Valanginian	43513	0.919	36.1	33.7		1.07	22.55	-25.74
70-04-74	Homogeneous mudstone	1153.24	Late Valanginian	20279	0.896	35.3	33.2		1.08	13.68	-24.27
72-01-92	Homogeneous mudstone	1166.92	Late Valanginian	145362	0.899	35.4	33.3		0.87	35.14	-25.74
73-01-80	Homogeneous mudstone	1175.8	Late Valanginian	27621	0.917	36.0	33.7		0.60	30.15	-24.78
73-04-19	Homogeneous mudstone	1179.63	Late Valanginian	24929	0.905	35.6	33.4		0.92	40.63	-25.36
74-05-90	Homogeneous mudstone	1190.9	Early Valanginian	8465	0.868	34.4	32.5		1.20	5.98	-24.01
75-02-120	Homogeneous mudstone	1195.7	Early Valanginian	20716	0.894	35.3	33.1		0.63	26.84	-26.72
75-06-09	Homogeneous mudstone	1200.28	Early Valanginian	160584	0.903	35.6	33.3		0.72	25.88	-27.47
77-02-29	Homogeneous	1212.79	Early	27174	0.910	35.8	33.5		0.41	8.51	-27.37

	Mudstone		Valanginian								
80-04-60	Homogeneous mudstone	1238.6	Late Berriasian	16673	0.892	35.2	33.1		1.37	37.58	-28.43
55-01-134	Laminated Marl	1018.84	Late Hauterivian	517068	0.915	36.0	33.6	0.014	0.91	60.62	-26.48
59-01-127	Laminated Marl	1054.77	Late Hauterivian	123625	0.927	36.3	33.9	0.015	0.52	77.55	-26.78
60-04-66	Laminated Marl	1067.66	Late Hauterivian	187666	0.914	35.9	33.6		0.42	75.74	-25.74
64-03-99	Laminated Marl	1102.44	Early Hauterivian	45317	0.905	35.7	33.4		0.63	59.19	-25.81
65-06-22	Laminated Marl	1115.22	Early Hauterivian	126371	0.909	35.8	33.5		0.40	85.61	-26.2
69-05-34	Laminated Marl	1145.34	Late Valanginian	120762	0.917	36.0	33.7		1.12	60.64	-26.39
70-02-58	Laminated Marl	1150.08	Late Valanginian	247252	0.919	36.1	33.7		0.74	90.56	-27.41
70-04-85	Laminated Marl	1153.35	Late Valanginian	92450	0.919	36.1	33.7		0.91	79.94	-27.45
72-01-91	Laminated Marl	1166.91	Late Valanginian	482807	0.914	35.9	33.6		0.69	79.53	-27.14
73-01-100	Laminated Marl	1176	Late Valanginian	90125	0.920	36.1	33.7		0.31	93.41	-26.48
73-04-25	Laminated Marl	1179.69	Late Valanginian	11864	0.919	36.1	33.7		0.23	85.69	-26.16
74-05-92	Laminated Marl	1190.92	Early Valanginian	93499	0.931	36.5	34.0	0.014	1.63	39.50	-27.32
75-02-102	Laminated Marl	1195.52	Early Valanginian	339097	0.937	36.7	34.1		1.61	59.22	-27.61
75-06-10	Laminated Marl	1200.29	Early Valanginian	528480	0.931	36.5	34.0		0.76	78.80	-27.66
77-02-21	Laminated Marl	1212.71	Early Valanginian	357739	0.934	36.6	34.1		0.76	69.88	-28.32
80-04-48	Laminated	1238.48	Late	15489	0.903	35.6	33.4		0.38	72.69	-28.87

	Marl		Berriasian								

***Appendix Table 2 (above)**. Site 534 geochemical data from Chapter 3. SST 1 = logarithmic calibration, TEX_{86}^{H} (Kim et al., 2010). SST 2 = reciprocal calibration, 1/ TEX_{86} (Kim et al., 2010; after Liu et al., 2009). TEX_{86} value, in some cases, represents an average of two or more analyses.*

Hole 603B, Core:	**Lithology**	**Depth (mbsf)**	**Age (stage)**	**[GDGT] g^{-1}**	**TEX_{86}**	**SST (°C)1**	**SST (°C)2**	**BIT Index**	**TOC %**	**$CaCO_3$ %**	**$\delta^{13}C_{org}$ ‰**
54-01-138	Homogeneous mudstone	1311.78	Late Hauterivian	115042	0.880	34.8	32.8		1.34	20.59	-25.98
54-04-132	Homogeneous mudstone	1316.22	Late Hauterivian	200879	0.875	34.6	32.7	0.046	1.43	24.02	
56-03-55	Homogeneous mudstone	1333.15	Late Hauterivian	72448	0.885	35.0	32.9	0.056	1.26	33.62	
58-03-111	Homogeneous mudstone	1352.91	Late Hauterivian	100487	0.859	34.1	32.3	0.039	1.28	35.12	
58-03-119	Homogeneous mudstone	1352.99	Late Hauterivian	80148	0.818	32.6	31.1		1.59	22.12	-25.00
59-02-125	Homogeneous mudstone	1360.97	Late Hauterivian	140049	0.881	34.8	32.8	0.038	0.99	32.66	-25.85
61-02-120	Homogeneous mudstone	1380.3	Late Hauterivian	82405	0.892	35.2	33.1	0.054	1.08	16.56	-24.64
62-03-38.5	Homogeneous mudstone	1390.23	Early Hauterivian	212891	0.880	34.8	32.8	0.035	1.14	20.47	-25.88
	Homogeneous	1392.33	Early	11254	0.873	34.5	32.6		1.03	16.48	-23.86

62-04-63	mudstone		Hauterivian								
64-01- 85	Homogeneous mudstone	1406.56	Early Hauterivian	55852	0.852	33.8	32.1	0.070	1.53	18.19	-24.10
64-05-105	Homogeneous mudstone	1412.75	Early Hauterivian	24820	0.878	34.7	32.8		1.39	13.24	-24.41
65-03-63	Homogeneous mudstone	1418.34	Early Hauterivian	213502	0.903	35.6	33.3	0.161	1.79	32.03	
65-04-121	Homogeneous mudstone	1420.41	Early Hauterivian	24269	0.878	34.8	32.8	0.026	1.65	20.26	-24.41
66-01-95	Homogeneous mudstone	1424.63	Early Hauterivian	86743	0.803	32.1	30.7		1.30	10.38	-24.13
66-02-77	Homogeneous mudstone	1425.97	Early Hauterivian	18133	0.869	34.4	32.5		1.94	16.58	
66-03-75	Homogeneous mudstone	1427.45	Early Hauterivian	21932	0.872	34.5	32.6		1.21	15.35	-25.55
67-01-57	Homogeneous mudstone	1433.27	Early Hauterivian	27995	0.886	35.0	32.9		1.46	20.33	
67-05-55	Homogeneous mudstone	1439.23	Late Valanginian	33174	0.876	34.7	32.7	0.052	1.41	17.10	
68-03-60	Homogeneous mudstone	1445.3	Late Valanginian	18966	0.888	35.1	33.0		1.44	29.49	
69-02-55	Homogeneous mudstone	1452.75	Late Valanginian	25296	0.875	34.6	32.7	0.050	1.24	14.35	-25.07
69-05-114	Homogeneous mudstone	1457.84	Late Valanginian	41702	0.859	34.1	32.3	0.056	1.69	17.95	-24.48
70-03-49	Homogeneous mudstone	1463.19	Late Valanginian	35795	0.869	34.4	32.5		1.41	16.27	-24.36
71-02-78	Homogeneous mudstone	1470.98	Late Valanginian	12898	0.858	34.0	32.2		1.13	26.27	-25.05
71-04-100	Homogeneous mudstone	1474.18	Late Valanginian	30701	0.890	35.1	33.0	0.034	1.75	14.87	-24.19
73-05-85	Homogeneous mudstone	1489.52	Late Valanginian	14883	0.875	34.6	32.7	0.069	1.58	15.01	-24.44
75-04-68	Homogeneous	1507.05	Late	64176	0.871	34.5	32.6		1.42	19.08	-25.24

	mudstone		Valanginian								
55-03-119	Laminated Marl	1324.19	Late Hauterivian	337750	0.903	35.6	33.3		1.13	87.32	-27.21
57-05-49	Laminated Marl	1345.69	Late Hauterivian	392203	0.891	35.2	33.1	0.010	1.94	71.07	-26.19
60-03-23	Laminated Marl	1371.23	Late Hauterivian	396284	0.911	35.8	33.5		1.44	75.63	-27.30
61-01-100	Laminated Marl	1378.6	Early Hauterivian	270783	0.909	35.8	33.5	0.010	1.26	68.66	
63-03-34	Laminated Marl	1399.51	Early Hauterivian	763428	0.912	35.9	33.6	0.012	0.95	78.99	-26.76
63-05-100	Laminated Marl	1403.2	Early Hauterivian	204448	0.921	36.2	33.8		1.96	70.18	-26.51
64-05-108	Laminated Marl	1412.78	Early Hauterivian	128938	0.914	35.9	33.6		1.83	80.31	-26.60
65-04-126	Laminated Marl	1420.46	Early Hauterivian	135942	0.897	35.4	33.2		0.85	81.38	-27.15
68-04-120	Laminated Marl	1447.4	Late Valanginian	164278	0.914	35.9	33.6	0.056	0.91	80.92	-27.12
74-06-13	Laminated Marl	1499.93	Late Valanginian	29174	0.902	35.5	33.3		0.84	80.50	-25.25
75-03-109	Laminated Marl	1505.99	Late Valanginian	67842	0.918	36.1	33.7		2.42	60.68	-26.54
76-05-45	Laminated Marl	1517.95	Early Valanginian	64206	0.902	35.5	33.3		1.63	59.84	-27.74
77-06-112	Laminated Marl	1529.72	Early Valanginian	67267	0.882	34.9	32.8		1.69	57.43	-28.68
78-03-88	Laminated Marl	1534.58	Early Valanginian	27092	0.904	35.6	33.4		0.85	53.51	
79-04-51	Laminated Marl	1545.21	Early Valanginian	25817	0.869	34.4	32.5		1.43	51.20	-28.19
81-02-98	Laminated Marl	1560.68	Late Berriasian	58994	0.909	35.8	33.5		1.49	58.03	-28.43
81-04-17	Laminated	1562.87	Late	34623	0.887	35.0	33.0			63.36	

	Marl		Berriasian						1.30		

***Appendix Table 3 (above)**. Site 603 geochemical data from Chapter 3. SST 1 = logarithmic calibration, TEX_{86}^{H} (Kim et al., 2010). SST 2 = reciprocal calibration, 1/ TEX_{86} (Kim et al., 2010; after Liu et al., 2009). TEX_{86} value, in some cases, represents an average of two or more analyses.*

***Appendix Table 4 (below)**. TEX_{86} and BIT Index data from Chapter 4. SST 1 = logarithmic calibration, TEX_{86}^{H} (Kim et al., 2010). SST 2 = reciprocal calibration, 1/ TEX_{86} (Kim et al., 2010; after Liu et al., 2009). TEX_{86} value, in some cases, represents an average of two or more analyses. Sediments from Site 603 and 534 are all laminated marls, sediments from Sites 766, 763, 692, 249 and 81/43 are mixed hemipelagic sediments. Data from BGS 81/43 should be regarded as very tentative estimates only.*

Major sites:

Leg	**Site**	**Hole**	**Core**	**Depth (mbsf)**	**Age (stage)**	**Age (ma)**	**[GDGT] g^{-1}**	**TEX_{86}**	**SST (°C)1**	**SST (°C)2**	**BIT index**
76	534	A	49-01-17	963.67	Early Barremian	129.02	3290297	0.919	36.1	33.7	0.018
76	534	A	49-03-122	967.6	Early Barremian	129.17	7411149	0.919	36.1	33.7	0.017
76	534	A	52-03-90	994.35	Late Hauterivian	130.23	1933036	0.917	36.0	33.7	0.016
76	534	A	53-02-83	1001.83	Late Hauterivian	130.52	924355	0.919	36.1	33.7	0.021
76	534	A	55-01-134	1018.84	Late Hauterivian	131.45	517068	0.916	36.0	33.7	0.014

76	534	A	59-01-127	1054.77	Late Hauterivian	131.83	123625	0.927	36.3	33.9	0.015
76	534	A	59-03-83	1057.03	Late Hauterivian	131.86	61753	0.913	35.9	33.6	
76	534	A	60-04-66	1067.66	Late Hauterivian	132.08	187666	0.914	35.9	33.6	
76	534	A	61-01-39	1071.89	Early Hauterivian	132.17	23141	0.920	36.1	33.7	0.046
76	534	A	61-04-52	1076.25	Early Hauterivian	132.25	60706	0.899	35.4	33.3	
76	534	A	63-01-136	1090.86	Early Hauterivian	132.50	77597	0.918	36.1	33.7	0.016
76	534	A	64-04-133	1104.28	Early Hauterivian	133.09	29526	0.921	36.2	33.8	
76	534	A	65-02-55	1109.55	Early Hauterivian	133.34	28351	0.919	36.1	33.7	
76	534	A	65-06-22	1115.03	Early Hauterivian	133.58	126371	0.909	35.8	33.5	
76	534	A	67-03-73	1129.15	Late Valanginian	134.34	1233895	0.927	36.3	33.9	0.006
76	534	A	69-03-147	1143.47	Late Valanginian	134.69	21200	0.921	36.2	33.8	
76	534	A	69-05-34	1145.34	Late Valanginian	134.74	120762	0.917	36.0	33.7	
76	534	A	70-02-58	1150.08	Late Valanginian	134.85	247252	0.919	36.1	33.7	
76	534	A	70-04-85	1153.35	Late Valanginian	134.93	82375	0.919	36.1	33.7	
76	534	A	71-03-72	1160.72	Late Valanginian	135.11	50216	0.920	36.1	33.7	
76	534	A	71-05-54	1163.51	Late Valanginian	135.18	70159	0.914	35.9	33.6	
76	534	A	72-01-91	1166.91	Late Valanginian	135.27	482807	0.914	35.9	33.6	

76	534	A	72-01-111	1167.11	Late Valanginian	135.27	251760	0.916	36.0	33.6	0.041
76	534	A	73-01-100	1176	Late Valanginian	135.97	90125	0.920	36.1	33.7	
76	534	A	73-04-25	1179.69	Late Valanginian	136.22	11864	0.919	36.1	33.7	
76	534	A	74-05-92	1190.92	Early Valanginian	137.01	93499	0.931	36.5	34.0	0.014
76	534	A	75-02-102	1195.52	Early Valanginian	137.33	339097	0.937	36.7	34.1	
76	534	A	75-06-10	1200.29	Early Valanginian	137.66	528480	0.931	36.5	34.0	
76	534	A	77-02-21	1212.71	Early Valanginian	138.53	357739	0.934	36.6	34.1	
76	534	A	77-04-60	1215.8	Early Valanginian	138.74	55949	0.935	36.6	34.1	
76	534	A	78-01-145	1216.95	Early Valanginian	138.82	130771	0.940	36.8	34.2	
76	534	A	78-03-77	1219.27	Early Valanginian	138.98	84950	0.940	36.8	34.2	
76	534	A	78-05-35	1221.85	Early Valanginian	139.16	46662	0.929	36.4	33.9	
76	534	A	79-03-08	1227.58	Early Valanginian	139.56	84913	0.919	36.1	33.7	
76	534	A	79-05-95	1231.45	Early Valanginian	139.83	60125	0.908	35.7	33.5	
76	534	A	80-02-136	1236.36	Early Valanginian	140.18	37157	0.923	36.2	33.8	
76	534	A	80-04-48	1238.48	Late Berriasian	140.32	15489	0.903	35.6	33.3	
76	534	A	80-05-45	1239.38	Late Berriasian	140.39	11273	0.908	35.7	33.5	
93	603	B	55-03-119	1324.19	Late Hauterivian	131.39	337750	0.903	35.6	33.3	

93	603	B	57-05-49	1345.69	Late Hauterivian	131.75	392203	0.891	35.2	33.1	0.010
93	603	B	60-03-23	1371.23	Late Hauterivian	132.09	396284	0.911	35.8	33.5	
93	603	B	61-01-100	1378.6	Early Hauterivian	132.18	270783	0.909	35.8	33.5	0.010
93	603	B	63-03-34	1399.51	Early Hauterivian	132.78	763428	0.912	35.9	33.6	0.012
93	603	B	63-05-100	1403.2	Early Hauterivian	132.98	204448	0.921	36.2	33.8	
93	603	B	64-05-108	1412.78	Early Hauterivian	133.32	128938	0.914	35.9	33.6	
93	603	B	65-04-126	1420.46	Early Hauterivian	133.46	135942	0.897	35.4	33.2	
93	603	B	68-04-120	1447.4	Late Valanginian	134.3	164278	0.914	35.9	33.6	0.056
93	603	B	74-06-13	1499.93	Late Valanginian	136.22	29174	0.902	35.5	33.3	
93	603	B	75-03-109	1505.99	Late Valanginian	136.71	67842	0.918	36.1	33.7	
93	603	B	76-05-45	1517.95	Early Valanginian	137.68	64206	0.902	35.5	33.3	
93	603	B	77-06-112	1529.72	Early Valanginian	138.64	67267	0.882	34.9	32.8	
93	603	B	78-03-88	1534.58	Early Valanginian	139.03	27092	0.904	35.6	33.4	
93	603	B	79-04-51	1545.21	Early Valanginian	139.9	25817	0.869	34.4	32.5	
93	603	B	81-02-98	1560.68	Late Berriasian	141.21	58994	0.909	35.8	33.5	
93	603	B	81-04-17	1562.87	Late Berriasian	141.41	34623	0.887	35.0	33.0	
123	766	A	28-03--88	262.485	Early Barremian	128.40	43885	0.690	27.6	26.8	0.089

123	766	A	29-03-108	272.38	Early Barremian	129.40	282030	0.660	26.3	25.6	0.057
123	766	A	31-01-60	288.105	Late Hauterivian	130.99	298413	0.642	25.4	24.7	0.044
123	766	A	32-01-13	297.335	Late Hauterivian	131.93	293609	0.656	26.1	25.4	0.031
123	766	A	33-01-69	307.49	Early Hauterivian	132.29	1430871	0.646	25.6	24.9	0.026
123	766	A	36-01-73	336.535	Early Hauterivian	132.67	250756	0.649	25.8	25.1	0.032
123	766	A	37-01-19	345.69	Early Hauterivian	132.78	118977	0.641	25.4	24.7	0.040
123	766	A	39-03-68	368.48	Early Hauterivian	133.12	164481	0.664	26.4	25.7	0.031
123	766	A	40-03-50	378	Early Hauterivian	133.24	68627	0.669	26.6	25.9	0.037
123	766	A	42-01-59	394.39	Early Hauterivian	133.43	86907	0.694	27.8	27.0	0.029
123	766	A	43-04-100	409	Early Hauterivian	133.88	80840	0.710	28.4	27.6	0.025
123	766	A	44-02-69	415.39	Late Valanginian	134.05	84469	0.646	25.6	24.9	0.043
123	766	A	44-06-52	421.22	Late Valanginian	134.20	163470	0.632	25.0	24.3	0.030
123	766	A	45-02-66	424.96	Late Valanginian	134.30	72830	0.640	25.3	24.7	0.031
123	766	A	45-04-66	427.96	Late Valanginian	134.54	94555	0.641	25.4	24.7	0.030
123	766	A	45-06-103	431.33	Late Valanginian	134.82	162189	0.642	25.4	24.8	0.036
123	766	A	46-02-91	434.91	Late Valanginian	135.11	79978	0.652	25.9	25.2	0.034
123	766	A	46-06-98	440.98	Late Valanginian	135.68	39058	0.643	25.5	24.8	

123	766	A	47-04-98	447.685	Late Valanginian	136.36	21728	0.664	26.4	25.7	

Minor sites:

Leg	Site	Hole	Core	Depth (mbsf)	Age (stage)	Age (ma)	[GDGT] g^{-1}	TEX_{86}	SST (°C)1	SST (°C)2	BIT index
123	763	B	50-03-69	636.19	Late Berriasian	/	32564	0.610	23.9	23.2	0.126
113	692	B	07-02-60	55.24	Valanginian-Hauterivian	/	3249158	0.744	29.8	28.8	0.021
113	692	B	08-01 67	59.97	Valanginian-Hauterivian	/	4658681	0.724	29.0	28.1	0.022
113	692	B	08-02-86	59.97	Valanginian-Hauterivian	/	6794442	0.732	29.3	28.4	0.020
113	692	B	08- 03-50	62.78	Valanginian-Hauterivian	/	383358	0.715	28.6	27.8	0.023
113	692	B	09-01-129	70.09	Valanginian-Hauterivian	/	2634954	0.688	27.5	26.7	
113	692	B	09-02-138	71.64	Valanginian-Hauterivian	/	948591	0.693	27.7	26.9	0.021
113	692	B	09-03-128	73.0	Valanginian-Hauterivian	/	354046	0.693	27.7	26.9	0.027
113	692	B	10-01-102	79.52	Valanginian-Hauterivian	/	777453	0.679	27.1	26.4	
113	692	B	10-02-131	81.15	Valanginian-Hauterivian	/	667018	0.695	27.8	27.0	0.019
113	692	B	10-05-108	84.9	Valanginian-Hauterivian	/	523814	0.736	29.5	28.5	
113	692	B	12 01-53		Valanginian-	/	448096	0.727	29.1	28.2	

				88.73	Hauterivian						
113	692	B	12-02-107	90.77	Valanginian-Hauterivian	/	398653	0.746	29.9	28.9	
25	249	/	24-01-104	295.04	Albian?	/	3972536	0.852	33.8	32.1	0.055
25	249	/	26-02 -86	315.36	Berriasian – Barremian?	/	1817703	0.671	26.8	26.1	0.066
25	249	/	27-02-120	324.7	Berriasian – Barremian?	/	1345243	0.601	23.5	22.7	0.065
25	249	/	28-02-47	333.97	Berriasian – Barremian?	/	4483334	0.607	23.8	23.0	0.084
25	249	/	29-01-82	351.82	Berriasian – Barremian?	/	2159174	0.585	22.7	21.9	0.077
25	249	/	30-04-145	375.95	Berriasian – Barremian?	/	61230	0.581	22.5	21.6	0.105
25	249	/	31-04 - 65	394.15	Berriasian – Barremian?	/	518475	0.586	22.7	21.9	0.056
/	*81/43*	*/*	*24*	*18.65*	*Barremian*	*/*	*10390*	*0.700*	*28.0*	*27.2*	
/	*81/43*	*/*	*37*	*27.2*	*Late Hauterivian*	*/*	*8639*	*0.728*	*29.2*	*28.3*	
/	*81/43*	*/*	*100*	*76.65*	*Early Valanginian*	*/*	*19837*	*0.634*	*25.0*	*24.4*	

Age?	Depth (mbsf)	$\delta^{13}C$ carbonate	$\delta^{18}O$ carbonate
Hauterivian?	1187.96	-5.02	-1.08
Valanginian?	1233.36	-2.51	-1.57
Valanginian?	1278.07	-1.48	-2.22
Valanginian?	1330.2	-0.04	-2.37
Valanginian?	1375.49	-4.61	-3.26
Valanginian?	1417.09	-1.80	-3.08
Valanginian?	1459.97	-0.73	-6.62
Valanginian?	1549.7	0.70	-3.32
Tithonian	1596.22	-2.63	-4.26

Appendix Table 5. *Low-resolution carbonate carbon-isotope ($\delta^{13}C_{carb}$) data from DSDP Site 416, in Chapter 4.*

***Appendix Table 6 (below)**. Lithologically-separated carbonate carbon-isotope data from Site 603, in Chapter 5.*

Site 603, Core:	Lithology	Depth	Age (stage)	Age (Ma)	$\delta^{13}C_{carb}$ ‰	$\delta^{18}O_{carb}$ ‰
58-06-26	Bioturbated Chalk	1356.41	Late Hauterivian	131.87	-2.00	-5.18
59-02-130	Bioturbated Chalk	1361.2	Late Hauterivian	131.94	-0.33	-4.16
60-04-88	Bioturbated Chalk	1373.38	Late Hauterivian	132.09	-0.90	-4.29
61-01-89	Bioturbated Chalk	1378.49	Early Hauterivian	132.16	-0.82	-4.61
62-05-34	Bioturbated Chalk	1393.54	Early Hauterivian	132.59	-1.20	-5.03
63-03-19	Bioturbated Chalk	1399.39	Early Hauterivian	132.77	-0.36	-5.05
64-05-82	Bioturbated Chalk	1412.52	Early Hauterivian	133.18	-0.24	-4.96
65-04-47	Bioturbated Chalk	1419.67	Early Hauterivian	133.41	-0.59	-5.20
66-03-03	Bioturbated Chalk	1426.73	Early Hauterivian	133.63	-0.46	-4.58
67-05-124	Bioturbated Chalk	1439.94	Late Valanginian	134.06	-0.12	-5.56
68-04-93	Bioturbated Chalk	1447.13	Late Valanginian	134.29	0.55	-4.68
69-02-66	Bioturbated Chalk	1452.86	Late Valanginian	134.47	0.85	-4.43
70-02-74	Bioturbated Chalk	1461.94	Late Valanginian	134.74	0.79	-5.47
70-05-14	Bioturbated Chalk	1465.84	Late Valanginian	134.85	0.80	-5.32

71-04-39	Bioturbated Chalk	1473.59	Late Valanginian	135.09	0.53	-5.38
73-04-105	Bioturbated Chalk	1488.25	Late Valanginian	135.53	1.45	-5.14
73-05-40	Bioturbated Chalk	1489.1	Late Valanginian	135.55	1.01	-5.12
74-01-72	Bioturbated Chalk	1493.02	Late Valanginian	135.67	1.47	-4.61
74-07-18	Bioturbated Chalk	1501.48	Late Valanginian	136.34	1.30	-5.17
75-01-13	Bioturbated Chalk	1502.03	Late Valanginian	136.38	1.77	-4.72
76-04-92	Bioturbated Chalk	1516.92	Early Valanginian	137.61	0.82	-4.23
76-05-35	Bioturbated Chalk	1517.85	Early Valanginian	137.69	0.75	-4.86
77-02-40	Bioturbated Chalk	1523	Early Valanginian	138.11	0.39	-4.42
77-05-106	Bioturbated Chalk	1528.16	Early Valanginian	138.54	-0.34	-5.74
78-03-47	Bioturbated Chalk	1534.17	Early Valanginian	139.03	0.29	-4.60
79-03-122	Bioturbated Chalk	1544.42	Early Valanginian	139.88	0.39	-4.96
80-03-58	Bioturbated Chalk	1552.78	Late Berriasian	140.56	0.50	-4.61
81-05-60	Bioturbated Chalk	1564.8	Late Berriasian	141.62	0.76	-4.33
82-02-133	Bioturbated Chalk	1570.03	Late Berriasian	142.08	0.89	-2.71
82-05-37	Bioturbated Chalk	1573.57	Late Berriasian	142.40	1.07	-4.00

Site 603, Core:	Lithology	Depth	Age (stage)	Age (Ma)	$\delta^{13}C_{carb}$ ‰	$\delta^{18}O_{carb}$ ‰
58-06-08	Laminated Marl	1356.23	Late Hauterivian	131.87	-0.62	-4.06
59-02-134	Laminated Marl	1361.24	Late Hauterivian	131.94	0.20	-2.73
60-04-66	Laminated Marl	1373.16	Late Hauterivian	132.09	0.41	-3.31
61-01-100	Laminated Marl	1378.6	Late Hauterivian	132.16	0.90	-2.94
62-04-96	Laminated Marl	1392.66	Early Hauterivian	132.57	0.36	-1.86
63-03-97	Laminated Marl	1400.17	Early Hauterivian	132.80	0.83	-4.04
64-04-52	Laminated Marl	1410.72	Early Hauterivian	133.13	1.71	-2.55
65-04-126	Laminated Marl	1420.46	Early Hauterivian	133.43	0.72	-4.43
66-04-01	Laminated Marl	1428.21	Early Hauterivian	133.68	1.15	-3.81
67-05-66	Laminated Marl	1439.36	Late Valanginian	134.04	1.60	-3.78
68-04-120	Laminated Marl	1447.4	Late Valanginian	134.30	1.09	-3.90
69-02-82	Laminated Marl	1453.02	Late Valanginian	134.47	0.93	-3.77
70-03-137	Laminated Marl	1464.07	Late Valanginian	134.80	1.67	-4.27
70-05-46	Laminated Marl	1466.16	Late Valanginian	134.86	1.33	-3.98
71-06-110	Laminated Marl	1471.5	Late Valanginian	135.02	1.29	-3.31
73-01-83	Laminated Marl	1483.53	Late Valanginian	135.38	1.46	-4.60

73-03-47	Laminated Marl	1486.17	Late Valanginian	135.46	2.29	-3.77
74-06-13	Laminated Marl	1499.93	Late Valanginian	136.21	2.09	-3.21
75-01-97	Laminated Marl	1502.87	Late Valanginian	136.45	2.18	-4.29
76-04-39	Laminated Marl	1516.39	Early Valanginian	137.57	1.59	-3.87
76-05-13	Laminated Marl	1517.63	Early Valanginian	137.67	1.45	-3.11
77-03-135	Laminated Marl	1525.45	Early Valanginian	138.31	1.05	-3.35
77-05-67	Laminated Marl	1527.77	Early Valanginian	138.51	1.15	-2.47
78-03-88	Laminated Marl	1534.58	Early Valanginian	139.07	1.13	-2.31
79-03-68	Laminated Marl	1543.88	Early Valanginian	139.83	1.25	-2.42
80-03-112	Laminated Marl	1553.32	Late Berriasian	140.61	0.93	-2.41
81-04-17	Laminated Marl	1562.87	Late Berriasian	141.45	1.34	-3.67
82-02-109	Laminated Marl	1569.79	Late Berriasian	142.06	1.56	-3.07
82-04-142	Laminated Marl	1573.12	Late Berriasian	142.36	1.49	-2.88

***Appendix Table 7 (below)**. Lithologically-separated bulk organic carbon-isotope data from Sites 534 and 603, in Chapter 5.*

Site 534, Core:	Lithology	Depth	Age (stage)	Age (Ma)	$\delta^{13}C_{org}$ ‰	TOC %	$CaCO_3$ %
49-01-17	Laminated marl	963.67	Barremian	129.02	-27.64	2.14	30.49
49-03-122	Laminated marl	967.6	Barremian	129.17	-27.97	1.43	67.11
52-03-90	Laminated marl	994.35	Hauterivian	130.23	-26.93	1.49	44.70
53-02-83	Laminated marl	1001.83	Hauterivian	130.52	-27.57	1.19	63.20
55-01-134	Laminated marl	1018.84	Hauterivian	131.45	-26.48	0.91	60.62
59-01-127	Laminated marl	1054.77	Hauterivian	131.83	-26.78	0.52	77.55
59-03-83	Laminated marl	1057.03	Hauterivian	131.86	-24.69	0.47	68.41
60-04-66	Laminated marl	1067.66	Hauterivian	132.08	-25.74	0.42	75.74
61-04-52	Laminated marl	1076.25	Hauterivian	132.25	-24.83	0.52	44.57
63-03-09	Laminated marl	1092.13	Hauterivian	132.52	-23.75	0.39	46.18
64-03-99	Laminated marl	1102.44	Hauterivian	133.01	-25.81		
65-02-55	Laminated marl	1109.55	Hauterivian	133.34	-24.82	0.75	27.97
65-06-22	Laminated marl	1115.03	Hauterivian	133.58	-26.20	0.40	85.61

67-03-73	Laminated marl	1129.15	Valanginian	134.34	-27.45	1.39	74.28
68-2-92	Laminated marl	1132.42	Valanginian	134.42	-26.98	0.65	84.64
69-01-101	Laminated marl	1140.01	Valanginian	134.60	-24.00	0.49	42.11
69-03-147	Laminated marl	1143.47	Valanginian	134.69	-25.37	0.61	44.31
69-05-34	Laminated marl	1145.34	Valanginian	134.74	-26.39	1.12	60.64
70-02-58	Laminated marl	1150.08	Valanginian	134.85	-27.41	0.74	90.56
70-04-85	Laminated marl	1153.35	Valanginian	134.93	-27.45	0.91	79.94
71-01-96	Laminated marl	1157.96	Valanginian	135.05	-25.39	0.20	78.49
71-03-72	Laminated marl	1160.72	Valanginian	135.11	-25.42	0.53	58.97
71-05-74	Laminated marl	1163.51	Valanginian	135.18	-26.68	1.18	10.82
72-01-91	Laminated marl	1166.91	Valanginian	135.27	-27.14	0.69	79.53
72-01-111	Laminated marl	1167.11	Valanginian	135.27	-26.72	1.36	52.13
72-04-112	Laminated marl	1171.33	Valanginian	135.63	-26.81	0.55	91.15
73-01-100	Laminated marl	1176	Valanginian	135.97	-26.48	0.31	93.41
73-02-80	Laminated marl	1177.24	Valanginian	136.05	-24.35	0.73	45.45
73-04-25	Laminated marl	1179.69	Valanginian	136.22	-26.16	0.23	85.69
73-cc-18	Laminated marl	1181.94	Valanginian	136.38	-25.66	0.28	83.91

74-05-92	Laminated marl	1190.92	Valanginian	137.01	-27.32	1.63	39.50
75-02-102	Laminated marl	1195.52	Valanginian	137.33	-27.61	1.61	59.22
75-04-69	Laminated marl	1198.19	Valanginian	137.51	-27.04		
75-06-10	Laminated marl	1200.29	Valanginian	137.66	-27.66	0.76	78.80
77-02-21	Laminated marl	1212.71	Valanginian	138.53	-28.32	0.76	69.88
77-04-60	Laminated marl	1215.8	Valanginian	138.74	-28.45	0.83	70.39
78-01-145	Laminated marl	1216.95	Valanginian	138.82	-28.79	0.73	47.07
78-03-77	Laminated marl	1219.27	Valanginian	138.98	-28.89	1.02	32.27
78-05-35	Laminated marl	1221.85	Valanginian	139.16	-28.46	0.96	60.49
79-03-08	Laminated marl	1227.58	Valanginian	139.56	-28.18	0.83	49.20
79-05-95	Laminated marl	1231.45	Valanginian	139.83	-28.22	0.93	52.10
80-02-136	Laminated marl	1236.36	Valanginian	140.18	-28.10	1.21	47.90
80-04-48	Laminated marl	1238.48	Berriasian	140.32	-28.87	0.38	72.69
81-04-86	Laminated marl	1247.56	Berriasian	140.60	-28.92	1.14	48.30
83-05-42	Laminated marl	1266.61	Berriasian	141.57	-27.08	0.19	49.71
84-01-110	Laminated marl	1269.1	Berriasian	141.95	-27.43	0.24	64.47
84-05-50	Laminated marl	1274.35	Berriasian	142.75	-28.58	0.61	56.96

49-05-44	Homogeneous Mudstone	969.82	Barremian	129.26	-27.08	1.22	29.51
55-01-61	Homogeneous Mudstone	1018.11	Hauterivian	131.40	-25.99	0.49	32.91
59-01-121	Homogeneous Mudstone	1054.71	Hauterivian	131.83	-25.70	0.74	44.17
60-04-63	Homogeneous Mudstone	1067.63	Hauterivian	132.08	-24.96	1.04	28.09
61-04-47	Homogeneous Mudstone	1076.2	Hauterivian	132.25	-24.25	0.70	25.66
64-03-102	Homogeneous Mudstone	1102.47	Hauterivian	133.01	-23.78	1.63	12.21
65-02-65	Homogeneous Mudstone	1109.65	Hauterivian	133.34	-24.85	1.17	19.53
65-06-03	Homogeneous Mudstone	1115.03	Hauterivian	133.58	-24.41	0.86	22.63
69-01-102	Homogeneous Mudstone	1140.02	Valanginian	134.60	-23.83	0.85	24.67
69-05-35	Homogeneous Mudstone	1145.35	Valanginian	134.74	-22.48	2.64	9.96
70-02-49	Homogeneous Mudstone	1149.99	Valanginian	134.85	-25.74	1.07	22.55
70-04-74	Homogeneous Mudstone	1153.24	Valanginian	134.93	-24.27	1.08	13.68
71-01-97	Homogeneous Mudstone	1157.97	Valanginian	135.05	-24.84	0.54	46.99
71-05-87	Homogeneous Mudstone	1163.64	Valanginian	135.19	-25.15	0.55	36.46
72-01-92	Homogeneous Mudstone	1166.92	Valanginian	135.27	-25.74	0.87	35.14
72-04-109	Homogeneous Mudstone	1171.3	Valanginian	135.63	-23.12	1.71	6.18
73-01-80	Homogeneous Mudstone	1175.8	Valanginian	135.95	-24.78	0.60	30.15

73-02-74	Homogeneous Mudstone	1177.18	Valanginian	136.05	-22.65	1.93	10.34
73-04-19	Homogeneous Mudstone	1179.63	Valanginian	136.22	-25.36	0.92	40.63
74-05-90	Homogeneous Mudstone	1190.9	Valanginian	137.01	-24.01	1.20	5.98
75-02-120	Homogeneous Mudstone	1195.7	Valanginian	137.34	-26.72	0.63	26.84
75-04-72	Homogeneous Mudstone	1198.22	Valanginian	137.52	-26.70	0.84	23.16
75-06-09	Homogeneous Mudstone	1200.28	Valanginian	137.66	-27.47	0.72	25.88
77-02-29	Homogeneous Mudstone	1212.79	Valanginian	138.53	-27.37	0.41	8.51
77-04-62	Homogeneous Mudstone	1215.82	Valanginian	138.74	-27.17	1.21	12.19
78-01-79	Homogeneous Mudstone	1216.29	Valanginian	138.78	-27.61	0.76	16.51
78-03-84	Homogeneous Mudstone	1219.34	Valanginian	138.99	-27.76	0.53	8.64
78-05-37	Homogeneous Mudstone	1221.87	Valanginian	139.17	-26.74	0.89	12.36
80-04-60	Homogeneous Mudstone	1238.6	Berriasian	140.33	-28.43	1.37	37.58

Site 603, Core:	**Lithology**	**Depth**	**Age (stage)**	**Age (Ma)**	**$\delta^{13}C_{org}$ ‰**	**TOC %**	**$CaCO_3$ %**
55-03-119	Laminated marl	1324.19	Hauterivian	131.36	-27.21	1.13	87.32
57-05-49	Laminated marl	1345.69	Hauterivian	131.73	-26.57	1.94	71.07

58-06-08	Laminated marl	1356.23	Hauterivian	131.87	-26.48		
59-02-134	Laminated marl	1361.24	Hauterivian	131.94	-27.04	1.05	69.62
60-03-23	Laminated marl	1371.23	Hauterivian	132.07	-27.30	1.44	75.63
62-04-96	Laminated marl	1392.66	Hauterivian	132.68	-26.01	0.75	64.77
63-03-34	Laminated marl	1399.51	Hauterivian	132.80	-26.76	0.95	78.99
63-05-100	Laminated marl	1403.2	Hauterivian	132.96	-26.51	1.96	70.18
64-05-108	Laminated marl	1412.78	Hauterivian	133.29	-26.60	1.83	80.31
65-04-126	Laminated marl	1420.46	Hauterivian	133.45	-27.15	0.93	82.45
66-04-01	Laminated marl	1428.21	Hauterivian	133.70	-27.02	0.51	90.62
67-05-66	Laminated marl	1439.36	Valanginian	134.06	-26.31	0.70	78.96
68-04-120	Laminated marl	1447.4	Valanginian	134.30	-27.12	0.93	82.70
69-02-82	Laminated marl	1453.02	Valanginian	134.47	-27.15	0.81	87.29
70-03-137	Laminated marl	1464.07	Valanginian	134.80	-26.28		
70-05-46	Laminated marl	1466.16	Valanginian	134.86	-26.19	0.44	67.22
73-01-83	Laminated marl	1483.53	Valanginian	135.38	-25.25	0.45	75.18
73-03-47	Laminated marl	1486.17	Valanginian	135.46	-24.64	0.36	77.09
74-06-13	Laminated marl	1499.93	Valanginian	136.21	-25.25	0.89	80.14

75-01-97	Laminated marl	1502.87	Valanginian	136.45	-25.38	0.72	79.48
75-03-109	Laminated marl	1505.99	Valanginian	136.71	-26.48	2.42	60.68
76-01-17	Laminated marl	1511.67	Valanginian	137.18	-26.36		
76-04-39	Laminated marl	1516.39	Valanginian	137.57	-27.97	1.30	76.18
76-05-45	Laminated marl	1517.95	Valanginian	137.70	-27.60	1.63	59.84
77-03-135	Laminated marl	1525.45	Valanginian	138.31	-28.81	1.02	75.10
77-05-67	Laminated marl	1527.77	Valanginian	138.51	-28.66	1.45	62.17
77-06-112	Laminated marl	1529.72	Valanginian	138.67	-28.55	1.69	57.43
78-02-120	Laminated marl	1533.4	Valanginian	138.97	-28.24	1.11	62.34
79-03-68	Laminated marl	1543.88	Valanginian	139.83	-28.74	1.59	43.46
79-04-51	Laminated marl	1545.21	Valanginian	139.94	-28.19	1.43	51.20
79-04-105	Laminated marl	1545.75	Valanginian	139.99	-28.42	1.22	62.55
80-03-22	Laminated marl	1552.42	Berriasian	140.54	-28.27	1.37	51.07
80-06-18	Laminated marl	1556.88	Berriasian	140.92	-28.19	1.24	40.98
81-01-83	Laminated marl	1559.03	Berriasian	141.11	-28.19	1.16	51.36
81-02-98	Laminated marl	1560.68	Berriasian	141.26	-28.43	1.49	58.03
81-04-15	Laminated marl	1562.85	Berriasian	141.45	-28.11	1.03	56.18

82-02-109	Laminated marl	1569.79	Berriasian	142.06	-26.74	0.36	60.24
82-04-142	Laminated marl	1573.12	Berriasian	142.36	-27.01	0.48	58.10
54-01-138	Homogeneous mudstone	1311.78	Hauterivian	131.04	-25.98	1.34	20.59
58-03-119	Homogeneous mudstone	1352.99	Hauterivian	131.83	-25.00	1.59	22.12
59-02-125	Homogeneous mudstone	1360.97	Hauterivian	131.93	-25.85	0.99	32.66
61-02-120	Homogeneous mudstone	1380.3	Hauterivian	132.18	-24.64	1.08	16.56
62-03-38.5	Homogeneous mudstone	1390.23	Hauterivian	132.64	-25.88	1.14	20.47
62-04-63	Homogeneous mudstone	1392.33	Hauterivian	132.67	-23.86	1.03	16.48
64-01-85	Homogeneous mudstone	1406.56	Hauterivian	133.15	-24.10	1.53	18.19
64-05-105	Homogeneous mudstone	1412.75	Hauterivian	133.29	-24.41	1.39	13.24
65-04-121	Homogeneous mudstone	1420.41	Hauterivian	133.45	-24.41	1.65	20.26
66-01-95	Homogeneous mudstone	1424.63	Hauterivian	133.54	-24.13	1.30	10.38
66-03-75	Homogeneous mudstone	1427.45	Hauterivian	133.67	-25.55	1.21	15.35
67-03-145	Homogeneous mudstone	1437.15	Valanginian	133.99	-24.56	1.29	13.31
68-03-20	Homogeneous mudstone	1444.9	Valanginian	134.23	-24.41	2.06	7.09
68-03-87	Homogeneous mudstone	1445.57	Valanginian	134.25	-24.20	2.48	7.00
69-02-55	Homogeneous mudstone	1452.75	Valanginian	134.46	-25.07	1.24	14.35

69-05-114	Homogeneous mudstone	1457.84	Valanginian	134.61	-24.48	1.69	17.95
69-06-145	Homogeneous mudstone	1459.65	Valanginian	134.67	-24.83	1.52	24.38
70-03-49	Homogeneous mudstone	1463.19	Valanginian	134.77	-24.36	1.41	16.27
70-04-45	Homogeneous mudstone	1464.65	Valanginian	134.82	-25.94	0.68	30.42
71-02-78	Homogeneous mudstone	1470.98	Valanginian	135.01	-25.05	1.13	26.27
71-04-100	Homogeneous mudstone	1474.18	Valanginian	135.10	-24.19	1.75	14.87
73-01-108	Homogeneous mudstone	1483.78	Valanginian	135.39	-24.68	1.50	19.61
73-01-111	Homogeneous mudstone	1483.81	Valanginian	135.39	-24.50	1.43	18.19
73-03-37	Homogeneous mudstone	1486.07	Valanginian	135.46	-24.04	1.61	20.51
73-05-85	Homogeneous mudstone	1489.52	Valanginian	135.56	-24.44	1.58	15.01
74-03-99	Homogeneous mudstone	1496.29	Valanginian	135.91	-24.54	1.47	10.99
74-05-116	Homogeneous mudstone	1499.46	Valanginian	136.17	-24.72	0.94	66.55
74-05-123	Homogeneous mudstone	1499.53	Valanginian	136.18	-23.98	1.47	19.55
75-03-89	Homogeneous mudstone	1505.79	Valanginian	136.69	-24.80	0.91	11.64
75-04-68	Homogeneous mudstone	1507.05	Valanginian	136.80	-25.24	1.42	19.08

***Appendix Table 8 (below)**. Delta-delta data from Sites 534 and 603, in Chapter 5. All samples are laminated marls. Italics indicate carbonate carbon-isotope data from Bornemann et al (2008), which is close to the bulk organic carbon-isotope data from this study, and which has been used to calculate additional $\Delta^{13}C$ points.*

Site 534, Core: ***(organic sample – this study)***	**Depth** ***(organic sample – this study)***	**Age (stage)**	**Age (Ma)** ***(organic sample – this study)***	**Depth** ***(carbonate sample – Bornemann et al., 2008)***	**$\delta^{13}C_{org}$ ‰**	**$\delta^{13}C_{carb}$ ‰**	**$\Delta^{13}C$ ‰**
49-01-17	963.67	Barremian	129.02		-27.64	1.57	29.21
49-03-122	967.6	Barremian	129.17		-27.97	0.54	28.51
52-03-90	994.35	Hauterivian	130.23		-26.93	1.88	28.81
53-02-83	1001.83	Hauterivian	130.52		-27.57	1.65	29.22
55-01-134	1018.84	Hauterivian	131.45		-26.48	1.72	28.20
59-03-83	1057.03	Hauterivian	131.86		-24.69	1.41	26.10
65-02-55	1109.55	Hauterivian	133.34		-24.82	1.59	26.40
67-03-73	1129.15	Valanginian	134.34		-27.45	1.74	29.19
69-01-101	1140.01	Valanginian	134.60		-24.00	1.90	25.90
69-03-147	1143.47	Valanginian	134.69		-25.37	2.28	27.65
69-05-34	1145.34	Valanginian	134.74	*1146.09*	-26.39	*2.04*	*28.43*
70-02-58	1150.08	Valanginian	134.85	*1150.04*	-27.41	*1.93*	*29.34*
70-04-85	1153.35	Valanginian	134.93	*1153.62*	-27.45	*1.88*	*29.33*
71-01-96	1157.96	Valanginian	135.05	*1157.13*	-25.39	*2.03*	*27.42*
71-03-72	1160.72	Valanginian	135.11		-25.42	2.26	27.68
71-05-74	1163.51	Valanginian	135.18		-26.68		26.68
72-01-91	1166.91	Valanginian	135.27	*1166.37*	-27.14	*2.09*	*29.23*
72-01-111	1167.11	Valanginian	135.27		-26.72	2.68	29.40
72-04-112	1171.33	Valanginian	135.63	*1171.01*	-26.81	*2.36*	*29.17*
73-01-100	1176	Valanginian	135.97	*1176.07*	-26.48	*2.43*	*28.91*
73-02-80	1177.24	Valanginian	136.05		-24.35	3.04	27.39
73-04-25	1179.69	Valanginian	136.22	*1179.99*	-26.16	*2.57*	*28.73*
73-cc-18	1181.94	Valanginian	136.38	*1180.98*	-25.66	*2.49*	*28.15*

74-05-92	1190.92	Valanginian	137.01	*1190.24*	-27.32	*2.36*	*29.68*
75-02-102	1195.52	Valanginian	137.33		-27.61	2.47	30.08
75-04-69	1198.19	Valanginian	137.51	*1198.32*	*-27.04*	*2.21*	*29.25*
75-06-10	1200.29	Valanginian	137.66		-27.66		27.66
77-02-21	1212.71	Valanginian	138.53	*1213.16*	*-28.32*	*1.30*	*29.62*
77-04-60	1215.8	Valanginian	138.74	*1215.69*	*-28.45*	*0.99*	*29.44*
78-01-145	1216.95	Valanginian	138.82		-28.79	1.11	29.90
78-03-77	1219.27	Valanginian	138.98		-28.89		28.89
78-05-35	1221.85	Valanginian	139.16	*1222.35*	*-28.46*	*0.72*	*29.18*
79-03-08	1227.58	Valanginian	139.56	*1227.04*	*-28.18*	*0.83*	*29.01*
79-05-95	1231.45	Valanginian	139.83	*1231.39*	*-28.22*	*0.92*	*29.14*
80-02-136	1236.36	Valanginian	140.18		-28.10	1.34	29.44
80-04-48	1238.48	Berriasian	140.32	*1238.44*	*-28.87*	*0.81*	*29.68*
81-04-86	1247.56	Berriasian	140.60		-28.92	1.31	30.24
83-05-42	1266.61	Berriasian	141.57		-27.08	1.67	28.75
84-05-50	1274.35	Berriasian	142.75		-28.58	1.49	30.07

Site 603, Core: ***(organic sample – this study)***	**Depth** ***(organic sample – this study)***	**Age (stage)**	**Age (Ma)** ***(organic sample – this study)***	**Depth** ***(carbonate sample – Bornemann et al., 2008)***	**$\delta^{13}C_{org}$ ‰**	**$\delta^{13}C_{carb}$ ‰**	**$\Delta^{13}C$ ‰**
59-02-134	1361.24	Hauterivian	131.94		-27.04	0.20	27.23
62-04-96	1392.66	Hauterivian	132.68		-26.01	0.36	26.36
65-04-126	1420.46	Hauterivian	133.45		-27.15	0.72	27.86
66-04-01	1428.21	Hauterivian	133.70		-27.02	1.15	28.17
67-05-66	1439.36	Valanginian	134.06		-26.31	1.60	27.91
68-04-120	1447.4	Valanginian	134.30		-27.12	1.09	28.21
69-02-82	1453.02	Valanginian	134.47		-27.15	0.93	28.08
70-03-137	1464.07	Valanginian	134.80		-26.28	1.67	27.95
70-05-46	1466.16	Valanginian	134.86		-26.19	1.33	27.52
73-01-83	1483.53	Valanginian	135.38		-25.25	1.46	26.71

73-03-47	1486.17	Valanginian	135.46		-24.64	2.29	26.93
74-06-13	1499.93	Valanginian	136.21		-25.25	2.09	27.34
75-01-97	1502.87	Valanginian	136.45		-25.38	2.18	27.56
75-03-109	1505.99	Valanginian	136.71	*1504.92*	-26.48	*2.51*	*28.99*
76-04-39	1516.39	Valanginian	137.57		-27.97	1.59	29.56
76-05-45	1517.95	Valanginian	137.70	*1518.20*	-27.60	*1.69*	*29.29*
77-03-135	1525.45	Valanginian	138.31		-28.81	1.05	29.86
77-05-67	1527.77	Valanginian	138.51		-28.66	1.15	29.81
77-06-112	1529.72	Valanginian	138.67	*1529.14*	-28.55	*1.21*	*29.76*
78-02-120	1533.4	Valanginian	138.97	*1533.46*	-28.24	*0.97*	*29.21*
79-03-68	1543.88	Valanginian	139.83		-28.74	1.25	29.99
79-04-51	1545.21	Valanginian	139.94	*1545.90*	-28.19	*0.86*	*29.05*
79-04-105	1545.75	Valanginian	139.99	*1545.90*	-28.42	*0.86*	*29.28*
80-03-22	1552.42	Berriasian	140.54	*1552.59*	-28.27	*1.42*	*29.69*
80-06-18	1556.88	Berriasian	140.92	*1556.51*	-28.19	*0.85*	*29.04*
81-01-83	1559.03	Berriasian	141.11	*1559.37*	-28.19	*1.03*	*29.22*
81-02-98	1560.68	Berriasian	141.26	*1560.95*	-28.43	*1.27*	*29.70*
81-04-15	1562.85	Berriasian	141.45	*1563.07*	-28.11	*1.20*	*29.31*
82-02-109	1569.79	Berriasian	142.06		-26.74	1.56	28.30
82-04-142	1573.12	Berriasian	142.36		-27.01	1.49	28.50